State of California
California Natural Resources Agency
DEPARTMENT OF WATER RESOURCES
Division of Engineering

CALIFORNIA AQUEDUCT SUBSIDENCE STUDY: SUPPLEMENTAL REPORT

San Luis Field Division

San Joaquin Field Division

March 2019

State of California
California Natural Resources Agency
DEPARTMENT OF WATER RESOURCES
Division of Engineering

CALIFORNIA AQUEDUCT SUBSIDENCE STUDY: SUPPLEMENTAL REPORT

Jeanne M. Kuttel ..... Division Chief

Joseph W. Royer ..... Chief, Geotechnical and Engineering Services Branch

Tru Van Nguyen ..... Supervising Engineer, General Engineering Section

G. Robert Barry ..... Supervising Engineering Geologist, Project Geology Section

By:

John M. Curless ..... Senior Engineering Geologist

Anna B. Gutierrez ..... Engineer, W.R.

Renato Torres ..... Engineer, HDR

Jeffrey Unruh ..... Geologist, Lettis Consultants International, Inc.

Assisted by:

Donald Walker ..... Supervising Engineer, W.R. (Operations and Maintenance)

Operations Control Office staff ..... Division of Operations and Maintenance

San Luis Field Division staff ..... Division of Operations and Maintenance

San Joaquin Field Division staff ..... Division of Operations and Maintenance

State of California
California Natural Resources Agency
DEPARTMENT OF WATER RESOURCES
Division of Engineering

CALIFORNIA AQUEDUCT SUBSIDENCE STUDY: SUPPLEMENTAL REPORT

ENGINEERING and GEOLOGY CERTIFICATION

John Curless
Certified Engineering Geologist 2188

Anna B. Gutierrez
Civil Engineer 72270

Renato Torres
Civil Engineer 83215

Jeffrey Unruh
Certified Engineering Geologist 2710

Contents

Tables

Figures

Acronyms and Abbreviations

Aqueduct	California Aqueduct
bsl	below sea level
BVPP	Buena Vista Pumping Plant
CASS	2017 California Aqueduct Subsidence Study
cfs	cubic feet per second
CVP	Central Valley Project
DAPP	Dos Amigos Pumping Plant
DEM	digital elevation model
DOE	California Department of Water Resources' Division of Engineering
DWR	California Department of Water Resources
GIS	geographic information system
HEC-RAS	Hydrologic Engineering Center's River Analysis System
LHOF	Lost Hills and Northwest Lost Hills
LiDAR	Light Detection and Ranging
mm	millimeters
MP	milepost
NAVD 88	North American Vertical Datum of 1988
NGVD 29	National Geodetic Vertical Datum of 1929
RS	river station
SAR	Synthetic Aperture Radar
SCADA	supervisory control and data acquisition
SLFD	San Luis Field Division
SJFD	San Joaquin Field Division
SWP	State Water Project
USGS	U.S. Geological Survey
Vc	compaction rate
Vs	sedimentation rate
WSE	water surface elevation

Executive Summary

This report presents new data compilation, analysis, and modeling to supplement the 2017 California Aqueduct Subsidence Study (CASS) report. This supplemental report addresses land use within a 10-mile-wide study corridor centered on the California Aqueduct (Aqueduct) in the San Luis Field Division (SLFD) and the San Joaquin Field Division (SJFD) south of San Luis Reservoir; subsidence in the Lost Hills oil field west of the Aqueduct; modeling of Aqueduct performance using the U.S. Army Corps of Engineers' Hydrologic Engineering Center's River Analysis System (HEC-RAS) hydraulic model; and predictions of future subsidence.

Agricultural Land Use

Data from county land use surveys document a multi-decade agricultural trend in the Aqueduct study corridor where row and field crops, which can be fallowed in dry years, have been progressively replaced by orchards and vineyards that require constant irrigation. As noted by researchers (Johnson and Cody 2015, Hanek et al. 2017), this long-term trend in agricultural land use has led to "demand hardening" for groundwater to sustain high-value crop producers, such as orchards and vineyards, that cannot be fallowed in dry years. Over the past several decades there has been a 10-fold increase in land planted in orchards and vineyards within the section of the Aqueduct study corridor that passes through western Fresno county, an area of well-documented historic land subsidence (Ireland et al. 1984). Land planted in orchards and vineyards also has increased by a factor of four in western Kings and Kern counties, including parts of known subsidence bowls traversed by the Aqueduct (California Department of Water Resources 2017a). These trends in agricultural land use are expected to exacerbate future demands on groundwater resources, with the potential for increased rates in land subsidence along the Aqueduct caused by groundwater pumping.

Deep Groundwater Levels

The model currently preferred by researchers to explain rapid land subsidence in the San Joaquin Valley relates groundwater withdrawal from a deep, confined aquifer below the Pleistocene Corcoran clay to increases in effective stress on the aquifer skeleton that drive compaction (Faunt et al. 2015). According to this model, the historic low elevation of the piezometric surface in the deep aquifer system can be considered a proxy for the state of pre-consolidation stress (i.e., the highest effective or inter-granular stress experienced by the aquifer to date). Any future groundwater withdrawals that reduce the piezometric surface below its historic low elevation will expose the aquifer skeleton to increased effective stress and non-elastic deformation, with associated non-recoverable compaction and permanent land subsidence.

Analysis of records from the State groundwater database indicates that from 2013 through 2016 the piezometric surface in the deep aquifer system beneath Pools 15 through 21 in western Fresno County (approximately Milepost [MP] 100 to MP 170) was drawn below historic low elevations recorded in 1967 (Ireland et al. 1984), prior to completion of Aqueduct construction and delivery of irrigation water to replace groundwater pumping. These data imply that at least some fraction of the measured subsidence of the Aqueduct during the 2013–2016 drought years is permanent and non-recoverable.

Water elevation records in the State database from other parts of the Aqueduct study corridor are limited in space and time. There is no readily available documentation of historic low elevations of the piezometric surface for Kings and Kern counties to compare with measurements during the 2013–2016 drought years. Data from a single deep well near MP 268 in western Kern Country, with more than 50 years of recorded water-level elevations, indicate that although the piezometric surface in the aquifer below the Corcoran clay declined during the 2013–2016 drought years, it did not reach or drop below the well's historic low elevation recorded in 1969 and 1970.

Land Subsidence at Lost Hills Oil Field

The Lost Hills and Northwest Lost Hills (collectively, LHOF) are two oilfields in northern Kern County that extend to within approximately one mile west of the Aqueduct. Land subsidence associated with oil production from a shallow (1,000-foot to 2,000-foot depth) reservoir has been observed at LHOF since the 1950s. Several lines of evidence indicate that oil-field subsidence in the LHOF does not extend east to the Aqueduct. Elevation change across the LHOF in the 1990s measured by synthetic aperture radar (SAR) interferometry shows that subsidence associated with oil extraction is localized across the main production area and decreases to background rates west of the Aqueduct. Long-term spatial patterns of subsidence measured by repeated land surveys along the Aqueduct are "anti-correlated" with the locus of oil-field subsidence, consistent with the SAR data showing that LHOF subsidence is localized across the main production area. Average rates of subsidence along the reach of the Aqueduct adjacent to the LHOF are similar to those in the surrounding agricultural areas to the east. They do not reflect influence of the much higher rates of subsidence documented across the LHOF to the west by SAR data.

Hydraulic Modeling

The HEC-RAS model used for the hydraulic analysis presented in the 2017 CASS report was updated with more recent topographic information; including 2016 Light Detection and Ranging and 2017 Precise Survey. The updated model is herein referred to as the 2017 Conditions CASS model. The 2017 Conditions CASS model was also updated to include additional geometric features such as updates for previous liner raises, updated check gate operations, and critical hydraulic structures such as overcrossings that may affect the capacity of the Aqueduct. The 2017 Conditions CASS model can perform unsteady- and steady-flow computations.

The 2017 Conditions CASS model was calibrated using a flow/stage dataset which extends from September 20, 2017, to October 4, 2017 — approximately 14 days. Model gates were automated to target water surface elevations (WSEs) within the range of typical operations. With this added functionality the 2017 Conditions CASS model could closely mimic observed stages and flows throughout the system.

The 2017 Conditions CASS model was used to perform various types of analyses including:

- A series of pool flow capacity calculations for Pools 14 through 30. This analysis included a comparison between capacities for 2017 conditions, 2015 conditions, and the design conditions. The findings from this assessment indicate there is a significant decrease in capacity downstream from Pool 20 and downstream from Pool 25 because of subsidence.
- An evaluation of potential impacts on flow capacity caused by overcrossings. This analysis included various simulations to estimate the hydraulic impacts of submerged overcrossings.

The findings from this assessment indicate the flow impacts of overchutes and other overcrossings are negligible as long as some headwater encroachment is allowed at the structures.

- An evaluation to estimate the impacts of projected subsidence to the aqueduct's delivery capacity. This analysis included an assessment of how subsidence will affect delivery schedules and estimates on how subsidence will affect the absolute maximum delivery capacity of the aqueduct downstream from Pools 20 and 25. The findings from this assessment indicate future subsidence may force delivery schedules to be much flatter, and ultimately may impede the ability of the system to deliver Table A allocations and even historical maximum deliveries.

Subsidence Predictions

California Department of Water Resources (DWR) land surveys along the Aqueduct through 2017 provide a 50-year history of subsidence. These data are used to derive long-term average model subsidence rates for the lowest points in subsidence bowls in the SLFD and the SJFD. A site-specific, long-term average subsidence rate is determined by fitting a linear trend line to the survey data that is constrained to pass through the origin (i.e., zero subsidence at the beginning of the survey record). This model assumes that multi-year variations in rainfall and Central Valley Project (CVP) water deliveries are random, and that future variations will be similar, on average, to those of previous decades. Consequently, the average annual groundwater withdrawal for irrigation that drives subsidence, will be similar as well. The regression statistics are used to calculate 95 percent prediction confidence intervals, which reflect the misfits between the linear subsidence trend and the observed subsidence during extended periods of wet weather (e.g., lower subsidence rates in the early 1980s, and possible local rebound) and dry weather (e.g., higher rates of subsidence in the late 2000s to the early 2010s).

In addition to the long-term average rate model, a short-term high-rate model is derived from the survey data by fitting a linear trend line to survey data measured between 2013 and 2017, when relatively rapid subsidence was measured along the Aqueduct during an extended drought period in 2013–2016. The motivation for deriving a more conservative, higher rate model is the observation that relatively lower subsidence rates measured in the early 1970s to mid-1980s reflect past patterns of agricultural land use and CVP allocations that have since changed, possibly permanently, to favor higher rates of groundwater extraction. The data from these low-subsidence-rate years may not be representative of future decades, which could potentially lead to underestimating subsidence in the next decade. Additionally, future climate trends in California are uncertain. It is unknown if the extremes in dry and wet years observed between 2013 and 2017 will continue into the next decade (e.g., Swain et al., 2014).

For the SLFD, mean subsidence predictions based the long-term average linear rate model (derived using survey data from 1967 to 2017) suggest that the most rapidly subsiding parts of the subsidence bowls will lose an additional 2 feet of freeboard within the next several decades, with the lowest areas in Pools 17 and 20 being most critically exposed to rapid subsidence. Predicted cumulative subsidence in 2040, using the long-term average rate model, ranges from approximately 5 feet in Pools 16 and 19, to approximately 9 feet in Pool 20. In contrast, predicted subsidence based on the high-rate model suggests that the low points in most SLFD pools could lose an additional 2 feet of freeboard within the next five to 10 years if the 2013–2017 patterns of California climate, CVP allocations, land use, and groundwater withdrawal continue into the next decade.

Subsidence rates in the SJFD generally are lower than those in the SLFD. A long-term average rate model (derived using data from 1986 to 2017) predicts that it will take several decades or longer for the lowest, most rapidly subsiding points in the three main subsidence bowls in SJFD to lose 2 feet of freeboard. Total cumulative subsidence in 2040 at these points is predicted to range between 2 feet and 5 feet, based on the long-term average rate model. The short-term high-rate model generally predicts loss of 2 feet of freeboard within two to five decades for the low points in Pools 23 through 26, and Pools 31 and 32. The high-rate model predicts that the low point in Pool 35 at MP 275 could lose 2 feet of freeboard within approximately 14 years, based on the rapid and relatively linear subsidence trend exhibited in the survey data from 2013 to 2017.

Based on results of the HEC-RAS hydraulic modeling, 1 foot of additional subsidence in Pool 20, relative to the elevations measured in 2017, will limit the capacity of the system to 3.8 million acre-feet of deliveries south of Pool 20 (i.e., the Maximum Table A volume). The Aqueduct will no longer be able to provide historical maximum deliveries of 3.4 million acre-feet after an additional 2.1 feet of subsidence relative to 2017. The HEC-RAS analysis assumes a flat delivery schedule with maximum flows 85 percent of the time year-round. Using mean values from the long-term average rate model for MP 163.69 in Pool 20, the 1-foot additional subsidence threshold could be exceeded within approximately 11 years, and the 2.1-foot threshold in approximately 24 years. In contrast, the mean value from the short-term high rate regression predicts exceeding 2.1 feet of additional subsidence of MP 163.69 within approximately three years.

The HEC-RAS model also indicates that cumulative subsidence as of 2017 limits conveyance of the Aqueduct system to approximately 3.1 million acre-feet across Pool 25 (assuming the system is operating 85 percent of the time annually). The HEC-RAS modeling further suggests that the volume capacity of the Aqueduct system would be reduced to the historical maximum limit of 2.6 million acre-feet with an additional 2.2 feet of subsidence in Pool 25. The long-term average-rate model derived from the time series at MP 208.11 in Pool 25 predicts that the mean time to accumulate an additional 2.2 feet of subsidence is 36 years. The high-rate model for the same time series predicts a mean time of approximately two decades (22 years) to accumulate 2.2 feet of additional subsidence.

In addition to anthropogenic subsidence associated with groundwater withdrawal, differential subsidence of the San Joaquin Valley floor because of natural processes has occurred over geologic time and presumably continues into the present. Based on analysis of geologic data, this natural or “background” subsidence is one to two orders of magnitude slower than the maximum historical rates associated with groundwater withdrawal. The natural or “background” subsidence rate will not impact future performance of the Aqueduct.

Chapter 1. Introduction

The purpose of this report is to present supplementary data and analysis to the 2017 California Aqueduct Subsidence Study (CASS) (California Department of Water Resources 2017a). This supplemental report specifically addresses the following topics:

- Land use within a 10-mile-wide corridor centered on the California Aqueduct (Aqueduct) (Chapter 2).
- Subsidence in the Lost Hills oil field, adjacent to the Aqueduct (Chapter 3).
- Results of an analysis of the hydraulic performance of the Aqueduct with the CASS Model developed using U.S. Army Corps of Engineers' Hydrologic Engineering Center's River Analysis System (HEC-RAS) software (Chapter 4).
- 2017 updates to survey data in the CASS report (Chapter 5).
- Predictions of future subsidence based on 50 years of survey data collected along the Aqueduct (Chapter 6).

This supplemental report focuses on an approximately 220-mile-long reach of the Aqueduct in the San Luis Field Division (SLFD) and the San Joaquin Field Division (SJFD) that extends from the latitude of San Luis Reservoir in the north to the Edmonston Pumping Plant in the south (Figure 1-1). As discussed in the CASS report (California Department of Water Resources 2017), this section of the Aqueduct traverses areas of known historical land subsidence (Ireland et al. 1984) and is affected by several long-wavelength, spatially-stable loci of subsidence, herein referred to as subsidence "bowls," that are well-documented by repeated surveying along the Aqueduct since the late 1960s. The maximum subsidence values cited in this report are relative to a post-construction 1967 precise survey elevation, and do not include subsidence that occurred during construction (see Section 5.3 for discussion). The main subsidence bowls discussed in this report include the following as shown in Figure 1-1.

- An approximately 47-mile reach of the Aqueduct between Milepost (MP) 96 and MP 143 in the SLFD, encompassing Pools 15 through 18, with a maximum subsidence of approximately 5.5 feet since 1967 near MP 127 (Pool 17). This subsidence feature is referred to as the "Panoche bowl" because of its proximity to Panoche Creek.
- An approximately 27-mile reach between MP 143 and MP 170 in the SLFD, encompassing Pools 19, 20, and the northern part of Pool 21, with a maximum subsidence of approximately 6 feet since 1967 at MP 160.45. This subsidence feature is referred to as the "Los Gatos bowl" because of its proximity to Los Gatos Creek.
- An approximately 32-mile reach of the Aqueduct between MP 192 and MP 224 in the SJFD that encompasses the southern part of Pool 23, all of Pools 24 and 25, and the northern half of Pool 26. This subsidence feature is referred to as the "Kern bowl" because it is bordered on the east by the Kern River channel. There are two maxima of 3.0 feet and 3.3 feet of total subsidence near MP 198 and MP 208, respectively, separated by a subsidence minimum or "divide" near MP 204, exhibiting approximately 1.0 foot of cumulative subsidence since 1967.
- An approximately 13-mile reach of the Aqueduct between MP 250 and MP 263 in the SJFD that encompasses the southern end of Pool 30, all of Pools 31 and 32, and the northern end of Pool 33. This subsidence feature is referred to as the "Maricopa bowl" because it is adjacent to the Maricopa Plain near the town of Taft. Maximum subsidence within this bowl since 1967 is approximately 1.6 feet near MP 256.

- An approximately 9-mile reach of the Aqueduct between MP 269 and MP 278 in the SJFD that encompasses the southern part of Pool 34 and all of Pool 35. This subsidence feature is referred to as the "Pleito bowl" because of its proximity to Pleito Creek. Maximum subsidence within this bowl since 1967 is approximately 1.7 feet near MP 275.

The CASS report (California Department of Water Resources 2017) presents a full description of the study area, the construction history of the Aqueduct, a summary of previous studies of land subsidence in the San Joaquin Valley, and subsidence data and analysis for the Aqueduct through 2015.

Figure 1-1 Land Use Study Corridor Along the California Aqueduct

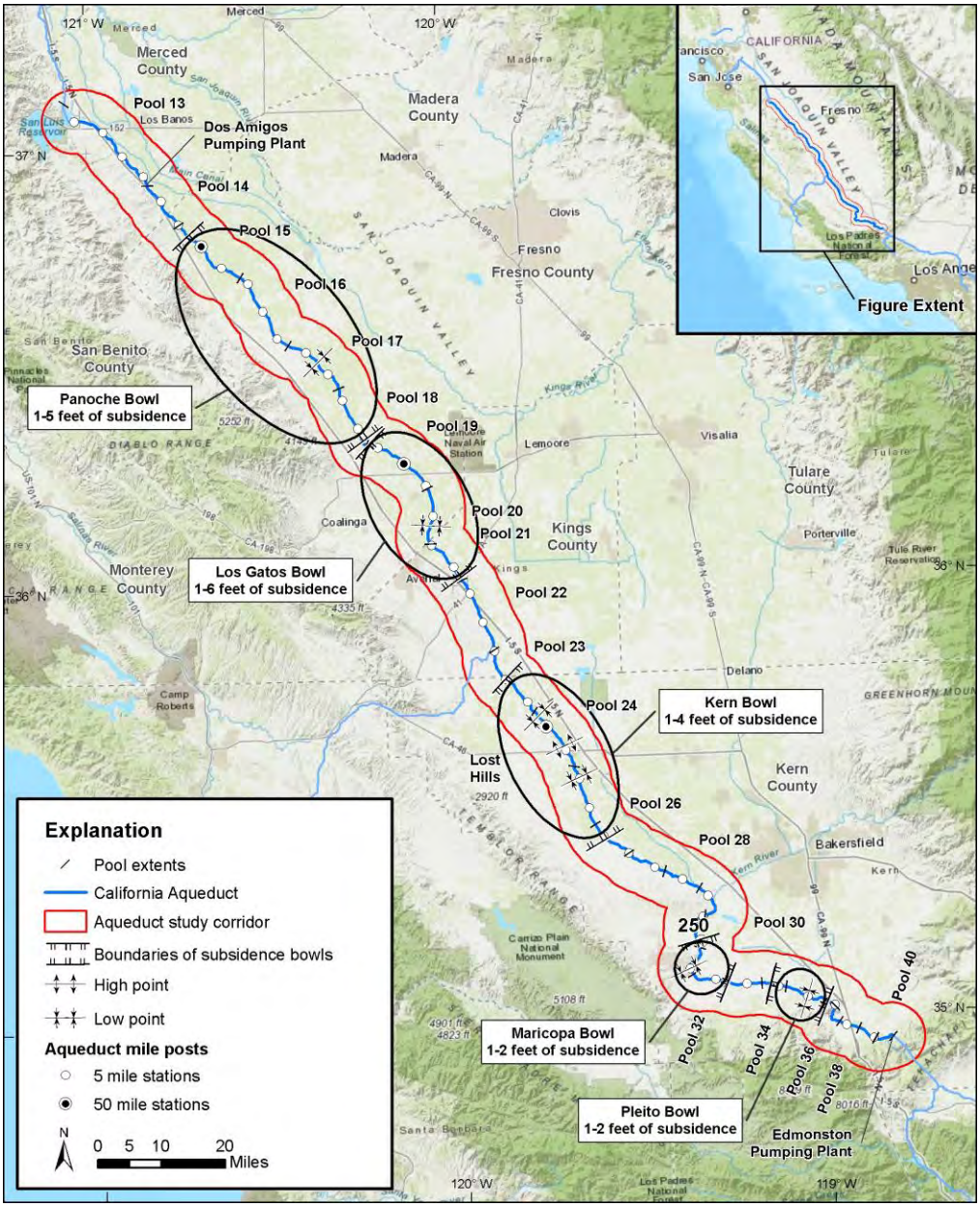

Chapter 2. Agricultural Land and Water Use

2.1 Agricultural Land Use

2.1.1 Introduction

This section presents an analysis of spatial and temporal changes in land use within the Aqueduct study corridor (Figure 1-1). This analysis uses data from periodic land-use surveys for Merced, Fresno, Kings, and Kern counties to evaluate changes through time in acreage dedicated to orchards and vineyards relative to vegetables and row crops within the study corridor. The analysis of land-use data within the study corridor is supplemented with information from annual county crop reports to assess whether countywide changes in agricultural land use over time have resulted in an average per-acre increase in the use of irrigation water. Because rates of land subsidence in the San Joaquin Valley are correlated with rates of groundwater withdrawal (Faunt et al. 2016), changes in land use that affect demand for irrigation water will potentially affect future subsidence.

The distinction between orchards and vineyards, and vegetables and row crops, reflects potential differences in long-term agricultural water use because increases in permanent crop producers, such as orchards and vineyards contribute to "demand hardening" for irrigation water (Faunt et al. 2016). Johnson and Cody (2015) described changes in agricultural land use that result in demand hardening for water as follows:

> "Attention has…focused on trends in California toward growing more permanent orchard crops, such as fruit and nut trees and vineyard crops, as well as production of grain and pasture crops, much of which is used to support the state's meat and dairy industries. Orchard crops refer to tree or vineyard crops that are planted once, require continuous watering to reach maturation, and cannot be fallowed during dry years without loss of investment. In contrast, most vegetables and other row crops (including grain and pasture crops) are annual crops that are sown and harvested during the same production year, sometimes more than once, and may be fallowed in dry years."

Land use surveys for San Joaquin Valley counties conducted over multiple years by the California Department of Water Resources (DWR), and a statewide survey in 2014 by Land IQ (an independent geographic analysis firm), provide the basic data for determining total acreage devoted to orchards and vineyards, vegetables and row crops, and all "other" land use (both agricultural and urban) in the 10-mile-wide Aqueduct study corridor for the given year that the survey was performed (Table 2-1). For the DWR land-use surveys, analysts interpreted aerial photos, satellite imagery, and other remote sensing data to map land use and crop type. Field reconnaissance was performed to verify the interpretation and mapping, and acreage for the various mapped land-use classes during the survey year was tallied and reported. The

Table 2-1 Percentage of Land Use Classes in the Study Corridor

Year	Row/Field Crops	Orchards/Vineyards	Other Land Uses
Merced County			
1995	67.4%	7.2%	25.4%
2002	66.8%	6.8%	26.4%
2012	61.6%	8.5%	29.9%
2014	51.0%	13.6%	35.4%
Fresno County			
1986	94.4%	3.7%	1.9%
1994	90.3%	5.6%	4.1%
2000	84.3%	14.2%	1.4%
2008	64.7%	30.1%	5.3%
2014	27.6%	39.9%	32.5%
Kings County			
1991	59.0	10.2%	30.8%
1996	81.7%	10.9%	7.4%
2003	54.9%	28.5%	16.6%
2013	40.9%	41.5%	17.6%
2014	20.6%	40.6%	38.8%
Kern County			
1990	68.9%	15.4%	15.7%
1998	68.7%	22.5%	8.8%
2006	45.9%	42.0%	12.1%
2014	26.2%	56.1%	17.8%
2015	32.1%	56.9%	11.0%

2014 Land IQ survey employed computer algorithms to analyze digital remote sensing data and classify land use and crop type for the entire state of California. Field reconnaissance also was performed for the Land IQ survey to evaluate accuracy of the classification. See Land IQ (2017) for additional details about the methodology and results of the 2014 statewide survey. For the purposes of the present analysis, all land use and crop-type classes reported for the DWR and Land IQ surveys were grouped into three general classes:

1. Orchards and vineyards (hereafter referred to as "Orchards/Vineyards"), which include deciduous fruits and nuts, citrus and subtropical fruits, and vineyards.
2. Row crops and vegetables ("Row/Field Crops"), which include grain and hay, rice, field crops, pasture, and truck crops.
3. All other land use ("Other"), including idle land, semi-agricultural and incidental land, urban land, native vegetation, and unclassified.

This analysis expands on a previous study of land use along the Aqueduct by Guillen (2016), which evaluated the percentage of land under cultivation for all "row and tree crops" versus "empty" land. The

present analysis explicitly distinguishes orchards and vineyards, from row and field crops, and permits evaluation of relative changes in acreage planted in these two different classes of crops over time.

Changes in acreage devoted to these three land-use classes, through time, are illustrated by a series of maps for each county derived from the DWR and Land IQ surveys. The land-use maps are presented in Appendix A. The maps are snapshots of annual land use in the study corridor separated by intervals of time that vary between approximately 6 and 10 years, and spanning total periods ranging from 17 years (Merced County) to 28 years (Fresno County). The total acreage devoted to Orchards/Vineyards, Row/Field Crops and Other land use within the study corridor were determined for each county survey with standard geographic information system (GIS) methods, and used to evaluate relative changes in these land-use categories over time. Additional GIS maps were created to display changes in crop types between the earliest and most recent land surveys.

For additional context on changing agricultural land use through time, annual crop reports for Merced, Fresno, Kings, and Kern counties were reviewed for supplementary data on acreage devoted to specific crops in a given year, rather than the three generalized classes of land use shown in the maps in Appendix A. Although the agricultural reports provide additional information on individual crops grown in each county, and their relative economic importance, the data are reported for the entire county and are not specific to the Aqueduct study corridor. It is assumed here that the patterns and trends of land use documented in the countywide reports generally apply to the reach of the study corridor that passes through each county.

To assess the potential effect of land-use changes on agricultural water use in the four counties of the study corridor, data from the annual county crop reports were combined with typical agricultural water use in California to evaluate whether changes in the mix of crop types, over time, has resulted in a change in the average annual use of irrigation water on a per-acre basis. The county crop reports commonly list the annual top ten, or more, crops in terms of their total revenue, along with the total acreage harvested for each crop. The “top-value” crops highlighted in the annual reports collectively represent the majority of agricultural land devoted to crops in a given county. Using the county crop data, the total annual agricultural water usage for the top-value crops was estimated by multiplying the total acres harvested of a given crop by the average annual per-acre water usage for the crop as reported in Johnson and Cody (2015) (Table 2-2), and then summing the usage for all the top-value crops. This provides an estimate of the total agricultural water used in the county for each year of interest. The summed total water use for all top-value crops was divided by the total acres harvested to estimate an average annual water use, on a per-acre basis, for the mix of top-value crops in a given year.

These estimates (total water applied and average per-acre application for the top-value crops) were calculated for the most recent year that a crop report is available for a given county, as well as the year, or closest year, corresponding to the earliest available land-use survey for the county. Because the types of crops grown in a given county have changed over time, comparing the average annual water use per acre for the top crops from different years provides a means of assessing whether the change in agricultural land use over time has resulted in a mix of crop types that requires more or less irrigation water, on average.

Although this analysis provides a basis for assessing potential changes in water usage over time, in tandem with changes in the mix of crops grown, it should be noted that irrigation practices also have

changed over time, and that the modern per-acre water usage for crops reported by Johnson and Cody (2015; Table 2-2) is likely different than it was one to three decades ago (see discussion in Hanak et al., 2017). The estimates of past water usage discussed in this report are most accurately interpreted as estimates of what irrigation water usage would be now if there had been no changes in agricultural land use, and if the mix of crop types had remained constant over time.

Table 2-2 Annual Water Use for Selected Crops

Crop Group	Average Acre-Feet Applied per Acre
Alfalfa	5
Rice	4.6
Irrigated Pasture	4.1
Almonds and Pistachios	3.5
Deciduous Fruits and Vegetables	3.3
Cotton	3.1
Corn	2.8
Onions and Garlic	2.8
Other Field Crops	2.6
Processing Tomato	2.4
Vine	1.9
Fresh Tomato	1.8
Vegetables/Non-Tree Fruits	1.5
Grain	1.4

Source: California Water Production and Irrigated Water Use, 2015.
https://www.everycrsreport.com/files/20150630_R44093_126291b87754c75f5965cae138b0363371948f61.pdf

2.1.2 Merced County

2.1.2.1 Land Use, 1995–2014, Aqueduct Study Corridor

Land-use surveys in Merced County are available for 1995, 2002, 2012, and 2014 (Table 2-1). Maps based on the survey data (Figures A-1, A-2, A-3, and A-4 in Appendix A), and a plot of relative percentage of the three primary land-use classes through time (Figure 2-1), reveal modest changes in agricultural land use over the past two decades. Land planted in Orchards/Vineyards increased from approximately 7 percent to 9 percent within the study corridor between 1995 and 2012, whereas Row/Field Crops decreased from 67 percent to 62 percent of the total survey area (Table 2-1 and Figure 2-1). The surveys show relatively abrupt changes between 2012 and 2014 as acreage reported for Orchards/Vineyards and Other uses both increased by approximately 5 percent of the total area in the study corridor. The percentage of acreage devoted to Row/Field Crops correspondingly decreased by approximately 10 percent (Figure 2-1).

Patterns of agricultural land use in 2014 relative to 1995 are illustrated in Figure 2-2. Most of the change from Row/Field Crops to Orchards/Vineyards directly adjacent to the Aqueduct occurred between MP 81 and MP 92; this reach of the study corridor does not lie within a recognized subsidence bowl (see discussion in Chapter 1). In general, the majority of land-use change directly adjacent to the Aqueduct north of MP 80 is characterized by conversion of Orchards/Vineyards to Row/Field Crops and Other use.

In contrast, Pool 13 and an area near MP 90 have dominantly changed from Row/Field Crops to Orchards/Vineyards (Figure 2-2).

2.1.2.2 Estimated Average Agricultural Water Use, 2004 and 2014, Merced County

According to an annual Merced County agricultural report, the top-value crops produced in 2015 include (in descending order of acres harvested) silage (corn), almonds, silage (other), alfalfa, tomatoes (for processing), irrigated pasture, sweet potatoes, wine grapes, cotton, tomatoes (for market), and miscellaneous vegetables (Merced County 2015) (Figure 2-3). Total acreage planted in these crops in 2015 was approximately 499,000 acres, out of approximately 652,000 acres planted in all crops (exclusive of rangeland grazing), or approximately 77 percent of all agricultural land devoted to crops in Merced County. Based on typical annual agricultural water usage for these crops reported by Johnson and Cody (2015), estimated total water use for the top-value crops in Merced County in 2015 was approximately 1.689 million acre-feet (Figure 2-4). The average water usage, per acre harvested, for the top-value crops in 2015 was approximately 3.4 acre-feet. Based on the annual water requirements and total acreage devoted to individual crops, hay, almonds, and silage accounted for approximately 82 percent of the total water applied to all top crops in Merced County in 2015.

Figure 2-1 Changes in Land Use Over Time in the Study Corridor, Merced County

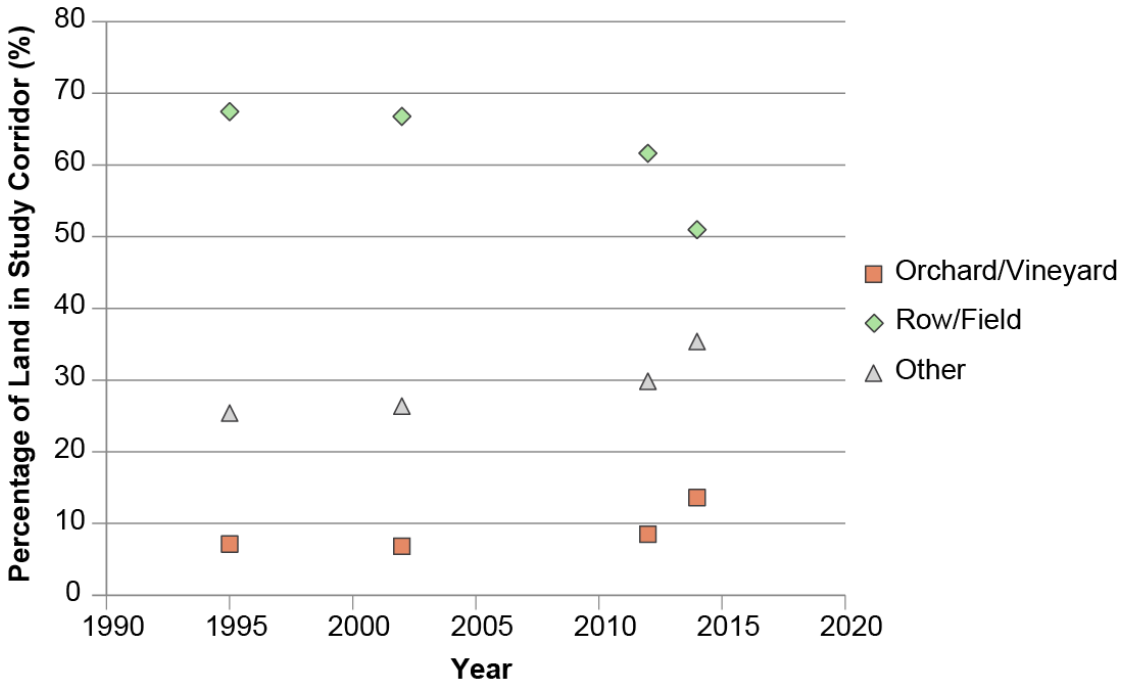

Figure 2-2 Agricultural Land Use in 2014 Relative to 1995, Aqueduct Study Corridor, Merced County

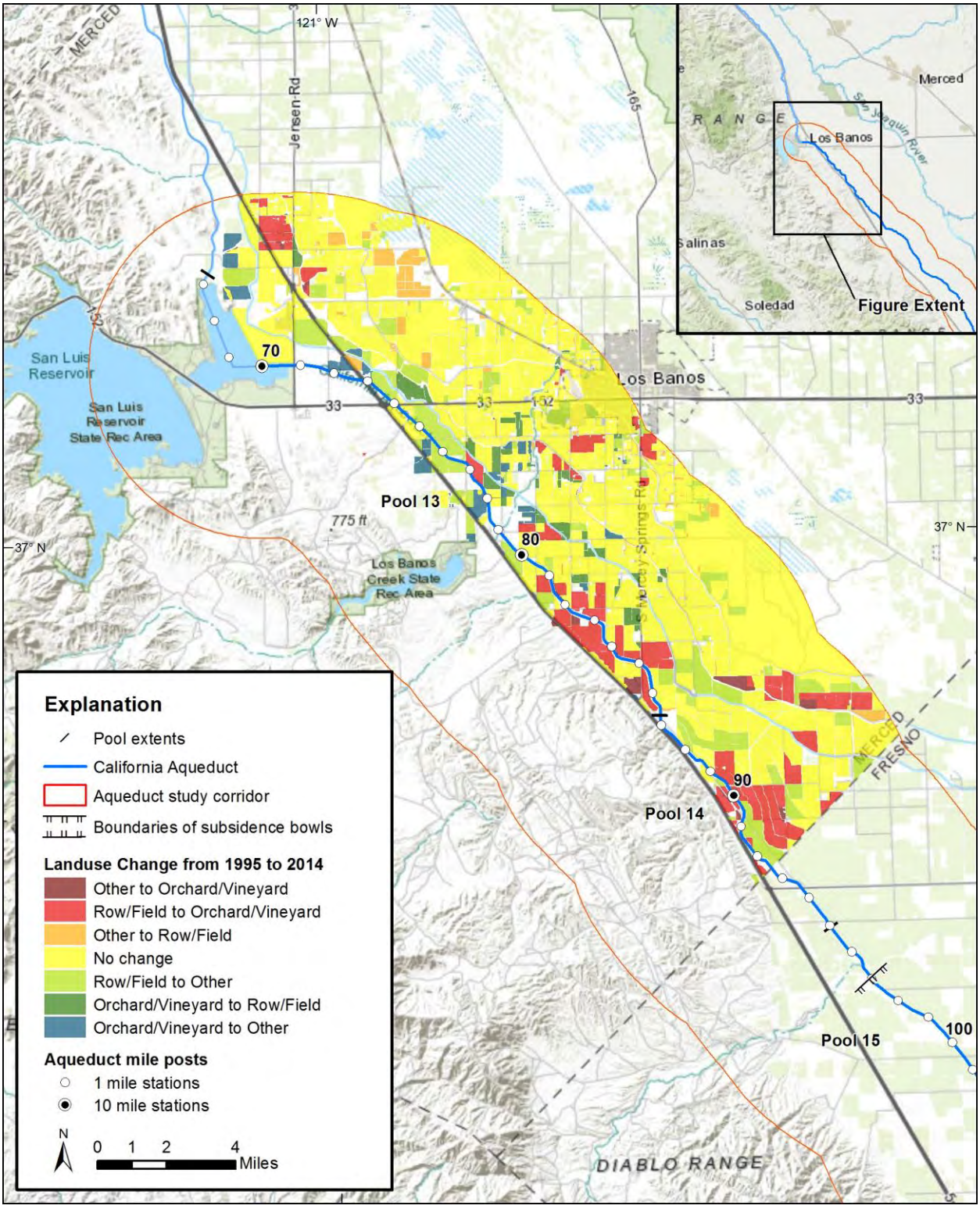

For comparison, the top-value crops produced in Merced County in 2004 included (in descending order of acres harvested) almonds, alfalfa, silage (corn), cotton, irrigated pasture, tomatoes (for processing and market), sweet potatoes, and nursery products (Merced County 2004) (Figure 2-5). Total acreage planted in these crops in 2004 was approximately 408,000 acres, out of approximately 587,000 acres planted in all crops (exclusive of rangeland), or approximately 70 percent of all agricultural land devoted to crops in Merced County in 2004. Based on typical annual agricultural water usage for these crops reported by Johnson and Cody (2015), estimated total water use for the top-value crops in Merced County in 2004 was approximately 1.468 million acre-feet (Figure 2-6). The average water usage per acre harvested was approximately 3.6 acre-feet in 2004. Based on the annual water requirements and total acreage devoted to individual crops, almonds, alfalfa (hay), silage (corn), cotton, and irrigated pasture accounted for approximately 95 percent of the total water applied to all top-value crops in Merced County in 2004.

This review of data from the annual Merced County reports indicates that total agricultural land in the entire county devoted to crops (including field, seed, vegetable and fruit/nut crops, and exclusive of rangeland) increased by approximately 65,000 acres between 2004 and 2015, representing an approximately 16 percent increase in 11 years. Almonds, hay, and silage occupied the top tier of countywide top-value crops in both 2004 and 2015, consistent with relatively small changes in land dedicated to Orchards/Vineyards versus Row/ Field crops in the study corridor (Figure 2-2). Total estimated agricultural water usage for the top-value crops in all of Merced County increased between 2004 and 2015, consistent with the countywide increase in total land dedicated to all crops. Estimated average agricultural water use on a per-acre basis for top-value crops declined slightly from 3.6 acre-feet in 2004, to 3.4 acre-feet in 2015, but this difference probably is not significant given the uncertainty in the assumptions used in the calculations.

Figure 2-3 Top-Value Crops, Merced County, 2015

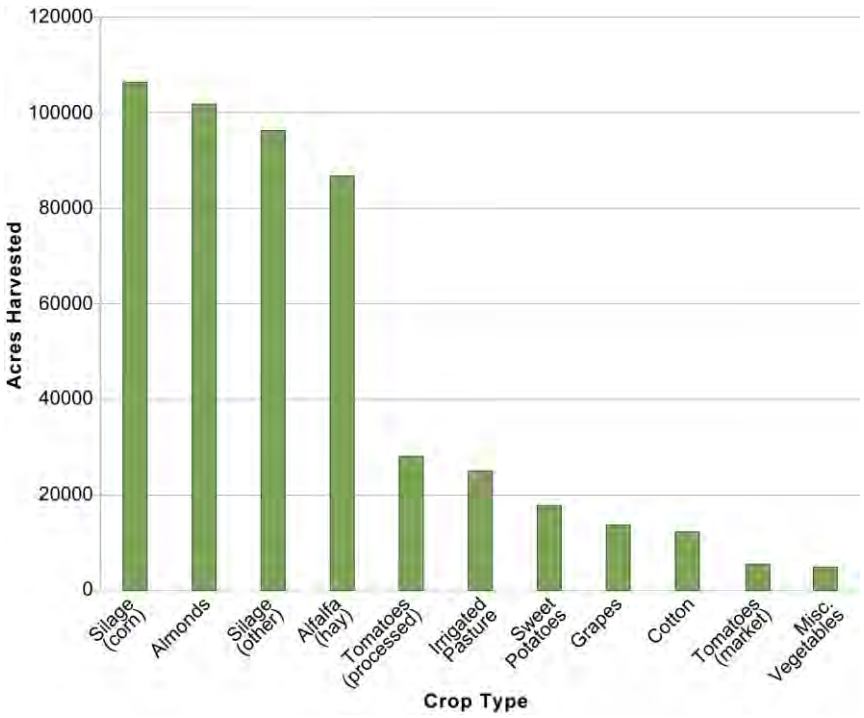

Figure 2-4 Relative Water Use by Top-Value Crops, Merced County, 2015

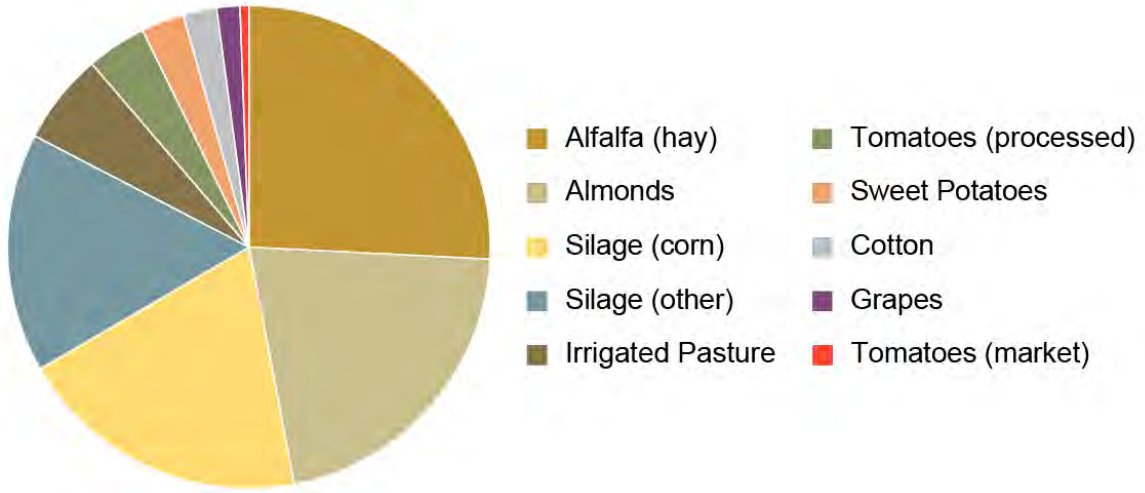

Note: Total estimated water use represented by this chart is 1.7 million acre-feet.

Figure 2-5 Top-Value Crops, Merced County, 2004

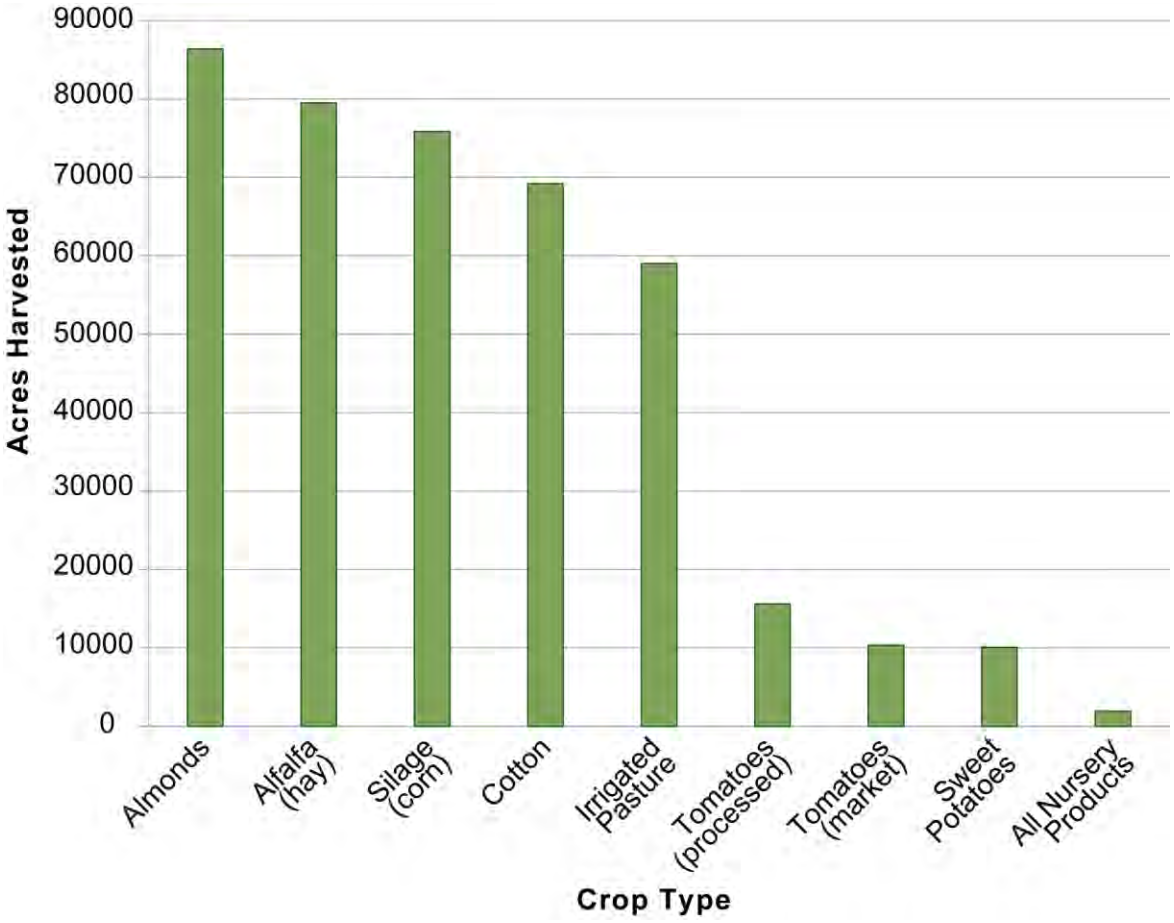

Figure 2-6 Relative Water Use by Top-Value Crops, Merced County, 2004

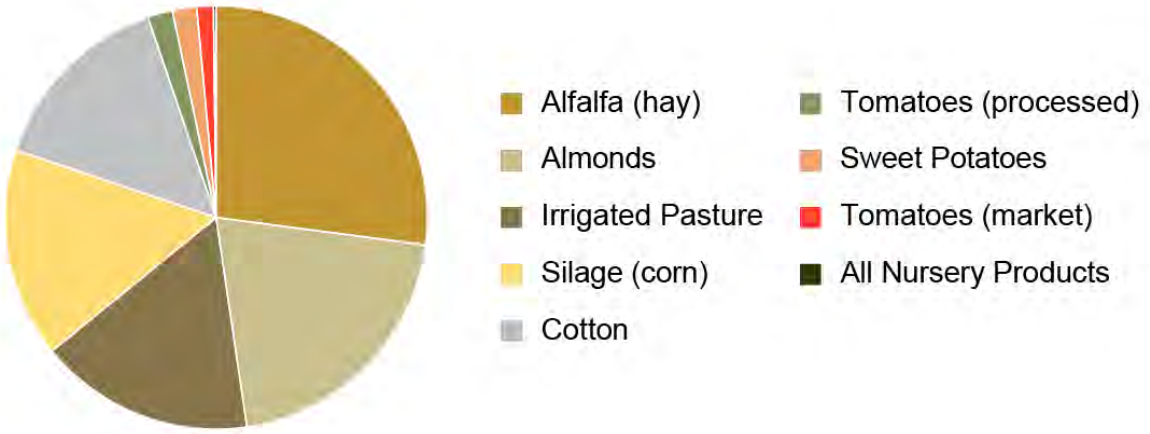

Note: Total estimated water use represented by this chart is 1.5 million acre-feet.

2.1.3 Fresno County

2.1.3.1 Land Use, 1986–2014, Aqueduct Study Corridor

Land-use surveys in Fresno County are available for 1986, 1994, 2000, 2008, and 2014 (Table 2-1). Maps based on the survey data (Figures A-5, A-6, A-7, A-8 and A-9 in Appendix A), and a plot of relative percentage of the three primary land-use classes through time (Figure 2-7), reveal that land planted in Orchards/Vineyards progressively increased from 1986 to 2014, primarily at the expense of Row/Field Crops. The acreage planted in Orchards/Vineyards over the 28-year period increased from approximately 4 percent of the study corridor area in 1986, to approximately 40 percent in 2014 (Table 2-1).

Figure 2-7 Changes in Land Use Over Time in the Study Corridor, Fresno County

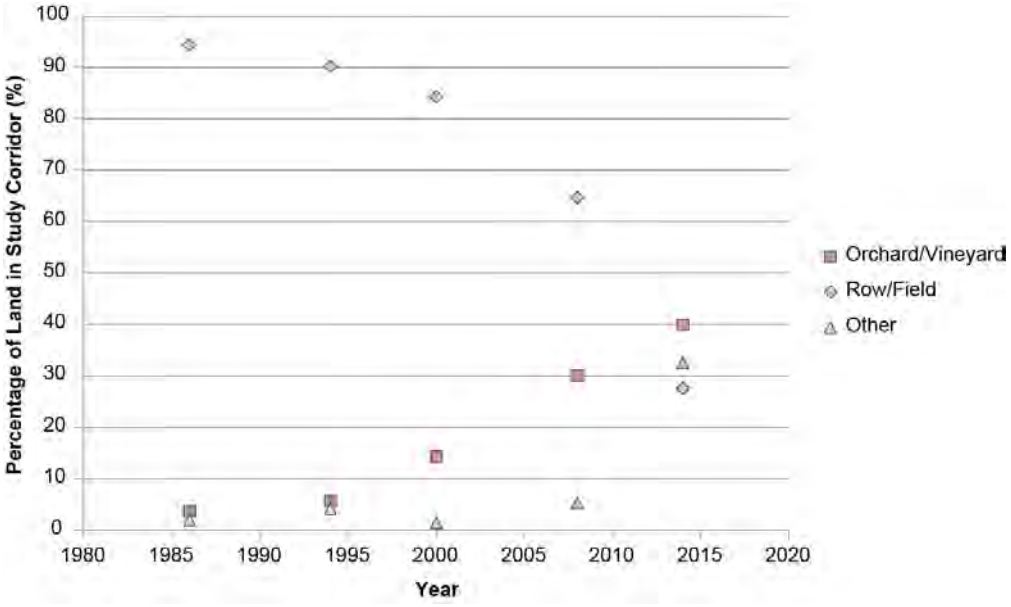

The surveys indicate that Row/Field Crops declined from approximately 65 percent of the study corridor area in 2008, to approximately 28 percent in 2014. Land classified in Other uses increased during the same period, from approximately 5 percent in 2008, to 33 percent in 2014 (Figure 2-7). Land devoted to Orchards/Vineyards increased approximately 9 percent during the same period; therefore, most of the change between 2008 and 2014 was in row/field acreage being switched to Other uses.

The different patterns of agricultural land use in 2014, relative to 1986, are illustrated in Figure 2-8. Notable areas of land, directly adjacent to the Aqueduct, that converted from Row/Field Crops to Orchards/Vineyards between 1986 and 2014 include reaches of Pools 15, 16, and 17 within the Panoche bowl, and Pool 19 in the northern part of the Los Gatos bowl.

2.1.3.2 Estimated Average Agricultural Water Use, 1994 and 2016, Fresno County

According to a 2016 annual agricultural report, the top-value crops produced in Fresno County included (in descending order of acres harvested) almonds, grapes, pistachios, tomatoes (for processing), cotton, oranges, garlic, peaches, and tomatoes (for market) (Fresno County Farm Bureau 2016) (Figure 2-9). Total acreage planted in these crops in 2016 was approximately 697,000 acres, out of approximately 991,000 acres planted in all crops (exclusive of rangeland), or approximately 70 percent of all agricultural land devoted to crops in Fresno County. Based on annual agricultural water usage for these crops reported by Johnson and Cody (2015), estimated total water use for the top-value crops in Fresno County in 2016 was approximately 1.974 million acre-feet (Figure 2-10). The average water usage per acre harvested for the top-value crops in 2016 was approximately 2.8 acre-feet. Based on the annual water requirements and total acreage devoted to individual crops, almonds, grapes, pistachios and tomatoes (processed) accounted for approximately 83 percent of the total water applied to all top crops in Fresno County in 2016.

For comparison, the top-value crops produced in Fresno County in 1994 included (in descending order of acres harvested) cotton (lint), grapes, tomatoes (processed), almonds, cotton (Pima), oranges, lettuce, garlic, nectarines, and tomatoes (cherry and market tomatoes) (Fresno County 1994) (Figure 2-11). Total acreage planted in these crops in 1994 was approximately 814,000 acres, out of approximately 1.238 million acres planted in all crops (exclusive of rangeland), or approximately 66 percent of all agricultural land devoted to crops in Fresno County in 1994. Based on typical annual agricultural water usage for these crops reported by Johnson and Cody (2015), estimated total water use for the top-value crops in Fresno County in 1994 was approximately 2.169 million acre-feet (Figure 2-12). The average water usage per acre harvested was approximately 2.7 acre-feet in 1994. Based on the annual water requirements and total acreage devoted to individual crops, cotton (lint), grapes, and tomatoes (processed) accounted for approximately 80 percent of the total water applied to all top-value crops in 1994.

This review of annual crop reports indicates that total agricultural land in Fresno County devoted to all crops (including field, seed, vegetable and fruit/nut crops, and exclusive of rangeland) decreased by approximately 247,000 acres between 1994 and 2016, representing an approximately 20 percent decrease in 22 years. Some of this decrease is likely because of an expansion of urban areas into former agricultural land (Hanak et al., 2017). The primary water-intensive crops in Fresno County changed over time, from cotton, grapes, and tomatoes in 1994; to almonds, grapes, pistachios, and tomatoes in 2016. Total estimated agricultural water usage for the top-value crops decreased between 1994 and 2016, likely related to the countywide decrease in land dedicated to all crops. Estimated average agricultural water use per acre for top-value crops may have increased slightly from 2.7 acre-feet in 1994 to 2.8 acre-feet in

2016, but the difference is probably not significant given the uncertainty in the assumptions used in the calculations.

Figure 2-8 Agricultural Land Use in 2014 Relative to 1986, Aqueduct Study Corridor, Fresno County

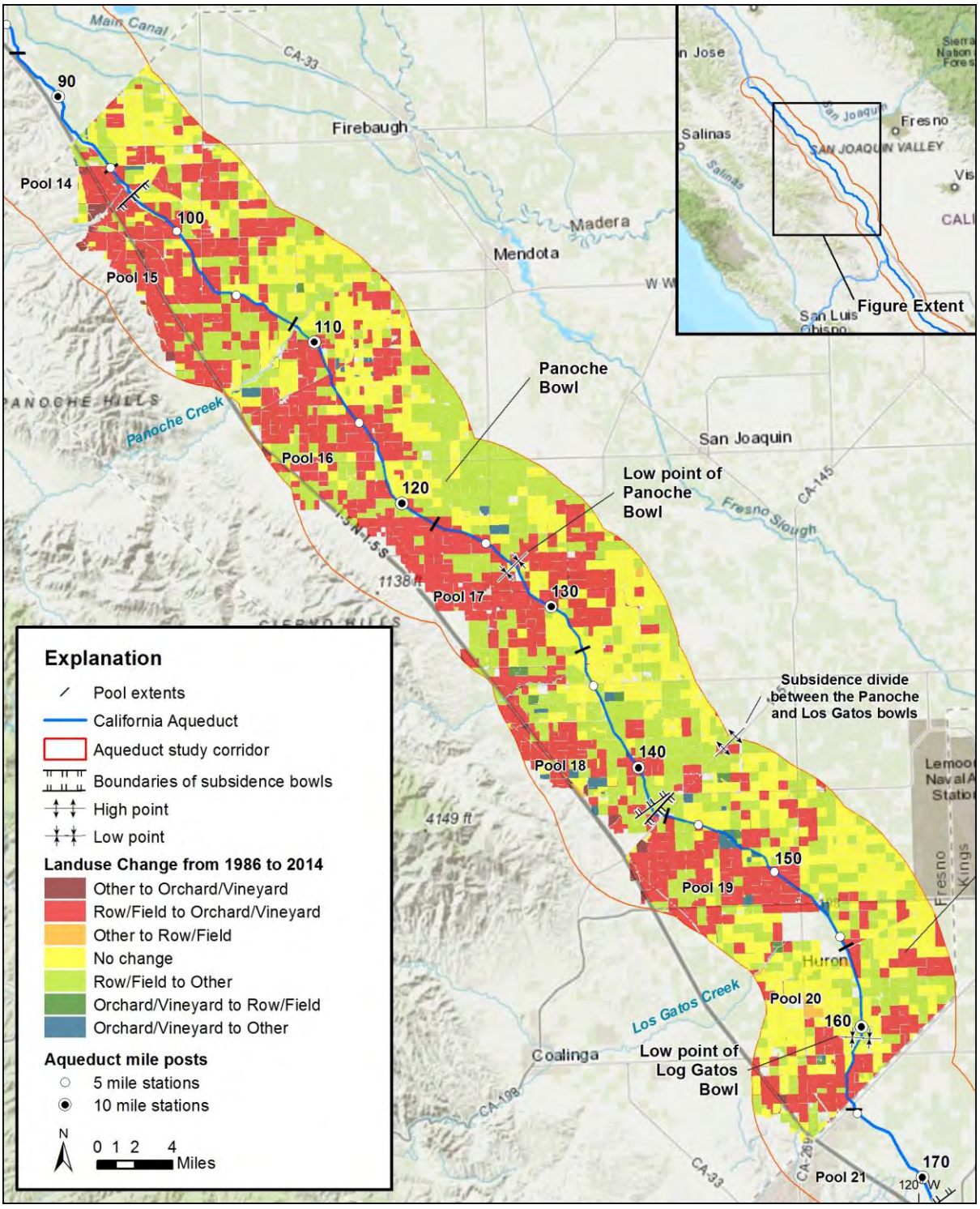

Figure 2-9 Top-Value Crops in Fresno County, 2016

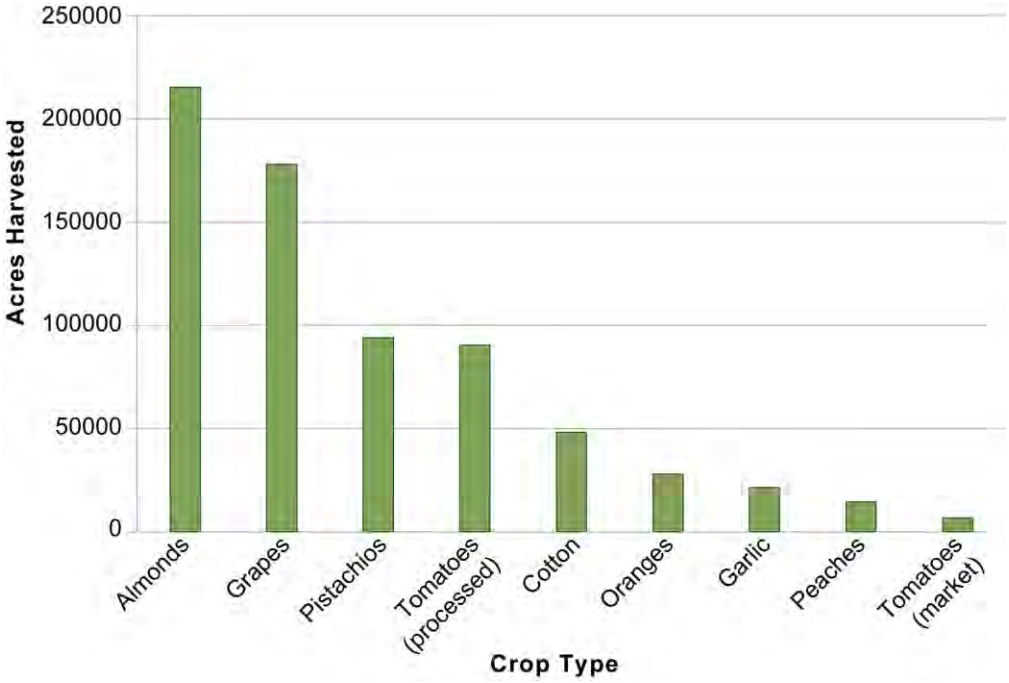

Figure 2-10 Relative Water Use by Top-Value Crops, Fresno County, 2016

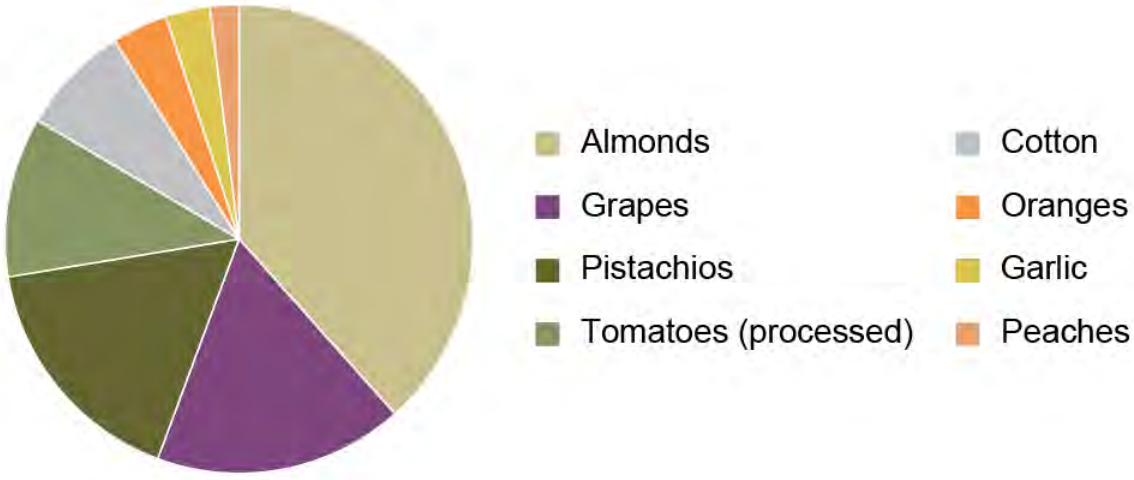

Note: Total estimated water use represented by this chart is 2.0 million acre-feet.

Figure 2-11 Top-Value Crops in Fresno County, 1994

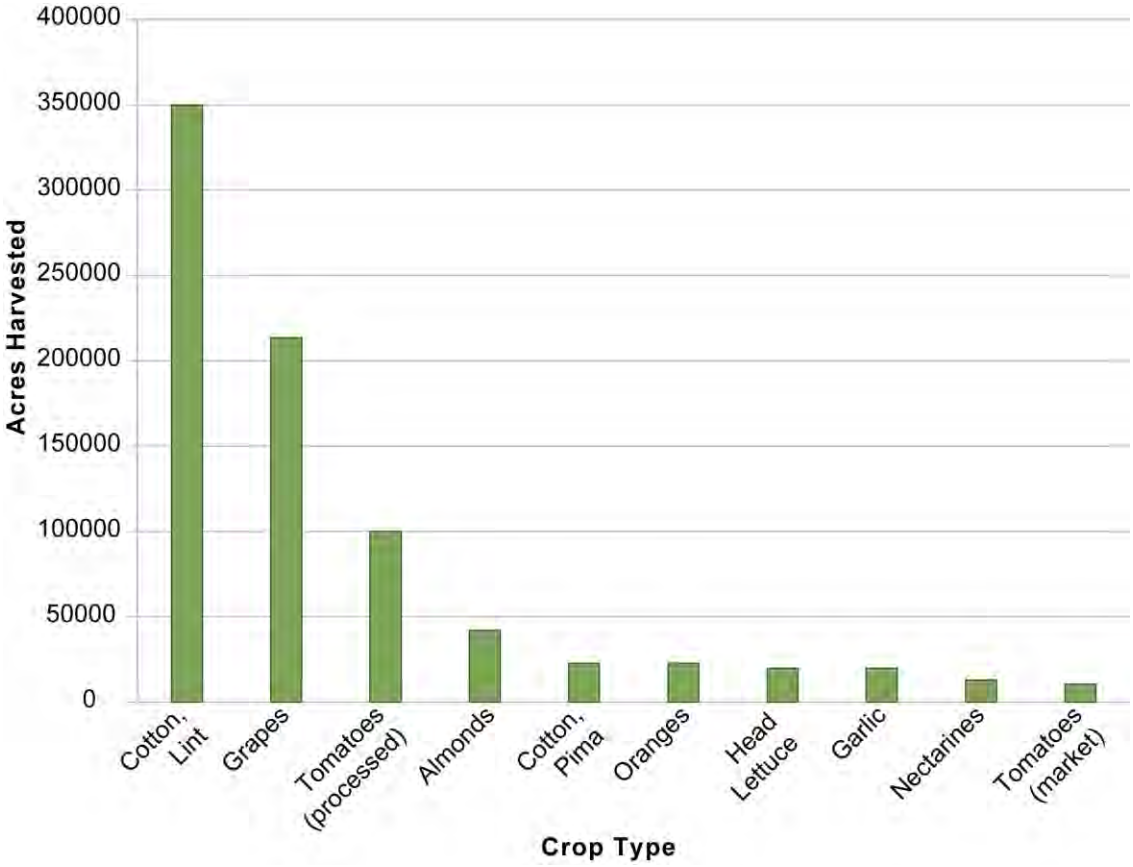

Figure 2-12 Relative Water Use by Top-Value Crops, Fresno County, 1994

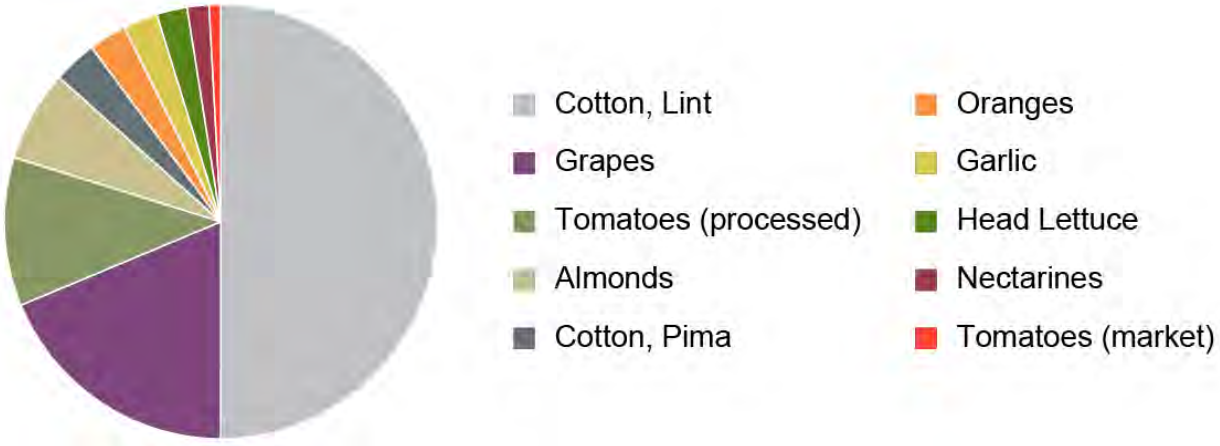

Note: Total estimated water use represented by this chart is 2.2 million acre-feet.

2.1.4 Kings County

2.1.4.1 Land Use, 1991–2014, Aqueduct Study Corridor

Land-use surveys in Kings County are available for 1991, 1996, 2003, 2013, and 2014 (Table 2-1). Maps based on the survey data (Plates A-10, A-11, A-12, A-13 and A-14) and a plot of relative percentage of the three primary land-use classes through time (Figure 2-13) reveal a relatively steady increase in land planted in Orchards/Vineyards along the study corridor in Kings County after 1996. The surveys also show increases in land dedicated to Other uses after 1996, with a commensurate overall decrease in Row/Field Crops. The surveys indicate an abrupt one-year decrease in row/field acreage from approximately 41 percent of the study corridor in 2013, to approximately 21 percent in 2014. The decrease primarily represented a change from Row/Field Crops to Other uses.

The different patterns of agricultural land use in 2014, relative to 1991, are illustrated in Figure 2-14. Notable areas of land directly adjacent to the Aqueduct that converted from Row/Field Crops to Orchards/Vineyards between 1991 and 2014 include the northeast side of Pool 21 between MP 164 and MP 168, and both sides of Pool 21 between MP 170 and 172. These areas lie within the southern part of the Los Gatos bowl (Figure 2-14). Other conversions of Row/Field Crops to Orchards/Vineyards include the east side of Pool 22 between MP 176 and MP 180, and discontinuous areas on the east side of Pool 23 between MP 184 and MP 188.

2.1.4.2 Estimated Average Agricultural Water Use, 1996 and 2015, Kings County

According to a 2015 crop report, the top-value crops in Kings County included (in descending order of acres harvested) cotton (Pima), silage (corn), alfalfa (hay), tomatoes (for processing), almonds, pistachios, almonds, walnuts, alfalfa (stubble), grapes, cotton (Acala), and alfalfa (other) (Kings County 2015) (Figure 2-15). The distinctions between alfalfa as a hay crop, a stubble crop, “silage,” “silage all year,” and “other” crops are unique to the Kings County agricultural reports. They are listed without explanation. The distinctions are retained here for consistency with the source reports. Total acreage planted in these crops in 2015 was approximately 257,000 acres, out of approximately 439,000 acres planted in all crops (exclusive of rangeland), or approximately 59 percent of all agricultural land devoted to crops in Kings County. Based on typical annual agricultural water usage for these crops reported by Johnson and Cody (2015), estimated total water use for the top crops in Kings County in 2015 was approximately 883,000 acre-feet (Figure 2-16). The average water usage for the top-value crops in 2015 was approximately 3.4 acre-feet, per acre harvested. Based on the annual water requirements and total acreage devoted to individual crops, cotton (Pima), alfalfa (hay), corn (silage), almonds, tomatoes (processed), and pistachios accounted for approximately 85 percent of the total water applied to all top-value crops in Kings County in 2015.

For comparison, the top-value crops produced in Kings County in 1996 included (in descending order of acres harvested) cotton (Acala), cotton (Pima), alfalfa (hay), tomatoes (for processing), walnuts, grapes, peaches, alfalfa (other), and tomatoes (for market) (Kings County 1996) (Figure 2-17). Total acreage planted in these crops in 1994 was approximately 308,000 acres, with an additional 10,000 acres devoted to irrigated rangeland. Approximately 318,000 acres were devoted to the top crops and irrigated pasture in 1996, out of approximately 547,000 total acres planted in crops (exclusive of non-irrigated rangeland). The top crops and irrigated pasture accounted for approximately 58 percent of total agricultural land in

Kings County for 1996, exclusive of rangeland grazing. Based on typical annual agricultural water usage for these crops reported by Johnson and Cody (2015), estimated total water use for the top-value crops in Kings County in 1996 was approximately 1.045 million acre-feet (Figure 2-18). The average water usage per acre harvested was approximately 3.3 acre-feet. Cotton (Acala and Pima) and alfalfa (hay) accounted for approximately 90 percent of the total water applied to the top-value crops in Kings County in 1994.

The review of data from the annual Kings county crop reports indicates that total agricultural land devoted to crops (including field, seed, vegetable and fruit/nut crops, and exclusive of rangeland) decreased by approximately 108,000 acres between 1996 and 2015, representing an approximately 20 percent decrease in 19 years. The primary water-intensive crops changed over time, from cotton and alfalfa in 1996, to cotton, almonds, tomatoes, and pistachios in 2015. Total estimated agricultural water usage for the top-value crops decreased between 1996 and 2015, consistent with the county-wide decline in total acreage devoted to all crops, as well as a greater than 50 percent decline of total cotton acreage during this period (approximately 252,000 acres in 1996, versus approximately 107,000 acres in 2015). Estimated average agricultural water use per acre for top-value crops possibly increased slightly from 3.3 acre-feet in 1996, to 3.4 acre-feet in 2015, but the difference probably is not significant given the uncertainty in the assumptions used in the calculations.

Figure 2-13 Changes in Land Use Over Time in the Study Corridor, Kings County

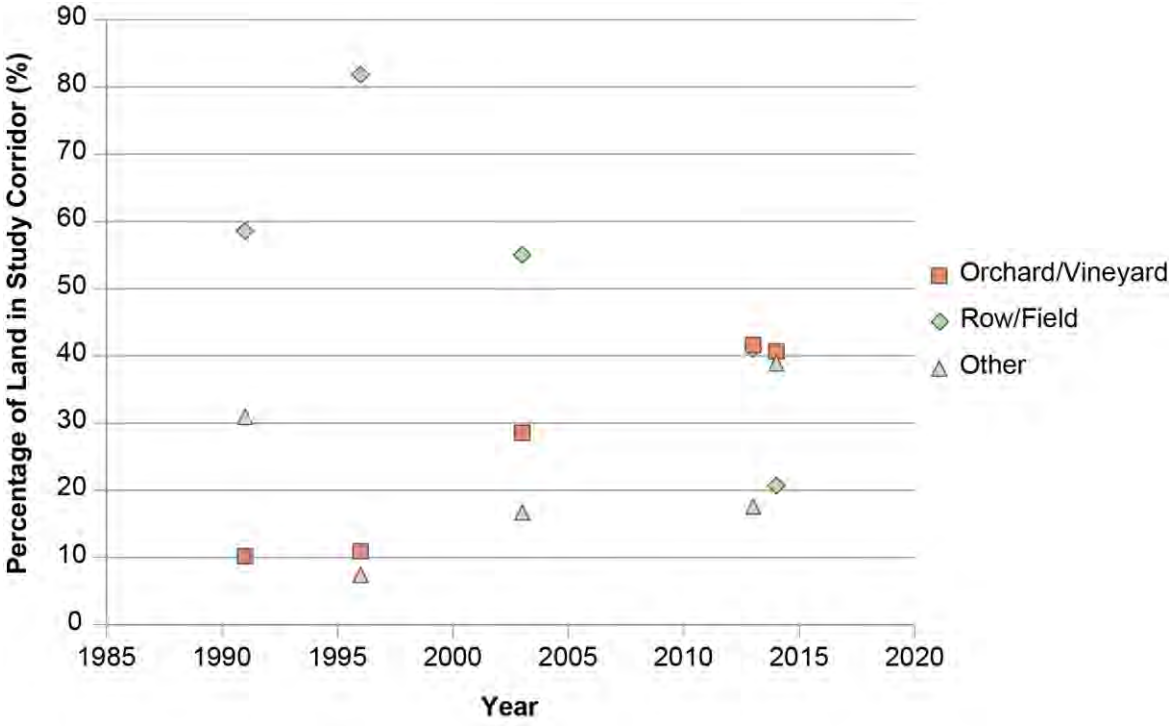

Figure 2-14 Agricultural Land Use in 2014 Relative to 1991, Aqueduct Study Corridor, Kings County

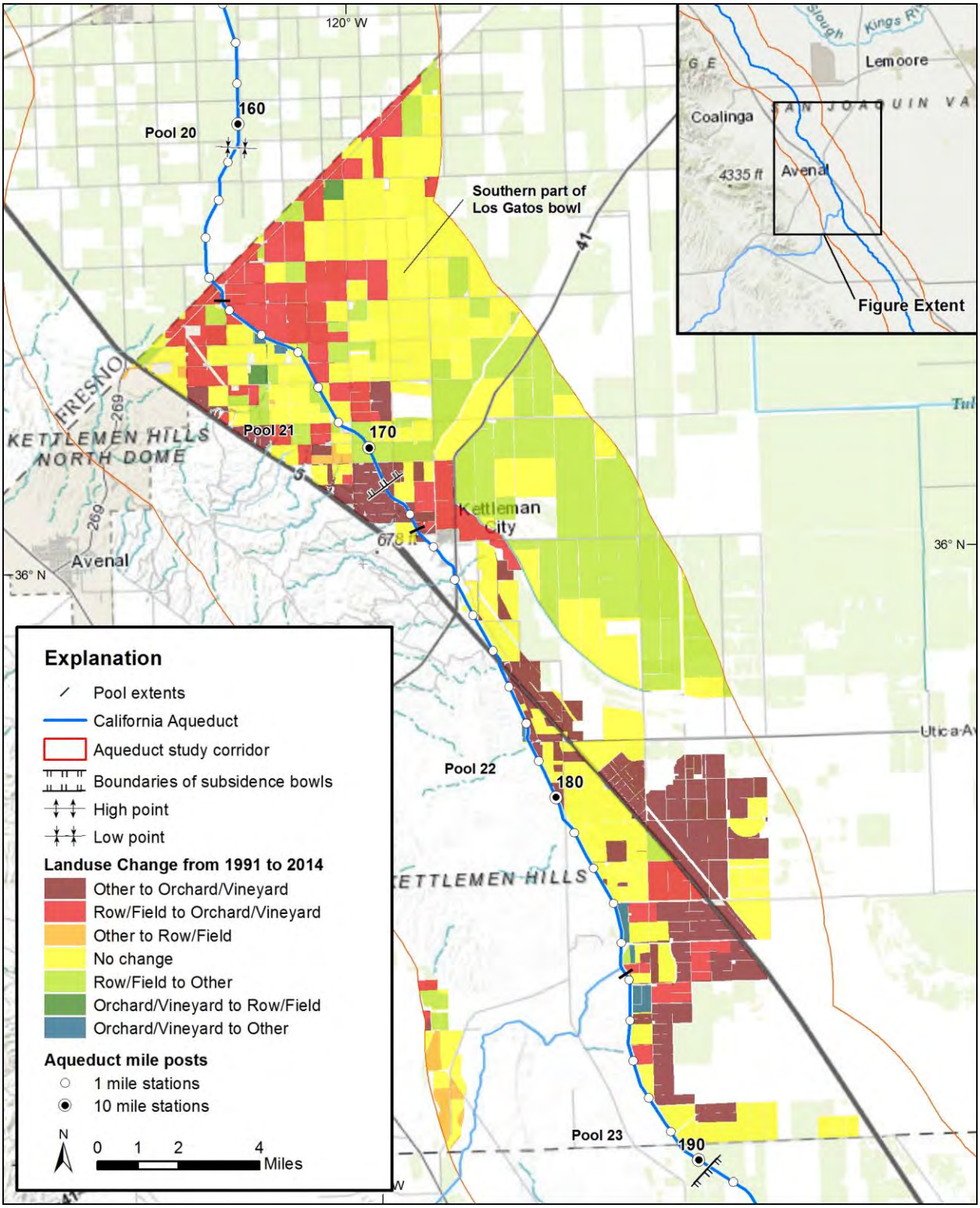

Figure 2-15 Top-Value Crops in Kings County, 2015

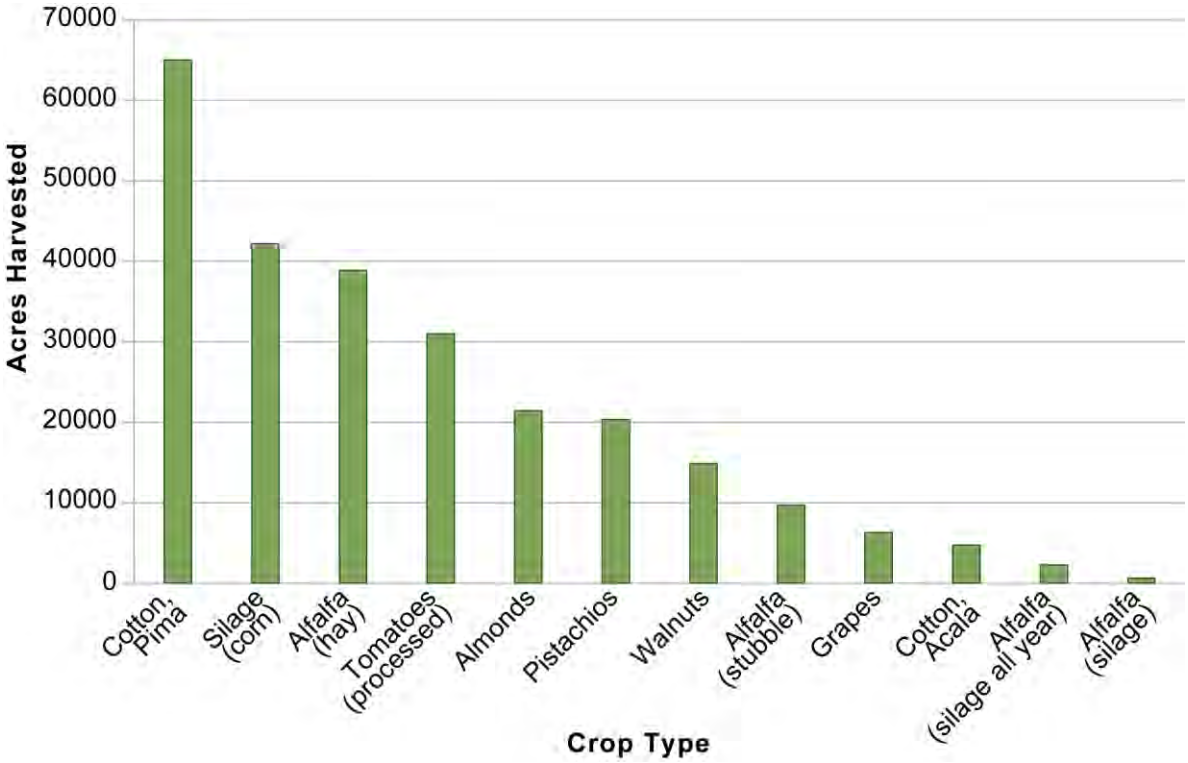

Figure 2-16 Relative Water Use by Top-Value Crops, Kings County, 2015

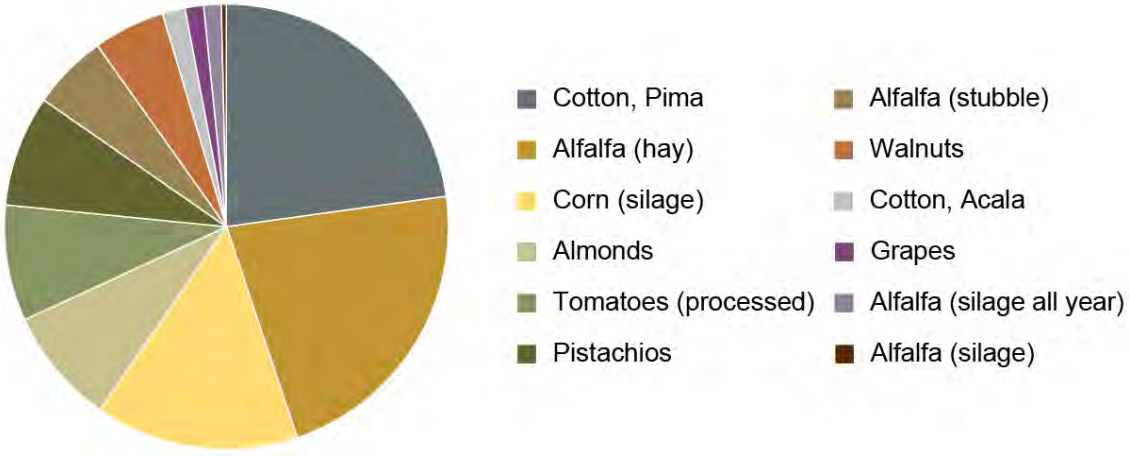

Note: Total estimated water use represented by this chart is 0.9 million acre-feet.

Figure 2-17 Top-Value Crops in Kings County, 1996

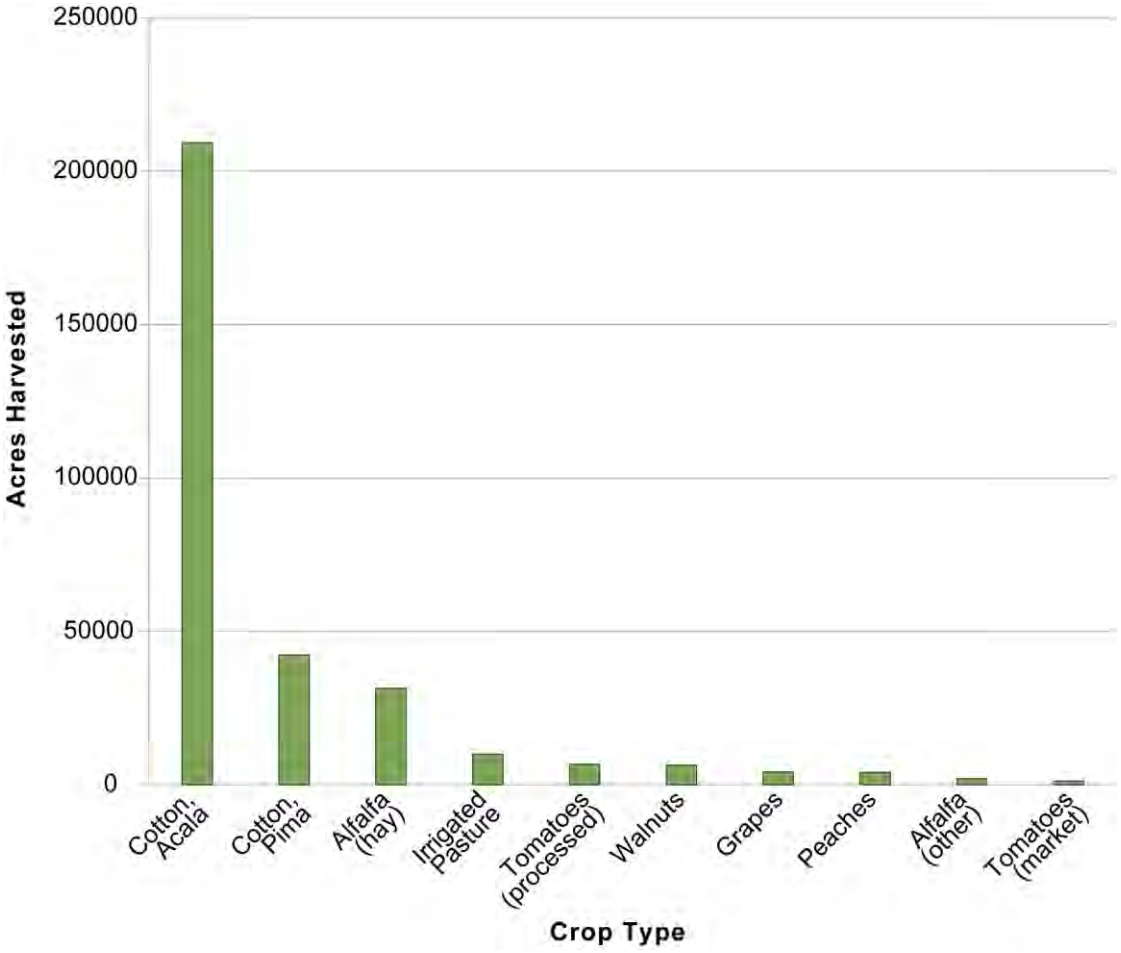

Figure 2-18 Relative Water Use by Top-Value Crops, Kings County, 1996

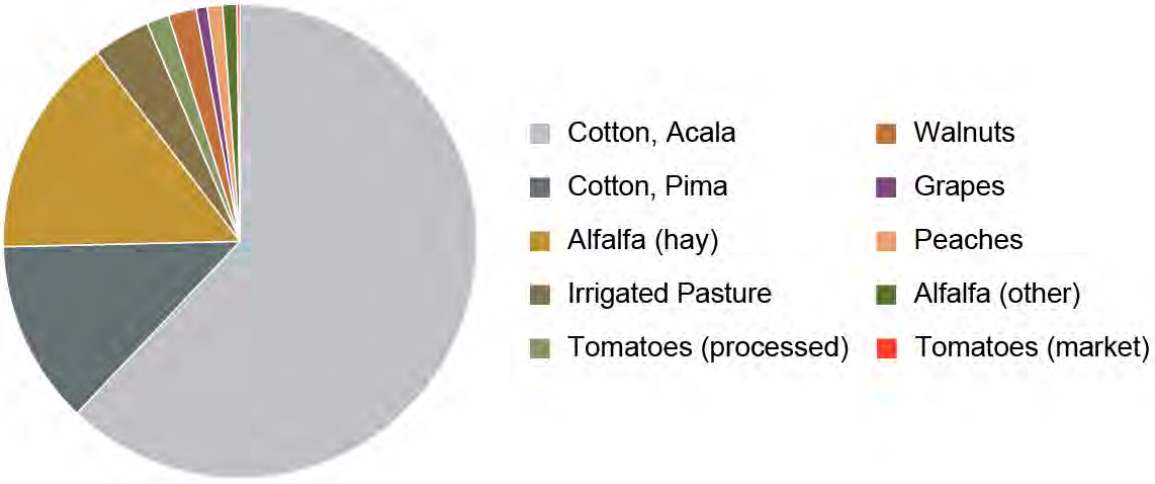

Note: Total estimated water use represented by this chart is 1.0 million acre-feet.

2.1.5 Kern County

2.1.5.1 Land Use, 1990–2015, Aqueduct Study Corridor

Land-use surveys in Kern County are available for 1990, 1998, 2006, 2014, and 2015 (Table 2-1). The 2015 survey is missing data for an approximately 15-mile section of the study corridor between the Kern County line to the north, and California State Route 46 on the south. Maps based on the survey data (Plates A-15, A-16, A-17, A-18, and A-19 in Appendix A), and a plot of relative percentage of the three primary land-use classes through time (Figure 2-19), reveal an increase in Orchards/Vineyards along the study corridor in Kern County since 1990, primarily at the expense of acreage in Row/Field Crops. The surveys show a large increase in Other land use between 2006 and 2014 (from 12 percent in 2006, to 20 percent in 2014), accompanied by a large decrease in the percentage of land dedicated to Row/Field Crops (from 46 percent in 2006, to 22 percent in 2014). These changes were abruptly reversed in 2015, with Other land use decreasing to approximately 11 percent and Row/Field Crops increasing to approximately 32 percent of the Kern County study corridor area.

Figure 2-19 Changes in Land Use Over Time in the Study Corridor, Kern County

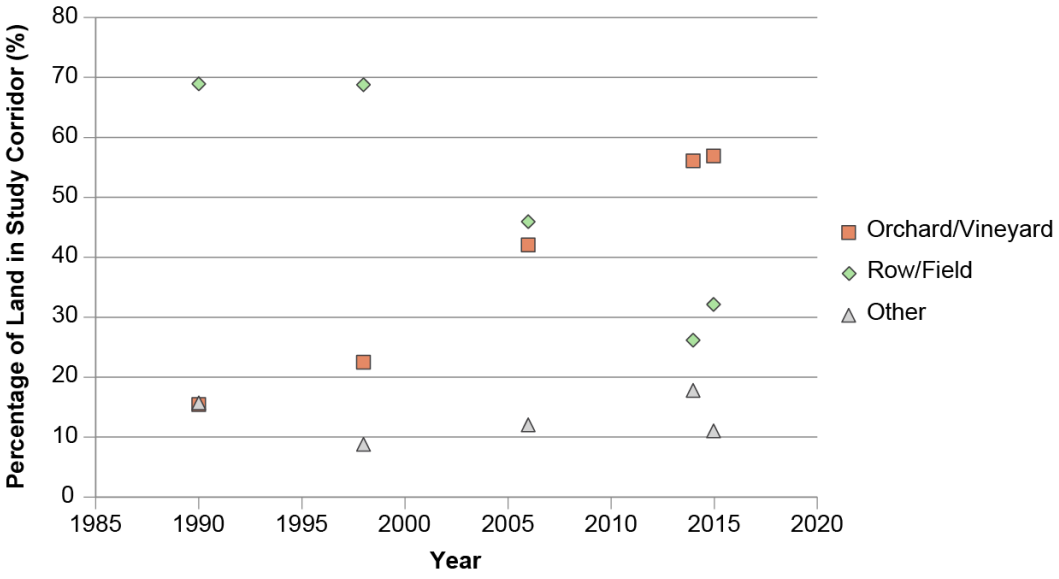

The different patterns of agricultural land use in 2014, relative to 1990, are illustrated in Figure 2-20. Most of the change in land use directly adjacent to the Aqueduct within the Kern bowl (MP 190 to MP 221) has been from Row/Field Crops to Orchards/Vineyards. Other areas of land directly adjacent to the Aqueduct that converted from Row/Field Crops to Orchards/Vineyards between 1990 and 2014 include Pool 32 in the southern part of the Maricopa bowl, Pools 33 and 34, and the northeast side of the Aqueduct in the Pleito bowl between MP 269 and MP 276 (Figure 2-20).

Figure 2-20 Agricultural Land Use in 2014 Relative to 1990, Aqueduct Study Corridor, Kern County

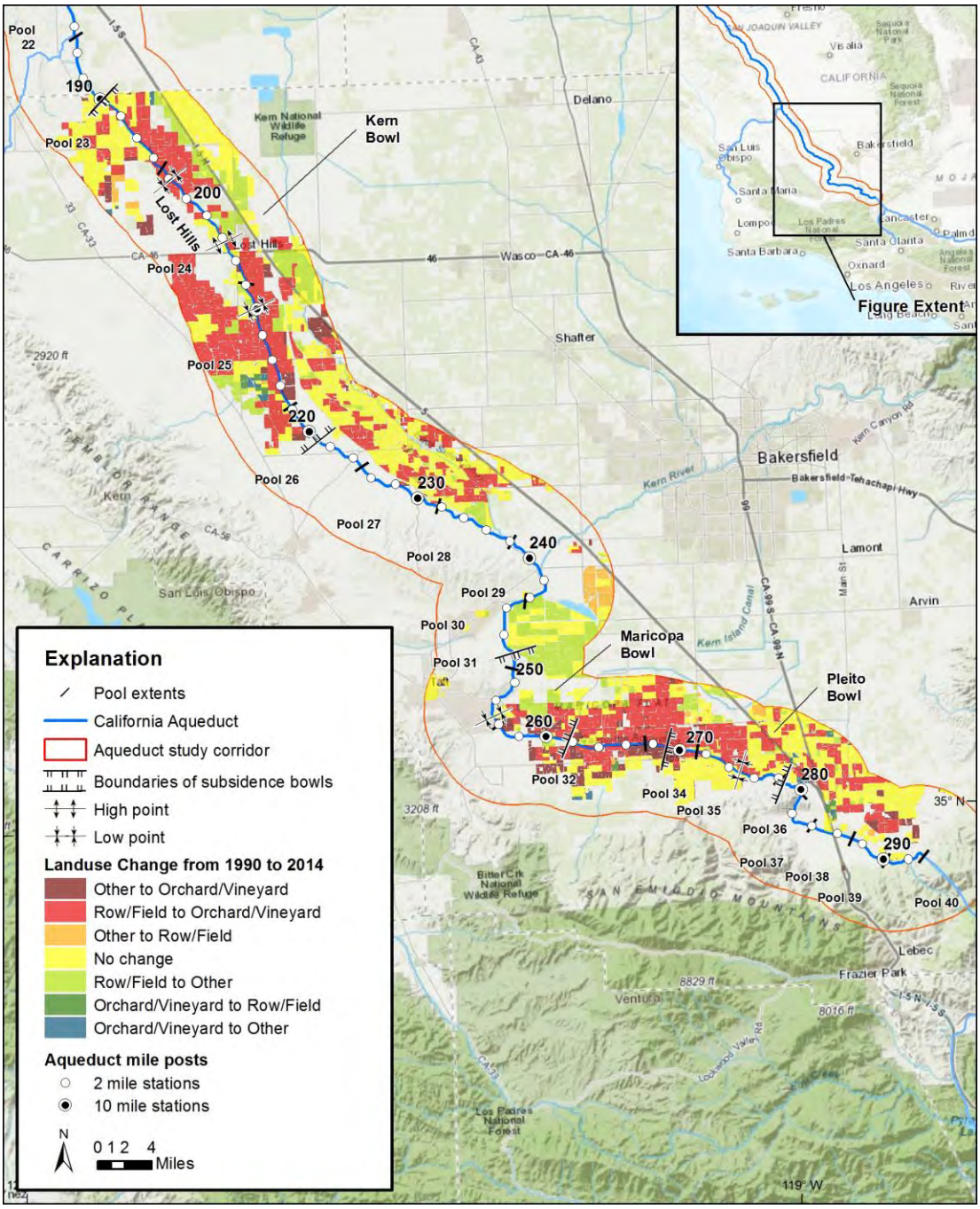

2.1.5.2 Estimated Average Agricultural Water Use, 1998 and 2015, Kern County

According to the 2015 county agricultural report, the top-value crops in Kern County included (in descending order of acres harvested) almonds, pistachios, grapes, alfalfa, silage, citrus, cotton (all varieties), tomatoes (for processing), potatoes, pomegranates, cherries, and garlic (Kern County 2015) (Figure 2-21). Total acreage planted in these crops in 2015 was approximately 750,000 acres, out of approximately 886,000 acres for all crops, or approximately 85 percent of all agricultural land devoted to

crops in Kern County (exclusive of rangeland). Based on typical annual agricultural water usage for these crops reported by Johnson and Cody (2015), estimated total water use for these top-value crops in Kern County in 2015 was approximately 2.647 million acre-feet (Figure 2-22). The average water usage for the top-value crops in 2015 per acre harvested was approximately 3.5 acre-feet. Based on the annual water requirements and total acreage devoted to individual crops, almonds, alfalfa, silage, and pistachios accounted for approximately 78 percent of the total water applied to all top-value crops in Kern County in 2015.

For comparison, the top agricultural crops produced in Kern County in 1998 included (in descending order of acres harvested) cotton (all), alfalfa (hay), grapes, almonds, wheat, citrus, pistachios, potatoes (all), tomatoes (for processing), and onions (Kern County 1998) (Figure 2-23). Total acreage planted in these crops in 1998 was approximately 664,000 acres, which accounted for approximately 76 percent of total agricultural land in Kern County for 1996 (approximately 868,500 acres, exclusive of rangeland grazing). Based on typical annual agricultural water usage reported by Johnson and Cody (2015), estimated total water use for these top-value crops in Kern County in 1998 was approximately 2.113 million acre-feet (Figure 2-24). The average water usage per acre harvested was approximately 3.2 acre-feet. Cotton, alfalfa, almonds, and grapes accounted for approximately 75 percent of the total water applied to the top-value crops in Kern County in 1998.

Figure 2-21 Top-Value Crops in Kern County, 2015

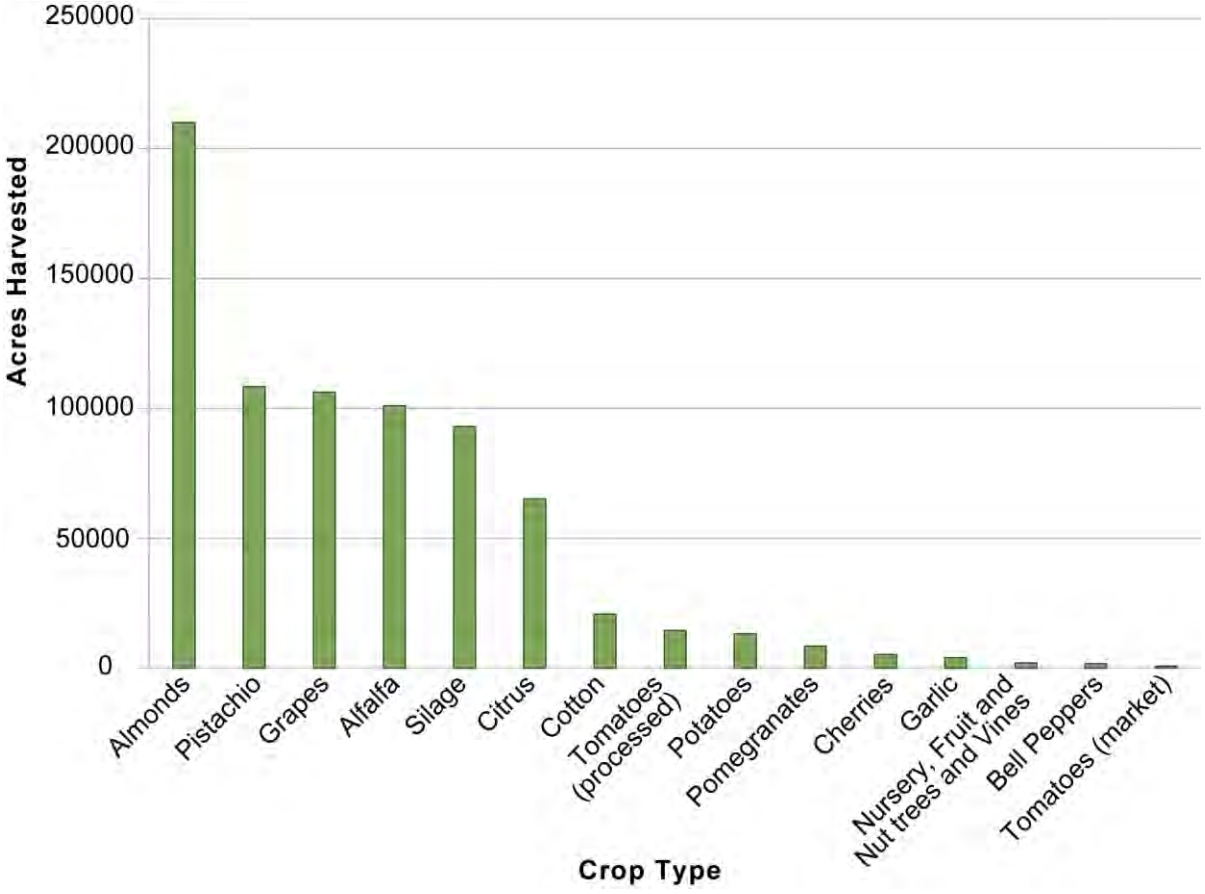

Figure 2-22 Relative Water Use by Top-Value Crops, Kern County, 2015

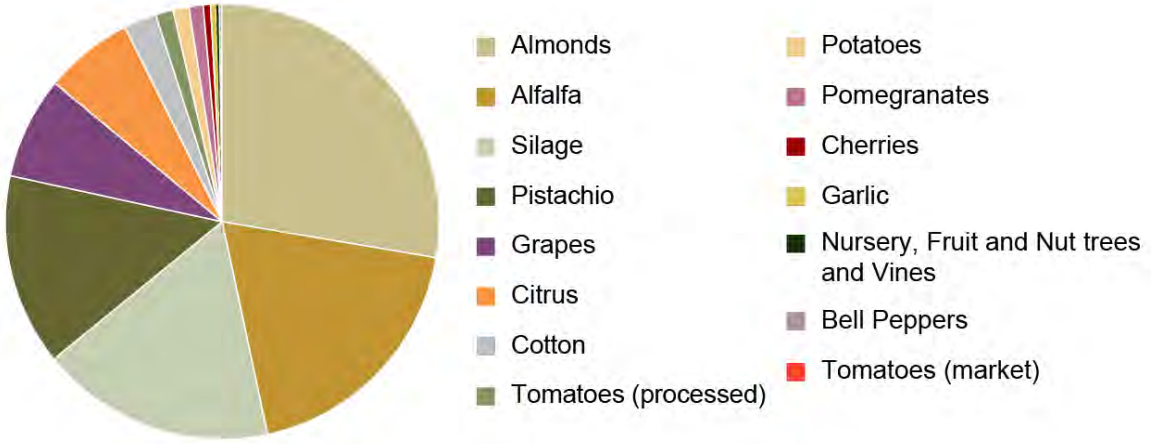

Note: Total estimated water use represented by this chart is 2.6 million acre-feet.

Figure 2-23 Top-Value Crops in Kern County, 1998

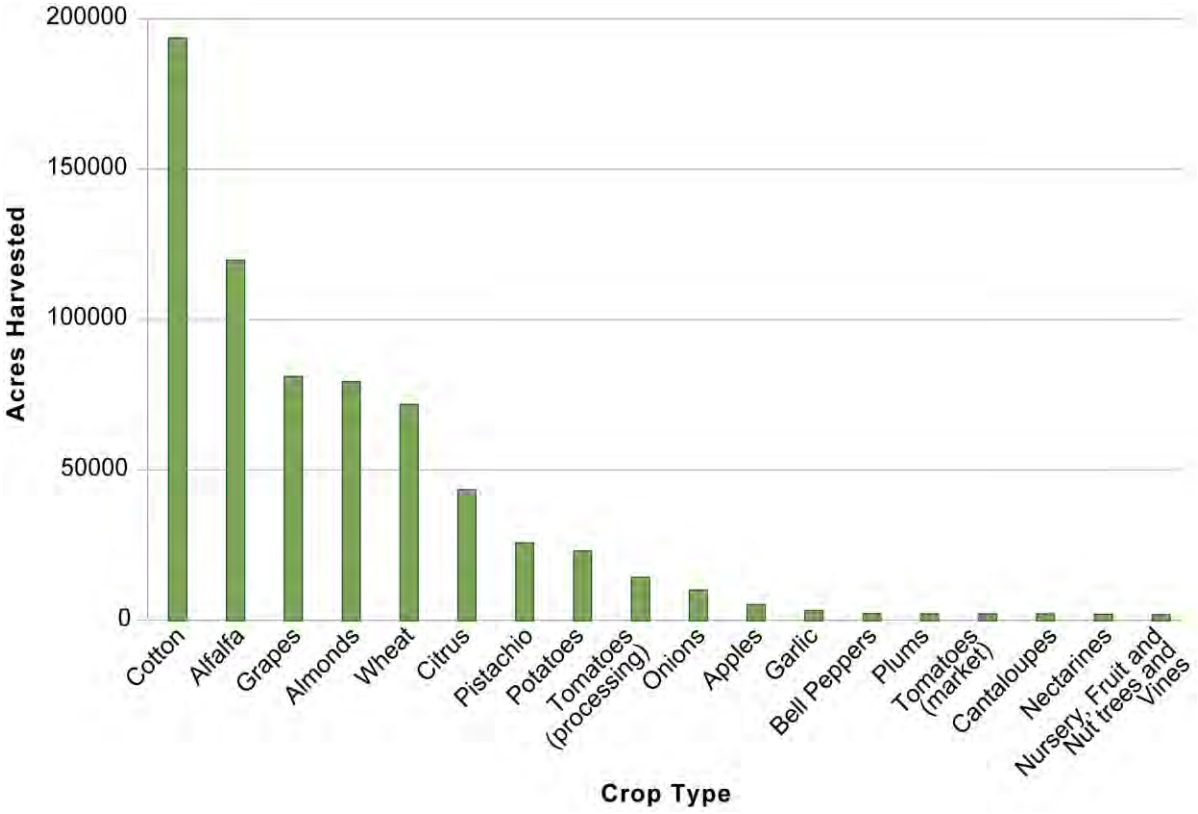

Figure 2-24 Relative Water Use by Top-Value Crops, Kern County, 1998

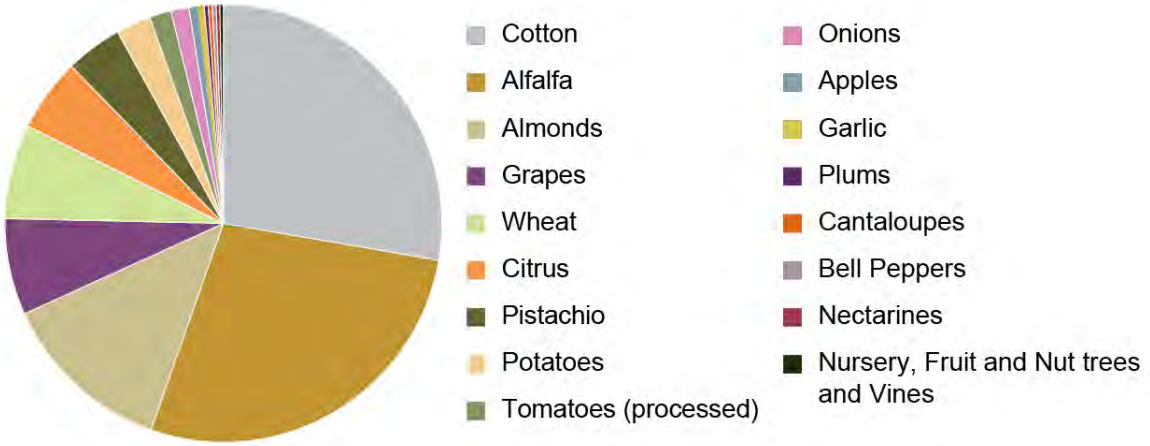

Note: Total estimated water use represented by this chart is 2.1 million acre-feet.

The review of data from the annual Kern County crop reports presented above indicates that total agricultural land devoted to crops (including field, seed, vegetable and fruit/nut crops, and exclusive of rangeland) increased by approximately 17,500 acres between 1998 and 2015, representing an approximately 2 percent increase in 17 years. The mix of water-intensive crops changed over time, from cotton, alfalfa, and almonds in 1998, to almonds, alfalfa, silage, and pistachios in 2015. Total estimated agricultural water usage for the top-value crops increased between 1998 and 2015. Estimated average agricultural water use per acre for top-value crops increased from approximately 3.2 acre-feet in 1998, to 3.5 acre-feet in 2015, which represents an approximately 9 percent increase over 17 years.

2.1.6 Discussion

Changes in agricultural land use in the Aqueduct study corridor over the past several decades (Figures 2-2, 2-8, 2-14, and 2-20) generally are characterized by replacing row and field crops with high-value orchards and vineyards, similar to the countywide trends described in the previous sections and observed elsewhere in the San Joaquin Valley (Johnson and Cody, 2015; Faunt et al. 2016, Hanak et al. 2017). In contrast to the relatively steady increase in orchards and vineyards over time, acreage dedicated to Row/Field Crops and Other uses has fluctuated sharply over short time periods. For example, Row/Field crop acreage in Kings County decreased by approximately 20 percent between 2013 and 2014, with nearly all the change going into Other land use (Figure 2-13). Between 2014 and 2015, acreage in Row/Field Crops in Kern County increased by 6 percent, with a comparable decline in Other land uses, while acreage in Orchards/Vineyards was approximately constant (Figure 2-19). These examples illustrate that land planted in row and field crops can be fallowed or rapidly changed to other uses depending on the availability of irrigation water (Hanak et al. 2017).

As discussed previously, estimating differences in total agricultural water use associated with changes in land use is problematic because irrigation methods have changed over time. Average water use per acre

for the top-value crops in Kern County may have increased slightly over the past two decades, but there is no clear indication of a similar increase or significant change in average water usage per acre for the top-value crops in Merced, Fresno, and Kings counties. This implies, on the average, that orchards and vineyards do not use significantly more water on an annual basis than the crops they have replaced, which include water-intensive crops such as cotton, alfalfa, and irrigated pasture (Table 2-1). But, the trend in agricultural land use within the Aqueduct study corridor over the past two decades has been toward replacing crops that can be fallowed in dry years with trees and vines that must be continually watered to preserve investment, contributing to "demand hardening" for irrigation water (Johnson and Cody 2015, Hanak et al. 2017), as discussed in Section 2.1.1. The most dramatic increase in Orchards/Vineyards within the study corridor has been in western Fresno County (Figure 2-7), an area of historic significant subsidence (Ireland et al. 1984) that includes the Panoche and Los Gatos bowls (Figures 2-8 and 2-14). Land planted in orchards and vineyards also has increased by an approximate factor of four over the past two decades within the study corridor in western Kings and Kern counties, including parts of the Kern, Maricopa, and Pleito bowls (Figure 2-20). The increase in acreage planted in orchards and vineyards directly adjacent to the Aqueduct increases the possibility that groundwater will need to be pumped for irrigation during drought years, potentially increasing local subsidence rates.

2.2 Deep Groundwater Elevations Along the Study Corridor

2.2.1 Introduction

Data from water wells in the California Aqueduct study corridor were analyzed to determine the lowest recorded elevation of the piezometric surface in the confined aquifer system below the Pleistocene Corcoran clay (Figure 2-25), a buried lacustrine deposit and aquitard that is present in the subsurface beneath the Aqueduct alignment at elevations ranging from sea level to 700 feet below sea level (Frink and Kues 1954). Following terminology employed by the U.S. Geological Survey (USGS) (Ireland et al. 1980), this report will refer to the confined aquifer system below the Corcoran clay as the *lower water-bearing zone*. Water from this unit has relatively low salinity and is preferred for irrigation. The aquifer system above the Corcoran clay is referred to as the *upper water-bearing zone*.

As summarized by Galloway and Riley (1999), historic permanent land subsidence in the San Joaquin Valley is primarily associated with aquifer-system compaction driven by groundwater withdrawal from the lower water-bearing zone. *Aquifer system compaction* refers to elastic (recoverable) and inelastic (non-recoverable) thickness reduction in response to increases in effective vertical normal stress. According to data reported in Ireland et al. (1984), 1967 marked historic low elevations of the piezometric surface in the lower water-bearing zone in the western San Joaquin Valley, specifically in SLFD, because of groundwater pumping for agriculture in the early to middle 20th century (Figure 2-26). The piezometric surface in the lower water-bearing zone began to recover in the 1970s when the delivery of irrigation water by the California Aqueduct and Delta-Mendota Canal reduced the need for groundwater pumping and allowed for recharge of the lower water-bearing zone (Ireland et al. 1980) (Figure 2-26). As noted by Faunt et al. (2015), the historic low elevation of the piezometric surface can be considered a proxy for the state of pre-consolidation stress in the deep aquifer system (i.e., the highest effective or inter-granular stress experienced by the aquifer). Any future withdrawals that reduce water-surface elevation in the lower water-bearing zone below the historic low elevation will expose the aquifer

skeleton to increased effective vertical normal stress and non-elastic deformation, with associated non-recoverable compaction and permanent land subsidence.

The objective of this analysis is to review available water well records within the Aqueduct study corridor for data on water-level elevations (elevation of the piezometric surface) in the lower water-bearing zone, and determine if increased groundwater pumping during the recent dry periods (2007–2016) and significantly reduced allocations reduced piezometric surface elevations below the 1967 elevations (see discussion in Section 5.3).

2.2.2 Analytical Approach

Water-level elevations used in this analysis were taken from the statewide groundwater data library (a public database) maintained by DWR. This database was queried to select data for wells within the California Aqueduct study corridor (Figure 1-1). This query returned 66,960 individual records associated with 4,212 wells (Figure A-20 in Appendix A). A review of this data revealed that most individual well records are incomplete, and that information on water-level elevations, where available, varies significantly in space and time. The groundwater well data within the study corridor were further parsed, as follows:

1. Records that contain no data entries for the total depth of the well or the depth(s) of perforation intervals were eliminated (54,897 records).
2. The remaining records were searched for wells with screened perforation intervals exclusively below the base of the Corcoran clay. As part of this evaluation, a review was conducted on the ground surface elevations for wells as reported in the DWR database and compared them with elevations of the well locations extracted from a USGS digital elevation model (DEM). In cases where multiple surface elevations are listed for an individual well in the DWR database, the reported elevation closest to the USGS DEM elevation of the well location was selected, provided that the chosen DWR elevation was within 10 feet of the USGS elevation (this criterion applied to 95 wells). In other cases, where the well elevations in the DWR database differed from the USGS elevations by more than 10 feet, the USGS elevations were selected and used as the well elevations (this criterion applied to 214 wells). After making these adjustments to the well surface elevations in the database, a search of the 54,897 records from step 1 returned 297 wells with screened perforation intervals exclusively below the base of the Corcoran clay.
3. Of the 297 wells with documented perforation intervals exclusively below the Corcoran clay, 281 wells had one or more readings of water-level elevation from this interval (Figure 2-27).
4. Water-level elevations for the 281 wells that passed this screening process were reviewed, and the lowest recorded water-level elevation and its associated date were extracted from the database for further analysis.

Figure 2-25 Subsurface Extent of the Corcoran Clay

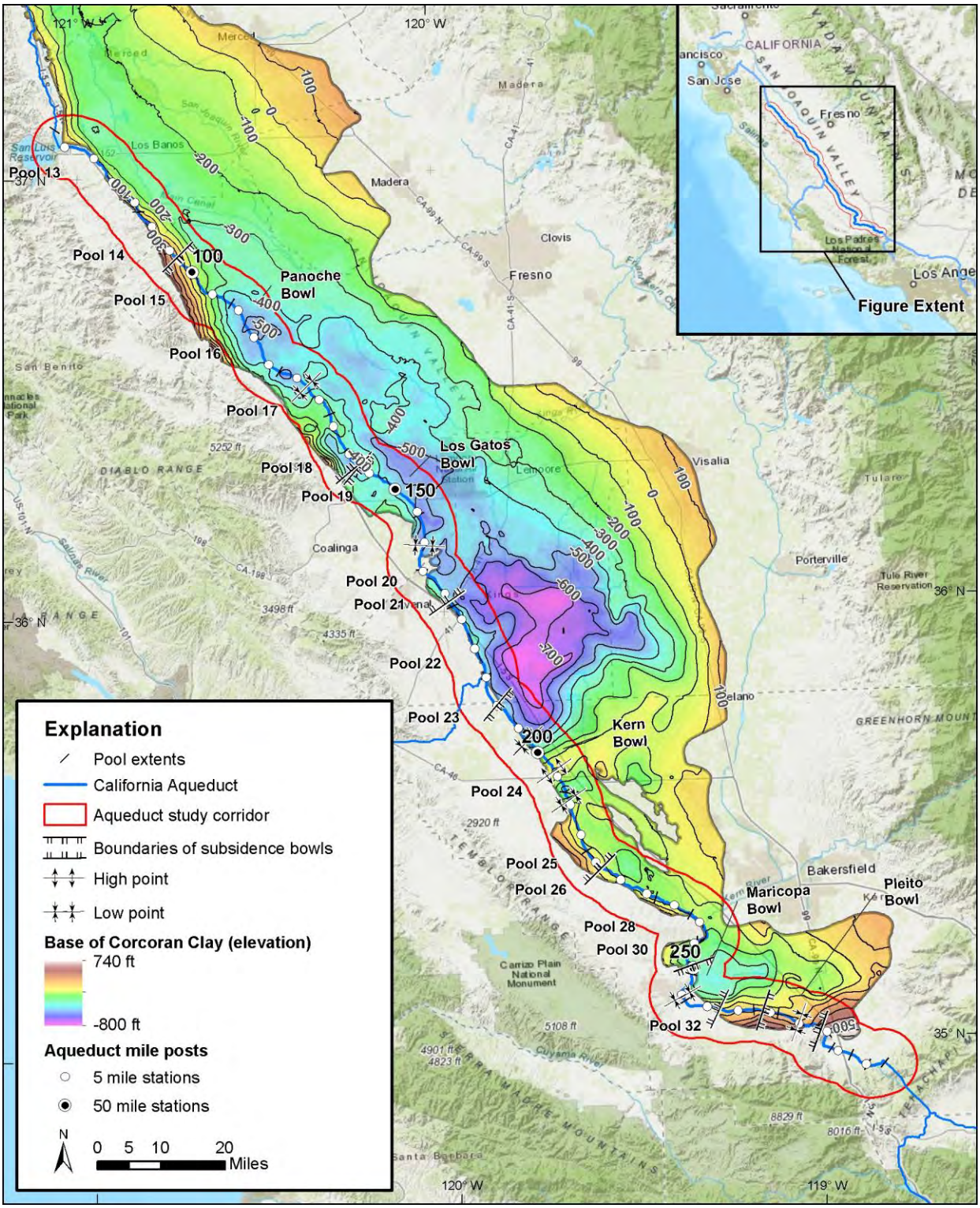

Figure 2-26 Historic Changes in Artesian Head in the Lower Water-Bearing Zone along the California Aqueduct, Western Fresno County

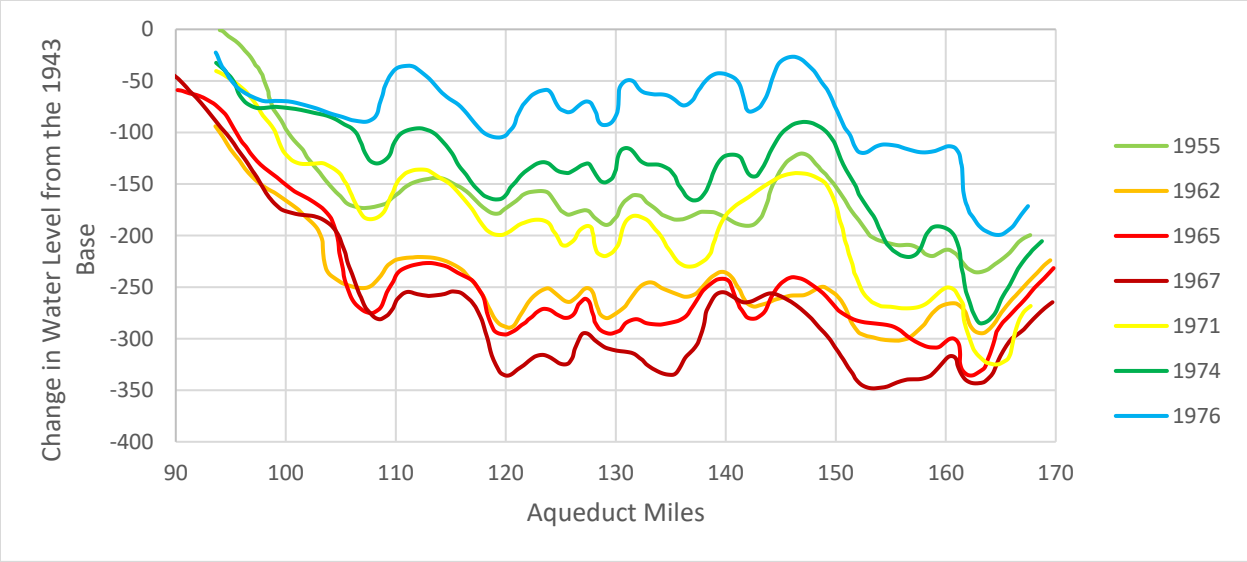

Note: Adapted from Ireland et al. 1984

2.2.3 Results

From inspection of Figure 2-27, the greatest number of wells drawing from the lower water-bearing zone are concentrated in the Panoche bowl and the northern part of the Los Gatos bowl, encompassing the southern end of Pool 14 and extending south to an area near Pool 20. Wells with screened intervals exclusively below the Corcoran clay are sparse south of Pool 21 and in the SJFD.

A map plotting the locations of wells screened below the Corcoran clay along with contours of the 1967 potentiometric surface in the lower water-bearing zone from Ireland et al. (1984) is provided in Figure 2-28. These wells also are shown in Figure A-21 and numbered and cross-referenced to Table A-1 in Appendix A, which lists for each numbered well the minimum water-level elevation, the date that the minimum elevation was recorded, the elevation of the 1967 potentiometric surface at the well location, and the difference between the recorded minimum water-level and the 1967 potentiometric surface elevations. Wells with recorded water-level elevations below the 1967 potentiometric surface are highlighted with a yellow ring in both Figure 2-28 and Figure A-21. A histogram of the dates of lowest water-level elevation in Table A-1, plotted in Figure 2-29, shows that most were recorded during the 2013 to 2016 drought years.

Figure 2-27 Wells Screened Exclusively Below the Corcoran Clay, Aqueduct Study Corridor

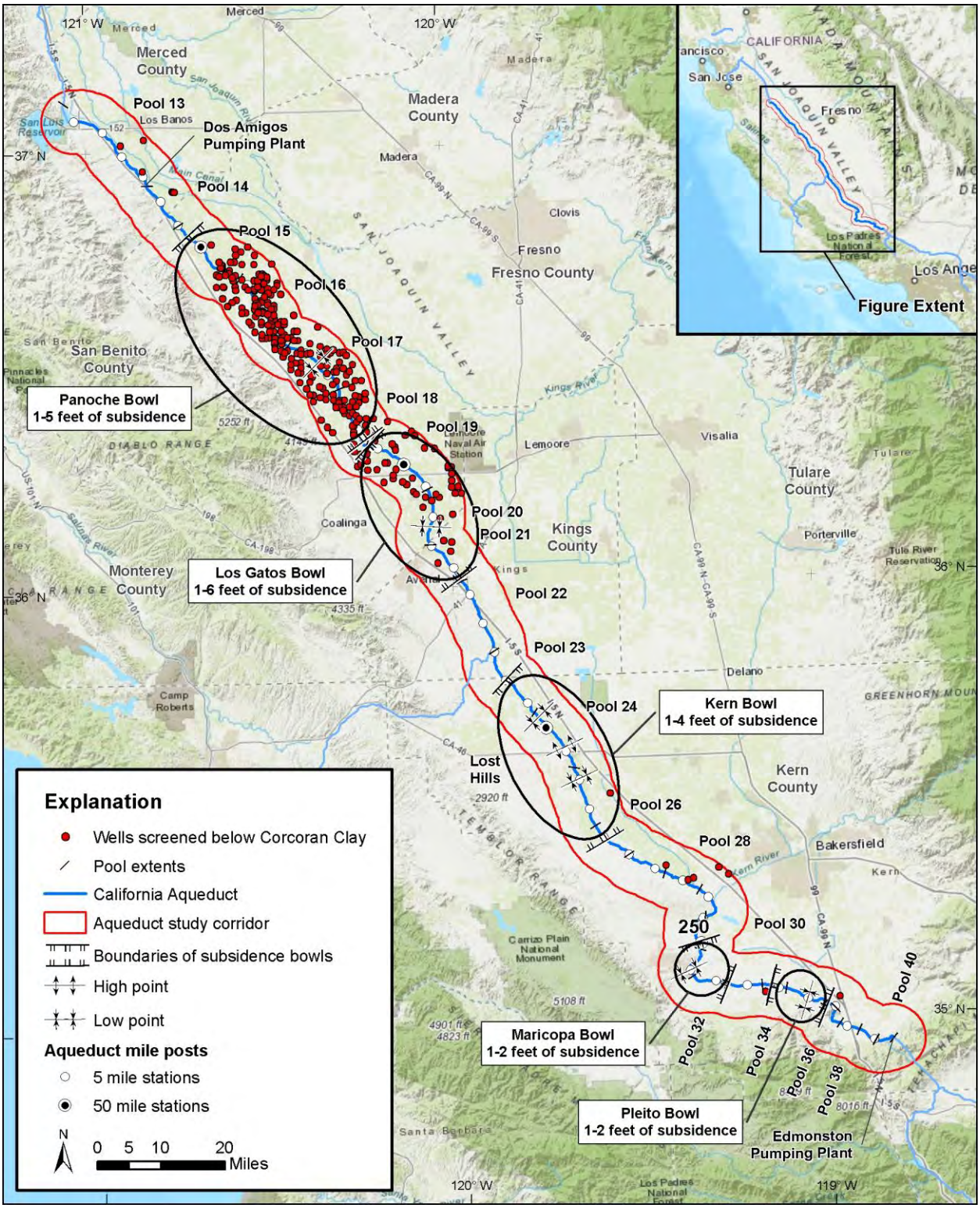

Figure 2-28 Wells in the Lower Water-Bearing Zone with Water-Level Elevations Below the 1967 Potentiometric Surface, Western Fresno County

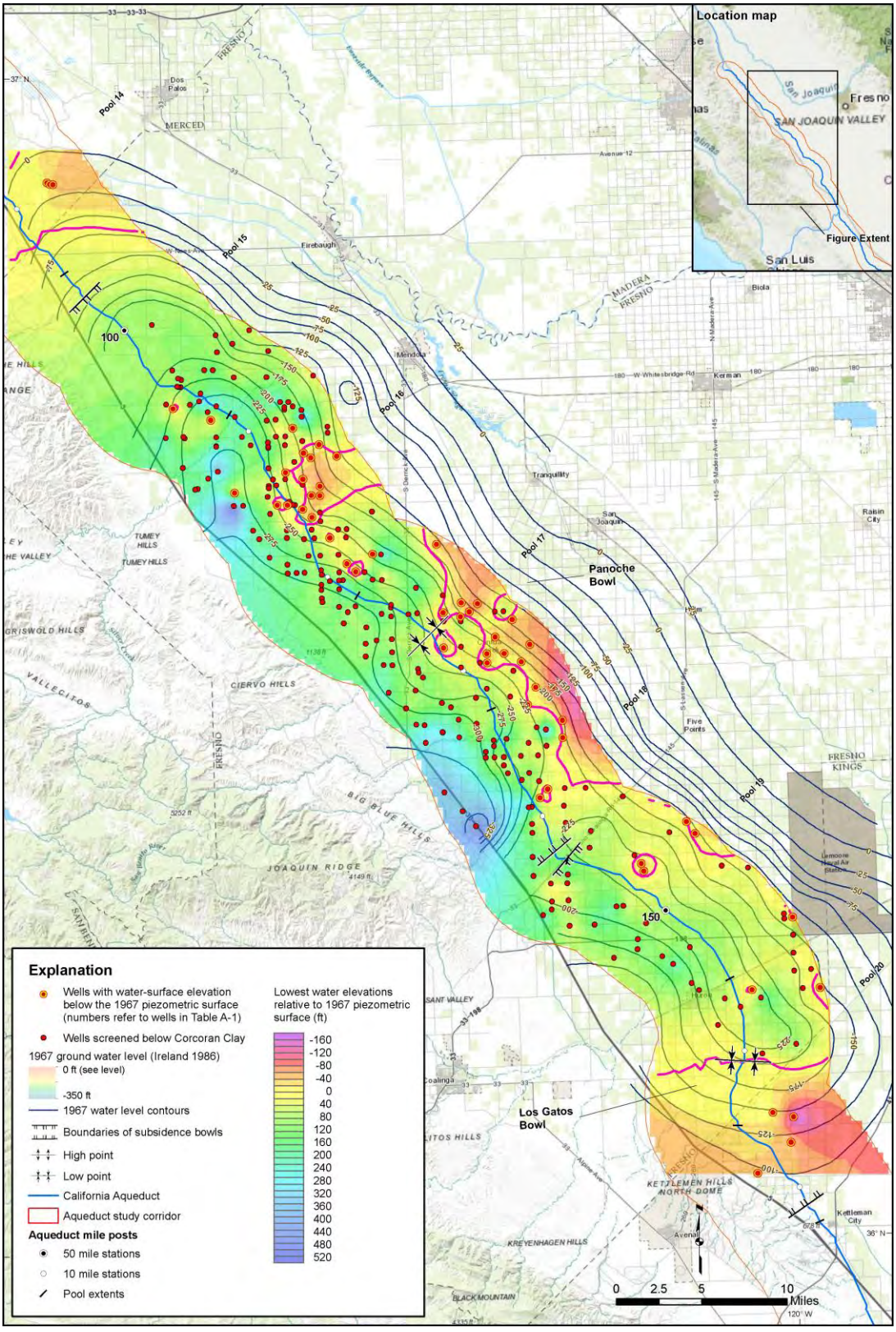

Figure 2-29 Dates of the Deepest Recorded Water-Surface Elevation in the Lower Water-Bearing Zone, Western Fresno County

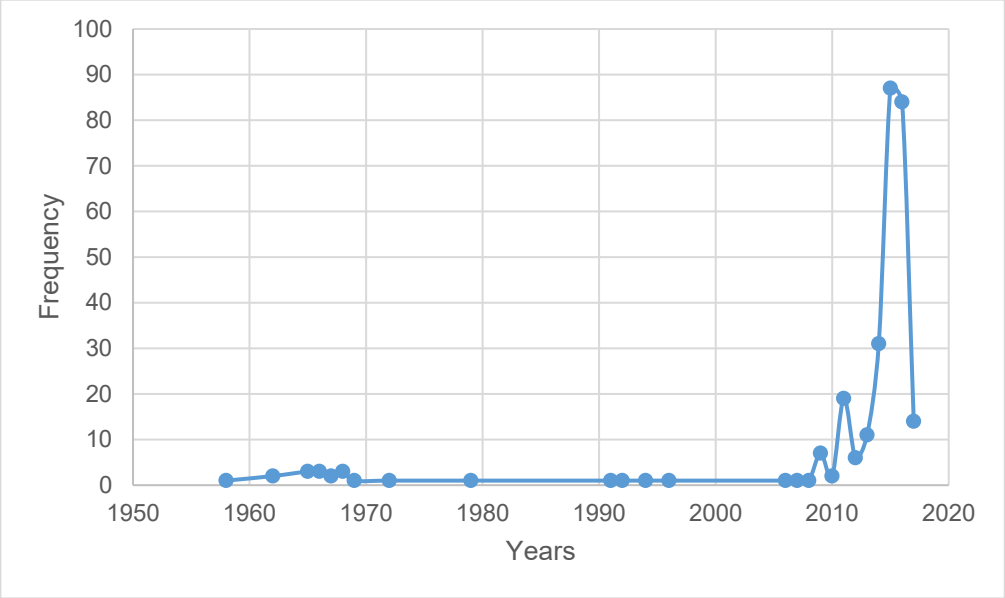

The color contours on Figures 2-28 and A-21 show the difference between the recorded minimum water-level elevation in the wells and that of the 1967 potentiometric surface. Areas where the water-level elevation dropped below the 1967 potentiometric surface are highlighted in warm colors (yellow through red) and include the following:

- A cluster of wells adjacent to and east of MP 115, Pool 16, where water-level elevations in 2014 to 2017 generally dropped 40 feet to 60 feet below the 1967 elevations, including a single well (Well 86, Table A-1) where the water-level elevation dropped approximately 62 feet below the 1967 elevation.
- Numerous wells east of the Aqueduct in the southern part of the Panoche bowl, where water-level elevations in 2014 through 2017 were recorded approximately 20 feet to 110 feet below the 1967 potentiometric surface. The red contours approach the Aqueduct most closely near the low point in the Panoche bowl near MP 127, which subsided more than 1 foot between 2013 and 2017 (see subsidence time history for MP 127.07 in Figure 5-1).
- A cluster of several wells near MP 165 in the Los Gatos bowl where water elevations in 2015 and 2016 were recorded approximately 45 feet to 167 feet below the 1967 potentiometric surface. The area near MP 165 experienced a significant increase in subsidence rate after 2013 relative to the previous 46 years (e.g., subsidence time history for MP 166.45 in Figure 5-1). This area also is close to a prominent "subsidence hot spot" imaged by Uninhabited Aerial Vehicle Synthetic Aperture Radar between 2013 and 2016 in the vicinity of Check 20 (Farr, Jones, and Liu 2016).

If it is assumed that the 1967 potentiometric surface is a proxy for the maximum pre-consolidation stress in the aquifer below the Corcoran clay (Galloway and Riley 1999, Faunt et al. 2015), then the areas in Figure 2-28 where water-level elevations declined significantly below that surface during the 2013–2016 drought likely experienced additional permanent compaction and land subsidence.

Water-surface elevation records for SJFD wells below the Corcoran clay generally are limited in space and time (Figure 2-27). The well in the Aqueduct study corridor with the longest and best-documented record of water-level elevations below the Corcoran clay is Well 12154, located in western Kern County near MP 268. A time series of water-level elevations from Well 12154 is presented in Figure 2-30. The water-level data in Figure 2-30 show that the potentiometric surface in the lower water-bearing zone decreased from approximately 150 feet above sea level in 1958, to a minimum of approximately 0 feet (sea level) in 1969 and 1970, then increased over the next 40 years to reach a maximum of approximately 250 feet in 2009, where it remained relatively constant for several years (excluding a one-year transient increase of approximately 100 feet in 2011). Water-level elevation in the lower water-bearing zone subsequently began to decline after 2013. Aside from the 2011 transient spike, the changes in water-level elevation in Well 12154 have been relatively steady and uniform since 1972.

A time history of subsidence from a nearby survey benchmark on the Aqueduct (MP 268.08) is also plotted against the water-level elevations in Well 12154 for comparison in Figure 2-30. An apparent episode of uplift or rebound is reflected in the survey data for MP 268.08 between 1980 and 1986. The source of this apparent rebound is not known, but similar abrupt increases in elevation are observed in nearly all survey data from SJFD Pools 22 to 38 during this time interval (see discussion in Section 5.1.3 of DWR's 2017 CASS report, for additional details). Because of the uncertainty in the origin of the 1980–1986 elevation increase in SJFD, only survey data collected after 1986 in the time series for MP 268.08 are considered in the following discussion. The red line in Figure 2-30 corresponding to the elevation changes measured for MP 268.08 is queried for the period 1980–1986 to highlight the uncertainty in the survey data.

The time series of water-level elevation (blue line in Figure 2-30) is interpreted to show a progressive decrease in artesian head because of groundwater production from the lower water-bearing zone prior to availability of surface irrigation water from the State Water Project (SWP) in the late 1960s and early 1970s. The sustained recovery in artesian head after 1970 is attributed to replacement of groundwater for irrigation by surface water. The DWR survey data for MP 268.08 (red line) indicate that subsidence of the Aqueduct occurred at a low, irregular rate during an approximately 20-year period between 1986 and the early 2000s, as water levels recovered steadily. The decline in artesian head after 2013, which reversed the previous 40-year increasing trend, is attributed to groundwater withdrawal during the 2012–2016 dry years. The decrease in artesian head after 2013 was accompanied by an abrupt increase in the subsidence rate measured along the Aqueduct. To date, the elevation of the potentiometric surface in the lower water-bearing zone has not been drawn below the low elevation of 0 feet (sea level) recorded in 1969–1970 (Figure 2-30).

In summary, well data within the study corridor that include water-level elevations for the lower water-bearing zone (the confined aquifer system below the Corcoran clay) are available between Pools 14 and 21, and indicate local decline below the 1967 potentiometric surface during the 2013–2016 drought years. This reach of the Aqueduct encompasses the Panoche bowl and the northern part of the Los Gatos bowl, both of which experienced increased subsidence rates during 2013–2016. Data from a single, well-documented, deep well near the southern end of the Aqueduct in western Kern County (Well 12154; Figure A-21 and Figure 2-30) indicate that while water-level elevation in the lower water-bearing zone there declined after 2013, it did not reach or drop below the historic low elevation recorded in the well in 1969–1970. The onset of water-elevation decline in the well after 2013 is temporally correlated with a distinct increase in the rate of subsidence measured along the Aqueduct nearby (Figure 2-30).

Figure 2-30 Historic Variations in Artesian Head, Well 12154, Western Kern County, and Time Series of Elevation Change at Milepost 268.08 Along the Aqueduct

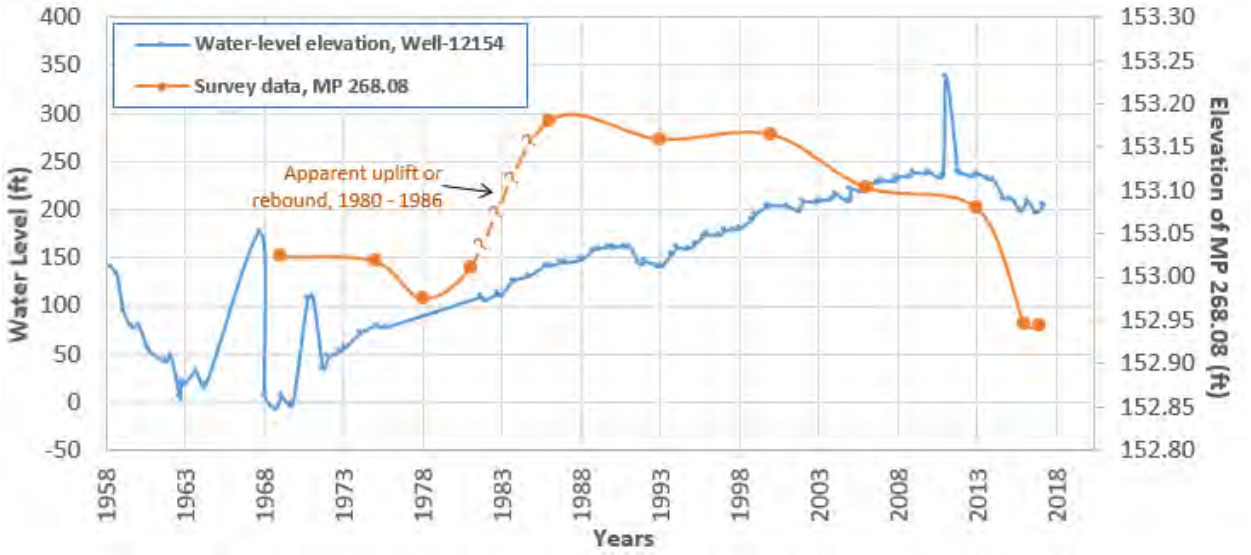

Note: ft=feet, MP=milepost

Chapter 3. Land Subsidence at the Lost Hills Oil Field

3.1 Introduction

This chapter presents data on subsidence related to oil production at the Lost Hills and Northwest Lost Hills oil fields (collectively, LHOF) east of the Aqueduct (Figure 3-1). As described in detail below, oil field subsidence is localized over the main production area and does not extend east to the Aqueduct. Measured historical subsidence along the Aqueduct at Lost Hills and Northwest Lost Hills oil fields is likely related to groundwater withdrawal, and spatial variations in historical subsidence along the Aqueduct. It mirrors patterns of deep, long-term subsidence that are probably controlled by geologic conditions directly below the Aqueduct, rather than oil production in the LHOF to the west.

Figure 3-1 Location Map of the Lost Hills and Northwest Lost Hills Oil Fields, Kern County

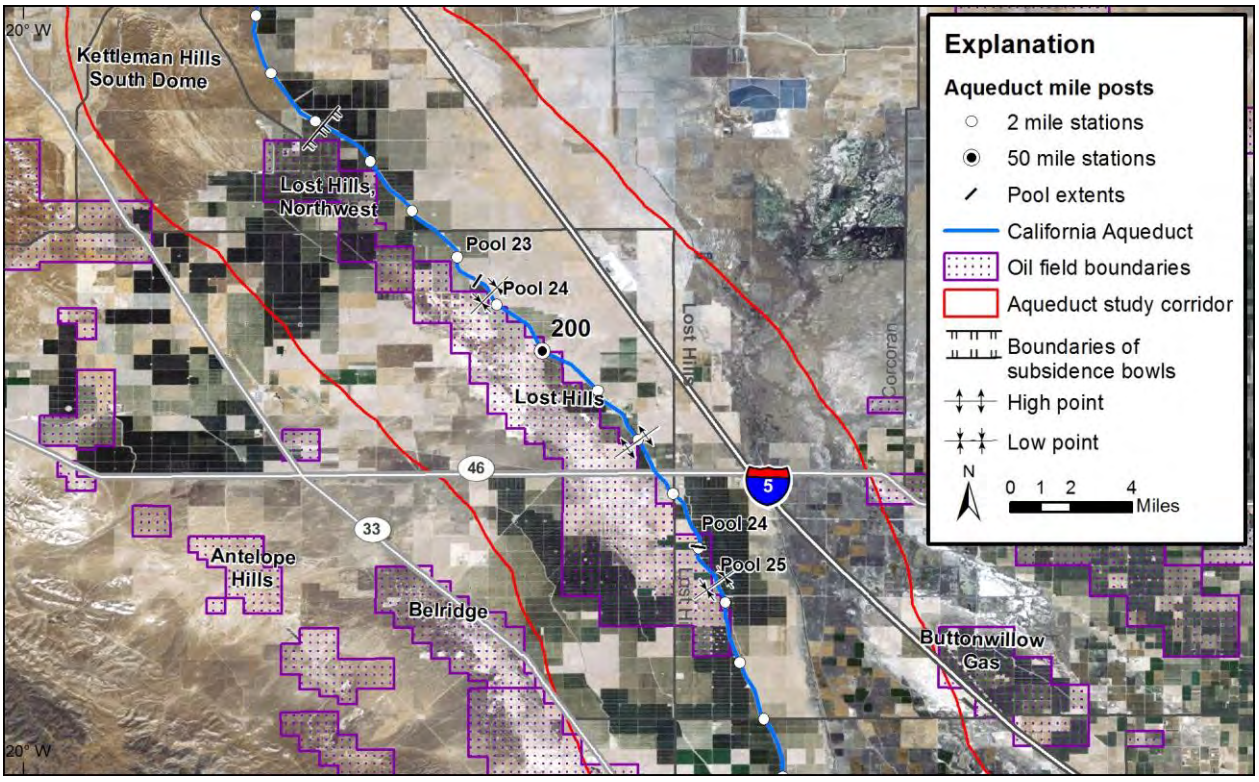

3.2 Oil-Field Subsidence

The LHOF in Kern County extend to within one mile west of the Aqueduct (Figure 3-1). The boundaries of the two fields collectively define a northwest-trending zone that is approximately 15 miles long, 2- to 4-miles wide, and on trend with the Kettleman Hills South Dome to the north. The map in Figure 3-1 shows the geographic boundaries of the LHOF as recognized by the Division of Oil, Gas and

Geothermal Resources. From inspection of Google Earth imagery, the distance between the eastern margin of the LHOF production area (as distinguished by the presence of production pads and pump jacks) and the Aqueduct generally varies between approximately 0.5 mile and 1.0 mile, with the closest approach being near MP 196.5. Pool 24 of the Aqueduct (between MP 197 and MP 208) flanks most of the northwest-southeast extent of the LHOF (Figure 3-1).

Oil production at the LHOF generally is from a northwest-southeast-trending anticlinal closure in Quaternary and Tertiary strata (Division of Oil Gas and Geothermal Resources 1998a, 1998b; Land 1984; Medwedeff 1989). The larger Lost Hills oil field to the south is associated with a doubly plunging anticline with a relatively broad, flat crest (Medwedeff 1989). The smaller Northwest Lost Hills field to the north is located along the northwest-plunging nose of the structure (Land 1984).

According to Bruno and Bovberg (1992), much of the production from the LHOF, and other nearby oil fields in the southwestern San Joaquin Valley (Figure 3-1), comes from thick, shallow, and relatively compactible beds of late Neogene diatomite and mudstone. In the LHOF, the producing diatomite zone that is susceptible to compaction is in the depth range of approximately 1,000 feet to 2,000 feet below the land surface (Bruno and Bovberg 1992, Division of Oil, Gas and Geothermal Resource 1998a, 1998b). The diatomite is porous but relatively less permeable than other producing zones within the LHOF. Enhanced recovery methods, such as hydraulic fracture stimulation, are required for economic oil production from this unit (Land, 1984, Bruno and Bovberg 1992).

Land subsidence has been documented above the LHOF and at other oil fields in the southern San Joaquin Valley where production occurs from shallow diatomite reservoirs (Bruno and Bovberg 1992). Subsidence above the LHOF began in the early 1950s and accelerated because of expanded well development in the late 1980s (Bruno and Bovberg 1992). Subsidence rates in excess of approximately 1.3 feet/year (400 millimeters [mm]/year) were measured at LHOF in the mid-1990s by Fielding et al. (1998) using Synthetic Aperture Radar (SAR) interferometry.

3.3 Extent of Oil-Field Subsidence

Patterns of land subsidence imaged by SAR interferometry were analyzed to assess whether subsidence related to oil production at the LHOF is potentially affecting the Aqueduct. Figure 3-2 is a SAR interferogram from Fielding et al. (1999) that images subsidence over the LHOF during an eight-month period in 1995. Inspection of Google Earth imagery indicates that the subsidence maximum is located over one of the most densely developed parts of the LHOF (based on the number and distribution of well pads, access roads, and pump jacks). The 1995 SAR subsidence maximum is adjacent to an approximately 7-mile-long section of the Aqueduct between MP 201 and MP 208.

The locus of maximum subsidence in the SAR data is approximately centered on, or slightly south of, State Route 46, which crosses the LHOF producing area at the latitude of Aqueduct MP 205 (Figure 3-1). Inspection of Figure 3-2 shows that the area of localized subsidence represented by closed contours in the SAR interferogram decreases to background rates approximately 1 mile west of the Aqueduct. The subsidence rates along the Aqueduct are no higher than those in surrounding farmland regions, where presumably the main contributing factor to subsidence is groundwater withdrawal. Fielding et al. (1999) published an east-west subsidence profile at the latitude of State Route 46 derived from the SAR data

(Figure 3-3). The profile also indicates that subsidence across the LHOF, as measured over an eight-month period in 1995, decreases to background rates west of the Aqueduct.

Land survey data collected along the Aqueduct demonstrate that there is no spatial correlation between localized high rates of subsidence in the LHOF to the east, and historic subsidence along the Aqueduct. Figure 3-4 presents the long-term subsidence profile of the Aqueduct between Pools 23 and 26, directly east of the LHOF. The profile shows that Pools 24 and 25 are located within the historic Kern bowl (Chapter 1) that extends from near MP 190 to near MP 220 (Figure 3-4). The Kern bowl can be subdivided into two smaller subsidence bowls with a divide or subsidence minimum between them located near MP 204. Maximum subsidence within the two smaller bowls, relative to a 1967 baseline, is approximately 3.25 feet and 3.0 feet near MP 198 and MP 208, respectively. Maximum subsidence at the divide, or minimum between them, near MP 204 in the same time period is approximately 1.0 foot.

The locus of maximum subsidence in the LHOF (Figure 3-2) lies directly west of the local minimum within the Kern bowl (Figure 3-4). If the high rates of production-related subsidence in the LHOF (as much as 400 mm/year in the mid-1990s, or approximately 1.3 feet/year) (Fielding et al. 1999) extended eastward to the Aqueduct, then it would be expected to see evidence of localized high rates of subsidence in the survey profile at the same latitude as the SAR subsidence maximum between MP 201 and MP 208. But, as shown on Figure 3-4, the locus of maximum subsidence in the LHOF is approximately at the same latitude as the local minimum subsidence within the Kern bowl, as shown in the Aqueduct survey profile. Additionally, the subsidence profile in Figure 3-4 shows that the highest rates of subsidence in the Kern bowl are located near MP 198 and MP 208, which are north and south, respectively, of the maximum subsidence rates over the LHOF imaged by the SAR data (Figure 3-2). These relations show that there is no spatial correlation between historical patterns of subsidence along the Aqueduct and LHOF subsidence to the west.

The average rate of subsidence at MP 203.92, derived from the DWR survey data (Figure 3-5), is 0.0125 feet/year (approximately 4 mm/year) for the 1993–2017 period, two orders of magnitude lower than the rate of subsidence observed in the LHOF directly to the west during 1995–1996 by Fielding et al. (1999). The 4 mm/year long-term subsidence rate at MP 203.92 is equivalent to approximately 0.01 mm/day, which is comparable to the 35-day average rate measured by SAR interferometry in 1995 where State Route 46 crosses the Aqueduct (Figure 3-3). The subsidence rate at MP 203.92 along the Aqueduct has been relatively uniform from 1993 through 2017 and shows no evidence of higher rates in the mid- to late-1990s corresponding to the higher rate of subsidence in the LHOF during that same period (Fielding et al., 1999). This data, along with the east-west profile through the SAR data in Figure 3-3, indicates that high rates of subsidence related to oil production in the LHOF, die out west of the Aqueduct.

Figure 3-2 SAR Interferogram Imaging Subsidence Over the Lost Hills Oil Field

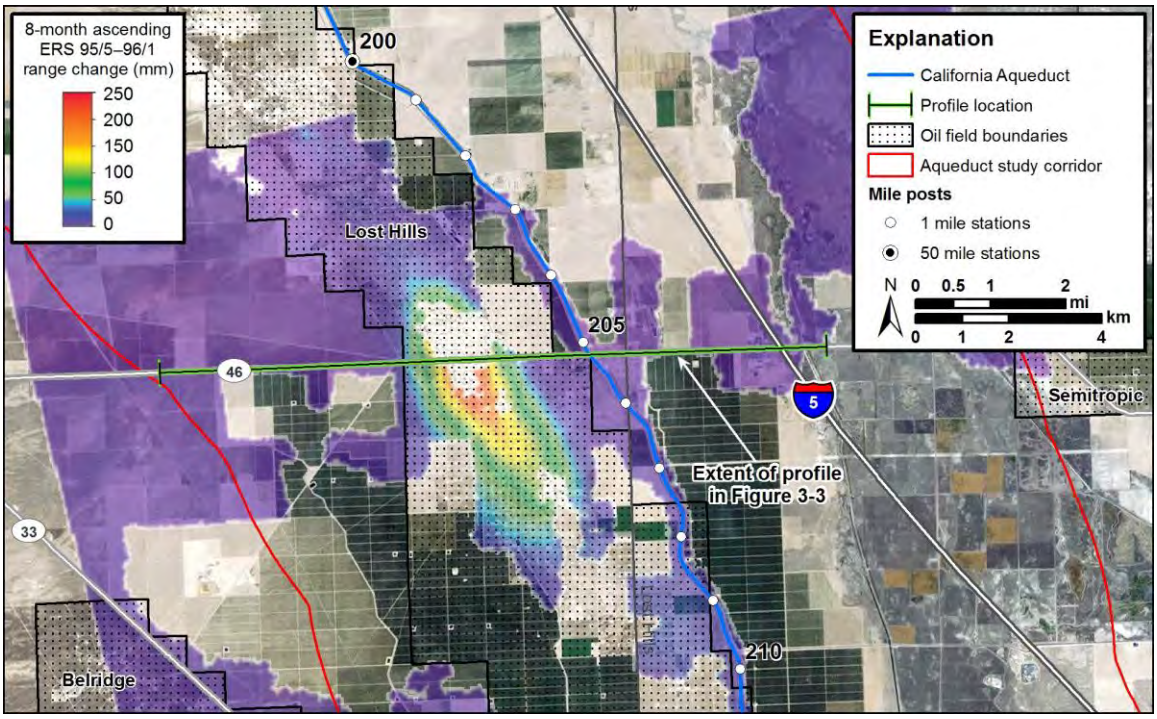

Note: Modified from Fielding et al. 1999.

Figure 3-3 East-West Profile of Subsidence Over the Lost Hills Oil Field, Kern County

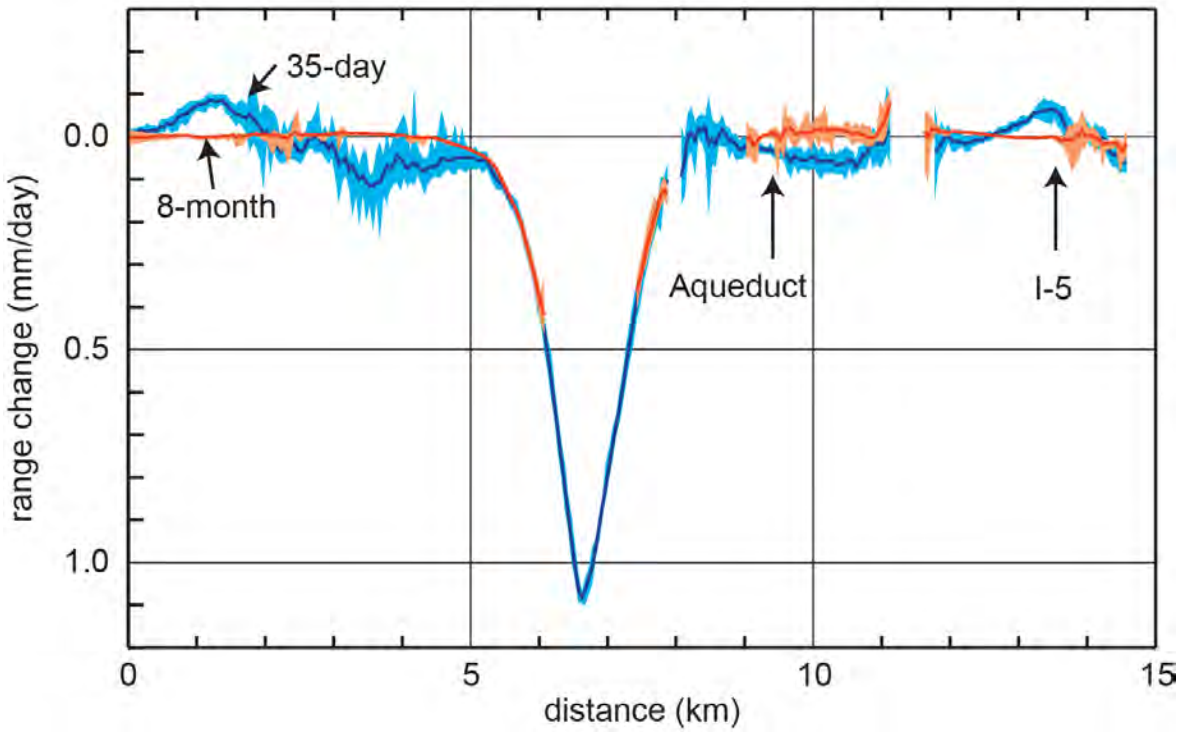

Note: Modified from Fielding et al. 1999.

Figure 3-4 Historic Subsidence Profile of the California Aqueduct East of the Lost Hills Oil Field

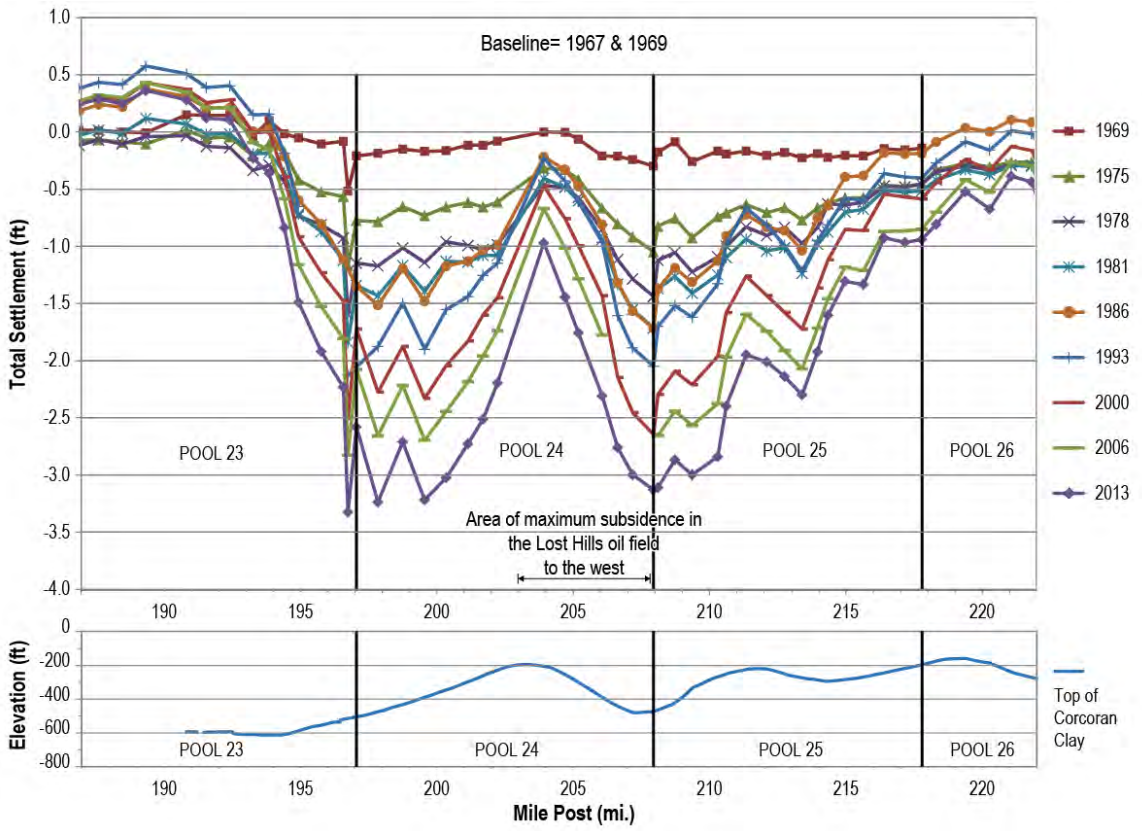

Figure 3-5 Subsidence History at Milepost 203.92, 1993–2017

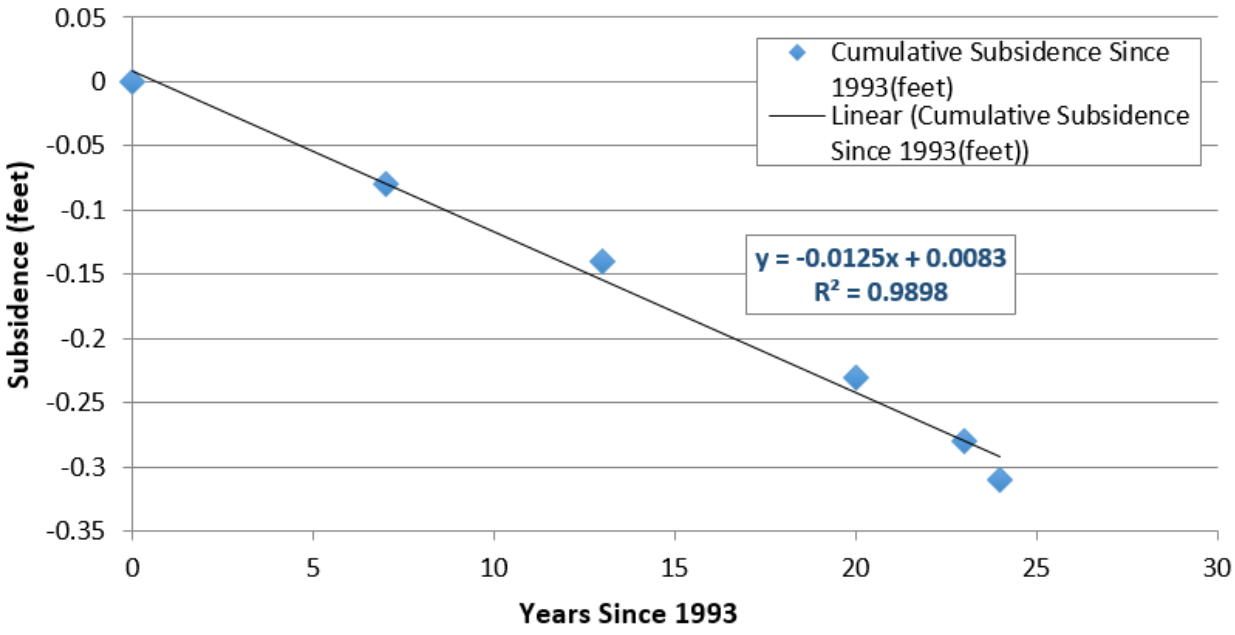

3.4 Discussion

The spatial pattern of subsidence in the Kern bowl, including the local subsidence minimum or "high" at MP 204 in the Aqueduct profile, may be controlled in part by patterns of deep natural subsidence below the Corcoran clay. Figure 3-4 presents a profile of the elevation of the top of the Corcoran clay beneath the Aqueduct alignment. A visual comparison of the Corcoran clay profile with the Aqueduct survey profile reveals that the peaks and troughs in the buried Corcoran clay mimic, to some extent, the historic subsidence patterns in the Kern bowl. Specifically, the local subsidence minimum or "high" in the Kern bowl is coincident with a local high in the underlying Corcoran clay, the top of which is located at an elevation of approximately 200 feet beneath MP 204, and which decreases to depths of 500 feet or greater to the northwest and southeast beneath Pool 24 (Figure 3-4). The 300 feet of buried topography on the top of the Corcoran clay beneath Pool 24 developed over extended geologic time and is not a historic feature. These variations in the elevation of the Corcoran clay, and specifically localized depressions in the buried surface of the clay, likely reflect natural compaction and subsidence of the geologic deposits underlying the clay (see discussion in Section 6.2). The fact that the pattern of historic subsidence along the Aqueduct is similar to buried geologic relief on the Corcoran clay suggests that some deep geologic control, in combination with groundwater withdrawal, has influenced the spatial variation in historic land subsidence in the Kern bowl (Figure 3-4). The spatial pattern of historic subsidence in the Kern bowl is better correlated with the natural geologic subsidence beneath the Corcoran clay than with shallow oil field subsidence measured across the LHOF in Figures 3-2 and 3-3.

In conclusion, the preferred interpretation of data presented in this section is that subsidence related to oil production in the LHOF decreases to background rates west of the Aqueduct (Figures 3-2 and 3-3). Historic subsidence measured along the Aqueduct is most likely driven by groundwater withdrawal, and spatial variations in historic subsidence in the Kern bowl, such as the local subsidence minimum or "high" at MP 204 (Figure 3-4), likely reflects the influence of natural geologic conditions directly beneath the Aqueduct.

Chapter 4. Hydraulic Analysis

4.1 HEC-RAS Hydraulic Model Development

A Hydrologic Engineering Center's River Analysis System (HEC-RAS) hydraulic model was developed for the 2017 California Aqueduct Subsidence Study (CASS), referred to herein as the 2017 Conditions CASS Model. The 2017 Conditions CASS Model was an update to the model documented in DWR's CASS report dated June 2017, referred to herein as the 2015 Conditions CASS model.

The 2017 Conditions CASS Model was used for the evaluations presented in this report including computation of current delivery capacities, evaluation of hydraulic structure impacts, and analyses of the potential impacts of subsidence to future deliveries. This section outlines the model development.

4.1.1 Model Background

The 2015 Conditions CASS Model was used as the starting point to develop the 2017 Conditions CASS Model, which in turn was modified to include more recent terrain data, refined gate operations, geo-referenced line work, and additional geometric components such as critical overchutes and canal raises. A detailed description of features in the 2017 Conditions CASS Model is included in subsequent sections. The extent of the 2017 Conditions CASS Model is presented in Figure 4-1.

4.1.2 Model Geometric Data

The following sections describe the model geometric features.

4.1.2.1 Horizontal Projection

The geographic information system (GIS) line work for the 2017 Conditions CASS Model is projected using the North American Datum of 1927, State Plane — California IV.

The detail, orientation, and length of the line work in the 2015 Conditions CASS Model indicate that it was developed in a geo-referenced environment using terrain data, aerial imagery, and/or elevation contours. But, the horizontal data used in its development were not explicitly documented. Several issues were identified when the stream centerline and cross sections from the model were imported into a GIS environment. First, the projected line work, as exported from the model, was shifted by more than 250 feet to the northeast. Second, the model line work was rotated counterclockwise about a point near the cross section at River Station (RS) 86.1406 (MP 164.77). That is, the line work north of this point was offset, but parallel to aerial imagery of the Aqueduct. The line work south of this point diverged from the Aqueduct alignment, moving further east as it moved south toward the downstream model boundary.

To correct the observed offsets, the line work in the 2015 Conditions CASS Model was adjusted manually in GIS. First, a global offset of the stream centerline and all cross sections was implemented so that the line work upstream of RS 86.1406 coincided with aerial imagery of the Aqueduct. Second, the line work downstream of RS 86.1406 was rotated clockwise so the centerline and cross sections coincide with the

Aqueduct. Third, manual adjustments were implemented to “fine tune” the cross sections along the Aqueduct channel.

Figure 4-1 2017 Conditions California Aqueduct Subsidence Study Model Extents

4.1.2.2 Vertical Datum

The 2017 Conditions CASS Model elevations are referenced to the National Geodetic Vertical Datum of 1929 (NGVD 29).

The 2015 Conditions CASS Model was initially assembled using as-built data for the Aqueduct. Subsequently, the model elevations for features such as cross sections and inline (check) structures were updated using DWR precise survey, which is referenced in NGVD 29. Survey points in the DWR precise survey dataset are generally spaced several hundred feet, or even thousands of feet, apart. The survey dataset also does not coincide with all model cross section locations, so when model elevations were updated, they were typically interpolated between survey points.

A Light Detection and Ranging (LiDAR) survey was conducted on July 29 through August 3, and August 26 and 27, 2016. The nominal point density of the LiDAR survey is 9 points per square meter. The 2017 Conditions CASS Model elevations were updated using the LiDAR dataset because of its high point density and the continuous dataset through the extent of the model. But, LiDAR elevations were referenced to the North American Vertical Datum of 1988 (NAVD 88), so a conversion factor of -2.82 feet was used to convert the model elevations back to NGVD 29. The difference between NGVD 29 and NAVD 88 is generally within the range of -2.64 feet and -2.94 feet within the model extents. The value of -2.82 feet was used because it is the mean difference in vertical datum within the range of the model and it creates for a maximum discrepancy of -0.18 foot.

The elevation update using LiDAR helped implement a general adjustment to model elevations to represent current terrain trends and slopes more accurately. To incorporate the latest elevation data, the model was adjusted again using 2017 precise survey. Elevation differences were calculated between the 2016 and 2017 precise survey datasets. Interpolated values were then calculated for model features between survey points. The interpolated elevation adjustments were then applied to model elevations to reflect 2017 conditions.

4.1.2.3 Cross Sections

There are more than 840 cross sections in the 2017 Conditions CASS Model. The vast majority of these represent the trapezoidal channel of the Aqueduct; a smaller subset of these represents the rectangular channel approach at check structures or siphons.

Bank stations for the 2017 Conditions CASS Model cross sections were set to represent the top of liner. Because the Aqueduct is operated to keep water surface elevations (WSEs) below the top of the concrete liner, the model is intended to convey flow in the main channel only. The model is not intended to convey flow in what HEC-RAS refers to as “overbanks,” which convey flow outside of the bank stations.

Manning’s “n” roughness coefficients for the main channel were set to a value of 0.02. This is consistent with recommendations made by DWR’s Division of Engineering (DOE) for current conditions (June 2017). Manning’s n values for the overbanks were also set to a value of 0.02. Manning’s roughness coefficients for concrete lined channels typically range from 0.011 to 0.027 depending on the smoothness of the finish (U.S. Army Corps of Engineers 2010).

Channel base widths, side slopes, and depths (vertical distance between the base and the top of liner) were initially developed for the 2015 Conditions CASS Model using as-built drawings for Aqueduct typical sections. For the 2017 Conditions CASS Model, some cross sections were updated to account for liner raises. Liner raises provide for a wider top width, increasing the flow capacity of the Aqueduct in these reaches.

Cross section spacing should be selected based on the characteristics of the channel being modeled. Cross sections should be included to capture variations in the channel which may include widening, narrowing, bends, and changes in slope, roughness, or depth. Because the California Aqueduct is a generally uniform channel, larger distances between cross sections are acceptable. Cross sectional spacing in the 2017 Conditions CASS Model varies from tens of feet to more than a mile. Regardless of these variations, model tests and calibration runs showed that observed flow rates, volumes, and stages could be simulated with the current model cross section layout.

4.1.2.4 Check Structures

Sixteen check structures (14 through 29) are included in the model. The check structures are modeled as inline structure weirs with radial gate openings. For this narrative, inline structures and check structures may be used interchangeably. Gate parameters include a trunnion exponent, a gate opening exponent, and a head exponent set to typical values of 0.16, 0.72, and 0.62, respectively. Radial discharge and orifice coefficient values were set to 0.7 and 0.8, respectively. These typical values are outlined in the HEC-RAS hydraulic manual.

4.1.2.5 Overcrossings

Overcrossings include overchutes, bridges, and pipelines. Within the model extents, approximately 70 overcrossings with soffits below the top of liner have been identified through field observations. It has also been observed that the soffits of some of these overcrossings are now below the maximum allowable WSE. Because of subsidence, the low chord of some of these overcrossings is now encroaching below the hydraulic grade line for some flow conditions. Some of the issues with this condition include lateral hydrodynamic forces, uplift from buoyancy effects, flow restrictions, and backwater effects that can potentially damage the overcrossing or upstream embankment. As a result, the maximum allowable WSEs for the Aqueduct are being reevaluated.

Critical locations were identified at each pool and included in the model. In general, critical locations were identified as the feature that encroached farthest into the maximum allowable WSEs. In some cases, it was the top of liner; in other cases, it was overcrossings. Additionally, where the second most critical feature in a pool was another overcrossing, a second overcrossing was included in the model. A summary of the overcrossings included in the model is presented in Table 4-1.

4.1.2.6 Lateral Structures

Lateral structures were included in the model along the entire modeled reach. Lateral structures are included to give users the option to model turnouts explicitly as gates along the Aqueduct. But, this option

Table 4-1 Modeled Overcrossings

Pool	Milepost	River Station	Structure	Quantity	Calculated Bottom of Structure Elevation (feet) NGVD 29	Number of Piers	Pier Width (feet)
17	132.96	117.9500	Trunnion Deck	1	317.59	3	3.50
22	179.50	71.4167	Overchute	1	313.38	1	1.50
23	196.58	54.3382	Overchute	1	308.05	3	1.50
24	197.84	53.0731	Overchute	1	306.62	2	1.50
24	207.18	43.7330	Overchute	1	304.58	1	1.50
25	208.11	42.8068	Overchute	1	304.24	1	1.50
25	209.36	41.5522	Overchute	1	304.30	1	1.50
26	224.18	26.7319	Overchute	1	302.85	1	1.50
27	225.05	25.8625	Overchute	1	303.51	1	1.50
28	232.96	17.9572	Overchute	1	301.98	1	1.50
29	240.07	10.8416	Pipeline Bridge	1	299.91	2	1.75
30	246.51	4.4065	Overchute	1	297.96	2	1.50

Note: NGVD 29 = North Geodetic Vertical Datum of 1929

was not used for the analyses summarized in this report. Lateral structures can have three functions: weir, gate, or culvert. To use the weir function correctly, it is necessary to capture the high ground along the channel. If the channel is overtopped, flow would be diverted away from the channel. A basic example of this is a leveed channel; once the levee crown is overtopped, flow is diverted away from the main channel. It is critical to capture the high ground alignment to model lateral structures correctly for overtopping flows. The lateral structures in the 2017 Conditions CASS Model do not capture the high ground alignment at all places. As a result, they should not be used as a weir to model overtopping flows. This model limitation is acceptable for the 2017 Conditions CASS Model because it is not intended to simulate excess flow above the top of liner. But, the user may include gates or culverts along a lateral structure between cross sections. These functions of the lateral structure feature can be used to explicitly model turnouts along the Aqueduct.

4.1.3 Model Flow Data

The sections below describe the flow data used for the hydraulic analyses presented in this report.

4.1.3.1 Boundary Conditions

Boundary conditions allow the user to enter known settings at various locations within the model to calculate hydraulic conditions elsewhere within the system. At a minimum, boundary conditions are needed at the upstream and downstream ends of the modeled reach. Typically, flows are entered at the upstream end of an open channel system and stages are entered at the downstream boundary. Both steady and unsteady model simulations were performed for this report, each using different boundary conditions.

An unsteady flow simulation was performed for model calibration. For this simulation, a flow hydrograph was used for the upstream boundary condition. The flow hydrograph was derived from flow rates at Dos Amigos Pumping Plant (DAPP) over a period of 16 days. A flow/stage hydrograph was used as the downstream boundary condition. The flow hydrograph was derived from flow rates at Buena Vista Pumping Plant (BVPP) over the same period of 16 days. The stage hydrograph was derived from stages measured just upstream of BVPP over the same period.

Additionally, for the unsteady flow simulation, internal boundary conditions were used to account for flow leaving the Aqueduct through turnouts. Flow rates at turnouts were not available for model calibration. But, flows are recorded at Check 21 and calculated at other check structures using historical relationships that are based on gate openings and WSEs. With this information, the flow leaving the Aqueduct via turnouts can be estimated quantitatively as the difference between flows at known flow locations. For the model calibration run, the flow leaving between two known flow locations was taken out of the system using uniform lateral inflow hydrographs. This internal boundary condition introduces, or removes (when set to negative values), flow out of a system between two points specified by the user. The flow leaving the system is uniformly distributed between the two points. It was observed in the calibration process that this approach to modeling flow at the turnouts produced results comparable to field data.

Another internal boundary used for the calibration run was the navigation dam option for gate operations. This is documented in greater detail in Section 4.1.3.3.

Various steady flow simulations were performed to evaluate the impacts of subsidence on the flow capacity of the Aqueduct. For these simulations, a single flow value is entered at the upstream end of the model. Additional flow changes can be specified by the user at known flow change locations. A known water surface was used as the downstream boundary for the steady flow simulations. Typically, the lowest allowable WSE at the downstream end of the model was used to allow the model to drive more flow through the system and capture maximum pool capacities.

4.1.3.2 Initial Conditions

During an unsteady flow simulation, the user may specify the initial conditions throughout a reach. The 2017 Conditions CASS Model includes Pools 14 through 30 as one reach. Typically, the user would specify the flow rate in a reach at the beginning of a simulation. But, because the flow varies widely between Pool 14 and Pool 30, a single flow doesn't reflect the initial conditions of the Aqueduct very well. HEC-RAS also allows the user to create a restart file at a particular time step during a simulation. The time step is selected at a moment when the conditions of the system reflect the way the conditions at the beginning of the simulation might appear. A preliminary simulation was performed to develop a restart file for the calibration simulation.

4.1.3.3 Gate Operations

There are various ways within HEC-RAS to operate gates at inline structures. For the analyses presented in this report, two primary methods of modeling gates at check structures were used: (1) navigation dam operations were used for calibration, and (2) fully open operations were used for pool capacity runs.

For model calibration, the gates were modeled using the navigation dams HEC-RAS boundary condition. This internal boundary condition opens and closes the gates to accommodate for varying flow rates while trying to maintain stages at a monitoring location established by the user at a set target WSE.

For pool capacity simulations, the gates were modeled as fully open to allow for maximum conveyance. This is consistent with the analysis performed by DOE to estimate pool capacities for the 2017 Conditions CASS Model.

4.1.4 Model Flow Analysis

For unsteady flow analyses, calculation options and tolerances were set to default. The simulation time for the calibration run extended 16 days from September 20, 2017, to October 5, 2017. Computational settings were set with a computational time step of six seconds, hydrograph output interval of one hour, and a detailed output interval of one hour.

For steady flow analyses, calculations options and tolerances were set to default. The flow regime was set to subcritical.

4.2 Model Simulations and Hydraulic Analyses

The 2017 Conditions CASS Model can serve to inform the user about many different aspects of the Aqueduct. Various types of simulations were carried out as part of the analyses presented in this report. The simulations that are summarized in this section generally can be categorized into the following types: calibration, capacity analysis, impact of overcrossings, and flow impacts resulting from projected subsidence. Simulations intended to assist operations will not be summarized in this report.

The findings presented in this section are based on the idealized Aqueduct configurations that were modeled. They are not a comprehensive evaluation of every potential scenario under which the Aqueduct system, or any of its components, can function. The Aqueduct is a complex system with many facilities and factors that can impact its hydraulics. Assumptions were made for the analysis presented herein; as a result, any application or conclusions derived from these findings should consider modeling limitations.

4.2.1 Model Calibration

Hourly stage and flow data for the SJFD and the SLFD reaches of the Aqueduct was compiled for a period of 16 days. The period of data extends from September 20, 2017, to October 5, 2017. This data are herein referred to as the calibration dataset.

The calibration dataset included flows and stages just downstream of DAPP and just upstream of BVPP. The flows at DAPP were used for the 2017 Conditions CASS Model upstream boundary condition. A flow/stage hydrograph was developed from the calibration dataset and used as the downstream boundary condition of the model.

Stage and flow data from DWR records were entered into the model just upstream of check structures as observed (measured) data. These data are not used to calculate results, but rather plotted along results for

comparison. Stage data were available at Check Structures 14 through 29. Flow data were available at Check Structures 18, 19, 20, 21, 22, and 25.

A series of model simulations were performed to check the validity of the model outputs against the observed data. After each subsequent simulation, adjustments were made to the model to refine the outputs and better replicate the observed data at the check structures. The main model function manipulated to target observed flows and WSEs was gate operations at check structures. Check gates are currently operated using operator experience, based on projected flow rates, and observing pool elevations directly upstream of the check structure. It would be very difficult to exactly duplicate the actual gate operations for the observed period. Instead, the navigation dam boundary condition was used to operate the gates. This feature allows the model to make decisions about the gate operations to target WSEs at the monitoring stations defined by the user.

Actual stages at the monitoring locations just upstream of the check structures vary randomly over time, as they are often based on operator preference. A particular operator can affect whether a pool is near the bottom, middle, or top of an allowable range. To overcome this variation, an average WSE was derived from the observed stage data. The average WSE values upstream of each check structure were then set as the target elevation for the navigation dam controls.

Figure 4-2 shows a typical profile within the simulation period compared to observed stages. Differences in elevations between model results and observed values were within 0.3 foot on average. Flow comparison plots were developed for Check Structures 18, 19, 20, 21, 22, and 25 (Appendix B – Flow Calibration Plots). Model results matched observed values with an average error ranging from 0.96 percent at Check 18, to 4.22 percent at Check 21.

Figure 4-2 Calibration Profile

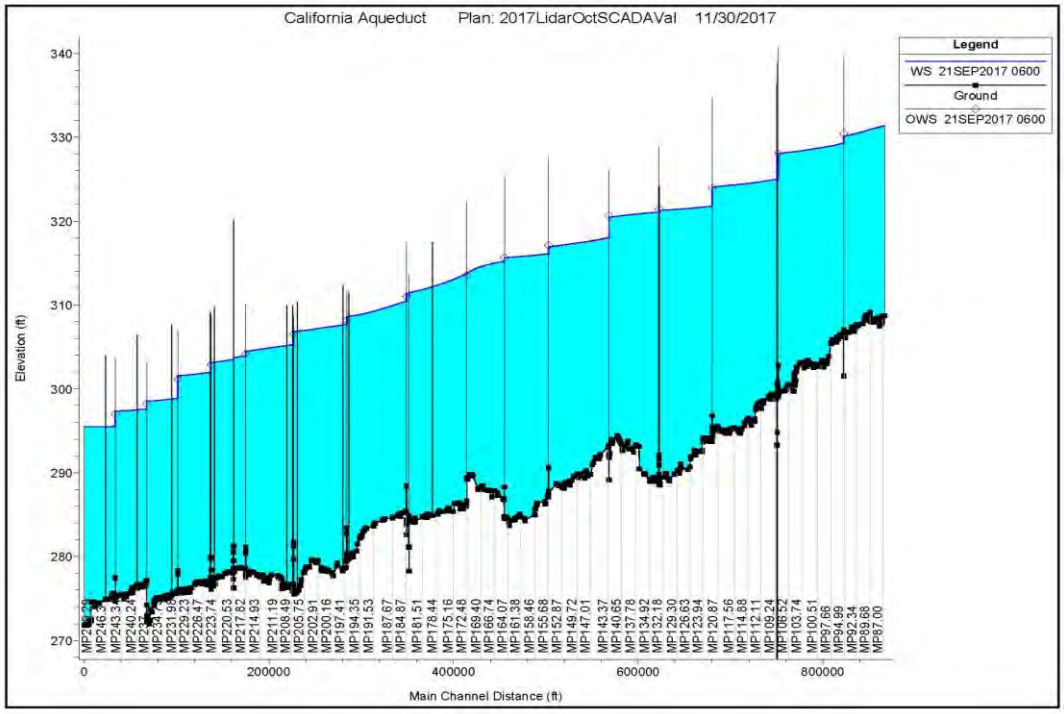

4.2.2 Pool Flow Capacity

The pool capacity simulations for 2017 conditions, carried out with the 2017 Conditions CASS Model, were performed using the same process presented in the June 2017 CASS report. The pool capacities presented for the June 2017 report were calculated using the 2015 Conditions CASS Model. In this process, the model is first run assuming design inflows at each pool and minimum pool elevation at the downstream end of the forebay of BVPP (water level at an elevation of 294.6 feet). The WSEs at each pool are then compared with the current top of liner elevations to determine the lined freeboard along the Aqueduct profile. If the freeboard at any point in the Aqueduct is less than the proposed minimum (0.5 foot), the inflow into the corresponding pool is reduced and the model is re-run. The trial is continued until the lined freeboard at each pool is within the specified limit. The resulting flow at this point is the estimated pool capacity.

For the analysis (performed using the 2017 Conditions CASS Model), headwater elevations at critical overcrossings and top of liner elevations were considered. The capacity simulation was carried out allowing WSEs to encroach as much as 2 feet above overcrossing soffits, except at locations identified for special operating conditions. Table 4-2 provides a list of locations with special operating conditions.

Table 4-2 Aqueduct Locations with Special Operating Conditions

Pool	Location	Structure	Condition
17	Check 17 (MP 132.97)	South Deck Radial Gates Anchor	3.8 feet in water
24	MP 197.84	Overchute	9 inches in water
25	MP 208.11	Overchute	1.3 feet in water

Note: MP = milepost

4.2.2.1 General Capacity Comparison

The analysis performed with the 2017 Conditions CASS Model indicates Pools 14 through 19 remain capable of conveying their design capacity. Reduced pool capacities begin in Pool 20, have a drop across Pool 24, another drop in Pool 25, and continue down to Pool 29. Also, the capacity for Pool 24 decreased compared to the findings presented in the June 2017 report. The reduced capacity for Pool 24 was reported at 6,650 cubic feet per second (cfs) in the June 2017 report. The latest analysis shows that Pool 24 has a capacity of 6,410 cfs. The capacities for Pools 25 through 29 also decreased compared to the findings presented in the June 2017 report. The reduced capacities listed in the June 2017 report were 5,500 cfs for Pools 25 through 28, and 5,350 cfs for Pool 29. The latest analysis shows these pools have a capacity of 5,160 cfs. Figure 4-3 presents a comparison between design capacities and modeled capacities for 2015 and 2017 conditions. Table 4-3 provides tabular results relating to Figure 4-3. It should be noted that differences in results between the 2015 and 2017 conditions models are not solely the result of changes in subsidence, but may be attributed to variability in detail between the two models.

Figure 4-4 shows the lined freeboard in Pools 14 through 30 measured from the 2017 conditions pool flow capacity simulation model. The 2017 conditions freeboard is plotted along the design freeboard. This comparison can be used to identify reaches of the Aqueduct that may benefit from concrete liner raises.

Figure 4-3 Capacity Comparison Including 2017 Conditions Max Flow

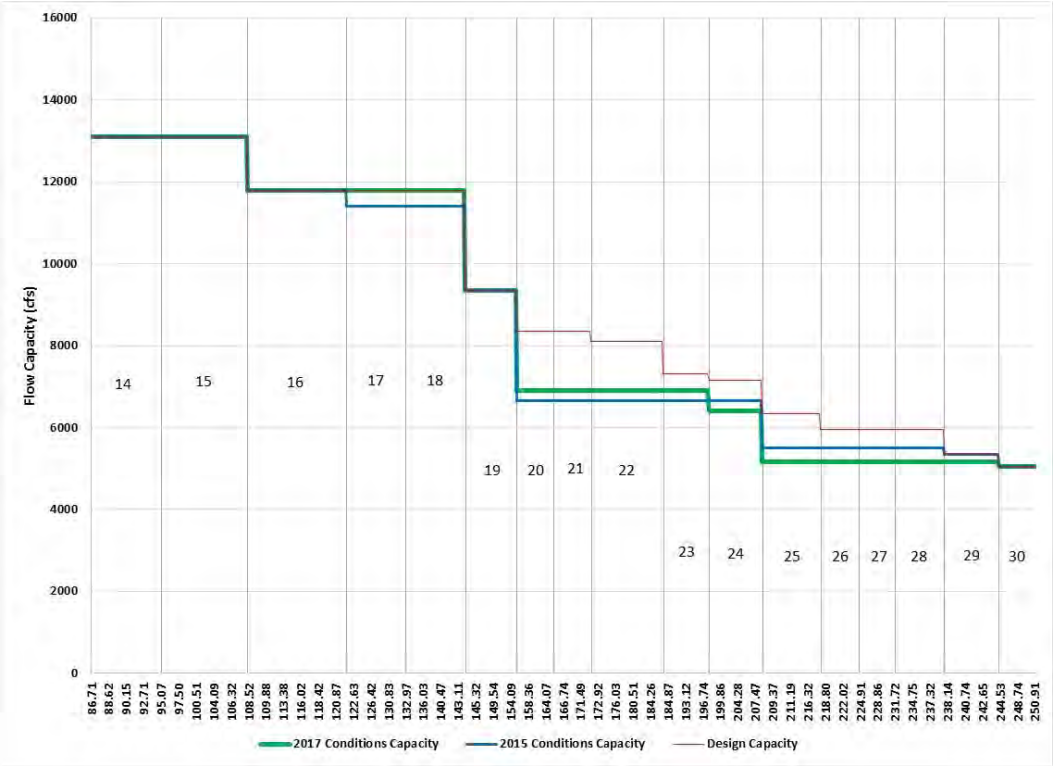

Figure 4-4 Lined Freeboard at Current Flow Capacity

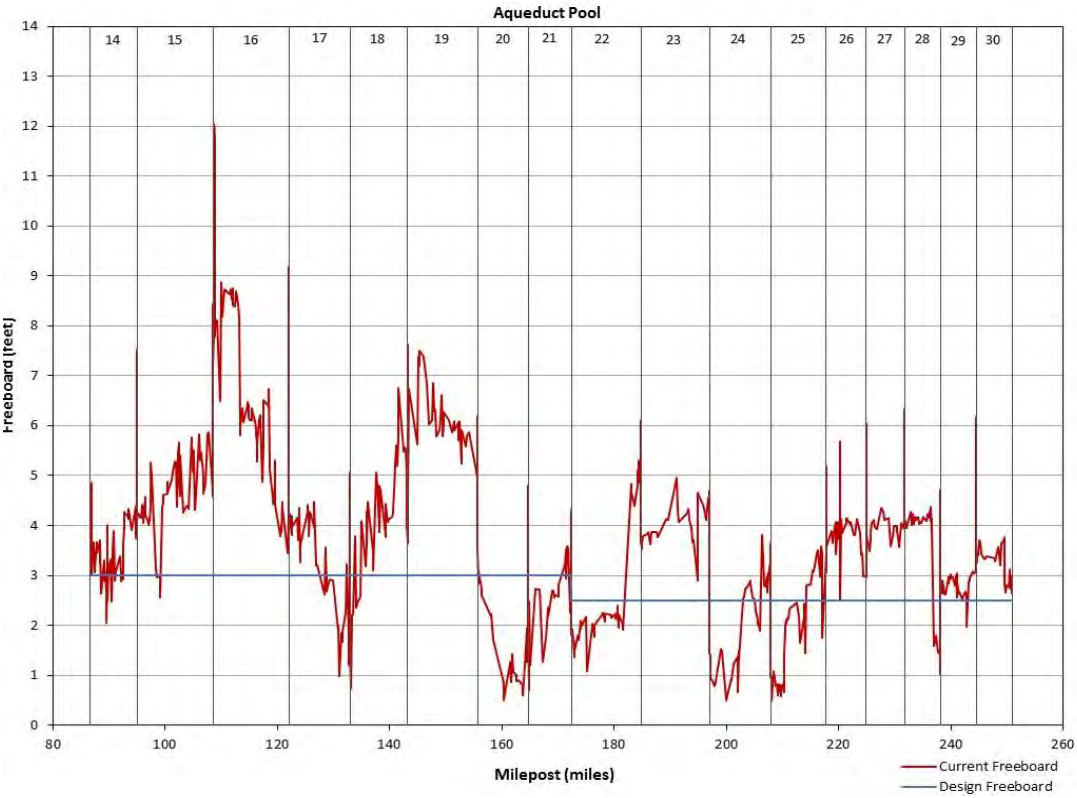

Table 4-3 Summary of Hydraulic Impacts

Pool Number	Design Capacity (cfs)	Design Freeboard (feet)	2015 Conditions Capacity (cfs)	2015 Conditions Reduction in Capacity[a] (cfs)	2015 Conditions Freeboard[b] (feet)	2017 Conditions Capacity (cfs)	2017 Conditions Reduction in Capacity[c] (cfs)	2017 Conditions Freeboard[d] (feet)
14	13100	3	13100	0	1.20	13100	0	2.06
15	13100	3	13100	0	2.02	13100	0	2.55
16	11800	3	11800	0	2.43	11800	0	3.45
17	11800	3	11400	400	0.50	11800	0	0.99
18	11800	3	11400	400	0.76	11800	0	0.75
19	9350	3	9350	0	5.14	9350	0	4.69
20	8350	3	6650	1700	0.50	6900	1450	0.50
21	8350	3	6650	1700	2.90	6900	1450	0.69
22	8100	2.5	6650	1450	2.22	6900	1200	1.08
23	7300	2.5	6650	650	2.17	6900	400	2.91
24	7150	2.5	6650	500	0.57	6410	740	0.50
25	6350	2.5	5500	850	0.50	5160	1190	0.50
26	5950	2.5	5500	450	1.45	5160	790	2.52
27	5950	2.5	5500	450	2.80	5160	790	3.49
28	5950	2.5	5500	450	1.40	5160	790	1.02
29	5350	2.5	5350	0	1.44	5160	190	1.98
30	5050	2.5	5050	0	3.12	5050	0	2.64

Note: cfs = cubic feet per second

[a] Reduction in capacity for 2015 conditions compared to design capacity. The 2015 conditions assume Manning's n values of 0.02 and a minimum freeboard of 0.5 foot. (June 2017 report).

[b] Minimum freeboard resulting from the pool flow capacity simulation performed using the 2015 Conditions California Aqueduct Subsidence Study Model (June 2017 report).

[c] Reduction in capacity for 2017 conditions compared to design capacity.

[d] Minimum freeboard resulting from the pool flow capacity simulation performed using the 2017 Conditions California Aqueduct Subsidence Study Model.

4.2.3 Overcrossing Impacts

An analysis was performed to quantify the hydraulic impacts of critical overcrossings in Pools 24 and 25. For this analysis, critical overcrossings encroaching farther into the hydraulic grade line were identified. The model geometry was then modified to exclude one overcrossing at a time. The process for determining pool capacities described in Section 4.2.2 was then executed with the new geometries to evaluate the changes to pool capacities. The process was repeated for three overcrossings. This process assumes that these overcrossings are raised sufficiently, such that they do not encroach on the hydraulic grade line. Findings from this evaluation show that the flow impacts of overchutes and other overcrossings are negligible as long as some headwater encroachment is allowed on the structure. With headwater at structures, impacts to flow rates are limited to within 10 cfs to 20 cfs. But, if 0.5 foot of clearance (distance between WSE and bottom of structure) is required, flow capacities at Pool 24 may be in the range of 2,000 cfs less.

4.2.4 Delivery Impacts of Projected Subsidence

An analysis was performed to estimate the maximum subsidence the Aqueduct system can experience before it affects water allocations. For this analysis, specific pools were identified as choke points (or locations) where the capacity of the Aqueduct is reduced because of subsidence. Model elevations were then lowered by discrete increments at these choke points for features such as cross sections, overcrossings, and check structures (where applicable). The model was then executed using the process described in Section 4.2.2 to determine the new reduced capacity of the subsided pools. This step was repeated at various increments in elevation drops to represent different stages of subsidence.

Two choke points were evaluated. One centered near Pool 20 and the other centered near Pools 24 and 25. For the evaluation centered near Pool 20, elevations in Pool 19 were also reduced (by two-thirds the reduction value of Pool 20). For the evaluation centered near Pools 24 and 25, two segments of the modeled Aqueduct were lowered. These segments extend approximately from MP 195 to 203, and MP 205 to 216. The segments of the Aqueduct where cross sections were lowered were identified based on historical subsidence profiles presented in the June 2017 report. The simulation of subsidence was simplified by assuming a constant elevation drop across each segment lowered.

4.2.4.1 Impacts of Subsidence to Month Distribution of Flow

Datasets from DWR's State Water Project webpage containing historical data were evaluated to identify the maximum historical deliveries. Historical annual maximums through Check 20 and Check 25 were calculated using data presented in the State Water Project Annual Reports of Operations and monthly State Water Project Operations Data reports. The historical maximum deliveries were then compared against the projected impacts of subsidence on Checks 20 and 25. This comparison was used to estimate when the ability to deliver historical volumes might be hindered by subsidence.

A historical monthly distribution of flows was also evaluated for the analyses and is presented in subsequent sections. The purpose of this evaluation was to understand the distribution of monthly deliveries over a typical year, and then evaluate the potential affect subsidence may have on the monthly distribution of deliveries. Monthly distributions (by percent of total volume) of deliveries made between 1990 and 2014, south of Pool 20, are plotted in Figure 4-5.

Figure 4-5 Distribution of Aqueduct Deliveries South of Pool 20, per Month, by Year

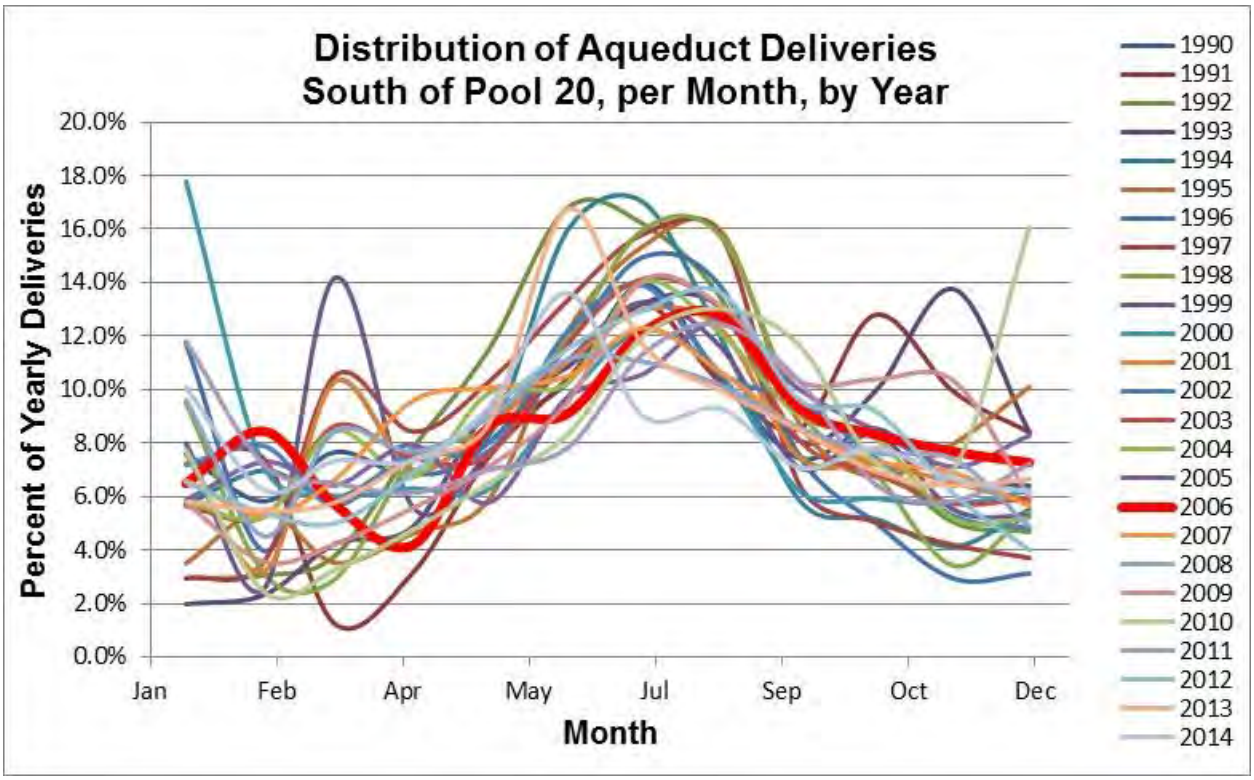

The 2006 monthly delivery distribution was used to model the progressive effects of subsidence on a typical delivery schedule. The 2006 distribution fits the general trend of delivery in a typical year. Normally, high delivery months are from May through September, while the lowest delivery months are March and April.

Flow capacity reductions caused by subsidence have the potential to affect the ability to meet allocations using a typical monthly distribution (such as seen in 2006). If the peak-flow capacity is reduced beyond a certain point, some of the flow from the peak months will have to be redistributed to low-delivery months to pass the same yearly volume (Appendix B). For the evaluation presented in subsequent sections, it was assumed that the volumes would be redistributed to adjacent months first. As the capacity was further reduced by future subsidence, additional volume was distributed to the next adjacent month and so on, until a flat distribution was reached. This level of subsidence was then noted as the point beyond which a particular flow allocation (or volume) could no longer be delivered.

Monthly flow/volume redistribution plots were developed for each of the choke points assessed (Appendix B). The plots show how flow/volumes would need to be redistributed for the allocation volumes that were evaluated at different subsidence stages.

Two types of allocations were evaluated:

- The *historical maximum* (referenced from online SWP annual and monthly reports), which includes every type of water delivery (e.g., Table A, Article 21, etc.).
- The *Maximum Table A*, which is the sum of the maximum Table A allocations south of Pools 20 and 25 (see Table 4-4 for Table A allocations below pool 20).

Table 4-4 Maximum Table A Volumes in Acre-Feet, South of Pool 20

San Joaquin Valley	
Oak Flat Water District	5,700
County of Kings	9,305
Dudley Ridge Water District	45,350
Empire West Side Irrigation District	3,000
Kern County Water Agency	982,730
Tulare Lake Basin Water Storage District	87,471
San Joaquin Valley Subtotal	**1,133,556**
Central Coast	
San Luis Obispo County Flood Control & Water Conservation District	25,000
Santa Barbara County Flood Control & Water Conservation District	45,486
Central Coast Subtotal	**70,486**
Southern California	
Antelope Valley-East Kern Water Agency	144,844
Castaic Lake Water Agency	95,200
Coachella Valley Water District	138,350
Crestline-Lake Arrowhead Water Agency	5,800
Desert Water Agency	55,750
Littlerock Creek Irrigation District	2,300
The Metropolitan Water District of Southern California	1,911,500
Mojave Water Agency	85,800
Palmdale Water District	21,300
San Bernardino Valley Municipal Water District	102,600
San Gabriel Valley Municipal Water District	28,800
San Gorgonio Pass Water Agency	17,300
Ventura County Watershed Protection District	20,000
Southern California Subtotal	**2,629,544**
Total	**3,833,586**

Source: California Water Data Library 2017

4.2.4.2 Delivery Impacts of Projected Subsidence Centered at Pool 20

To estimate the maximum subsidence the Aqueduct system can experience at Pool 20 before it affects allocations, the model was run at various increments of subsidence centered at Pool 20. The pool capacity was then recalculated at each increment. This process yielded a linear relationship between subsidence and a decrease in pool capacity. Assuming the system is operating 85 percent of the time year-round, it was estimated that approximately 4.2 million acre-feet could be conveyed across Pool 20 with 2017 conditions (running flat for the entire year). The system's capacity through Check 20 will be equal to the Maximum Table A volume of 3.8 million acre-feet after 1 foot of additional subsidence (beyond that measured in 2017). The historical maximum limit of 3.4 million acre-feet will be reached after

approximately 2 feet of additional subsidence (beyond that measured in 2017). Figure 4-6 shows the relationship between subsidence and maximum yearly volume capacity at Pool 20.

Figure 4-6 Volume Capacity vs. Subsidence Relationship for Pool 20

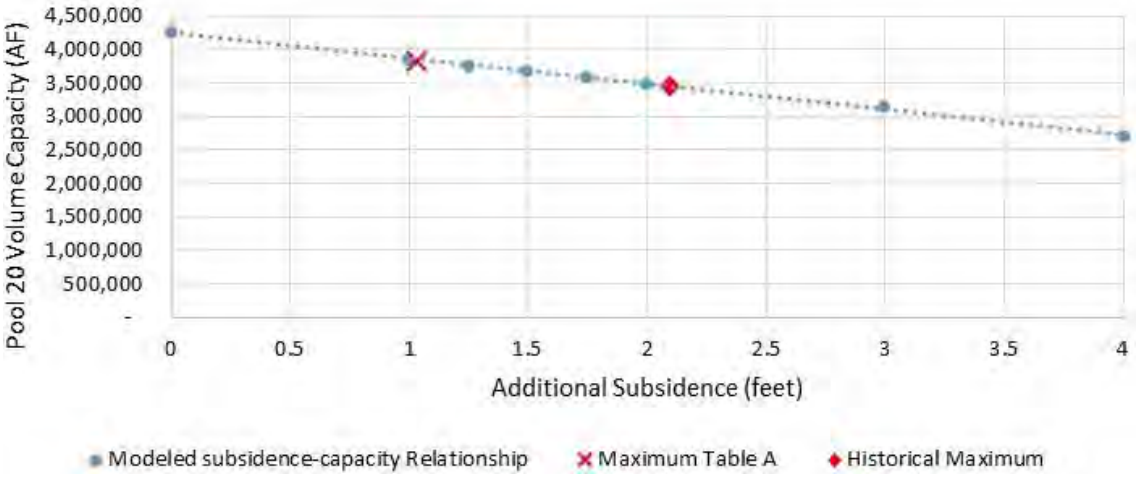

Note: AF = acre-feet

4.2.4.3 Delivery Impacts of Projected Subsidence Centered at Pools 24 and 25

To estimate the maximum subsidence the Aqueduct system can experience at Pools 24 and 25 before it impacts water allocations, the model was run at various increments of subsidence centered at Pools 24 and 25. The pool capacity was then recalculated at each increment. Assuming that the system is operating 85 percent of the time year-round, it was estimated that just more than 3.1 million acre-feet could be conveyed across Pool 25 with 2017 conditions. This is less than estimated Maximum Table A volume of 3.6 million acre-feet (assumed to be equal to [Table 4-4 total] – [Central Coast Subtotal] – [Tulare Lake Basin + Dudley Ridge + County of Kings]). The historical maximum limit of 2.6 million acre-feet will be reached after approximately 2.2 feet of additional subsidence. Figure 4-7 shows the relationship between additional subsidence (relative to 2017 elevations) and maximum yearly volume capacity at Pool 25.

Figure 4-7 Volume Capacity vs. Subsidence Relationship for Pool 25

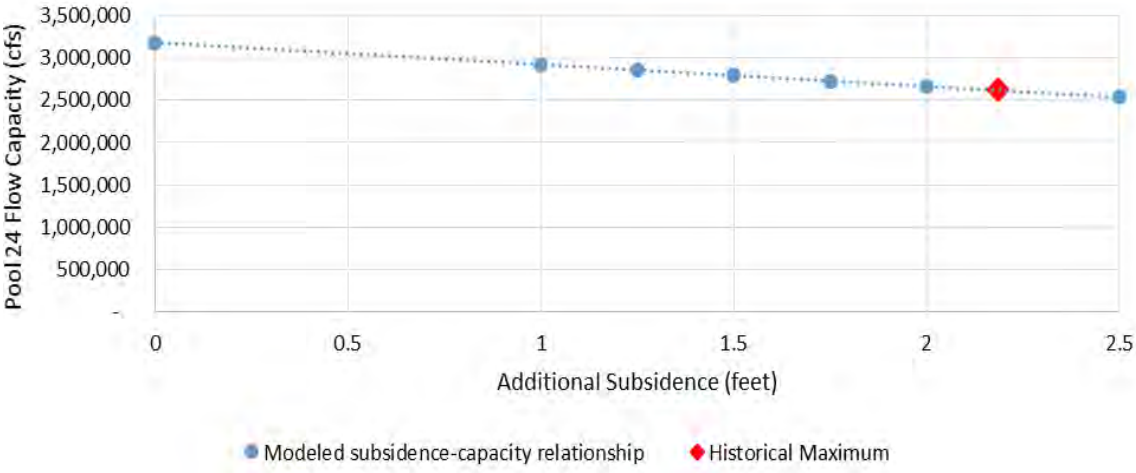

Note: cfs = cubic feet per second

Chapter 5. 2016–2017 Data Updates

In January and February of 2016 and 2017, Precise Survey conducted two new land surveys along the Aqueduct in the SLFD and the SJFD (Pools 14 through 40). The survey data was released in June of 2016 and 2017. The following graphs and figures from the CASS report, released in June of 2017, were updated (page numbers and plates cited below in parentheses refer to DWR's 2017 CASS report):

- Figure 6-3 Central Valley Project Water Allocations versus San Luis Field Division Subsidence (page 6-11)
- Figure 6-4 State Water Project Water Allocations versus San Joaquin Field Division Subsidence (page 6-12)
- Table 6-5 Historic Subsidence Rates in San Luis Field Division, Inches per Year (page 6-17). The updated version of Table 6-5 is included at the end of this chapter.
- Table 6-6 Historic Subsidence Rates in San Joaquin Field Division, Inches per Year (1 of 2) (page 6-19). The updated version of Table 6-6 is included at the end of this chapter.
- Table 6-7 Historic Subsidence Rates in San Joaquin Field Division, Inches per Year (2 of 2) (page 6-21). The updated version of Table 6-7 is included at the end of this chapter.
- Plates 1-29 Subsidence, Operation, & Geologic Profiles. The revised plates are included in Appendix C of this report.

And the following graphs were created with new survey data from 2017 (Plates 31-33 in Appendix C):

- Plate 31 SLFD & SJFD Top of Lining magnitude of Subsidence from As-Built to 2017
- Plates 32-33 SLFD & SJFD Top of Lining Subsidence Profiles from As-Built to 2017

5.1 Subsidence Monitoring

Figures 6-3 and 6-4 from the CASS report were updated with survey data from 2016 and 2017. The updated figures are presented here as Figure 5-1 (SLFD) and Figure 5-2 (SJFD), respectively. Previously, the figures included data from 1967 to 2015 for the SLFD, and from 1967 to 2013 for the SJFD. When DOE originally analyzed subsidence versus time at MPs 98.67, 116.27, 127.07, 136.05, 148.56, 160.45, 160.99, and 166.45 (Figure 5-1), it made a correlation between subsidence and allocation. Between 1977 and 1989, allocations were constant and subsidence was minor. When allocations dropped in 1990, subsidence increased. When allocations picked up again, between 1995 and 2006, subsidence decreased. But, with allocations picking up again in 2017, subsidence appears to have slowed to something less than the recent trends (Figure 5-1).

When analyzing subsidence versus time in the SJFD, at MPs 196.74, 207.94, 222.89, 256.56, and 275, the long-term trend from 1986 to 2017 (Figure5-2) is generally more linear and uniform than in the SLFD (Figure 5-1), with subsidence rates apparently less sensitive to variations in allocation.

Figure 5-1 Central Valley Project Water Allocations versus San Luis Field Division Subsidence

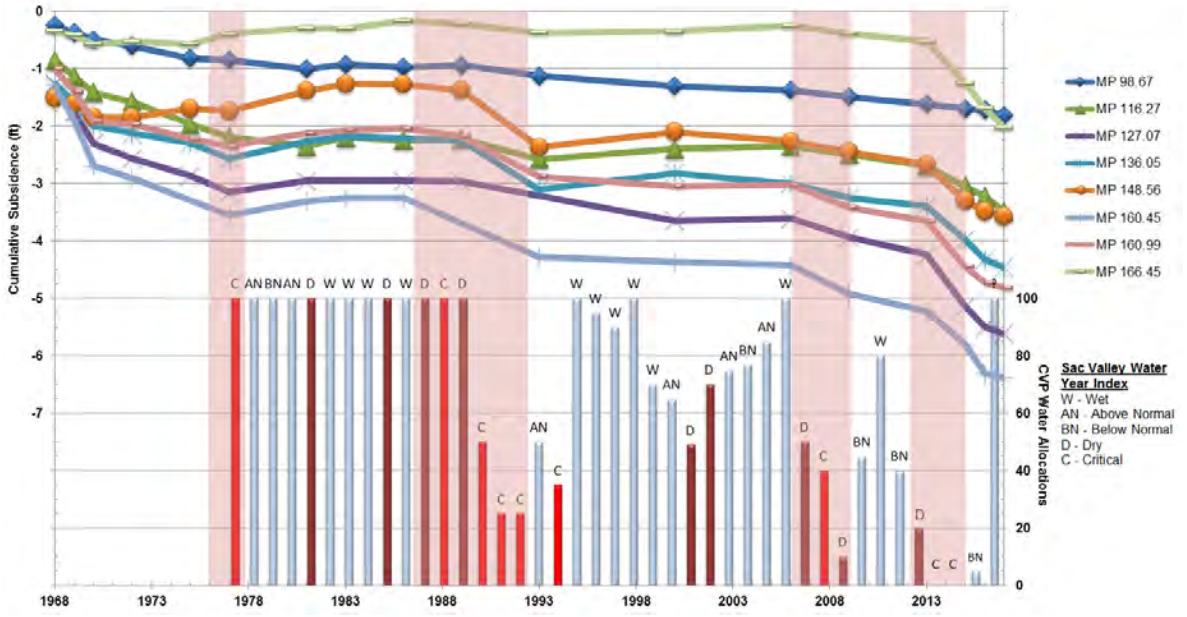

Note: Figure 5-1 is a revision of Figure 6-3 in DWR's CASS report (June 2017).

Figure 5-2 State Water Project Water Allocations versus San Joaquin Field Division Subsidence

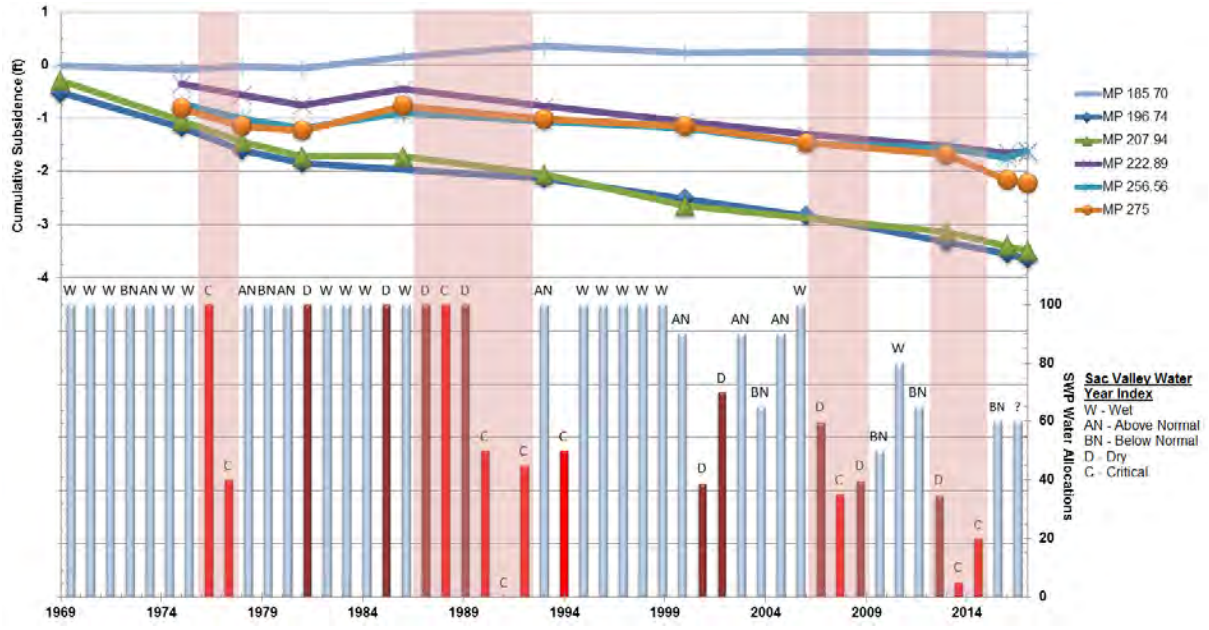

Note: Figure 5-2 is a revision of Figure 6-4 in DWR's CASS report (June 2017).

5.2 Subsidence Rates

Tables 6-5, 6-6, and 6-7 from the CASS report were updated with survey data from 2016 and 2017 (the updated versions are presented at the end of this chapter as Tables 5-2, 5-3, and 5-4, respectively).

Previously, DOE calculated subsidence rates for Pools 14 to 38 (MP 91.75 to 287.09) from 1967 to 2015 for the SLFD, and from 1967 to 2013 for the SJFD. The rates were determined by using historical subsidence values in feet (the same values that were used to plot the subsidence profiles), divided by the number of years between each data set, and then multiplied by 12 to get a subsidence rate in inches per year.

For the SLFD (Pools 14 to 21), the subsidence rates were the highest in critically dry years, from 1975 to 1977, 1989 to 1993, 2006 to 2009, 2013 to 2016 (in red), and a few years after the canal was built from 1967 to 1970 (in green). Rates during wet years (in gray) from 1970 to 1975, 1977 to 1989, 1993 to 2006, and 2009 to 2013, had very little subsidence, except from 2016 to 2017. During this time, Pools 16, 17, 20, and 21 experienced subsidence rates comparable to rates during critically dry years from 2013 to 2016. The maximum subsidence rates between 2015 and 2017 were at MP 163.69 (Pool 20), with 9.8 inches per year (2015–2016) and 8 inches per year (2016–2017).

For SJFD (Pools 22 to 38), the highest rates of subsidence were also in critically dry years from 1975 to 1978, 1986 to 1993, and from 2006 to 2016 (in red). The maximum subsidence rate from 2013 to 2016 was 4.8 inches per year at MP 270.5 (Pool 34). Rates during wet years (in gray) from 1978 to 1986, and 1993 to 2006 had very little subsidence, except from 2016 to 2017. The maximum subsidence rate from 2016 to 2017 was 2.1 inches per year at MP 206.63 (Pool 24).

When comparing subsidence rates between field divisions, subsidence rates were higher in the SLFD than in the SJFD. In general, the SJFD had more uplift, especially from 2016 to 2017, than the SLFD. The greatest subsidence rate between 2013 and 2017 in the SLFD was 9.8 inches per year (Pool 20), while in SJFD, it was 4.8 inches per year (Pool 34).

5.3 Plates 1–33

Plates 1 through 29 from the CASS report were updated with survey data from 2016 and 2017 (Appendix C). Previously, subsidence and operational profiles for Pools 14 to 38 (MP 86.94 to 287.09) were created with data from 1967 to 2015 for the SLFD, and from 1967 to 2013 for the SJFD. Subsidence profiles in Plates 1 through 28 show a progression of subsidence (of structures and on top of the liner) from 1967 to 2017 for the SLFD and the SJFD, while operational profiles show the total subsidence on top of the liner from 1967 to 2017. Plate 29 shows subsidence profiles for the SLFD and the SJFD for 2016 and 2017. Plate 30 was not updated because current Uninhabited Aerial Vehicle Synthetic Aperture Radar data were not available, but is included herein for completeness.

For both the SLFD and the SJFD, Plate 31 shows the total magnitude of subsidence for all top-of-liner survey points from as-built 1967 values to current 2017 values. The difference between the as-built elevations and the initial1967 survey elevations is the result of subsidence that occurred during construction, and prior to conducting the first precise leveling survey in 1967. The pools with the largest magnitude of subsidence in the SLFD, relative to the as-built elevations, are Pools 16 to 20 with a maximum of 7.11 feet (MP 113.29), 14.26 feet (MP 132.81), 11.27 feet (MP 133.81), 5.1 feet (MP 148.56), and 7.1 feet (MP 163.26) of subsidence, respectively. In SJFD the largest magnitude of subsidence relative to the as-built elevations occurred in Pools 24, 25, 31, and 35, with 3.6 feet (MP 199.55), 3.49 feet (MP 207.94), 3.99 feet (MP 255.77) and 3.12 feet (MP 275.56) of subsidence, respectively. Overall, the magnitude of subsidence in the SLFD is higher than in the SJFD.

Plates 32 and 33 show the top of liner elevations for as-built conditions in 1967 versus current conditions in 2017, for the SLFD and the SJFD (Pools 14 through 40). The graphs were created using top of liner elevations from precise survey data.

5.4 SCADA vs. LiDAR

In 2016, DOE obtained WSEs upstream and downstream of Check Structures 14 through 40 from LiDAR terrain surface models. DOE obtained supervisory control and data acquisition (SCADA) elevations from the Operations Control Office for the same dates and times the LiDAR was collected, and then compared them. Table 5-1 provides the comparison.

Table 5-1 Supervisory Control and Data Acquisition compared to LiDAR Water Surface Elevations, 2016

Check Number	Location	Time Zone and Date	SCADA Elevation (feet) NGVD 29	LiDAR Elevation (feet) NGVD 29	Difference (feet)
14	Upstream	Local Time: Fri. July 29, 2016, 13:17:46 GMT-0700 (Pacific Daylight Time) UTC Time: Fri. July 29, 2016, 20:17:46 GMT	330.56	330.77	-0.21
	Downstream		328.69	328.93	-0.23
15	Upstream	Local Time: Fri. July 29, 2016, 12:53:00 GMT-0700 (Pacific Daylight Time) UTC Time: Fri. July 29, 2016, 19:53:00 GMT	328.64	328.54	0.10
	Downstream		325.23	325.02	0.22
16	Upstream	Local Time: Fri. July 29, 2016, 12:37:54 GMT-0700 (Pacific Daylight Time) UTC Time: Fri. July 29, 2016, 19:37:54 GMT	325.27	324.54	0.74
	Downstream		322.48	321.84	0.64
17	Upstream	Local Time: Fri. July 29, 2016, 10:44:30 GMT-0700 (Pacific Daylight Time) UTC Time: Fri. July 29, 2016, 17:44:30 GMT	323.03	321.77	1.26
	Downstream		322.70	321.39	1.31
18	Upstream	Local Time: Fri. July 29, 2016, 10:33:01 GMT-0700 (Pacific Daylight Time) UTC Time: Fri. July 29, 2016, 17:33:01 GMT	321.41	320.74	0.67
	Downstream		318.59	317.99	0.60
19	Upstream	Local Time: Fri. July 29, 2016, 10:18:45 GMT-0700 (Pacific Daylight Time) UTC Time: Fri. July 29, 2016, 17:18:45 GMT	318.43	317.35	1.08
	Downstream		317.22	316.06	1.16
20	Upstream	Local Time: Fri. July 29, 2016, 10:08:28 GMT-0700 (Pacific Daylight Time) UTC Time: Fri. July 29, 2016, 17:08:28 GMT	317.03	315.59	1.44
	Downstream		316.26	314.93	1.33
21	Upstream	Local Time: Fri. July 29, 2016, 10:00:26 GMT-0700 (Pacific Daylight Time) UTC Time: Fri. July 29, 2016, 17:00:26 GMT	313.91	314.31	-0.40
	Downstream		313.76	314.18	-0.42
22	Upstream	Local Time: Sun. July 31, 2016, 10:43:33 GMT-0700 (Pacific Daylight Time) UTC Time: Sun. July 31, 2016, 17:43:33 GMT	311.34	312.50	-1.17
	Downstream		308.93	309.08	-0.14
23	Upstream	Local Time: Sun. July 31, 2016, 10:30:02 GMT-0700 (Pacific Daylight Time) UTC Time: Sun. July 31, 2016, 17:30:02 GMT	308.57	307.31	1.26
	Downstream		307.22	305.54	1.68

Check Number	Location	Time Zone and Date	SCADA Elevation (feet) NGVD 29	LiDAR Elevation (feet) NGVD 29	Difference (feet)
24	Upstream	Local Time: Sun. July 31, 2016, 10:17:07 GMT-0700 (Pacific Daylight Time) UTC Time: Sun. July 31, 2016, 17:17:07 GMT	306.31	304.82	1.49
	Downstream		306.21	304.69	1.52
25	Upstream	Local Time: Sun. July 31, 2016, 10:05:27 GMT-0700 (Pacific Daylight Time) UTC Time: Sun. July 31, 2016, 17:05:27 GMT	304.39	303.96	0.44
	Downstream		303.23	302.77	0.46
26	Upstream	Local Time: Sun. July 31, 2016, 09:56:33 GMT-0700 (Pacific Daylight Time) UTC Time: Sun. July 31, 2016, 16:56:33 GMT	303.22	302.03	1.18
	Downstream		301.83	301.54	0.30
27	Upstream	Local Time: Sun. July 31, 2016, 09:49:45 GMT-0700 (Pacific Daylight Time) UTC Time: Sun. July 31, 2016, 16:49:45 GMT	301.81	301.17	0.64
	Downstream		299.19	299.15	0.04
28	Upstream	Local Time: Sun. July 31, 2016, 09:41:32 GMT-0700 (Pacific Daylight Time) UTC Time: Sun. July 31, 2016, 16:41:32 GMT	298.56	298.53	0.03
	Downstream		298.37	298.27	0.10
29	Upstream	Local Time: Sun. July 31, 2016, 09:32:49 GMT-0700 (Pacific Daylight Time) UTC Time: Sun. July 31, 2016, 16:32:49 GMT	297.48	297.47	0.01
	Downstream		296.66	296.53	0.13
30 BVPP	Upstream	Local Time: Sun. July 31, 2016, 09:25:53 GMT-0700 (Pacific Daylight Time) UTC Time: Sun. July 31, 2016, 16:25:53 GMT	295.90	295.92	-0.02
	Downstream		499.60	499.71	-0.11
31	Upstream	Local Time: Sun. July 31, 2016, 09:12:41 GMT-0700 (Pacific Daylight Time) UTC Time: Sun. July 31, 2016, 16:12:41 GMT	498.91	499.15	-0.24
	Downstream		498.51	498.58	-0.07
32	Upstream	Local Time: Sun. July 31, 2016, 09:06:38 GMT-0700 (Pacific Daylight Time) UTC Time: Sun. July 31, 2016, 16:06:38 GMT	498.16	497.72	0.44
	Downstream		497.38	496.88	0.50
33	Upstream	Local Time: Sun. July 31, 2016, 09:00:56 GMT-0700 (Pacific Daylight Time) UTC Time: Sun. July 31, 2016, 16:00:56 GMT	496.13	496.23	-0.10
	Downstream		494.77	494.51	0.25
34	Upstream	Local Time: Sun. July 31, 2016, 08:55:14 GMT-0700 (Pacific Daylight Time) UTC Time: Sun. July 31, 2016, 15:55:14 GMT	494.80	493.94	0.86
	Downstream		494.19	493.39	0.80
35 TPP	Upstream	Local Time: Sun. July 31, 2016, 08:46:11 GMT-0700 (Pacific Daylight Time) UTC Time: Sun. July 31, 2016, 15:46:11 GMT	493.40	492.61	0.79
	Downstream		725.70	725.20	0.50
36 CPP	Upstream	Local Time: Sun. July 31, 2016, 12:20:34 GMT-0700 (Pacific Daylight Time) UTC Time: Sun. July 31, 2016, 19:20:34 GMT	723.06	722.32	0.74
	Downstream		1242.49	1242.39	0.11
37	Upstream	Local Time: Sun. July 31, 2016, 12:25:35 GMT-0700 (Pacific Daylight Time) UTC Time: Sun. July 31, 2016, 19:25:35 GMT	1242.17	1242.04	0.13
	Downstream		1242.40	1241.13	1.27
38	Upstream	Local Time: Sun. July 31, 2016, 12:28:22 GMT-0700 (Pacific Daylight Time) UTC Time: Sun. July 31, 2016, 19:28:22 GMT	1240.71	1240.72	0.00
	Downstream		1239.56	1240.18	-0.62

Check Number	Location	Time Zone and Date	SCADA Elevation (feet) NGVD 29	LiDAR Elevation (feet) NGVD 29	Difference (feet)
39	Upstream	Local Time: Sun. July 31, 2016, 12:31:26 GMT-0700 (Pacific Daylight Time) UTC Time: Sun. July 31, 2016, 19:31:26 GMT	1240.05	1239.86	0.19
	Downstream		1239.84	1239.73	0.11
40 EPP	Upstream	Local Time: Sun. July 31, 2016, 12:41:00 GMT-0700 (Pacific Daylight Time) UTC Time: Sun. July 31, 2016, 19:41:00 GMT	1238.77	1239.33	-0.56
	Downstream		–	–	–

Notes: BVPP = Buena Vista Pumping Plant, CPP = Chrisman Pumping Plant, EPP = Edmonston Pumping Plant, GMT = Greenwich Mean Time, LiDAR = light detection and ranging, NGVD 29 = North Geodetic Vertical Datum of 1929, SCADA = supervisory control and data acquisition, TPP = Teerink Pumping Plant, UTC = Universal Time Coordinated

The difference between LiDAR and SCADA elevations range from -0.62 feet to 1.68 feet. In general, SCADA elevations were higher than LiDAR elevations except in Pools 14, 21, 22, 30, 31, 33, 38, and 40. Very little difference was seen in Pools 14, 15, 21, 25, 27 through 33, 38, and 39. Pools 16, 18, 27, 34, 35, 36, 38, and 40 showed a difference between 0.5 foot and 1 foot. Pools 17, 19, 20, 22, 23, 24, 26, and 37 showed a difference between 1foot and 1.68 feet. These pools are some of the areas where significant subsidence has been observed over the years.

DOE recommends that the Operations Control Office review and re-evaluate SCADA values.

Table 5-2 Historic Subsidence Rates in San Luis Field Division, Inches per Year (Update of Table 6-5, 2017 California Aqueduct Subsidence Study)

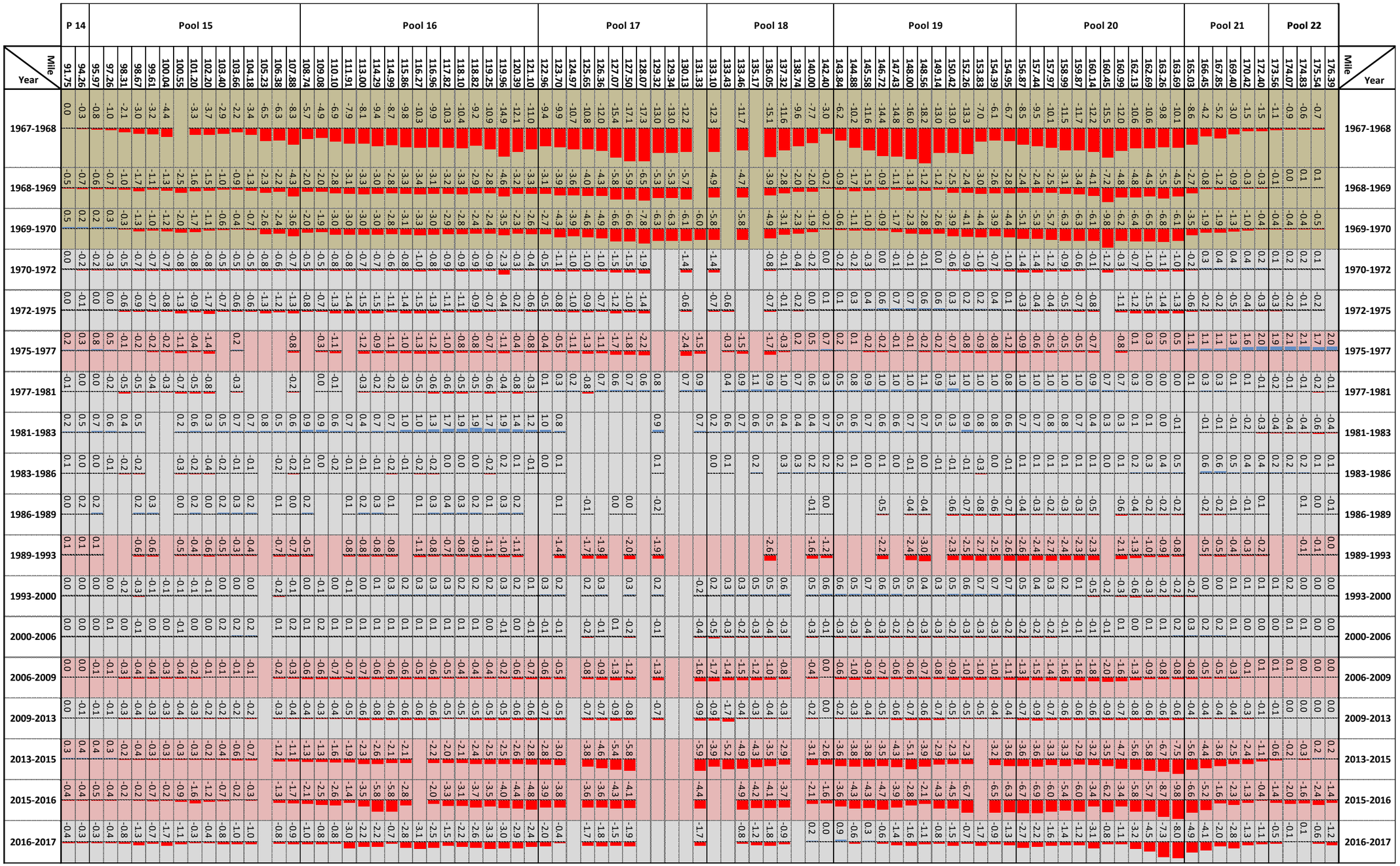

Table 5-3 Historic Subsidence Rates in San Joaquin Field Division, Inches per Year (1 of 2) (Update of Table 6-6, 2017 California Aqueduct Subsidence Study)

Pool	Mile \ Year	1967-1969	1969-1975	1975-1978	1978-1981	1981-1986	1986-1993	1993-2000	2000-2006	2006-2013	2013-2016	2016-2017
Pool 22	177.40	-0.2	-0.1	-0.1	0.1	0.7	0.3	-0.2	-0.1	0.0	0.0	-0.4
	178.53	0.6	-0.4	0.4	0.1	0.6	0.3	-0.2	-0.1	0.0	0.0	-0.2
	179.50	0.1	-0.1	-0.2	0.2	0.6	0.0	0.0	0.1	0.0	-0.1	-0.2
	180.64	0.6	-0.2	-0.1	0.2	0.6	0.3	-0.1	-0.1	0.0	-0.3	0.0
	181.14	0.0	-0.2	-0.2	0.2	0.6	0.3	-0.1	-0.1	0.0	-0.1	-0.3
	181.76	0.3	-0.1	-0.2	0.2	0.6	0.3	-0.1	-0.1	0.0	-0.1	-0.6
	182.39	0.0	-0.1	-0.2	0.3	0.6	0.3	-0.1	0.0	0.0	-0.1	-0.3
	183.19	-0.1	-0.1	-0.2	0.3	0.6			0.0	0.0	-0.3	0.1
	183.74	0.1	-0.1	-0.2	0.3	0.6			0.0	0.0	-0.2	-0.5
	184.29	0.6	0.0	-0.1	0.4	0.6			0.0	0.0	-0.1	-0.4
	184.82	-0.2	-0.1	-0.2	0.4	0.6			0.0	0.0	-0.4	0.9
Pool 23	185.70	-0.1	-0.2	-0.2	0.3	0.5	0.3	-0.2	0.0	0.0	-0.2	0.3
	186.30	0.1	-0.1	-0.1	0.4	0.5	0.3	-0.2	0.0	-0.1	-0.2	0.2
	186.88	0.1	-0.2	-0.2	0.3	0.5	0.3	-0.2	0.1	-0.1	-0.3	0.6
	187.60	0.1	-0.2	0.0	0.3	0.5	0.3	-0.2	0.0	-0.1	-0.1	0.2
	188.47	0.0	-0.2	-0.1	0.4	0.6	0.3	-0.2	0.0	-0.1	-0.1	0.1
	189.33	0.0	-0.2	0.3	0.6	0.6	0.3	-0.2	0.0	-0.1	-0.4	1.0
	190.82	0.9	-0.3	-0.2	0.4	0.6	0.3	-0.2	0.0	-0.1	-0.2	0.0
	191.55	0.9	-0.4	-0.3	0.4	0.5	0.3	-0.2	-0.1	-0.1	-0.3	-0.2
	192.41	0.9	-0.4	-0.4	0.5	0.5	0.3	-0.2	-0.1	-0.2	-0.4	-0.3
	193.26	-0.2	-0.3	-0.5	0.6	0.5	0.2	-0.3	-0.2	-0.2	-0.4	0.0
	193.85	0.6	-0.4	-0.7	0.4	0.5	0.2	-0.3	-0.3	-0.4	-0.5	-0.6
	194.41	-0.1	-0.3	-1.0	0.3	0.3	0.0	-0.4	-0.4	-0.4	-0.6	-0.2
	194.93	-0.3	-0.7	-1.3	0.1	0.3	-0.1	-0.5	-0.5	-0.6	-0.6	-0.6
	195.76	-0.6	-0.8	-1.1	-0.2	0.2			-0.6	-0.7	-0.9	-1.0
	196.57	-0.5	-1.0	-1.5	-0.8	0.0			-0.7	-0.7	-0.9	-0.3
	196.74	-3.1	-1.3	-1.7	-1.0			-0.7	-0.6	-0.9	-0.9	-1.2
	197.05	-1.3	-1.1	-1.5	-0.8	0.0			-0.7	-0.9	-1.0	-1.3
Pool 24	197.84	-1.1	-1.2	-1.6	-1.0	-0.2	-0.6	-0.7	-0.8	-1.0	-0.9	-1.3
	198.75	-0.9	-1.0	-1.4	-0.6	-0.1	-0.5	-0.6	-0.7	-0.8	-0.8	-1.2
	199.55	-1.0	-1.1	-1.6	-1.0	-0.2	-0.7	-0.7	-0.7	-0.9	-1.0	-1.6
	200.34	-1.0	-1.0	-1.2	-0.7	-0.1	-0.7	-0.8	-0.8	-1.0	-1.2	-1.9
	201.14	-0.7	-1.0	-1.5	-0.6	0.0	-0.5	-0.7	-0.7	-0.9	-1.5	-0.7
	201.69	-0.7	-1.1	-1.5	-0.2	0.1	-0.4	-0.6	-0.7	-0.9	-1.4	-1.9
	202.22	-0.5	-1.1	-1.5	-0.4	0.2	-0.3	-0.5	-0.6	-0.8	-1.0	-1.4
	203.92	0.0	-0.6	-0.6	0.2	0.5	0.0	-0.4	-0.4	-0.5	-0.6	-1.4
	204.70	0.0	-0.6	-0.6	0.0	0.4	-0.2	-0.6	-0.5	-0.7	-1.0	-1.5
	205.19	-0.4	-0.7	-0.6	-0.1	0.3	-0.2	-0.7	-0.6	-0.8	-1.1	
	206.06	-1.3	-0.9	-0.8	-0.3	0.3	-0.3	-0.8	-0.7	-0.9	-1.2	-1.1
	206.63	-1.3	-1.2	-1.3	-0.9	0.0	-0.5	-0.9			-1.3	-2.1
	207.18	-1.5	-1.4	-1.5	-1.1	0.0	-0.6	-1.0			-1.2	-1.6
	207.94	-1.8	-1.5	-1.6	-1.1	0.0	-0.6	-1.0			-1.1	-0.9
Pool 25	208.11	-1.1	-1.3	-1.2	-1.0	0.0	-0.6	-1.0	-0.7	-0.8	-0.7	-2.0
	208.73	-0.5	-1.3	-1.2	-0.8	0.2	-0.6	-1.0	-0.7	-0.7	-0.8	-1.5
	209.36	-1.6	-1.3	-1.2	-0.7	0.2	-0.5	-1.0	-0.7	-0.7	-0.8	-1.8
	210.30	-1.0	-1.1	-1.4	-0.6	0.3	-0.3	-1.1	-0.8	-0.8	-0.7	-1.4
	210.61	-1.2	-1.0	-1.2	-0.4	0.5	-0.1	-1.0	-0.8	-0.7	-0.6	-1.9
	211.34	-1.0	-0.9	-0.8	-0.4	0.5	0.1	-1.0	-0.7	-0.6	-0.4	-1.7
	212.10	-1.2	-1.0	-0.8	-0.5	0.5	0.0	-1.1	-0.6	-0.5	-0.2	-1.0
	212.75	-1.1	-1.0	-0.7	-0.7	0.4	-0.2	-1.0	-0.7	-0.4	-0.2	-0.8
	213.39	-1.4	-1.1	-0.8	-1.0	0.5	-0.3	-0.9	-0.7	-0.4	0.0	-1.0
	213.96	-1.1	-0.9	-0.7	-0.6	0.6	-0.3	-0.7	-0.7	-0.4	-0.2	-0.6
	214.34	-1.3	-0.8	0.0	-1.0	0.6	-0.3	-0.5	-0.7	-0.2	-0.2	0.2
	214.97	-1.2	-0.7	-0.2	-0.2	0.7	-0.3	-0.5	-0.7	-0.2	-0.1	-0.1
	215.64	-1.3	-0.7	-0.2	-0.3	0.7	-0.4	-0.5	-0.7	-0.2	-0.2	0.6
	216.40	-0.9	-0.6	0.0	-0.1	0.8	-0.3	-0.3	-0.7	-0.1	0.0	0.3
	217.16	-0.9	-0.6	0.0	-0.2	0.8	-0.3	-0.3	-0.6	-0.2	-0.1	0.0
	217.78	-0.8	-0.6	0.0	-0.2	0.8	-0.4	-0.3	-0.5	-0.2	-0.1	0.4
Pool 26	218.31			-0.1	-0.3	0.8	-0.3	-0.3	-0.5	-0.2	-0.2	0.4
	219.38			-0.1	-0.1	0.9	-0.2	-0.3	-0.4	-0.2	-0.2	0.5
	220.27			-0.1	-0.2	0.9	-0.3	-0.3	-0.4	-0.3	-0.3	0.0
	221.06			-0.1	0.0	1.0	-0.2	-0.2	-0.3	-0.2	-0.2	0.6
	221.81			-0.1	0.0	0.9	-0.2	-0.3	-0.3	-0.2	-0.3	0.5
	222.58			-0.2	-0.1	0.9	-0.4	-0.5	-0.4	-0.4	-0.5	0.9
	222.89			-0.8	-0.8	0.7	-0.5	-0.5	-0.5	-0.4	-0.5	0.3
	223.19			-0.1	0.0	1.0	-0.2	-0.2	-0.3	-0.2	-0.3	0.5
	224.05			-0.3	-0.1	1.0	-0.3	-0.3	-0.4	-0.4	-0.6	0.2
	224.73	-0.6	-0.6	-0.2	0.0	1.0	-0.3	-0.3	-0.4	-0.3	-0.5	0.2
Pool 27	225.05			-0.1	0.0	1.0	-0.2	-0.3	-0.2	-0.2	-0.5	-0.4
	225.89			-0.2	-0.1	1.0	-0.3	-0.3	-0.3	-0.3	-0.5	-0.5
	226.79			0.0	0.0	1.0	-0.1	-0.2	-0.2	-0.2	-0.5	-0.1
	227.64			0.0	0.0	1.1	-0.1	-0.2	-0.2	-0.2	-0.3	0.4
	228.06			0.0	0.0	1.0	-0.1	-0.2	-0.2	-0.2	-0.3	0.3
	228.67			0.0	0.0	1.1	-0.1	-0.2	-0.2	-0.2	-0.3	0.0
	229.06			-0.1	-0.1	1.0	-0.2	-0.3	-0.2	-0.3	-0.6	0.0
	229.71			-0.4	-0.2	1.1	-0.3	-0.3	-0.2	-0.3	-0.5	-0.6
	230.44			-0.1	-0.1	1.1	-0.2	-0.3	-0.2	-0.2	-0.4	0.1
	231.06			-0.1	0.0	1.1	-0.2	-0.2	-0.2	-0.2	-0.6	0.1
	231.60			-0.1	0.0	1.1	-0.2	-0.3	-0.2	-0.2	-0.5	0.1
Pool 28	232.24			-0.1	-0.1							
	232.96			0.0	0.0	1.1	-0.2	-0.2	-0.2	-0.2	-0.6	0.7
	233.56			0.0	0.0	1.1	-0.2	-0.2	-0.2	-0.2	-0.6	0.4
	234.10			0.0	0.0	1.1	-0.2	-0.3	-0.2	-0.2	-0.5	0.0
	234.71			-0.1	-0.1	1.1	-0.2	-0.3	-0.1	-0.2	-0.7	0.1
	235.06			0.0	-0.1	1.1	-0.2	-0.3	-0.1	-0.2	-0.6	0.4
	235.56			0.0	-0.1	1.0	-0.1	-0.3	-0.1	-0.2	-0.7	0.4
	236.27			0.1	-0.1	1.0	0.0	-0.4	-0.1	-0.2	-0.8	0.8
	237.00			0.1	0.0	1.1	-0.1	-0.3	-0.1	-0.2	-0.7	0.0
	237.50			0.0	0.1	1.1	0.1	-0.3	-0.1	-0.2	-0.7	0.0
	238.00			0.1	0.0	1.1	-0.1	-0.3	-0.1	-0.2	-0.7	0.3

-7 Subsidence Rate reported per location, per period. Data bar depicts relative magnitude of subsidence rates. Red is negative (bad).

Period During Aqueduct and Water Distribution Construction in San Joaquin Field Division.

Normal to Wet Hydrologic Years (Water Index).

Dry to Critical Hydrologic Years (Water Index).

Table 5-4 Historic Subsidence Rates in San Joaquin Field Division (2 of 2) (Inches per Year) (Update of Table 6-7, 2017 California Aqueduct Subsidence Study)

-7 Subsidence Rate reported per location, per period. Data bar depicts relative magnitude of subsidence rates. Red is negative (bad).

Period During Aqueduct and Water Distribution Construction in San Joaquin Field Division.

Normal to Wet Hydrologic Years (Water Index).

Dry to Critical Hydrologic Years (Water Index).

	Pool 29													Pool 30												
Mile / Year	238.50	239.00	239.50	240.07	240.50	241.06	241.50	242.00	242.50	243.00	243.50	244.00	244.53	245.09	245.50	246.00	246.50	247.00	247.50	248.00	248.50	248.97	249.65	250.00	250.50	250.99
1967-1969																										
1969-1975																										
1975-1978	0.2	0.3	0.4	0.6	0.6	0.5	0.4	0.7	0.1	0.1	0.1	0.0	-0.1	0.0	0.0	0.0	0.0	-0.1	-0.1	-0.1	-0.1	-0.1	0.0	0.1	0.1	0.0
1978-1981	0.1	0.1	0.2	0.3	0.3	0.3	0.3	-0.2	0.1	0.1	0.0	0.1	0.1	0.1	0.0	-0.1	-0.2	-0.2	-0.2	-0.1	0.0	-0.1	0.0	-0.1	-0.1	-0.1
1981-1986		1.1	1.1	1.3	1.3	1.3	1.3	1.2	1.2	1.2	1.2	1.3	1.3	1.3	1.2	1.2	1.0	1.1	1.2	1.2	1.2	1.2	1.2	1.2	1.1	1.1
1986-1993		-0.2	-0.2	-0.2	-0.1	-0.2	-0.2	-0.2	-0.2	-0.1	-0.1	-0.1	-0.1	-0.1	0.0	-0.3	-0.2	-0.2	-0.2	-0.1	-0.1	-0.1	0.0	0.0	0.0	0.0
1993-2000		-0.1	-0.1	-0.1	-0.1	-0.1	-0.1	-0.1	-0.1	-0.1	-0.1	0.0	0.0	-0.1	0.0	-0.1	-0.1	-0.1	-0.1	0.0	0.0	0.0	0.0	0.0	0.1	0.1
2000-2006		-0.4	-0.4	-0.4	-0.4	-0.5	-0.5	-0.5	-0.5	-0.5	-0.5	-0.5	-0.4	-0.4	-0.4	-0.5	-0.4	-0.5	-0.5	-0.5	-0.4	-0.4	-0.4	-0.4	-0.4	-0.5
2006-2013		-0.1	-0.1	-0.1	-0.1	-0.1	-0.1	-0.1	-0.1	-0.1	-0.1	-0.1	-0.1	-0.1	0.0	-0.1	-0.1	-0.2	-0.1	-0.1	-0.1	-0.1	0.0	0.0	0.0	0.0
2013-2016		-0.4	-0.5	-0.3	-0.4	-0.7	-0.5	-0.6	-0.5	-0.4	-0.6	-0.7	-0.6		-0.6	-0.5	-0.7	-0.8	-0.7	-0.8	-0.5		-0.6	-0.4	-0.4	-0.6
2016-2017		-0.1	0.2	-0.4	-0.4	-0.3	-0.8	-0.2	0.0	-0.5	0.3	0.3	0.0			-0.6	0.6	0.7	0.3	0.7	0.3		-0.1	0.5	0.6	0.2

	Pool 31											Pool 32										
Mile / Year	251.50	252.01	252.50	253.00	253.50	253.80	254.11	254.50	255.00	255.36	256.12	256.56	257.00	257.48	257.63	258.00	258.50	259.00	259.50	260.50	261.00	261.72
1967-1969																						
1969-1975																						
1975-1978	0.0	0.0	0.0	-0.1	-0.1	-0.2	-0.3	-0.2	-0.3	-0.2	-0.4	-1.1	-0.2	-0.5	-0.5	-0.4	-0.8	-0.4	-0.5	-0.5	-0.5	-0.6
1978-1981	-0.2	-0.3	-0.3	-0.3	-0.2	-0.3	-0.4	-0.3	-0.3	-0.3	-0.3	-0.7	-0.2	-0.4	-0.7	-0.2	-0.6	-0.1	-0.4	0.0	-0.1	0.0
1981-1986	1.0	1.0	0.9	0.9	0.9	0.9	0.8	0.8	0.9	0.8	0.8	0.7	1.0	0.9	0.7	1.0	0.8	1.1	1.0	1.0	1.2	1.1
1986-1993	0.0	0.0	0.0	0.0	0.0	0.0	-0.1	-0.1	0.0	0.0	0.0	-0.3	0.0	-0.1	-0.3	-0.2	-0.2	-0.2	-0.2	-0.3	-0.2	-0.3
1993-2000	0.0	0.0	0.0	0.0	0.0	0.0	-0.1	-0.1	-0.2	-0.1	-0.1	-0.2	0.0	-0.2	-0.3	-0.2	-0.2	-0.1	-0.2	-0.2	-0.2	-0.1
2000-2006	-0.5	-0.5	-0.4	-0.5	-0.5	-0.5	-0.6	-0.5	-0.7	-0.6	-0.5	-0.6	-0.4	-0.5	-0.7	-0.6	-0.6	-0.5	-0.6	-0.6	-0.5	-0.5
2006-2013	0.0	0.0	0.0	0.0	0.0	0.0	-0.2	-0.1	-0.2	-0.2	-0.1	-0.1	0.0	-0.1	-0.3	-0.2	-0.1	-0.1	-0.2	-0.2	-0.2	-0.1
2013-2016	-0.4	-0.5	-0.4	-0.3	-0.4	-0.4	-0.6	-0.4	-0.5	-0.5	-0.6	-0.7	-0.6	-0.8	-0.8	-0.8	-0.8	-0.9	-0.9	-0.5	-0.6	-0.5
2016-2017	-0.3	-0.1	0.8	1.1	0.6	0.6	0.7	0.3	1.1	0.0	0.3	1.6	1.2	1.3	0.9	1.1	0.4	0.6	1.4	-0.6	-0.7	0.2

	Pool 33											Pool 34				
Mile / Year	262.00	262.50	263.00	263.50	264.00	264.50	265.00	265.50	266.00	266.50	266.91	268.00	268.50	269.30	270.00	270.50
1967-1969																
1969-1975																
1975-1978	-0.4	-0.3	-0.3	-0.3	-0.7	-0.5	-0.5	-0.4	-0.4	-0.4	-0.5	-0.6	-0.6	-0.6	-0.7	-0.9
1978-1981	0.0	0.1	0.1	0.0	-0.1	0.0	0.1	0.1	0.2	0.3	0.4	0.5	0.5	0.6	0.6	0.5
1981-1986	1.2	1.2	1.2	1.2	1.0	1.0	1.1	1.2	1.3	1.3	1.3	1.3	1.3	1.3	1.4	1.3
1986-1993	-0.2	0.0	0.0	0.0	0.0	0.1	0.1	0.0	-0.1	-0.1	-0.1	-0.1	-0.1	-0.1	-0.2	-0.3
1993-2000	-0.2	0.0	0.0	0.0	0.0	0.0	0.0	0.0	0.0	0.0	0.0	0.0	0.0	0.0	0.0	0.0
2000-2006	-0.5	-0.4	-0.4	-0.4	-0.5	-0.4	-0.4	-0.4	-0.4	-0.4	-0.4	-0.4	-0.4	-0.4	-0.4	-0.4
2006-2013	-0.1	0.0	0.0	0.0	-0.1	-0.1	-0.1	-0.1	-0.1	-0.1	-0.1	-0.1	-0.2	-0.2	-0.2	-0.3
2013-2016	-0.5	-0.5	-0.5	-0.6	-0.6	-0.9	-0.9	-1.0	-1.1	-1.1	-1.3	-1.8	-1.9	-2.9	-4.0	-4.8
2016-2017	0.5	0.7	-0.6	-0.1	0.7	1.5	1.1	0.0	-0.2	-0.8	-0.4	0.0	-0.3	0.0	0.8	0.4

	Pool 35													P 36			37	P 38	
Mile / Year	271.50	272.00	273.00	273.75	274.04	274.50	275.00	275.50	276.00	276.50	277.13	277.50	278.00	279.05	279.45	280.06	282.44	284.96	287.09
1967-1969																			
1969-1975																			
1975-1978	-1.3	-1.2	-1.0			-1.2	-1.3	-1.2	-0.9	-0.6	-1.0	-0.8	-0.3	-0.4	-0.4	-0.3	-0.4	-0.2	-0.1
1978-1981	0.3	0.2	0.4	0.4	0.1	-0.5	-0.3	-0.4	-0.1	0.2	-0.6	-0.1	0.4	0.2	0.1	0.2	0.0	0.1	0.1
1981-1986	1.2	1.2	1.3	1.3	1.2	1.0	1.1	1.1	1.2	1.3	1.4	1.3	1.4	1.3	1.3	1.3	1.3	1.4	1.4
1986-1993	-0.4	-0.4	-0.3	-0.4	-0.4	-0.5	-0.4	-0.5	-0.3	-0.2	-0.4	-0.3	-0.2	-0.2	-0.2	-0.2	-0.2	-0.1	0.0
1993-2000	0.0	0.0	0.0	-0.1	-0.1	-0.2	-0.2	-0.2	-0.2	-0.1	-0.2	-0.2	-0.1	-0.2	-0.2	-0.2	-0.2	-0.1	-0.1
2000-2006	-0.4	-0.4	-0.5	-0.5	-0.6	-0.5	-0.6	-0.5	-0.5	-0.4	-0.5	-0.5	-0.5	-0.5	-0.5	-0.5	-0.6	-0.5	-0.5
2006-2013	-0.3	-0.2	-0.2	-0.2	-0.5	-0.4	-0.4	-0.3	-0.2	-0.2	-0.3	-0.2	-0.2	-0.1	-0.1	-0.1	-0.2	-0.1	0.0
2013-2016	-3.1	-2.6	-2.2	-1.9	-2.1	-2.2	-1.9	-1.6	-1.2	-1.2	-1.3	-1.2	-0.8	-0.8	-0.9	-0.8	-0.9	-1.1	-1.0
2016-2017	0.0	-0.1	0.1	-0.2	-0.4	-0.2	-0.8	0.2	-0.4	0.0	0.4	0.2	0.0	0.1	0.6	0.4	0.6	0.0	0.2

Chapter 6. Subsidence Predictions

6.1 Introduction

The time history of subsidence along the Aqueduct, measured by repeated precise leveling surveys and referenced to a 1967 baseline, provides a basis for deriving subsidence rates that can be used to make predictions of future subsidence. See Chapter 5 of this report for an update of the survey data presented in DWR's CASS report (California Department of Water Resources 2017a) that brings the long-term subsidence history of the Aqueduct current as of June 2017.

As documented in the 2017 CASS report, non-uniform land subsidence along the Aqueduct alignment has produced several distinct loci of subsidence or "bowls." They generally coincide with known areas of the greatest historical land subsidence in the San Joaquin Valley (Ireland et al. 1980, 1984). The historic subsidence bowls also are spatially associated with loci of deep natural subsidence related to geologic processes that have been active during the past 600,000 years or longer (see discussion in Section 6.2). The 50-year time history of subsidence within a given bowl is a function of the local geologic conditions and fluctuations in artesian head in the lower water-bearing zone because of groundwater withdrawal and natural recharge. The magnitude of total subsidence is greater in the SLFD (5 feet to 6 feet maximum in the lowest parts of the subsidence bowls since precise leveling began in 1967; see Section 5.3 for discussion) than in the SJFD (1.6 feet to 3.3 feet maximum since 1967) (California Department of Water Resources 2017a).

The following sections present an analysis of "background" subsidence rates caused by natural geologic processes that predate groundwater withdrawal and anthropogenic subsidence in the San Joaquin Valley (Section 6.2). The purpose of this discussion is to provide a basis for distinguishing long-term natural subsidence rates from historic anthropogenic rates. The discussion of "background" subsidence rates is followed by analysis of the time history of subsidence in the SLFD (Section 6.3) and the SJFD (Section 6.4). The two field divisions are treated separately because their patterns and rates of subsidence differ significantly. Data from subsidence time series at individual survey points are used to develop a range of site-specific subsidence rate models for predicting future subsidence in individual pools.

6.2 Natural or "Background" Subsidence Rates

Differential subsidence of the San Joaquin Valley caused by natural processes has occurred during Quaternary time and is recorded in relief on the middle Pleistocene Corcoran clay, which is buried beneath the modern valley floor. As discussed below, this natural subsidence probably is related, at least in large part, to slow compaction of underlying Tulare Formation sediments, and occurs at rates that are at least an order of magnitude lower than the maximum historic or anthropogenic rates that have been attributed to groundwater withdrawal. The low natural rates of "background" subsidence have not significantly impacted the performance of the Aqueduct.

The Corcoran clay is approximately 50 to 120 feet thick and consists of fine-grained diatomaceous sediments that originally accumulated at the bottom of a fresh water lake, which occupied much of the ancestral San Joaquin Valley approximately 600,000 to 800,000 years ago (Frink and Kues 1954, Lettis

1982). The lakebeds that now comprise the Corcoran clay were presumably sub-horizontal and sub-planar at the time they were deposited. They are now buried to depths ranging from approximately 200 feet to 900 feet beneath the modern San Joaquin Valley floor (Frink and Kues, 1954).

A contour map of the elevation of the Corcoran clay reveals significant relief on the buried surface of the deposit (Figure 6-1). The elevation of the top of the clay beneath the eastern San Joaquin Valley near the cities of Merced and Visalia is approximately sea level (0 feet). The top of clay slopes down in a southwest direction to an elevation of approximately 175 feet beneath the central and western parts of the valley at the latitude of Los Banos, and at the latitude of California State Route 46. The elevation of the top of clay beneath the Aqueduct drops to 600 feet (near MP 100) and -700 feet (near MP 200), defining a long-wavelength, irregular depression with a maximum relief of approximately 600 feet in Fresno County, generally centered beneath the playa of historical Tulare Lake east of the Aqueduct (Figure 6-1). This long-wavelength depression in the surface of the Corcoran clay encompasses the historic Panoche and Los Gatos bowls in the SLFD, and the northern part of the Kern bowl in the SJFD. Another distinct buried depression in the surface of the Corcoran clay is in west Kern County between MP 245 and MP 260 along the Aqueduct. It is spatially associated with the Maricopa bowl in the SJFD (compare Figure 1-1 with Figure 6-1).

A northwest-southeast profile of the buried surface of the Corcoran clay beneath the west-central San Joaquin Valley, east of the Aqueduct and the valley margin (Figure 6-2, see Figure 6-1 for profile location), shows that the maximum elevation of the top of clay to the north and south of the major subsidence depression is approximately 175 feet below sea level (bsl). If it is assumed that 175 feet bsl represents a reference elevation of the Corcoran clay for most of its mapped extent, then relief on the clay relative to that elevation can be used to evaluate natural or “background” subsidence within the long-wavelength depression between MP 100 and MP 200. At its lowest points beneath the Aqueduct alignment, the elevation of the top of clay ranges between approximately 600 feet bsl and 700 feet bsl, representing approximately 400 feet to 500 feet of negative relief relative to the reference elevation of 175 feet bsl. Maximum negative relief on the top of clay is approximately 600 feet beneath the Tulare Lake playa east of the Aqueduct alignment (Figure 6-2).

The negative relief on the Corcoran clay between MP 100 and MP 200 has accumulated since deposition of the clay ended. According to data and field relations summarized by Lettis (1982), the upper part of the Corcoran clay is locally inter-bedded with air-fall ash horizons that are chemically correlated with the Friant pumice, which is dated at 615,000 years, +/- 22,000 years, by K-Ar methods (Sarna-Wojcicki et al. 1984). Thicker water-laid deposits of the Friant pumice stratigraphically overlie the Corcoran clay (Lettis 1982), which presumably accumulated after the ancestral Corcoran lake drained and streams deposited sediment on the exposed playa. These relations indicate that the negative relief started accumulating approximately 615,000 years ago. For the range of maximum relief (-400 to -500 feet) and an age of 615,000 years for the top of the Corcoran clay, the long-term average natural subsidence rate between MP 100 and MP 200 is approximately 6.5 to 8.1 x 10^{-4} feet/year, or on the order of approximately 0.2 mm/year.

Figure 6-1 Buried Relief on the Surface of the Pleistocene Corcoran Clay, San Joaquin Valley

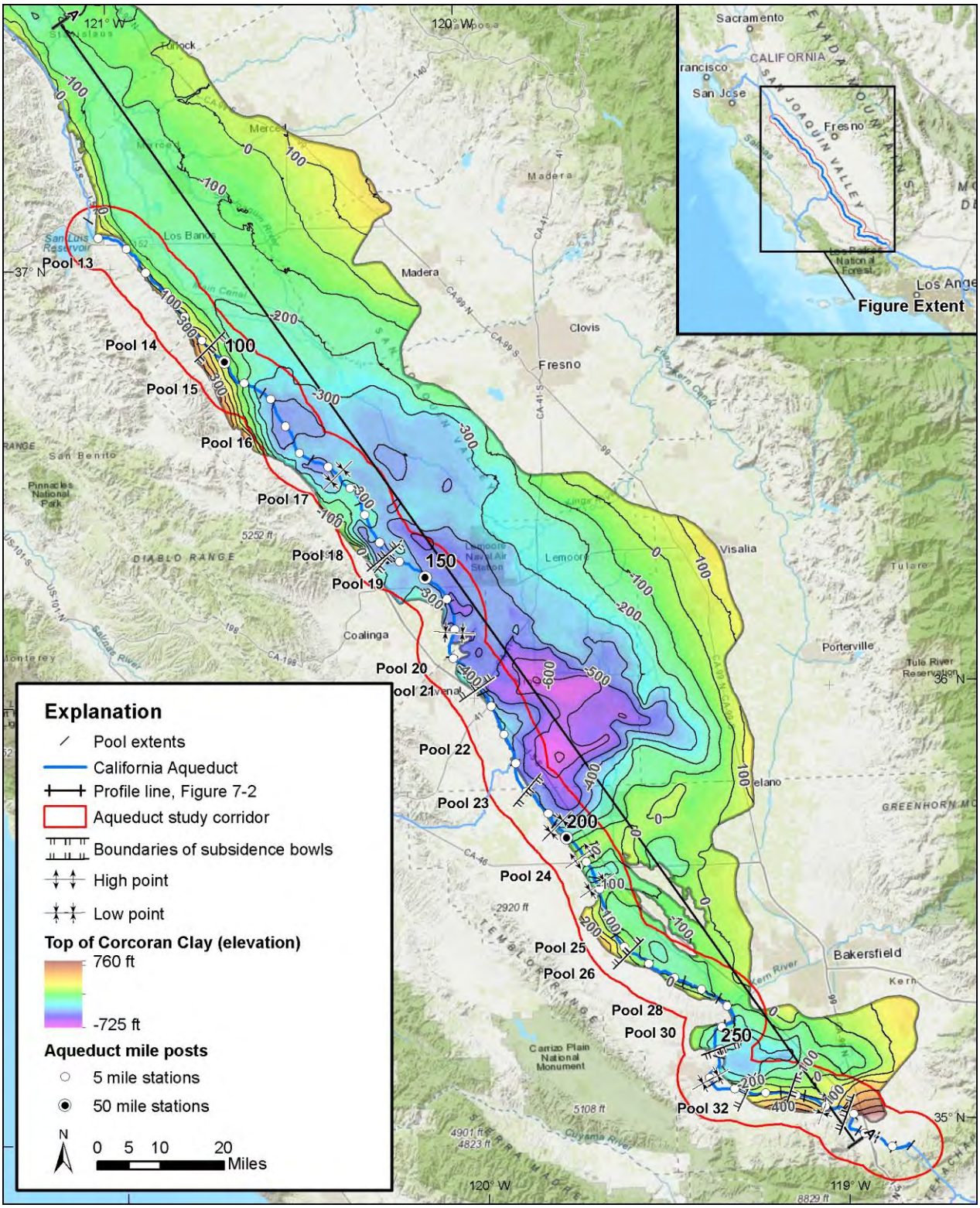

Figure 6-2 Profiles of the Surface of the Pleistocene Corcoran Clay Showing Magnitude of Natural Subsidence Beneath the California Aqueduct, and in the Center of the San Joaquin Valley

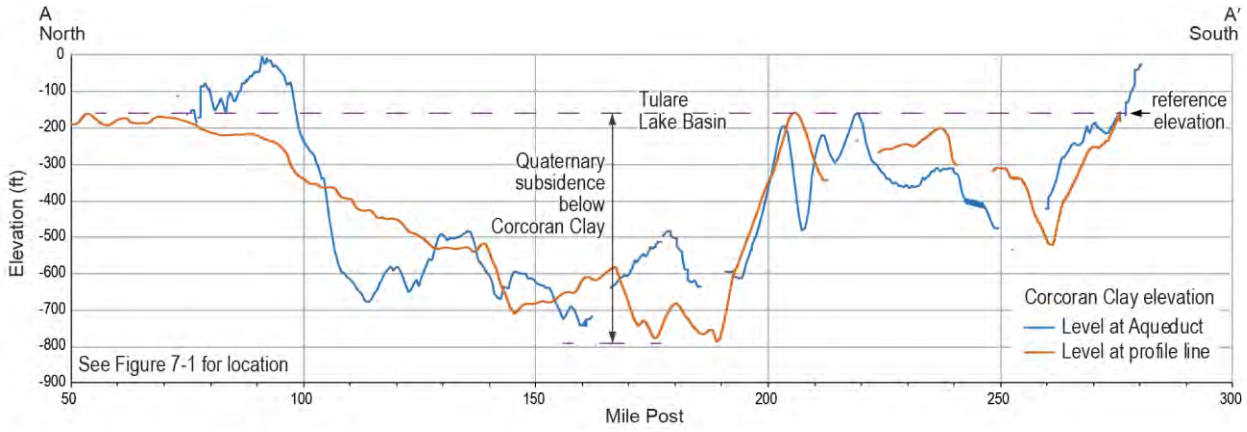

The relief on the Corcoran clay shown in Figures 6-1 and 6-2 is an order of magnitude greater than the maximum historical land subsidence in the early to middle 1900s that is attributed to groundwater withdrawal (approximately 30 feet, Ireland et al. 1984). As a result, it must have formed because of natural geological processes since middle to late Quaternary time. Although some of the relief on the Corcoran clay along the western margin of the San Joaquin Valley (particularly any net positive relief above the -175 feet reference elevation; Figure 6-2) may be because of folding and tectonic deformation along the western edge of the valley (Lettis 1982), the full eastward extent of the negative relief and its spatial distribution, as shown in Figures 6-1 and 6-2, suggest that compaction and consolidation of late Cenozoic sediments underlying the clay may explain its origin.

The 0.2 mm/year natural or "background" rate of Quaternary subsidence in the San Joaquin Valley is similar to theoretically predicted compaction rates associated with progressive porosity loss in saturated sandstones and clays in sedimentary basins (Kooi and de Vries 1998). Mechanical models for natural compaction (Kooi and de Vries 1998, and references therein) generally assume that the weight of deposited sediment increases the lithostatic normal stress on the aquifer skeleton at depth, and that the normal stress is moderated by pore fluid pressure. Compaction occurs when water flows out of the pore volume and releases excess pore pressure, which results in an increase in effective stress (normal stress minus the pore pressure) on the aquifer skeleton. The rate of pore volume loss, and the resulting rate of compaction in response to a step-increase in sedimentation rate, is a time-dependent process, but can reach steady state on the order of 10^4 years (tens of thousands of years) in active sedimentary basins (Kooi and de Vries 1998).

In their model, Kooi and de Vries (1998) found that a column of sediment hundreds of meters to kilometers thick, that is being progressively buried in a sedimentary basin, is predicted to compact at rates on the order of hundredths of millimeters per year, to the low tenths of millimeters per year, similar to the middle to late Quaternary subsidence rate measured from relief on the surface of the Corcoran clay. Kooi and de Vries (1998) also found that, under steady state conditions, their model predicts that the ratio of the compaction rate (Vc) to the sedimentation rate (Vs) scales with thickness of the compacting layer (L, in meters) by the following relationship:

$$Vc/Vs = F \times L, \quad (1)$$

where F is a constant given by the sediment porosity, the difference between the fluid and grain densities, and the drained pore compressibility. For a representative choice of these parameter values, Kooi and de Vries (1998) found that $F = 4.25 \times 10^{-4}$ /meter.

In an application of this model to the San Joaquin Valley, consider the subsidence of the Corcoran clay near MP 160, near the center of the Los Gatos bowl in the SLFD. From analysis of geologic cross sections in Miller et al. (1971), maximum net subsidence of the top of the Corcoran clay near MP 160 is approximately 250 feet, and the thickness of the overlying post-Corcoran clay sedimentary column is approximately 750 feet. Using these values to calculate Vc and Vs, and taking $F = 4.25 \times 10^{-4}$ (per Kooi and de Vries, 1998), solution of equation (1) gives the predicted thickness of the underlying compacting sediment column L to be approximately 2,600 feet. For comparison, the cross sections in Miller et al. (1971) indicate that the thickness of the Quaternary Tulare Formation below the Corcoran clay is approximately 2,400 feet. The Tulare Formation is underlain by older and more consolidated marine sedimentary rocks of the San Joaquin Formation, which are presumably less susceptible to compaction.

These results are consistent with the hypothesis that much of the cumulative natural subsidence of the Corcoran clay, as expressed in the structure contours in Figure 6-1, and profile in Figure 6-2, may be explained by compaction of the underlying continental Tulare Formation deposits. Some net subsidence of the Corcoran clay also may be driven by elastic loading of the western margin of the valley by Quaternary thrust faulting and associated growth of folds like the Panoche Hills, Coalinga Nose, and Kettleman Hills anticlines (Rentschler and Bloch 1988). It is also possible that net tectonic subsidence is occurring at Tulare Lake basin. It is important to note that the value of the parameter F derived by Kooi and de Vries (1998) is based on a single value for compressibility of the aquifer skeleton. Well-documented variations in the ratio of clay versus sand within the Tulare Formation beneath the western San Joaquin Valley (Miller et al. 1971, Faunt et al. 2010) suggest that the compressibility, and hence the value of the parameter F, probably varies laterally. If this is the case, then variations in compressibility could account for some of the variability in relief on the Corcoran clay as mapped in Figure 6-1.

The subsurface relief on the Corcoran clay provides evidence for maximum natural rates of “background” subsidence of approximately 0.2 mm/year along the Aqueduct alignment. Much of this natural subsidence may be explained by compaction of underlying Tulare Formation sediments. The subsidence occurs at rates that are one to two orders of magnitude slower than the maximum historic rates that have been attributed to groundwater withdrawal (approximately 30 feet in 60 years to 100 years, equivalent to approximately 0.04 feet/year, or approximately 10 mm/year). Given the rate of “background” subsidence in the San Joaquin Valley, it would take several thousand years to lose 2 feet of freeboard in the most rapidly compacting areas beneath the Aqueduct alignment.

6.3 Subsidence Predictions for the San Luis Field Division

As discussed in Chapter 1 of this report and in DWR’s 2017 CASS report, historic subsidence along the Aqueduct has formed the long-wavelength Panoche and Los Gatos bowls in the SLFD (Figure 1-1). Inspection of the time series of subsidence at selected points in the SLFD (Figure 5-1) from the precise leveling data prompts the following observations approximately temporal patterns of subsidence within

the Panoche and Los Gatos bowls, and their correlation with variations in annual rainfall and Central Valley Project (CVP) allocations:

- There was a short period of relatively rapid subsidence for several years immediately following construction of the Aqueduct, approximately from 1967 to 1970. Rainfall years during this period generally were above normal to wet (see Water Year Index for 1967 to 1970 reported on Figure 5-2).
- Subsidence continued, but at a lower rate, from 1970 to 1977, a period that included several years of drought in the middle 1970s.
- Minor rebound of the Aqueduct occurred during the late 1970s and early to middle 1980s in parts of the Panoche and Los Gatos bowls, coincident with above normal to wet rainfall years and full (100 percent) allocations of irrigation water from the CVP (Figure 5-1).
- The rate of subsidence increased from the middle to late 1980s into the early 1990s, coincident with dry to critically dry years. CVP allocations abruptly dropped from 100 percent in 1989, to less than 50 percent in 1990 and 1991 (Figure 5-1).
- Subsidence rates slowed in the middle 1990s to middle 2000s, and in some places (e.g., MP 136.05 and MP 148.56) the Aqueduct experienced a minor rebound. The majority of rainfall years during this period were above normal to wet. CVP allocations generally ranged from 50 percent to 100 percent (Figure 5-1).
- Subsidence rates generally increased in 2007 to 2009, coincident with several dry years. The rate of subsidence accelerated significantly after 2012 during several years of drought, and with CVP allocations of 20 percent or less (Figure 5-1).

As summarized above, the full 50-year precise survey record (1967–2017) encompasses several alternating wet-and-dry periods, as well as a wide range in CVP water allocations. If it is assumed that future multi-year variations in rainfall and water deliveries are random and similar, on average, to those of the previous 50 years, and consequently that future groundwater usage for irrigation is similar, then the long-term average subsidence rate derived from the precise leveling survey data may be appropriate for estimating future subsidence along the Aqueduct.

The long-term average subsidence rate for a given survey point in the SLFD was derived by fitting a linear trend line to the survey data from 1967 to 2017. The trend line was determined using the linear regression analysis package in Excel, and it was constrained to pass through the origin (subsidence in 1967 set to zero). The resulting slope of the trend line was adopted as the "long-term average subsidence rate" (Table 6-1). Constraining the trend line to pass through the origin results in a steeper slope and thus incorporates conservatism into the rate to account for uncertainty in future land use, climate variability, and water availability. This approach also results in larger misfits between the linear subsidence trend and the observed subsidence during extended periods of wet weather (lower subsidence rates in the early 1980s and possible local rebound) and dry weather (higher rates of subsidence in the late 2000s to early 2010s), which correspond to larger uncertainties when using the long-term rate to predict future subsidence. Regression statistics obtained from Excel were used to determine 95 percent prediction intervals for future subsidence using standard methods (Table 6-1).

As shown in Table 6-1, future subsidence predictions from extrapolating the long-term average rate suggest that the most rapidly subsiding areas in the SLFD will lose an additional 2 feet of freeboard or more by 2040, with the lowest areas in Pools 17 and 20 being the most critical. The mean predicted

Table 6-1 Predicted Cumulative Subsidence in 2040 for Selected Points in the San Luis Field Division Using the Long-Term Average Rate

MP	Pool	"Long-Term Average" Subsidence Rate, 1967–2017 (feet/year)	"Long-Term Average" Subsidence Rate, 1967–2017 (inches/year)	Additional Predicted Subsidence, 2018–2040 (feet)	Mean Predicted Cumulative Subsidence in 2040, relative to 1967 Baseline (feet)	95% Prediction Interval for Subsidence in 2040 (+/- feet)
98.67	15	0.038	0.5	0.8	2.7	0.4
116.27	16	0.073	0.9	1.6	5.2	1.1
127.07	17	0.111	1.3	2.4	8.2	1.7
136.05	18	0.0897	1.1	2.0	5.7	1.3
148.56	19	0.069	0.8	1.5	6.5	1.3
160.45	20	0.131	1.6	2.9	9.4	1.7
160.99	20	0.094	1.1	2.1	7.0	1.3

Note: MP = milepost

cumulative subsidence in 2040, relative to a 1967 baseline, ranges from approximately 5 feet in Pools 16 and 19 to approximately 9 feet in Pool 20. The 95 percent prediction uncertainties for total subsidence in 2040 range from approximately +/- 0.4 foot to +/- 1.7 feet (Table 6-1).

Although forcing the linear trend line of the 50-year dataset through the origin incorporates conservatism, the resulting long-term rate model still reflects conditions during the first two decades following construction of the Aqueduct when annual CVP water allocations were at or near 100 percent, and prior to most of the changes in agricultural land use along the Aqueduct study corridor described in Chapter 2 that contribute to demand hardening for irrigation water. These observations suggest that the relatively lower subsidence rates that prevailed from the early 1970s to the mid-1980s (Figure 5-1) are not likely to return in the next two decades. Future climate trends in California are uncertain, and it is unknown if the extremes in dry and wet years observed between 2013 and 2017 will continue for the next several decades (Swain et al. 2014).

Given these considerations, a more conservative approach for predicting future subsidence is to assume that the relatively high rates of subsidence observed between 2013 and 2017 are likely to continue for at least the next decade. Using the same approach described above to evaluate the long-term average subsidence rate, a linear trend line was fit to survey data measured between 2013 and 2017. This approach is referred to as the "short-term high rate." The regressions are based on four observation years (2013, 2015, 2016, and 2017) and encompass critically dry years when CVP allocations ranged from 0 percent to 20 percent, as well as the wet 2017 rainfall year when 100 percent of CVP allocations were available (Table 6-2). The resulting 2013–2017 short-term subsidence rates are approximately three to five times faster than the long-term average rates between 1967 and 2017. Predicted subsidence based on the short-term, high-rate regressions suggests that the low points in most SLFD pools could lose an additional 2 feet of freeboard in the next 5 to 10 years if the 2013–2017 patterns of California climate, CVP allocations, land use, and groundwater withdrawal continue into the next decade (Table 6-2).

Figure 6-3 Subsidence History at Milepost 98.67, 1967–2017

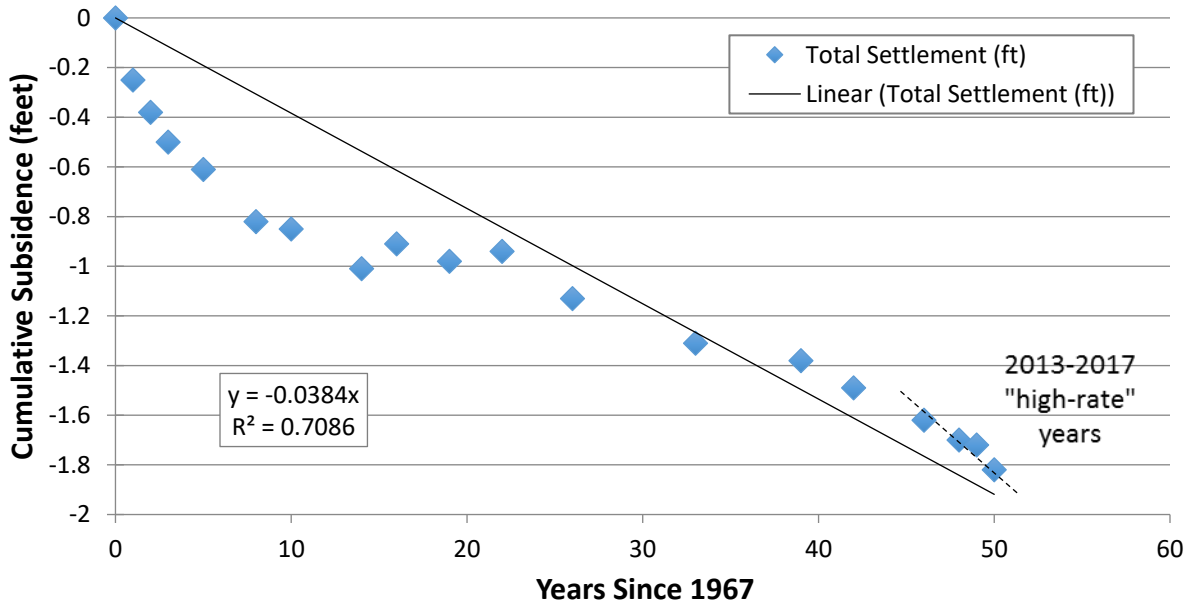

Figure 6-4 Subsidence History at Milepost 116.27, 1967–2017

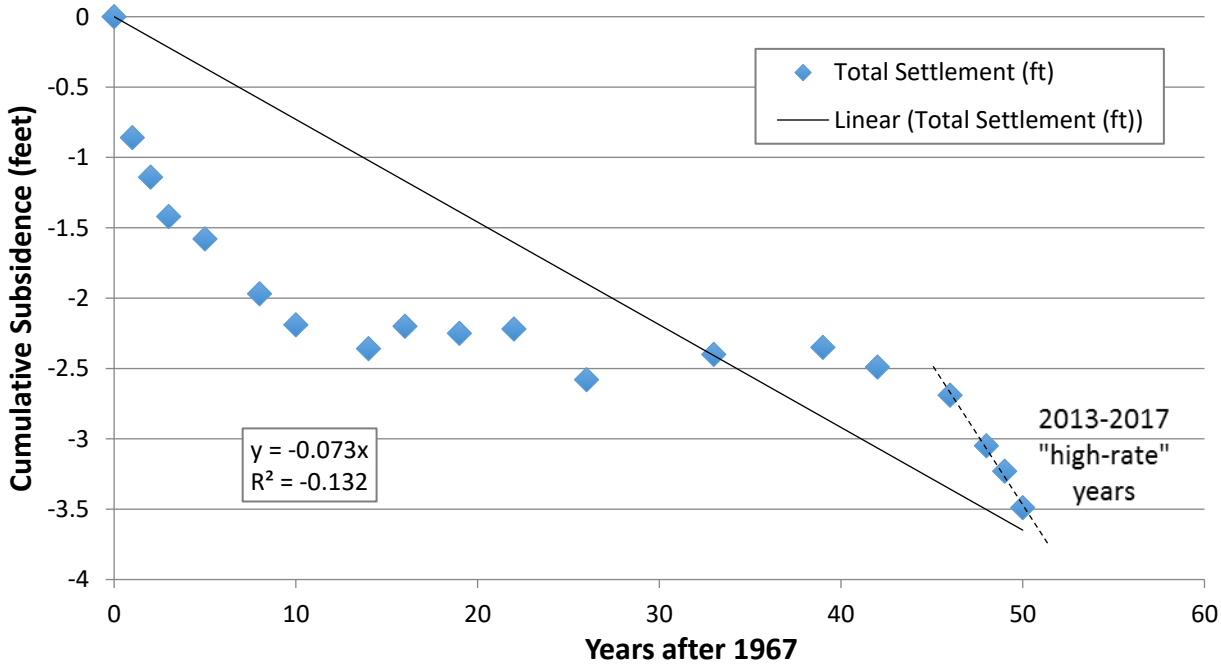

Figure 6-5 Subsidence History at Milepost 127.07, 1967–2017

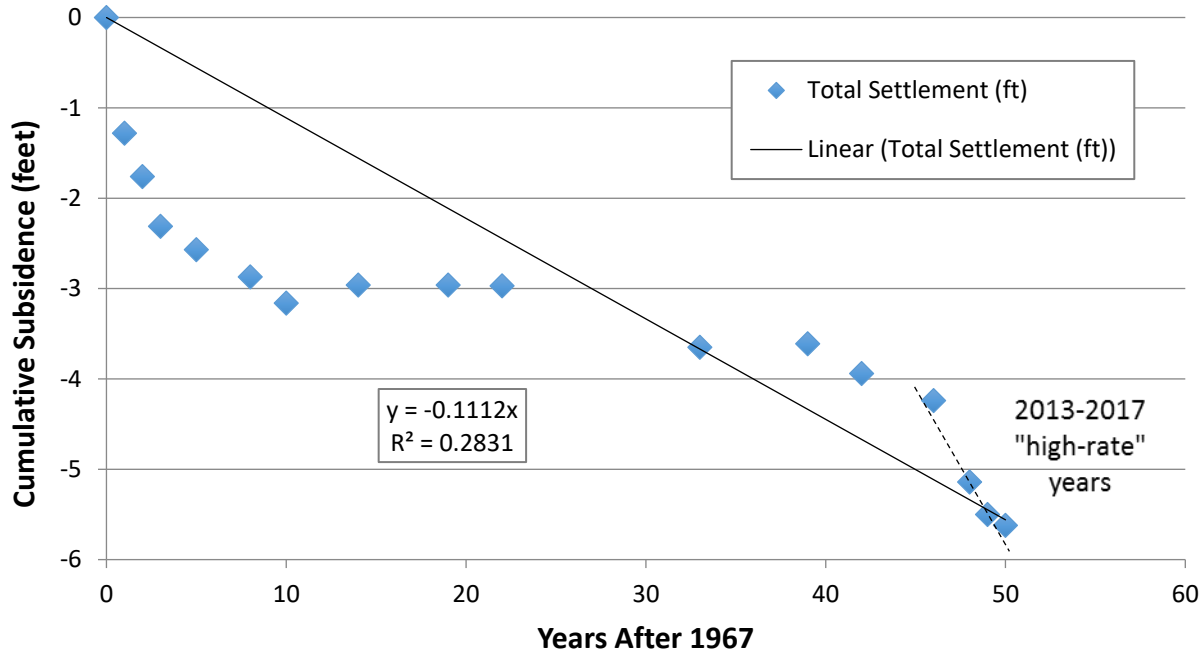

Figure 6-6 Subsidence History at Milepost 136.05, 1967–2017

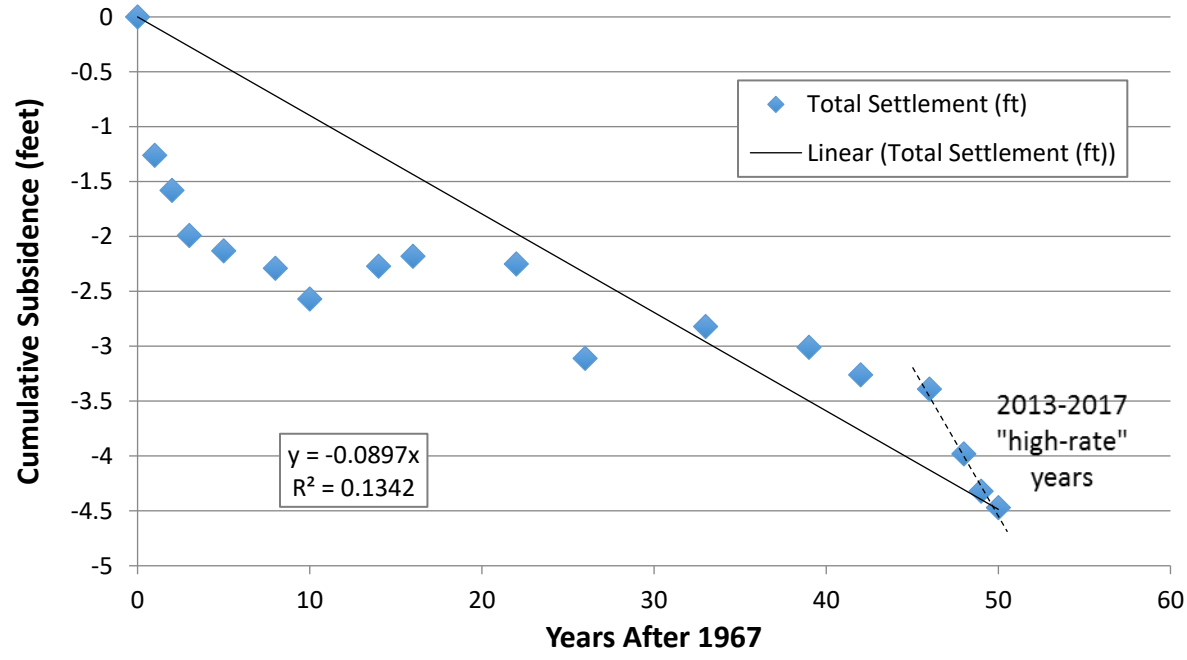

Figure 6-7 Subsidence History at Milepost 148.56, 1967–2017

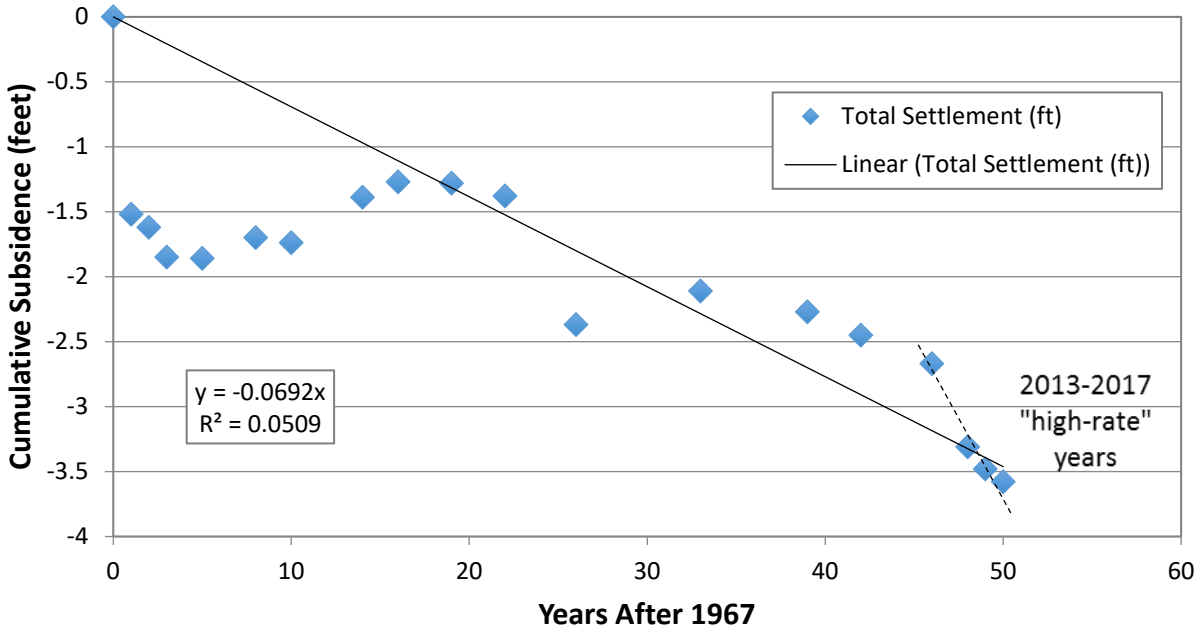

Figure 6-8 Subsidence History at Milepost 160.45, 1967–2017

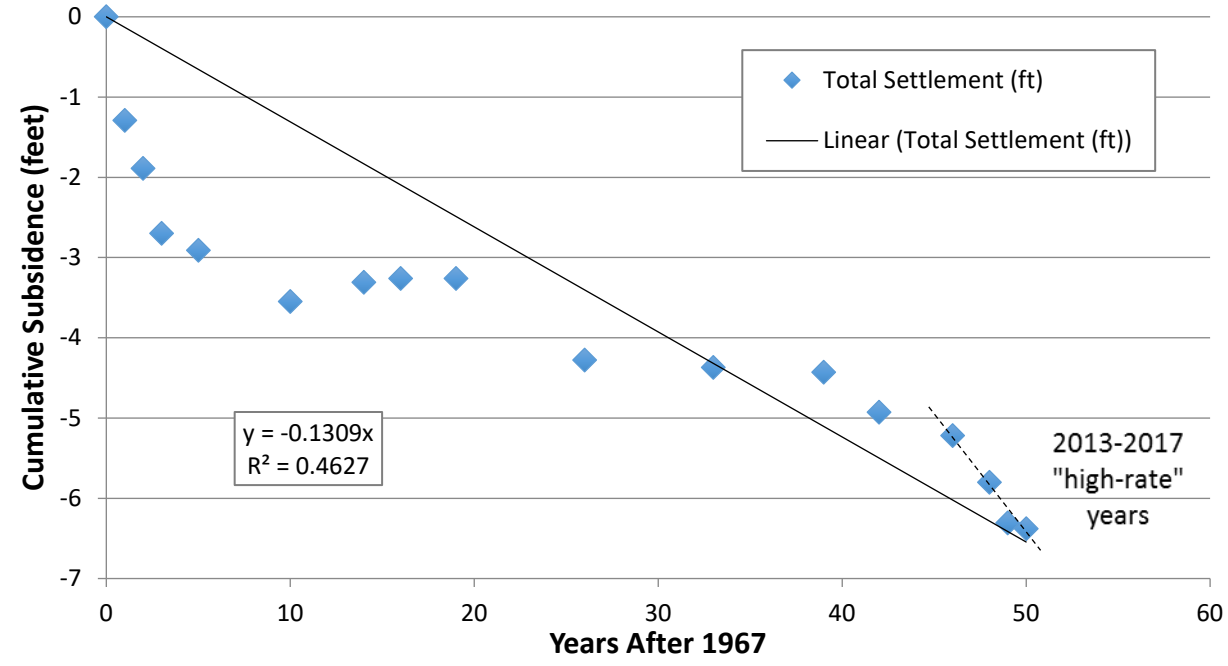

Figure 6-9 Subsidence History at Milepost 160.99, 1967–2017

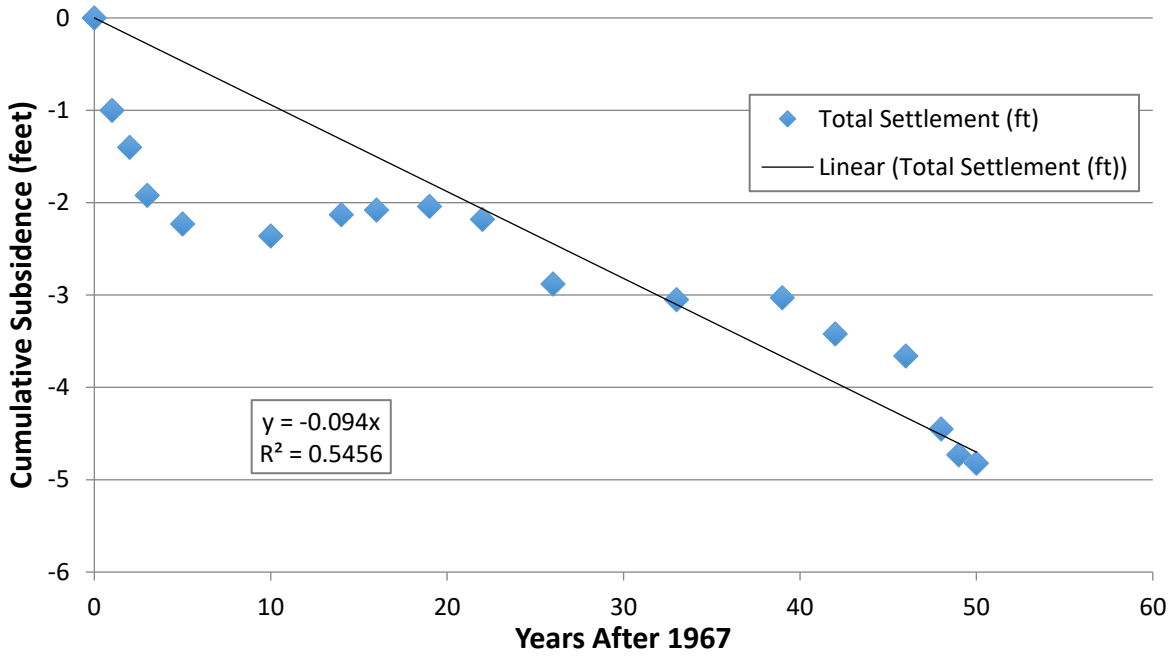

Table 6-2 Predicted Cumulative Subsidence in 5 Years for Selected Points in the San Luis Field Division Using the Short-Term High Rate

MP	Pool	"High" Subsidence Rate, 2013–2017 (feet/year)	"High" Subsidence Rate, 2013–2017 (inches/year)	Additional Predicted Subsidence Between 2018–2023 (feet)	Mean Predicted Cumulative Subsidence in 5 Years (2023), relative to 1967 Baseline (feet)	95% Prediction Interval for Subsidence in 2023 (+/- feet)
98.67	15	0.043	0.5	0.22	2.1	0.3
116.27	16	0.191	2.3	1.0	4.6	0.3
127.07	17	0.383	4.6	1.9	8.1	1.4
136.05	18	0.286	3.4	1.4	6.2	0.6
148.56	19	0.253	3.0	1.3	5.2	1.0
160.45	20	0.313	3.8	1.6	8.3	1.2
160.99	20	0.325	3.9	1.6	6.9	1.3

Note: MP = milepost

6.4 Subsidence Predictions for the San Joaquin Field Division

Examination of the subsidence time series for selected points within the SJFD (Figure 5-2) suggests that the subsidence history of the Kern, Maricopa, and Pleito bowls can be divided into several distinct periods:

- A period of relatively uniform subsidence rate from 1969 to 1981. Note that there was no obvious change in the subsidence rate during critical dry years in 1976–1977.
- A period of distinctly lower subsidence rate, or apparent rebound, between 1981 and 1986. The reduction in subsidence rate (and local reversal to net uplift) is not obviously related to a change in climate during this period. SWP allocations are reported to have been consistently at 100 percent during this period (Figure 5-2).
- Relatively constant subsidence rates from 1986 to 2013. Note that this period spans several multi-year wet and dry cycles, as well as varying allocations from the CVP.
- An increase in subsidence rate between 2013 and 2016 for some, but not all, observation points shown in Figure 5-2 (contrast the time series for MP 275 and MP 207.94 with that of MP 196.74). This period corresponds to a drought period in which allocations from the CVP were 40 percent or less.
- A reduction of subsidence rate between 2016 and 2017 for some observation points (MP 275), and local rebound for others (MP 222.89 and MP 256.56).

Using similar assumptions to those described in Section 6.3 for evaluating subsidence rate data in SLFD, the temporal patterns of subsidence illustrated in Figure 5-2 were used to develop the following subsidence rates for SJFD:

1. A long-term average rate based on subsidence measured between 1986 and 2017, which spans multiple wet-dry periods, as well as years with variable SWP allocations. This period specifically excludes the years between 1981 and 1986 that record an apparent uplift or rebound that extends for a minimum of 80 miles along the Aqueduct and is anomalous over the full 50-year leveling history in the SJFD (Figure 5-2). As discussed in Section 2.3.3 and in DWR's 2017 CASS report, DOE recommends not using SJFD survey data from 1981 to 1986 as part of any subsidence rate calculation.
2. A short-term high rate based on subsidence measured during the 2013-2017, during which SWP allocations consistently were below 40 percent. As discussed in Section 6.3, the short-term high rate conservatively assumes that climate trends and patterns of land use resulting in increased groundwater withdrawal from 2013 to 2016 will continue for at least the next decade.

With these assumptions, long-term average (Table 6-3) and short-term high (Table 6-4) rates of subsidence were derived for the survey points in the SJFD shown in Figure 5-2. These points are associated with areas of maximum cumulative subsidence within individual pools. In general, the long-term average rate predicts that it will take several decades or longer for the lowest, most rapidly subsiding points in the three main subsidence bowls in the SJFD to lose 2 feet of freeboard (Table 6-3). The short-term high rate generally predicts loss of 2 feet of freeboard within two to five decades for low points in Pools 23 through 26, Pool 31, and Pool 32 (Table 6-4). The high rate predicts that the low point in Pool 35 at MP 275 could lose 2 feet of freeboard within 14 years based on the rapid and relatively linear subsidence trend exhibited in the survey data from 2013 to 2017.

Figure 6-10 Subsidence History at Milepost 196.74, 1993–2013

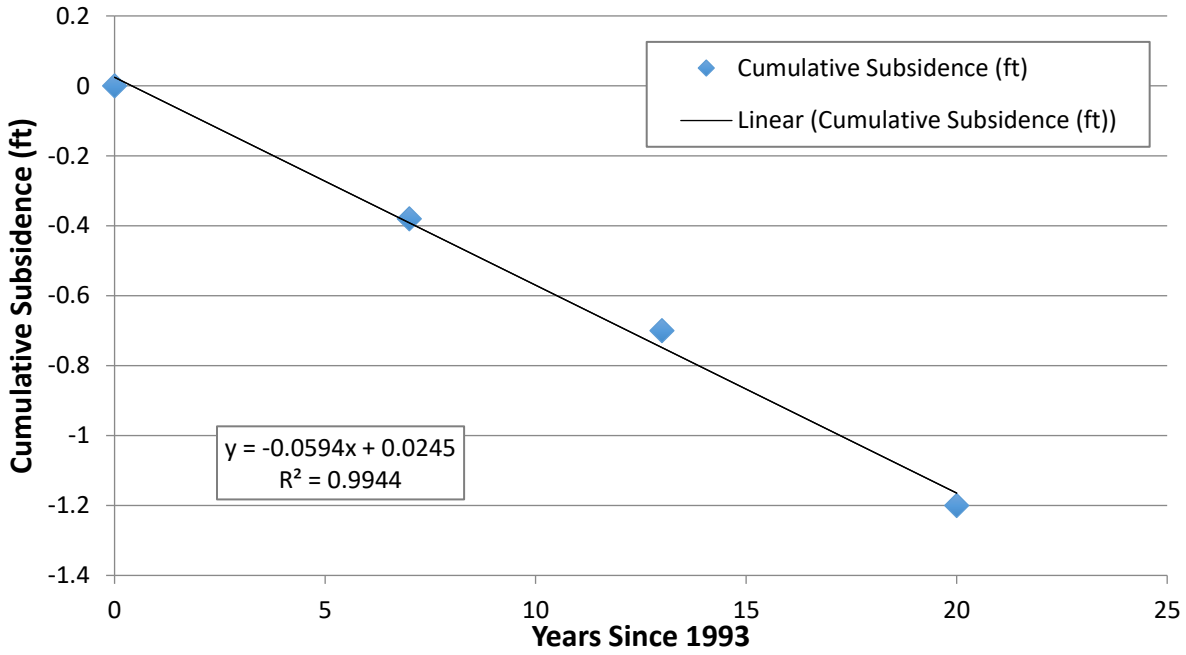

Figure 6-11 Subsidence History at Milepost 207.94, 1986–2013

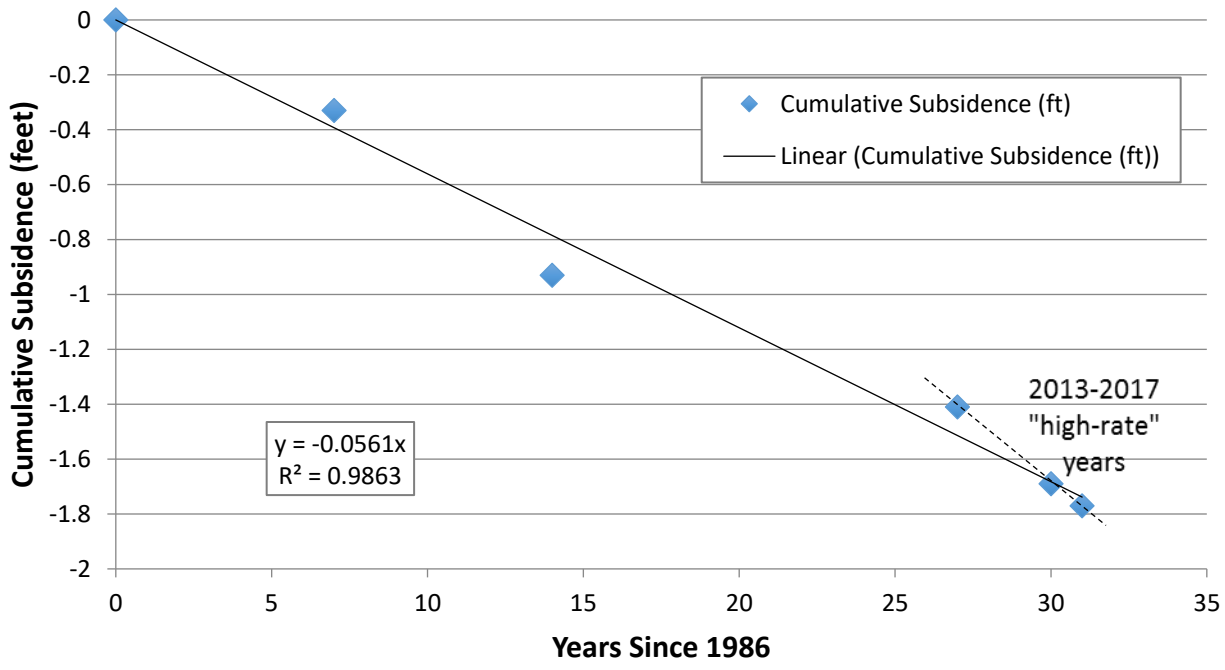

Figure 6-12 Subsidence History at Milepost 222.89, 1986–2013

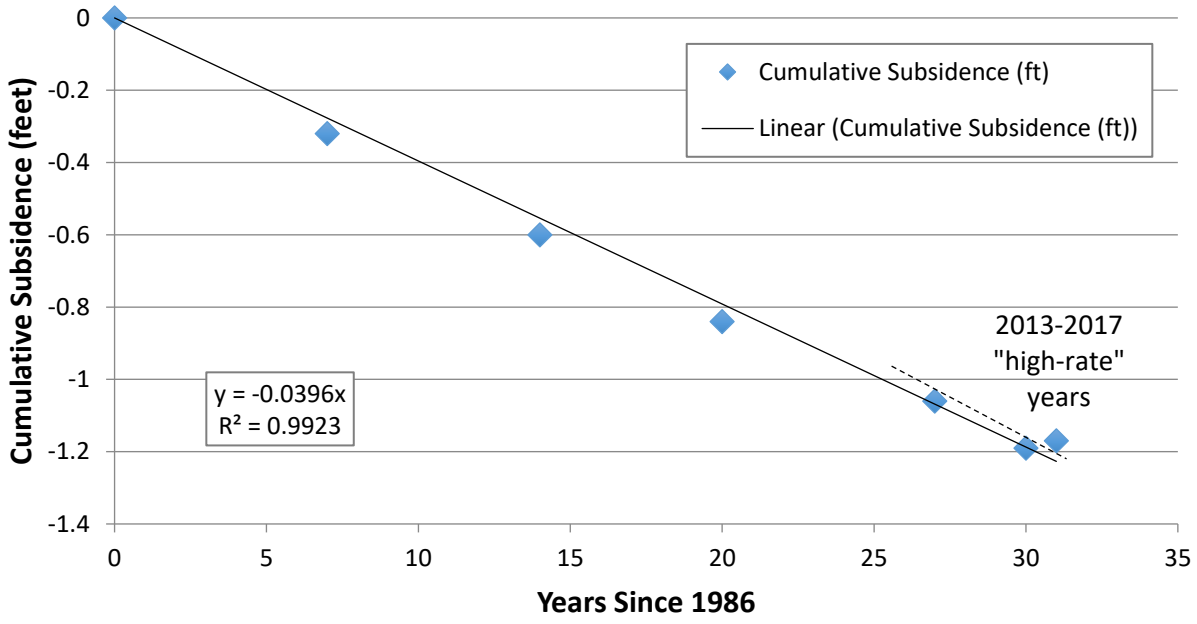

Figure 6-13 Subsidence History at Milepost 256.56, 1986–2013

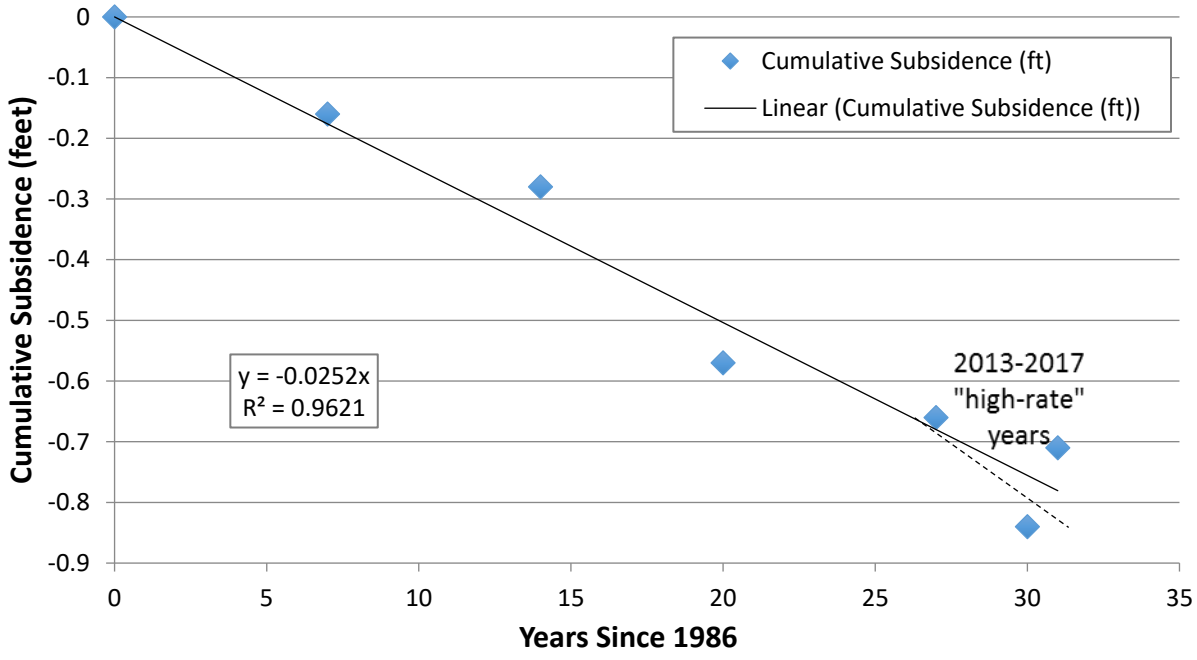

Figure 6-14 Subsidence History at Milepost 275, 1986–2013

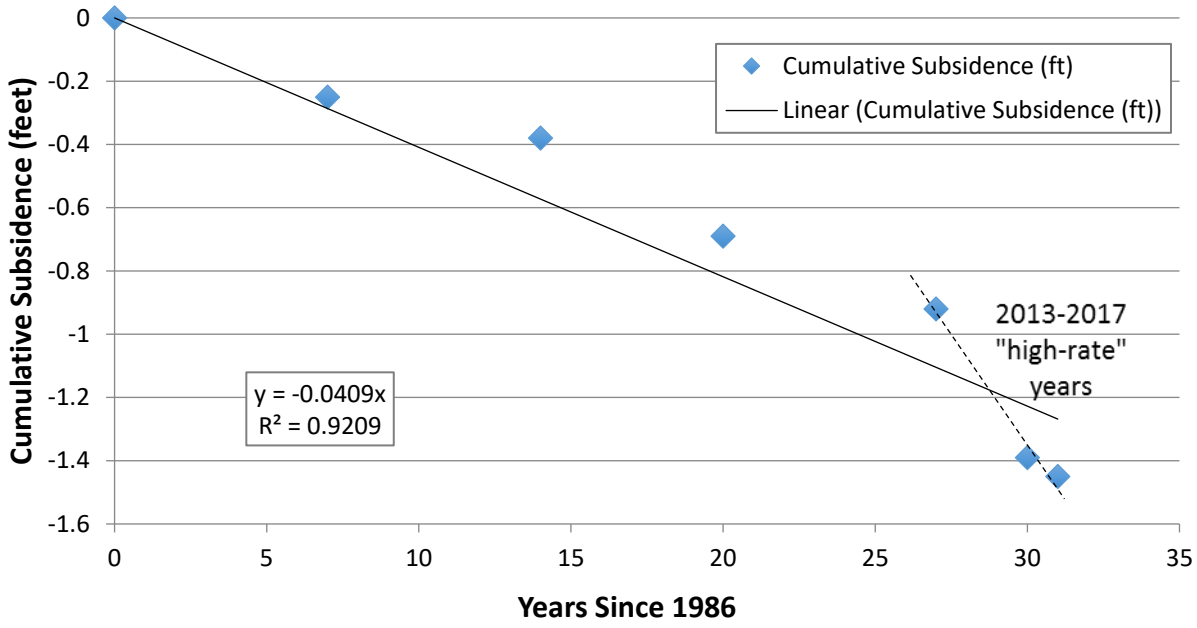

Table 6-3 Predicted Subsidence in 2040 for Selected Points in the San Joaquin Field Division Using the Long-Term Average Rate

MP	Pool	"Long-Term Average" Subsidence Rate, 1986–2017 (feet/year)	"Long-Term Average" Subsidence Rate, 1986–2017 (inches/year)	Additional Predicted Subsidence, 2018–2040 (feet)	Mean Predicted Cumulative Subsidence in 2040, relative to 1967 Baseline (feet)	95% Prediction Interval for Subsidence in 2040 (+/- feet)
196.74	23, 24	0.061	0.73	1.3	5.1	0.3
207.94	25	0.056	0.67	1.2	4.8	0.4
222.89	26	0.040	0.48	0.9	2.5	0.1
256.56	31,32	0.025	0.30	0.6	2.3	0.3
275	35	0.041	0.49	0.9	3.0	0.6

Note: MP = milepost

Table 6-4 Predicted Subsidence in 5 Years for Selected Points in the San Joaquin Field Division Using the Short-Term High Rate

MP	Pool	"High" Subsidence Rate, 2013–2017 (feet/year)	"High" Subsidence Rate, 2013–2017 (inches/year)	Additional Predicted Subsidence, 2018–2023 (feet)	Mean Predicted Cumulative Subsidence in 5 Years (2023), relative to 1967 Baseline (feet)	95% Prediction Interval for Subsidence in 2023 (+/- feet)
196.74	23, 24	0.078	0.9	0.4	4.1	0.2
207.94	25	0.091	1.1	0.5	4.0	0.1
222.89	26	0.033	0.4	0.2	1.9	0.5
256.56	31,32	0.030	0.36	0.15	1.9	1.4
275	35	0.141	1.7	0.7	3.1	0.7

Note: MP = milepost

6.5 Potential Impact of Subsidence on Future Deliveries

As discussed in Chapter 4, hydraulic modeling using HEC-RAS software suggests that the ability of the Aqueduct system to deliver future allocations is particularly sensitive to additional subsidence in Pools 20 and 25. The subsidence rate modeling approach presented in this chapter can be used to predict when critical thresholds of subsidence in these two pools will be exceeded.

For the following analysis, survey data from MP 163.69 and MP 208.11 are used to characterize the subsidence rates of low points of Pools 20 and 25, respectively. These mileposts are close to, but not equivalent to, the mileposts cited in Sections 5.1, 6.3, and 6.4 of this report to illustrate the time history of subsidence in the low points of Pools 20 and 25, which are presented here for continuity with the 2017 CASS report. From review of survey data collected through 2017, MP 163.69 and MP 208.11 were specifically selected to incorporate conservatism in the analysis because these mileposts exhibit some of the highest recent short-term subsidence rates in these two pools. In particular, MP 163.69 is very close to a "hot spot" of high subsidence rate in Pool 20, just north of the Avenal Cutoff Road that has been identified from analysis of Uninhabited Aerial Vehicle Synthetic Aperture Radar data (Farr, Jones, and Liu 2016). The mean long-term average and short-term high subsidence rates for these mileposts were derived from the survey data using the methodology described in Section 6.3, and are presented in Table 6-5.

Table 6-5 Subsidence Rates for Selected Low Points in Pools 20 and 25

Milepost	Pool	Mean Long-Term Average Subsidence Rate, 1967–2017 (feet per year)	Mean Short-Term "High" Subsidence Rate, 2013–2017 (feet per year)
163.69	20	0.088	0.677
208.11	25	0.058	0.1

Based on results of the HEC-RAS modeling discussed in Section 4.2.4.2, 1 foot of additional subsidence in Pool 20, relative to the elevations measured in 2017, will limit the capacity of the system to 3.8 million

acre-feet of deliveries south of Pool 20 (i.e., the Maximum Table A volume, described in Section 4.2.4.1). The Aqueduct will no longer be able to provide historical maximum deliveries of 3.4 million acre-feet after an additional 2.1 feet of subsidence relative to 2017 (Section 4.2.4.2). The HEC-RAS analysis assumes a flat delivery schedule with maximum flows 85 percent of the time year-round. Using mean values from the long-term average rate model for MP 163.69 in Pool 20 (Table 6-5), the 1-foot additional subsidence threshold could be exceeded within approximately 11 years, and the 2.1-foot threshold in approximately 24 years. In contrast, the mean value from the short-term high rate regression (Table 6-5) predicts exceeding 2.1 feet of additional subsidence of MP 163.69 within approximately three years.

Cumulative subsidence as of 2017 limits conveyance of the Aqueduct system to approximately 3.1 million acre-feet across Pool 25, which is less than the total Maximum Table A allocations of 3.8 million acre-feet (Section 4.2.4.3). HEC-RAS modeling suggests an additional 2.2 feet of subsidence in Pool 25, below the 2017 surveyed elevations, would reduce the capacity of the Aqueduct system to the historical maximum of 2.6 million acre-feet. The long-term average rate model derived from the time series at MP 200.11 in Pool 25 (Table 6-5) predicts approximately 38 years to accumulate an additional 2.2 feet of subsidence. The short-term high-rate model for the same time series (Table 6-5) predicts approximately 22 years to accumulate 2.2 feet of additional subsidence.

The predicted time remaining before maximum historical deliveries cannot be met is summarized in Table 6-6. The estimates in Table 6-6 conservatively assume that MP 163.69 and MP 208.11 act as "choke points" for flow through Pools 20 and 25, respectively. In detail, the ability of the Aqueduct to meet historical maximum deliveries may depend on differential subsidence of finite reach of the canal rather than a single discrete point. Additional HEC-RAS modeling is being performed to test the sensitivity of Aqueduct capacity to lateral variations in the subsidence rate across the low points of Pools 20 and 25, and whether MP 163.69 and MP 208.11 are good proxies for evaluating performance of these pools. The results of these analyses can be used to refine the estimates in Table 6-6.

Based on rate extrapolations from the survey data, the major uncertainty for evaluating near-term impact on performance of the Aqueduct is whether the very rapid subsidence rate in Pool 20 (more than 0.5 foot per year in the "Avenal hot spot;" see Figure 8 in Farr, Jones, and Liu 2016) during the 2013–2016 drought period will continue for the next several years. As discussed in Section 2.2.3, this is an area where the potentiometric surface in the lower water-bearing zone declined below 1967 low elevations in 2015 and 2016, contributing to the possibility that much of the additional subsidence at MP 163.69 that accumulated in 2013–2016 is permanent and non-recoverable. In addition, the predictions in Table 6-6 are based on using mean subsidence rates from the survey data regressions; within uncertainty, there is a 50 percent probability that the future rate of subsidence will be higher than the mean rate, and thus the critical subsidence thresholds at MP 163.69 and MP 208.11 could be exceeded within a shorter time span than shown by the forecasts in Table 6-6.

Table 6-6 Estimation of When Historical Maximum Deliveries Cannot be Met[a]

Pool Number (Milepost)	Additional Subsidence to Reach Historical Maximum Delivery Threshold	Time Remaining (Mean Estimate) At 2013–2017 Subsidence Rate	Time Remaining (Mean Estimate) At 1967–2017 Subsidence Rate
20 (163.69)	2.1 feet	3 years	24 years
25 (208.11)	2.2 feet	22 years	38 years

Note:
[a] Assumes running flat 85 percent of the time year-round.

It is important to note that the subsidence predictions in Table 6-6, as well as those discussed in Section 6.3 (San Luis Field Division), and Section 6.4 (San Joaquin Field Division), are based on extrapolating past trends into the future. The subsidence predictions herein assume that the contributing factors to anthropogenic subsidence (long-term agricultural land use change, multi-year drought, variations in annual SWP and CVP deliveries, etc.) will continue, with the same trends and temporal variations observed in the past. Any changes in the contributing factors will presumably affect predictions of future subsidence. For example, the Sustainable Groundwater Management Act (SGMA), which was signed into law in 2014, requires that groundwater use be managed to eliminate its contribution to land subsidence by 2040. Assuming that implementation of SGMA is successful, the subsidence rate models derived in this study will not be valid for predicting subsidence beyond 2040. As groundwater sustainability agencies progressively adopt practices leading to full implementation of SGMA, changes to the contributing factors of subsidence may render the subsidence rate models in this report obsolete before 2040.

References

Bruno MS, and Bovberg CA. 1992. Reservoir compaction and surface subsidence above Lost Hills field, California, in Tillerson, JR and Wawersik, WR, eds, Rock Mechanics, Proceedings of the 33rd U.S. Symposium: June 3–5 1992, Sweeney Convention Center, Santa Fe, New Mexico. A.A. Balkema, Rotterdam, pp. 263–272.

California Department of Water Resources. 1979a. *Water Operations Manual OP-450R*. Division of Operations and Maintenance, Sacramento, California.

California Department of Water Resources. 1979b. *Milepost at Structure Sites San Luis Canal*. Division of Operations and Maintenance.

California Department of Water Resources. June 1989. *Water Operations Manual OP-350R*. Division of Operations and Maintenance, Sacramento, California.

California Department of Water Resources. 2009. *Data Handbook State Water Project*. Division of Operations and Maintenance.

California Department of Water Resources. September 2012. "California Aqueduct Strip Maps by Field Division," Division of Operations and Maintenance, Sacramento, California.

California Department of Water Resources. 2013. *Standing Operating Order PC 600.22*. Division of Operations and Maintenance.

California Department of Water Resources. 2016a. Precise Survey Data, Division of Operations and Maintenance.

California Department of Water Resources. 2016b. LiDAR Data, Division of Engineering.

California Department of Water Resources. 2017a. *California Aqueduct Subsidence Study*, Division of Engineering.

California Department of Water Resources. 2017b. Precise Survey Data, Division of Operations and Maintenance.

Division of Oil, Gas and Geothermal Resources. 1998a. Lost Hills Oil Field: Volume 1-Central California Oil and Gas Fields, Fourth Edition, California Department of Conservation Publication No. TR11.

Division of Oil, Gas and Geothermal Resources. 1998b. North Lost Hills Oil Field: Volume 1-Central California Oil and Gas Fields, Fourth Edition, California Department of Conservation Publication No. TR11.

Farr TG, Jones CE, and Liu Z. 2016. *Progress Report: Subsidence in California, March 2015–2016*. Prepared by the Jet Propulsion Laboratory for the California Department of Resources, 37 pp.

Faunt CC, Belitz K, and Hanson RT. 2010. Development of a three-dimensional model of sedimentary texture in valley-fill deposits Central Valley, California: Hydrogeology Journal, v. 18, pp. 625–649.

Faunt CC, Sneed M, Traum J, and Brandt JT. 2016. Water Availability and land subsidence in the Central Valley, California, USA: Hydrogeology Journal, v. 24, no. 3, pp. 675–684.

Fielding EJ, Blom RG, and Goldstein RM. 1998. Rapid subsidence over oil fields measured by SAR interferometry: Geophysical Research Letters, v. 25, no. 17, pp. 3215–3218.

Fresno County. 1994. Fresno County Annual Crop and Livestock Report. Department of Agriculture, 20 pp. Viewed online at: http://www.co.fresno.ca.us/Home/ShowDocument?id=16886. Accessed: Sept. 7, 2017.

Fresno County Farm Bureau. 2016. Fresno County Annual Crop and Livestock Report: prepared by County of Fresno, Department of Agriculture, 29 pp. Viewed online at: http://www.co.fresno.ca.us/WorkArea/DownloadAsset.aspx?id=74037. Accessed: Sept. 7, 2017.

Frink JW, and Kues HA. 1954. *Corcoran Clay—a Pleistocene lacustrine deposit in the San Joaquin Valley, California*. American Association of Petroleum Geologists Bulletin, v. 38, no. 11, p. 2353-2371.

Galloway DL, and Riley FS. 1999. San Joaquin Valley, California: largest human alteration of the Earth's surface, in Galloway DL, Jones DR. and Ingebritsen SE. eds., Land subsidence in the United States: United States Geological Survey Circular 1182, pp. 23–34.

Guillen A. 2016. Land use history along the Aqueduct between Dos Amigos and Buena Vista; California Department of Water Resources internal memo, 8 pp.

Hanak E, Lund J, Arnold B, Escriva-Bou A, Gray B, Green S, Harter T, Howitt R, MacEwan D, Medellin-Azuara J, Moyle P, Seavy N. 2017. *Water Stress and a Changing San Joaquin Valley*. Public Policy Institute of California, 50 pp. Viewed online at: http://www.ppic.org/content/pubs/report/R_0317EHR.pdf. Accessed: Jan. 15, 2018.

Ireland RL, Poland JF, and Riley FS. 1980. Land subsidence in the San Joaquin Valley, California, as of 1980: United States Geological Survey Professional Paper 437-I, 93 pp.

Johnson R, and Cody BA. 2015. California Water Production and Irrigated Water Use. Congressional Research Service. CRS Report R44093, 25 pp. Submitted June 20, 2015. Viewed online at: https://www.everycrsreport.com/files/20150630_R44093_126291b87754c75f5965cae138b0363371948f61.pdf. Accessed: Nov. 14, 2017.

Kern County. 1998. Crop Report: Department of Agriculture, Kern County, California, 18 pp. Viewed online at: http://www.kernag.com/caap/crop-reports/crop90_99/crop1998.pdf. Accessed: Dec. 8, 2017.

Kern County. 2015. Kern County Agricultural Report: prepared by the Department of Agriculture and Measurement Standards, Kern County, California, 15 pp. Viewed online at: http://www.kernag.com/caap/crop-reports/crop10_19/crop2015.pdf. Accessed: Sept. 7, 2017.

Kings County. 1996. Agricultural Crop Report: prepared by the Agricultural Commissioner, Sealer of Weights and Measures, 14 pp. Viewed online at: https://www.countyofkings.com/home/showdocument?id=2786. Accessed: Dec. 8, 2017.

Kings County. 2016. Annual Agricultural Crop Report: prepared by Department of Agriculture, Measurement Standards, 23 pp. Viewed online at: https://www.countyofkings.com/home/showdocument?id=16141. Accessed: Sept. 7, 2017.

Kooi H, and de Vries JJ. 1998. Land subsidence and hydrodynamic compaction of sedimentary basins: Hydrology and Earth System Sciences, v.2, no. 2–3, pp. 159–171.

Land PE. 1984. Lost Hills Oil Field: Publication no. TR32, California Department of Conservation, Division of Oil and Gas, pp. 1–16.

Land IQ. 2017. Draft Report, *2014 Statewide Land Use Mapping*. Prepared for the California Department of Water Resources, 17 pp.

Lettis WR. 1982. Late Cenozoic stratigraphy and structure of the western margin of the central San Joaquin Valley, California: Ph.D. dissertation, University of California, Berkeley, 202 p. plus plates.

Medwedeff DE. 1989. Growth fault-bend folding at southeast Lost Hills, San Joaquin Valley, California: American Association of Petroleum Geologists Bulletin, v. 73, no. 1, pp. 54–67.

Merced County. 2004. Annual Report of Agriculture: Merced County Department of Agriculture, 15 pp. Viewed online at: https://www.co.merced.ca.us/ArchiveCenter/ViewFile/Item/243. Accessed: Dec. 8, 2017.

Merced County. 2015. Annual Report on Agriculture: Merced County Department of Agriculture, 13 pp. Viewed online at: https://www.co.merced.ca.us/ArchiveCenter/ViewFile/Item/521. Accessed: Sept. 7, 2017.

Miller RE, Green JH, and Davis GH. 1971. Geology of the compacting deposits in the Los Banos-Kettleman City subsidence area, California: United States Geological Survey Professional Paper 497-E, 43 pp.

Rentschler MS, and Bloch RB. 1988. Flexural subsidence modeling of the San Joaquin basin, California, in Graham, S.A., and Olson, H.C., eds., Studies of the Geology of the San Joaquin Basin: Society

of Economic Paleontologists and Mineralogists, Pacific Section Field Trip Guidebook, v. 60, pp. 29–57.

Sarna-Wojcicki AM, Bowman HR, Meyer CE, Russell PC, Woodward MJ, McCoy G, Rowe JJ Jr, Baedecker PA, Asaro F, and Michael H. 1984. Chemical analyses, correlations, and ages of Upper Pliocene and Pleistocene ash layers of east-central and southern California: United States Geological Survey Professional Paper 1293, 40 pp.

Swain, DL, Tsiang M, Haugen M, Singh D, Charland A, Rajaratnam B, and Diffenbaugh NS. 2014. The extraordinary California drought of 2013/2014: character, context and the role of climate change. Bulletin of the American Meteorological Society, v. 95, no. 9, pp. S3–S7

U.S. Army Corps of Engineers. 2010. Hydraulic Engineering Center-River Analysis System (HEC-RAS) Applications Guide, Version 4.1, CPD-70, January 2010, 351 pp.

Appendix A. Geology Figures

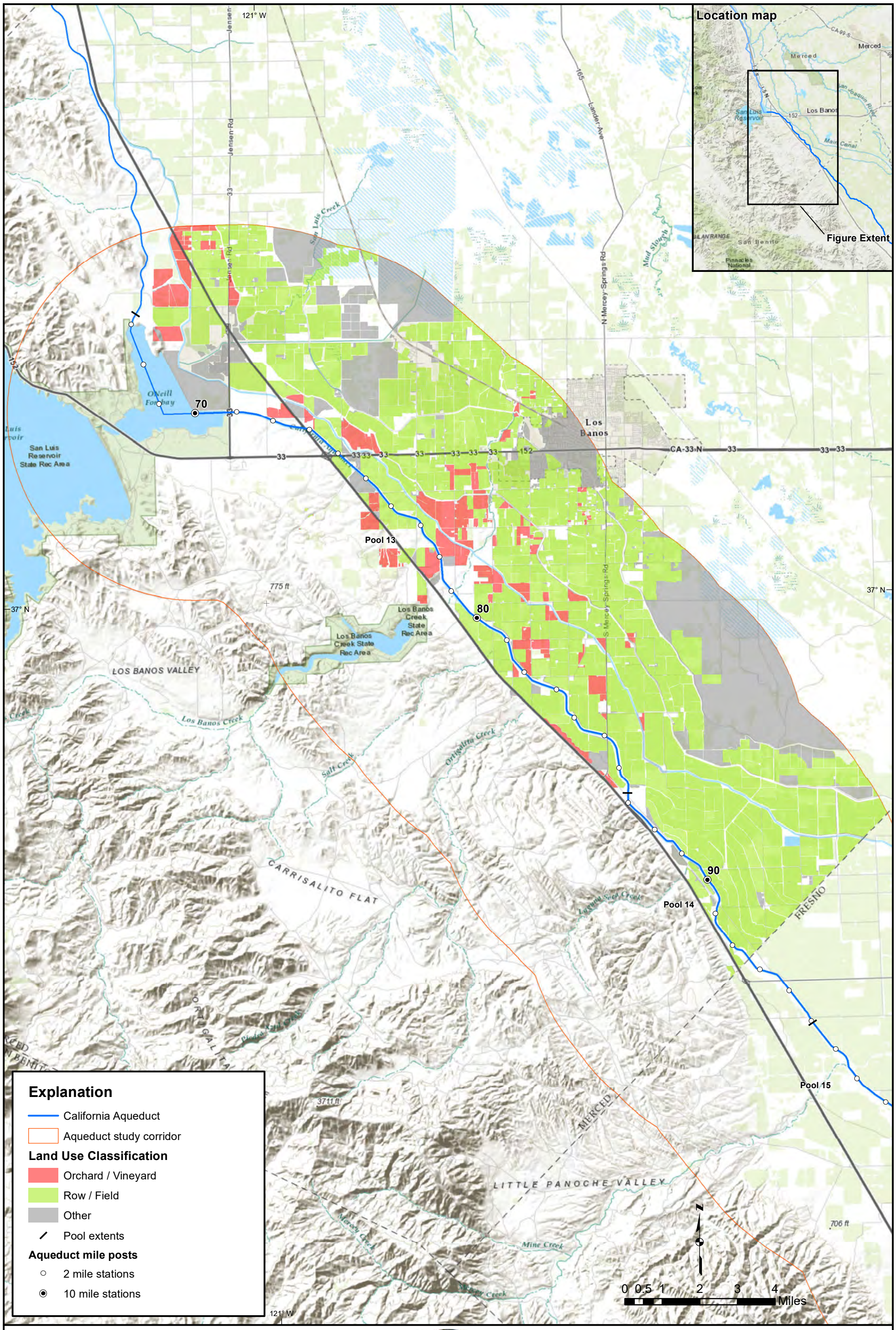

DEPARTMENT OF WATER RESOURCES
STATE WATER PROJECT
CALIFORNIA AQUEDUCT SUBSIDENCE STUDY

FIGURE A-1
LAND USE MAPS
MERCED COUNTY 1995

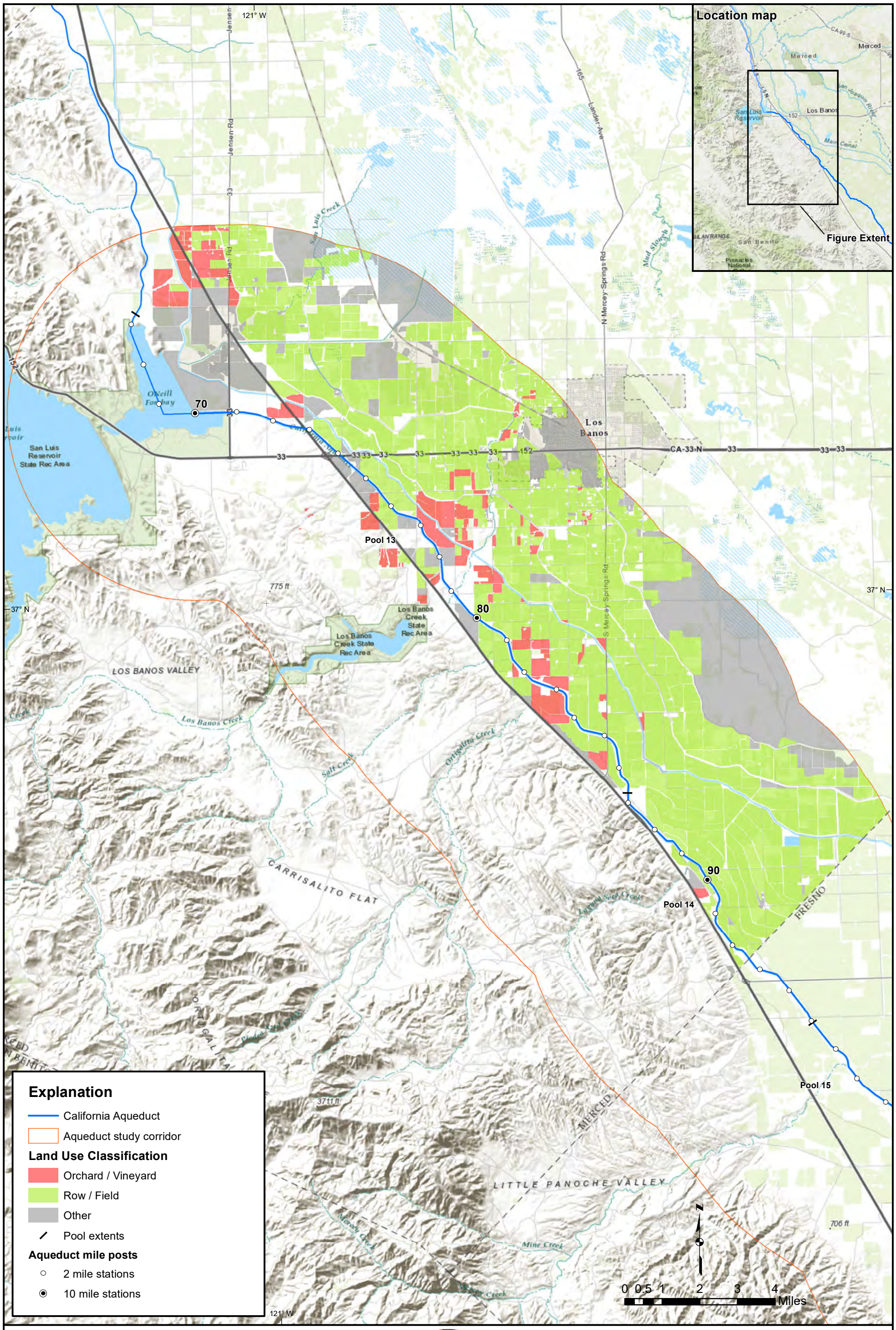

DEPARTMENT OF WATER RESOURCES
STATE WATER PROJECT
CALIFORNIA AQUEDUCT SUBSIDENCE STUDY

FIGURE A-2
LAND USE MAPS
MERCED COUNTY 2002

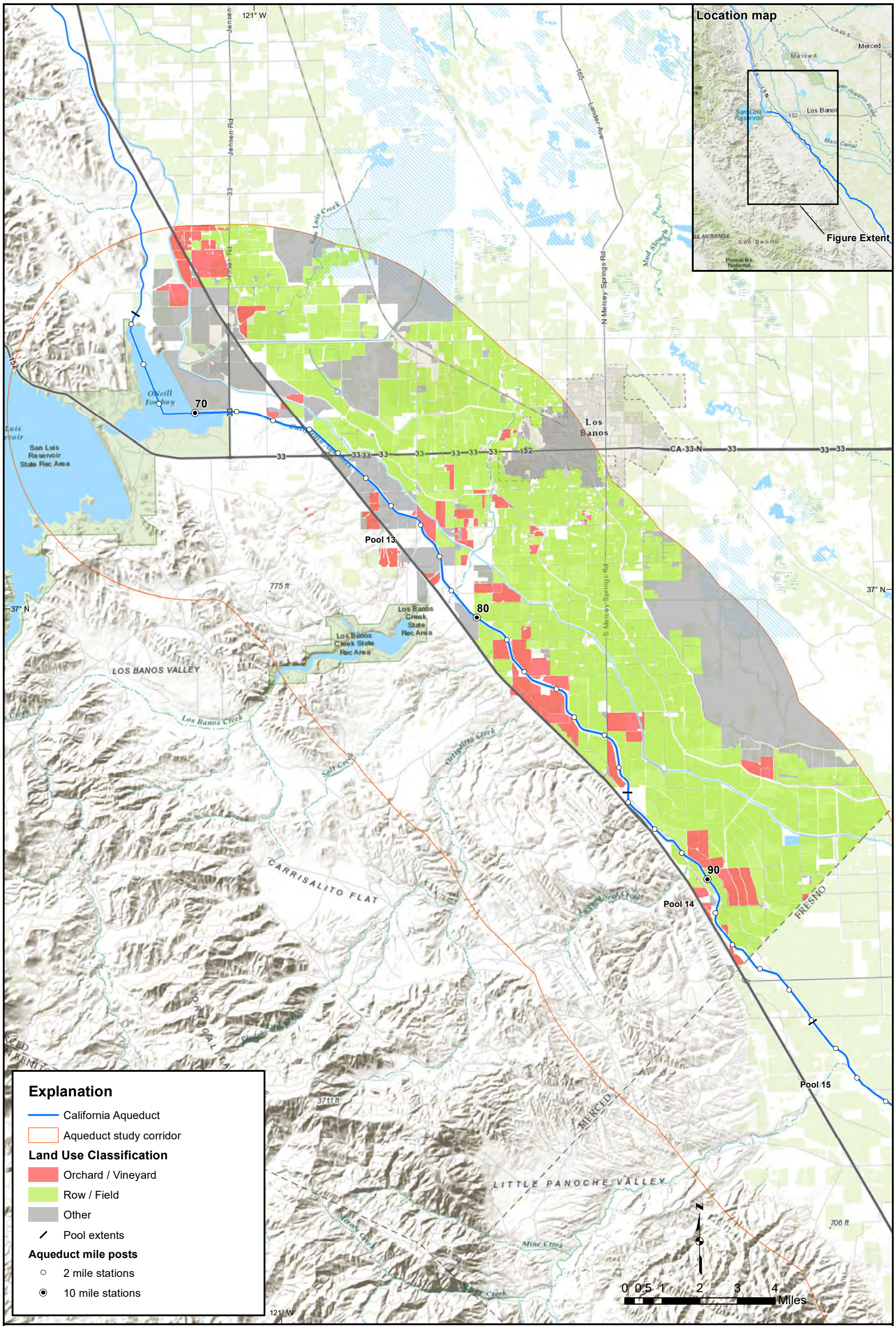

DEPARTMENT OF WATER RESOURCES
STATE WATER PROJECT
CALIFORNIA AQUEDUCT SUBSIDENCE STUDY

FIGURE A-3
LAND USE MAPS
MERCED COUNTY 2012

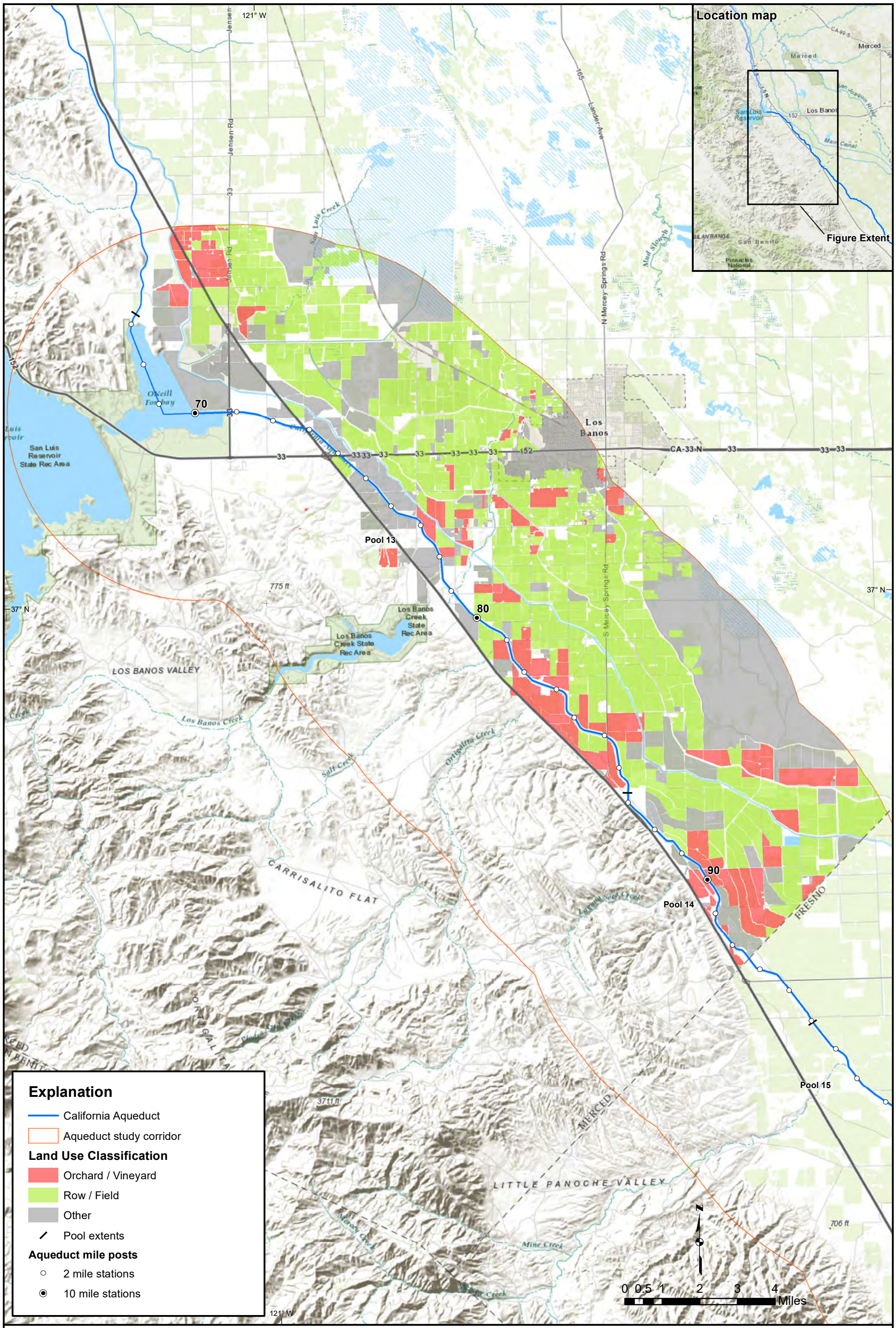

DEPARTMENT OF WATER RESOURCES
STATE WATER PROJECT
CALIFORNIA AQUEDUCT SUBSIDENCE STUDY

FIGURE A-4
LAND USE MAPS
MERCED COUNTY 2014

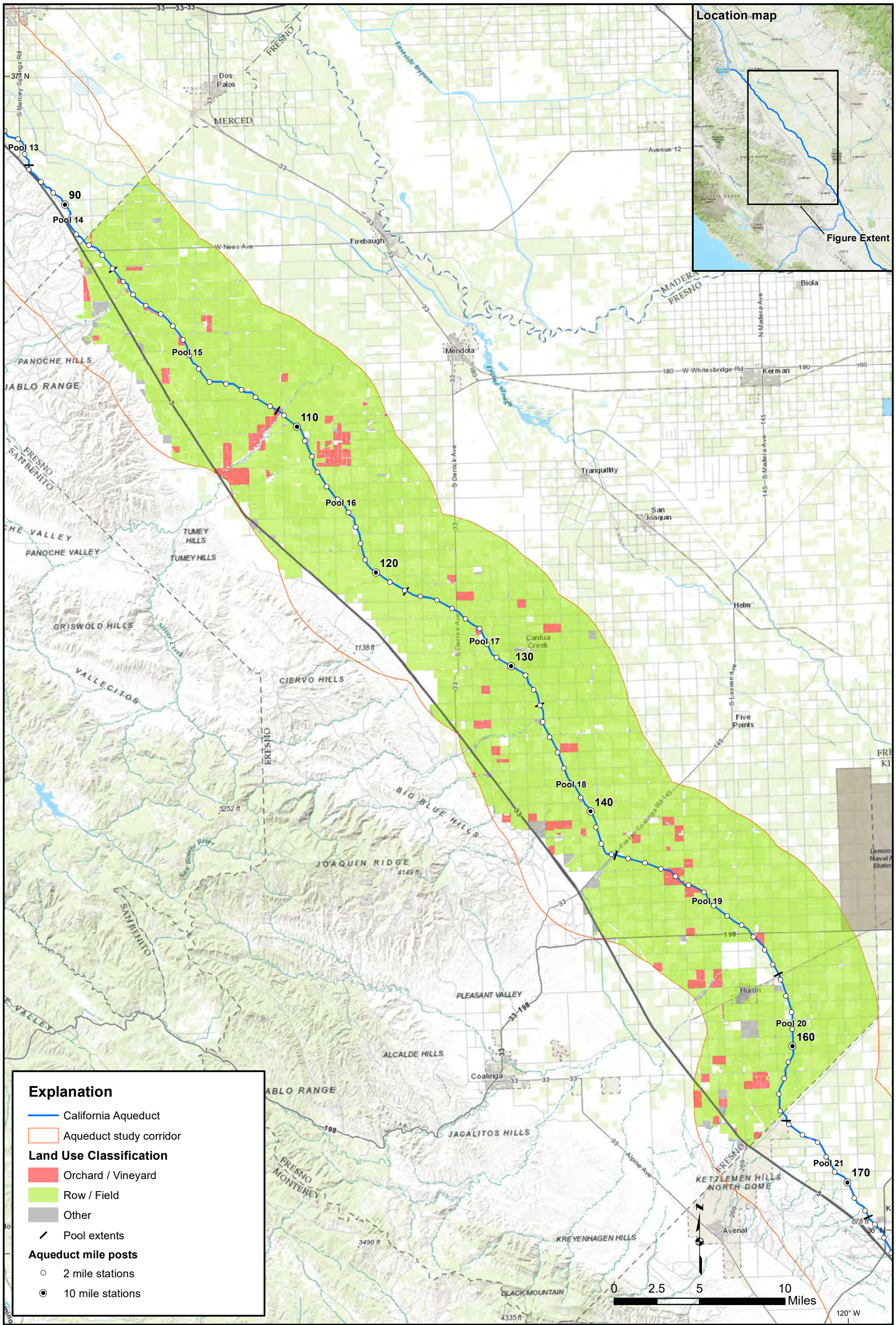

DEPARTMENT OF WATER RESOURCES
STATE WATER PROJECT
CALIFORNIA AQUEDUCT SUBSIDENCE STUDY

FIGURE A-5
LAND USE MAPS
FRESNO COUNTY 1986

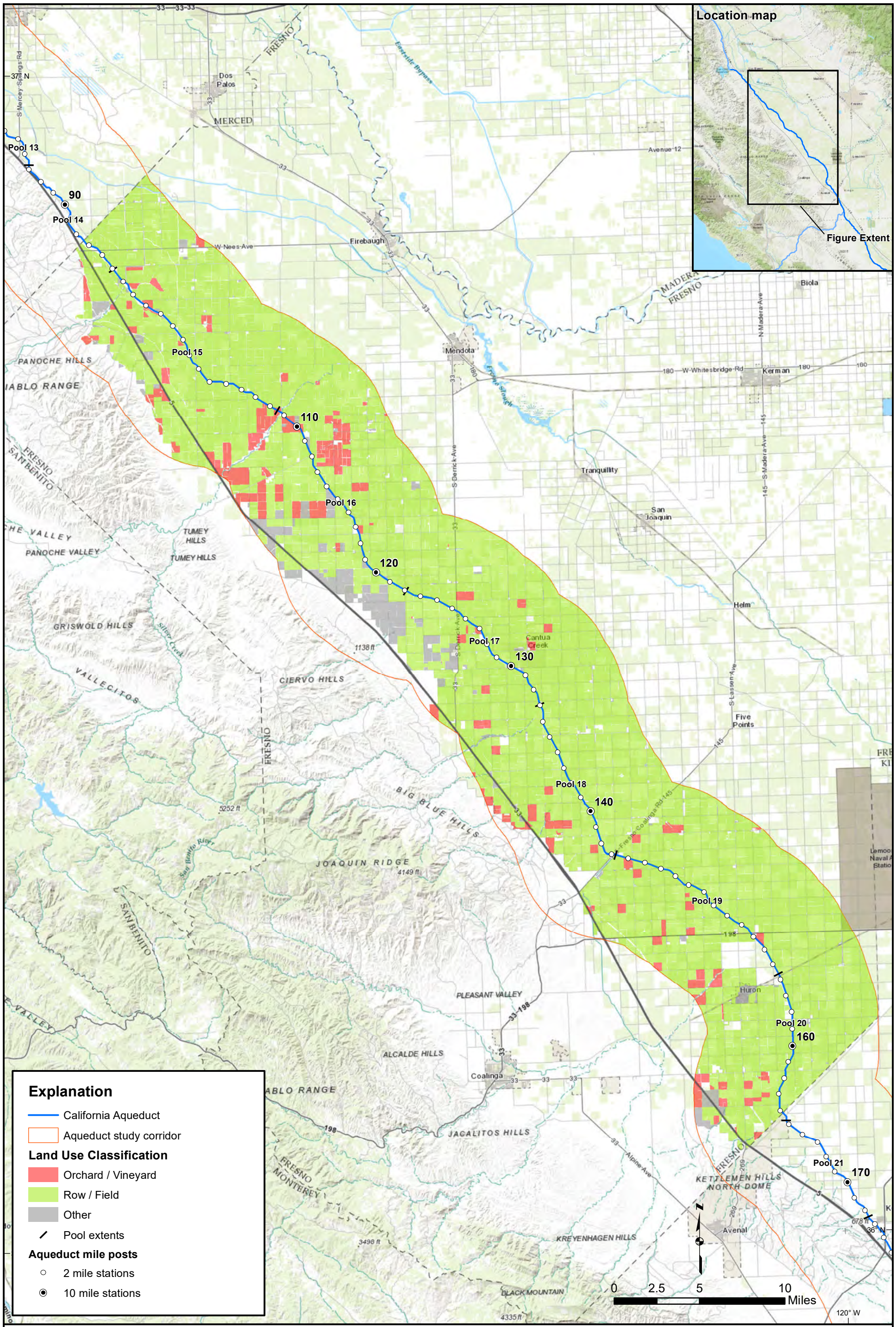

DEPARTMENT OF WATER RESOURCES
STATE WATER PROJECT
CALIFORNIA AQUEDUCT SUBSIDENCE STUDY

FIGURE A-6
LAND USE MAPS
FRESNO COUNTY 1994

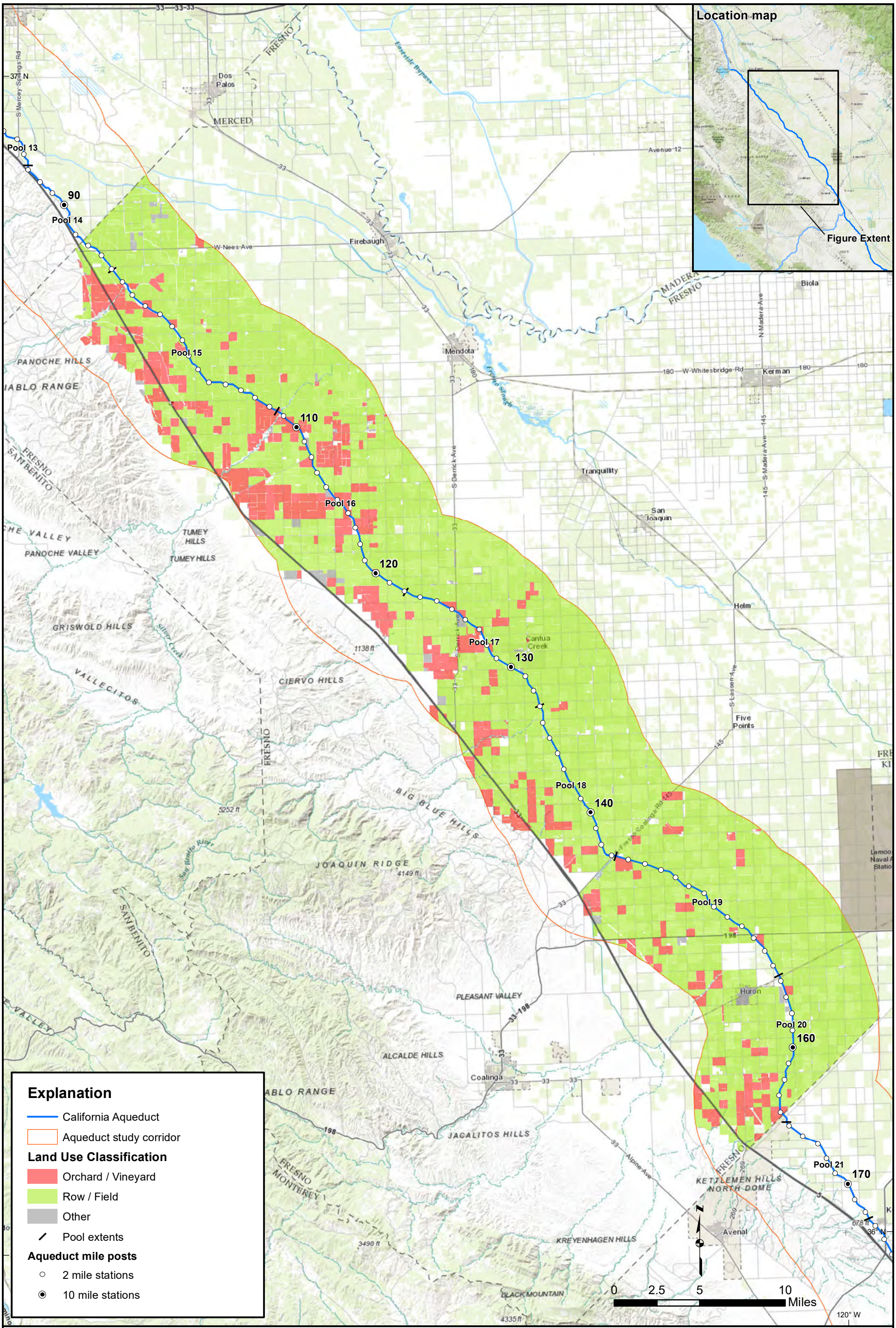

DEPARTMENT OF WATER RESOURCES
STATE WATER PROJECT
CALIFORNIA AQUEDUCT SUBSIDENCE STUDY

FIGURE A-7
LAND USE MAPS
FRESNO COUNTY 2000

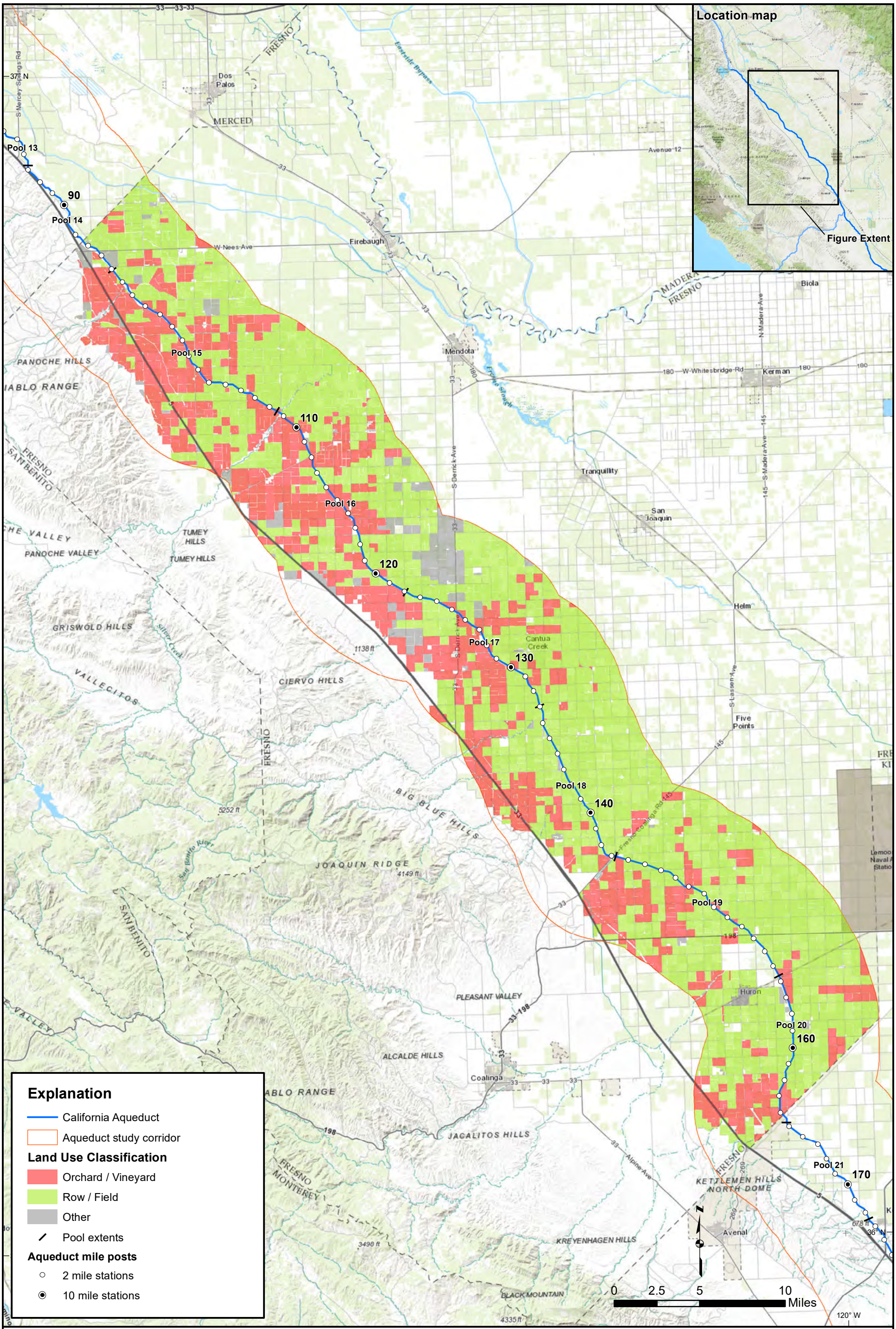

DEPARTMENT OF WATER RESOURCES
STATE WATER PROJECT
CALIFORNIA AQUEDUCT SUBSIDENCE STUDY

FIGURE A-8
LAND USE MAPS
FRESNO COUNTY 2008

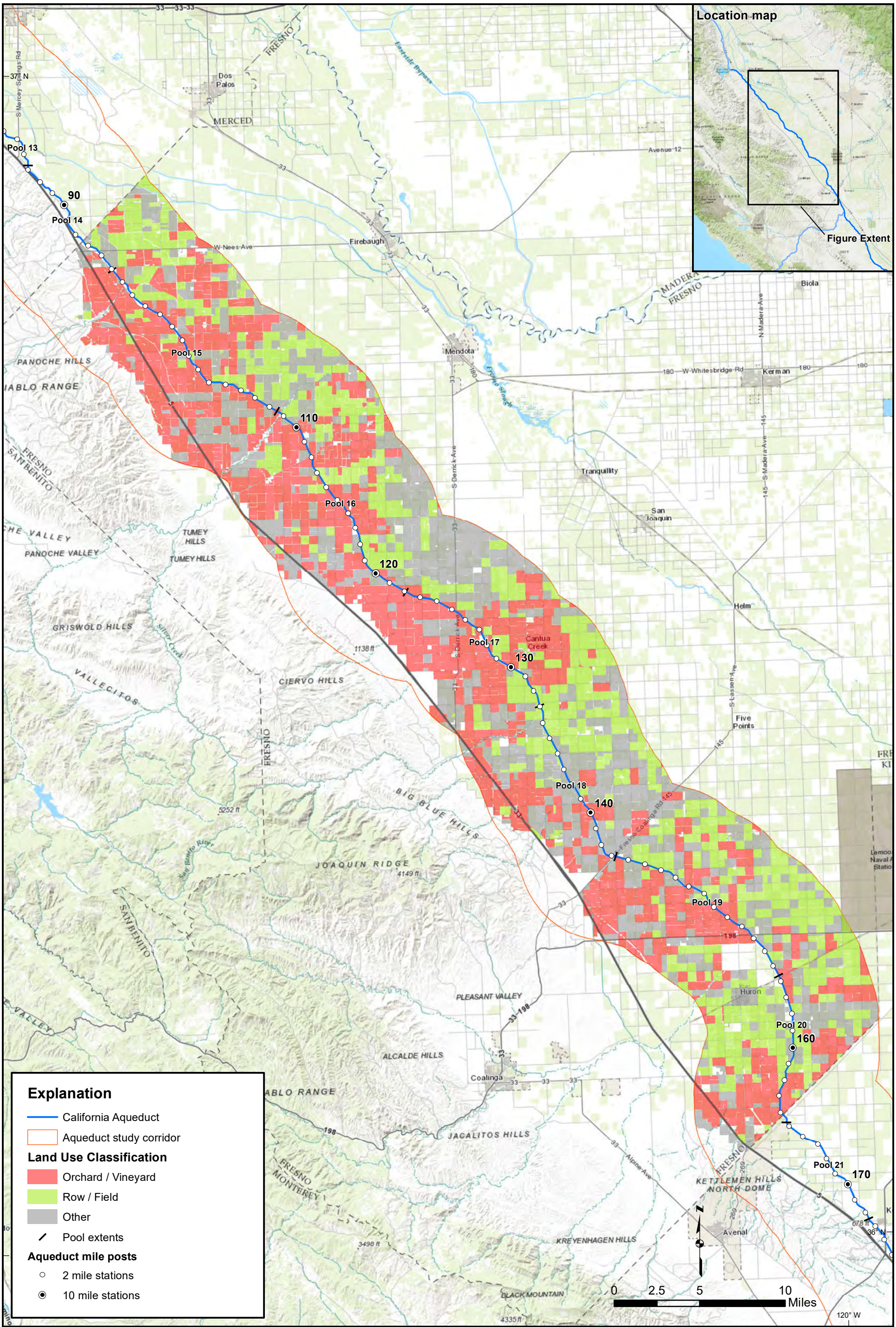

DEPARTMENT OF WATER RESOURCES
STATE WATER PROJECT
CALIFORNIA AQUEDUCT SUBSIDENCE STUDY

FIGURE A-9
LAND USE MAPS
FRESNO COUNTY 2014

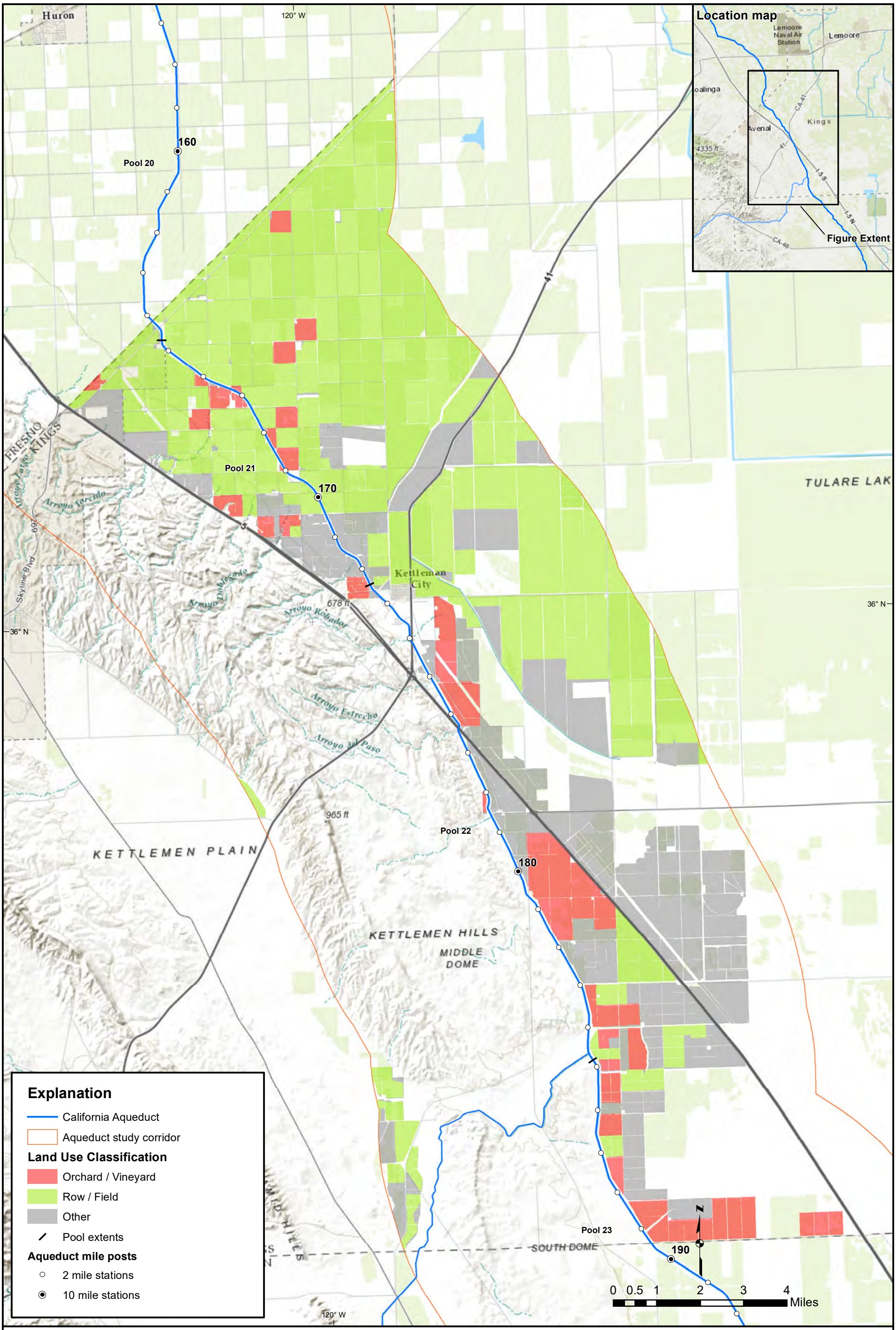

DEPARTMENT OF WATER RESOURCES
STATE WATER PROJECT
CALIFORNIA AQUEDUCT SUBSIDENCE STUDY

FIGURE A-10
LAND USE MAPS
KINGS COUNTY 1991

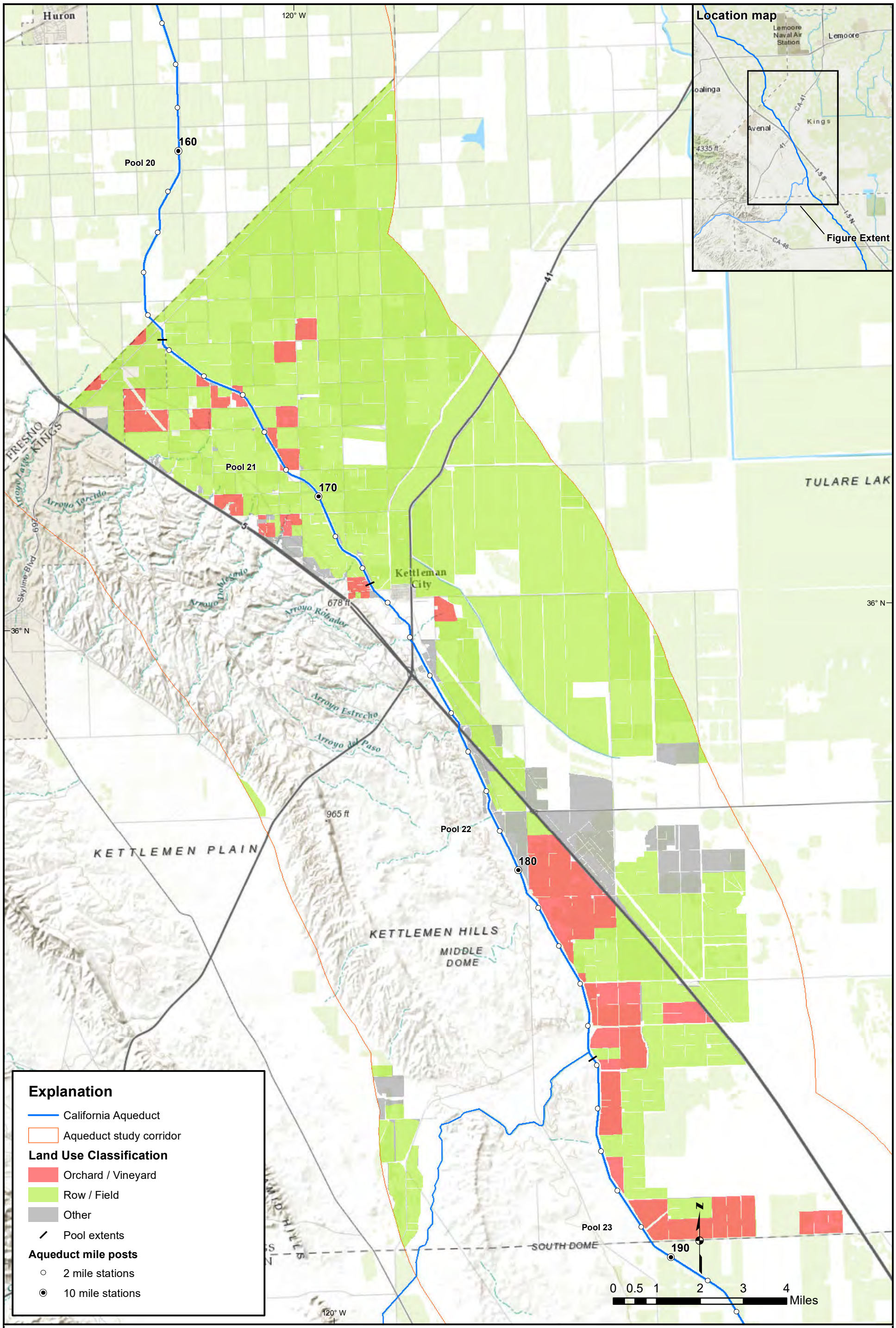

DEPARTMENT OF WATER RESOURCES
STATE WATER PROJECT
CALIFORNIA AQUEDUCT SUBSIDENCE STUDY

FIGURE A-11
LAND USE MAPS
KINGS COUNTY 1996

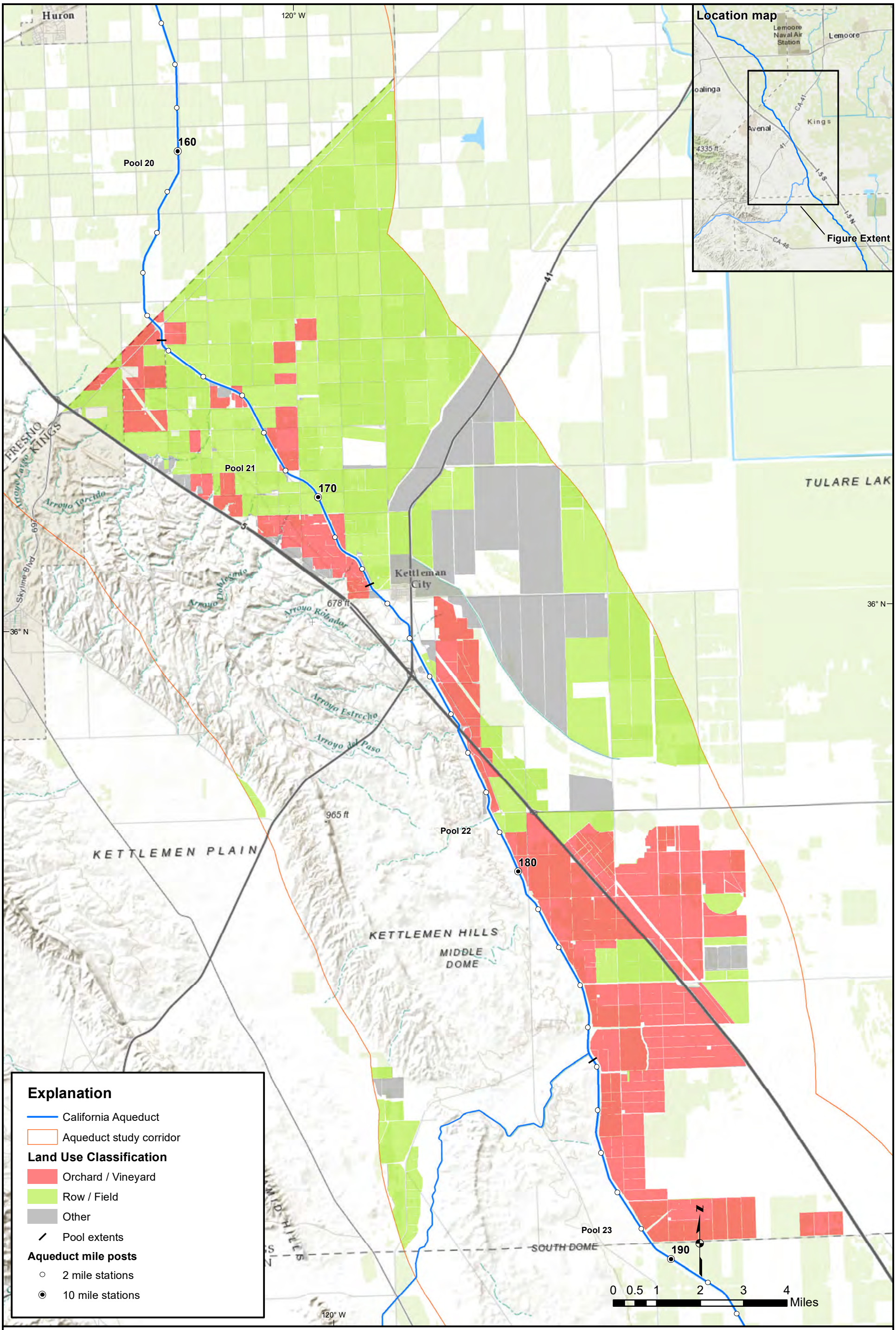

DEPARTMENT OF WATER RESOURCES
STATE WATER PROJECT
CALIFORNIA AQUEDUCT SUBSIDENCE STUDY

FIGURE A-12
LAND USE MAPS
KINGS COUNTY 2003

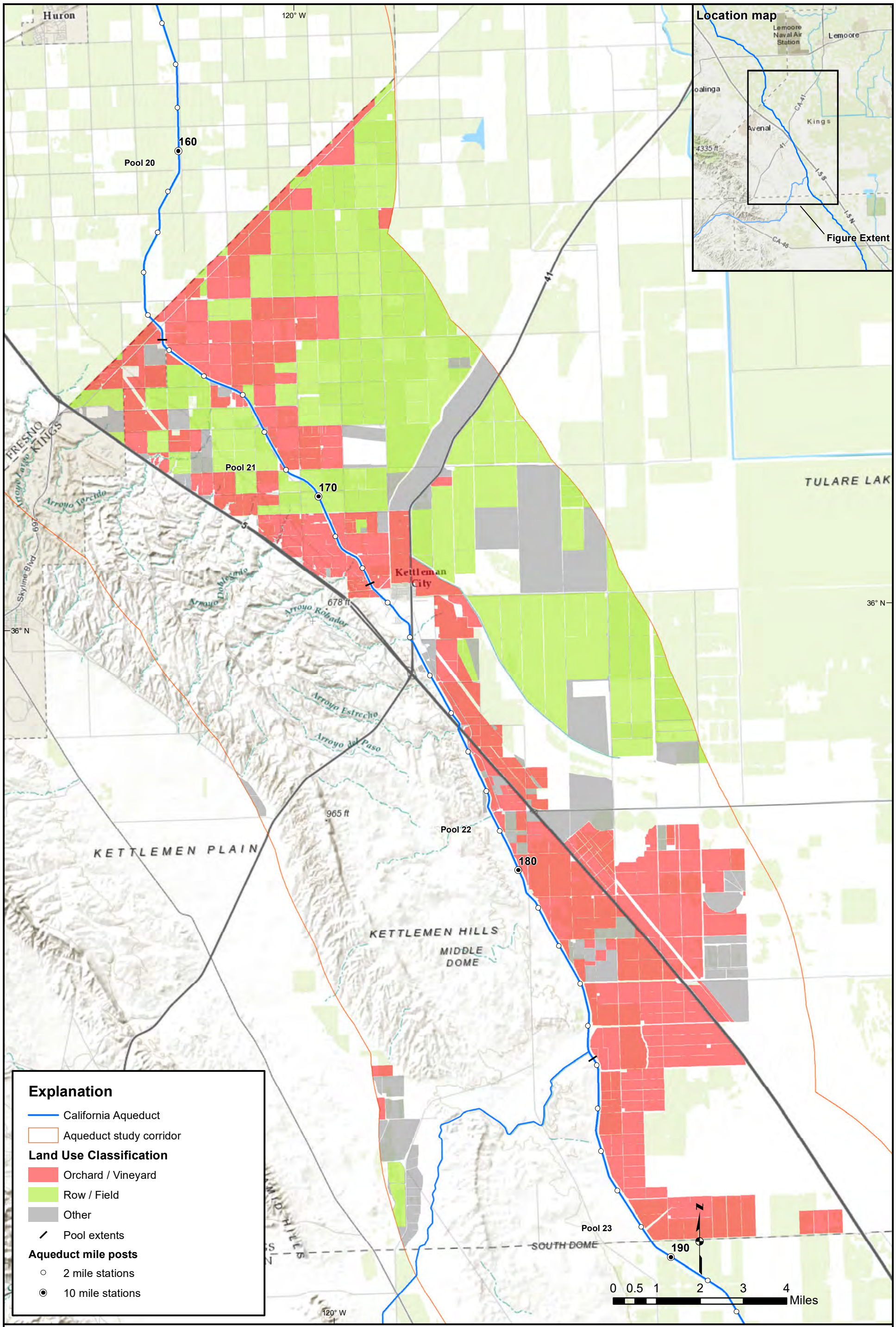

DEPARTMENT OF WATER RESOURCES
STATE WATER PROJECT
CALIFORNIA AQUEDUCT SUBSIDENCE STUDY

FIGURE A-13
LAND USE MAPS
KINGS COUNTY 2013

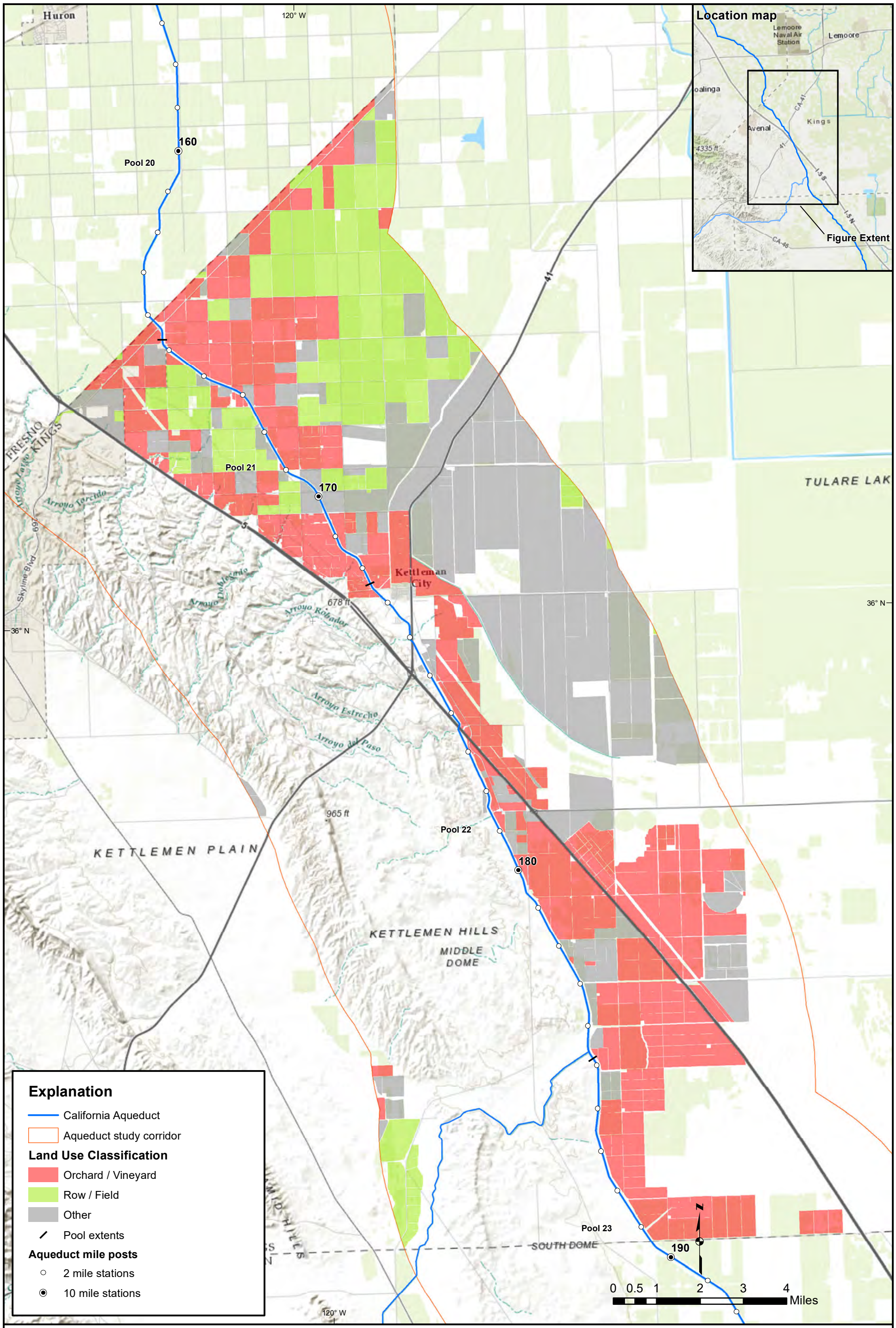

DEPARTMENT OF WATER RESOURCES
STATE WATER PROJECT
CALIFORNIA AQUEDUCT SUBSIDENCE STUDY

FIGURE A-14
LAND USE MAPS
KINGS COUNTY 2014

Location map

Figure Extent

Explanation

California Aqueduct

Aqueduct study corridor

Land Use Classification

Orchard / Vineyard

Row / Field

Other

Pool extents

Aqueduct mile posts

2 mile stations

10 mile stations

0 2 4 8 12 16 Miles

DEPARTMENT OF WATER RESOURCES
STATE WATER PROJECT
CALIFORNIA AQUEDUCT SUBSIDENCE STUDY

FIGURE A-15
LAND USE MAPS
KERN COUNTY 1990

Location map

Figure Extent

Explanation

California Aqueduct

Aqueduct study corridor

Land Use Classification

Orchard / Vineyard

Row / Field

Other

Pool extents

Aqueduct mile posts

2 mile stations

10 mile stations

0 2 4 8 12 16 Miles

DEPARTMENT OF WATER RESOURCES
STATE WATER PROJECT
CALIFORNIA AQUEDUCT SUBSIDENCE STUDY

FIGURE A-16
LAND USE MAPS
KERN COUNTY 1998

Location map

Figure Extent

Explanation

California Aqueduct

Aqueduct study corridor

Land Use Classification

Orchard / Vineyard

Row / Field

Other

Pool extents

Aqueduct mile posts

2 mile stations

10 mile stations

0 2 4 8 12 16 Miles

DEPARTMENT OF WATER RESOURCES
STATE WATER PROJECT
CALIFORNIA AQUEDUCT SUBSIDENCE STUDY

FIGURE A-17
LAND USE MAPS
KERN COUNTY 2006

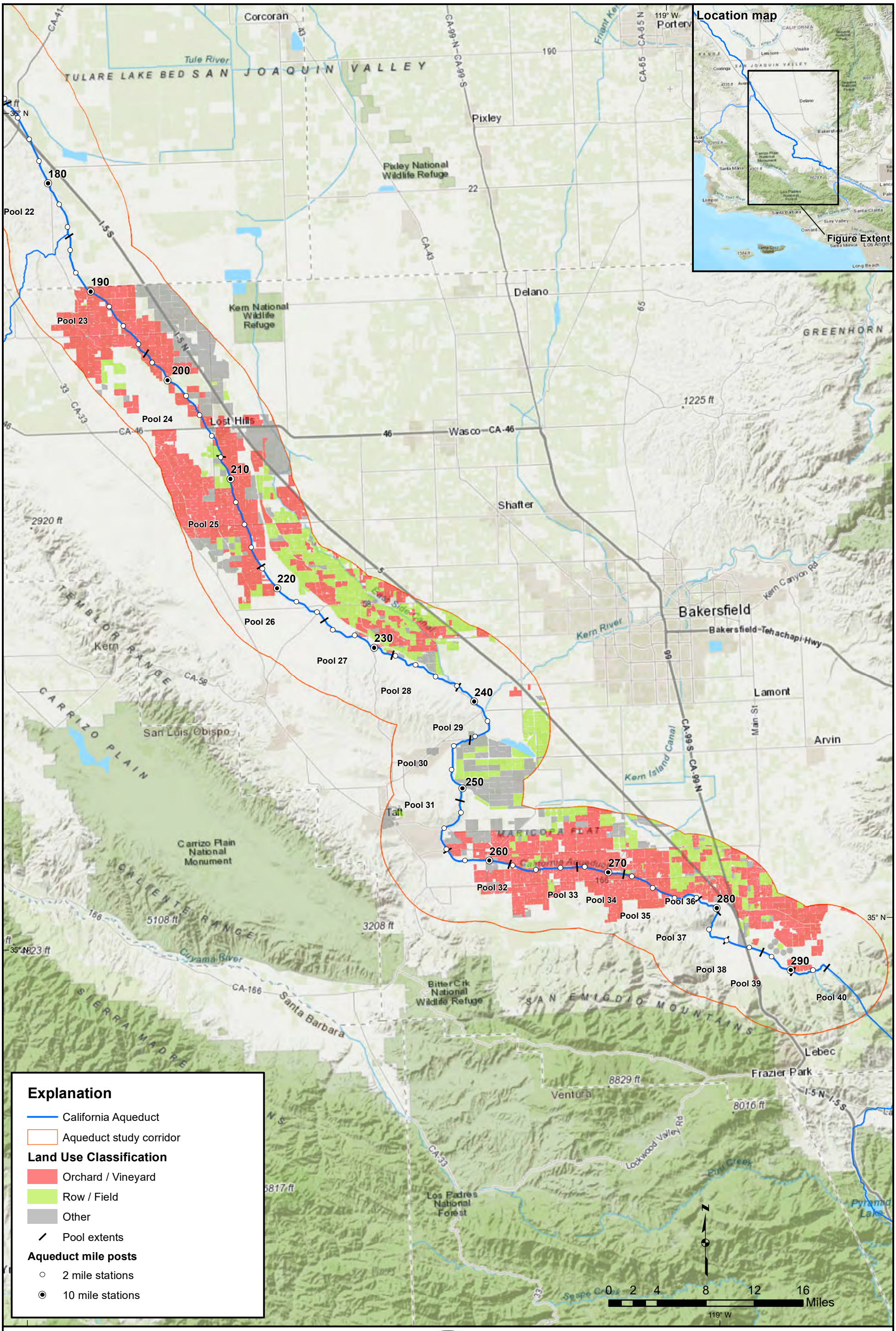

DEPARTMENT OF WATER RESOURCES
STATE WATER PROJECT
CALIFORNIA AQUEDUCT SUBSIDENCE STUDY

FIGURE A-18
LAND USE MAPS
KERN COUNTY 2014

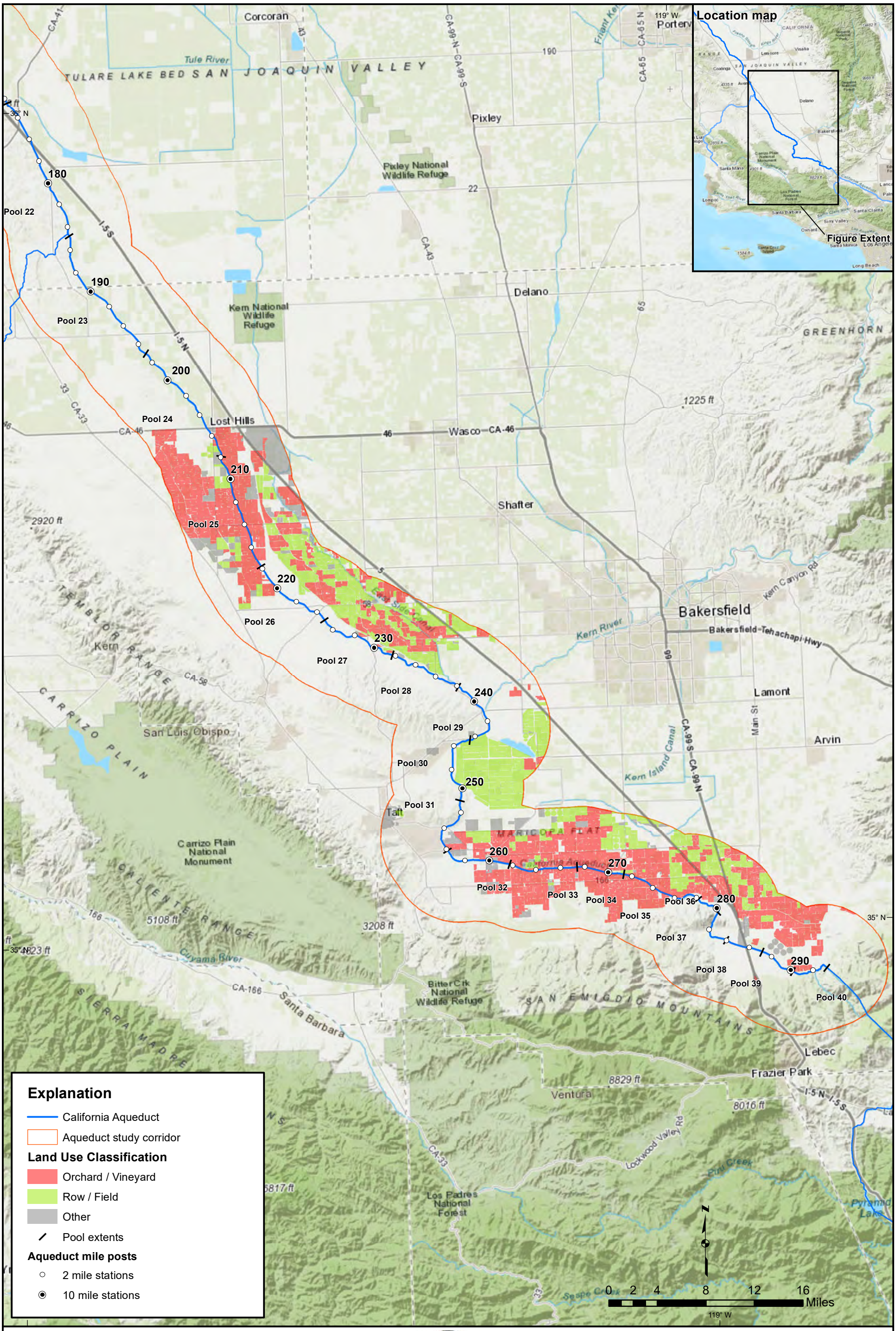

DEPARTMENT OF WATER RESOURCES
STATE WATER PROJECT
CALIFORNIA AQUEDUCT SUBSIDENCE STUDY

FIGURE A-19
LAND USE MAPS
KERN COUNTY 2015

DEPARTMENT OF WATER RESOURCES
STATE WATER PROJECT
CALIFORNIA AQUEDUCT SUBSIDENCE STUDY

FIGURE A-20
ALL WELLS IN DWR DATABASE
STUDY AREA

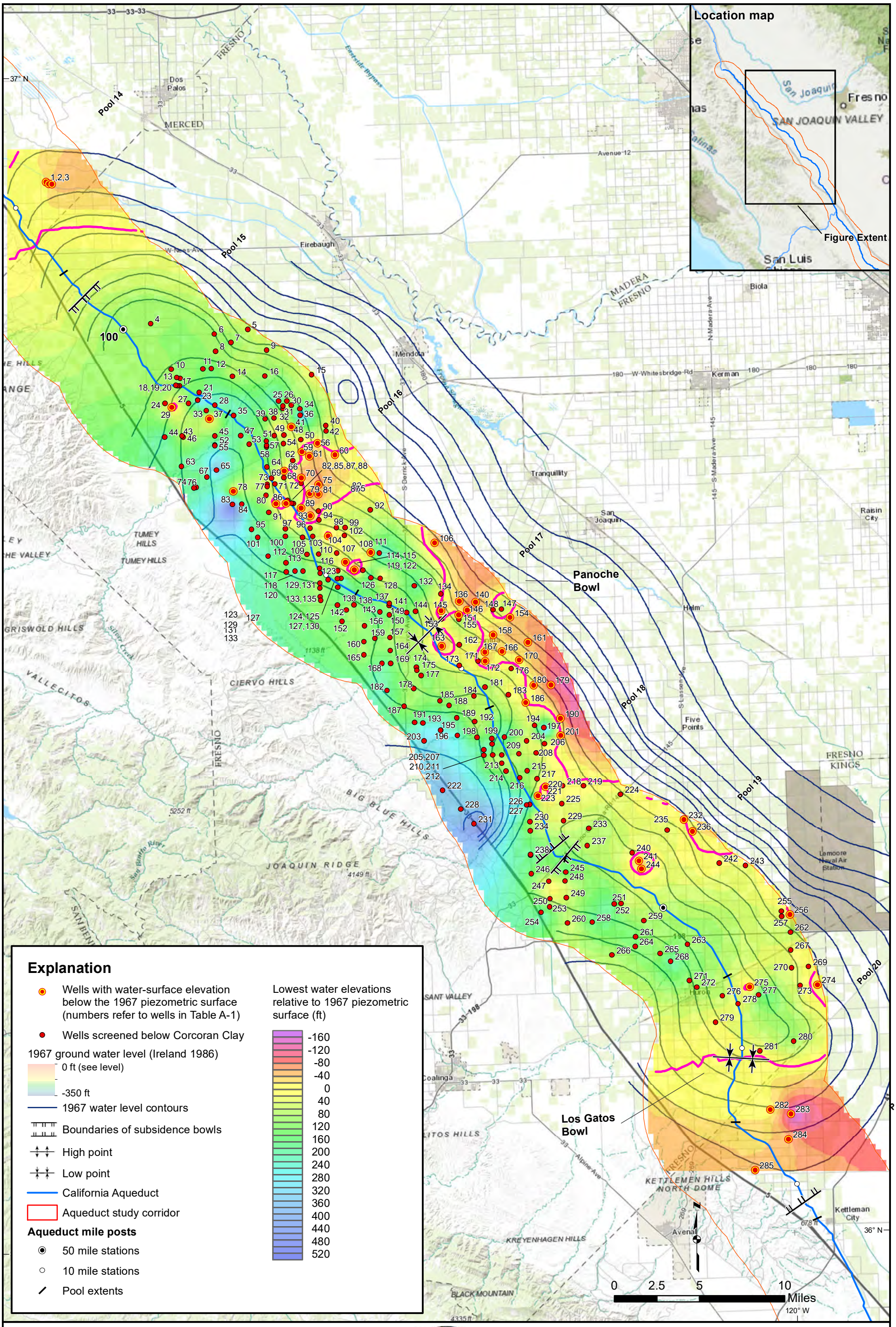

DEPARTMENT OF WATER RESOURCES
STATE WATER PROJECT
CALIFORNIA AQUEDUCT SUBSIDENCE STUDY

FIGURE A-21

WELLS WITH SCREENED INTERVALS
BELOW CORCORAN CLAY

Table A-1: Wells with water-surface elevation below the 1967 piezometric surface

Label	Site ID	Ground Surface Elevation	Depth of Well (BGS)	Top of perforated section (BGS)	Bottom of perforated section (BGS)	Base of Corcoran Clay (BGS)	1967 low water level (BGS)	Low water level (BGS)	Date of lowest recorded water level	Feet below 1967 piezometric surface
1	93034	167.3	700	400	680	359.3	180.8	194.75	10/19/2016	14.0
2	93035	166.3	615	365	615	361.7	181.6	229.85	10/14/2015	48.3
3	93037	164.0	600	360	600	365.9	180.3	230.56	10/14/2015	50.3
4	87263	265.1	1002	542	982	461.4	458.0	360.9	10/13/2016	
5	91200	240.3	1330	600	1050	583.2	347.2	294	12/7/2015	
6	60841	256.3	1323	602	1323	575.4	432.0	339	12/13/2013	
7	51765	259.4	1050	670	920	581.0	406.0	302	11/21/2011	
8	51768	274.4	1200	678	1196	577.4	461.7	374	9/30/2015	
9	51759	249.4	1500	708	1450	614.6	389.3	310	9/30/2015	
10	94830	318.6	1000	740	950	550.3	520.1	420	1/2/2015	
11	95419	302.8	1200	678	1200	626.9	515.4	372	12/11/2015	
12	95418	300.2	1202	682	1202	629.6	512.4	354	12/7/2015	
13	91204	330.6	1002	642	1002	610.5	542.2	N/A	11/21/2011	
14	95394	294.0	1224	728	1210	681.6	508.1	441	6/24/2015	
15	94968	240.0	1170	620	1110	608.0	375.6	361	9/23/2014	
16	91214	274.5	1160	660	1140	654.5	459.3	372	10/29/2015	
17	91203	326.3	1042	642	1042	614.5	541.1	N/A	11/21/2011	
18	91211	340.6	992	632	992	593.7	559.3	N/A	11/21/2011	
19	50888	337.6	980	750	960	593.7	558.0	450	6/10/2016	
20	50887	332.6	1150	700	1150	595.5	554.7	N/A	11/21/2011	
21	50872	337.3	1250	743	1250	707.0	580.4	451	1/3/2017	
22	50874	341.0	2180	869	2180	694.3	591.2	128	12/5/2013	
23	53816	344.0	1838	809	1838	697.3	594.2	454	5/12/2016	
24	50843	366.3	1768	606	1768	502.7	583.7	493.9	5/6/1958	
25	53844	279.0	1458	695	1458	678.9	473.7	167	11/14/2011	
26	53847	275.5	1520	700	1400	668.7	461.5	379	5/12/2016	
27	94826	351.6	1242	722	1242	630.6	597.6	456	10/29/2015	
28	53809	336.6	1300	980	1300	752.6	596.7	355	11/27/2012	
29	50844	363.8	1220	603	1220	551.9	590.9	612	3/27/1962	21.1
30	53850	275.3	1360	700	1352	686.6	459.4	326	12/6/2013	
31	93983	283.5	1042	682	1042	686.4	477.4	N/A	12/5/2013	
32	53849	284.3	1405	703	1405	697.2	480.0	469	12/29/1966	
33	95975	349.5	1230	817	1220	723.6	611.0	438	2/11/2016	
34	91237	270.3	1080	680	1080	672.8	446.0	295	11/27/2012	
35	53808	338.6	1263	783	1263	790.7	603.7	399	1/2/2015	
36	50709	282.0	1483	712	1483	714.4	461.4	134	11/27/2012	
37	53819	358.7	1840	819	1840	738.9	625.2	666.5	12/16/1968	41.3
38	53853	301.3	1130	770	970	737.2	515.6	438	10/29/2015	
39	53830	313.5	1400	800	1400	779.3	545.3	422	12/19/2016	
40	50710	260.5	988	768	988	695.0	397.7	382	11/22/2013	
41	96151	293.1	1200	740	1200	740.1	490.3	500	4/26/2016	9.7

Table A-1: Wells with water-surface elevation below the 1967 piezometric surface

Label	Site ID	Ground Surface Elevation	Depth of Well (BGS)	Top of perforated section (BGS)	Bottom of perforated section (BGS)	Base of Corcoran Clay (BGS)	1967 low water level (BGS)	Low water level (BGS)	Date of lowest recorded water level	Feet below 1967 piezometric surface
42	91238	258.3	1162	722	1162	700.3	397.9	305	11/27/2012	
43	91213	394.4	962	642	962	592.3	646.0	N/A	1/6/2011	
44	91212	422.9	720	520	720	518.0	650.9	439	12/9/2009	
45	53824	372.7	1373	790	1373	768.3	645.5	526	1/25/1979	
46	50849	396.7	1001	649	1001	599.3	649.8	591.6	4/27/2017	
47	91216	348.6	1050	840	1040	818.8	619.1	423	1/5/2015	
48	48716	306.5	879	863	873	777.4	519.0	468.8	5/6/2014	
49	95378	316.1	1259	803	1245	799.1	543.0	542	8/26/2015	
50	50681	287.5	1503	797	1503	765.8	479.3	453.5	12/20/1968	
51	53842	328.6	1526	809	1526	818.5	576.9	251	1/11/2011	
52	53798	381.7	1200	800	1200	767.3	655.9	385	11/20/1996	
53	91226	353.6	1042	842	1042	822.7	621.3	543	5/12/2016	
54	53837	310.5	1487	799	1487	803.1	527.4	489	5/10/2016	
55	91229	382.7	1222	822	1222	769.0	656.9	478	12/4/2015	
56	91240	266.3	1430	740	1410	739.0	427.8	449	5/2/2016	21.2
57	53781	329.6	1408	857	1408	823.7	577.8	521	12/20/1968	
58	53780	329.6	1516	830	1508	825.0	578.2	N/A	12/17/1965	
59	91241	287.5	1190	805	1165	796.5	481.4	490	5/2/2016	8.6
60	50687	255.5	1292	707	1292	712.8	388.1	389	12/19/2016	0.9
61	50684	280.5	1406	802	1406	790.0	462.0	503	12/17/1965	41.0
62	94818	300.0	1420	850	1414	816.8	508.8	460	5/10/2016	
63	50855	435.8	1035	654	1035	622.6	686.0	510	6/10/2016	
64	53758	333.6	1945	832	1945	839.3	585.7	468	5/10/2016	
65	74578	403.7	1200	800	1200	790.6	681.1	317	1/3/2007	
66	74628	313.5	1920	825	1920	829.3	536.1	540.4	3/28/1962	4.3
67	74581	422.7	1200	760	1160	723.2	695.7	521	6/2/2016	
68	91243	317.3	1244	884	1244	823.3	542.5	491	11/24/2014	
69	91244	336.3	1202	882	1202	845.1	585.8	558	12/9/2016	
70	63959	295.5	1505	808	1505	803.7	496.3	564	12/29/1966	67.7
71	91245	336.3	1244	884	1244	831.8	581.5	527	12/9/2016	
72	91242	298.5	1142	842	1142	801.9	501.0	486	12/9/2016	
73	74631	350.3	1959	880	1959	852.5	606.0	585	9/30/2015	
74	74616	450.7	1183	640	1100	637.1	712.3	486	12/3/2015	
75	91383	276.5	1340	900	1300	778.8	456.3	515	10/29/2015	58.7
76	74621	452.7	1115	730	950	621.5	711.8	554.69	5/4/2017	
77	95620	355.3	1204	914	1190	852.6	611.4	587	5/16/2015	
78	74538	421.6	1426	842	1426	825.2	700.0	710	12/30/1966	10.0
79	94965	286.0	1240	840	1220	792.2	480.2	532	6/25/2014	51.8
80	91246	375.6	1209	907	1209	857.9	634.6	556.2	5/4/2017	
81	91384	277.6	1202	802	1202	776.5	462.9	510	5/24/2016	47.1
82	74550	337.6	1220	905	1220	820.7	567.4	510	12/7/2016	

Table A-1: Wells with water-surface elevation below the 1967 piezometric surface

Label	Site ID	Ground Surface Elevation	Depth of Well (BGS)	Top of perforated section (BGS)	Bottom of perforated section (BGS)	Base of Corcoran Clay (BGS)	1967 low water level (BGS)	Low water level (BGS)	Date of lowest recorded water level	Feet below 1967 piezometric surface
83	91380	460.0	1280	910	1260	816.5	740.3	97	12/3/2013	
84	91379	447.6	1250	910	1230	851.0	725.4	628	9/30/2015	
85	91247	331.6	1310	890	1290	814.1	557.2	443	12/4/2013	
86	91249	369.6	1170	920	1160	847.6	619.1	681	9/30/2015	61.9
87	91248	344.6	1207	906	1207	824.2	578.9	622.2	5/2/2017	43.3
88	74554	326.3	1611	860	1611	810.0	549.5	469.4	1/7/1972	
89	95941	311.6	1160	840	1160	811.9	527.4	549	1/22/2016	21.6
90	95976	287.1	1200	780	1180	759.0	485.1	474	2/27/2016	
91	74560	406.3	1613	930	1613	892.6	667.0	542	6/2/2016	
92	95942	222.1	1920	860	1900	709.2	387.7	341	2/14/2016	
93	94967	311.6	1270	810	1250	790.8	526.8	578	10/17/2014	51.2
94	91389	293.6	1480	820	1460	760.2	509.5	463	11/25/2014	
95	74574	494.7	1765	918	1765	912.7	779.6	595.5	5/4/2017	
96	91387	322.6	1270	850	1250	800.0	557.4	512	12/6/2016	
97	91381	392.6	1490	930	1490	885.5	647.1	625	6/2/2016	
98	63894	261.6	1942	714	1942	709.4	484.9	435	10/28/2015	
99	95956	248.1	1970	790	1950	703.7	463.4	405	3/13/2016	
100	63978	400.7	1849	917	1849	896.0	661.1	496	9/28/2015	
101	63974	483.7	1770	920	1770	916.2	768.7	583	12/5/2016	
102	63895	249.6	1458	743	1262	694.4	478.9	477	10/28/2015	
103	63892	332.6	1265	865	1265	810.5	577.8	504	11/25/2014	
104	94829	285.6	1162	842	1162	744.6	525.2	526	10/28/2015	0.8
105	96073	353.3	1505	880	1505	835.6	603.5	531	12/5/2016	
106	93972	189.3	1162	600	1162	607.4	322.8	369	10/28/2015	46.2
107	94834	272.7	1400	780	1380	744.1	528.6	519	10/23/2015	
108	63903	230.7	1500	700	1500	649.4	451.6	456	10/23/2015	4.4
109	91391	353.7	1242	842	1242	822.6	622.6	539	12/5/2016	
110	91390	315.7	1220	862	1220	790.9	581.6	512	12/6/2016	
111	74429	227.3	1130	700	1130	650.3	440.4	165	5/7/2014	
112	95809	480.7	2195	968	2195	924.1	773.2	572.55	5/4/2017	
113	94937	431.0	2471	893	2455	894.6	719.1	600	10/28/2015	
114	91388	266.7	1530	910	1510	725.4	527.2	586	5/27/2016	58.8
115	91393	267.7	1320	800	1280	726.5	528.3	335	4/9/2010	
116	91392	327.8	1310	848	1310	747.2	610.8	519	12/6/2016	
117	74532	402.8	1926	884	1926	819.7	696.4	466	12/5/2016	
118	74425	372.8	1800	915	1800	771.7	663.1	556	10/28/2015	
119	91394	262.7	1040	720	1040	701.2	524.5	643.31	5/11/2017	118.8
120	91406	452.9	2445	920	1820	886.6	751.2	620.14	5/4/2017	
121	73764	294.8	1747	731	1747	729.7	573.8	536	10/28/2015	
122	73761	257.7	1558	760	1558	687.1	509.2	450	12/6/2016	
123	94832	340.8	2390	847	2380	741.3	629.3	486	12/22/2014	

Table A-1: Wells with water-surface elevation below the 1967 piezometric surface

Label	Site ID	Ground Surface Elevation	Depth of Well (BGS)	Top of perforated section (BGS)	Bottom of perforated section (BGS)	Base of Corcoran Clay (BGS)	1967 low water level (BGS)	Low water level (BGS)	Date of lowest recorded water level	Feet below 1967 piezometric surface
124	73765	306.4	1743	734	1743	730.1	591.6	287	12/5/2011	
125	94831	317.8	2030	967	2010	736.9	605.4	555	9/25/2014	
126	73763	275.7	2018	718	2018	727.3	528.6	338	12/5/2011	
127	73775	340.8	1769	813	1769	741.7	633.4	452	1/2/2013	
128	73759	272.7	1120	750	960	730.4	519.2	515	10/28/2015	
129	95121	378.9	2010	905	1989	756.2	677.9	577	12/22/2014	
130	94406	354.8	2120	860	2100	770.1	650.6	515	12/22/2014	
131	91407	405.9	2305	925	2165	768.7	708.3	636	12/12/2016	
132	73735	256.7	1900	734	1890	684.0	487.8	303	12/10/2009	
133	95324	444.8	2230	846	2210	803.0	753.0	645	12/2/2015	
134	73739	246.7	1380	656	1380	619.0	446.9	444	11/9/2016	
135	95325	458.3	2131	855	2120	816.6	768.8	674	12/12/2016	
136	94828	244.7	1395	680	1385	627.8	404.3	433	11/9/2016	28.7
137	73790	327.7	1340	940	1340	821.0	600.8	537	4/28/2016	
138	91409	382.8	2190	880	1510	859.8	685.9	546	12/22/2014	
139	91410	420.8	2230	930	2110	857.1	729.5	590	12/22/2014	
140	93779	243.7	1162	682	1142	637.0	378.3	444	10/23/2015	65.7
141	63232	332.8	1634	880	1634	826.5	608.1	532	12/1/2015	
142	95977	431.8	2260	927	2250	868.0	740.9	652	5/3/2016	
143	63237	358.8	2803	1000	2803	859.4	650.0	479	12/22/2014	
144	91421	309.7	1262	942	1262	737.1	561.9	490	12/4/2014	
145	91420	267.7	1200	840	1200	650.8	475.6	501	10/23/2015	25.4
146	91419	253.7	1125	725	1125	651.2	413.9	478	11/9/2016	64.1
147	92446	234.7	1075	680	1075	639.8	350.9	270	12/3/2010	
148	63138	240.7	1100	676	1076	645.9	365.8	337	1/3/2014	
149	63096	328.7	1980	806	1980	782.6	590.1	446	10/23/2015	
150	95132	356.8	2386	1092	2370	844.7	636.3	542	12/1/2015	
151	95982	263.1	1220	800	1200	658.5	444.7	465	11/9/2016	20.3
152	63142	498.0	2027	900	2027	870.2	813.7	N/A	12/5/2011	
153	95957	286.3	1180	701	1160	680.5	500.0	498	11/9/2016	
154	95777	237.3	1302	682	1282	666.5	355.6	396	11/18/2015	40.4
155	63111	269.7	1816	750	1801	688.5	460.0	360	1/3/2014	
156	91411	417.9	1855	1335	1835	834.2	727.0	628	12/1/2015	
157	91412	414.8	1700	907	1700	822.8	695.1	624	12/12/2016	
158	91424	265.7	1120	760	1120	722.6	439.7	475	10/23/2015	35.3
159	91414	435.9	2220	840	2200	820.4	736.9	620	12/22/2014	
160	91415	461.9	1880	1380	1860	802.2	770.5	667	12/2/2015	
161	73549	244.8	995	675	995	679.9	378.3	426	11/5/2015	47.7
162	63130	302.7	1180	680	1160	682.6	525.4	499	11/23/2015	
163	91427	320.4	2270	795	2250	695.2	555.2	602	12/1/2016	46.8
164	91413	452.8	2100	840	1400	829.1	733.3	629	12/12/2016	

Table A-1: Wells with water-surface elevation below the 1967 piezometric surface

Label	Site ID	Ground Surface Elevation	Depth of Well (BGS)	Top of perforated section (BGS)	Bottom of perforated section (BGS)	Base of Corcoran Clay (BGS)	1967 low water level (BGS)	Low water level (BGS)	Date of lowest recorded water level	Feet below 1967 piezometric surface
165	63163	504.9	2050	964	1695	811.3	810.7	725	12/2/2015	
166	91425	274.0	1202	802	1202	726.1	467.7	488	11/14/2016	20.3
167	63127	288.8	1198	738	1197	722.9	501.8	506	11/14/2016	4.2
168	91416	502.9	1770	909	1770	818.1	793.5	603	12/22/2014	
169	63165	477.9	2200	841	2104	826.1	759.7	634	12/22/2014	
170	91444	267.8	1202	802	1202	697.3	451.2	473	12/10/2014	21.8
171	63037	304.0	1817	722	1817	642.4	532.9	N/A	12/9/2011	
172	91428	297.8	1300	700	1300	672.3	522.0	551	11/14/2016	29.0
173	63082	325.0	2792	1013	2792	610.1	568.6	N/A	12/9/2011	
174	63077	401.8	2607	802	2131	789.1	662.9	551	12/26/2014	
175	95609	398.7	1900	795	1900	779.0	661.2	603	4/30/2015	
176	73553	280.8	1270	722	1246	690.0	490.0	464	11/14/2016	
177	60230	387.8	1490	828	1490	752.9	650.5	520	11/4/2016	
178	95039	420.5	2121	770	2101	728.0	697.3	620	11/4/2016	
179	93739	247.9	1202	742	1202	675.4	423.7	535	11/5/2015	111.3
180	91476	268.8	1340	800	1180	681.1	472.8	488	10/26/2015	15.2
181	91469	324.8	1322	962	1322	613.8	587.0	497	12/8/2014	
182	95423	510.6	2320	803	2310	754.7	808.1	604	11/3/2016	
183	91475	307.9	1570	1000	1400	662.8	551.0	538	11/7/2016	
184	94624	343.9	1455	680	1442	619.5	621.3	568	10/26/2015	
185	60246	392.9	2529	861	2529	627.3	673.9	559	10/26/2015	
186	94311	288.9	1340	800	1320	686.0	512.4	514	11/5/2015	1.6
187	60268	440.9	1982	954	1982	682.7	740.8	645	11/5/2015	
188	60197	384.0	2600	902	2600	619.9	672.7	N/A	12/8/2011	
189	60199	386.0	2953	902	2953	616.8	690.6	N/A	12/8/2011	
190	93751	248.9	1200	802	1200	685.2	449.5	540	11/9/2016	90.5
191	95084	447.3	2207	866	2190	630.7	758.2	570	11/4/2016	
192	60219	362.9	1500	842	1500	619.3	661.5	602	10/26/2015	
193	60206	441.0	1512	850	1512	620.5	752.3	509	11/4/2016	
194	95044	278.6	1420	660	1400	653.7	503.8	500	11/7/2016	
195	95135	428.3	2860	960	2780	614.9	744.0	521	3/15/2015	
196	60214	427.9	2823	924	2823	614.5	743.7	450	11/5/2015	
197	51447	264.0	806	670	806	653.5	483.9	160	12/5/2012	
198	60216	409.9	3000	860	3000	609.8	723.7	497	11/4/2016	
199	60222	374.9	1765	714	1765	645.8	675.8	594	12/9/2009	
200	60224	325.0	2382	603	2382	588.2	575.1	383	12/9/2009	
201	51464	252.0	1385	900	1365	671.2	456.7	483	11/9/2016	26.3
202	60227	347.9	1773	621	1773	615.6	628.0	473	12/26/2014	
203	51551	470.0	1819	840	1819	680.6	791.7	496	11/7/2016	
204	95025	293.9	1410	890	1390	586.7	525.4	500	11/9/2016	
205	60229	354.0	3000	1019	3000	631.8	630.4	466	12/26/2014	

Table A-1: Wells with water-surface elevation below the 1967 piezometric surface

Label	Site ID	Ground Surface Elevation	Depth of Well (BGS)	Top of perforated section (BGS)	Bottom of perforated section (BGS)	Base of Corcoran Clay (BGS)	1967 low water level (BGS)	Low water level (BGS)	Date of lowest recorded water level	Feet below 1967 piezometric surface
206	91833	270.0	1330	860	1300	655.5	493.2	489	11/9/2016	
207	51544	375.0	2818	920	2809	717.4	668.3	419	11/17/2008	
208	91834	285.0	1430	860	1090	658.2	512.8	484	11/9/2016	
209	51477	313.0	1481	645	1470	567.0	551.7	488	11/12/2014	
210	95424	377.0	3000	1570	3000	746.0	672.8	581	10/26/2015	
211	95022	360.9	2570	1290	2550	696.7	634.7	590	11/7/2016	
212	51506	345.0	2600	1136	2600	638.3	602.0	514	10/26/2015	
213	95049	352.0	3000	1290	3000	677.5	616.7	543	11/7/2016	
214	51509	347.1	2900	1615	2900	708.7	613.1	511	10/26/2015	
215	60439	303.1	1690	800	1600	626.1	538.3	423	10/30/2015	
216	60396	323.1	2996	1203	2690	681.6	570.7	480	12/7/2016	
217	95222	293.6	2040	950	2020	660.5	518.6	468	9/11/2015	
218	91860	270.1	1480	800	1480	668.8	485.7	485	10/30/2015	
219	95161	267.6	1370	979	1350	724.9	472.9	462	4/4/2015	
220	95422	287.8	1840	940	1820	659.7	506.9	532	7/9/2015	25.1
221	60436	287.1	1760	942	1720	659.3	506.1	478	12/7/2016	
222	60413	508.1	2495	1513	2495	557.0	854.5	483.6	4/21/2017	
223	93974	310.1	1450	1122	1442	690.9	529.9	560	12/7/2016	30.1
224	91864	271.1	1604	1004	1604	795.8	448.7	420	12/8/2016	
225	57567	284.1	1840	960	1680	670.5	503.7	475	11/19/2014	
226	57564	332.0	2550	1990	2550	725.1	555.3	N/A	11/10/2011	
227	60373	340.0	2175	725	1642	721.7	567.1	268	11/16/2011	
228	60423	541.4	2583	1788	2488	620.7	891.8	565	11/9/2015	
229	57576	295.2	2050	763	2009	688.8	519.6	490	12/7/2016	
230	95072	358.7	2410	820	2410	818.4	576.6	539	10/30/2015	
231	96086	518.0	1505	600	1505	480.3	869.6	411	4/21/2017	
232	57474	269.0	1750	850	1750	833.1	425.2	429	10/20/2015	3.8
233	60393	294.1	1750	1150	1750	557.6	523.2	450	12/8/2016	
234	95073	368.0	2505	840	1945	836.2	583.9	500	12/8/2016	
235	57471	293.0	1750	1200	1750	838.0	480.6	438	12/12/2016	
236	91869	271.0	1640	850	1020	819.1	428.9	442	10/20/2015	13.1
237	57506	305.5	2022	814	2022	695.1	533.7	472	12/12/1969	
238	95980	400.2	2423	830	2403	806.1	611.6	451	11/1/2015	
239	57509	402.2	2500	1300	2200	806.1	613.6	430	12/8/2016	
240	95984	307.9	1830	860	1800	748.2	533.8	508	2/24/2016	
241	70532	312.1	1873	800	1873	763.3	540.3	584	12/19/1967	43.7
242	68875	278.0	1996	896	1996	798.9	435.4	424	10/13/2015	
243	91883	272.5	1675	875	1655	814.9	411.2	389.4	1/3/2017	
244	70533	315.1	1730	744	1730	737.9	544.7	564	12/19/1967	19.3
245	57523	337.1	2000	800	2000	756.4	553.9	396	5/13/2016	
246	91884	424.1	2302	1497	2280	797.8	631.3	N/A	9/8/2009	

Table A-1: Wells with water-surface elevation below the 1967 piezometric surface

Label	Site ID	Ground Surface Elevation	Depth of Well (BGS)	Top of perforated section (BGS)	Bottom of perforated section (BGS)	Base of Corcoran Clay (BGS)	1967 low water level (BGS)	Low water level (BGS)	Date of lowest recorded water level	Feet below 1967 piezometric surface
247	94403	400.1	1960	800	1940	752.5	607.2	595.3	5/17/2017	
248	95768	355.6	2040	900	2020	752.3	568.4	527	10/24/2015	
249	70872	384.9	2301	860	2186	742.5	590.1	544	11/9/2015	
250	91885	454.9	1910	840	1860	750.5	655.4	635	11/9/2015	
251	74522	355.1	2124	872	2124	737.3	571.5	521	12/15/1965	
252	91895	356.0	1265	763	1243	748.8	569.2	385	12/2/2009	
253	94402	461.0	2120	889	2100	750.1	657.5	529	6/7/2013	
254	74476	508.1	1720	860	1700	757.4	700.1	508	12/1/2006	
255	94408	270.9	2016	755	2016	761.7	410.4	395	12/6/2016	
256	94308	267.9	1718	750	1718	759.1	403.7	416	10/13/2015	12.3
257	91914	271.9	1180	760	1160	760.3	415.7	384	12/4/2013	
258	94404	381.0	2100	1030	2080	773.3	573.2	410	12/5/2013	
259	71150	355.0	2072	800	2072	713.9	568.5	492	10/15/2015	
260	70886	397.9	2350	878	2350	768.3	583.2	540	10/15/2015	
261	74453	374.0	2004	800	2004	672.3	565.3	432	1/6/1992	
262	91915	271.9	1710	750	1690	749.9	426.0	350.4	5/12/2017	
263	94398	341.5	2040	840	2020	737.2	566.5	468	5/11/2016	
264	71119	378.0	2070	777	2070	668.5	558.9	438	10/20/2015	
265	71115	368.0	2018	716	2005	657.0	555.0	458	12/2/1991	
266	74488	402.9	2117	742	2117	742.2	563.5	486	11/29/1994	
267	91918	273.9	2410	1550	2390	728.9	445.3	437	10/13/2015	
268	71073	365.9	2151	820	2151	656.3	554.3	360	12/3/2009	
269	91962	266.9	2370	1570	2350	710.5	426.4	415	10/13/2015	
270	94307	278.9	2414	746	2400	740.1	457.6	428	10/13/2015	
271	73673	362.0	2356	745	2356	690.4	559.2	N/A	11/22/2011	
272	73675	356.0	2045	760	2045	687.5	562.7	N/A	11/22/2011	
273	91977	272.9	2435	1280	2420	739.7	444.0	429	10/13/2015	
274	91978	260.9	2190	710	2180	699.9	414.5	434	10/13/2015	19.5
275	95082	311.8	2020	945	2000	888.3	543.1	560	9/11/2014	16.9
276	93981	336.9	2200	812	2162	760.2	571.6	511	11/23/2015	
277	91974	306.9	1420	870	1390	877.9	537.5	366	12/10/2012	
278	91973	324.9	1450	940	1410	848.7	562.1	535	11/20/2014	
279	93971	352.9	1610	860	1590	773.9	571.0	564	10/21/2015	
280	70223	277.8	1150	1000	1150	777.9	492.9	411	1/7/2014	
281	95369	306.7	2410	781	2400	769.1	525.0	518	5/11/2015	
282	52889	272.9	1945	1156	1945	767.9	420.5	431	11/19/2015	10.5
283	95970	258.8	1870	950	1850	771.7	401.1	568	8/15/2015	166.9
284	96101	257.0	2110	760	2100	749.7	375.8	434.2	12/19/2016	58.4
285	93980	423.1	1730	790	1730	722.3	519.9	564.8	12/19/2016	44.9

Appendix B. Subsidence Model Plots

Calibration Plots

Calibration Plots

Flows

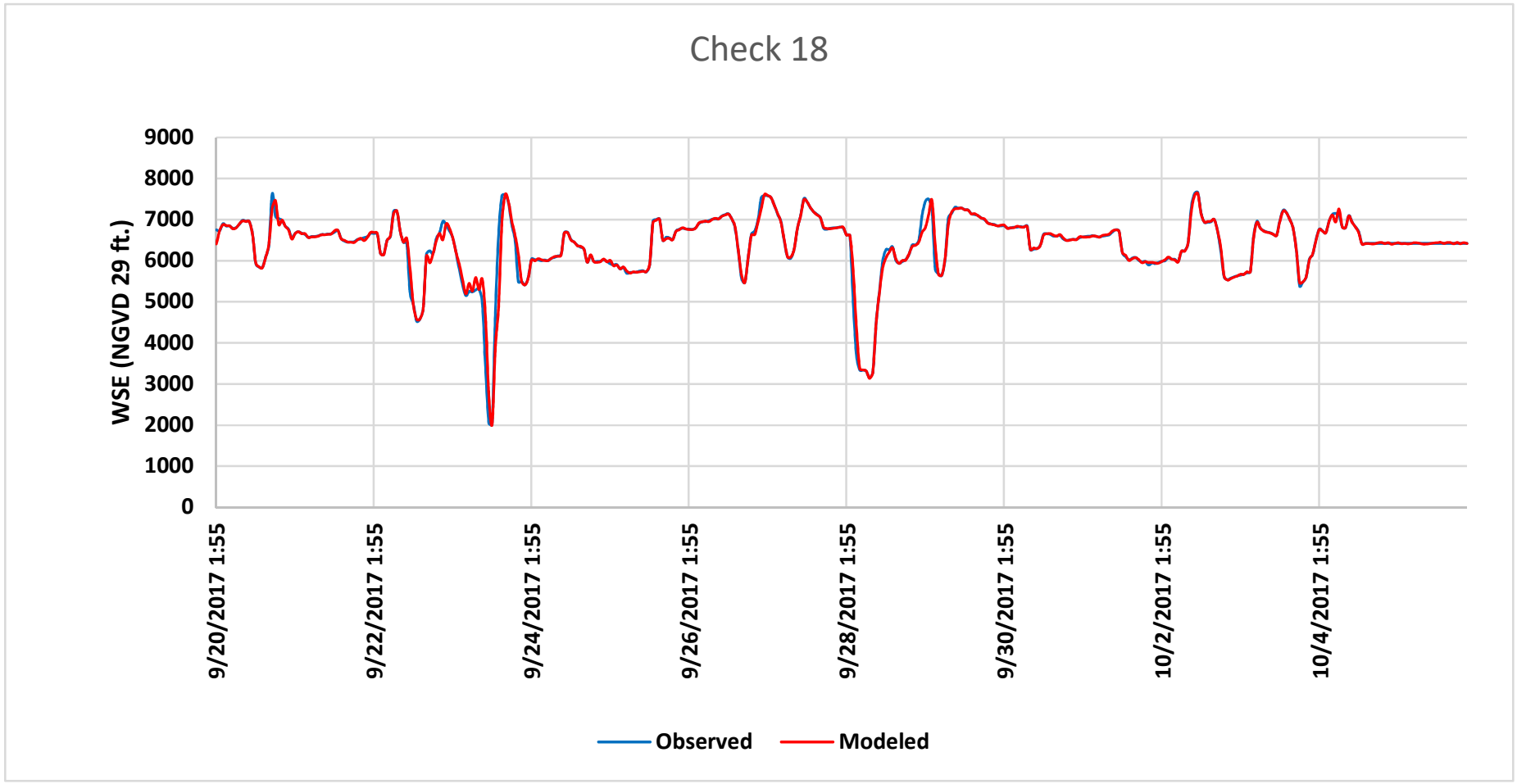
Check 18
WSE (NGVD 29 ft.)
9000
8000
7000
6000
5000
4000
3000
2000
1000
0
9/20/2017 1:55
9/22/2017 1:55
9/24/2017 1:55
9/26/2017 1:55
9/28/2017 1:55
9/30/2017 1:55
10/2/2017 1:55
10/4/2017 1:55
Observed
Modeled

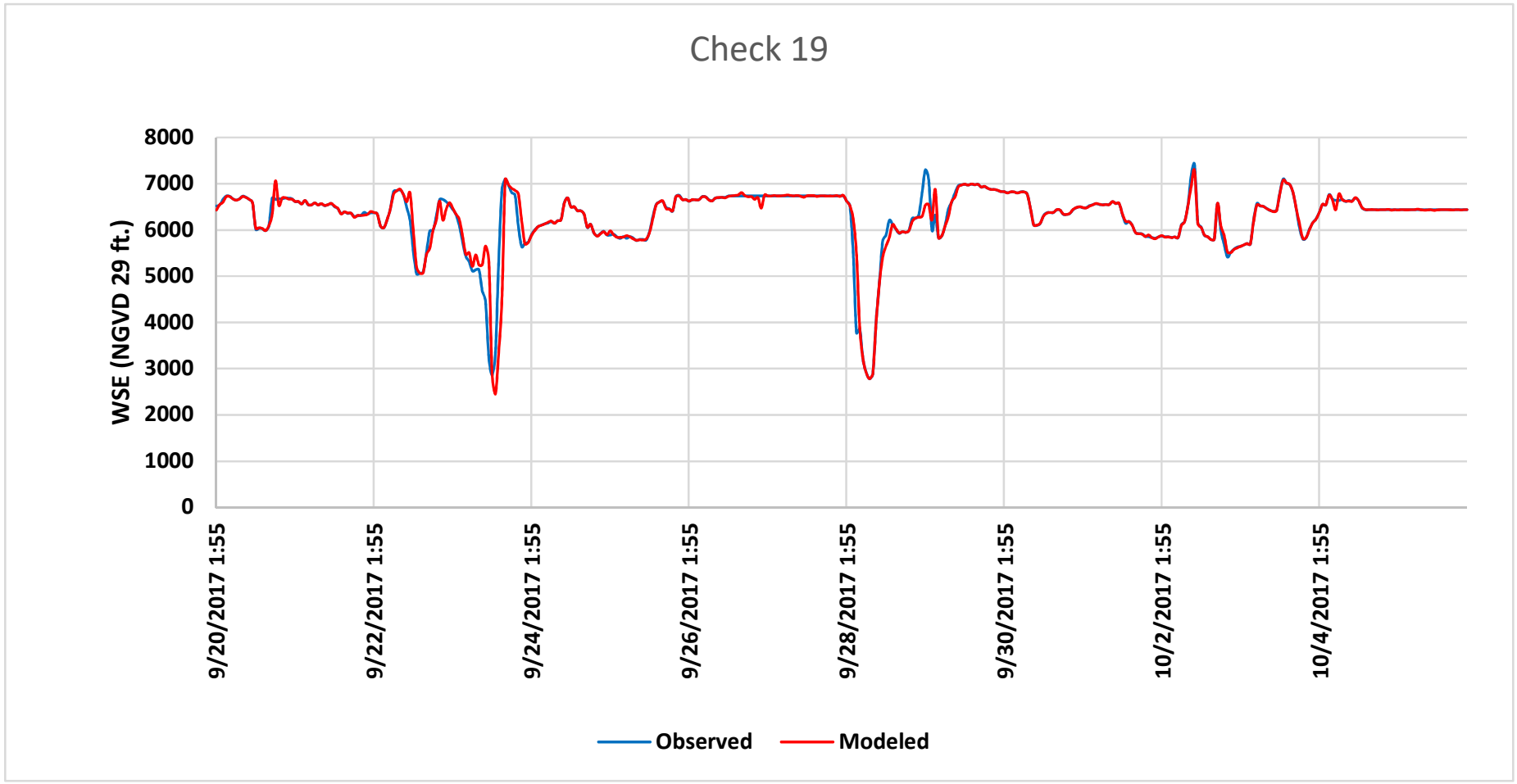
Check 19
WSE (NGVD 29 ft.)
8000
7000
6000
5000
4000
3000
2000
1000
0
9/20/2017 1:55
9/22/2017 1:55
9/24/2017 1:55
9/26/2017 1:55
9/28/2017 1:55
9/30/2017 1:55
10/2/2017 1:55
10/4/2017 1:55
Observed
Modeled

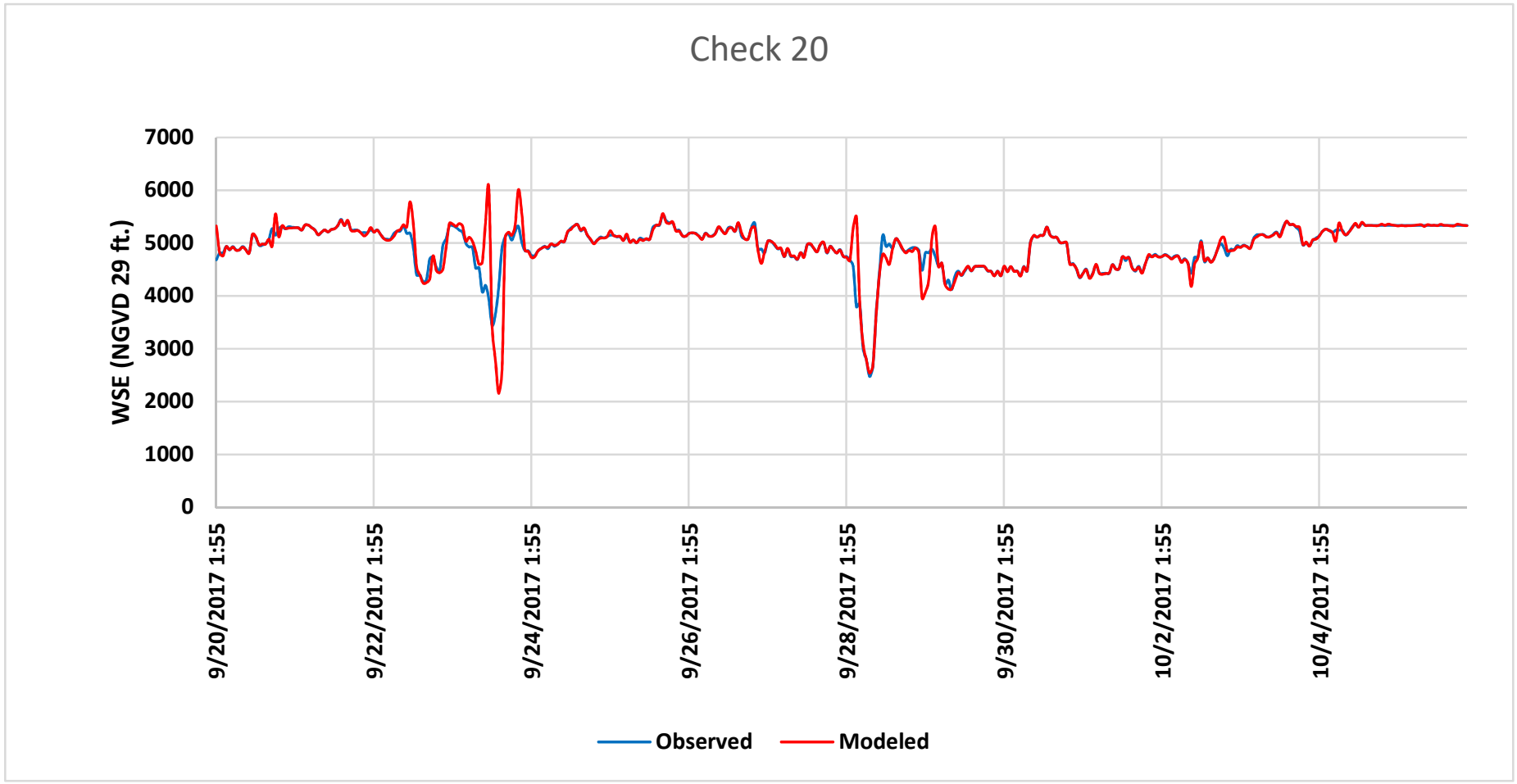
Check 20
WSE (NGVD 29 ft.)
7000
6000
5000
4000
3000
2000
1000
0
9/20/2017 1:55
9/22/2017 1:55
9/24/2017 1:55
9/26/2017 1:55
9/28/2017 1:55
9/30/2017 1:55
10/2/2017 1:55
10/4/2017 1:55
Observed
Modeled

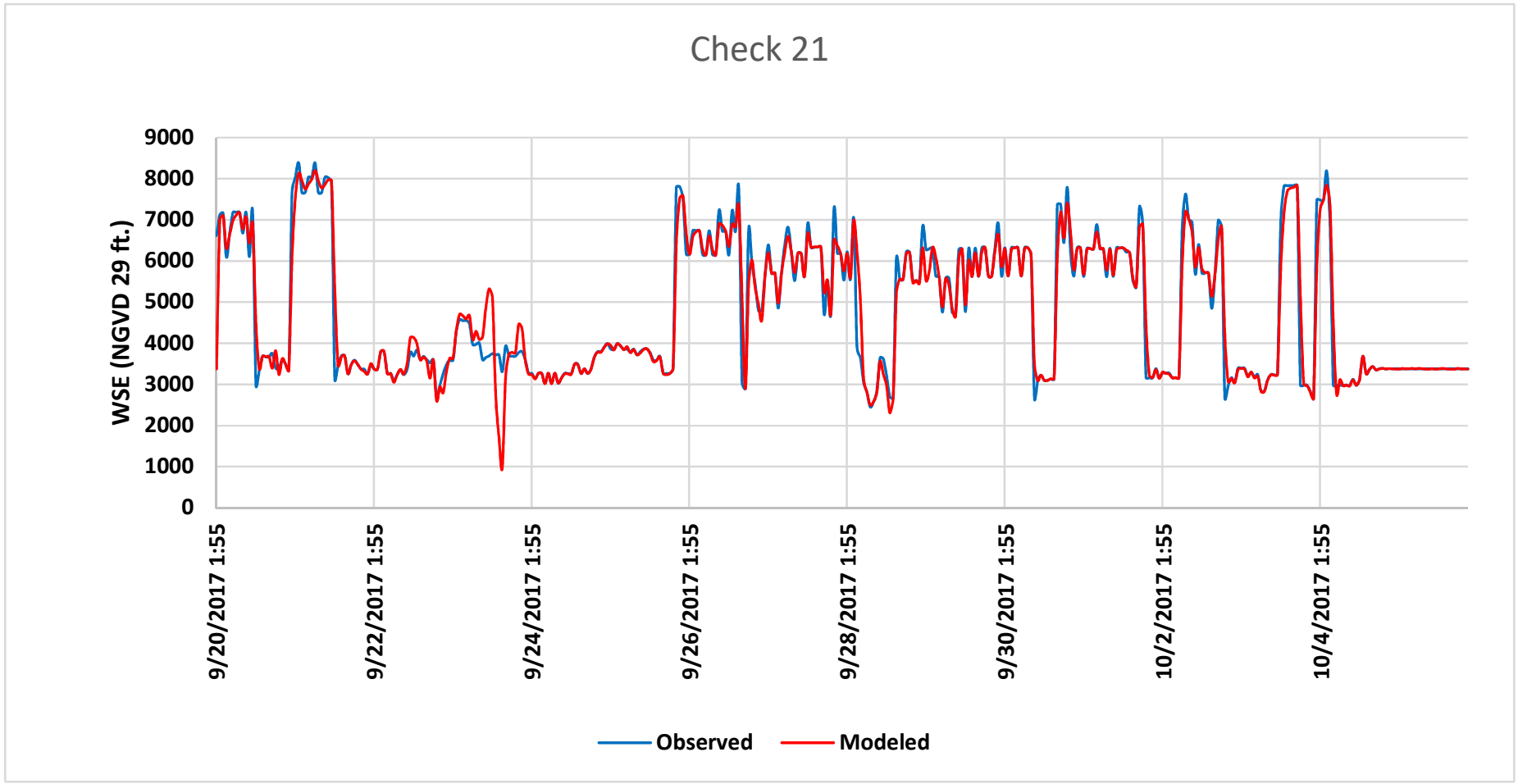
Check 21
WSE (NGVD 29 ft.)
9000
8000
7000
6000
5000
4000
3000
2000
1000
0
9/20/2017 1:55
9/22/2017 1:55
9/24/2017 1:55
9/26/2017 1:55
9/28/2017 1:55
9/30/2017 1:55
10/2/2017 1:55
10/4/2017 1:55
Observed
Modeled

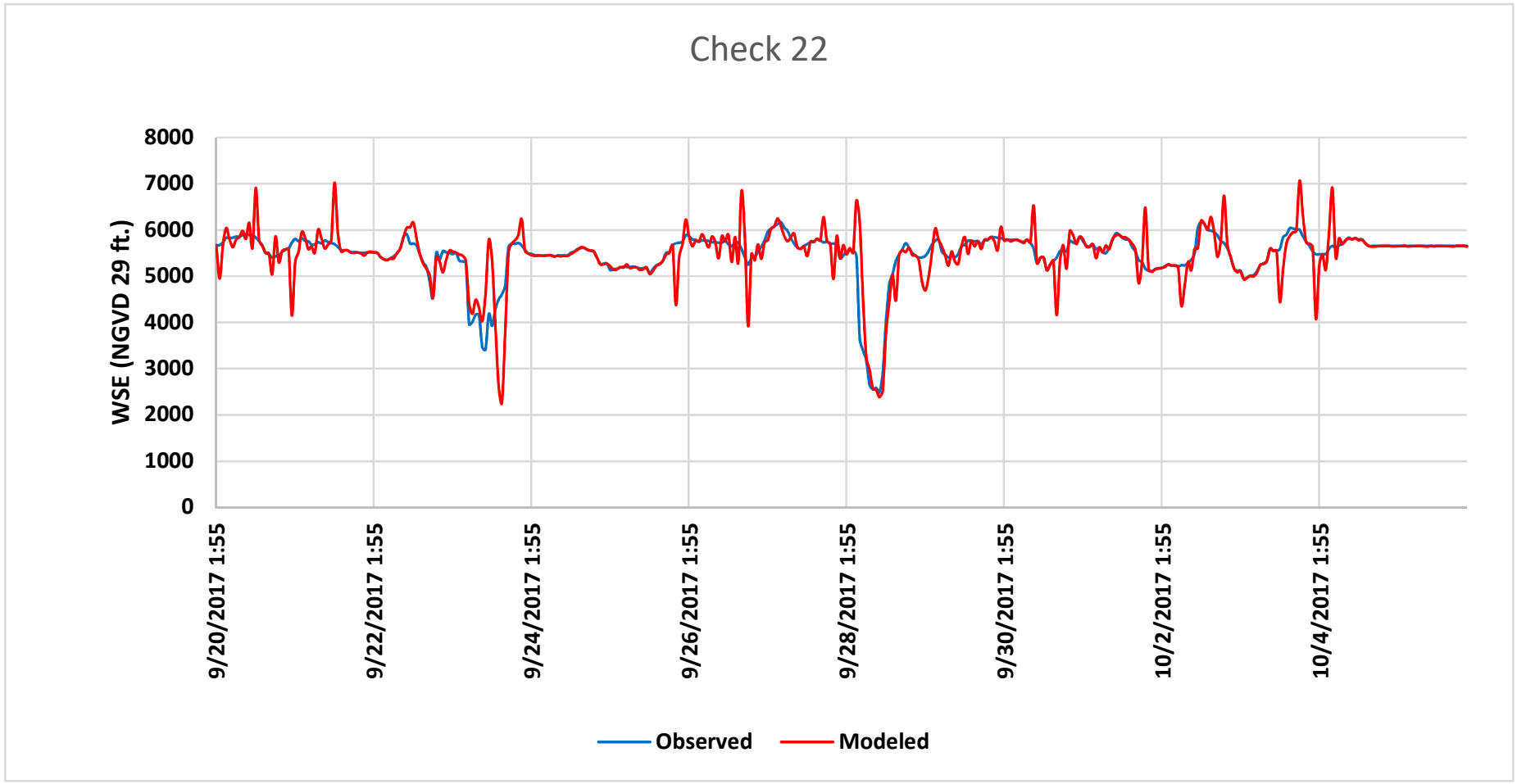
Check 22
WSE (NGVD 29 ft.)
8000
7000
6000
5000
4000
3000
2000
1000
0
9/20/2017 1:55
9/22/2017 1:55
9/24/2017 1:55
9/26/2017 1:55
9/28/2017 1:55
9/30/2017 1:55
10/2/2017 1:55
10/4/2017 1:55
Observed
Modeled

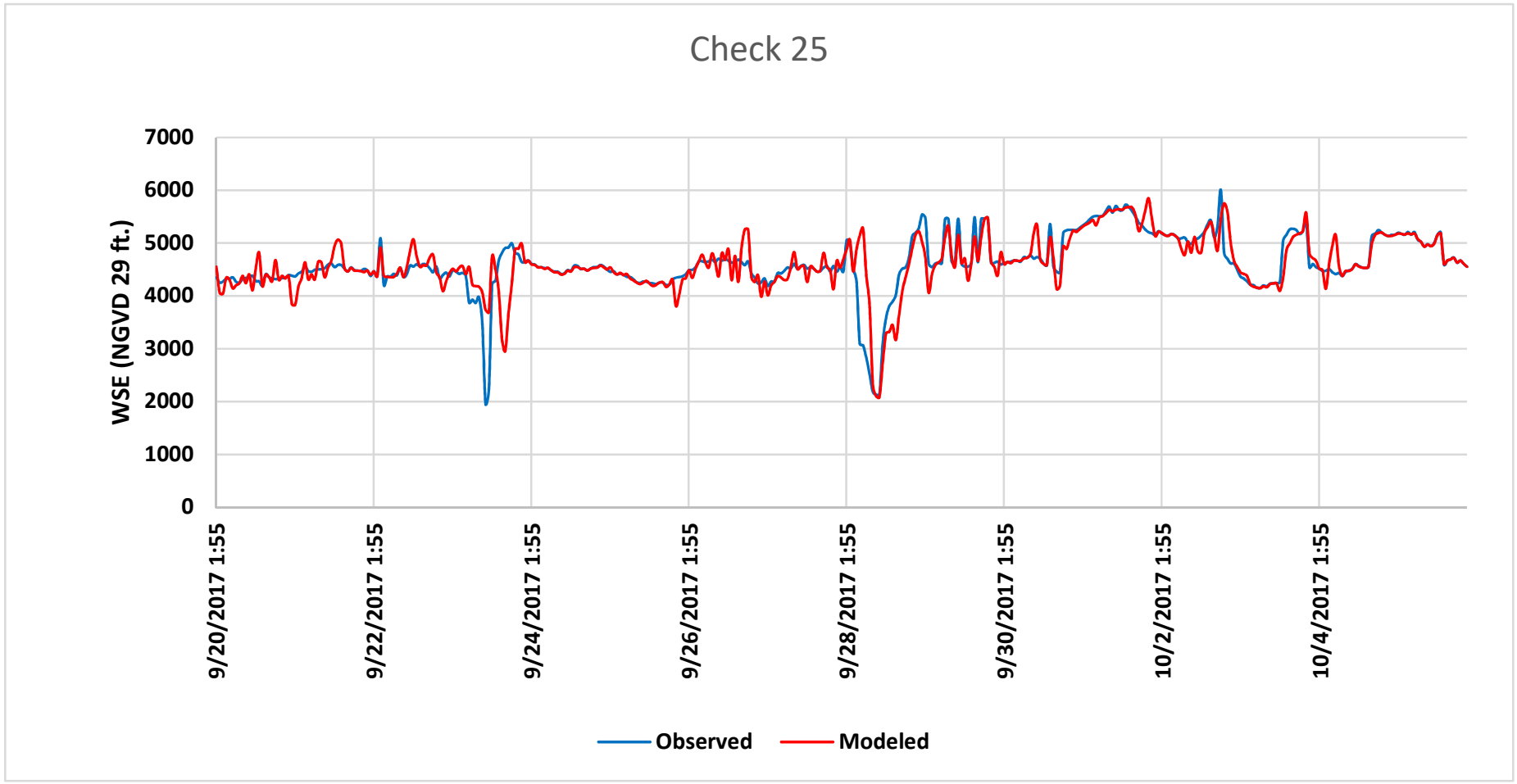
Check 25
WSE (NGVD 29 ft.)
7000
6000
5000
4000
3000
2000
1000
0
9/20/2017 1:55
9/22/2017 1:55
9/24/2017 1:55
9/26/2017 1:55
9/28/2017 1:55
9/30/2017 1:55
10/2/2017 1:55
10/4/2017 1:55
Observed
Modeled

Calibration Plots

Stages

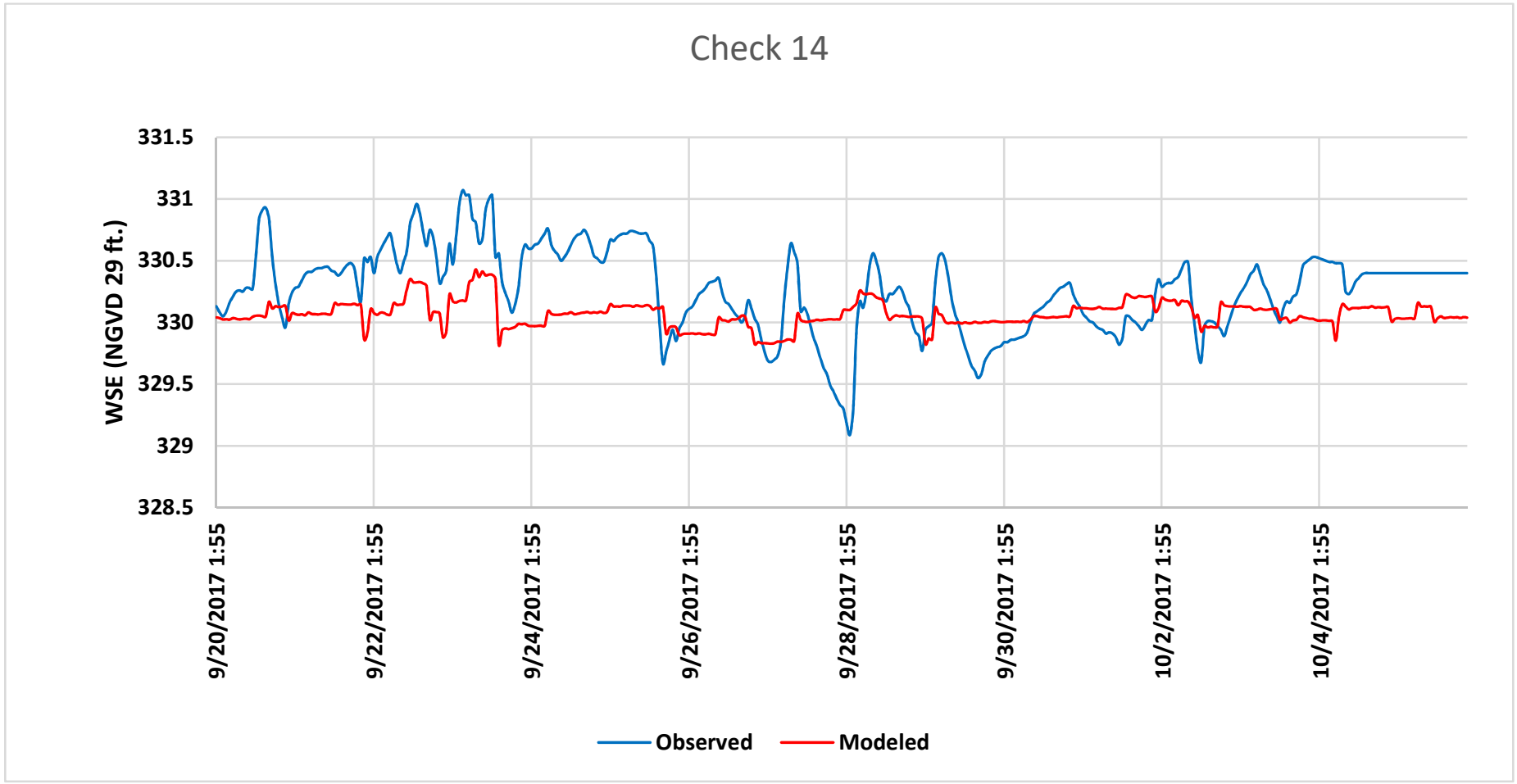
Check 14
331.5
331
330.5
330
329.5
329
328.5
WSE (NGVD 29 ft.)
9/20/2017 1:55
9/22/2017 1:55
9/24/2017 1:55
9/26/2017 1:55
9/28/2017 1:55
9/30/2017 1:55
10/2/2017 1:55
10/4/2017 1:55
Observed
Modeled

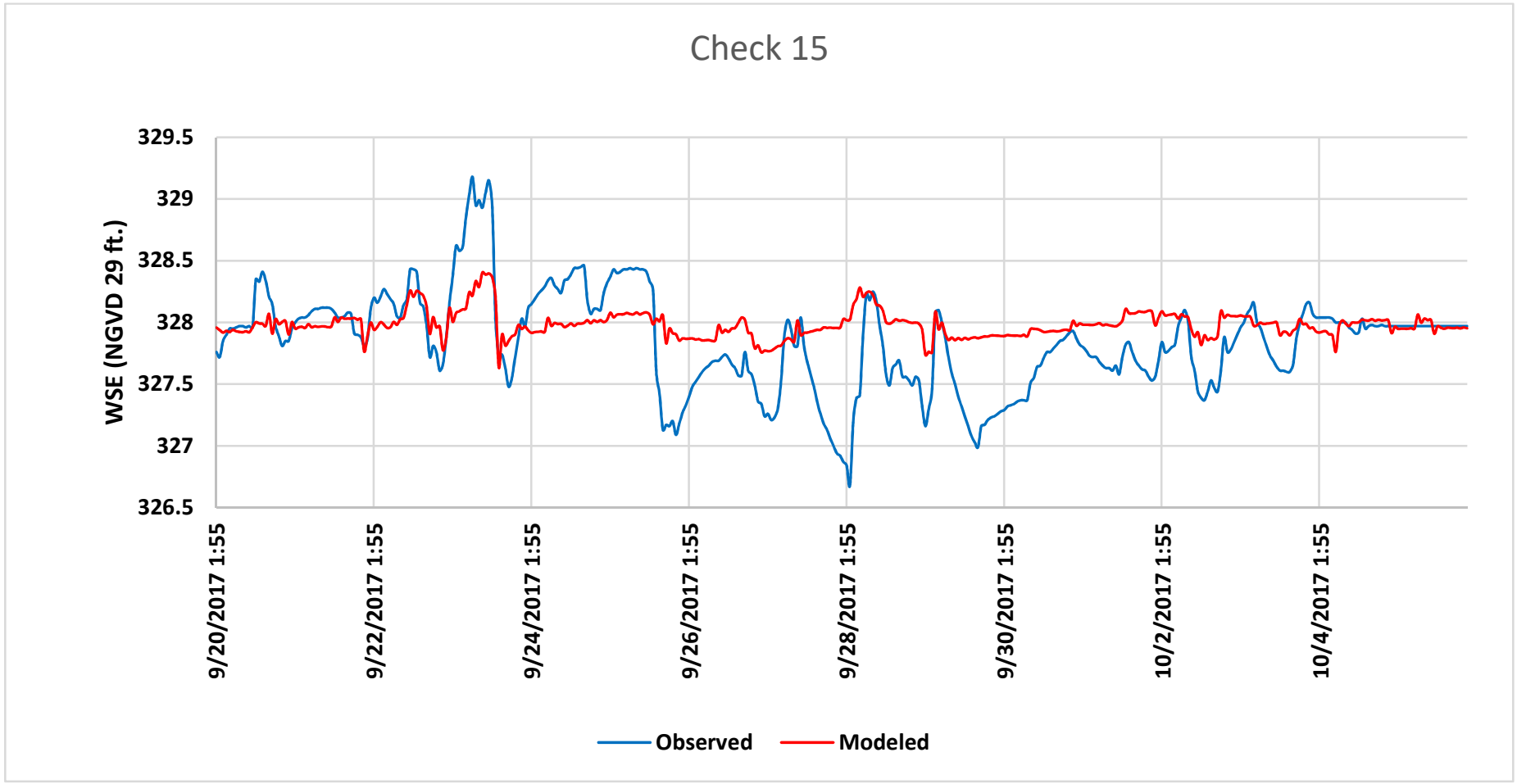
Check 15
WSE (NGVD 29 ft.)
329.5
329
328.5
328
327.5
327
326.5
9/20/2017 1:55
9/22/2017 1:55
9/24/2017 1:55
9/26/2017 1:55
9/28/2017 1:55
9/30/2017 1:55
10/2/2017 1:55
10/4/2017 1:55
Observed
Modeled

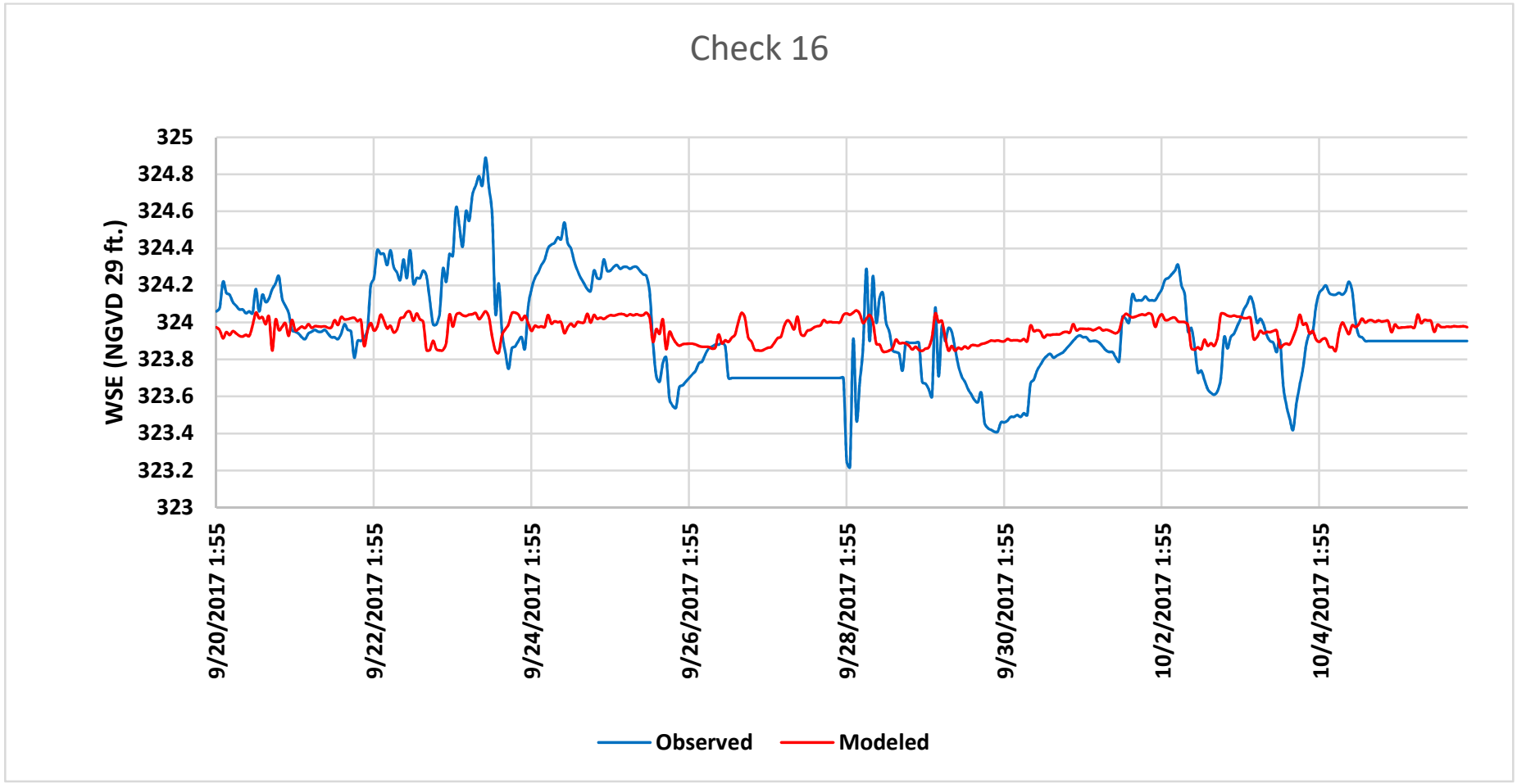
Check 16
WSE (NGVD 29 ft.)
325
324.8
324.6
324.4
324.2
324
323.8
323.6
323.4
323.2
323
9/20/2017 1:55
9/22/2017 1:55
9/24/2017 1:55
9/26/2017 1:55
9/28/2017 1:55
9/30/2017 1:55
10/2/2017 1:55
10/4/2017 1:55
Observed
Modeled

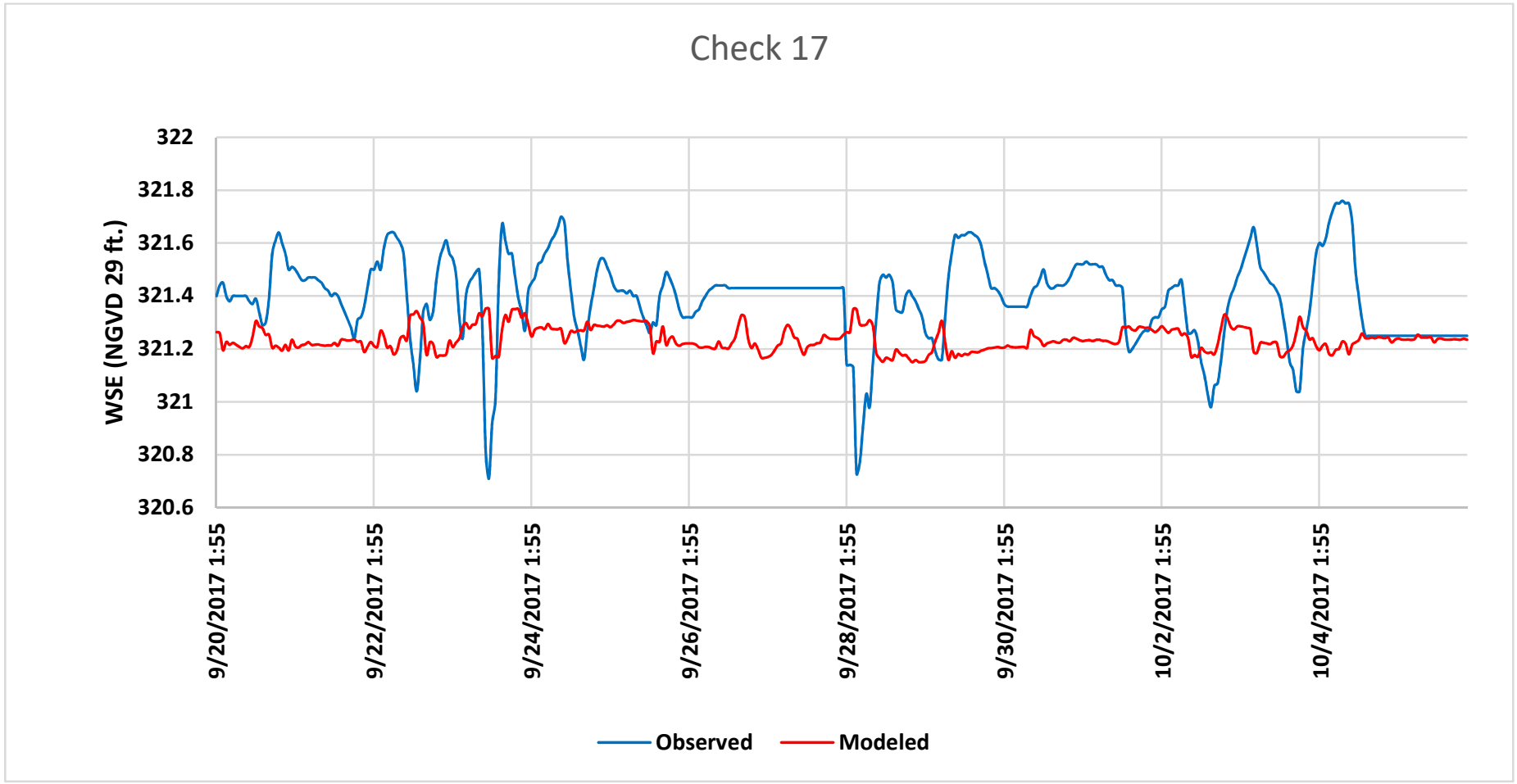
Check 17
WSE (NGVD 29 ft.)
322
321.8
321.6
321.4
321.2
321
320.8
320.6
9/20/2017 1:55
9/22/2017 1:55
9/24/2017 1:55
9/26/2017 1:55
9/28/2017 1:55
9/30/2017 1:55
10/2/2017 1:55
10/4/2017 1:55
Observed
Modeled

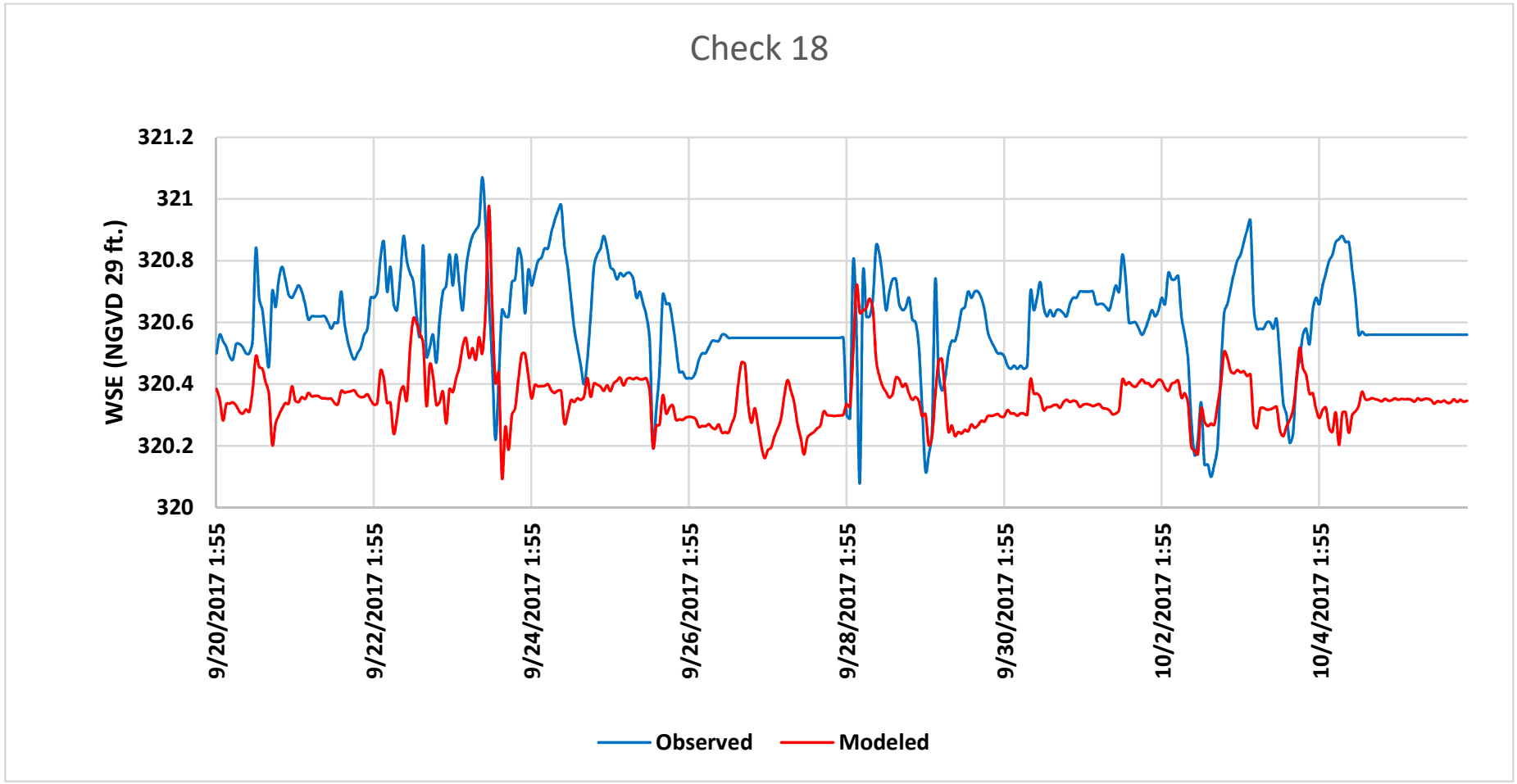
Check 18
WSE (NGVD 29 ft.)
321.2
321
320.8
320.6
320.4
320.2
320
9/20/2017 1:55
9/22/2017 1:55
9/24/2017 1:55
9/26/2017 1:55
9/28/2017 1:55
9/30/2017 1:55
10/2/2017 1:55
10/4/2017 1:55
Observed
Modeled

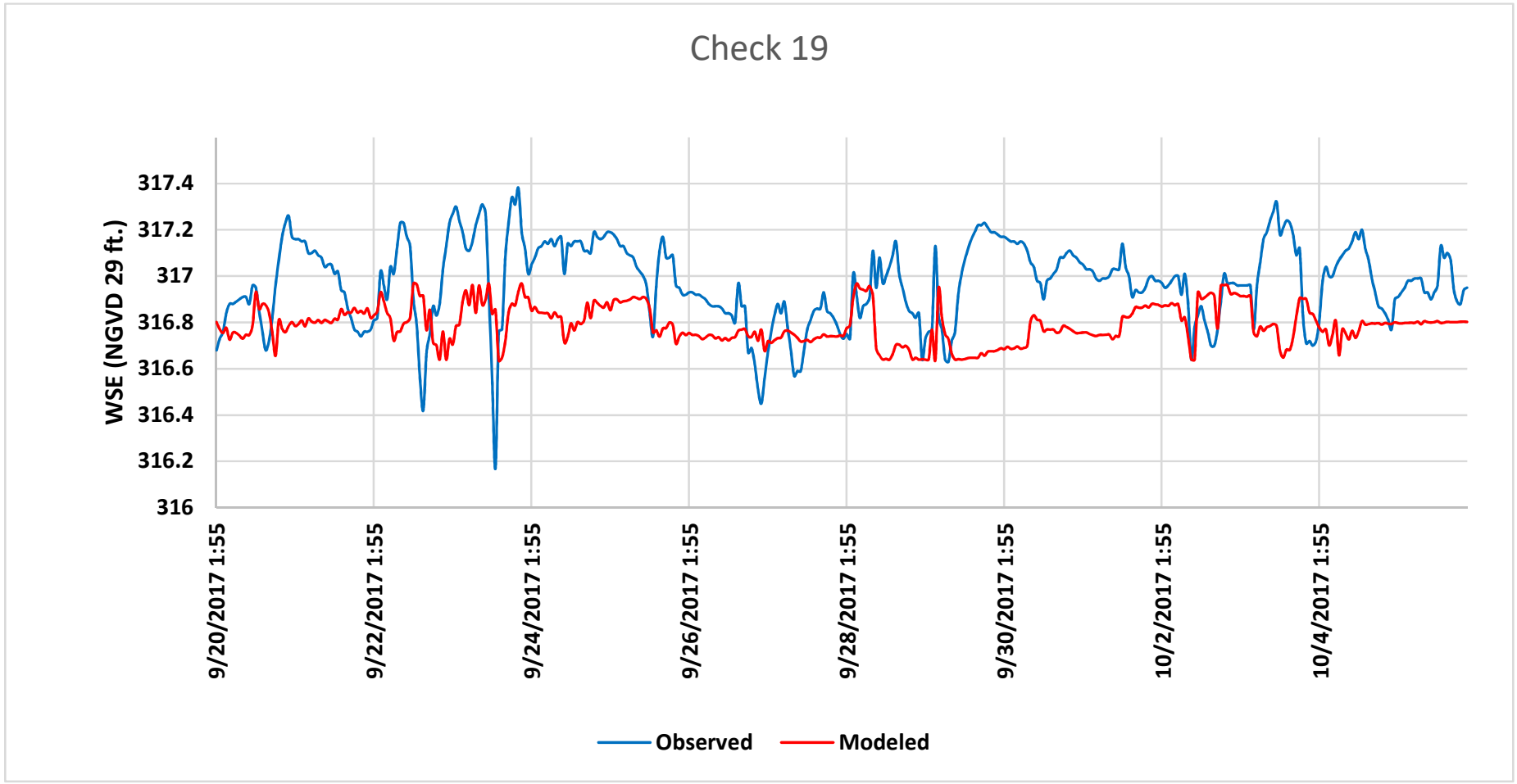
Check 19
WSE (NGVD 29 ft.)
317.4
317.2
317
316.8
316.6
316.4
316.2
316
9/20/2017 1:55
9/22/2017 1:55
9/24/2017 1:55
9/26/2017 1:55
9/28/2017 1:55
9/30/2017 1:55
10/2/2017 1:55
10/4/2017 1:55
Observed
Modeled

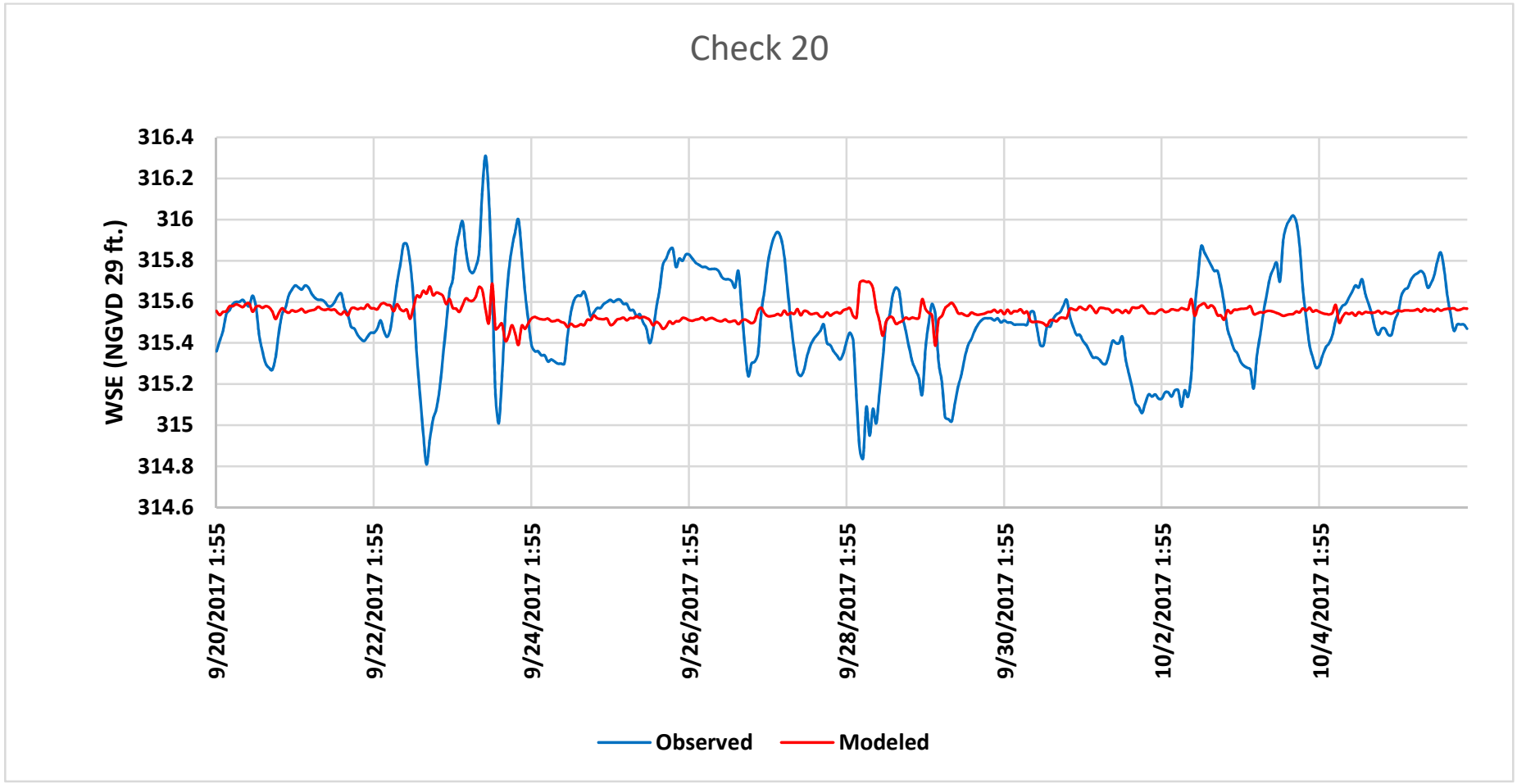
Check 20
WSE (NGVD 29 ft.)
316.4
316.2
316
315.8
315.6
315.4
315.2
315
314.8
314.6
9/20/2017 1:55
9/22/2017 1:55
9/24/2017 1:55
9/26/2017 1:55
9/28/2017 1:55
9/30/2017 1:55
10/2/2017 1:55
10/4/2017 1:55
Observed
Modeled

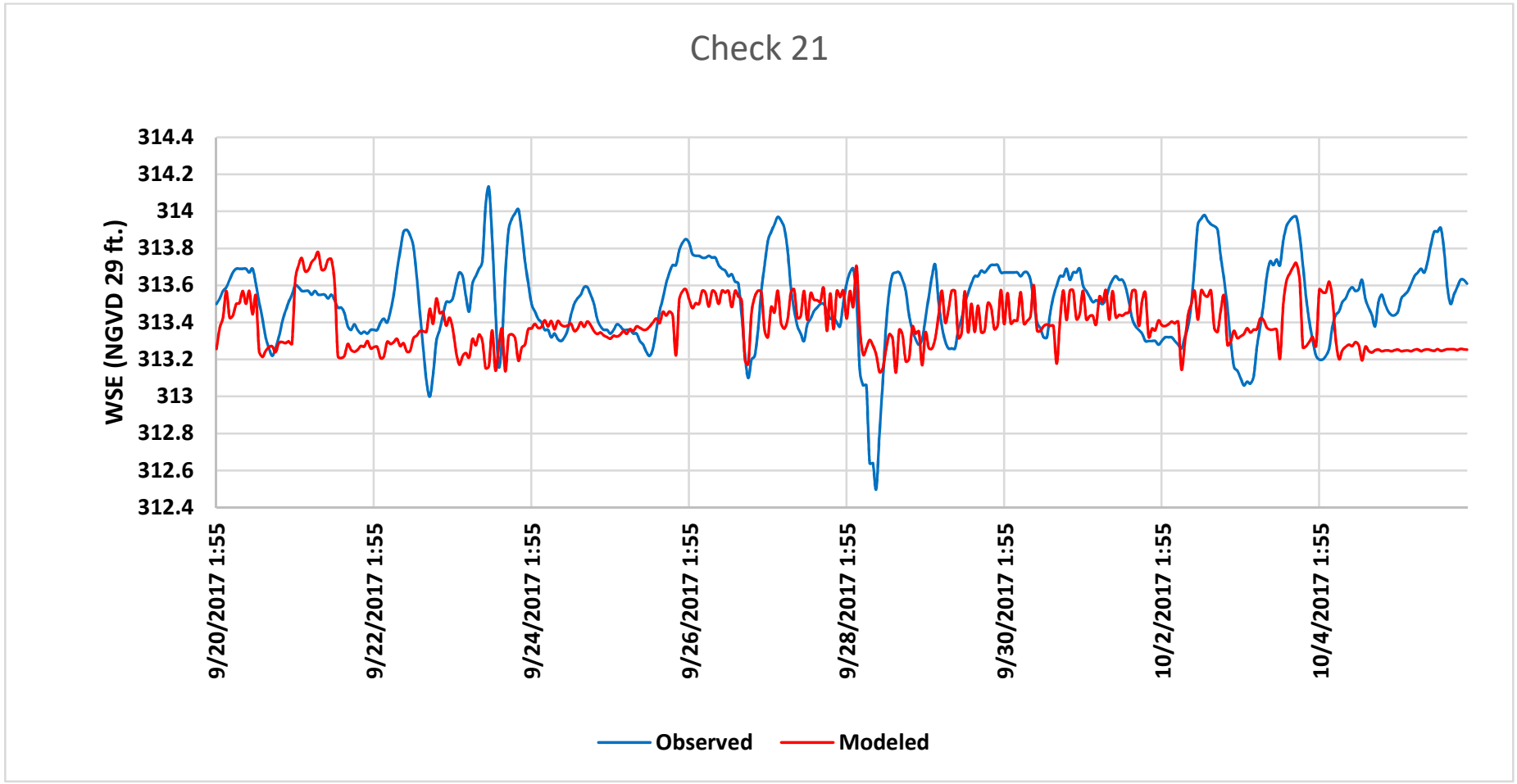
Check 21
WSE (NGVD 29 ft.)
314.4
314.2
314
313.8
313.6
313.4
313.2
313
312.8
312.6
312.4
9/20/2017 1:55
9/22/2017 1:55
9/24/2017 1:55
9/26/2017 1:55
9/28/2017 1:55
9/30/2017 1:55
10/2/2017 1:55
10/4/2017 1:55
Observed
Modeled

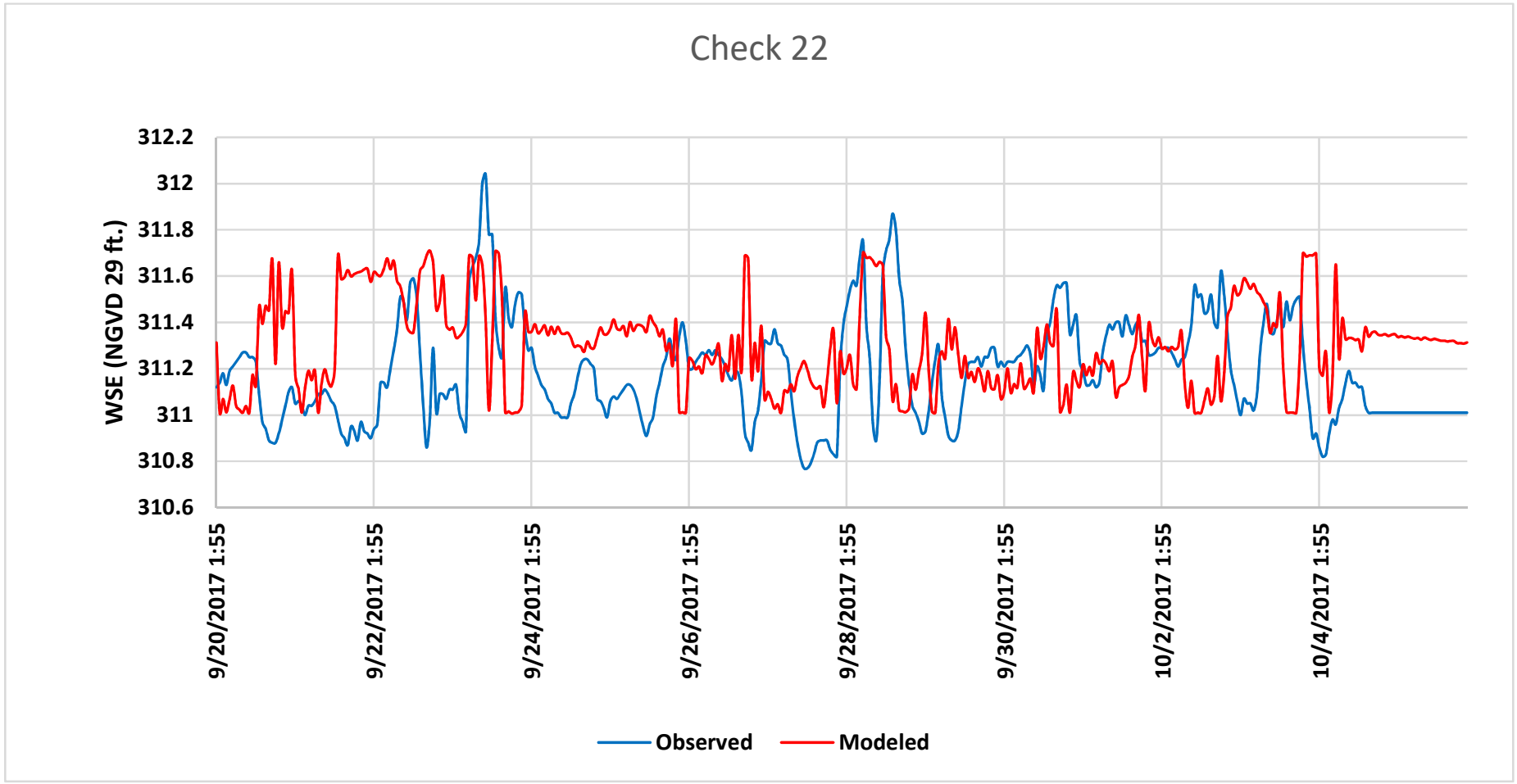
Check 22
WSE (NGVD 29 ft.)
312.2
312
311.8
311.6
311.4
311.2
311
310.8
310.6
9/20/2017 1:55
9/22/2017 1:55
9/24/2017 1:55
9/26/2017 1:55
9/28/2017 1:55
9/30/2017 1:55
10/2/2017 1:55
10/4/2017 1:55
Observed
Modeled

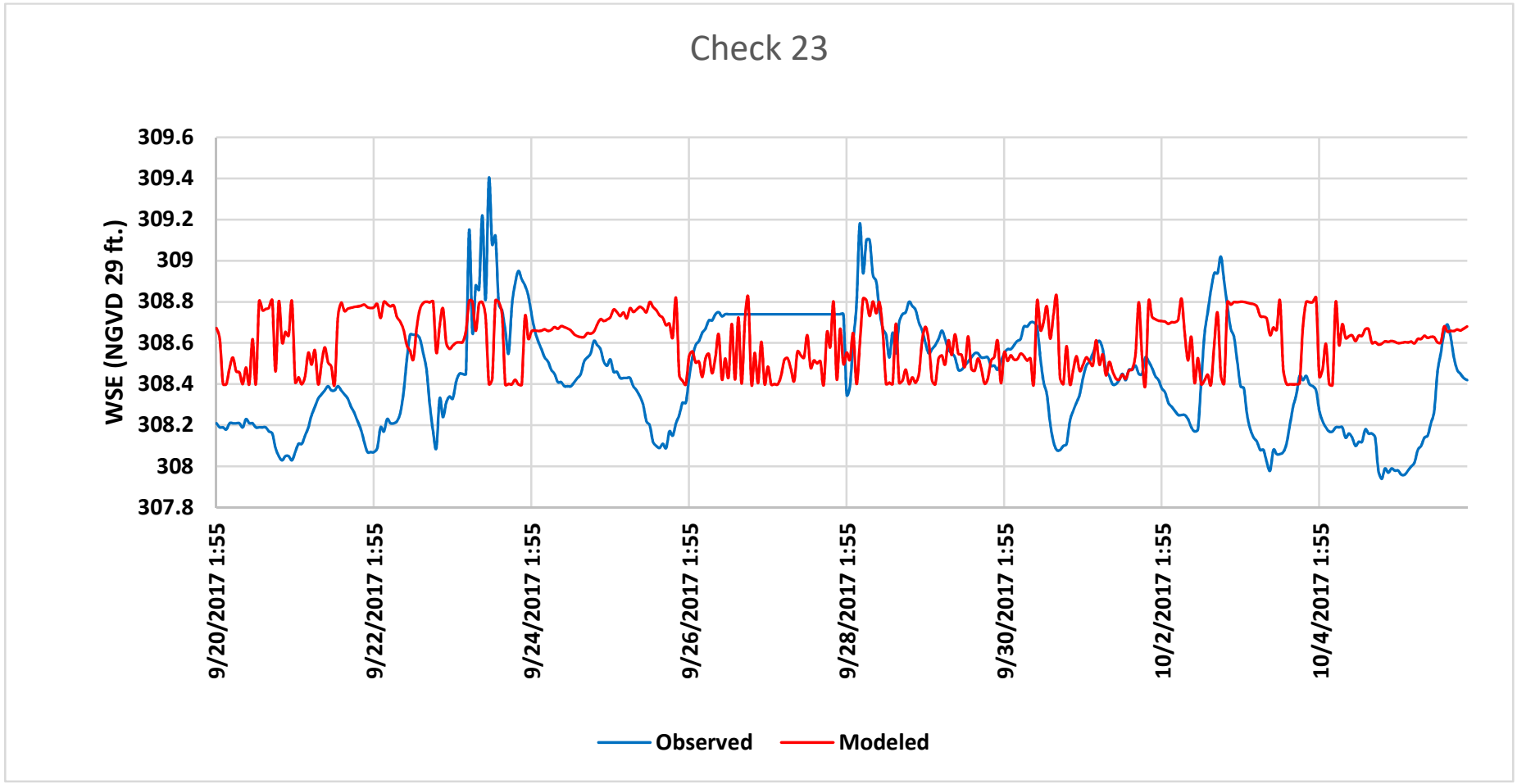
Check 23
WSE (NGVD 29 ft.)
309.6
309.4
309.2
309
308.8
308.6
308.4
308.2
308
307.8
9/20/2017 1:55
9/22/2017 1:55
9/24/2017 1:55
9/26/2017 1:55
9/28/2017 1:55
9/30/2017 1:55
10/2/2017 1:55
10/4/2017 1:55
Observed
Modeled

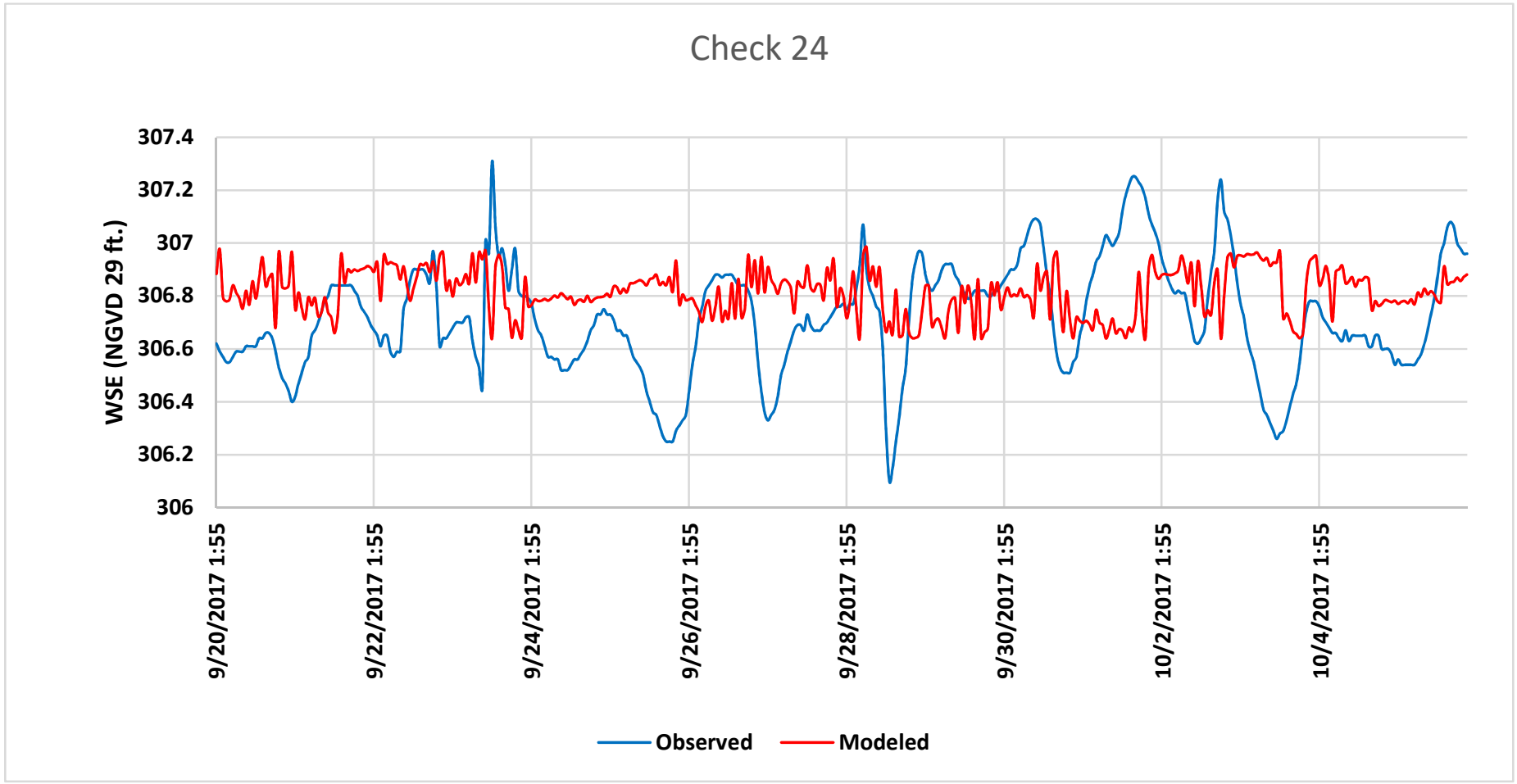
Check 24
WSE (NGVD 29 ft.)
307.4
307.2
307
306.8
306.6
306.4
306.2
306
9/20/2017 1:55
9/22/2017 1:55
9/24/2017 1:55
9/26/2017 1:55
9/28/2017 1:55
9/30/2017 1:55
10/2/2017 1:55
10/4/2017 1:55
Observed
Modeled

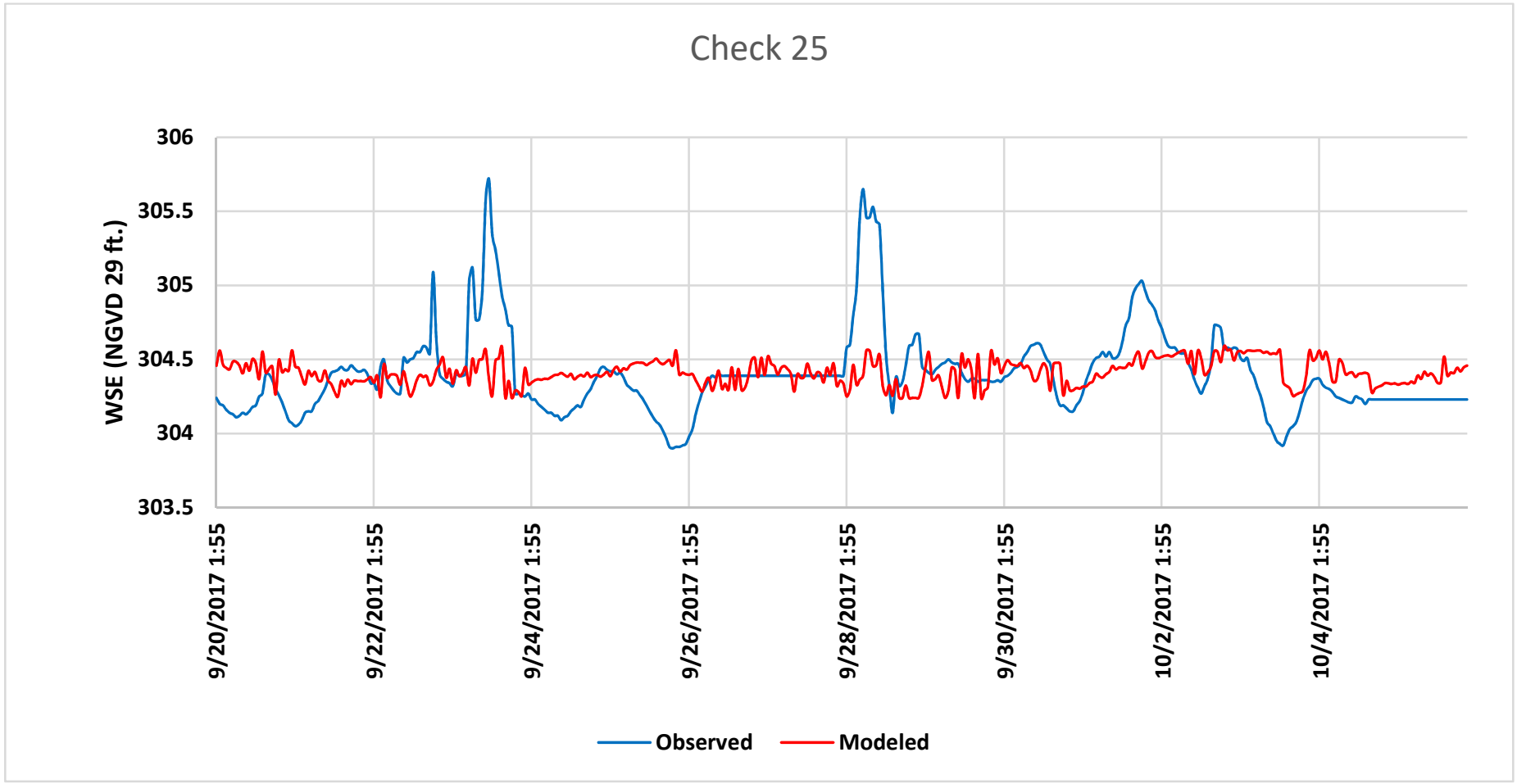
Check 25
WSE (NGVD 29 ft.)
306
305.5
305
304.5
304
303.5
9/20/2017 1:55
9/22/2017 1:55
9/24/2017 1:55
9/26/2017 1:55
9/28/2017 1:55
9/30/2017 1:55
10/2/2017 1:55
10/4/2017 1:55
Observed
Modeled

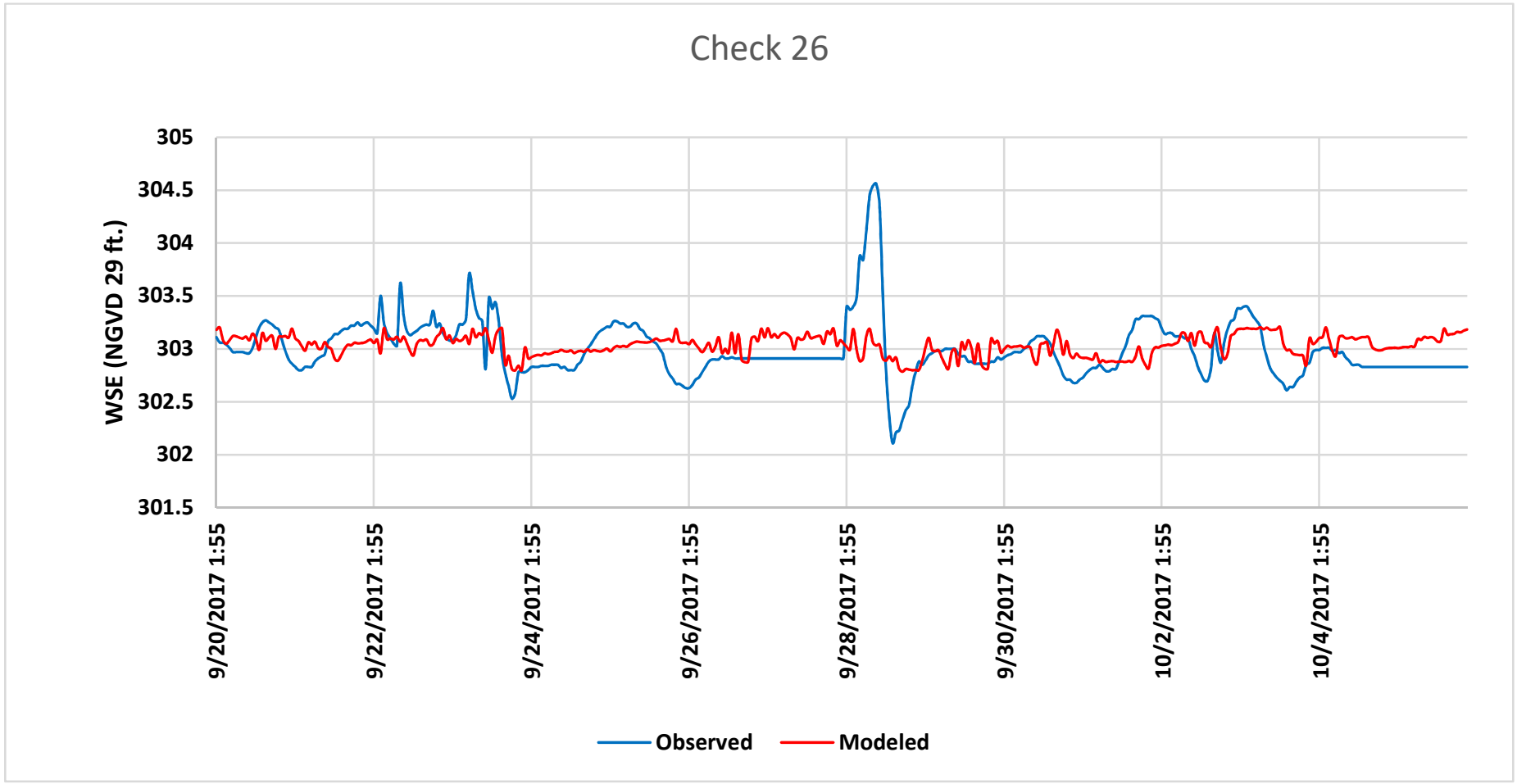
Check 26
WSE (NGVD 29 ft.)
305
304.5
304
303.5
303
302.5
302
301.5
9/20/2017 1:55
9/22/2017 1:55
9/24/2017 1:55
9/26/2017 1:55
9/28/2017 1:55
9/30/2017 1:55
10/2/2017 1:55
10/4/2017 1:55
Observed
Modeled

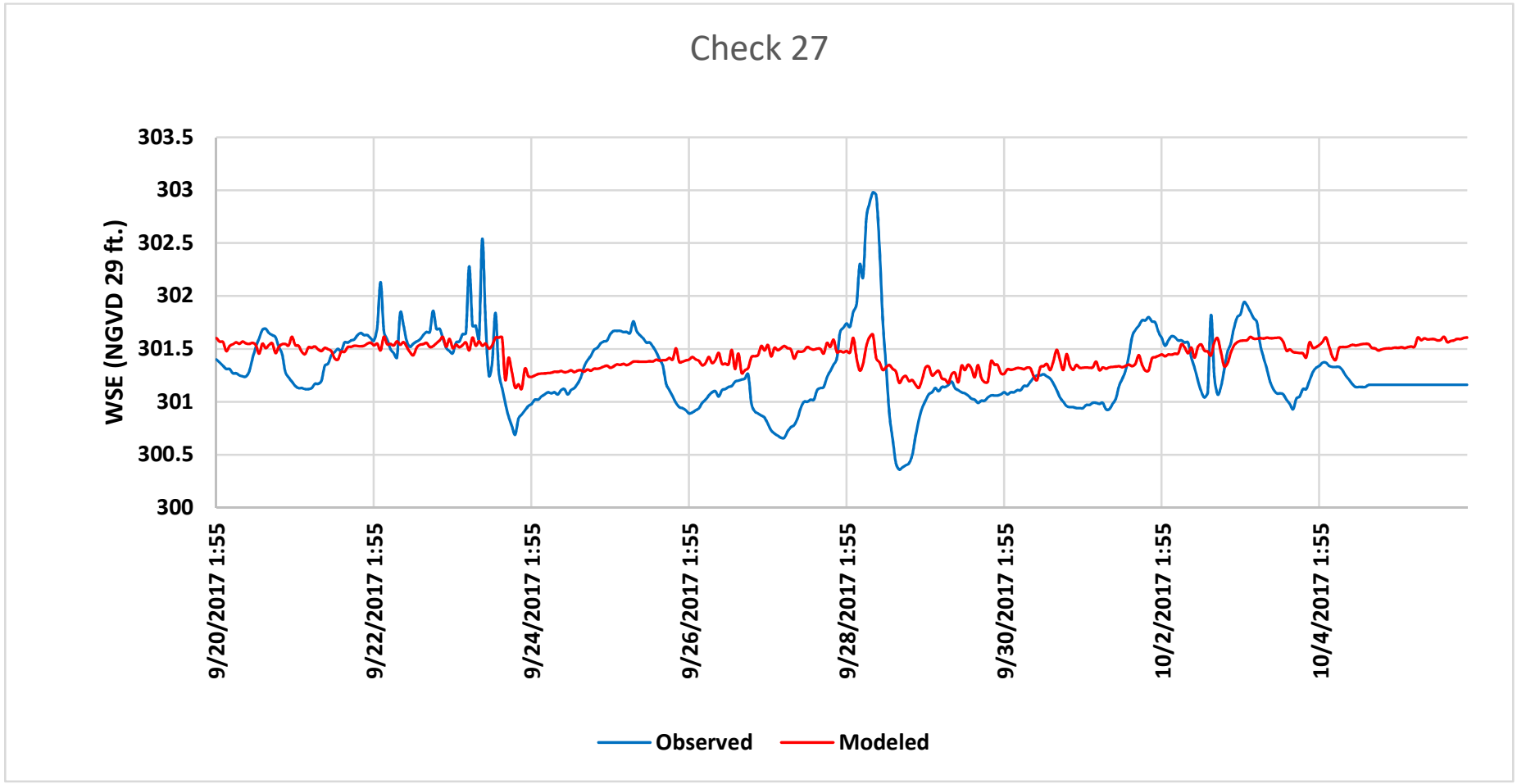
Check 27
WSE (NGVD 29 ft.)
303.5
303
302.5
302
301.5
301
300.5
300
9/20/2017 1:55
9/22/2017 1:55
9/24/2017 1:55
9/26/2017 1:55
9/28/2017 1:55
9/30/2017 1:55
10/2/2017 1:55
10/4/2017 1:55
Observed
Modeled

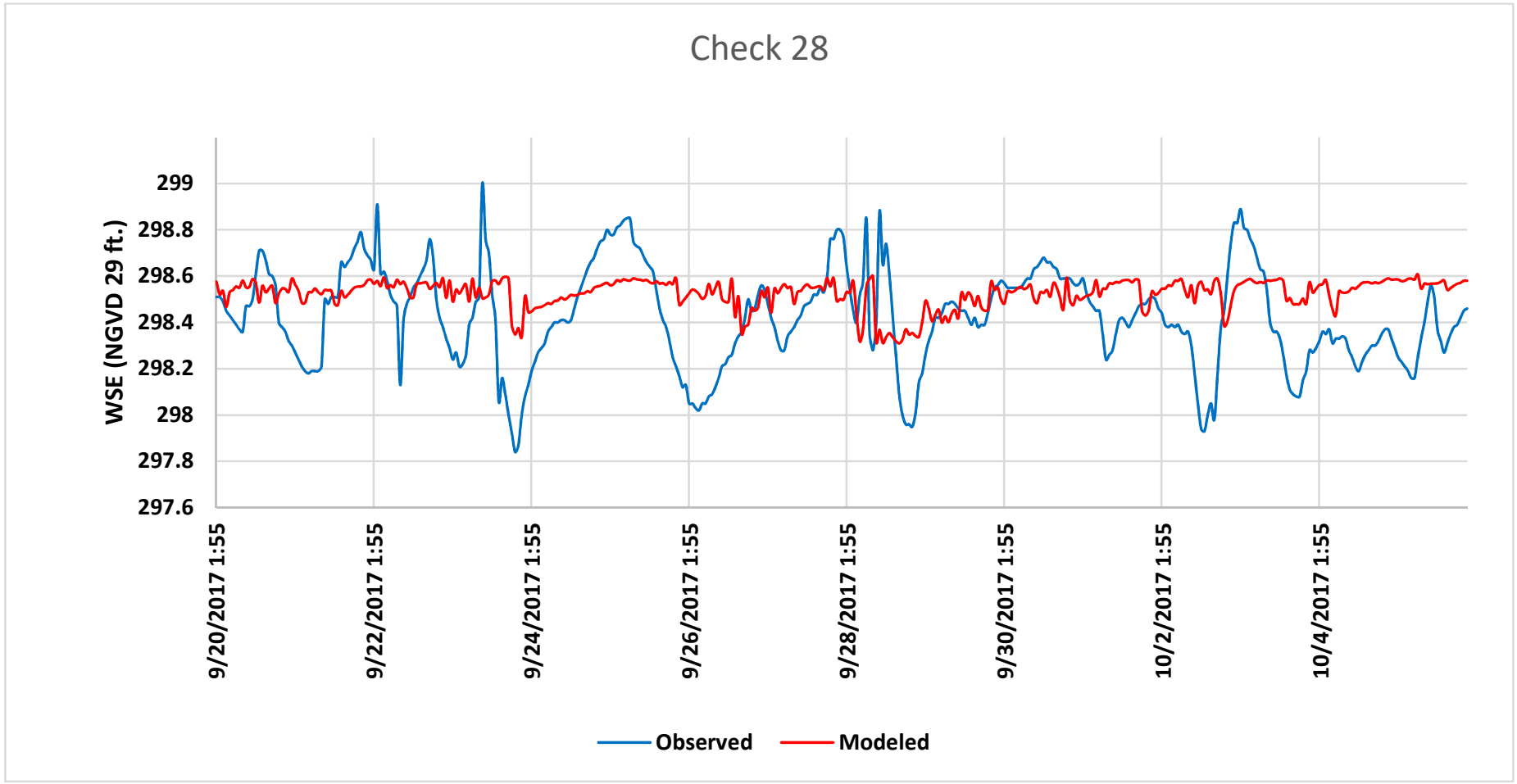
Check 28
WSE (NGVD 29 ft.)
299
298.8
298.6
298.4
298.2
298
297.8
297.6
9/20/2017 1:55
9/22/2017 1:55
9/24/2017 1:55
9/26/2017 1:55
9/28/2017 1:55
9/30/2017 1:55
10/2/2017 1:55
10/4/2017 1:55
Observed
Modeled

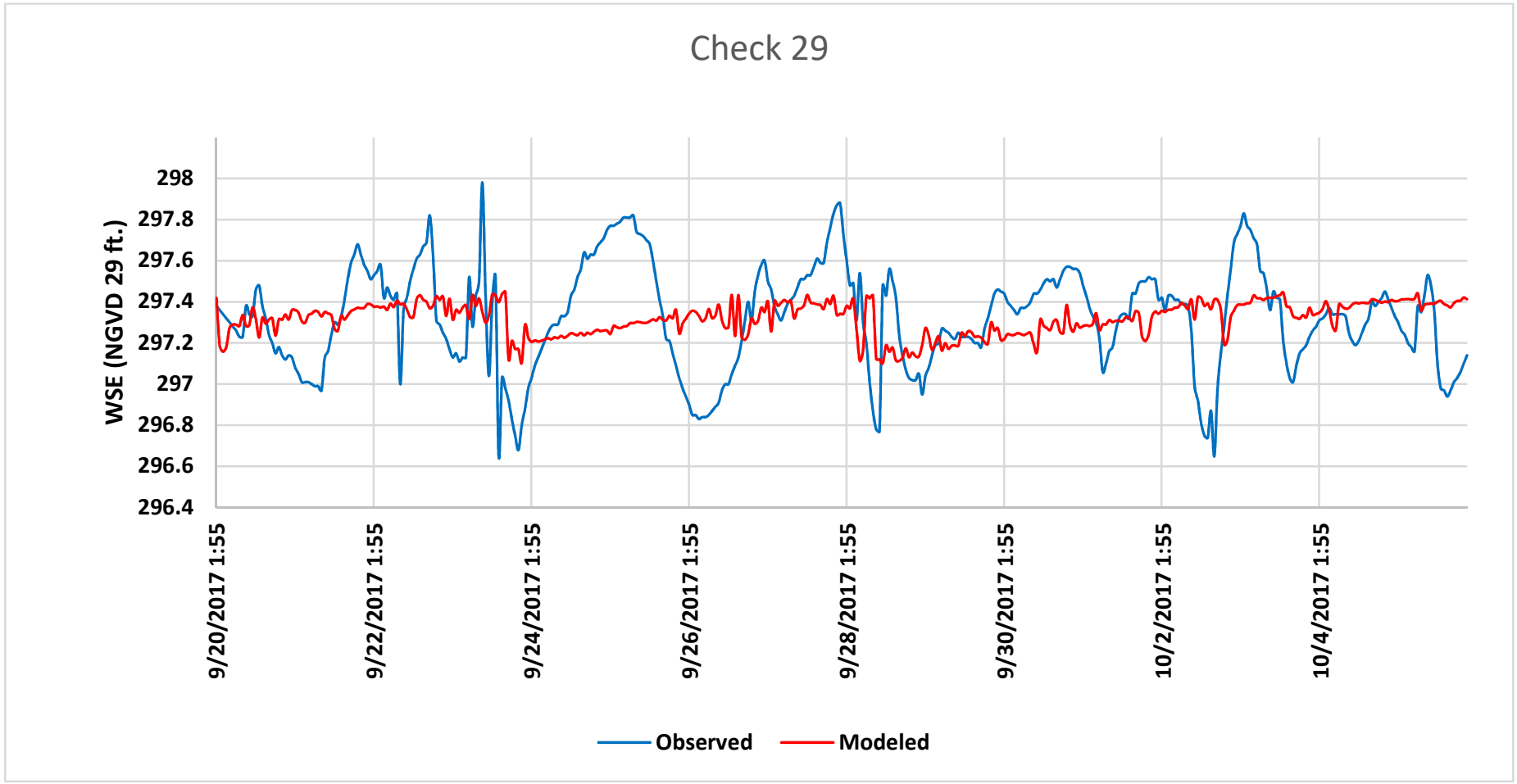
Check 29
WSE (NGVD 29 ft.)
298
297.8
297.6
297.4
297.2
297
296.8
296.6
296.4
9/20/2017 1:55
9/22/2017 1:55
9/24/2017 1:55
9/26/2017 1:55
9/28/2017 1:55
9/30/2017 1:55
10/2/2017 1:55
10/4/2017 1:55
Observed
Modeled

Pool 20 Redistributions

Pool 20 subsidence effects on deliveries

1 ft subsidence

<u>Historical Maximum</u>

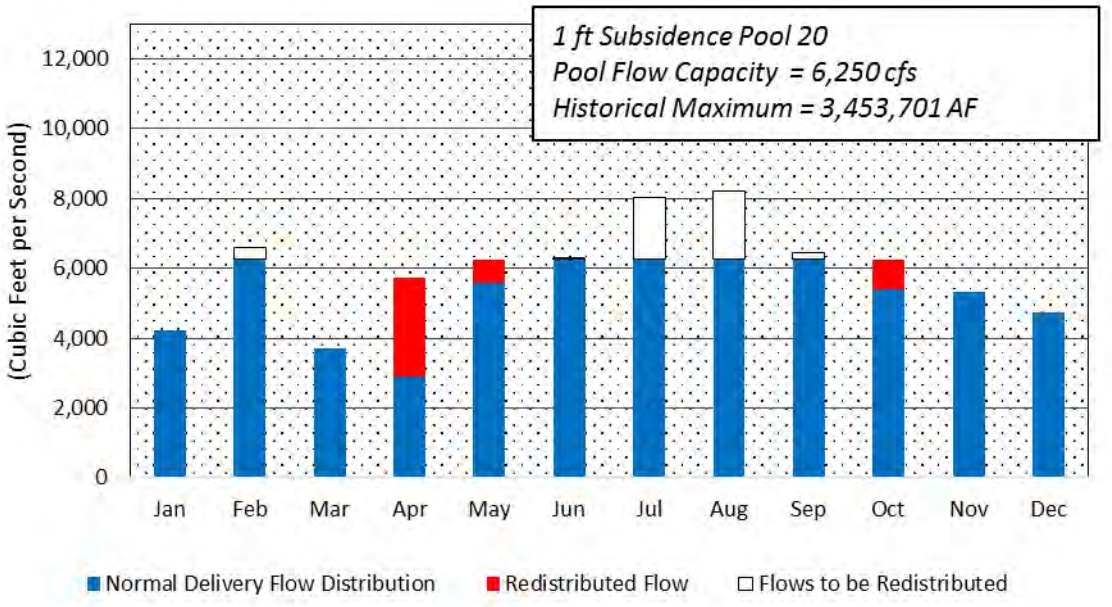

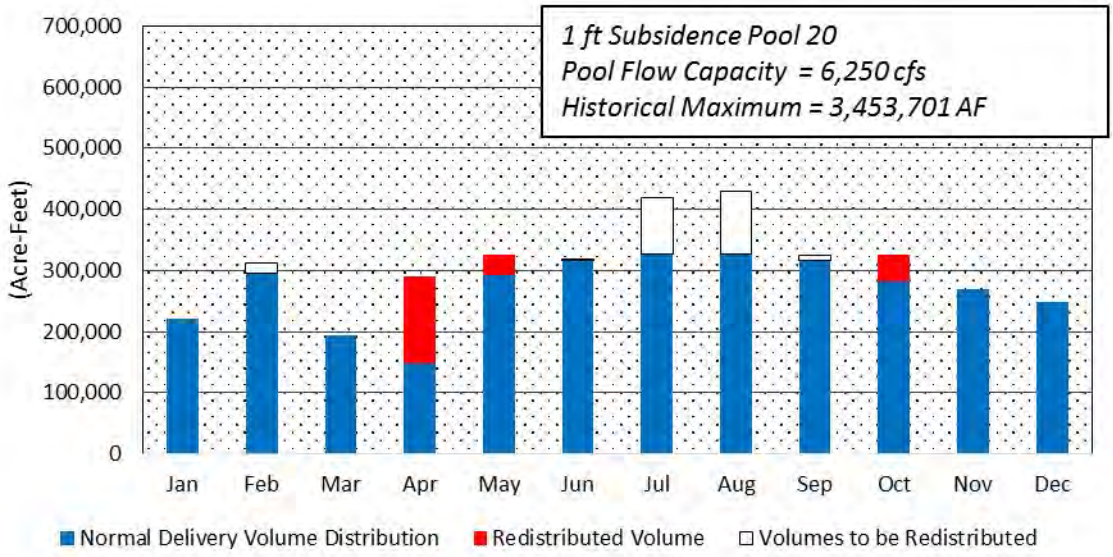

****All Volume Redistributed***

Maximum Table A

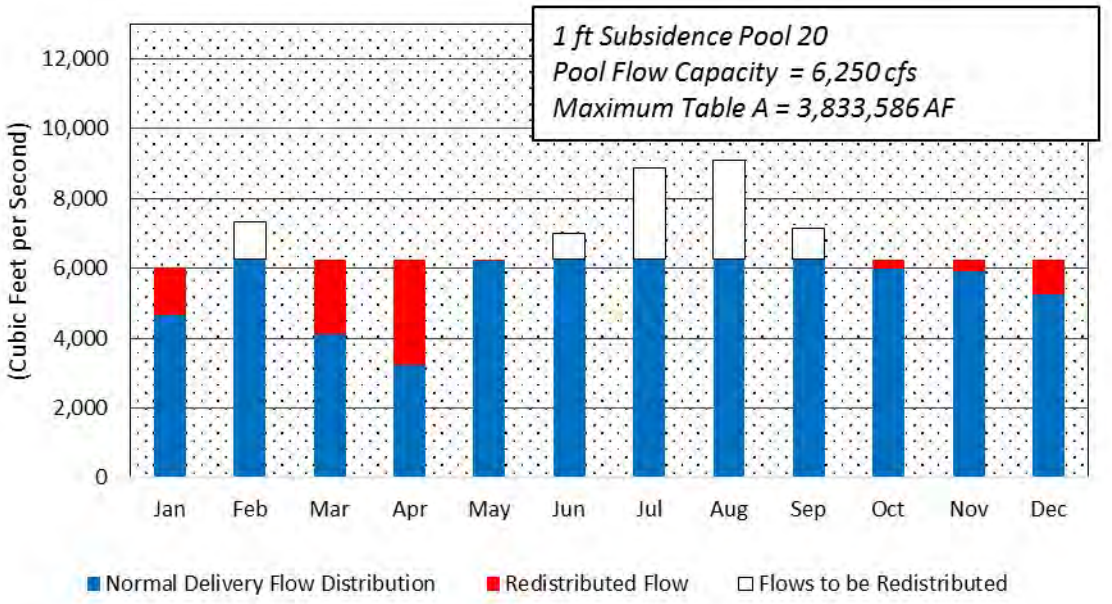

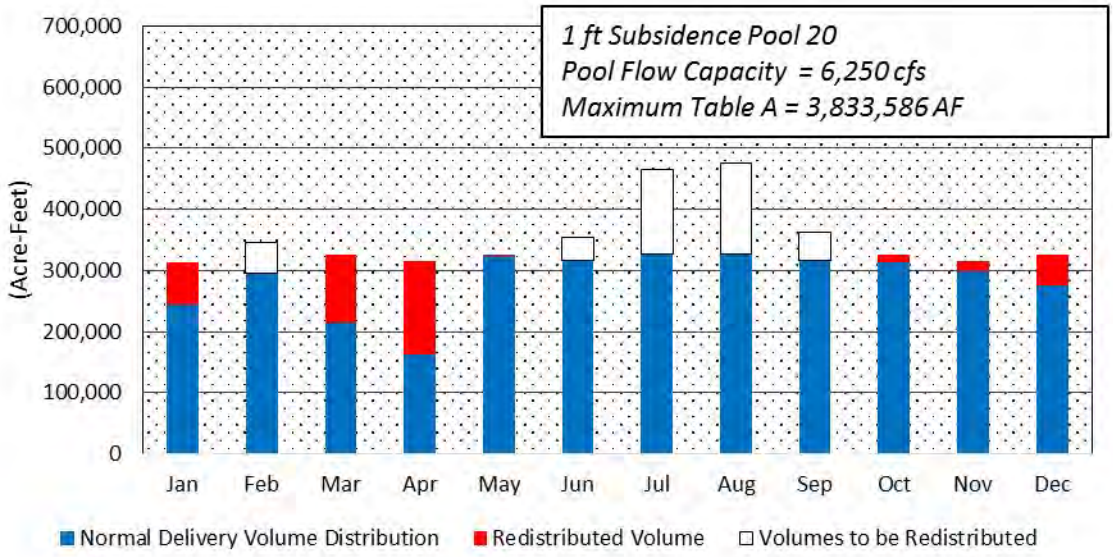

All Volume Redistributed

1.25 ft subsidence

<u>Historical Maximum</u>

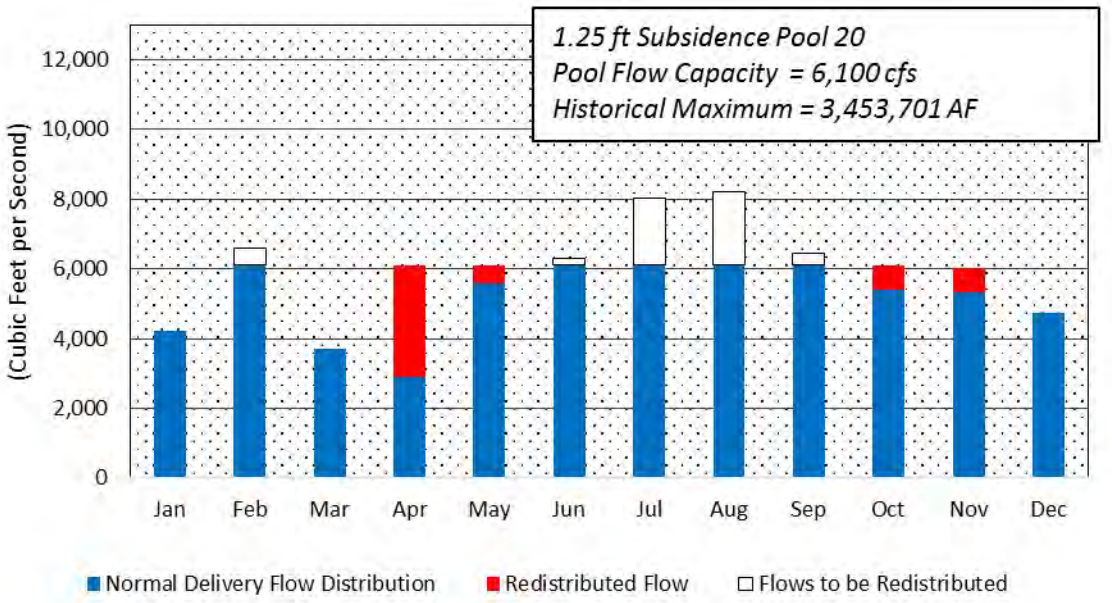

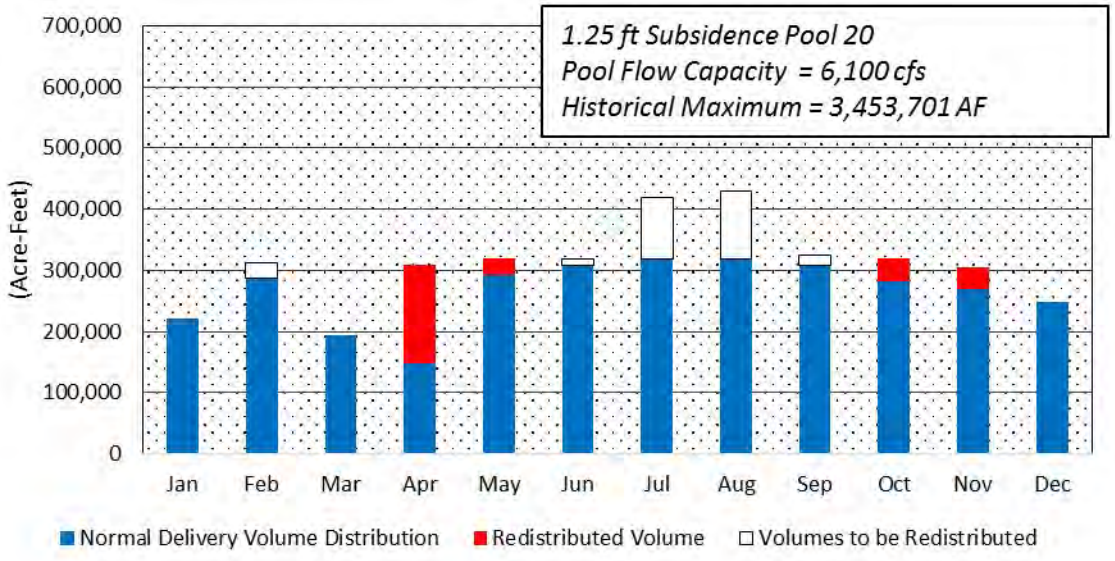

****All Volume Redistributed***

Maximum Table A

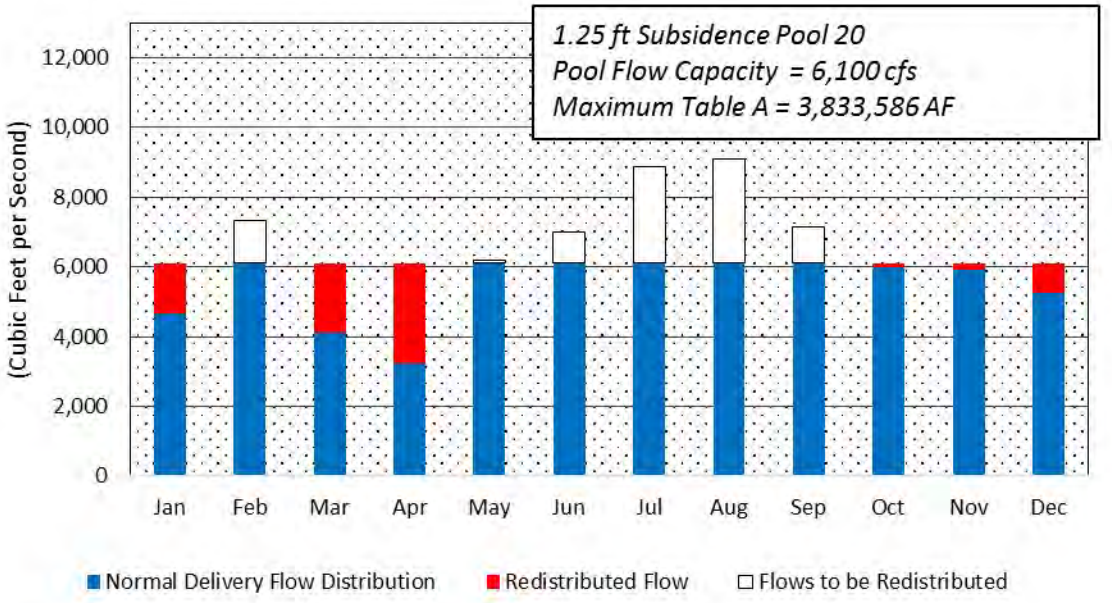

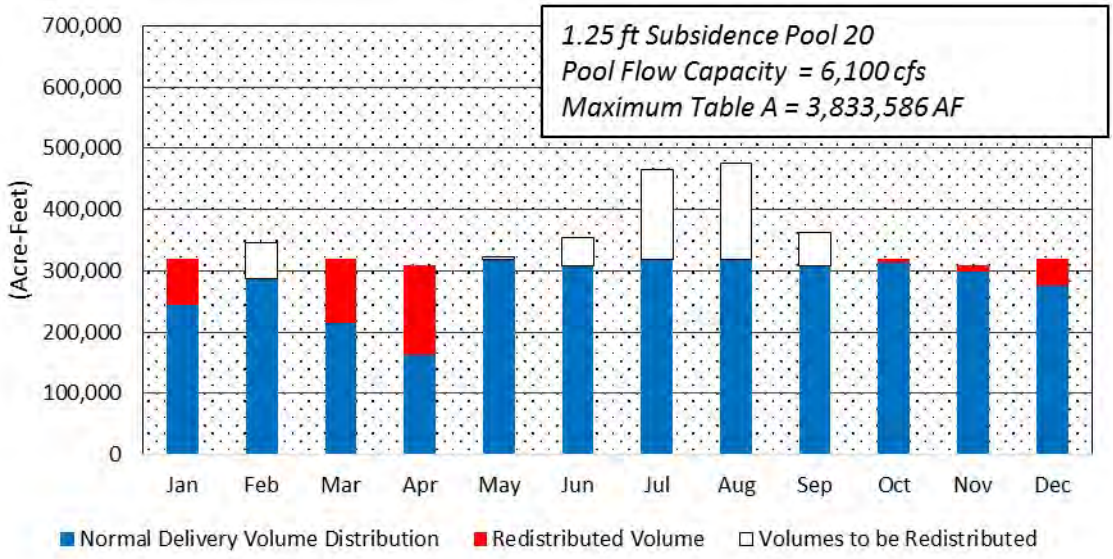

****79,817 AF not able to be redistributed***

1.5 ft subsidence

<u>Historical Maximum</u>

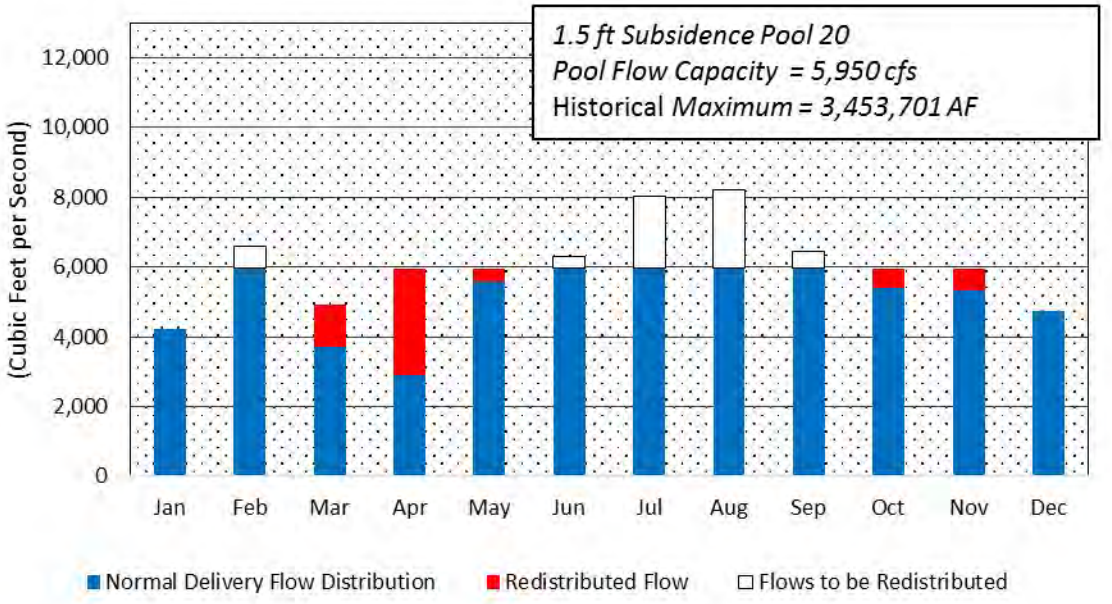

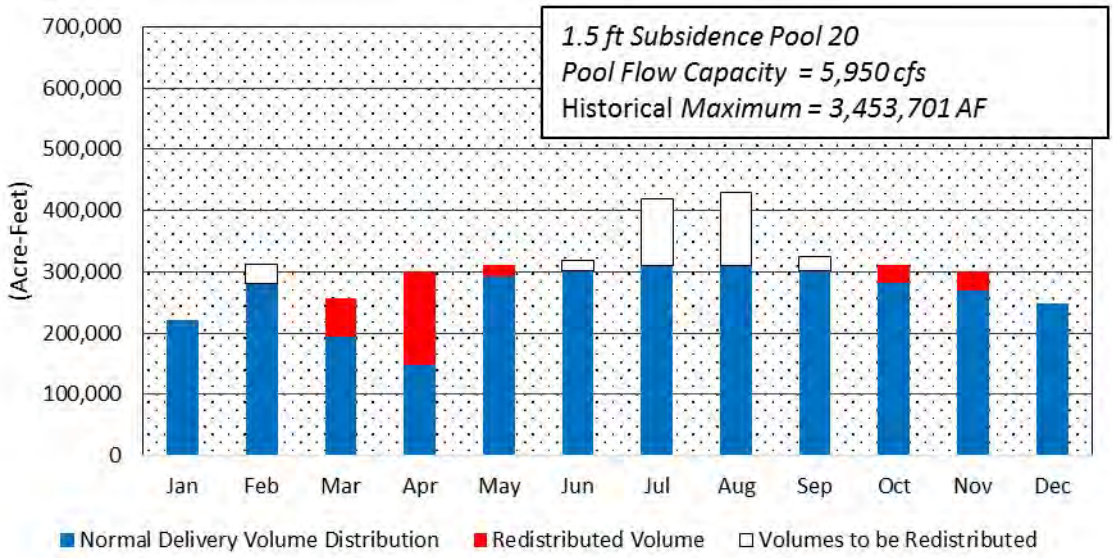

****All Volume Redistributed***

Maximum Table A

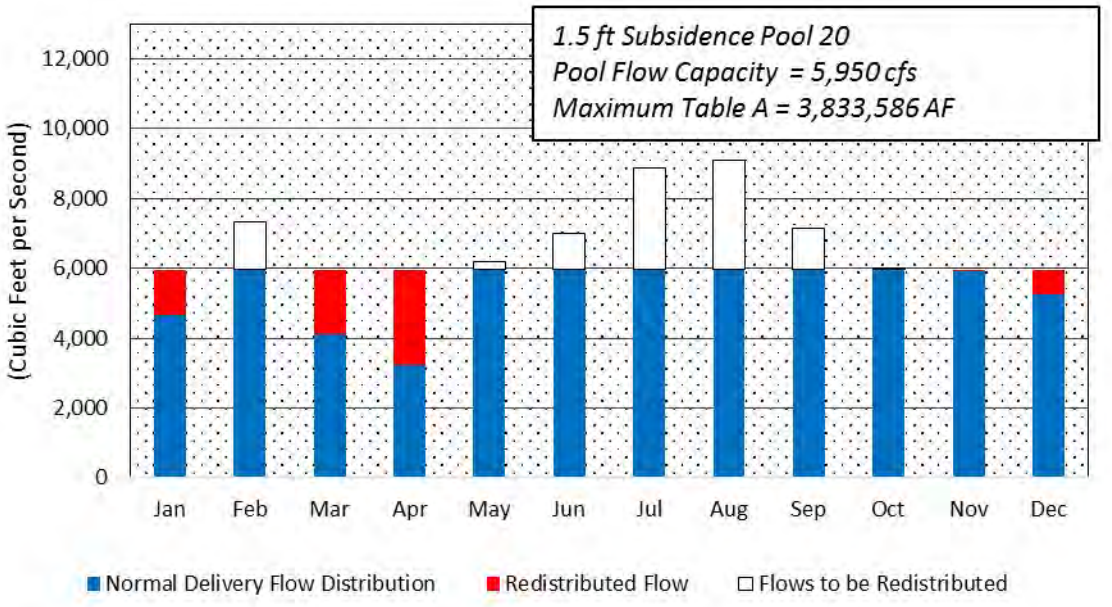

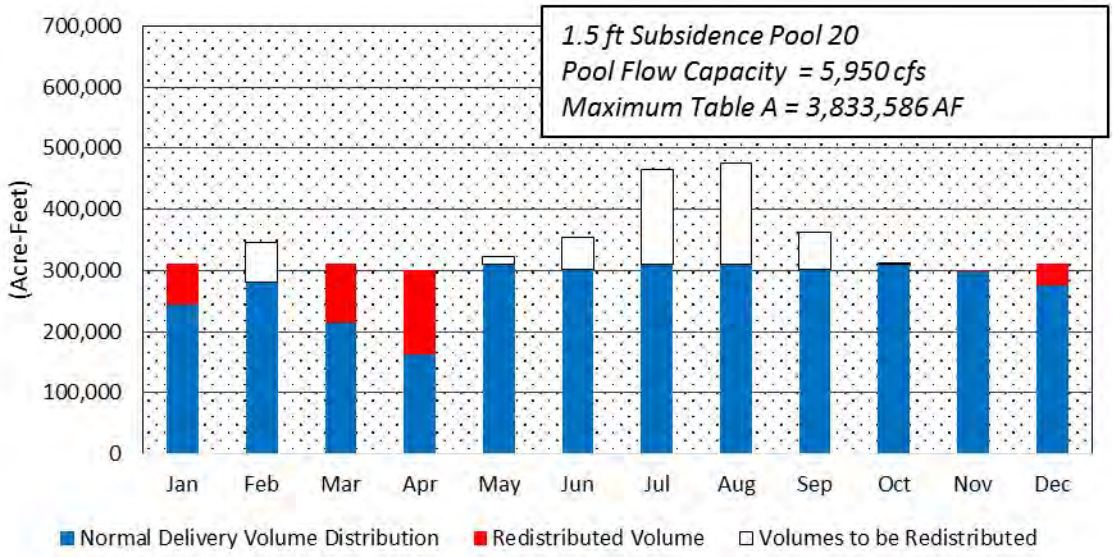

172123 AF not able to be redistributed

1.75 ft subsidence

<u>Historical Maximum</u>

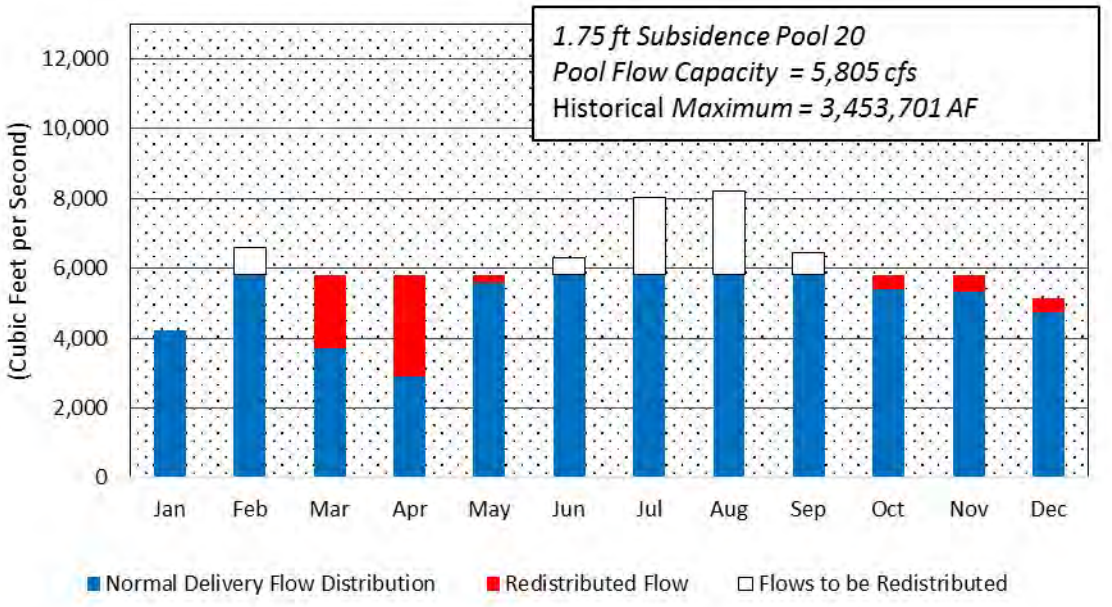

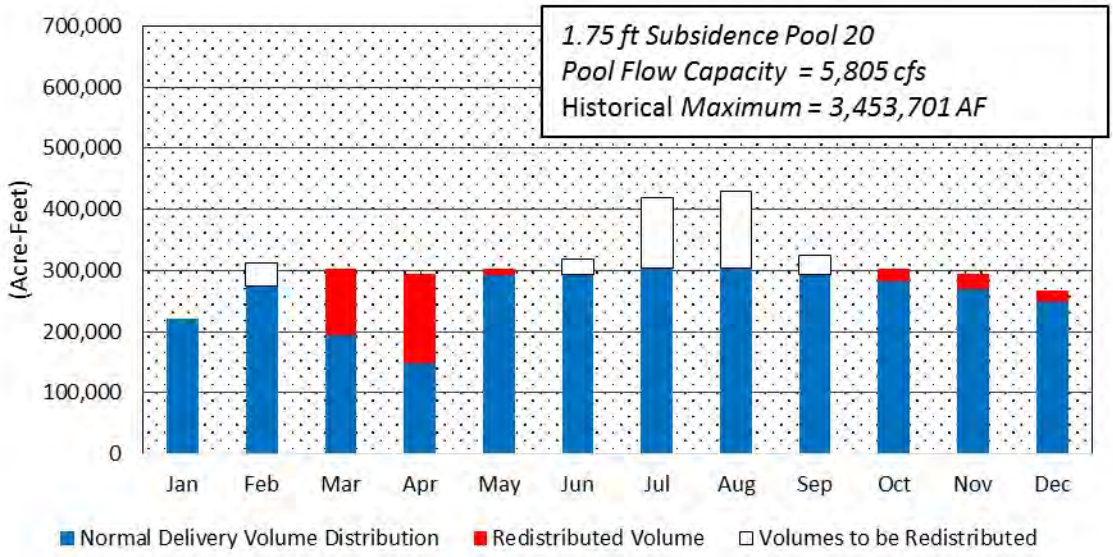

****All Volume Redistributed***

Maximum Table A

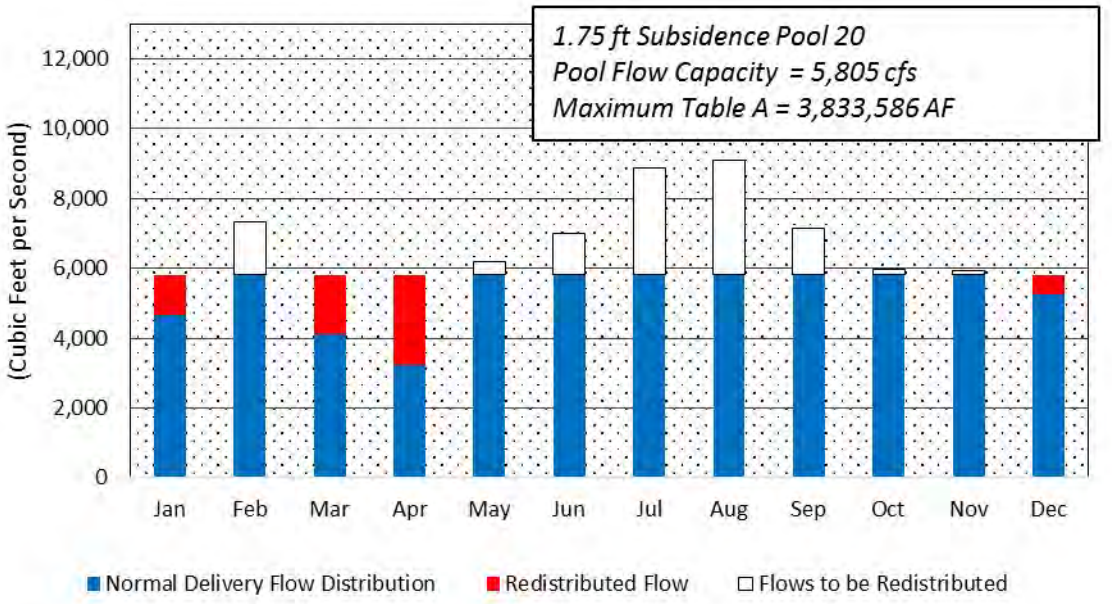

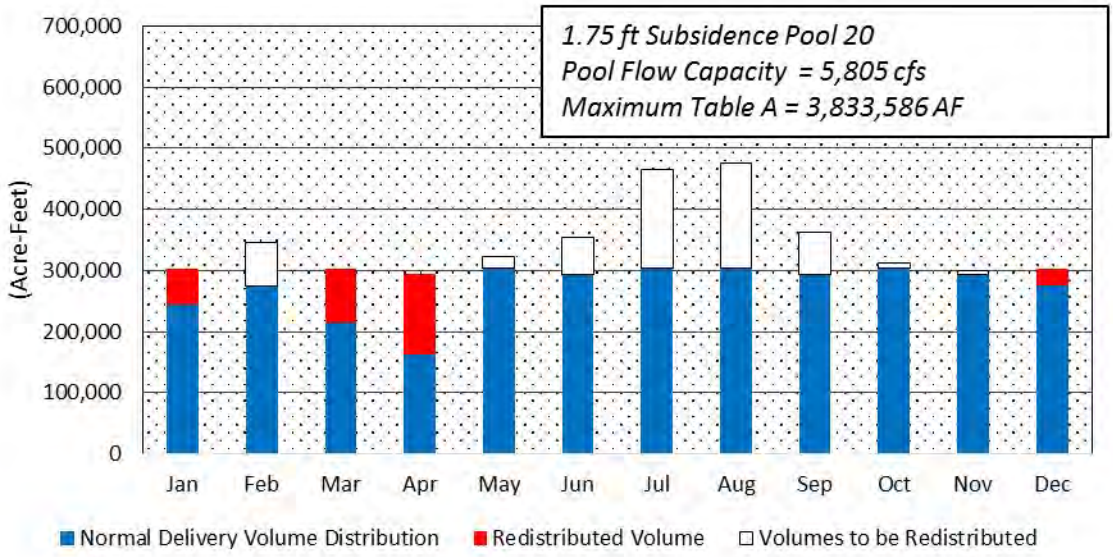

****261,352 AF not able to be redistributed***

2 ft subsidence

<u>Historical Maximum</u>

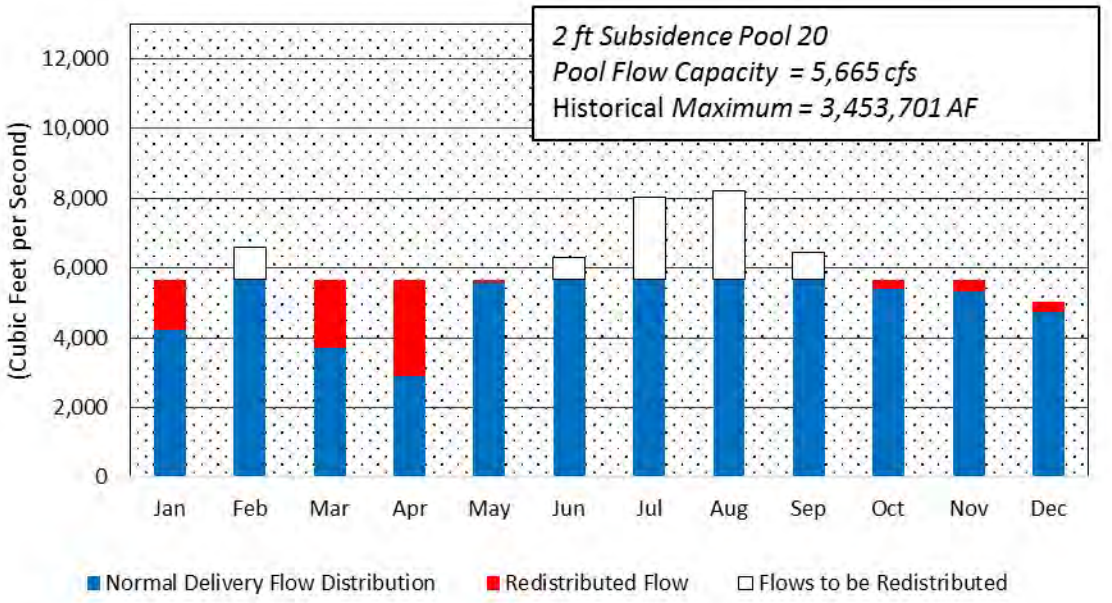

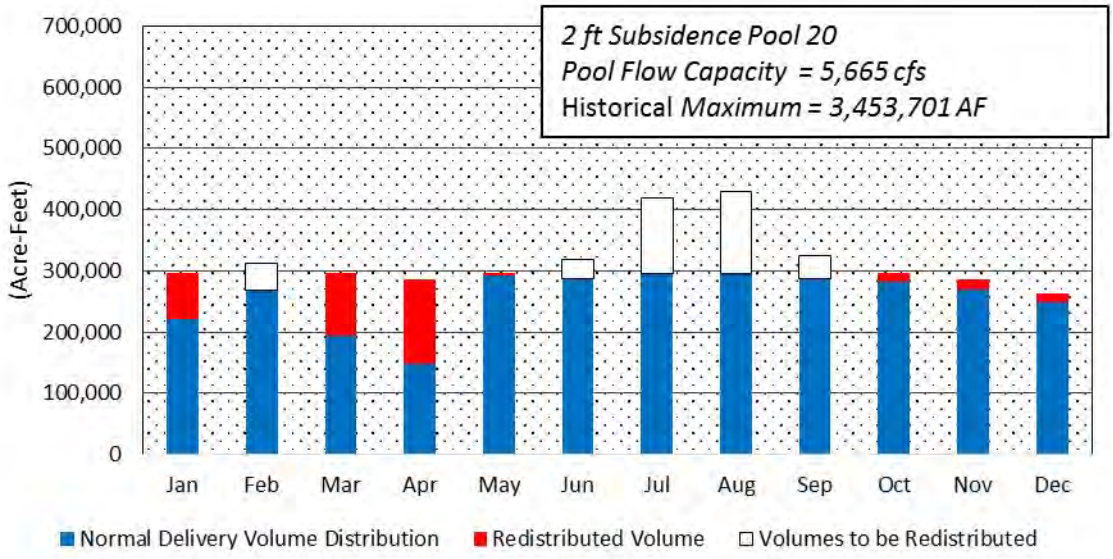

****All Volume Redistributed***

Maximum Table A

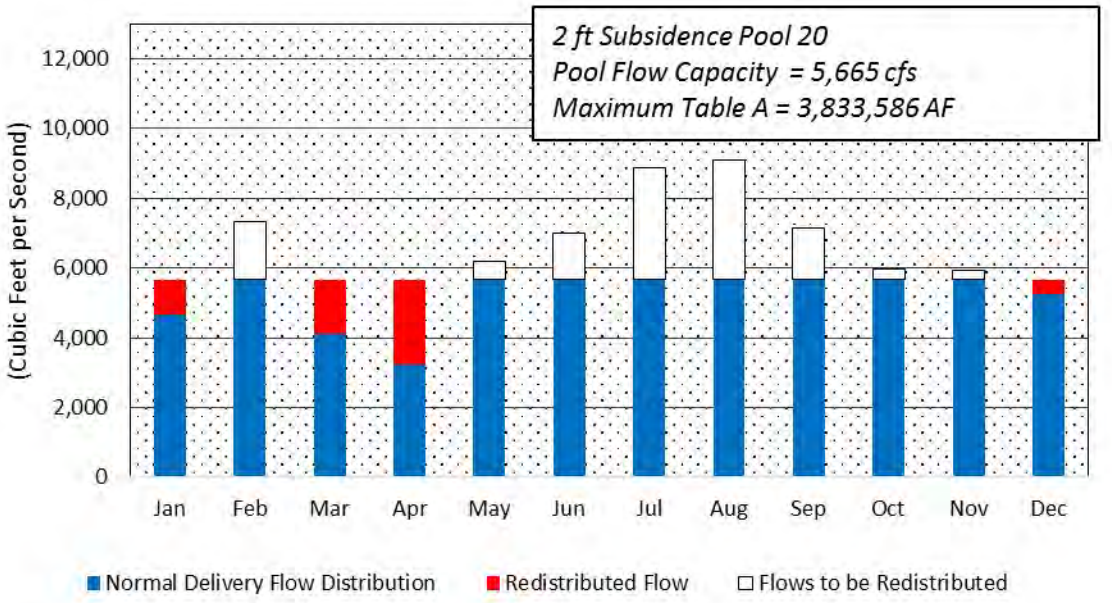

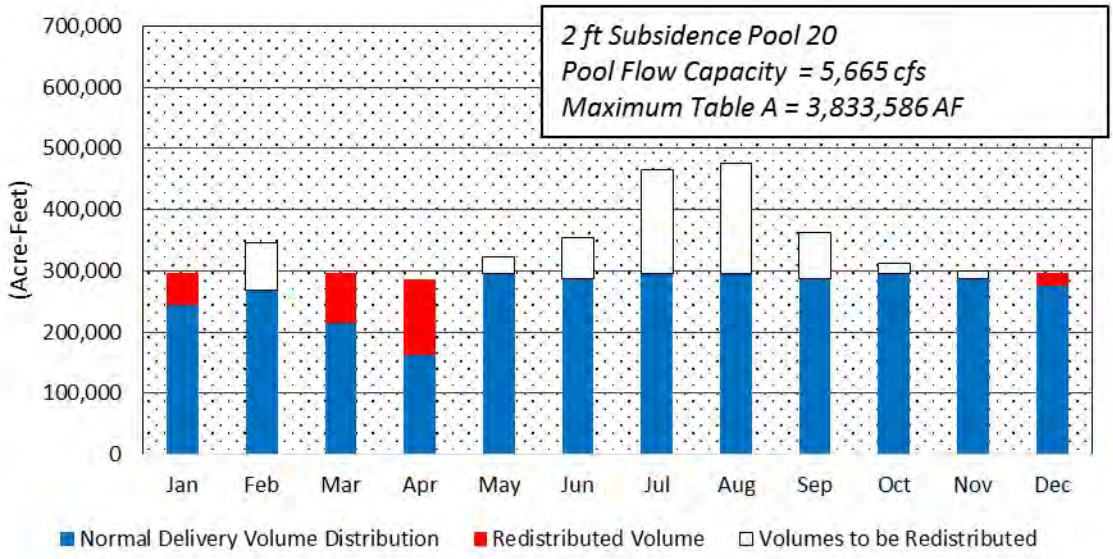

****452,117 AF not able to be redistributed***

3 ft subsidence

<u>Historical Maximum</u>

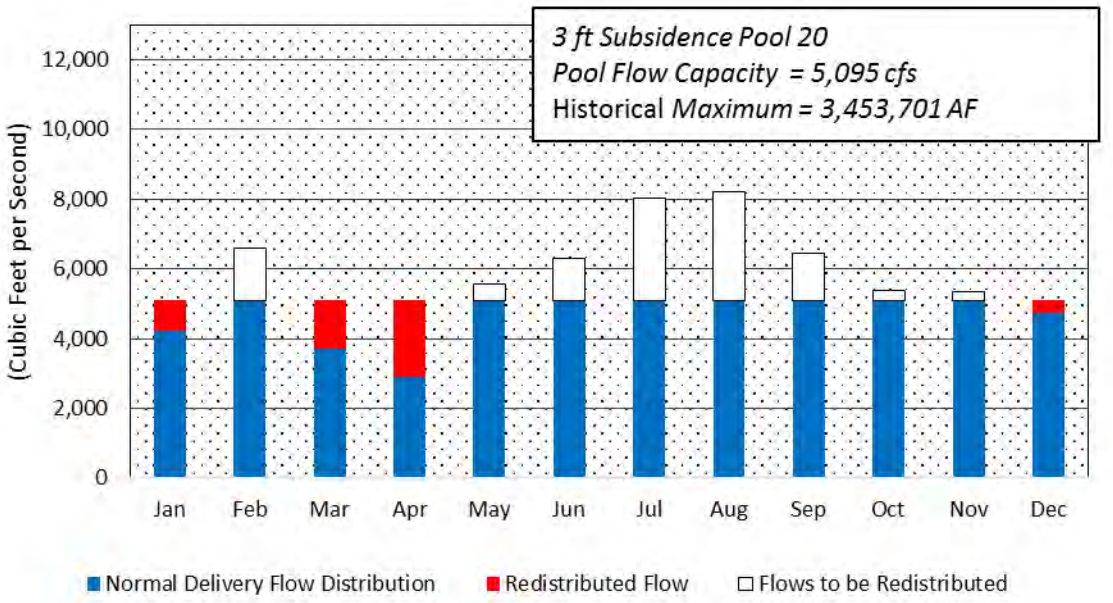

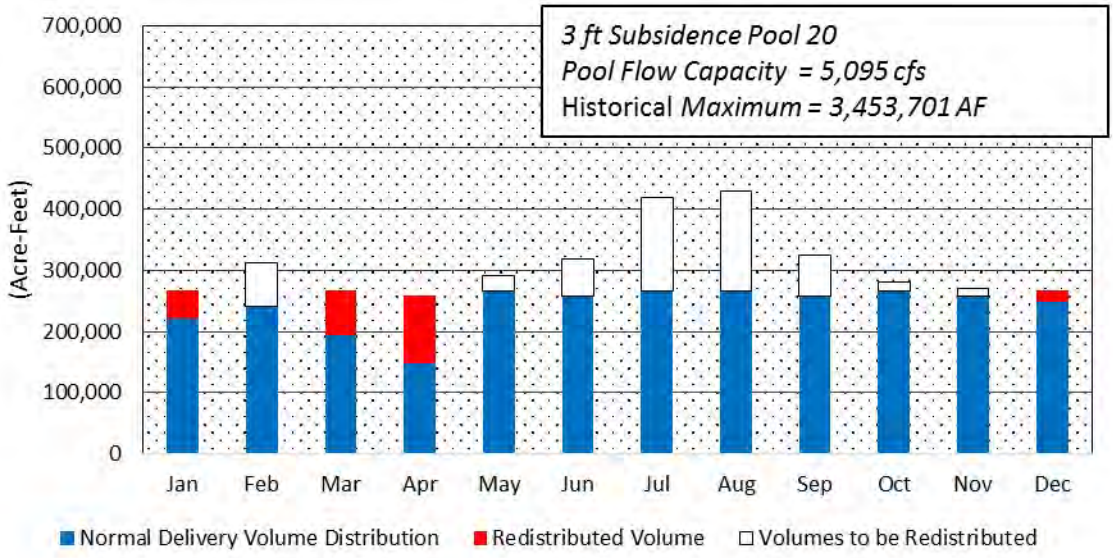

****318,381 AF not able to be redistributed***

Maximum Table A

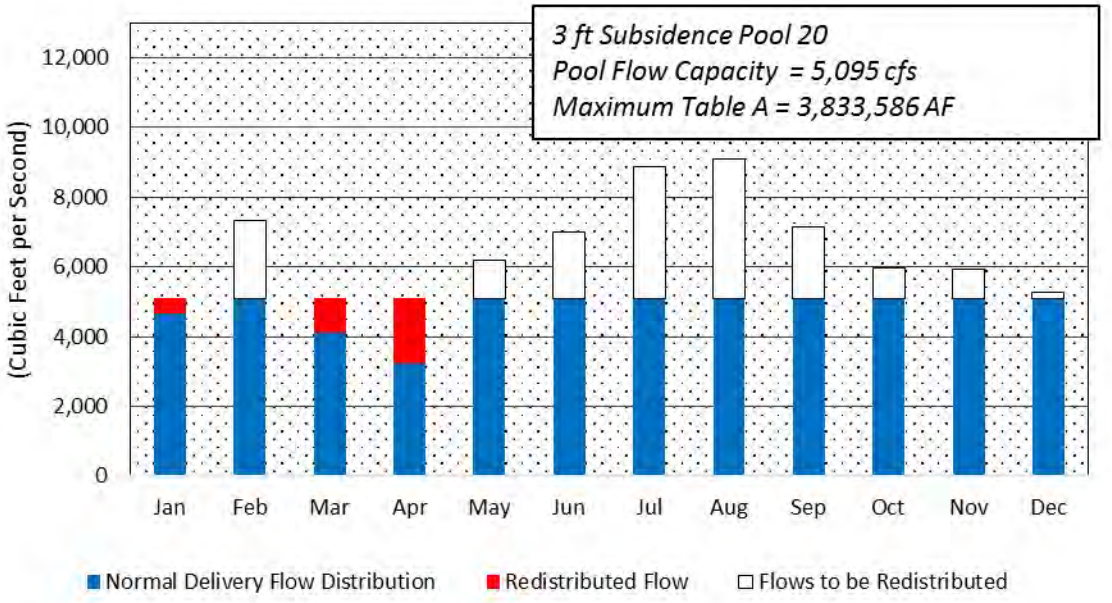

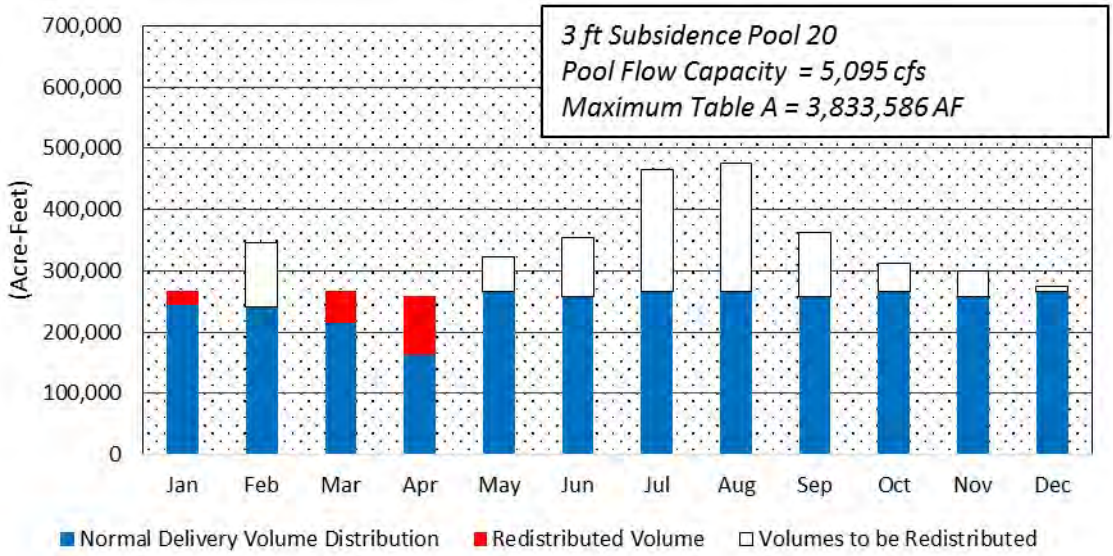

698,266 AF not able to be redistributed

Pool 25 Redistributions

Pool 24 & 25 subsidence effects on deliveries

1 ft subsidence

<u>Historical Maximum</u>

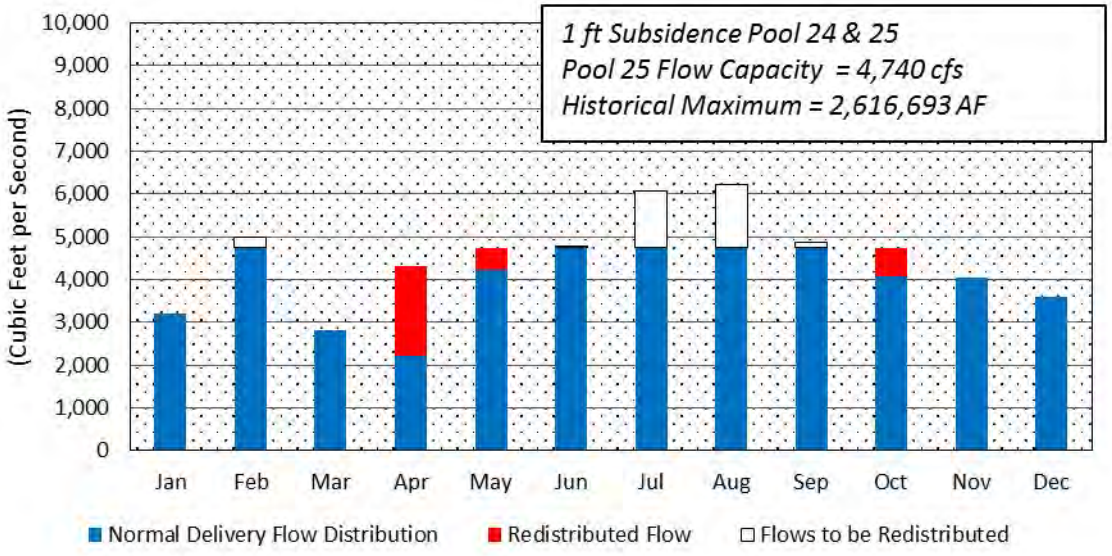

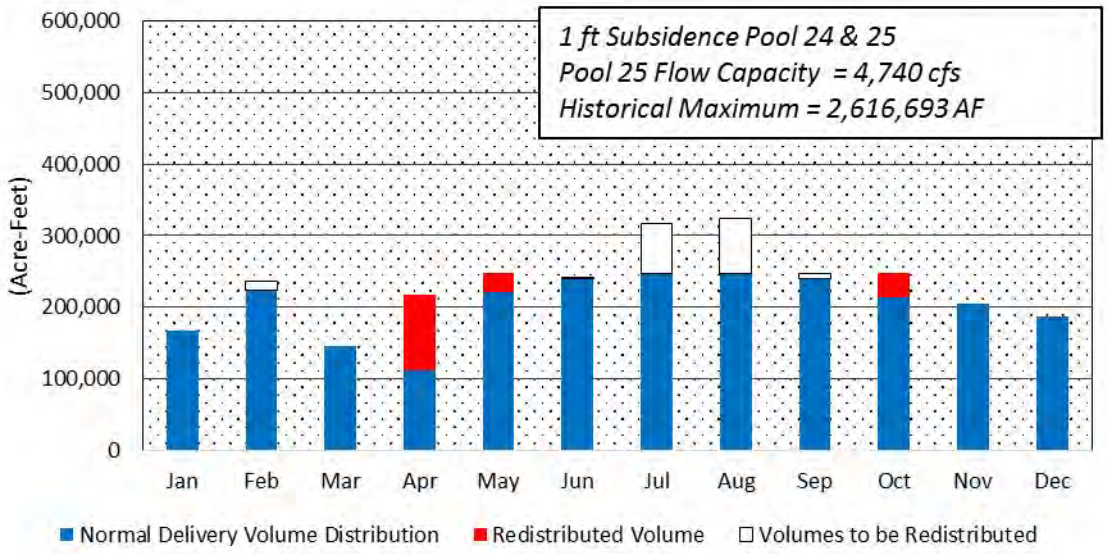

****All Volume Redistributed***

Maximum Table A

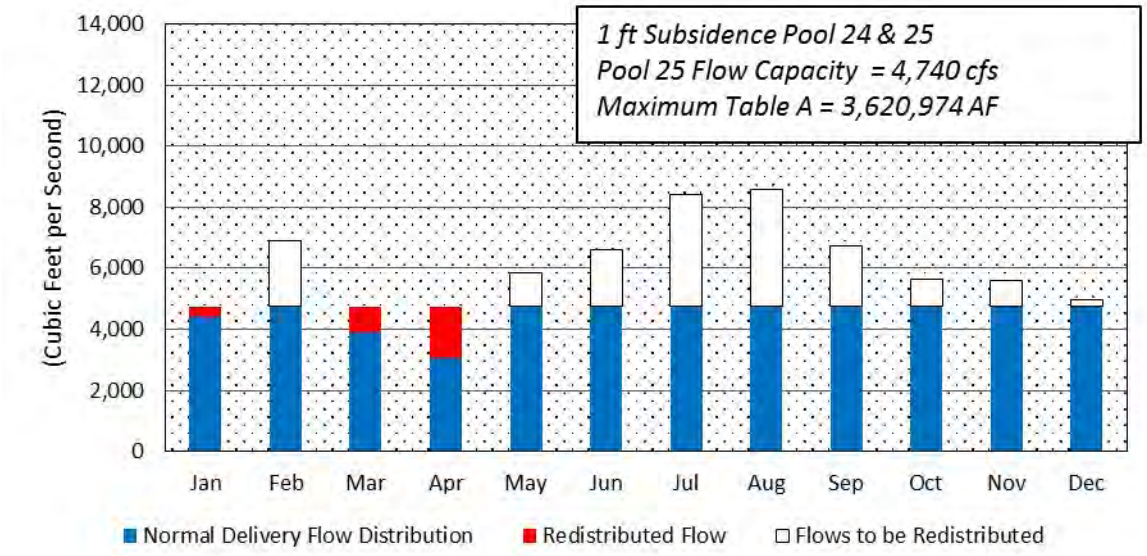

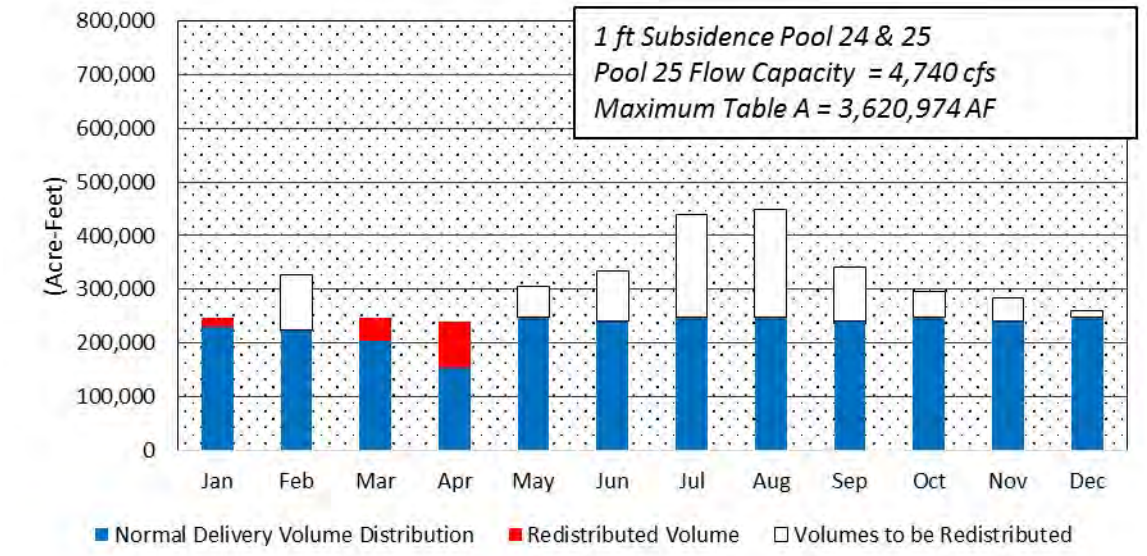

704,111 AF not able to be redistributed

1.25 ft subsidence

Historical Maximum

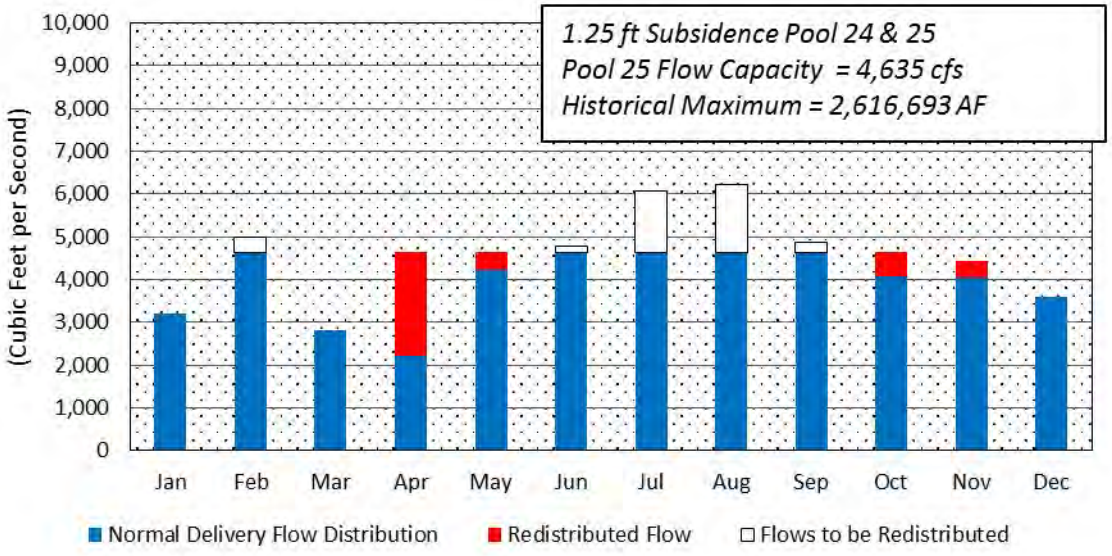

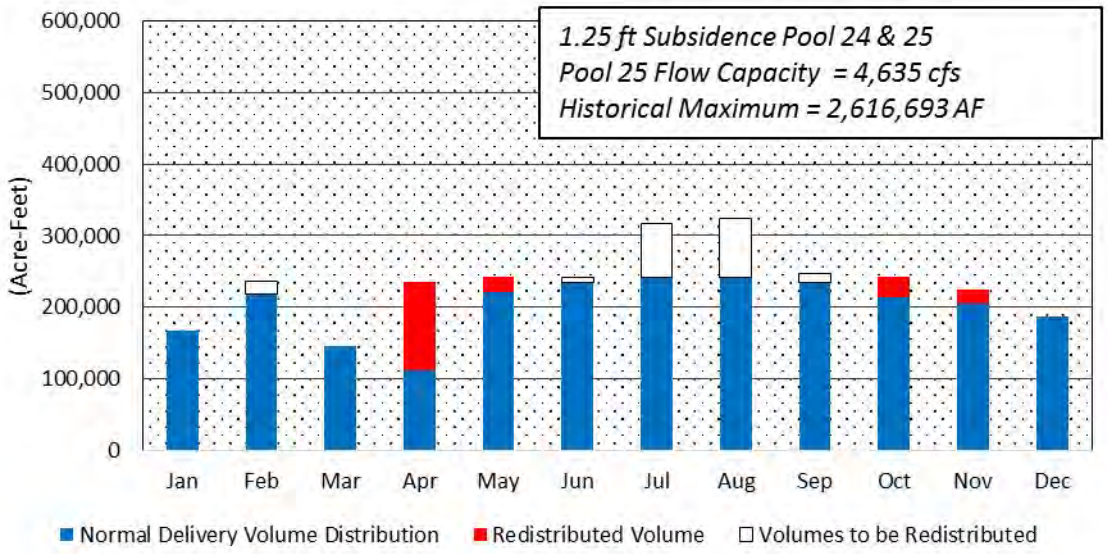

****All Volume Redistributed***

Maximum Table A

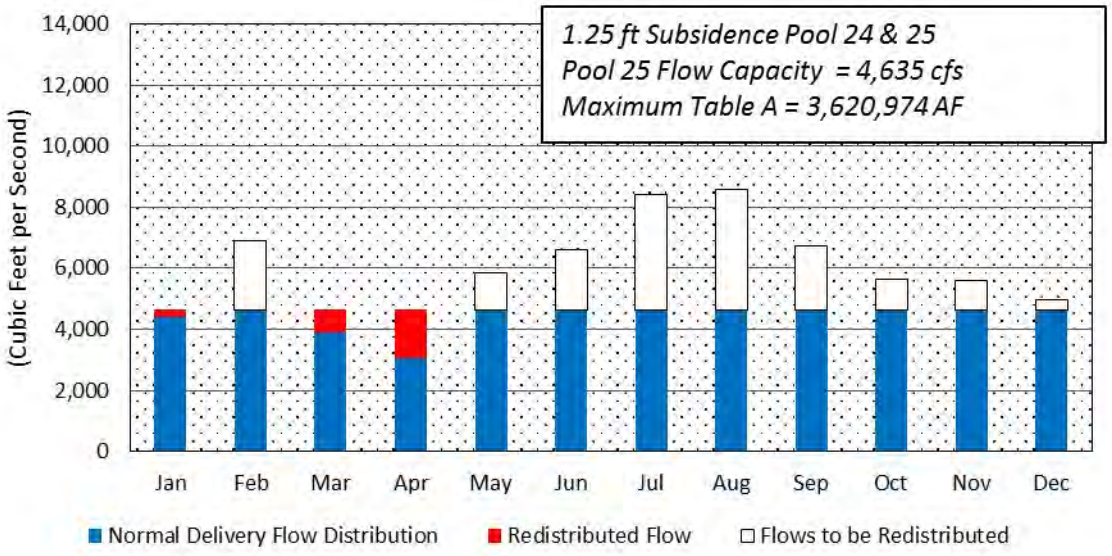

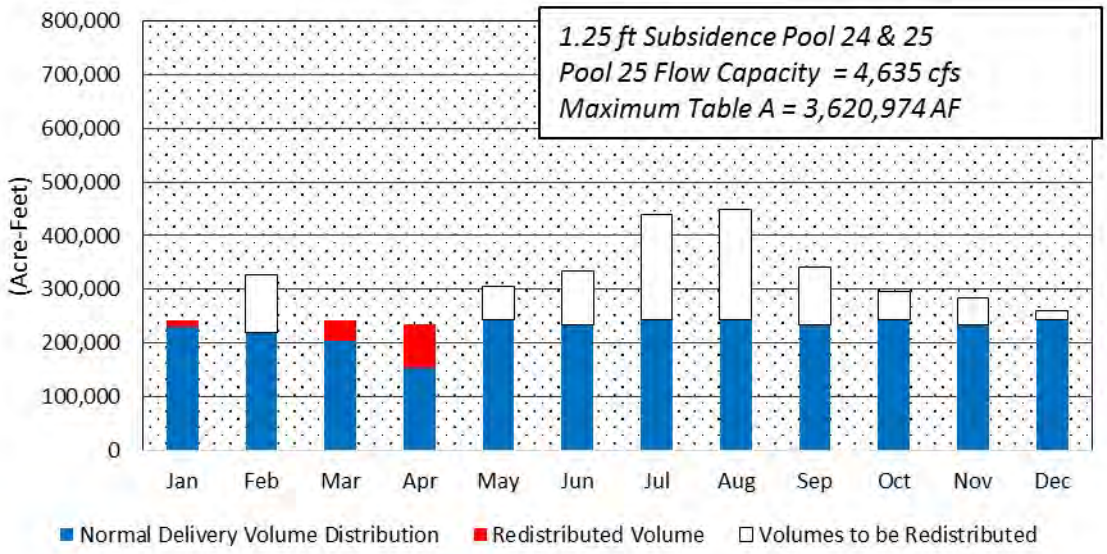

768,725 AF not able to be redistributed

1.5 ft subsidence

Historical Maximum

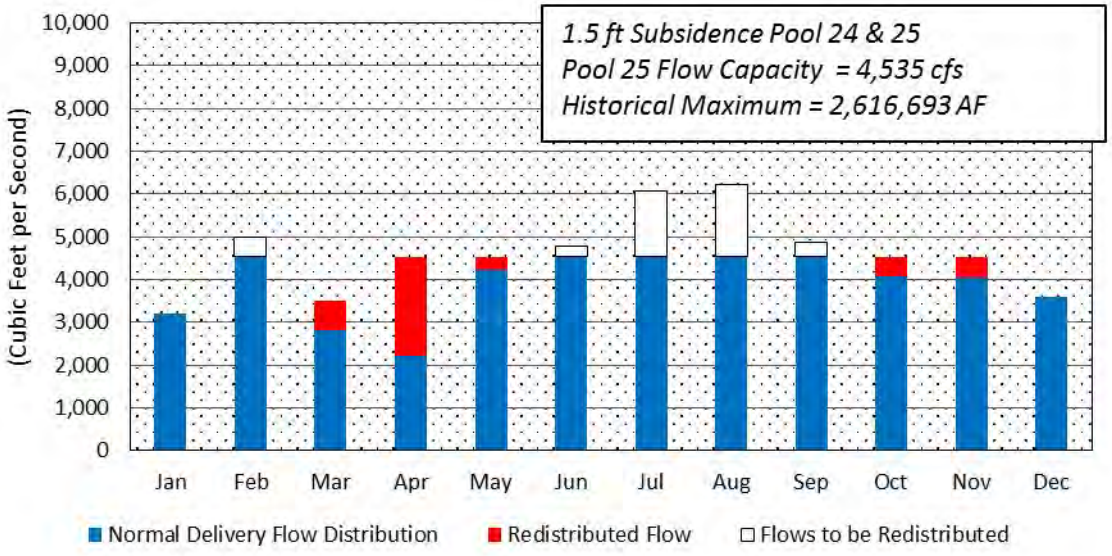

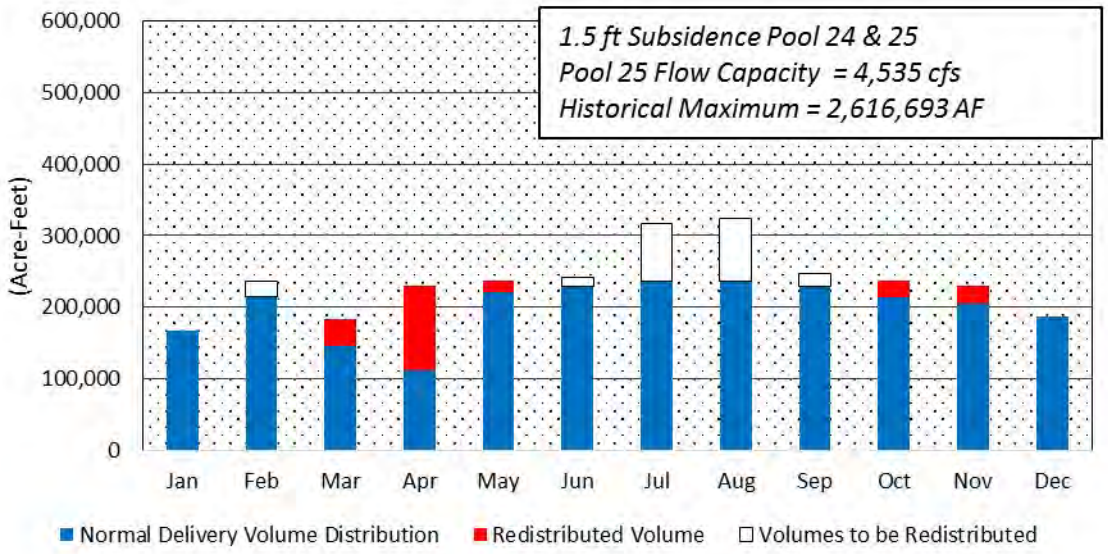

****All Volume Redistributed***

Maximum Table A

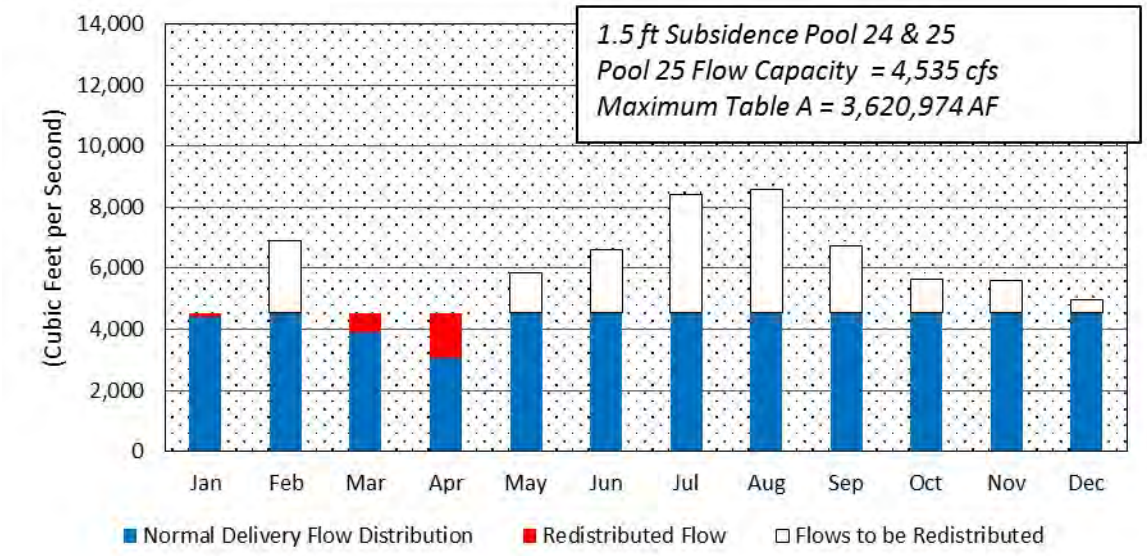

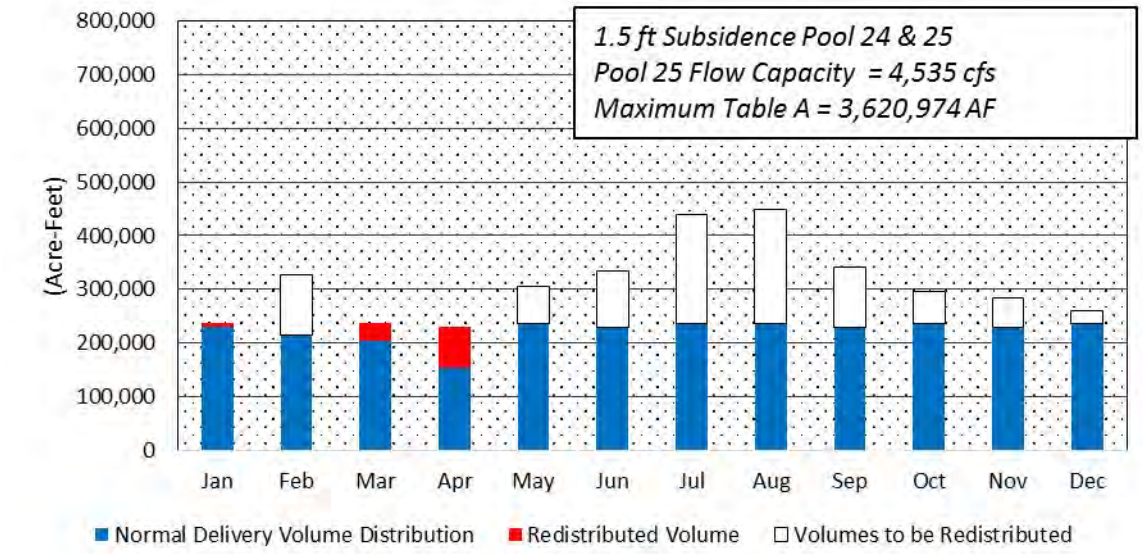

830,262 AF not able to be redistributed

1.75 ft subsidence

Historical Maximum

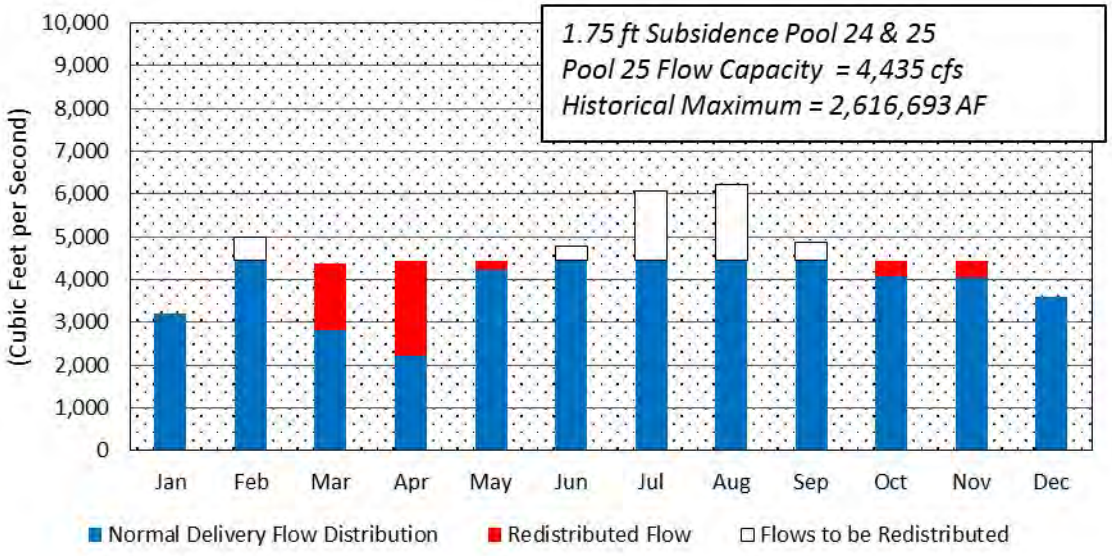

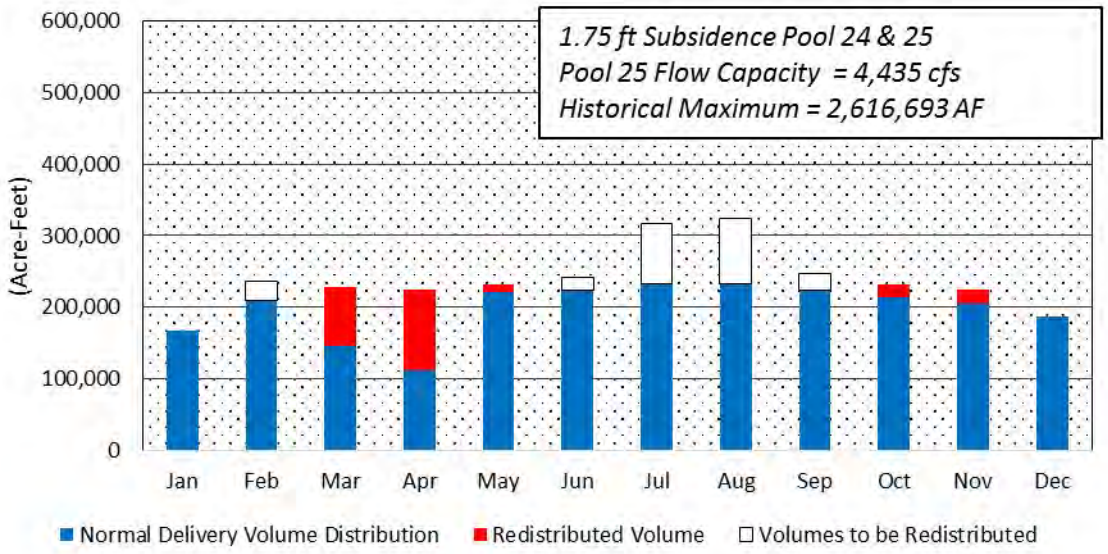

****All Volume Redistributed***

Maximum Table A

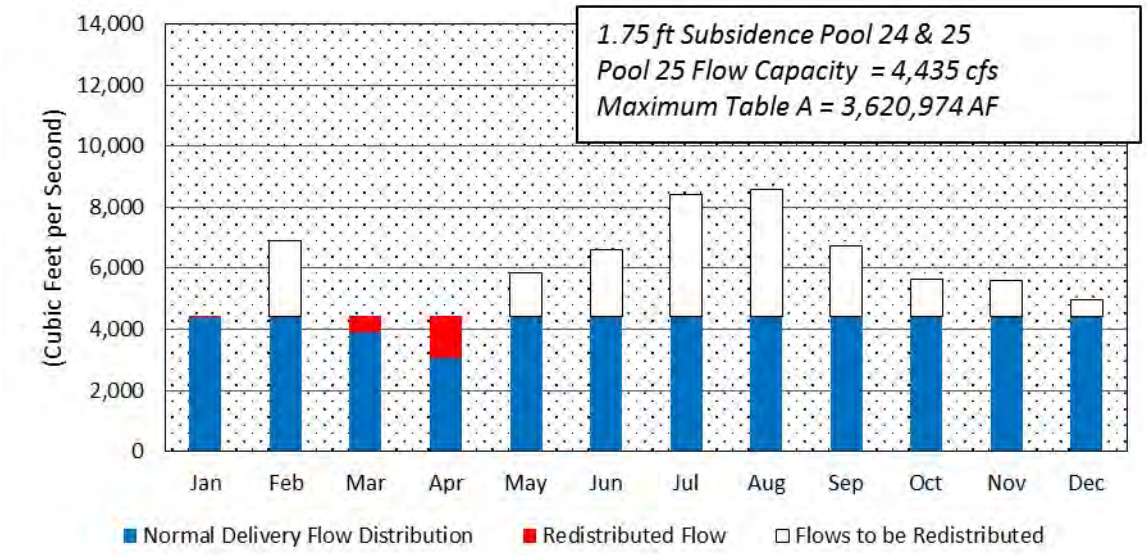

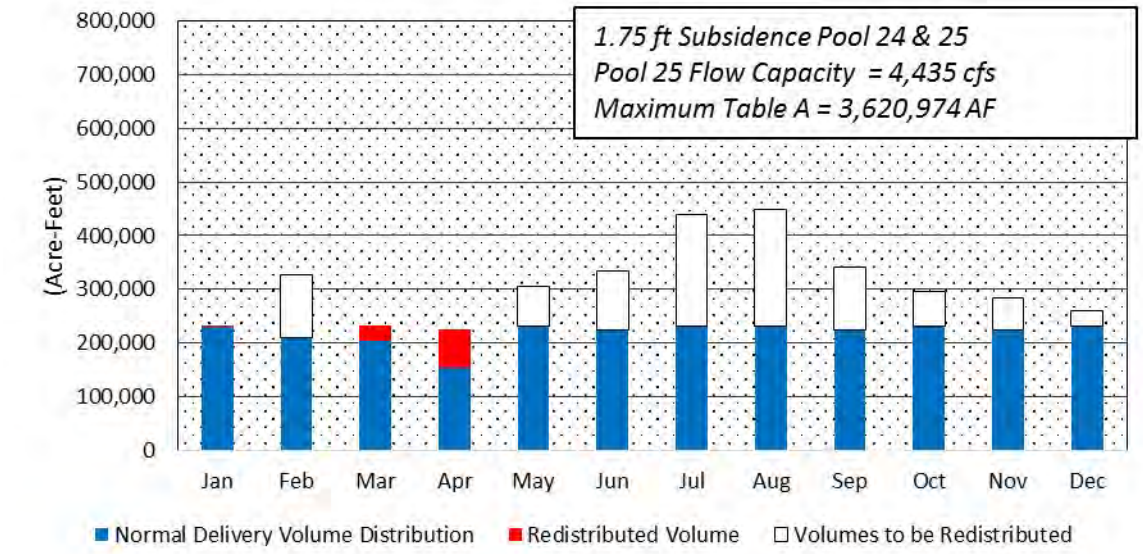

****891,800 AF not able to be redistributed***

2 ft subsidence

Historical Maximum

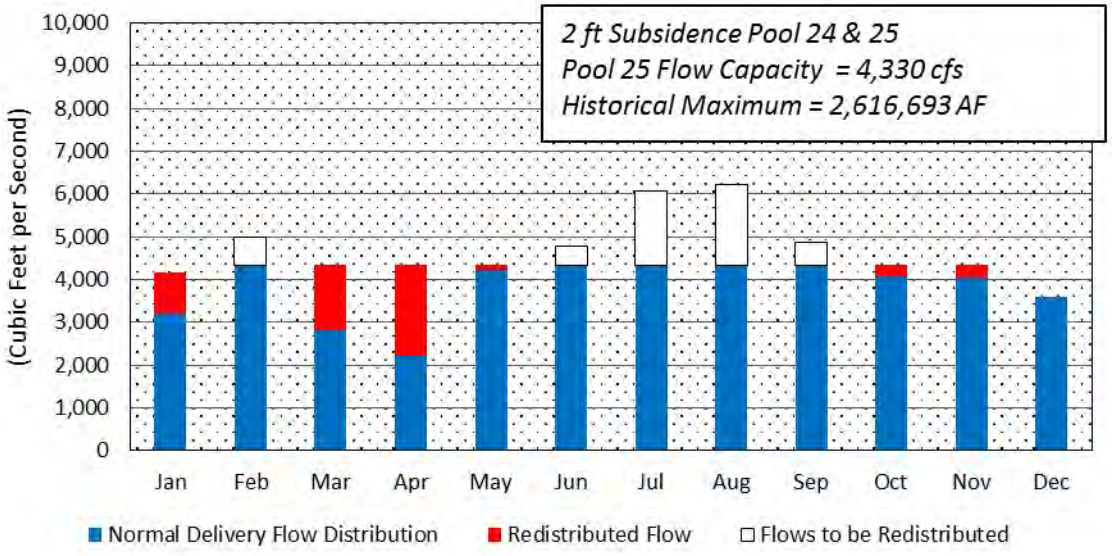

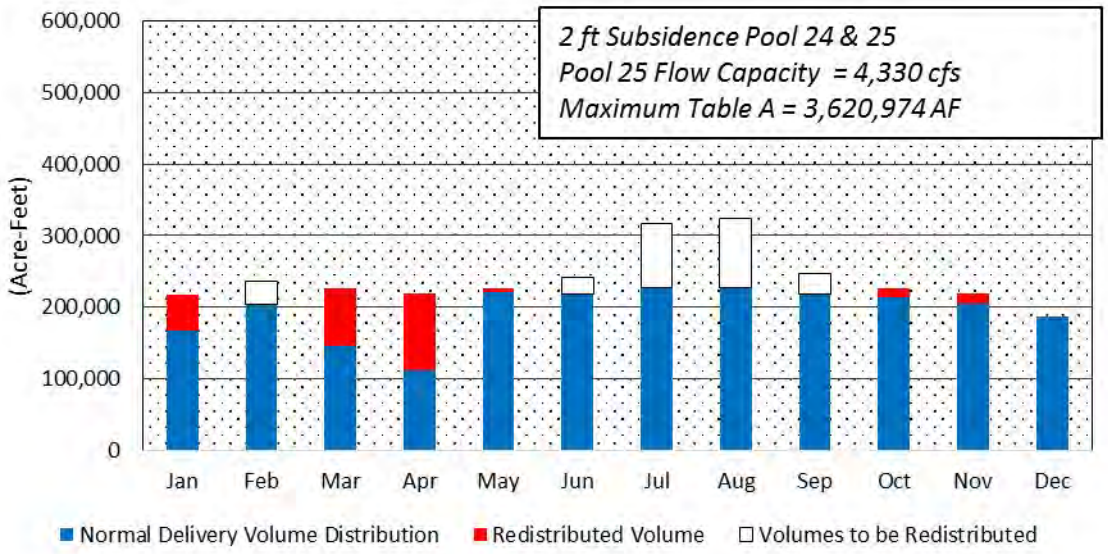

****All Volume Redistributed***

Maximum Table A

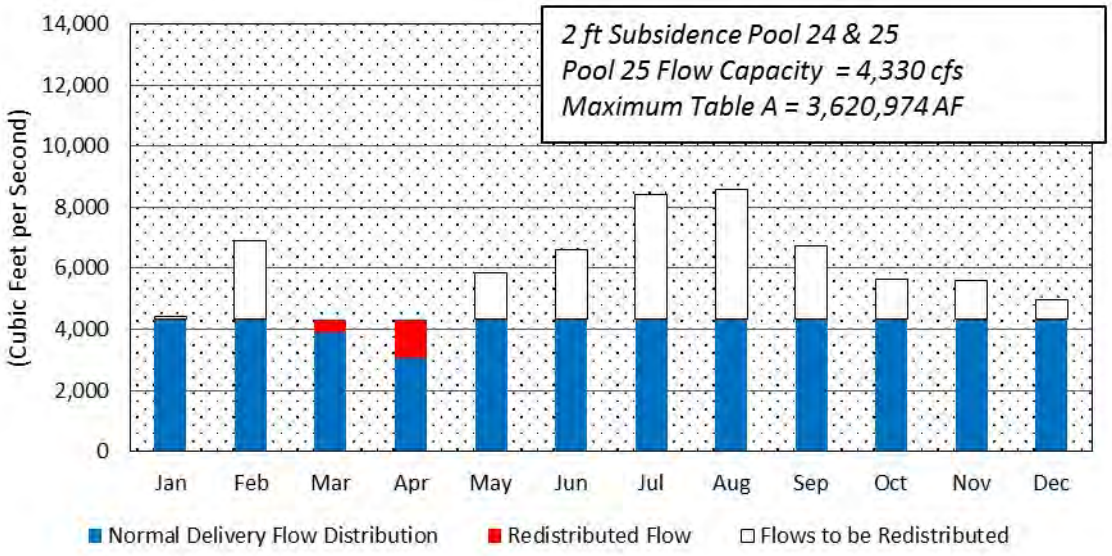

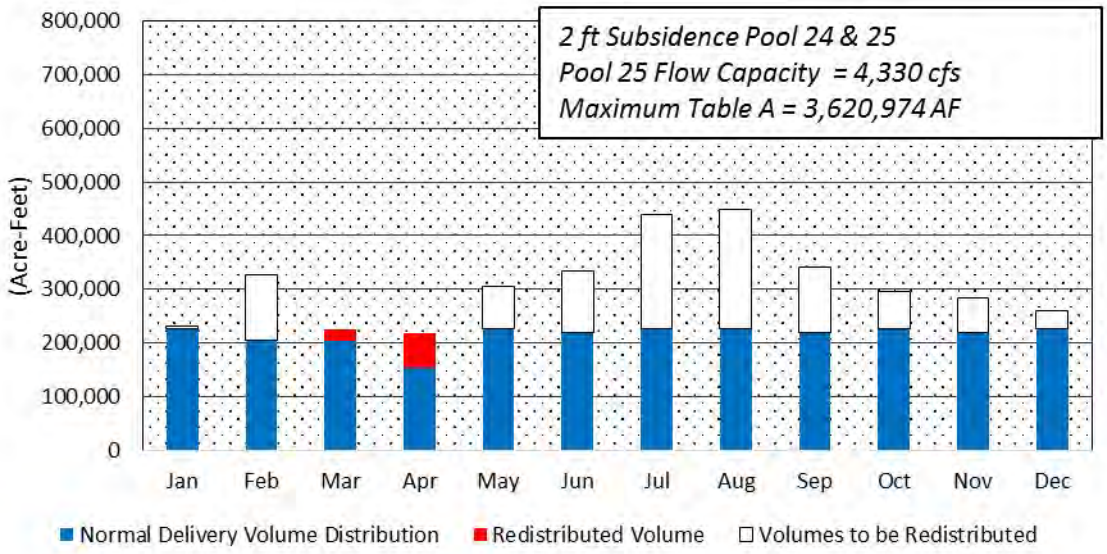

956,414 AF not able to be redistributed

Appendix C. Updated Subsidence Plates

Dos Amigos Pumping Plant to Kettleman City Operational Profile

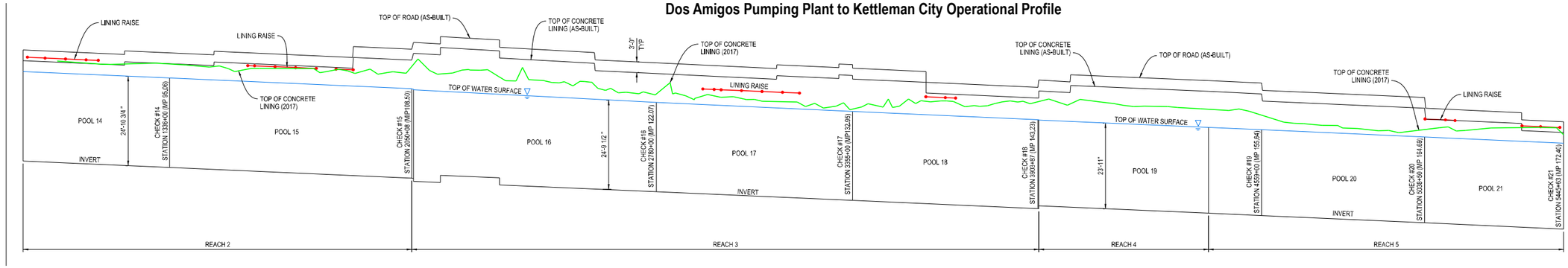

Dos Amigos Pumping Plant to Kettleman City Subsidence Profile

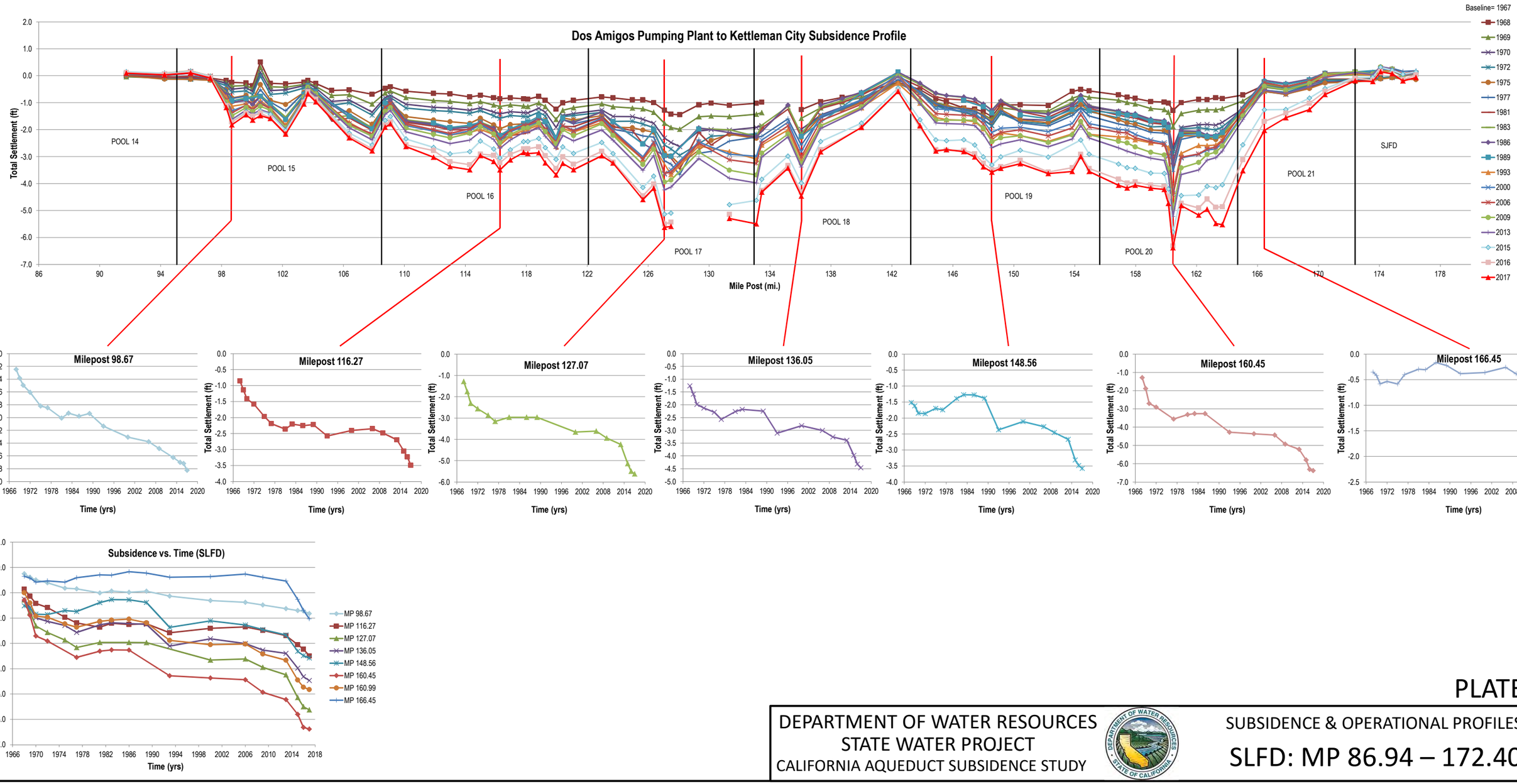

PLATE 1

DEPARTMENT OF WATER RESOURCES
STATE WATER PROJECT
CALIFORNIA AQUEDUCT SUBSIDENCE STUDY

SUBSIDENCE & OPERATIONAL PROFILES

SLFD: MP 86.94 – 172.40

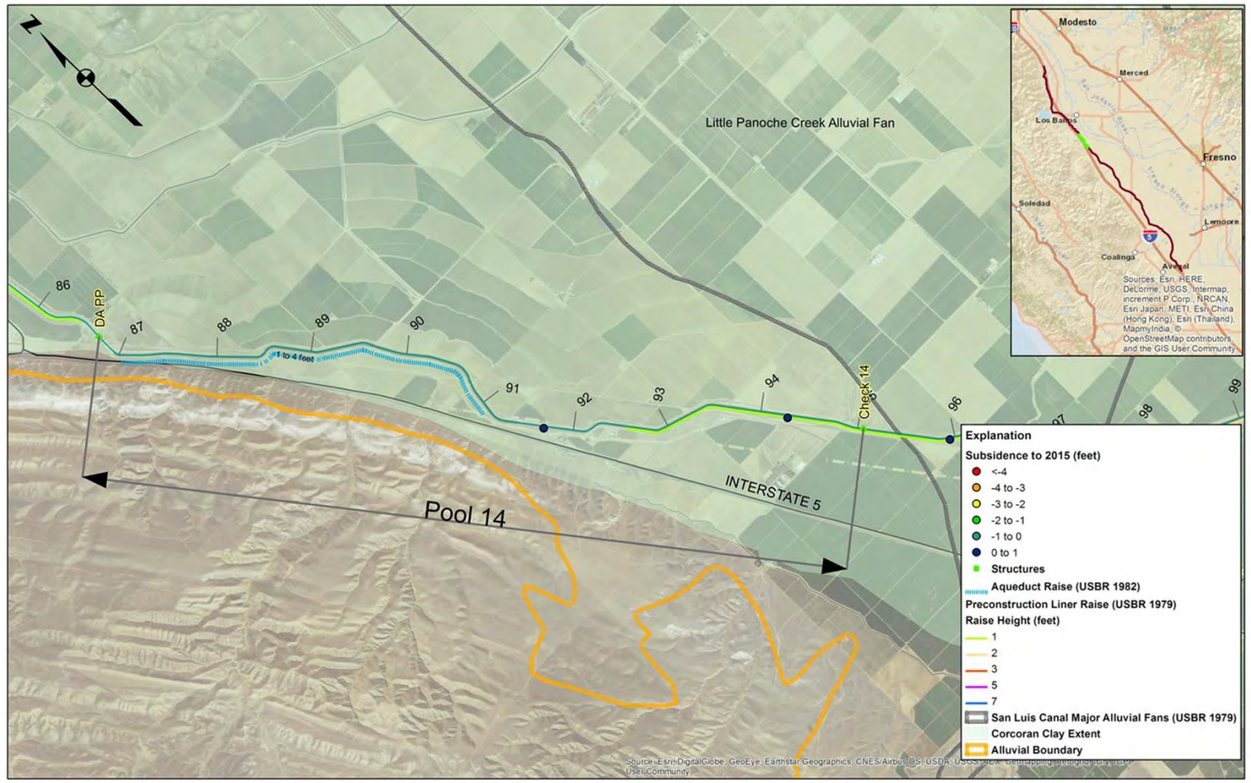

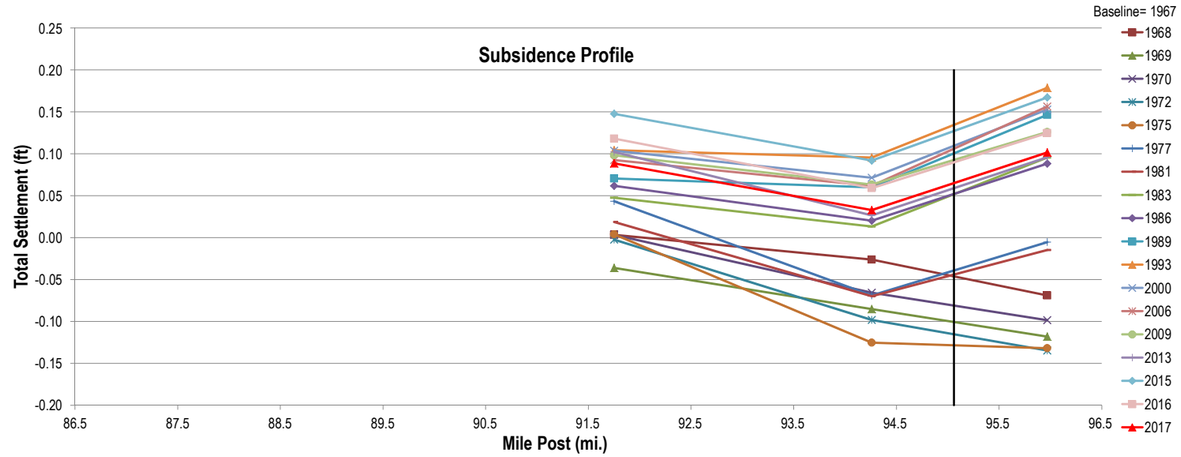

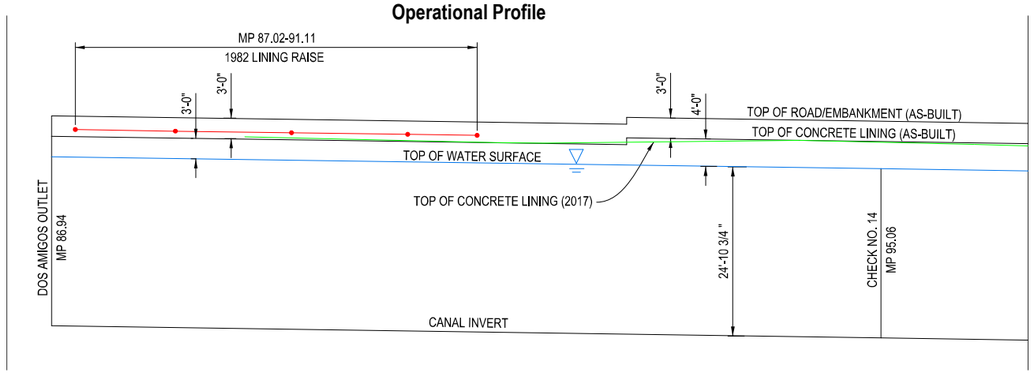

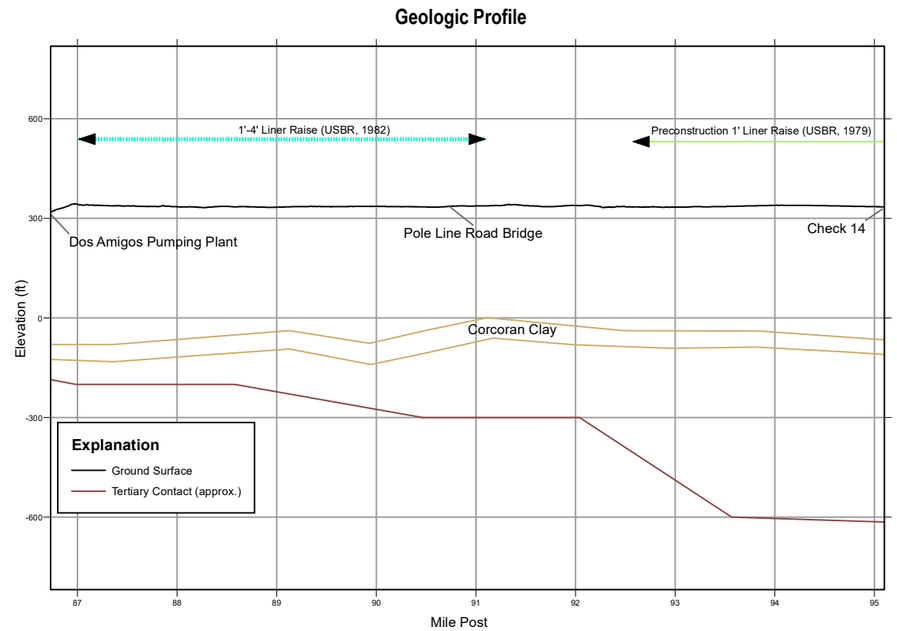

STRUCTURE	SIDE OF EMBANKMENT	MP
OUTLET 6 DISCHARGE LINES		86.94
DRAIN INLET	R	86.97
START LINING RAISE (1982)		87.02
BERM DRAIN		87.16
RECORDER STATION	L	87.17
DRAIN INLET	R	87.30
DRAIN INLET	R	87.45
WATERLINE CROSSING		87.67
TURNOUT	R	87.78
DRAIN INLET	R	87.98
DRAIN INLET	R	88.38
OIL & GASLINE CROSSINGS		88.44
BRIDGE		88.51
TEMP. TURNOUT	R	89.03
TEMP. TURNOUT	L	89.15
TEMP. TURNOUT	L	89.16
DRAIN INLET	R	89.27
TEMP. TURNOUT	L	89.66
TEMP. TURNOUTS	L	89.67

STRUCTURE	SIDE OF EMBANKMENT	MP
TEMP. TURNOUT	L	89.68
IRRIGATION CROSSING		89.68
BRIDGE		89.68
POWERLINE		89.68
TEMP. TURNOUT	R	89.68
TURNOUT	R	89.69
TEMP. TURNOUT	L	89.69
TURNOUT	L	89.70
GASLINE CROSSING		90.37
DRAIN INLET	R	90.47
BRIDGE		90.72
OIL & GASLINE CROSSINGS		90.78
END LINING RAISE (1982)		91.11
POWERLINE		91.25
IRRIGATION CROSSING		91.35
IRRIGATION CROSSING		91.36
IRRIGATION CROSSING		91.92
TURNOUT	R	92.16
TEMP. TURNOUT	R	92.16
POWERLINE		92.26
POWERLINE		92.40

STRUCTURE	SIDE OF EMBANKMENT	MP
DRAIN INLET	R	92.58
IRRIGATION CROSSING		92.72
TURNOUT	L	92.73
TEMP. TURNOUT	L	92.73
POWERLINE		93.23
IRRIGATION CROSSING		93.24
OIL & GASLINE CROSSINGS		93.27
REGEN. STATION		93.37
DRAIN INLET	R	93.41
TURNOUT	L	93.46
IRRIGATION CROSSING/GASLINE		93.67
BRIDGE		93.67
BERM DRAIN		93.75
BERM DRAIN		93.96
IRRIGATION CROSSING		94.05
TURNOUT	L	94.06
BERM DRAIN		94.11
BERM DRAIN		94.30
BERM DRAIN		94.47
DRAIN INLET	R	94.85
IRRIGATION CROSSING		94.89
POWERLINE		94.90
RECORDER STATION	L	95.05
BEGIN CHECK NO. 14		95.06

PLATE 2

DEPARTMENT OF WATER RESOURCES
STATE WATER PROJECT
CALIFORNIA AQUEDUCT SUBSIDENCE STUDY

SUBSIDENCE, OPERATION, & GEOLOGIC PROFILES

POOL 14: MP 86.94 – 95.06

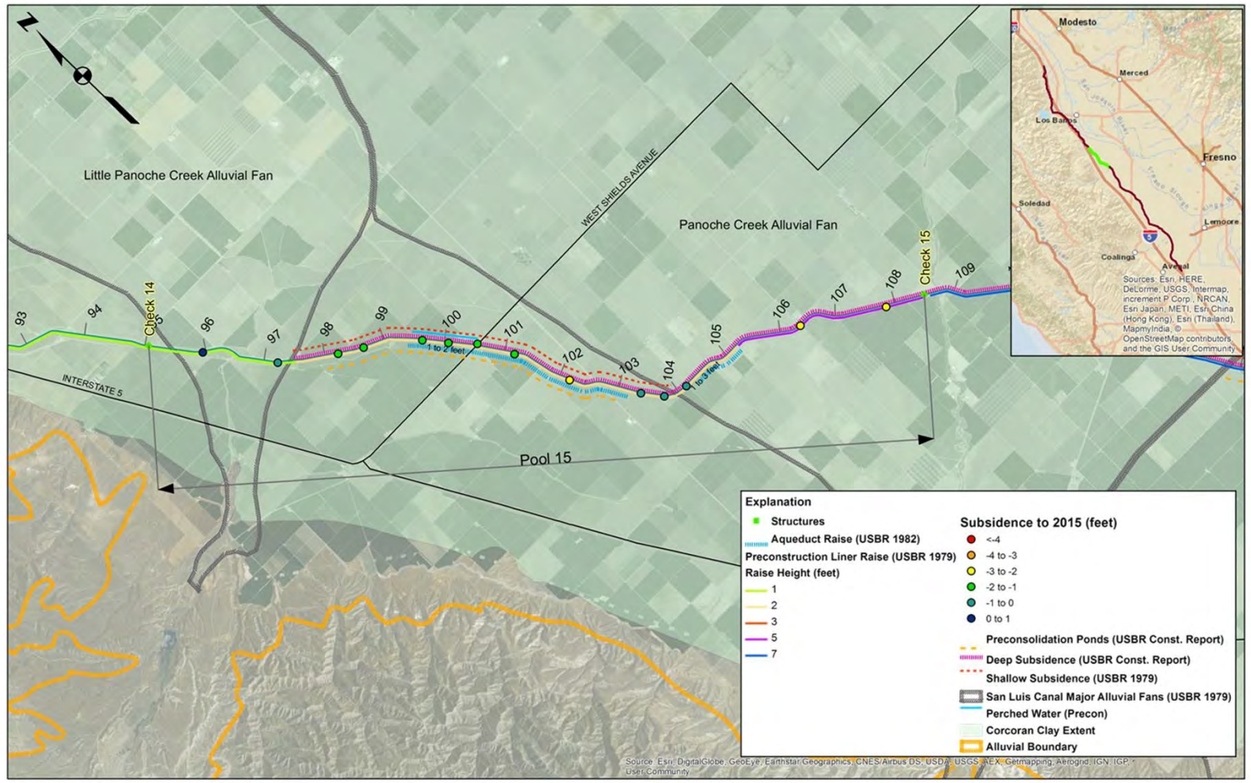

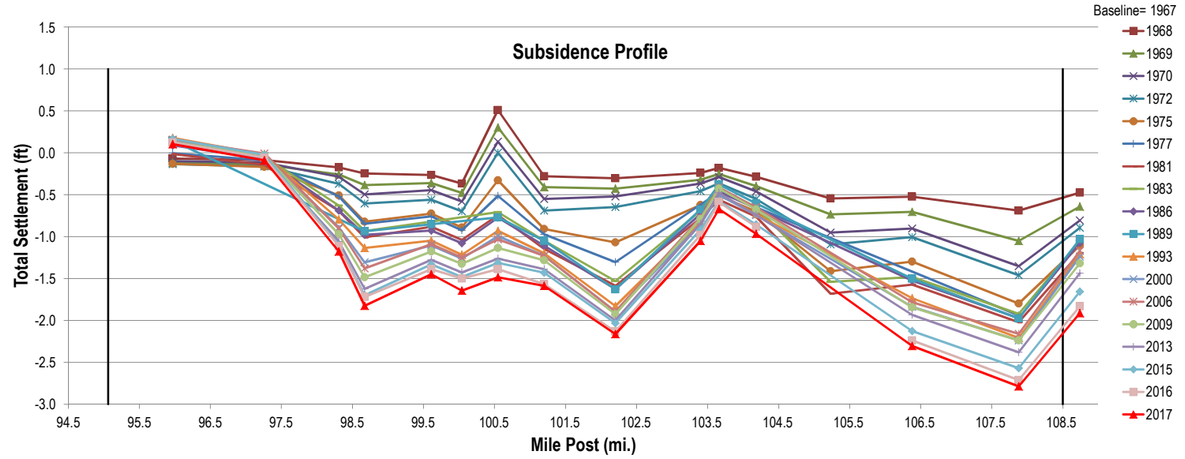

Operational Profile

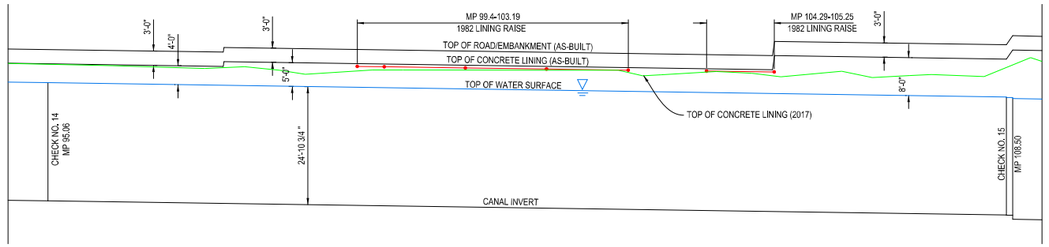

STRUCTURE	SIDE OF EMBANKMENT	MP
CHECK NO. 14		95.06
RECORDER STA.	L	95.21
TURNOUT	L	96.15
POWERLINE		96.20
TEMP. TURNOUT	R	96.55
BOX CULVERT		96.56
DRAIN INLET	R	96.57
BRIDGE		96.78
TEMP. TURNOUT	L	96.85
TURNOUT	L	97.51
POWERLINE		97.53
POWERLINE		97.80
IRRIGATION CROSSING		98.14
TURNOUT	L	98.15
BRIDGE		99.16
POWERLINE		99.22
START LINING RAISE (1982)		99.40
IRRIGATION CROSSING		99.60
TURNOUT	L	99.61
POWERLINE		100.40
TURNOUT	L	100.48
TEMP. TURNOUTS	L	100.48
BRIDGE/POWERLINE		100.55
IRRIGATION CROSSING		100.62
TEMP. TURNOUT	R	101.70

STRUCTURE	SIDE OF EMBANKMENT	MP
TURNOUT	L	102.20
TURNOUT	R	102.20
TEMP. TURNOUT	L	102.20
TEMP. TURNOUT	R	102.20
POWERLINE		102.22
DRAIN INLET	R	102.24
DRAIN INLET	R	102.63
BRIDGE/ELECTRICAL CONTEL		102.64
TURNOUT	L	102.64
TEMP. TURNOUTS	L	102.64
DOMESTIC WATERLINE		102.64
POWERLINE		102.65
POWERLINE		102.87
IRRIGATION CROSSING		102.88
END LINING RAISE (1982)		103.19
TURNOUT	L	103.40
TURNOUT	R	103.40
TEMP. TURNOUT	L	103.40
PUMP PAD	R	103.93
IRRIGATION CROSSING		103.95
TURNOUT	R	104.18
TURNOUT	R	104.20
TEMP. TURNOUT	R	104.20
START LINING RAISE (1982)		104.29
IRRIGATION CROSSING		104.44

STRUCTURE	SIDE OF EMBANKMENT	MP
IRRIGATION CROSSING		104.98
TURNIN (ABANDON)	L	105.00
TURNIN (ABANDON)	L	105.21
TEMP. TURNOUT	L	105.21
TURNOUT	L	105.22
TURNOUT	R	105.23
END LINING RAISE (1982)		105.25
PUMP PAD	R	105.55
TURNIN (ABANDON)	L	105.60
TURNIN	R	106.02
TURNOUT	L	106.35
IRRIGATION CROSSING		106.36
BRIDGE/POWERLINE		106.38
TURNIN (ABANDON)	R	107.10
IRRIGATION CROSSING		107.15
POWERLINE		107.16
IRRIGATION CROSSING		107.58
POWERLINE		107.60
TURNIN (ABANDON)	R	107.63
IRRIGATION CROSSING		108.09
POWERLINE		108.15
TURNOUT	L	108.39
TURNOUT	R	108.46
RECORDER STA.	L	108.49
CHECK NO. 15		108.50

Geologic Profile

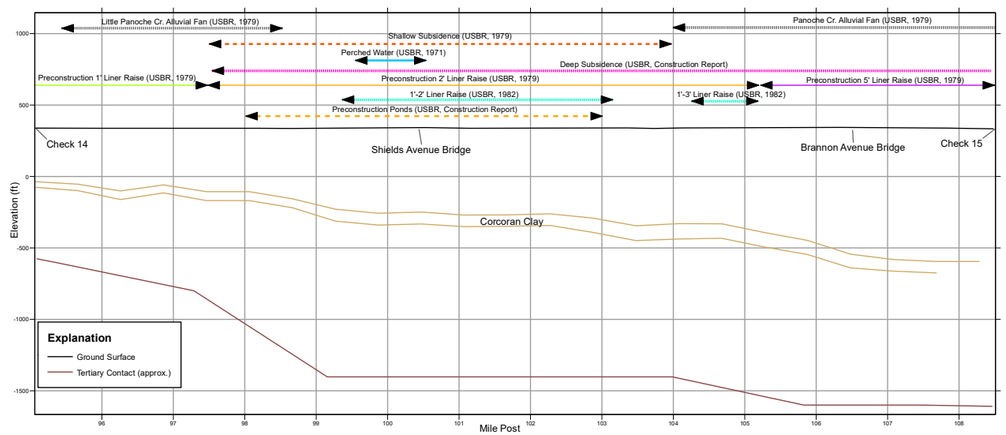

PLATE 3

DEPARTMENT OF WATER RESOURCES
STATE WATER PROJECT
CALIFORNIA AQUEDUCT SUBSIDENCE STUDY

SUBSIDENCE, OPERATION, & GEOLOGIC PROFILES

POOL 15: MP 95.06 – 108.50

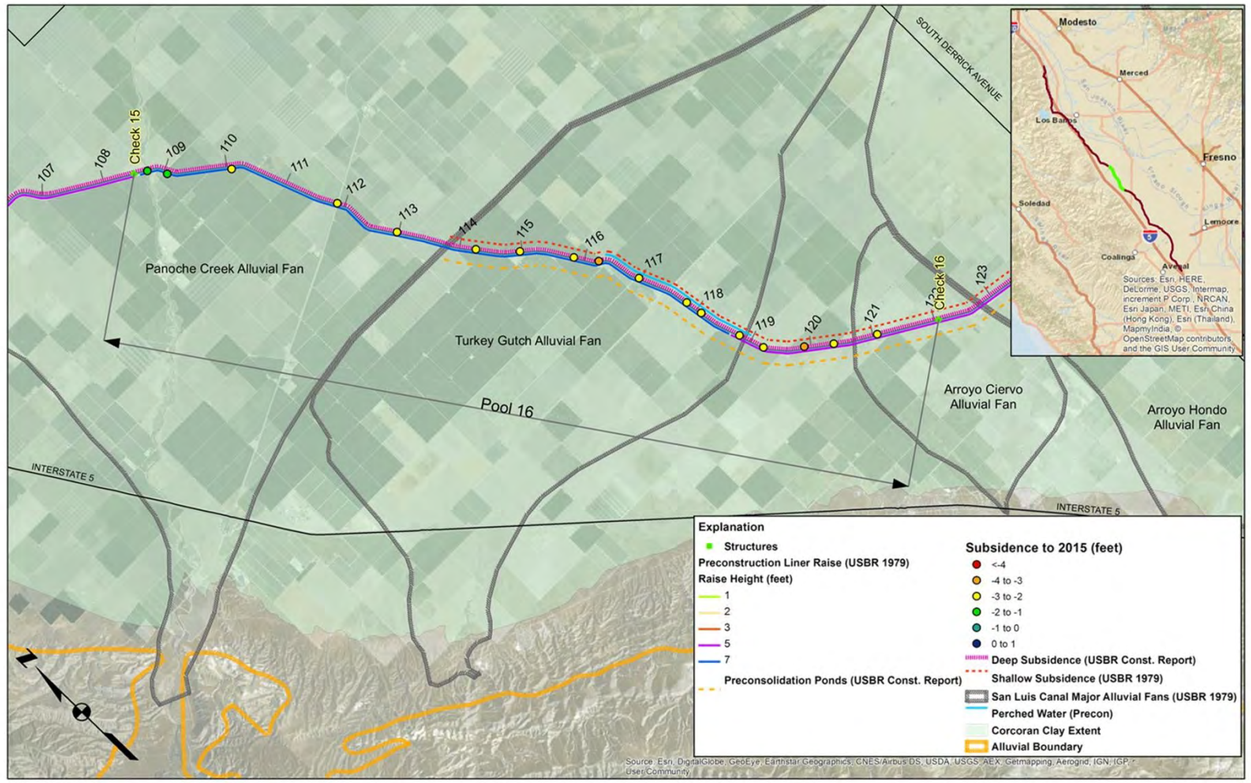

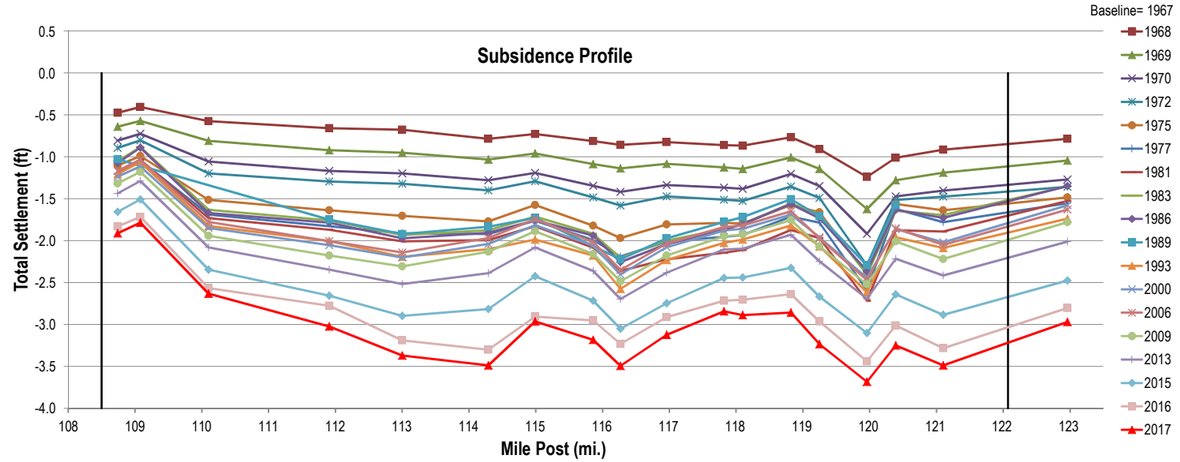

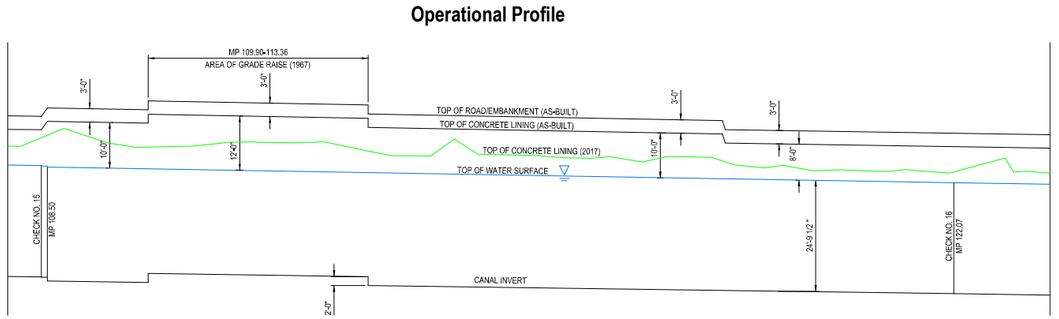

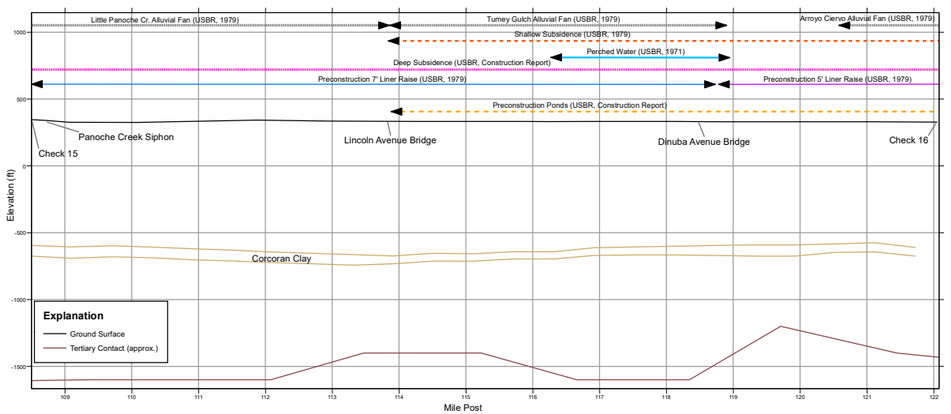

STRUCTURE	SIDE OF EMBANKMENT	MP
CHECK NO. 15		108.50
RECORDER STATION	L	108.65
BEGIN PANOCHE CREEK SIPHON/ BRIDGE		108.71
POWERLINE		108.80
TURNIN (ABANDON)	L	108.85
END PANOCHE CREEK SIPHON		108.87
TURNIN	L	108.95
RECORDER STATION	R	109.01
POWERLINE		109.02
IRRIGATION CROSSING		109.08
IRRIGATION CROSSING		109.09
BEGIN AREA OF GRADE RAISE IN ANTICIPATION OF IMMINENT DEEP SUBSIDENCE.		109.90
BEGIN AREA OF GRADE RAISE IN ANTICIPATION OF IMMINENT DEEP SUBSIDENCE.		110.09
IRRIGATION CROSSING		110.10
IRRIGATION CROSSING		110.10
IRRIGATION CROSSING		110.47
IRRIGATION CROSSING		110.47
TURNIN (ABANDON)	L	110.49
POWERLINE		110.50
TURNOUT/TURNIN	L	110.52
TURNIN (ABANDON)	R	111.02
IRRIGATION CROSSING		111.30
IRRIGATION CROSSING		111.87

STRUCTURE	SIDE OF EMBANKMENT	MP
POWERLINE		111.90
IRRIGATION CROSSING		111.91
BRIDGE		111.91
GASLINE CROSSING		111.91
TURNIN (ABANDON)	R	111.91
POWERLINE		111.92
TURNOUT	L	111.93
TURNIN (ABANDON)	L	111.93
PUMP PAD	R	112.23
IRRIGATION CROSSING		112.53
POWERLINE		112.56
POWERLINE		112.90
TURNOUT	L	113.00
IRRIGATION CROSSING		113.02
END AREA OF GRADE RAISE IN ANTICIPATION OF IMMINENT DEEP SUBSIDENCE.		113.17
END AREA OF GRADE RAISE IN ANTICIPATION OF IMMINENT DEEP SUBSIDENCE.		113.36
IRRIGATION CROSSING		113.44
TURNIN (ABANDON)	R	113.65
PUMP PAD	R	113.72
TURNOUT	R	113.77
BRIDGE		113.82
PIPELINE		113.84
TURNIN (ABANDON)	R	114.00
TEMP. TURNOUT	R	114.00
PUMP PAD	R	114.07

STRUCTURE	SIDE OF EMBANKMENT	MP
IRRIGATION CROSSING		114.64
TEMP. TURNOUT	R	114.64
POWERLINE		114.80
TEMP. TURNOUT	R	114.90
TURNOUT	R	114.90
TEMP. TURNOUT	R	114.92
TURNIN (ABANDON)	L	115.00
POWERLINE		115.25
POWERLINE		115.41
TURNOUT	L	115.43
TURNIN (ABANDON)	L	115.43
TEMP. TURNOUT	R	115.44
TURNIN (ABANDON)	R	115.44
PUMP PAD	R	115.70
IRRIGATION CROSSING		115.83
TEMP. TURNOUT	R	116.02
DOMESTIC WATERLINE		116.30
POWERLINE		116.30
TEMP. TURNOUT	R	116.32
PUMP PAD	R	116.38
IRRIGATION CROSSING		116.55
TURNIN (ABANDON)	R	116.91
TEMP. TURNOUT	R	116.91
TEMP. TURNOUT	R	117.42
TURNOUT	R	117.42
BRIDGE		117.47
IRRIGATION CROSSING		117.47
POWERLINE		117.47
IRRIGATION CROSSING		117.51
TURNOUT	L	117.51
TURNIN (ABANDON)	L	117.53
PUMP PAD	R	118.17

STRUCTURE	SIDE OF EMBANKMENT	MP
POWERLINE		118.25
TURNOUT	R	118.44
TURNIN (ABANDON)	L	118.46
TEMP. TURNOUT	R	118.46
IRRIGATION CROSSING		118.49
BRIDGE		118.49
POWERLINE		118.49
PUMP PAD	R	119.50
IRRIGATION CROSSING		119.56
TEMP. TURNOUT	L	119.56
TURNIN (ABANDON)	R	119.56
POWERLINE		119.58
TEMP. TURNOUT	R	119.60
TURNOUT	R	119.63
TEMP. TURNOUT	R	119.63
PUMP PAD	R	119.96
IRRIGATION CROSSING		120.50
TURNOUT	L	120.77
TURNIN (ABANDON)	L	120.80
POWERLINE		120.83
REGEN. STA.	R	120.84
TEMP. TURNOUT	L	120.86
TEMP. TURNOUT	R	120.87
TURNOUT	L	121.92
PUMP PAD	R	121.93
BRIDGE		121.97
IRRIGATION CROSSING		121.97
POWERLINE		122.00
TEMP. TURNOUT	R	122.01
TEMP. TURNOUT	R	122.02
TEMP. TURNOUT	R	122.05
TURNOUT	R	122.05
RECORDER STATION	L	122.07
CHECK NO. 16		122.07

PLATE 4

DEPARTMENT OF WATER RESOURCES
STATE WATER PROJECT
CALIFORNIA AQUEDUCT SUBSIDENCE STUDY

SUBSIDENCE, OPERATION, & GEOLOGIC PROFILES

POOL 16: MP 108.50 – 122.07

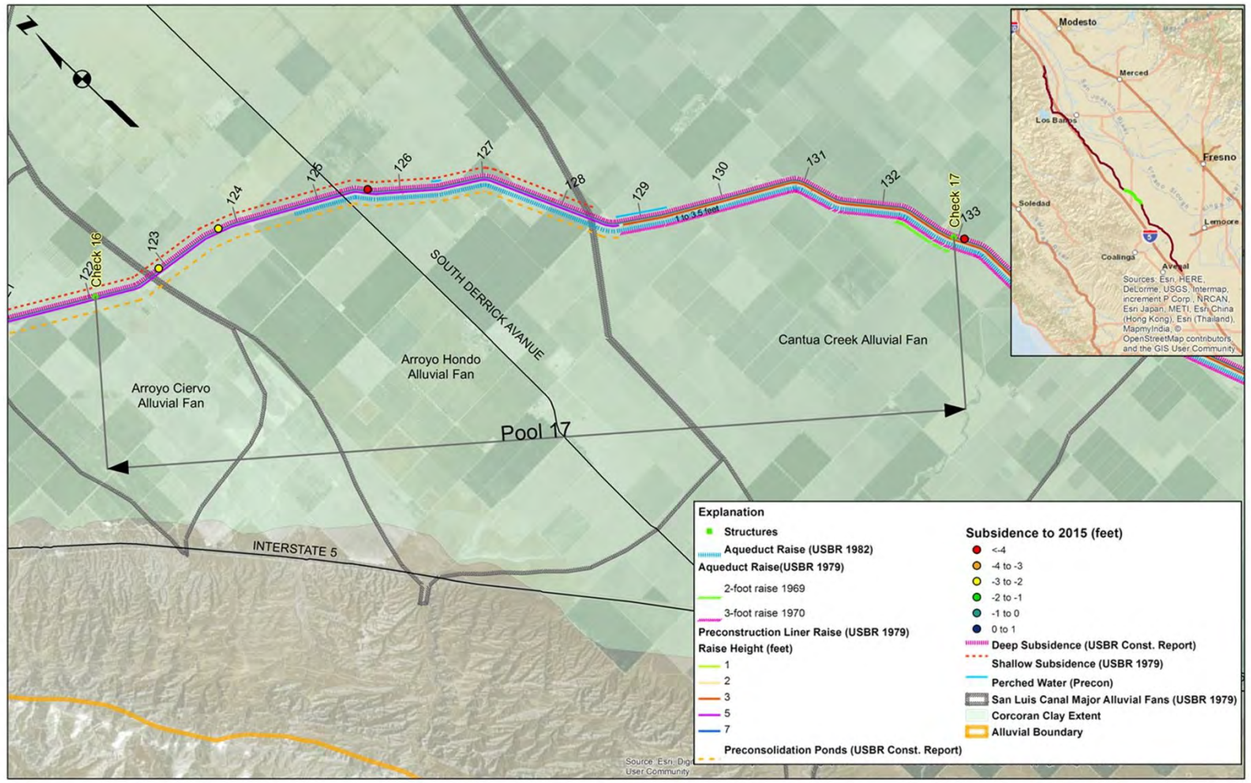

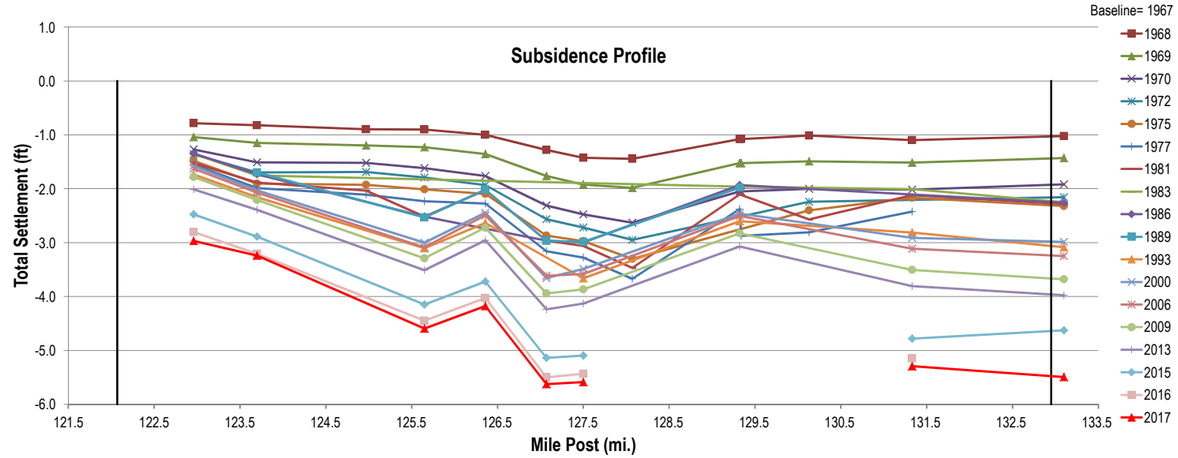

Operational Profile

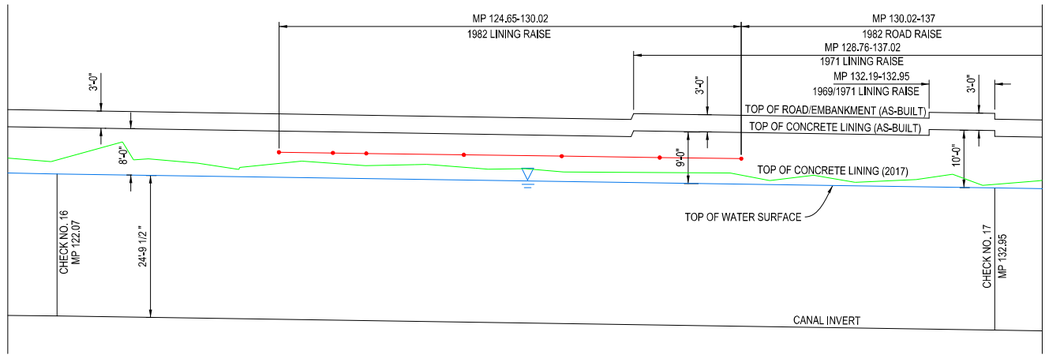

Geologic Profile

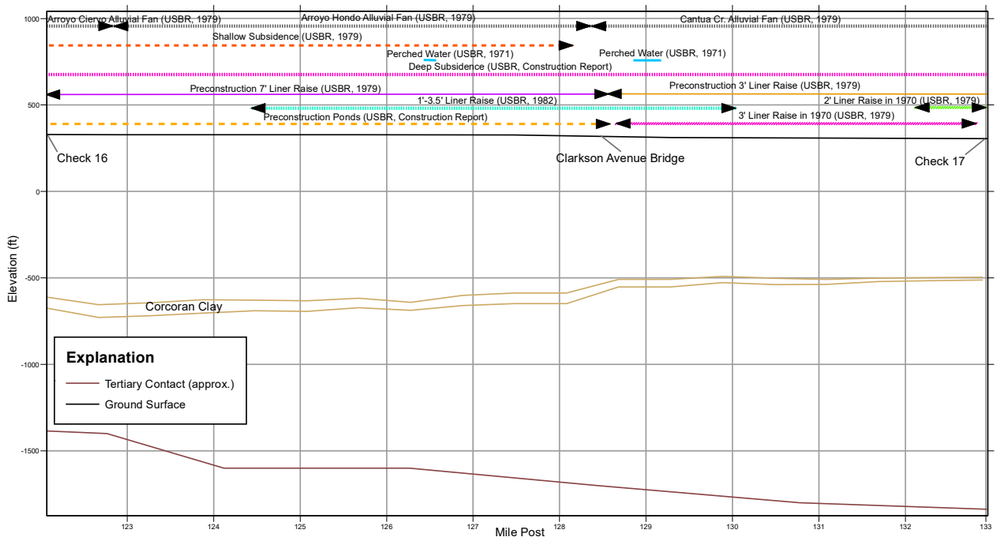

STRUCTURE	SIDE OF EMBANKMENT	MP
CHECK NO. 16		122.07
RECORDER STA.	L	122.22
TURNIN (ABANDON)	R	122.59
TEMP. TURNOUT	R	122.59
PUMP PAD	R	122.65
IRRIGATION CROSSING		122.83
TURNIN (ABANDON)	L	123.05
TURNIN (ABANDON)	R	123.89
TEMP. TURNOUT	R	123.89
POWERLINE		123.89
PUMP PAD	R	123.95
POWERLINE		124.12
OIL LINE CROSSING		124.16
TURNIN (ABANDON)	R	124.16
TEMP. TURNOUT	R	124.16
TURNOUT	L	124.16
TURNOUT	R	124.18
TURNOUT	R	124.19
TEMP. TURNOUT	R	124.19
START LINING RAISE (1982)		124.65
PUMP PAD	R	125.26
BRIDGE		125.31
IRRIGATION CROSSING		125.31
POWERLINE		125.32
TURNIN (ABANDON)	L	125.33
TEMP. TURNOUT	R	125.35

STRUCTURE	SIDE OF EMBANKMENT	MP
TEMP. TURNOUT	R	125.36
IRRIGATION CROSSING		125.81
BRIDGE		125.91
PUMP PAD	R	126.04
TURNOUT	L	126.65
POWERLINE		126.68
TURNIN (ABANDON)	L	127.40
PUMP PAD	R	127.61
PUMP PAD	R	127.83
POWERLINE		128.47
BRIDGE		128.48
CONDUIT		128.48
TEMP. TURNOUT	R	128.49
TURNIN (ABANDON)	R	128.49
TURNIN (ABANDON)	L	128.50
PUMP PAD	R	128.54
TURNIN (ABANDON)	L	128.54
TURNOUT	R	128.57
POWERLINE		128.69
3' LINING RAISE, DC-6859 (1971)		128.76
IRRIGATION CROSSING		128.89
IRRIGATION CROSSING		129.63
TURNOUT	L	129.88
POWERLINE		129.91
PUMP PAD	R	129.97
END LINING RAISE (1982)		130.02

STRUCTURE	SIDE OF EMBANKMENT	MP
START ROAD RAISE (1982)		130.02
IRRIGATION CROSSING		130.81
TURNIN (ABANDON)	R	130.81
BRIDGE		130.81
TURNOUT	L	130.85
PUMP PAD	R	131.46
POWERLINE		131.65
TURNOUT	L	131.70
START 2' LINING RAISE 200C-752 (1969)		132.19
START 2' LINING RAISE DC-6859 (1971)		132.19
POWERLINE		132.72
TURNOUT	R	132.74
IRRIGATION CROSSING		132.75
BRIDGE		132.77
TURNIN (ABANDON)	L	132.77
TURNOUT	L	132.81
GATED DRAIN INLETS	R	132.81
RECORDER STA.	L	132.94
END 2' LINING RAISE 200C-752 (1969)		132.95
END 2' LINING RAISE DC-6859 (1971)		132.95
CHECK NO. 17		132.95

PLATE 5

DEPARTMENT OF WATER RESOURCES
STATE WATER PROJECT
CALIFORNIA AQUEDUCT SUBSIDENCE STUDY

SUBSIDENCE, OPERATION, & GEOLOGIC PROFILES

POOL 17: MP 122.07 – 132.95

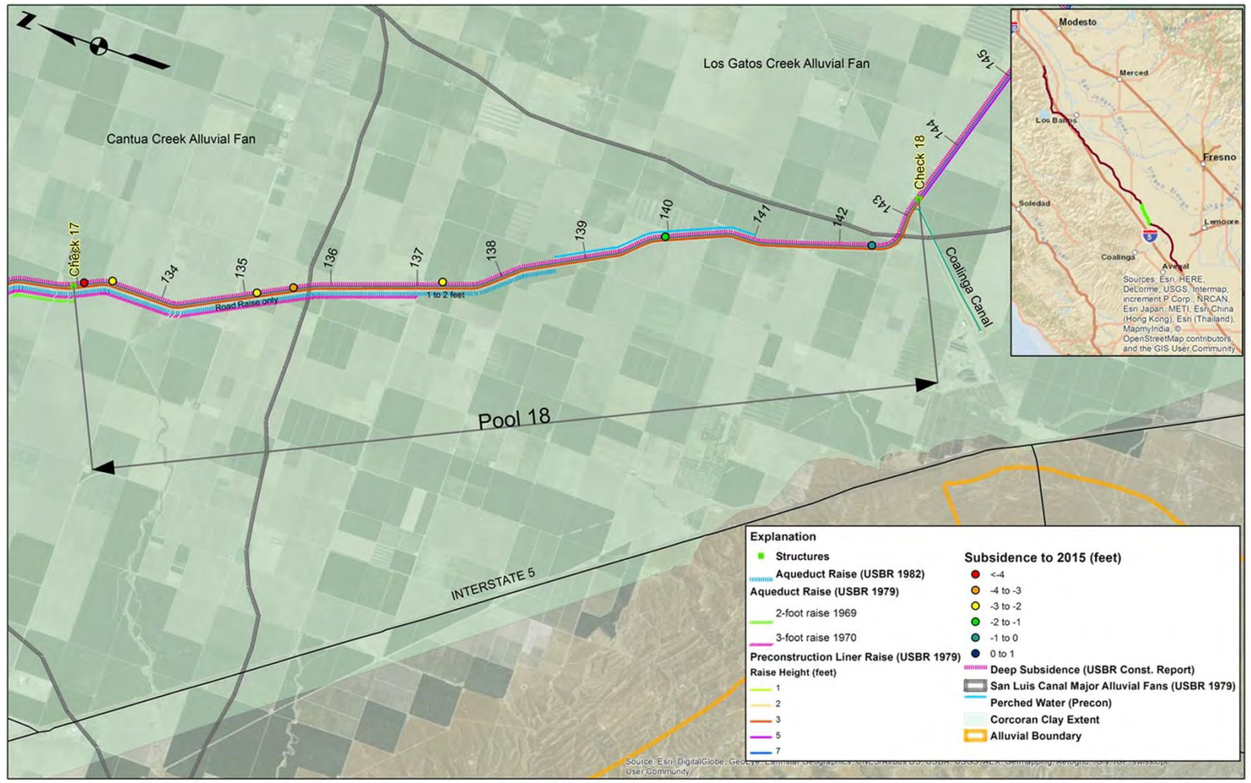

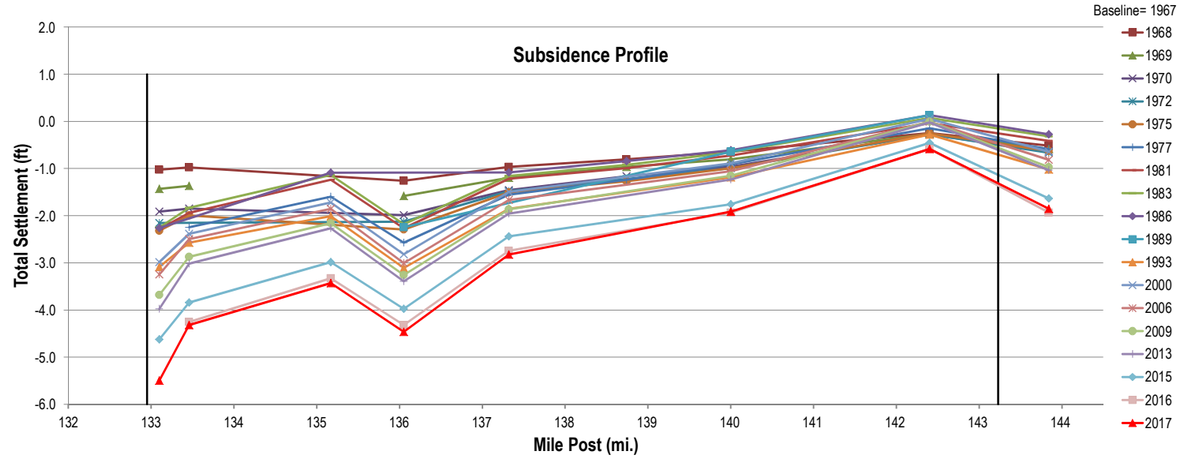

Operational Profile

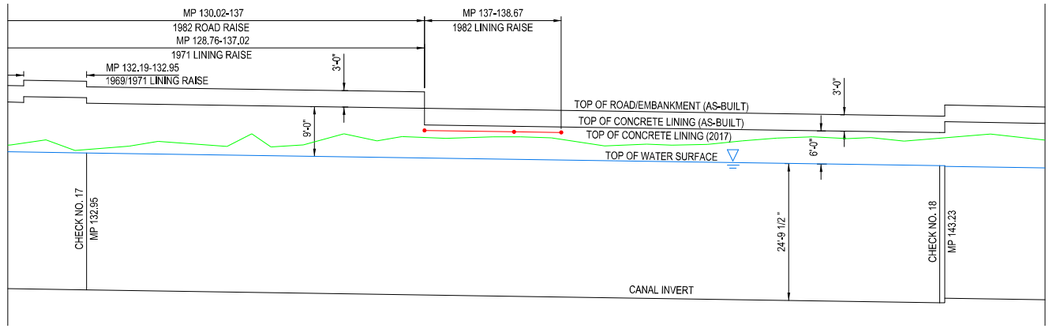

Geologic Profile

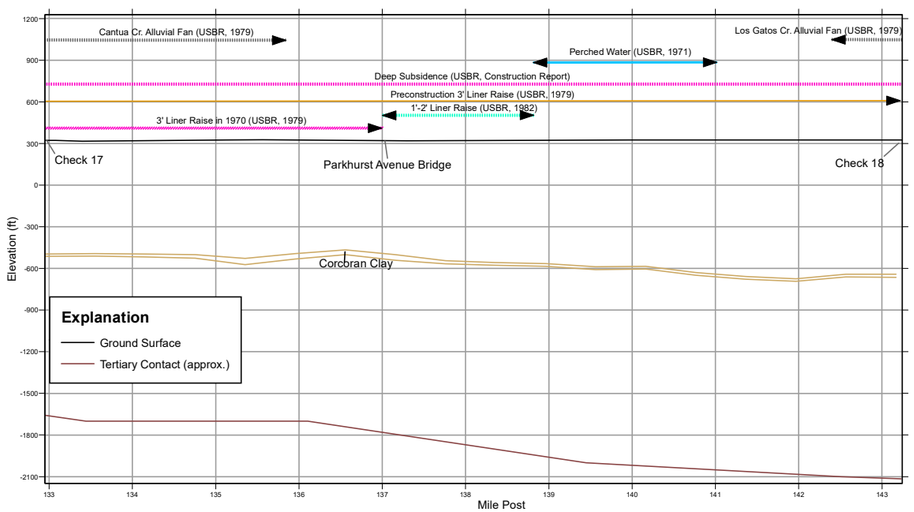

STRUCTURE	SIDE OF EMBANKMENT	MP
CHECK NO. 17		132.95
START 3' LINING RAISE DC-6859 (1971)		133.00
RECORDER STA.	L	133.10
DRAIN INLET	R	133.67
TURNIN (ABANDON)	L	133.80
TURNOUT	L	133.81
TURNOUT	R	133.81
TURNIN (ABANDON)	R	133.81
POWERLINE		133.82
TURNIN	R	133.83
POWERLINE		134.20
FLUME/ CANTUA CR.	R	134.81
POWERLINE		134.88
BRIDGE		134.89
POWERLINE		134.90
DRAIN INLET	R	134.91
IRRIGATION CROSSING		134.93
TURNOUT	L	134.94
DRAIN INLET/ CANTUA	R	134.94
TURNIN (ABANDON)	R	135.48
TURNOUT	R	135.96
IRRIGATION CROSSING		135.98
IRRIGATION CROSSING		135.98
DRAIN INLET/POWERLINE	R	136.00

STRUCTURE	SIDE OF EMBANKMENT	MP
TURNIN (ABANDON)	L	136.03
TURNOUT	L	136.05
END 3' LINING RAISE DC-6859 (1971)	R	137.00
END ROAD RAISE (1982)		137.00
START LINING RAISE (1982)		137.00
TURNOUT	R	137.00
END 3' LINING RAISE DC-6859 (1971)	L	137.02
POWERLINE		137.05
IRRIGATION CROSSING		137.06
BRIDGE		137.06
POWERLINE		137.07
DRAIN INLET	R	137.08
GASOLINE CROSSING		137.09
TURNOUT	L	137.11
TURNIN (ABANDON)	L	137.11
TURNIN (ABANDON)	L	137.31
IRRIGATION CROSSING		137.32
PUMP PAD	R	137.80
TURNIN	L	137.80
IRRIGATION CROSSING		137.83
TURNIN (ABANDON)	L	137.83

STRUCTURE	SIDE OF EMBANKMENT	MP
POWERLINE		138.13
TURNOUT	R	138.14
IRRIGATION CROSSING		138.24
TURNIN (ABANDON)	L	138.24
TURNOUT	L	138.29
PUMP PAD	R	138.29
END LINING RAISE (1982)		138.67
IRRIGATION CROSSING		138.95
PUMP PAD	R	138.96
TURNOUT	R	139.27
POWERLINE		139.31
IRRIGATION CROSSING		139.34
POWERLINE		139.34
BRIDGE		139.35
TURNOUT	L	139.39
TURNIN (ABANDON)	L	139.40
PUMP PAD	R	139.72
TURNOUT	R	140.48
IRRIGATION CROSSING		140.50
POWERLINE		140.52
TURNIN (ABANDON)	L	140.55
TURNOUT	L	140.57
PUMP PAD	R	140.95
TEMP. TURNOUT	R	140.99

STRUCTURE	SIDE OF EMBANKMENT	MP
TURNIN (ABANDON)	R	141.02
TEMP. TURNOUT	R	141.29
TURNOUT	R	141.53
TURNIN (ABANDON)	L	141.55
IRRIGATION CROSSING		141.55
POWERLINE		141.56
BRIDGE		141.57
TURNOUT	L	141.60
PUMP PAD	R	142.50
TEMP. TURNOUT	R	142.57
TURNIN (ABANDON)	R	142.58
TEMP. TURNOUT	R	142.60
TEMP. TURNOUT	R	142.61
POWERLINE		142.64
TURNIN (ABANDON)	L	143.00
POWERLINE		143.10
OIL LINE CROSSING/BRIDGE		143.12
POWERLINE		143.14
PUMP PAD	R	143.14
BRIDGE		143.16
TURNOUT	R	143.16
IRRIGATION CROSSING		143.21
TURNIN (ABANDON)	R	143.21
RECORDER STA.	L	143.23
CHECK NO. 18		143.23

PLATE 6

DEPARTMENT OF WATER RESOURCES
STATE WATER PROJECT
CALIFORNIA AQUEDUCT SUBSIDENCE STUDY

SUBSIDENCE, OPERATION, & GEOLOGIC PROFILES

POOL 18: MP 132.95 – 143.23

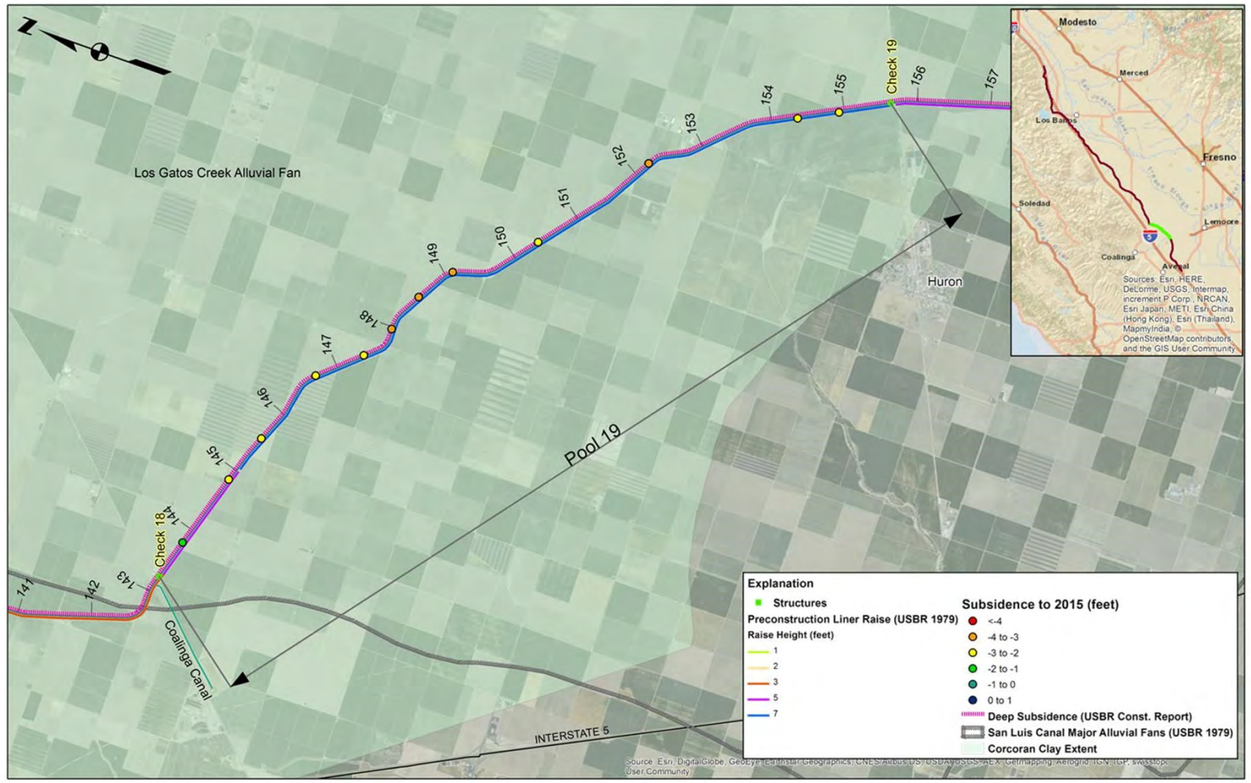

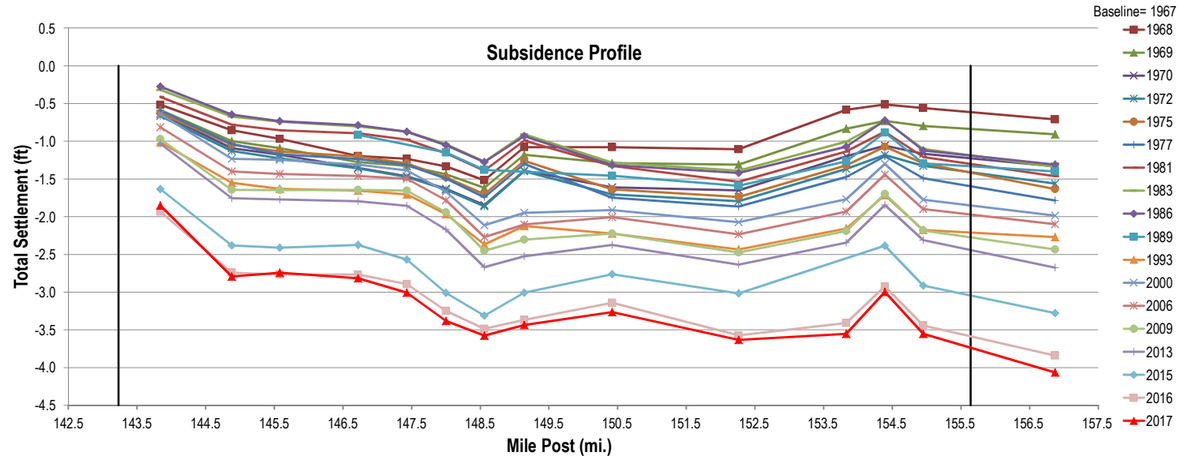

Operational Profile

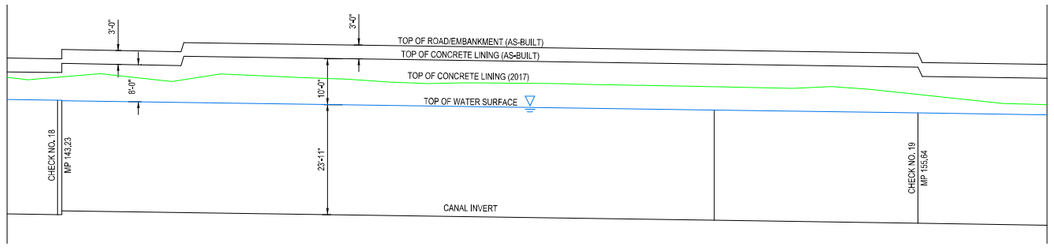

Geologic Profile

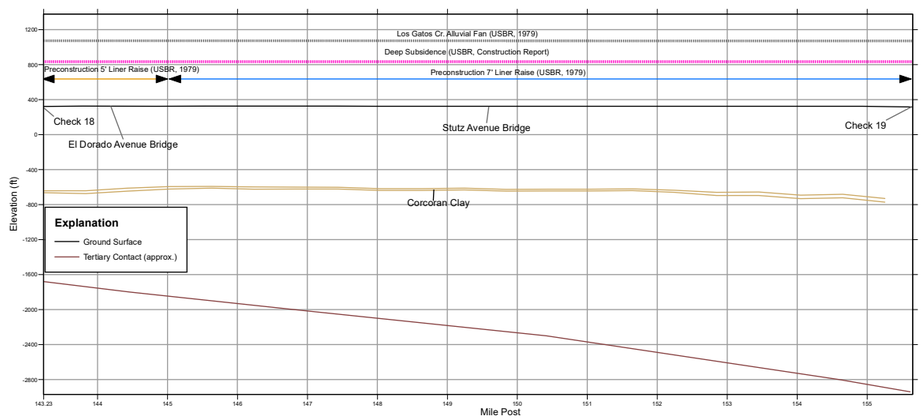

STRUCTURE	SIDE OF EMBANKMENT	MP
CHECK NO. 18		143.23
RECORDER STATION	R	143.39
IRRIGATION CROSSING		143.72
PUMP PAD	R	144.16
POWERLINE		144.24
BRIDGE		144.25
TURNIN (ABANDON)	L	144.25
IRRIGATION CROSSING		144.27
IRRIGATION CROSSING		144.77
TURNOUT	L	145.26
PUMP PAD	R	145.27
POWERLINE		145.30
TURNOUT	R	145.32
IRRIGATION CROSSING		145.74
POWERLINE		145.74
POWERLINE		146.02
IRRIGATION CROSSING		146.16
BRIDGE		146.17
POWERLINE		146.35
TURNOUT	L	147.02
TURNIN (ABANDON)	L	147.02
IRRIGATION CROSSING		147.03
PUMP PAD	R	147.05

STRUCTURE	SIDE OF EMBANKMENT	MP
REGEN. STA.	L	147.60
POWERLINE		147.71
TURNIN (ABANDON)	R	147.75
TEMP. TURNOUT	R	147.75
PUMP PAD	R	148.22
IRRIGATION CROSSING		148.47
POWERLINE		148.85
TURNOUT	L	149.12
TURNIN (ABANDON)		149.12
TURNOUT	R	149.55
IRRIGATION CROSSING		149.57
POWERLINE		149.58
BRIDGE		149.59
TEMP. TURNOUT	R	149.59
PUMP BACK		150.01
TEMP. TURNOUT	R	150.48
POWERLINE		150.51
TURNOUT	L	150.88
TURNOUT	R	151.19
IRRIGATION CROSSING		151.21
IRRIGATION CROSSING		151.21
PUMP PAD	R	151.65

STRUCTURE	SIDE OF EMBANKMENT	MP
BRIDGE		151.73
IRRIGATION CROSSING		151.73
POWERLINE		151.74
IRRIGATION CROSSING		151.77
TURNOUT	L	152.35
IRRIGATION CROSSING		152.71
IRRIGATION CROSSING		152.71
TURNIN (ABANDON)	L	152.75
BRIDGE		152.76
POWERLINE		152.76
IRRIGATION CROSSING		153.07
TURNIN (ABANDON)		153.10
POWERLINE		153.12
BRIDGE		153.30
TURNIN (ABANDON)	L	154.10
TURNOUT	L	154.11
IRRIGATION CROSSING		154.12
POWERLINE		155.06
TURNIN (ABANDON)	L	155.15
PUMP BACK		155.20
RECORDER STATION	L	155.63
CHECK NO. 19		155.64

PLATE 7

DEPARTMENT OF WATER RESOURCES
STATE WATER PROJECT
CALIFORNIA AQUEDUCT SUBSIDENCE STUDY

SUBSIDENCE, OPERATION, & GEOLOGIC PROFILES

POOL 19: MP 143.23 – 155.64

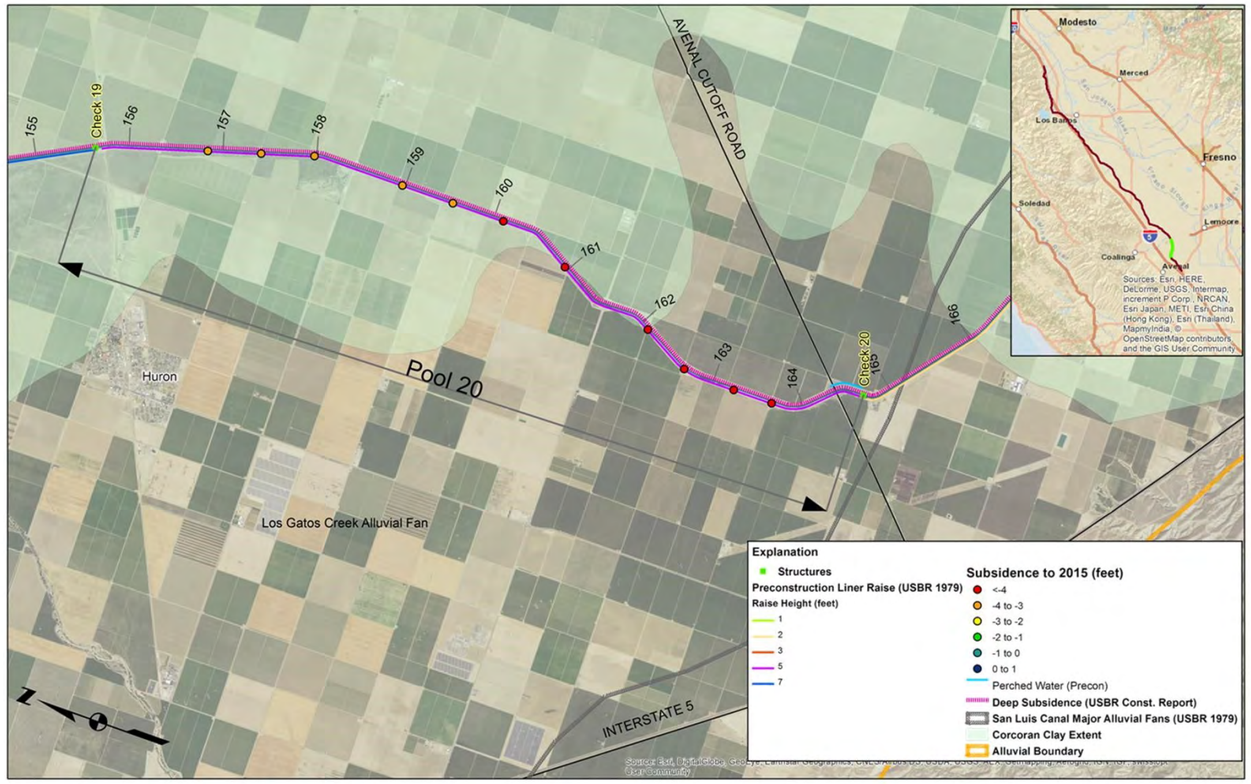

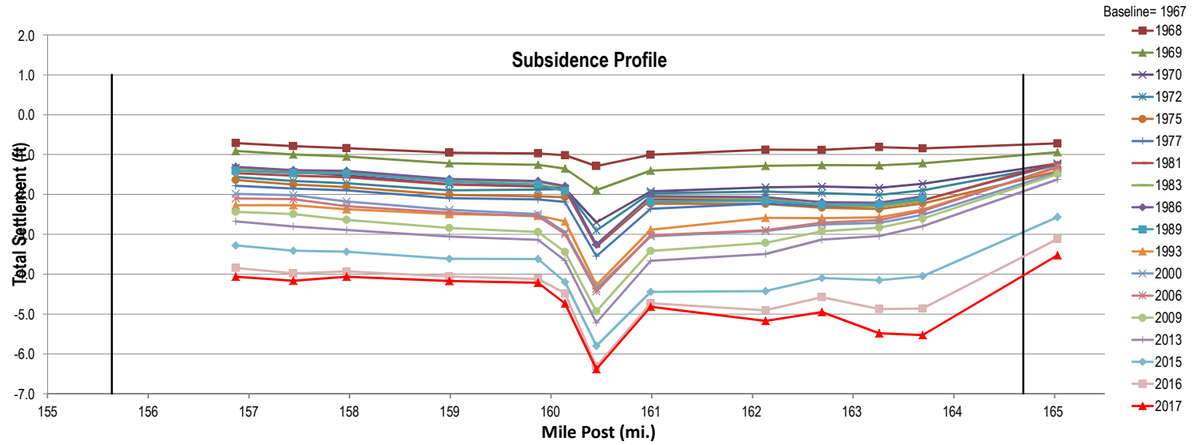

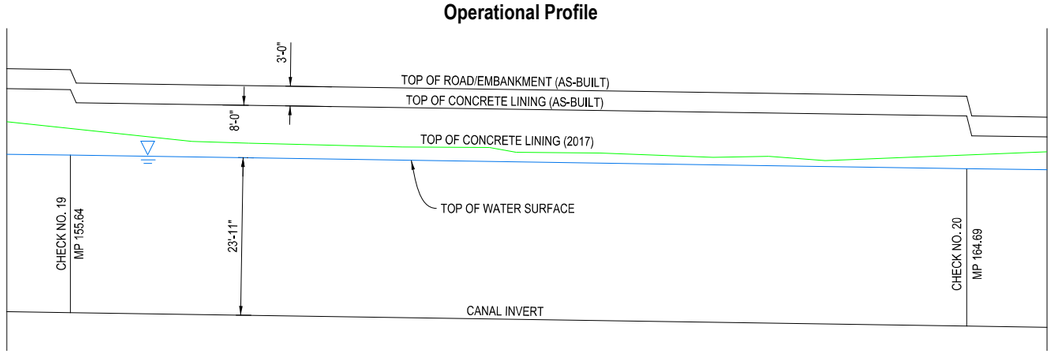

STRUCTURE	SIDE OF EMBANKMENT	MP
CHECK NO. 19		155.64
IRRIGATION CROSSING		155.71
GATED CULVERT		155.73
OIL LINE CROSSING		155.77
BRIDGE (2)		155.78
POWERLINE		155.79
RECORDER STA.	R	155.83
TURNOUT	R	156.34
IRRIGATION CROSSING		156.36
TURNIN (ABANDON)	L	156.37
TURNOUT	L	156.40
TURNIN (ABANDON)	L	156.40
POWERLINE		157.16
TURNIN (ABANDON)	R	157.40
IRRIGATION CROSSING		157.42
DRAIN INLET	R	158.36
DRAIN INLET	R	158.37
DRAIN INLET	R	158.38
DRAIN INLET	R	158.39
POWERLINE		158.44

STRUCTURE	SIDE OF EMBANKMENT	MP
BRIDGE		158.45
TURNOUT	L	158.47
TURNOUT	R	158.47
PUMP PAD	R	158.55
TURNIN (ABANDON)	L	158.95
POWERLINE		159.25
POWERLINE		159.45
TURNOUT	L	160.45
TURNOUT	R	160.45
IRRIGATION CROSSING		160.46
POWERLINE		160.48
TURNIN (ABANDON)	R	160.50
TURNIN (ABANDON)	L	160.68
PUMP PAD	R	161.52
POWERLINE		161.56
BRIDGE		161.57
POWERLINE		161.58
TURNOUT	L	161.60
TURNIN (ABANDON)	L	161.60
TURNOUT	R	161.60
IRRIGATION CROSSING		161.62
TURNIN (ABANDON)	L	161.63

STRUCTURE	SIDE OF EMBANKMENT	MP
PUMP PAD	R	161.64
IRRIGATION CROSSING		162.08
TURNIN (ABANDON)	L	162.08
TURNIN (ABANDON)	R	162.10
TURNOUT/TURNIN (ABANDON)	L	162.63
TURNIN (ABANDON)	L	162.64
IRRIGATION CROSSING		163.18
TURNIN (ABANDON)	R	163.20
TEMP. TURNOUT	L	163.59
IRRIGATION CROSSING		163.67
POWERLINE		163.67
TURNOUT	L	163.69
TURNOUT	R	163.69
TURNIN (ABANDON)	R	164.11
PUMP PAD	R	164.33
BRIDGE		164.40
TURNIN (ABANDON)	L	164.55
TURNIN (ABANDON)	R	164.63
RECORDER STA.	L	164.68
TEMP. TURNOUT	R	164.69
CHECK NO. 20		164.69

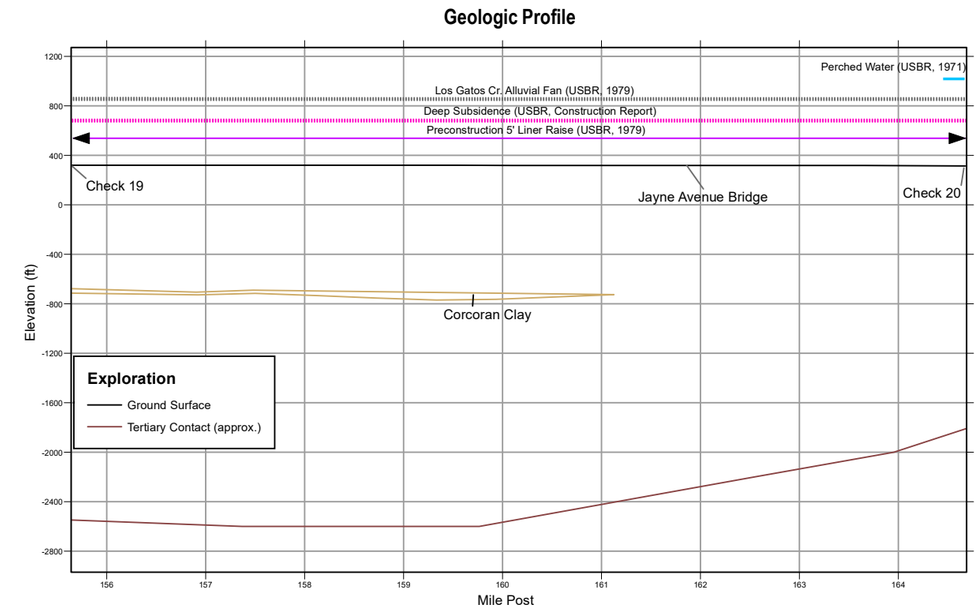

PLATE 8

DEPARTMENT OF WATER RESOURCES
STATE WATER PROJECT
CALIFORNIA AQUEDUCT SUBSIDENCE STUDY

SUBSIDENCE, OPERATION, & GEOLOGIC PROFILES

POOL 20: MP 155.64 – 164.69

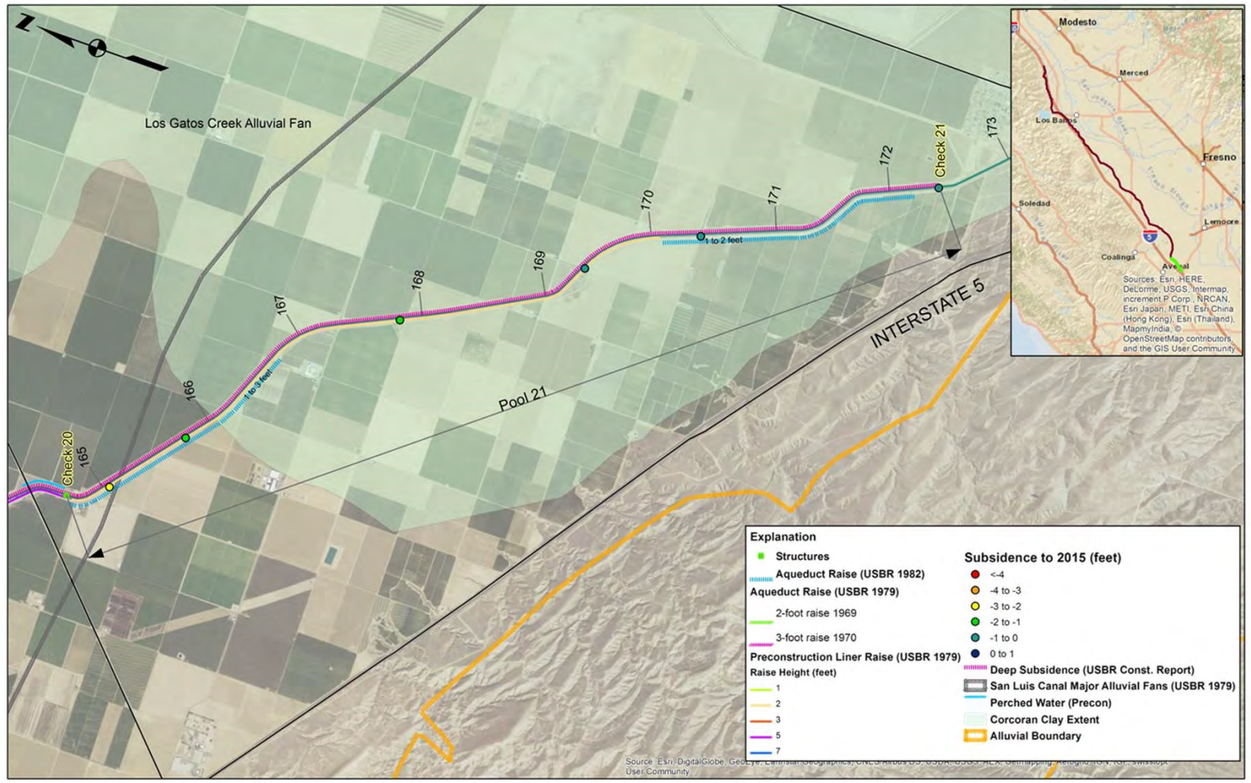

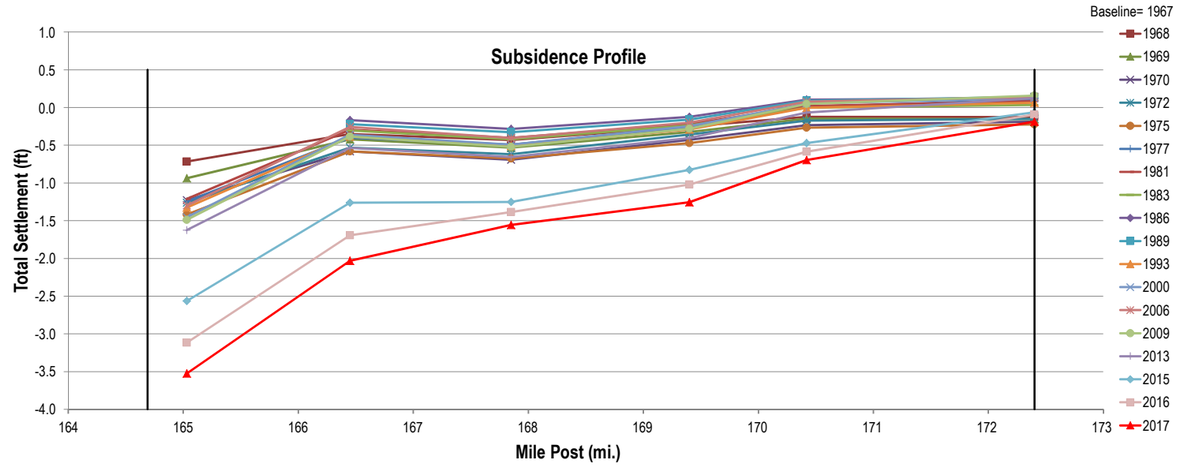

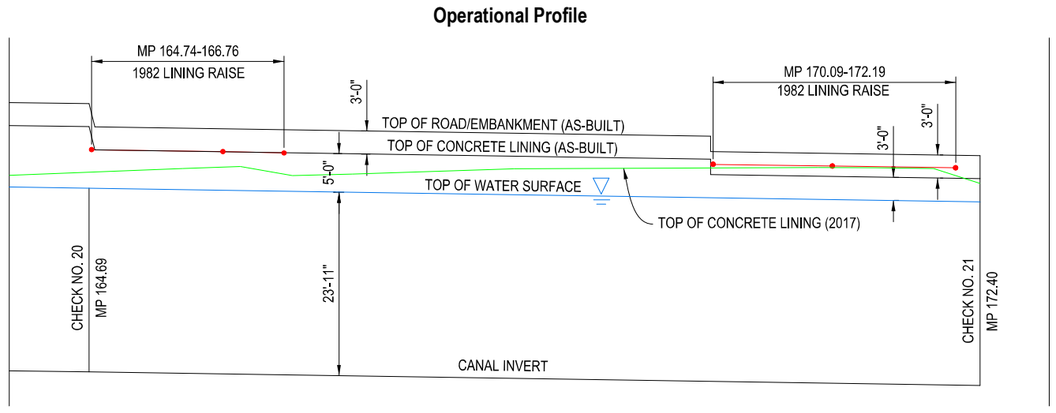

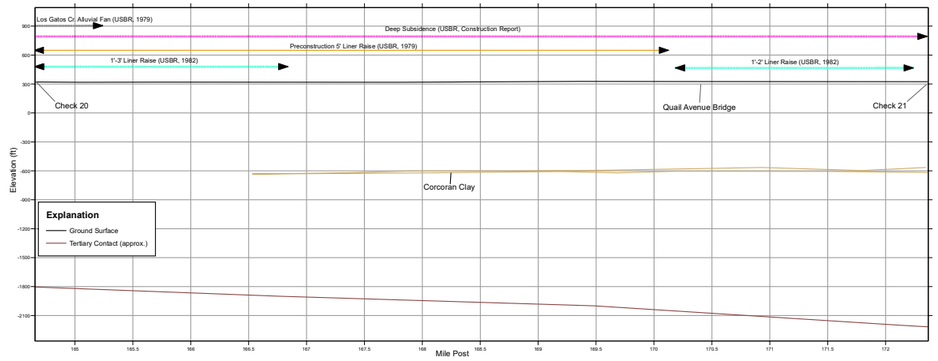

STRUCTURE	SIDE OF EMBANKMENT	MP
CHECK NO. 20		164.69
START CANAL LINING RAISE (1982)		164.74
TURNOUT	R	164.79
TEMP. TURNOUT	R	164.79
POWERLINE		164.80
POWERLINE		164.89
OIL LINE CROSSING		164.93
OIL LINE CROSSING		164.93
TURNIN (ABANDON)	R	164.95
IRRIGATION CROSSING		164.98
RECORDER STA.	R	165.03
DRAIN INLET	R	165.38
IRRIGATION CROSSING		165.59
GASLINE CROSSING		165.80
GASLINE CROSSING		165.80
DRAIN INLET	R	166.04
POWERLINE		166.21
POWERLINE		166.45
IRRIGATION CROSSING		166.69
POWERLINE		166.69
END CANAL LINING RAISE (1982)		166.76
DRAIN INLET	R	166.90
IRRIGATION CROSSING		166.99

STRUCTURE	SIDE OF EMBANKMENT	MP
TURNOUT	L	167.04
TURNIN (ABANDON)		167.04
DRAIN INLET	R	167.27
GASLINE CROSSING		167.36
BRIDGE		167.36
COMMUNICATION LINE		167.36
IRRIGATION CROSSING		167.64
DRAIN INLET	R	167.78
TURNOUT	R	167.84
TURNIN (ABANDON)	R	167.86
POWERLINE		167.90
GASLINE CROSSING		168.56
IRRIGATION CROSSING		168.56
IRRIGATION CROSSING		168.56
DRAIN INLET	R	168.62
POWERLINE		168.75
TURNIN (ABANDON)	R	169.21
TURNOUT	L	169.30
TURNIN	L	169.30
DRAIN INLET	R	169.37
POWERLINE		169.39
BRIDGE/COMM. LINE		169.40
POWERLINE		169.41
DRAIN INLET	R	169.72
POWERLINE		169.84
TURNIN (ABANDON)	L	169.88

STRUCTURE	SIDE OF EMBANKMENT	MP
PIPELINE		169.99
START CANAL LINING RAISE (1982)		170.09
DRAIN INLET	R	170.25
BRIDGE/COMM. LINE		170.42
IRRIGATION CROSSING		170.68
DRAIN INLET	R	170.83
POWERLINE		170.95
DRAIN INLET	R	171.48
TURNIN (ABANDON)	L	171.50
TURNOUT	R	171.51
POWERLINE		171.55
WATERLINE CROSSING		171.61
TEMP. TURNOUT	L	171.67
POWERLINE		171.79
POWERLINE		171.80
DRAIN INLET	R	171.85
IRRIGATION CROSSING		171.94
END CANAL LINING RAISE (1982)		172.19
ACOUSTIC VELOCITY METER FACILITIES/BRIDGE		172.25
RECORDER STA.	L	172.26
RECORDER STA.	L	172.39
CHECK NO. 21		172.40

PLATE 9

DEPARTMENT OF WATER RESOURCES
STATE WATER PROJECT
CALIFORNIA AQUEDUCT SUBSIDENCE STUDY

SUBSIDENCE, OPERATION, & GEOLOGIC PROFILES

POOL 21: MP 164.69 – 172.40

Kettleman City to Edmonston Pumping Plant Operational Profile

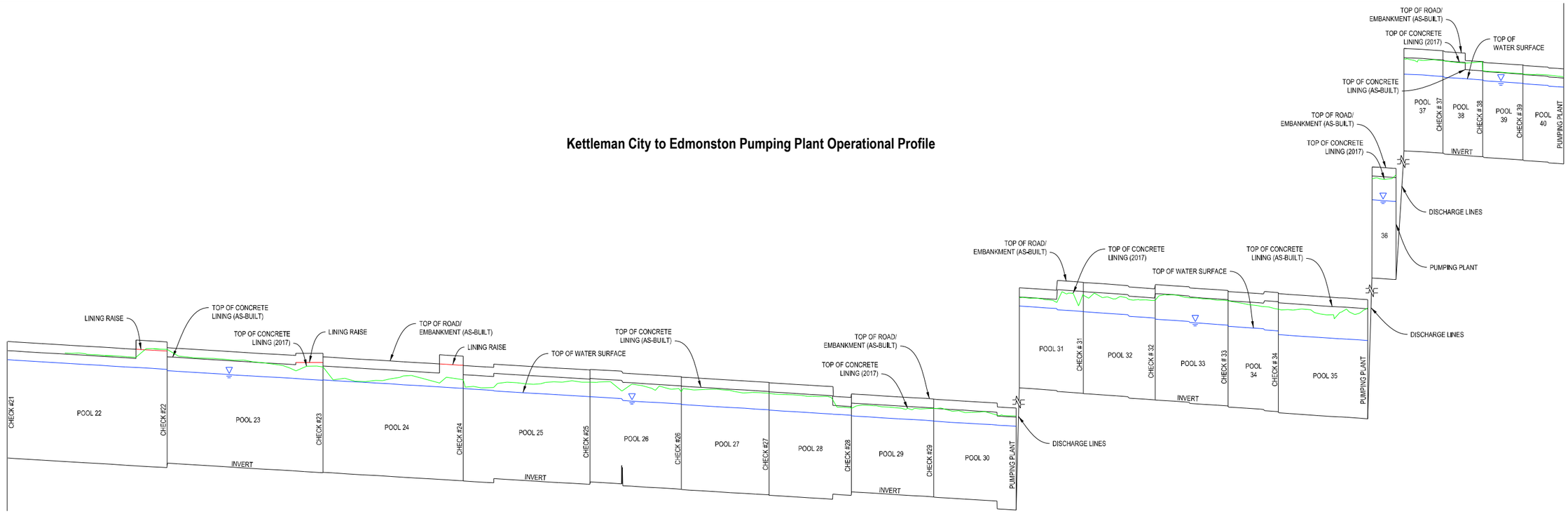

Kettleman City to Edmonston Pumping Plant Subsidence Profile

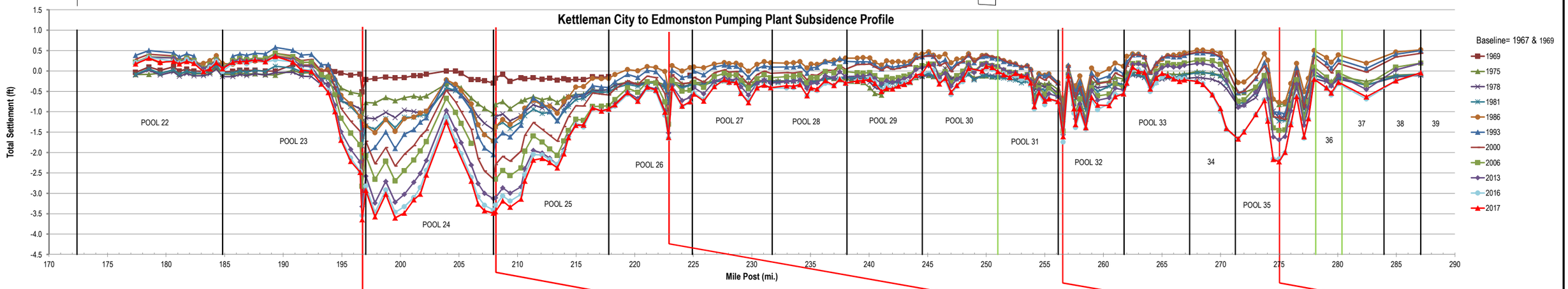

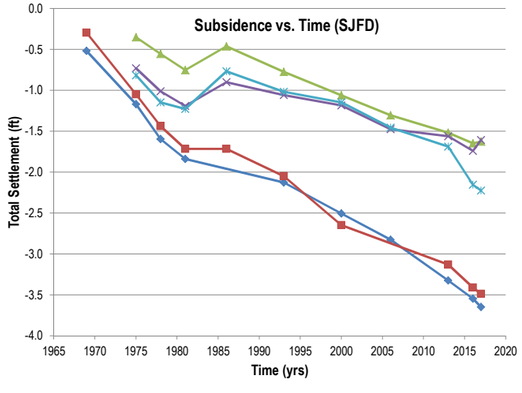

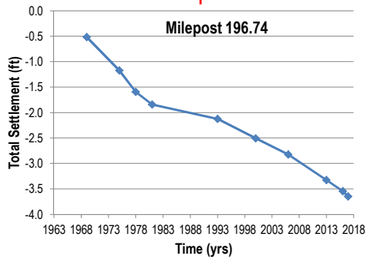

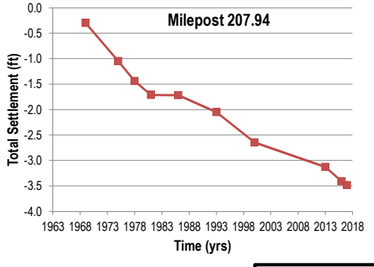

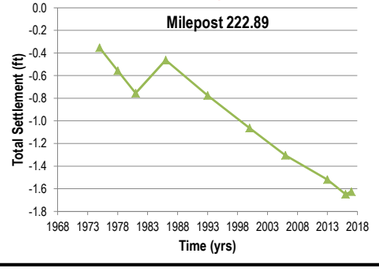

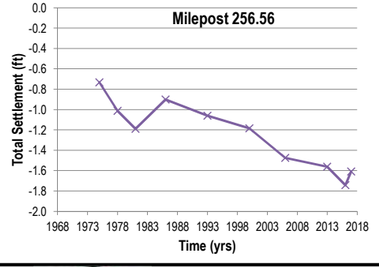

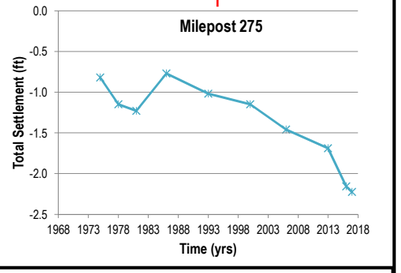

DEPARTMENT OF WATER RESOURCES
STATE WATER PROJECT
CALIFORNIA AQUEDUCT SUBSIDENCE STUDY

PLATE 10
SUBSIDENCE & OPERATIONAL PROFILES

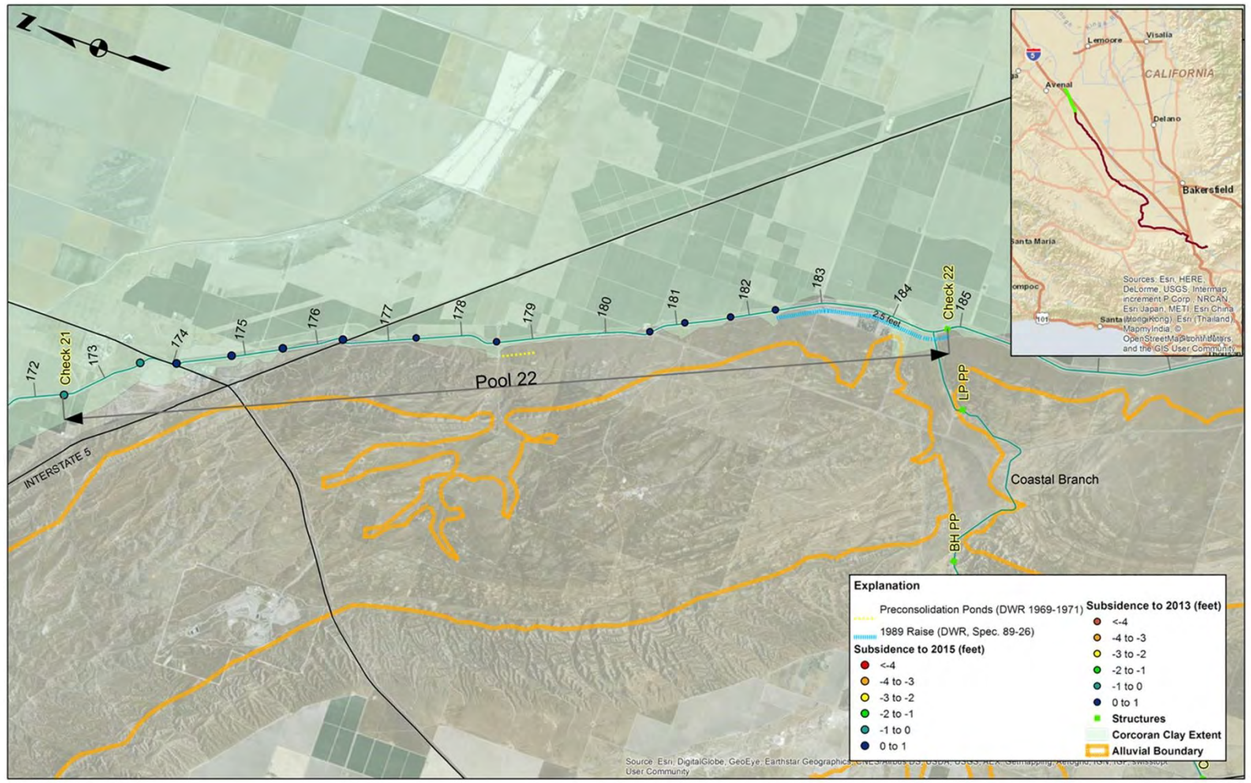

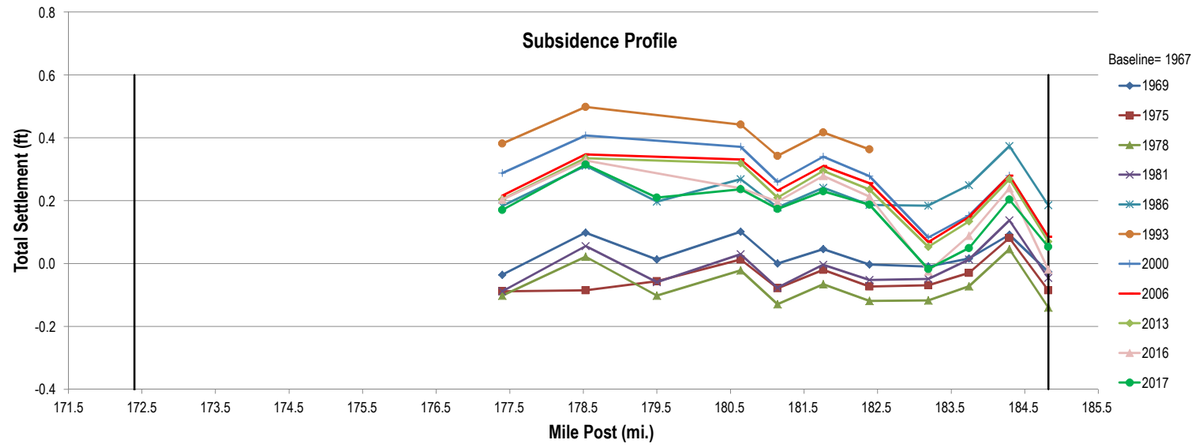

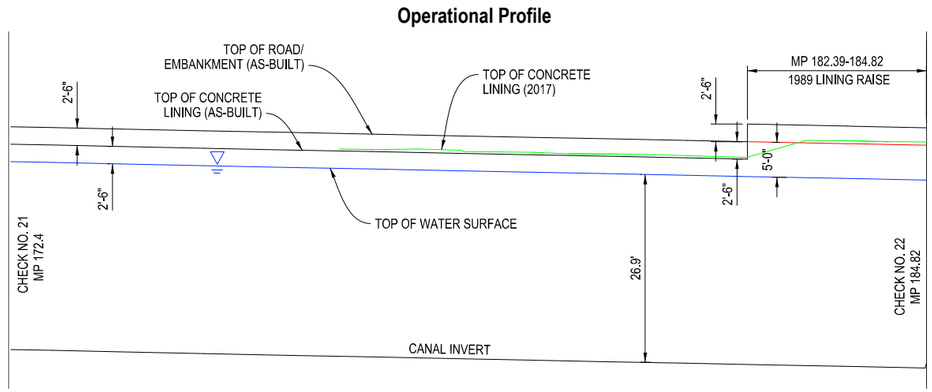

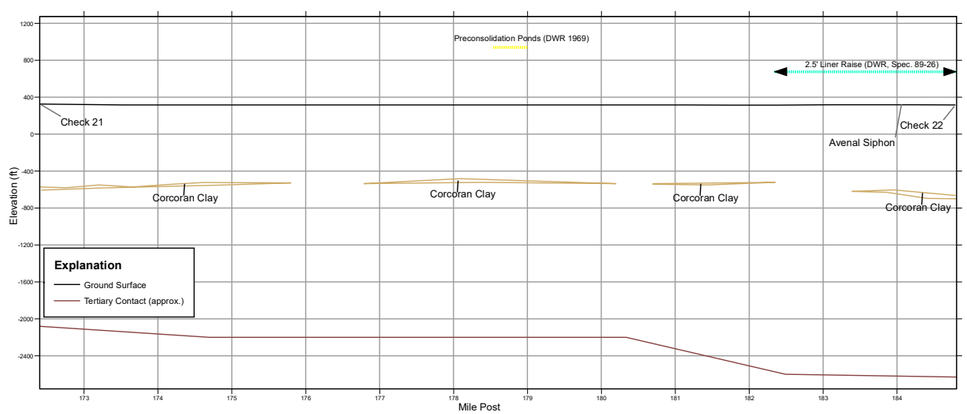

STRUCTURE	SIDE OF EMBANKMENT	MP
CHECK NUMBER 21		172.4
END OF SAN LUIS FIELD DIVISION		172.44
POWERLINE CROSSING		172.49
MILHAM AVE. BRIDGE		172.58
TURNOUT	L	172.66
CULVERT CROSSING		172.72
PIPELINE CROSSING (4)		172.8
POWERLINE CROSSING		172.84
PIPELINE CROSSING		172.93
CULVERT CROSSING		172.96
POWERLINE CROSSING		172.97
PIPELINE CROSSING		173.13
4TH STREET BRIDGE		173.13
POWERLINE CROSSING		173.36
CULVERT CROSSING		173.37
BRIDGE		173.56
POWERLINE CROSSING		173.65
POWERLINE CROSSING (2)		173.67
POWERLINE CROSSING (2)		173.68

STRUCTURE	SIDE OF EMBANKMENT	MP
POWERLINE CROSSING		173.7
POWERLINE CROSSING		173.77
PIPELINE CROSSING		173.78
PIPELINE CROSSING		173.91
OVERCHUTE CROSSING		174.07
POWERLINE CROSSING		174.08
HIGHWAY 41 BRIDGE		174.13
POWERLINE CROSSING		174.15
POWERLINE CROSSING		174.4
PIPELINE CROSSING		174.51
POWERLINE CROSSING		174.65
PIPELINE CROSSING (2)		175.03
TURNOUT	L	175.18
CULVERT CROSSING		175.2
PIPELINE CROSSING		175.2
OVERCHUTE CROSSING		175.55
INTERSTATE 5 BRIDGE		176.39
CULVERT CROSSING		176.52
OVERCHUTE CROSSING		177.41
TURNOUT	L	177.54
UTICA AVENUE BRIDGE		178.54

STRUCTURE	SIDE OF EMBANKMENT	MP
OVERCHUTE CROSSING		178.57
OVERCHUTE CROSSING		179.5
OVERCHUTE CROSSING		179.98
POWERLINE CROSSING		180
POWERLINE CROSSING		180.62
BRIDGE/POWERLINE		180.64
TURNOUT	R	180.64
TURNOUT	L	180.65
OVERCHUTE CROSSING		181.14
OVERCHUTE CROSSING		182.39
TURNOUT	L	182.99
TURNOUT	L	183
POWERLINE CROSSING		183.01
OVERCHUTE CROSSING		183.19
POWERLINE CROSSING		184.05
AVENAL GAP SIPHON/BRIDGE		184.3
BRIDGE		184.31
COASTAL BRANCH AQUEDUCT		184.63
TURNOUT	L	184.78
POWERLINE CROSSING		184.8
STILLING WELL	L	184.8
CHECK NUMBER 22		184.82

PLATE 11

DEPARTMENT OF WATER RESOURCES
STATE WATER PROJECT
CALIFORNIA AQUEDUCT SUBSIDENCE STUDY

SUBSIDENCE, OPERATION, & GEOLOGIC PROFILES

POOL 22: MP 172.4 – 184.82

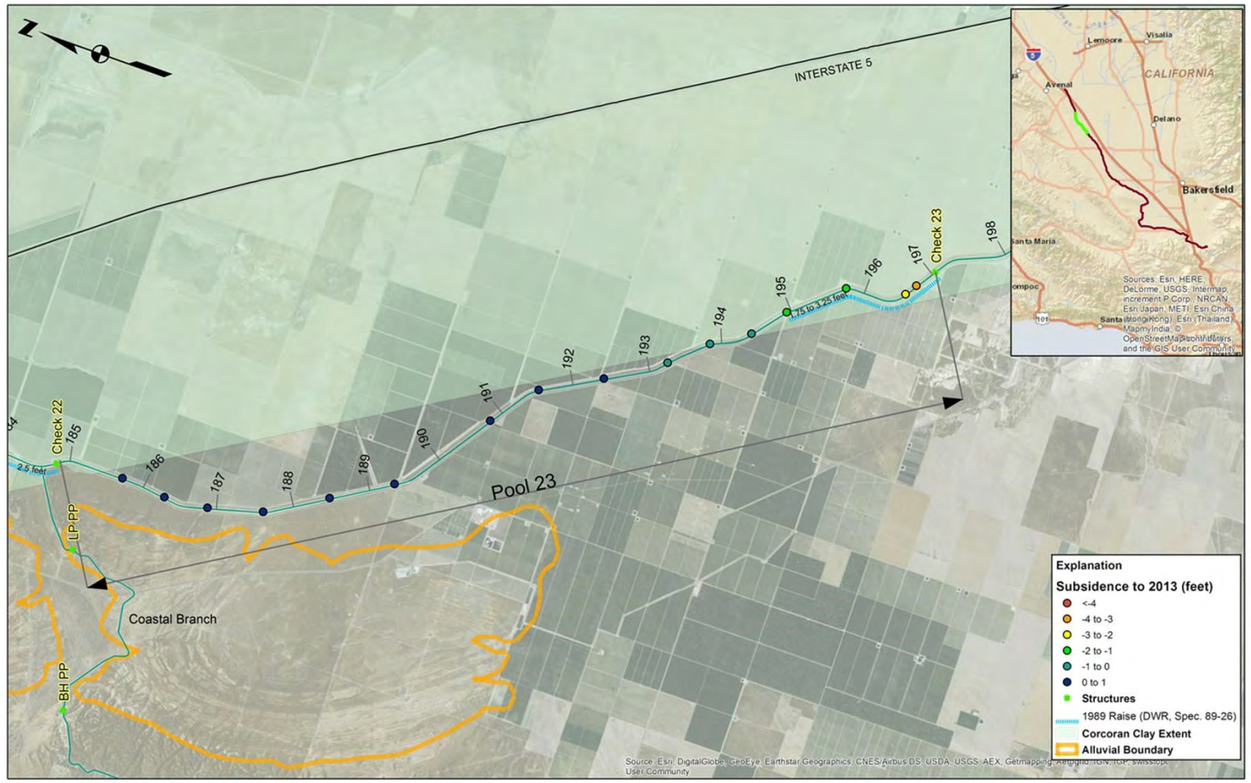

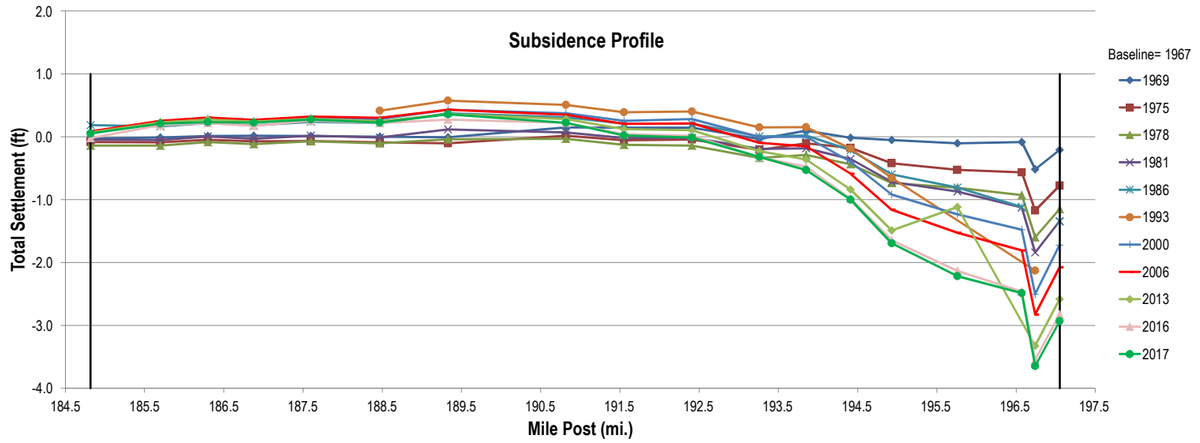

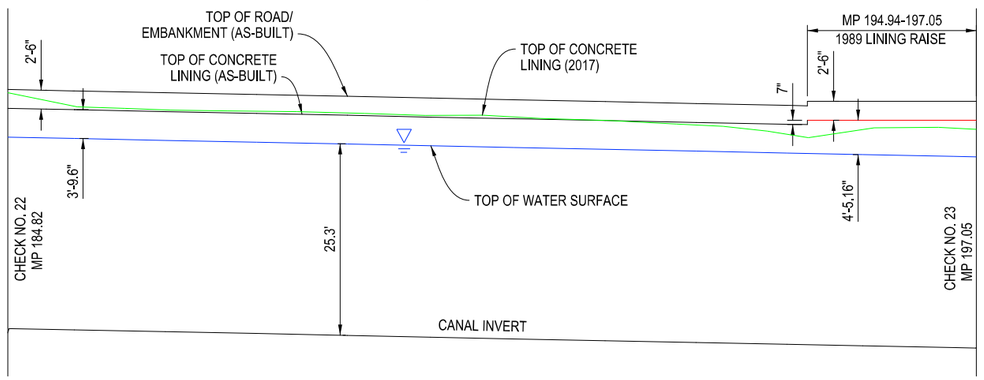

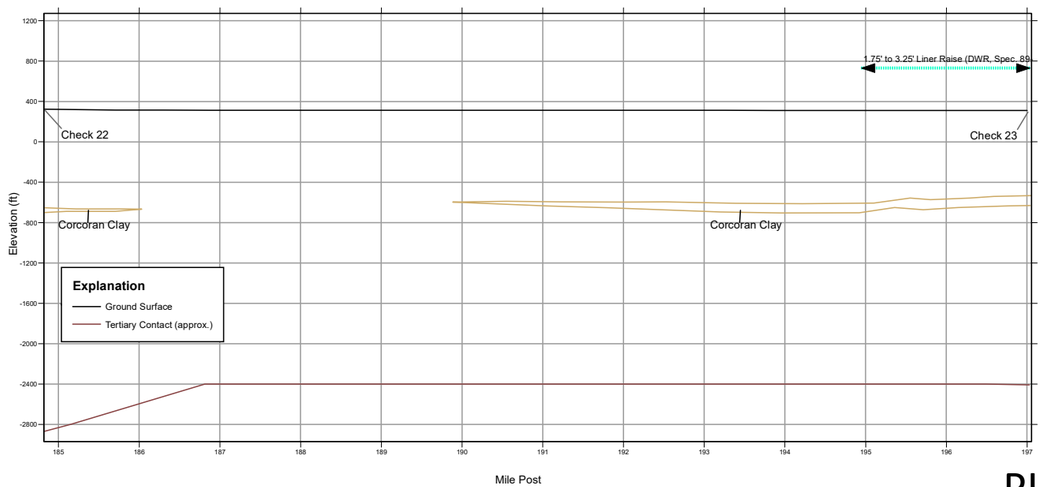

STRUCTURE	SIDE OF EMBANKMENT	MP
CHECK NUMBER 22		184.82
STILLING WELL	L	184.88
OVERCHUTE CROSSING		185.71
OVERCHUTE CROSSING		186.88
OVERCHUTE CROSSING		187.6
CULVERT CROSSING		189.1
POWERLINE CROSSING		189.12
BRIDGE		189.34
TURNOUT	R	189.69
OVERCHUTE CROSSING		190.09
TURNOUT	L	191.18
OVERCHUTE CROSSING		191.56
OVERCHUTE CROSSING		192.41
OVERCHUTE CROSSING		193.26
TURNOUT	L	194.22
OVERCHUTE CROSSING		194.42
POWERLINE CROSSING		194.93
TWISSELMAN ROAD BRIDGE		194.94
POWERLINE CROSSING		196.39
TURNOUT	R	196.4
OVERCHUTE CROSSING		196.58
TURNOUT	L	196.75
STILLING WELL	L	197.03
CHECK NUMBER 23		197.05

PLATE 12

DEPARTMENT OF WATER RESOURCES
STATE WATER PROJECT
CALIFORNIA AQUEDUCT SUBSIDENCE STUDY

SUBSIDENCE, OPERATION, & GEOLOGIC PROFILES

POOL 23: MP 184.82 – 197.05

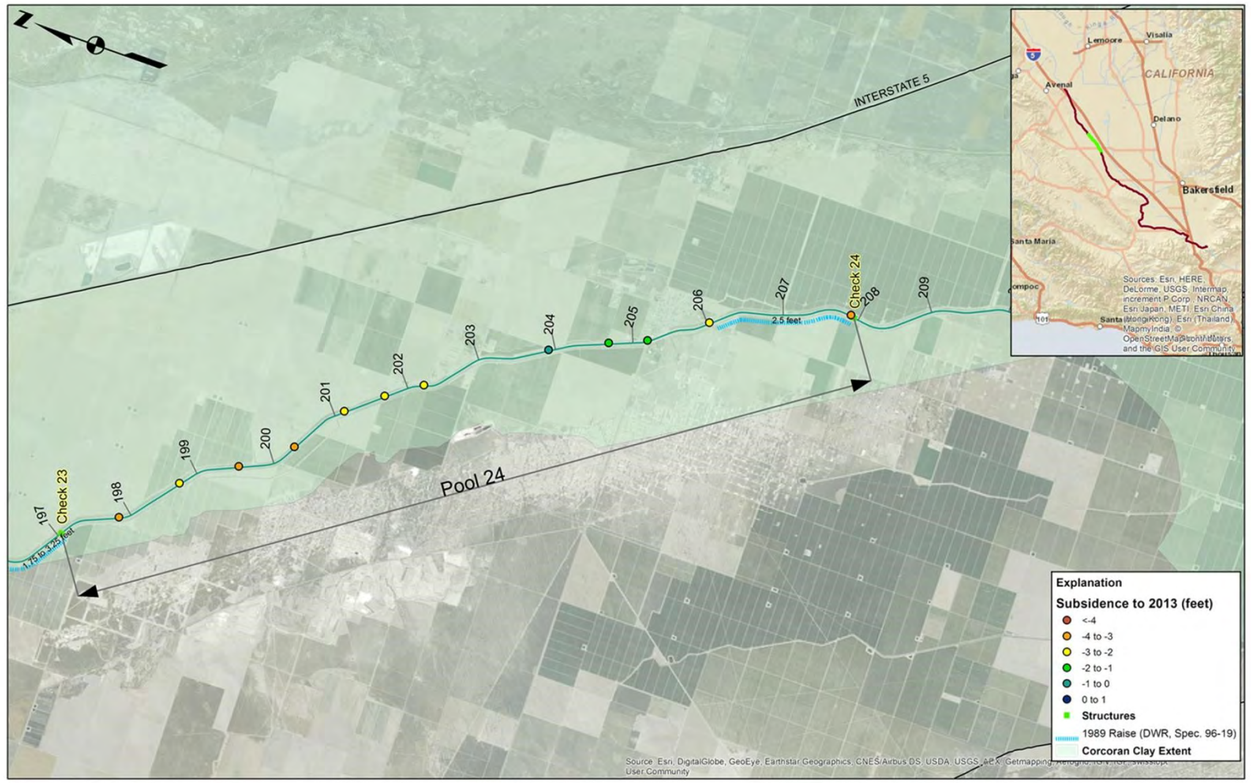

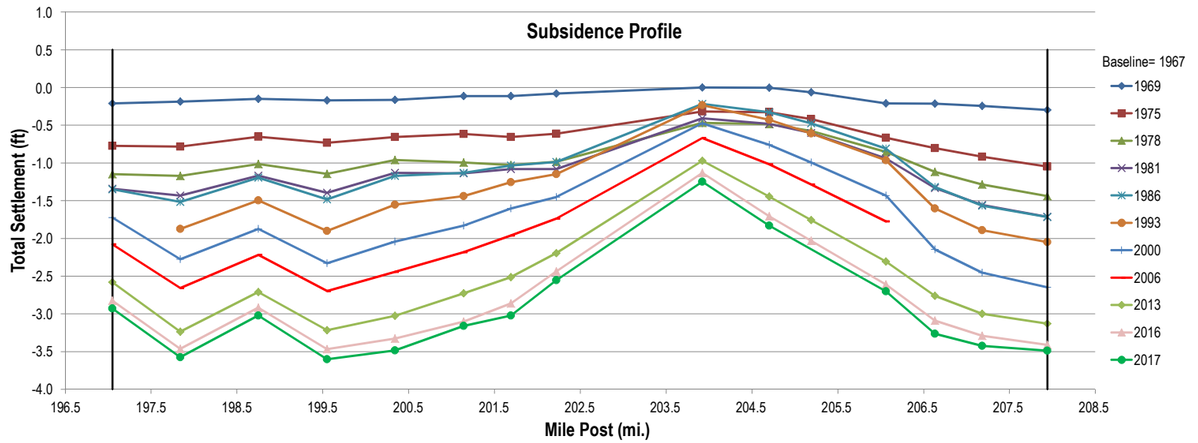

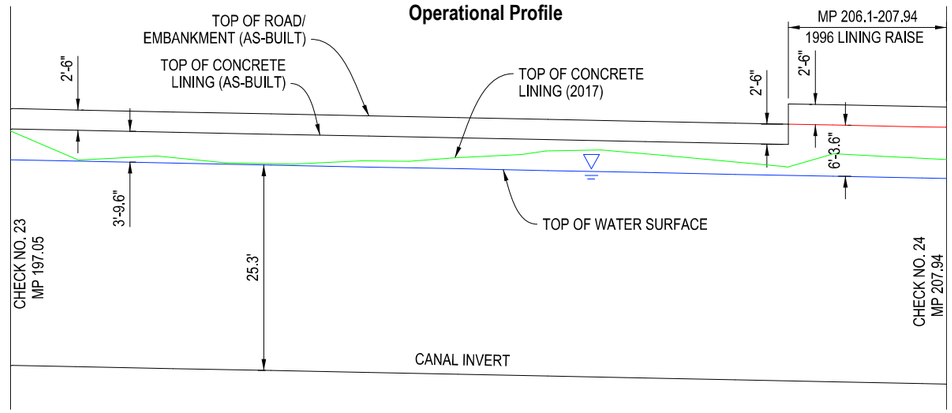

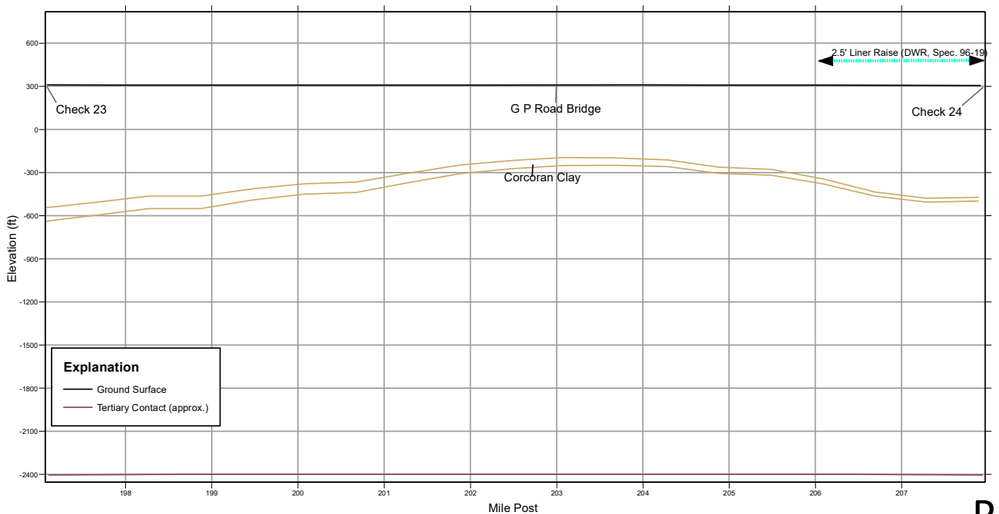

STRUCTURE	SIDE OF EMBANKMENT	MP
CHECK NUMBER 23		197.05
STILLING WELL	L	197.1
OVERCHUTE CROSSING		197.84
BRIDGE		198.75
POWERLINE CROSSING		198.92
CULVERT CROSSING		199.76
PIPELINE CROSSING		200.56
POWERLINE CROSSING		200.72
OVERCHUTE CROSSING		201.14
TURNOUT (2)	R	201.24
TURNOUT	L	202.05
OVERCHUTE CROSSING		202.22
PIPELINE CROSSING		202.77
POWERLINE CROSSING		202.99
G P ROAD BRIDGE		203
OVERCHUTE CROSSING		203.28
OVERCHUTE CROSSING		203.92
OVERCHUTE CROSSING		204.7

STRUCTURE	SIDE OF EMBANKMENT	MP
TURNOUT	L	204.7
POWERLINE CROSSING		205.18
PHONE LINES		205.19
PIPELINE CROSSING (3)		205.19
HIGHWAY 46 BRIDGE		205.19
PHONE LINES (2)		205.2
POWERLINE CROSSING		205.25
TURNOUT	R	205.26
POWERLINE CROSSING		206.05
LOST HILLS ROAD BRIDGE		206.06
OVERCHUTE CROSSING		206.1
POWERLINE CROSSING		206.43
TURNIN	L	206.99
TURNOUT	L	206.99
PHONE LINES		207.14
OVERCHUTE CROSSING		207.18
STILLING WELL	L	207.92
CHECK NUMBER 24		207.94

PLATE 13

DEPARTMENT OF WATER RESOURCES
STATE WATER PROJECT
CALIFORNIA AQUEDUCT SUBSIDENCE STUDY

SUBSIDENCE, OPERATION, & GEOLOGIC PROFILES

POOL 24: MP 197.05 – 207.94

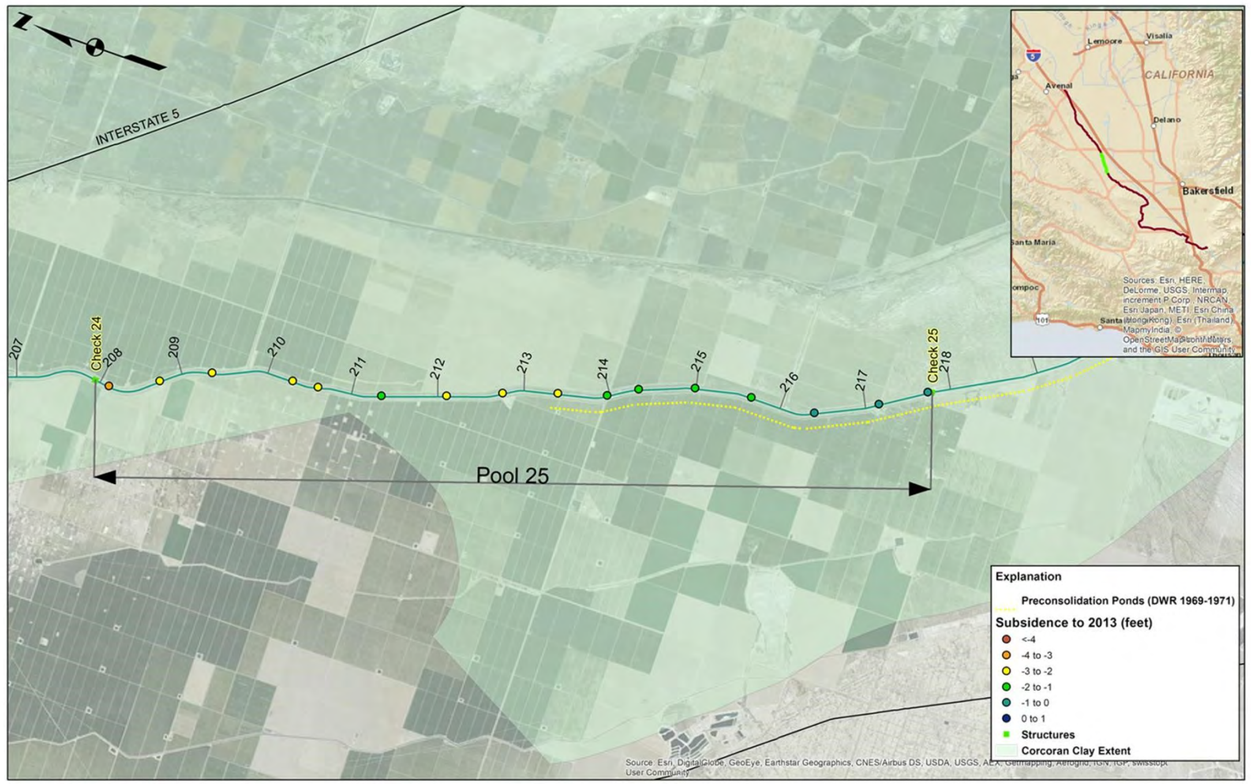

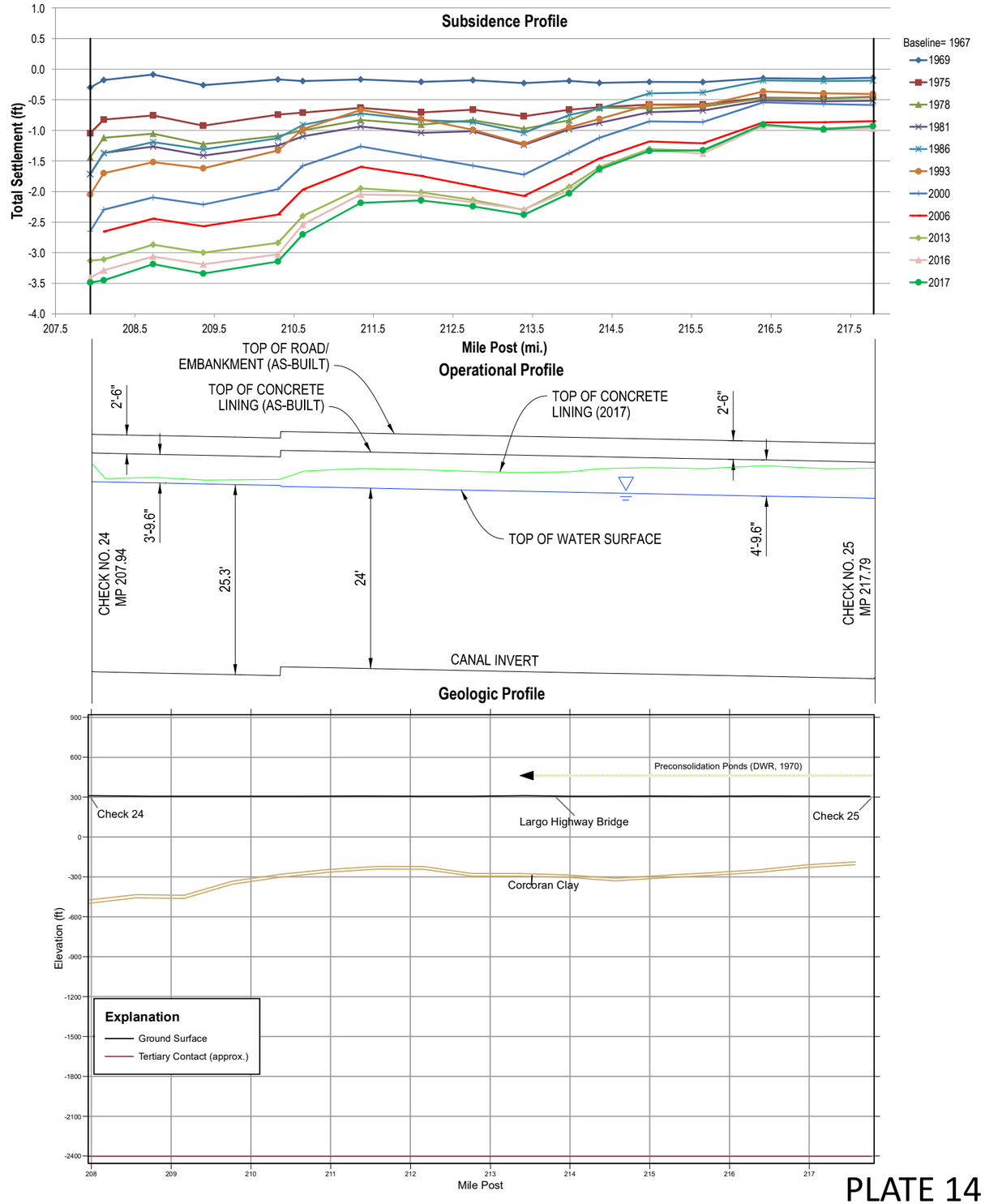

STRUCTURE	SIDE OF EMBANKMENT	MP
CHECK NUMBER 24		207.94
STILLING WELL	L	207.99
POWERLINE CROSSING		208.06
OVERCHUTE CROSSING		208.11
TURNOUT	L	208.85
POWERLINE CROSSING		209.2
OVERCHUTE CROSSING		209.36
TURNOUT	L	209.71
POWERLINE CROSSING		209.73
TURNOUT	L	209.78
TURNIN	L	209.8
TURNOUT	L	209.8
BRIDGE		210.31
OVERCHUTE CROSSING		210.61
TURNOUT	L	210.75
PIPELINE CROSSING (2)		211.8

STRUCTURE	SIDE OF EMBANKMENT	MP
OVERCHUTE CROSSING		212.11
PIPELINE CROSSING (4)		212.64
OVERCHUTE CROSSING		213.4
POWERLINE CROSSING		213.96
LERDO HIGHWAY BRIDGE/PIPELINE		213.97
POWERLINE CROSSING		213.98
TURNOUT	L	214.11
OVERCHUTE CROSSING		214.34
OVERCHUTE CROSSING		215.65
CANAL DRAIN		216.03
TURNOUT	L	216.62
TURNOUT	R	217.13
OVERCHUTE CROSSING		217.16
CONDUIT CROSSING		217.16
STILLING WELL	L	217.77
SAND TRAP		217.79
CHECK NUMBER 25		217.79

PLATE 14

DEPARTMENT OF WATER RESOURCES
STATE WATER PROJECT
CALIFORNIA AQUEDUCT SUBSIDENCE STUDY

SUBSIDENCE, OPERATION, & GEOLOGIC PROFILES

POOL 25: MP 207.94 – 217.79

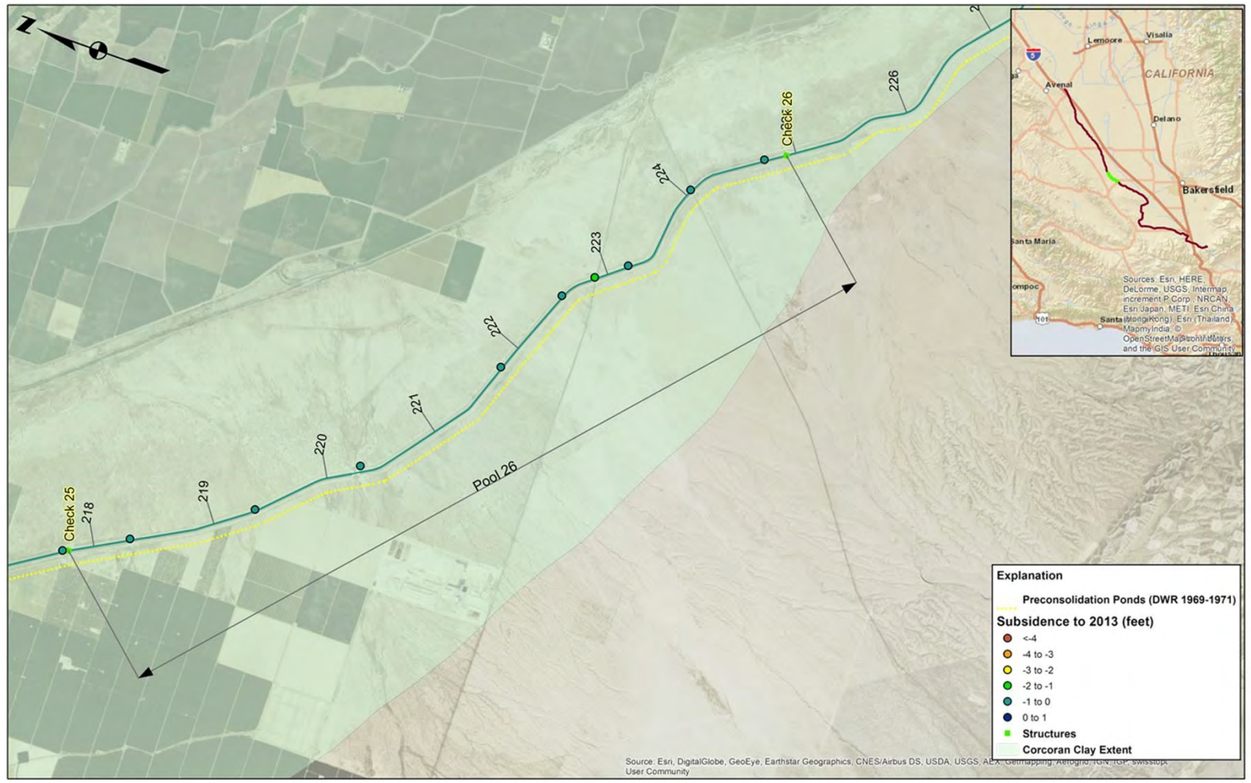

STRUCTURE	SIDE OF EMBANKMENT	MP
CHECK NUMBER 25		217.79
STILLING WELL	L	217.84
7TH STANDARD ROAD BRIDGE		218.32
POWERLINE CROSSING		218.33
OVERCHUTE CROSSING		218.49
TURNOUT	L	219.58
BRIDGE		220.28
TEMBLOR CREEK SIPHON		220.28
OVERCHUTE CROSSING		222.6
LOKERN ROAD BRIDGE		222.91
PIPELINE CROSSING (2)		222.91
PHONE LINE CROSSING (2)		222.96
OVERCHUTE CROSSING		223.2
POWERLINE CROSSING		223.27
POWERLINE CROSSING		224.04
HIGHWAY 58 BRIDGE		224.06
POWERLINE CROSSING		224.15
OVERCHUTE CROSSING		224.18
PIPELINE CROSSING		224.45
POWERLINE CROSSING		224.8
STILLING WELL	L	224.87
CHECK NUMBER 26		224.92

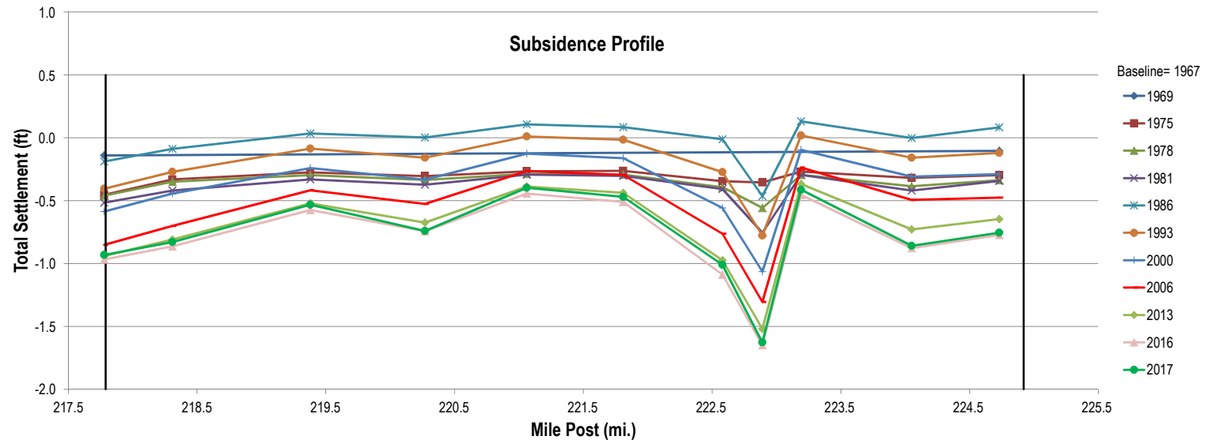

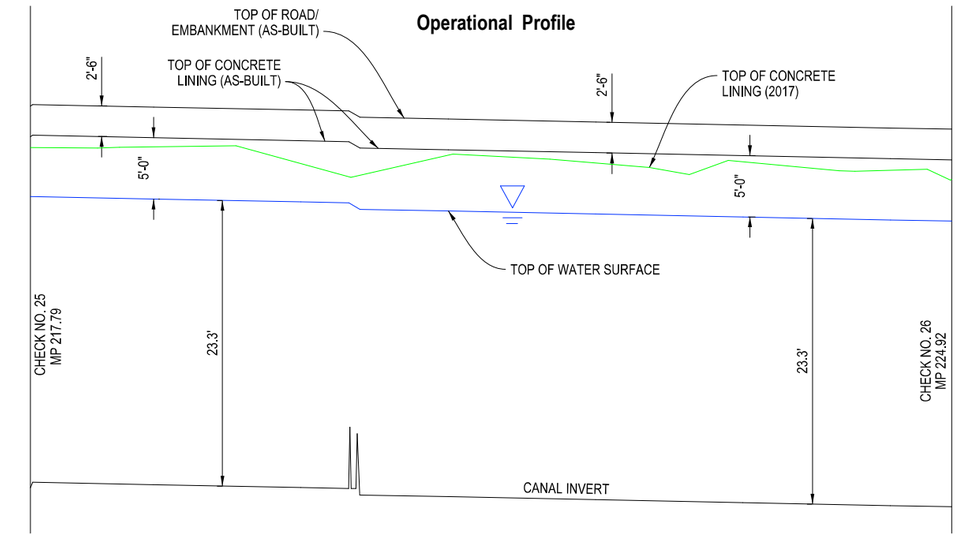

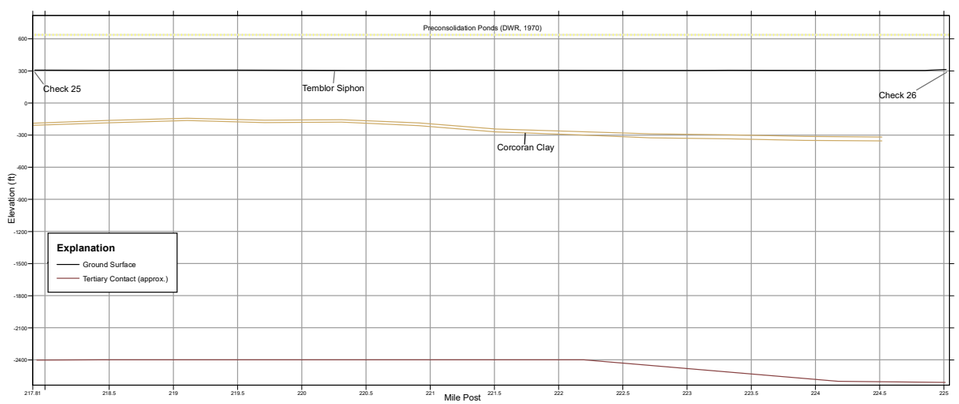

PLATE 15

DEPARTMENT OF WATER RESOURCES
STATE WATER PROJECT
CALIFORNIA AQUEDUCT SUBSIDENCE STUDY

SUBSIDENCE, OPERATION, & GEOLOGIC PROFILES

POOL 26: MP 217.79 – 224.92

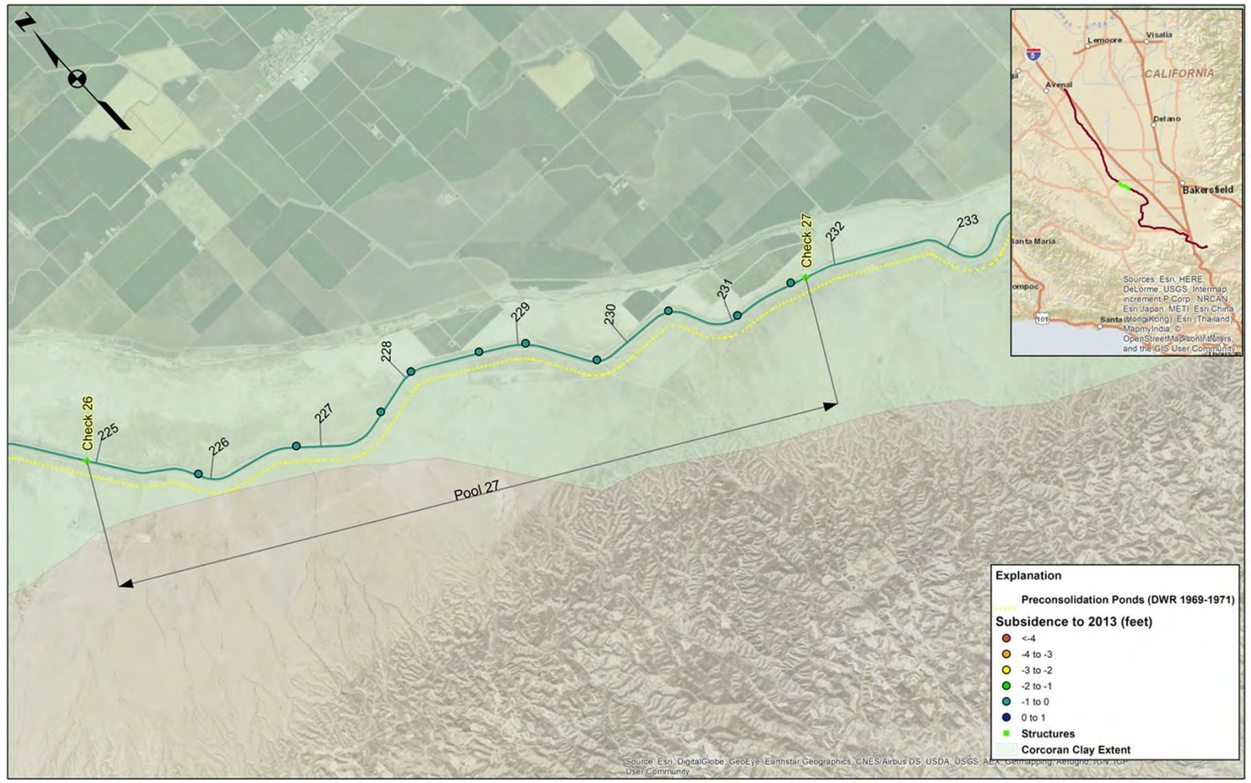

STRUCTURE	SIDE OF EMBANKMENT	MP
CHECK NUMBER 26		224.92
STILLING WELL	L	224.94
OVERCHUTE CROSSING		225.05
POWERLINE CROSSING		225.45
POWERLINE CROSSING		225.55
OVERCHUTE CROSSING		225.89
PHONE LINE CROSSING		226.06
OVERCHUTE CROSSING		226.79
OVERCHUTE CROSSING		227.64
OVERCHUTE CROSSING		228.67
POWERLINE CROSSING		229.05
PIPELINE CROSSING		229.15
ELK HILLS ROAD BRIDGE		229.71
PHONE LINE CROSSING		229.75
TURNOUT	L	230.37
OVERCHUTE CROSSING		230.44
PIPELINE CROSSING		230.44
PIPELINE CROSSING		230.7
POWERLINE CROSSING		231.09
POWERLINE CROSSING		231.14
POWERLINE CROSSING		231.17
OVERCHUTE CROSSING		231.59
STILLING WELL	L	231.69
CHECK NUMBER 27		231.73

Subsidence Profile

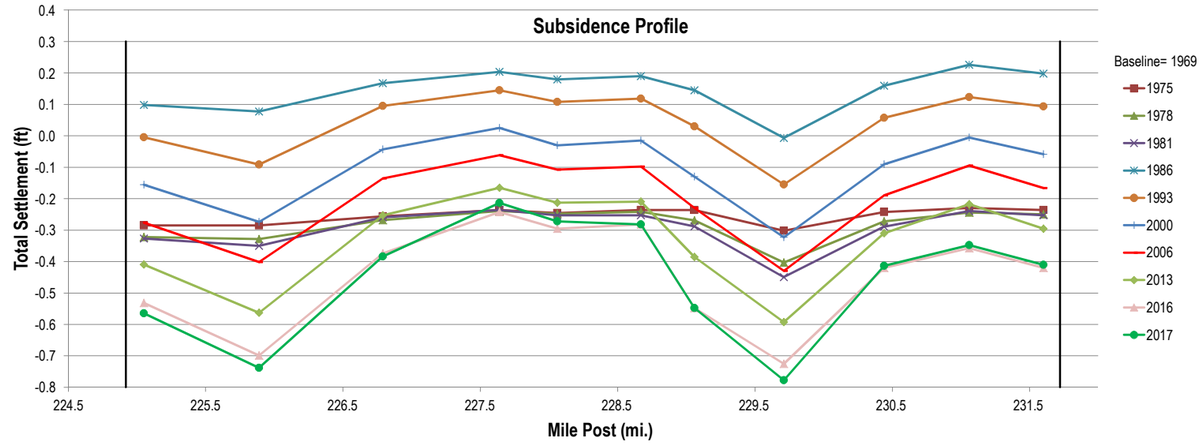

Operational Profile

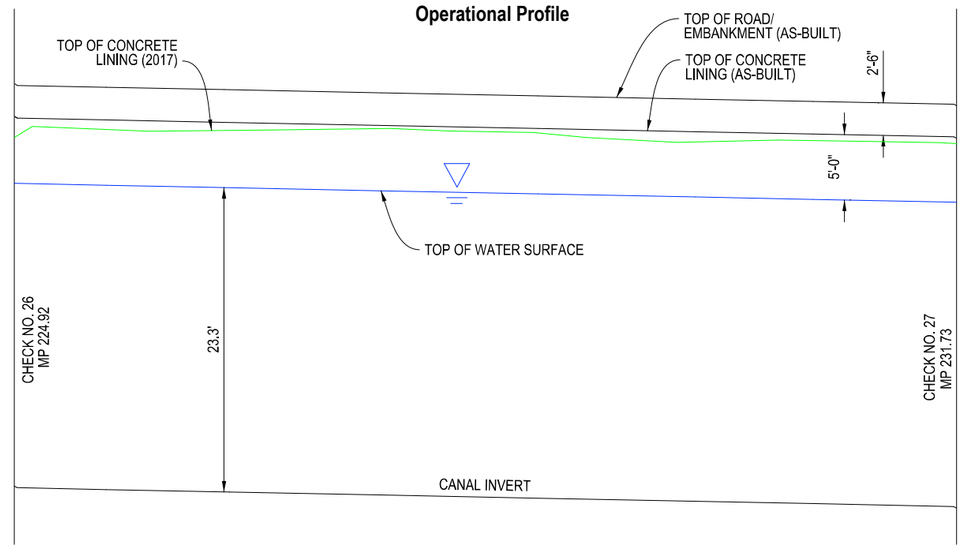

Geologic Profile

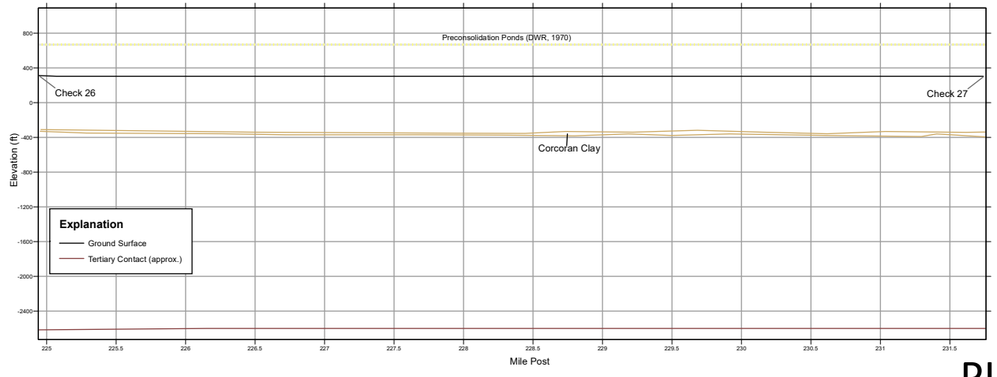

PLATE 16

DEPARTMENT OF WATER RESOURCES
STATE WATER PROJECT
CALIFORNIA AQUEDUCT SUBSIDENCE STUDY

SUBSIDENCE, OPERATION, & GEOLOGIC PROFILES

POOL 27: MP 224.92 – 231.73

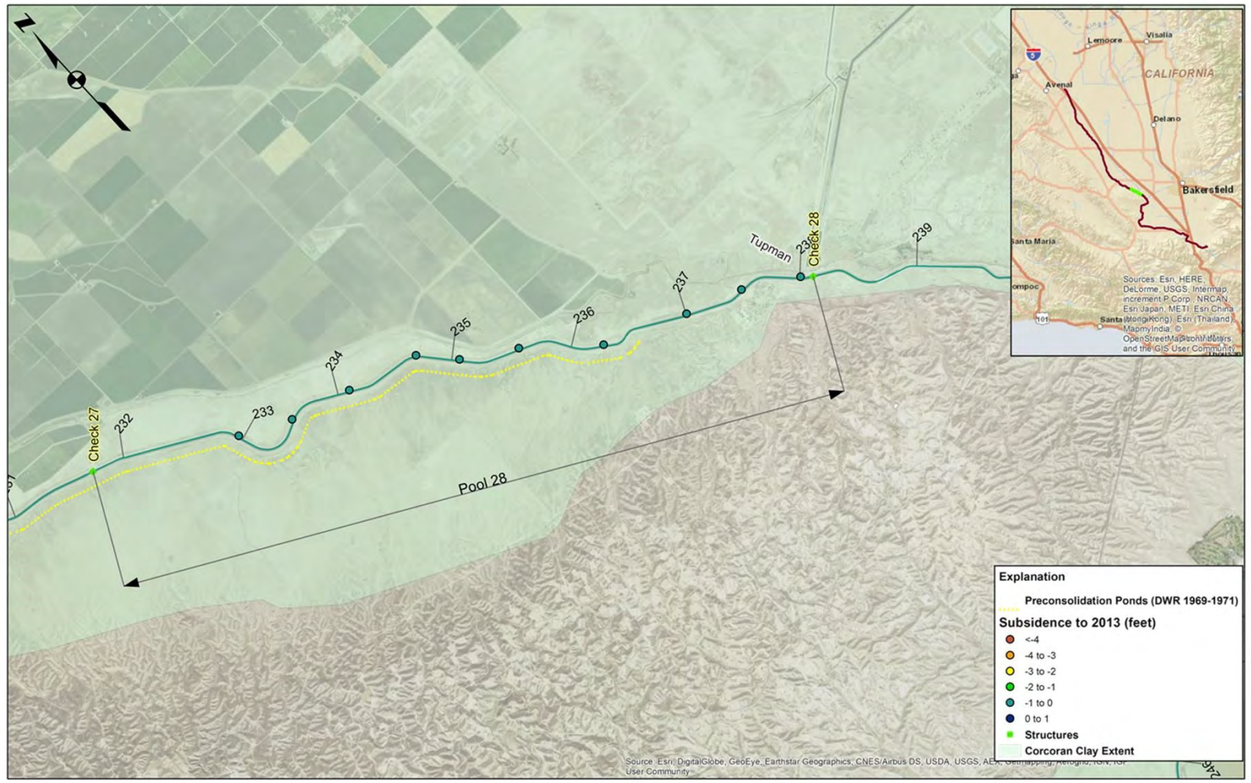

STRUCTURE	SIDE OF EMBANKMENT	MP
CHECK NUMBER 27		231.73
STILLING WELL	L	231.76
BRIDGE		232.23
PIPELINE CROSSING		232.77
POWERLINE CROSSING		232.81
OVERCHUTE CROSSING		232.96
OVERCHUTE CROSSING		234.09
OVERCHUTE CROSSING		235.06
TURNOUT	L	235.75
POWERLINE CROSSING		235.78
POWERLINE CROSSING		235.88
OVERCHUTE CROSSING		236.27
TUPMAN ROAD BRIDGE		236.47
POWERLINE CROSSING		237.11
PHONE LINE CROSSING		237.12
PIPELINE CROSSING		237.12
PHONE LINE CROSSING		237.13
SUMP PUMP	R	237.16
OVERCHUTE CROSSING		237.16
POWERLINE CROSSING		237.75
PIPELINE CROSSING (2)		237.8
CROSS VALLEY CANAL TURNIN	L	238.04
CROSS VALLEY CANAL TURNOUT	L	238.04
TURNOUT	L	238.06
STILLING WELL	L	238.07
POWERLINE CROSSING		238.08
CHECK NUMBER 28		238.11

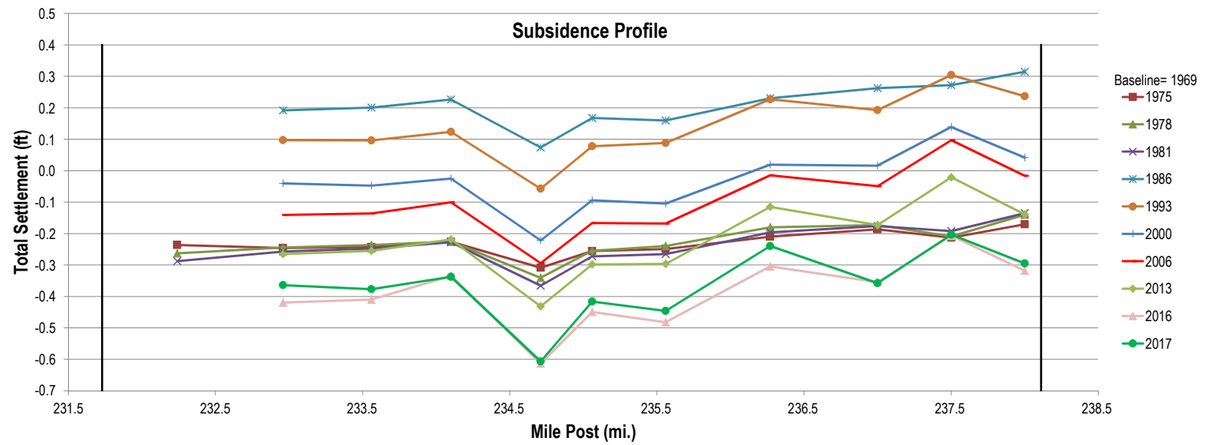

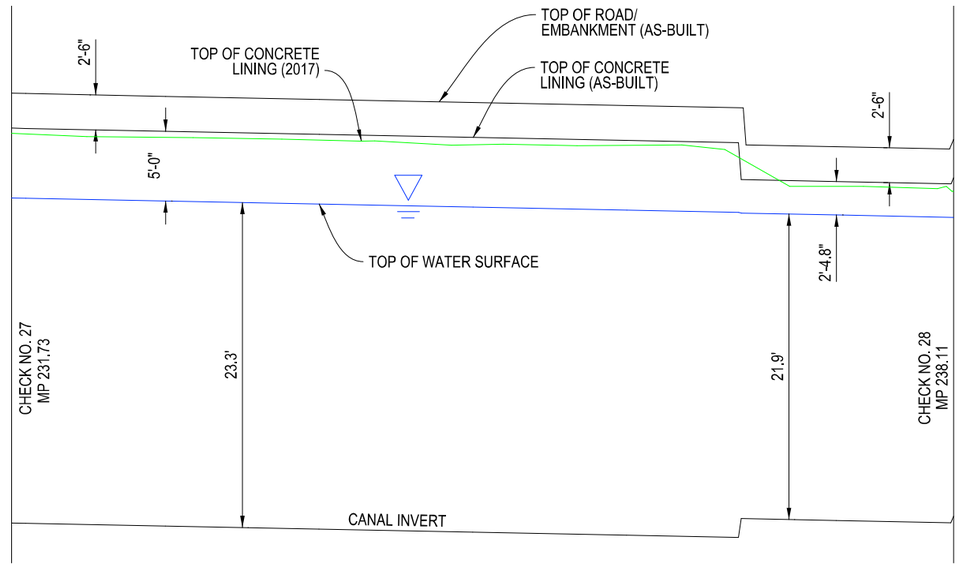

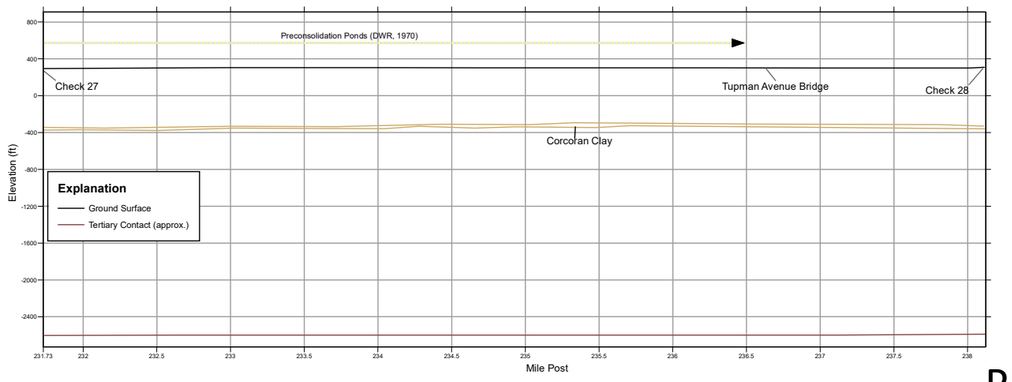

PLATE 17

DEPARTMENT OF WATER RESOURCES
STATE WATER PROJECT
CALIFORNIA AQUEDUCT SUBSIDENCE STUDY

SUBSIDENCE, OPERATION, & GEOLOGIC PROFILES

POOL 28: MP 231.73 – 238.11

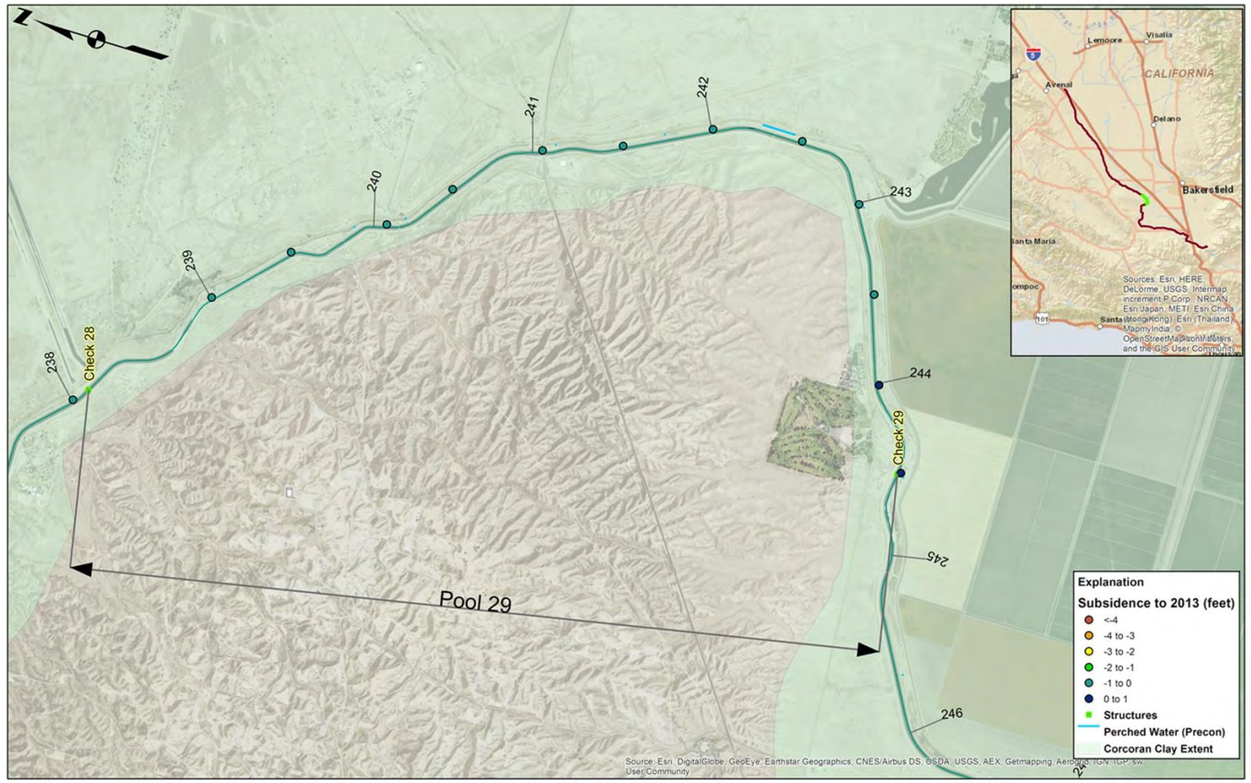

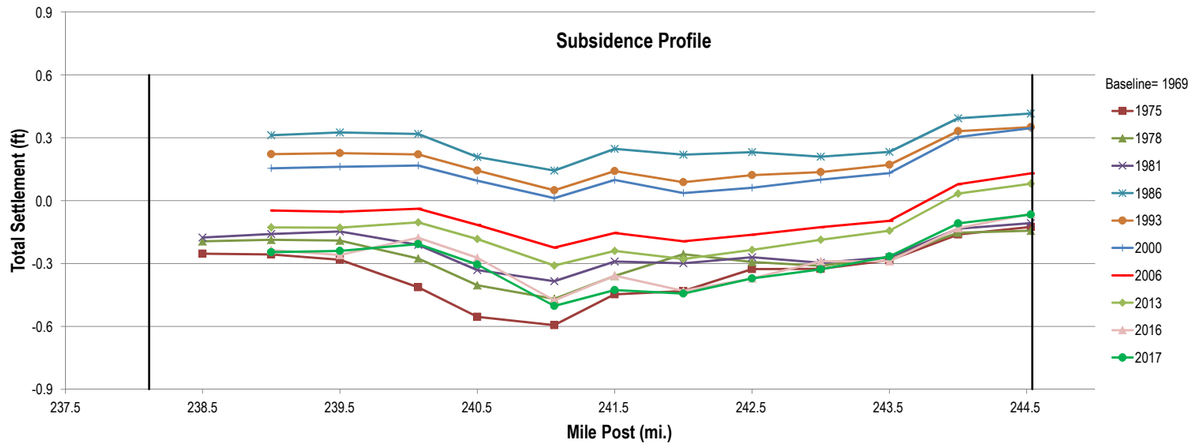

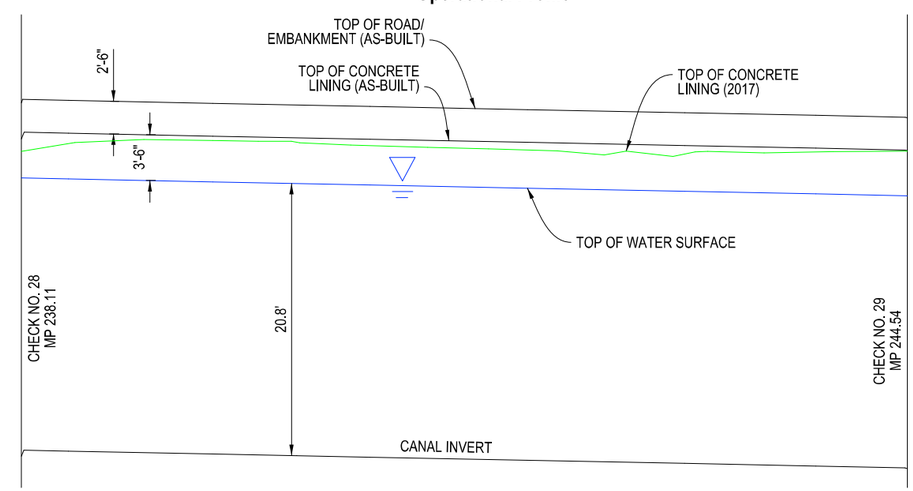

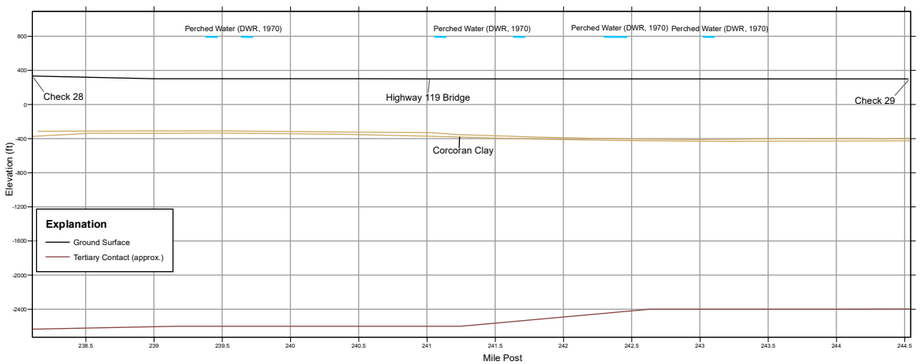

STRUCTURE	SIDE OF EMBANKMENT	MP
CHECK NUMBER 28		238.11
STILLING WELL	L	238.14
OVERCHUTE CROSSING		238.54
SUMP PUMP	R	238.54
POWERLINE CROSSING		238.83
PIPELINE CROSSING (3)		238.97
POWERLINE CROSSING		239.06
OVERCHUTE CROSSING		239.26
SUMP PUMP	R	239.26
PIPELINE CROSSING (10)		239.81
SUMP PUMP	R	240.05
OVERCHUTE CROSSING		240.05
PIPELINE CROSSING (17)		240.07
POWERLINE CROSSING		240.1
BRIDGE		240.14
PIPELINE CROSSING		240.2
TURNIN	R	240.2
PHONE LINE CROSSING		240.24
OVERCHUTE CROSSING		240.35
SUMP PUMP	R	240.35
POWERLINE CROSSING		240.6

STRUCTURE	SIDE OF EMBANKMENT	MP
KERN RIVER INTERTIE		241
HIGHWAY 119 BRIDGE		241.06
TURNOUT	R	241.17
SUMP PUMP	R	241.39
OVERCHUTE CROSSING		241.39
PIPELINE CROSSING		241.61
PIPELINE CROSSING (2)		241.74
POWERLINE CROSSING		242.06
PIPELINE CROSSING (4)		242.35
BRIDGE		242.35
TURNOUT	L	242.65
TURNOUT	L	242.85
IRONBARK ROAD BRIDGE		243.01
TURNOUT	L	243.09
PHONE LINE CROSSING		243.14
PHONE LINE CROSSING		243.15
POWERLINE CROSSING		243.57
STILLING WELL	L	244.47
CHECK NUMBER 29		244.54

PLATE 18

DEPARTMENT OF WATER RESOURCES
STATE WATER PROJECT
CALIFORNIA AQUEDUCT SUBSIDENCE STUDY

SUBSIDENCE, OPERATION, & GEOLOGIC PROFILES

POOL 29: MP 238.11 – 244.54

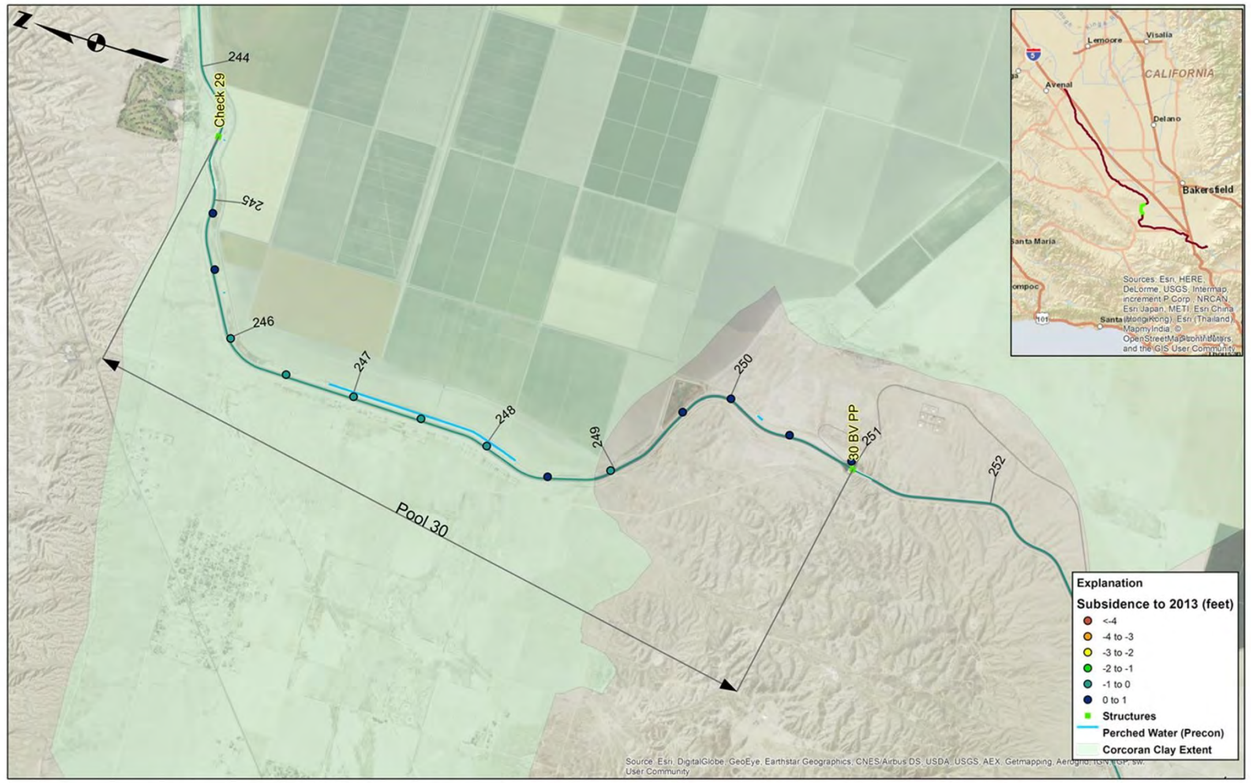

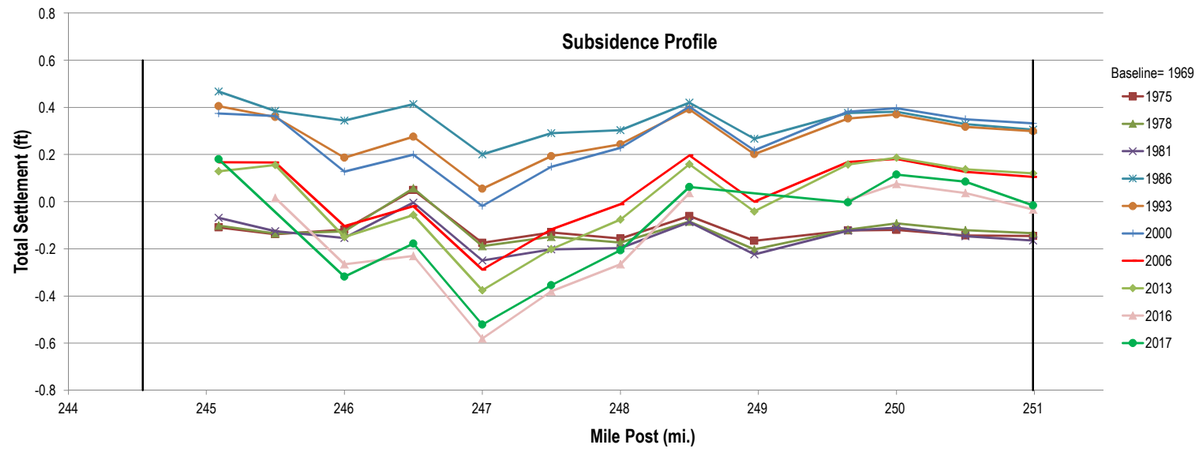

Operational Profile

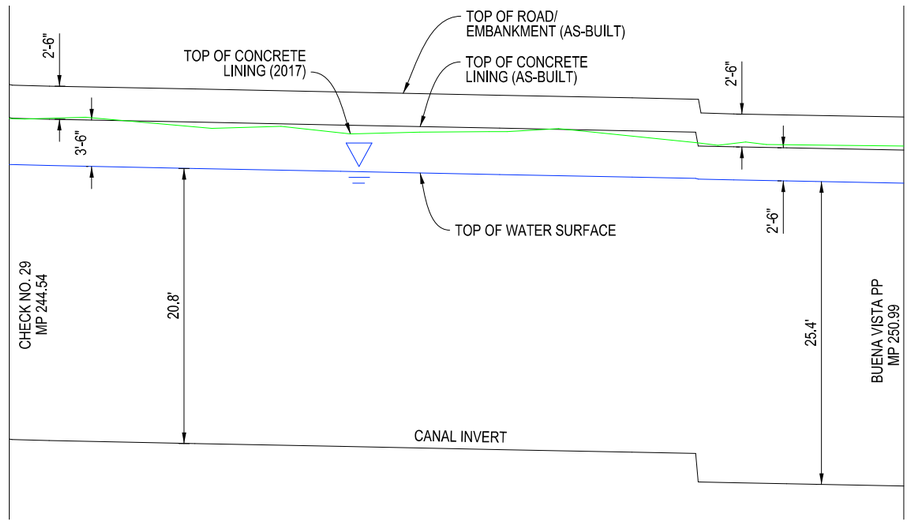

Geologic Profile

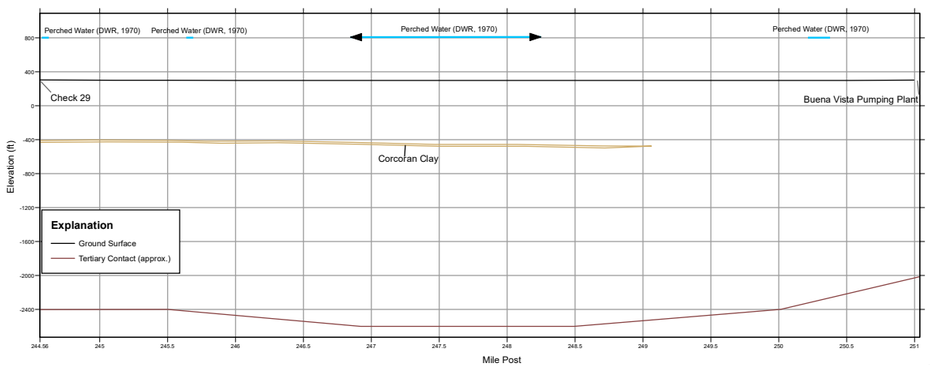

STRUCTURE	SIDE OF EMBANKMENT	MP
CHECK NUMBER 29		244.54
STILLING WELL	L	244.55
OVERCHUTE CROSSING		244.65
PIPELINE CROSSING		245.09
BRIDGE		245.09
POWERLINE CROSSING		245.15
SUMP PUMP	R	245.71
SUMP PUMP	R	245.85
SUMP PUMP	R	245.98
SUMP PUMP	R	246.11
SUMP PUMP	R	246.24
SUMP PUMP	R	246.38
SUMP PUMP	R	246.5
OVERCHUTE CROSSING		246.51
SUMP PUMP	R	246.61
SUMP PUMP	R	246.73
SUMP PUMP	R	246.84
SUMP PUMP	R	246.95
SUMP PUMP	R	247.07
SUMP PUMP	R	247.18
SUMP PUMP	R	247.3
SUMP PUMP	R	247.41

STRUCTURE	SIDE OF EMBANKMENT	MP
SUMP PUMP	R	247.52
SUMP PUMP	R	247.64
SUMP PUMP	R	247.75
SUMP PUMP	R	247.86
SUMP PUMP	R	247.98
SUMP PUMP	R	248.07
OVERCHUTE CROSSING		248.13
SUMP PUMP	R	248.19
SUMP PUMP	R	248.3
SUMP PUMP	R	248.41
SUMP PUMP	R	248.54
SUMP PUMP	R	248.67
SUMP PUMP	R	248.8
BRIDGE		248.97
PIPELINE CROSSING		248.97
OVERFLOW WEIR/BRIDGE	L	249.65
SAND TRAP		249.71
TURNOUT	L	249.85
POWERLINE CROSSING		249.97
SUMP PUMP	R	250.23
BUENA VISTA PUMPING PLANT		250.99

PLATE 19

DEPARTMENT OF WATER RESOURCES
STATE WATER PROJECT
CALIFORNIA AQUEDUCT SUBSIDENCE STUDY

SUBSIDENCE, OPERATION, & GEOLOGIC PROFILES

POOL 30: MP 244.54 – 250.99

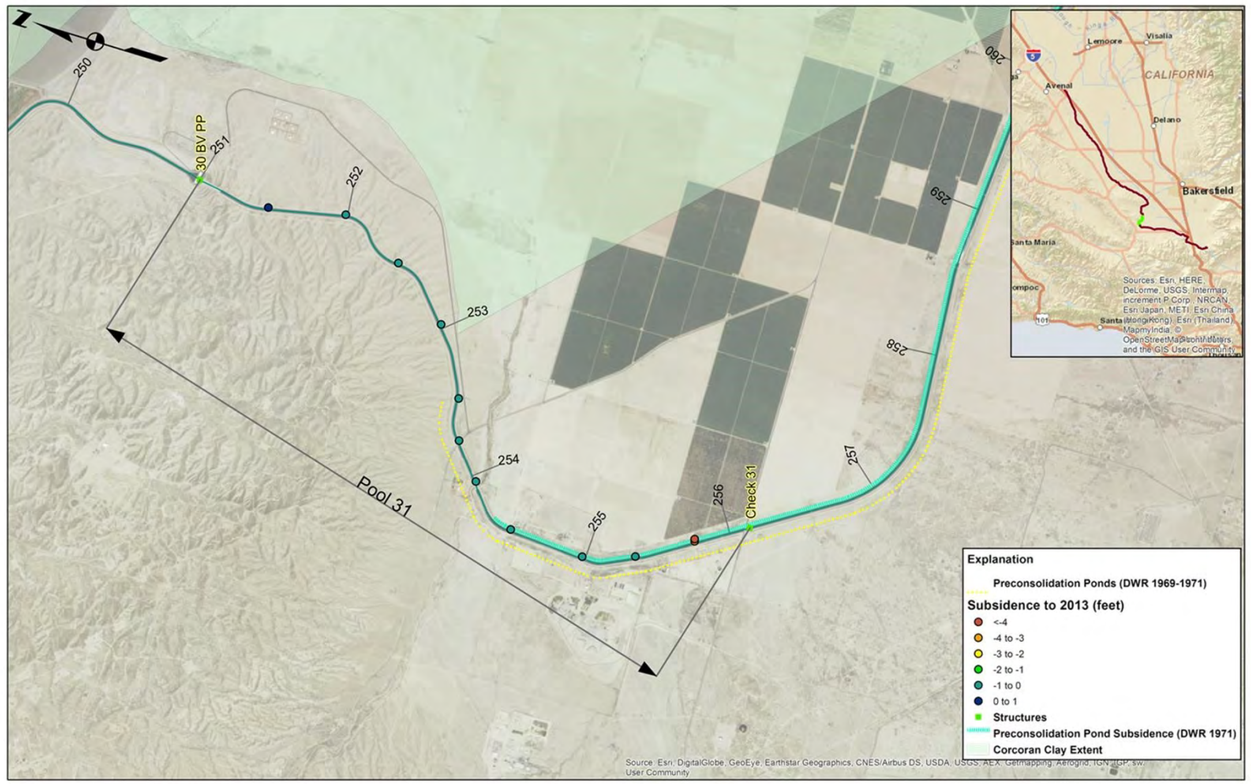

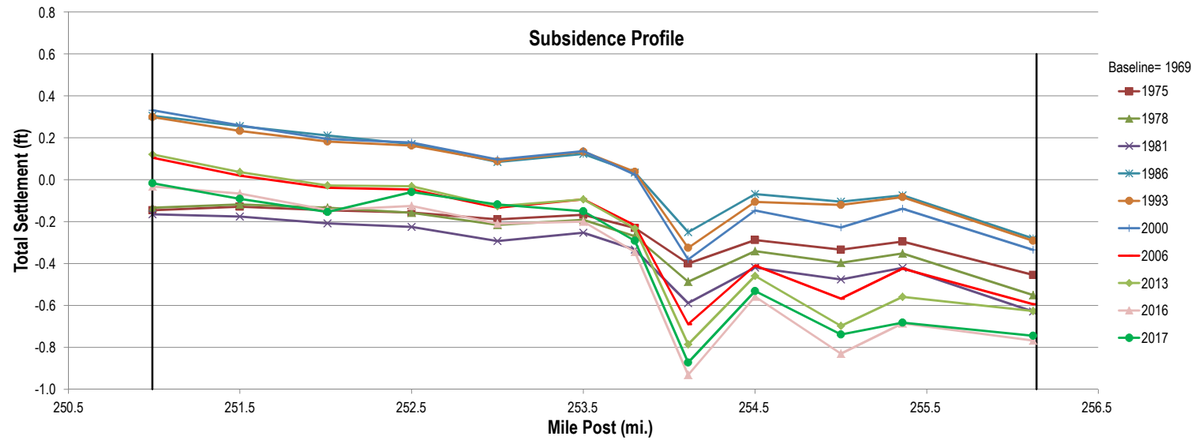

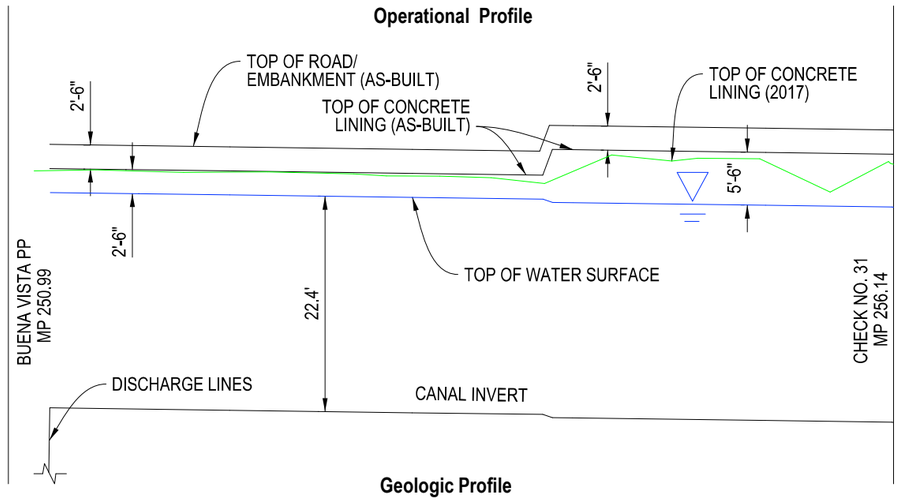

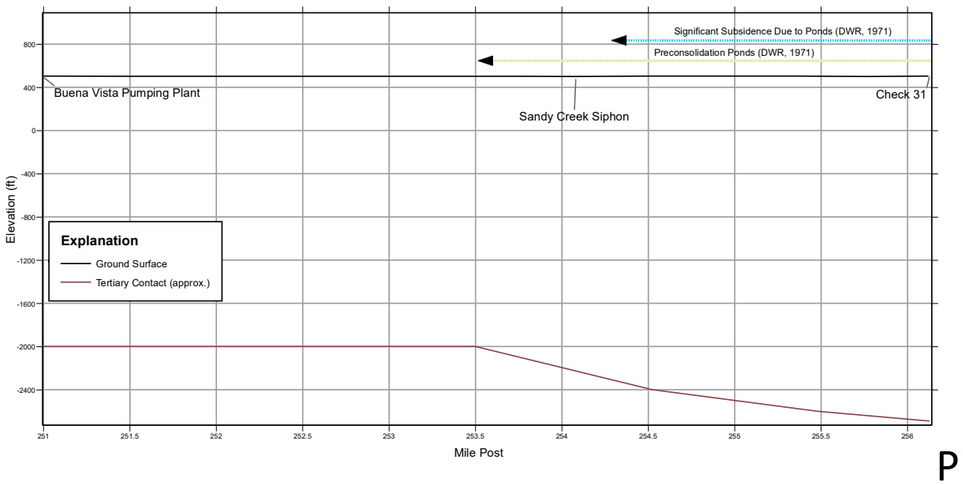

STRUCTURE	SIDE OF EMBANKMENT	MP
BUENA VISTA PUMPING PLANT		250.99
PIPELINE CROSSING (4)		251.16
CULVERT CROSSING		251.35
PHONE LINE CROSSING		251.43
CULVERT CROSSING		251.54
SUMP PUMP	R	251.66
CULVERT CROSSING		251.73
CULVERT CROSSING		251.84
PIPELINE CROSSING		252.01
CULVERT CROSSING		252.03
CULVERT CROSSING		252.36
SUMP PUMP	R	252.63
CULVERT CROSSING		252.95
PIPELINE CROSSING		253.19
CULVERT CROSSING		253.26
CULVERT CROSSING		253.49

STRUCTURE	SIDE OF EMBANKMENT	MP
SUMP PUMP	R	253.6
PIPELINE CROSSING		253.8
GARDNER FIELD ROAD BRIDGE		253.8
BRIDGE		254.11
SANDY CREEK SIPHON		254.11
PIPELINE CROSSING		254.12
TURNOUT	R	254.47
POWERLINE CROSSING		254.83
PIPELINE CROSSING		254.85
PHONE LINE CROSSING		255.34
PIPELINE CROSSING		255.36
POWERLINE CROSSING		255.55
OVERCHUTE CROSSING		255.78
TURNOUT	L	256.11
CADET ROAD BRIDGE		256.13
STILLING WELL	L	256.14
CHECK NUMBER 31		256.14

PLATE 20

DEPARTMENT OF WATER RESOURCES
STATE WATER PROJECT
CALIFORNIA AQUEDUCT SUBSIDENCE STUDY

SUBSIDENCE, OPERATION, & GEOLOGIC PROFILES

POOL 31: MP 250.99 – 256.14

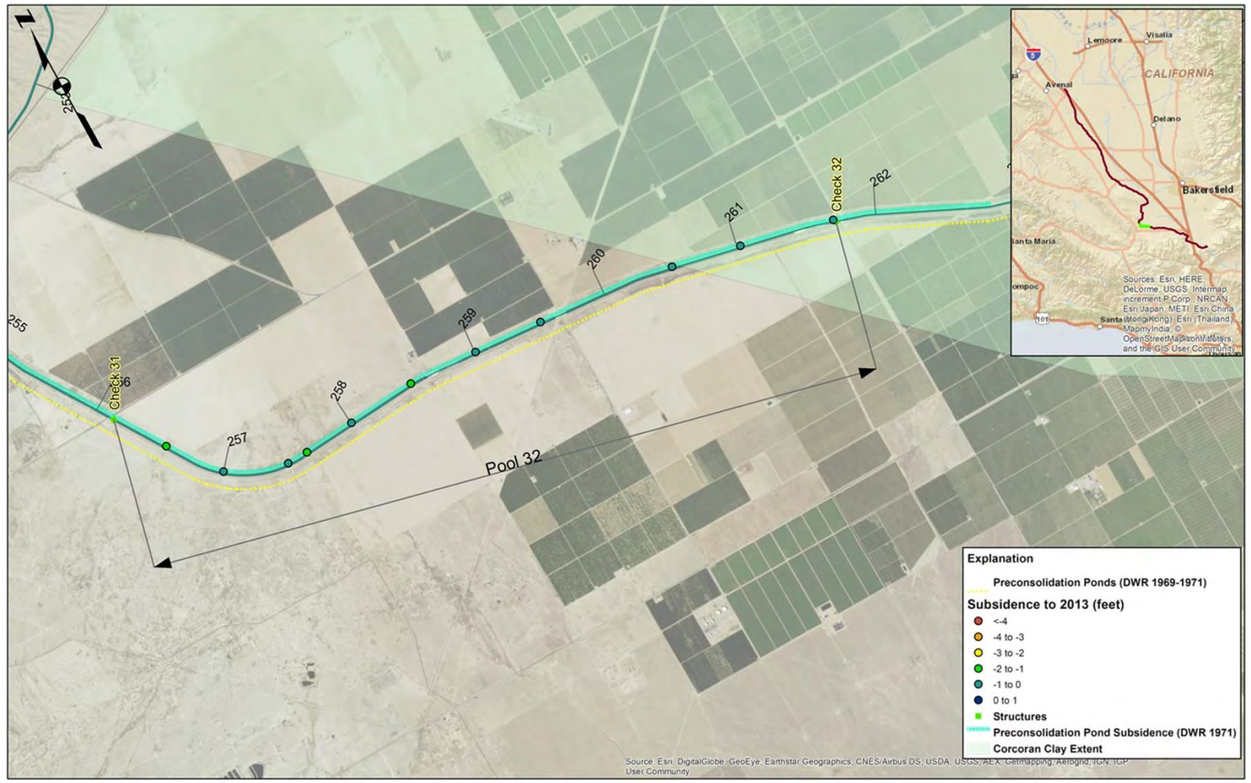

STRUCTURE	SIDE OF EMBANKMENT	MP
CHECK NUMBER 31		256.14
STILLING WELL	L	256.21
POWERLINE CROSSING		256.36
OVERCHUTE CROSSING		256.56
OVERCHUTE CROSSING		257.48
PIPELINE CROSSING		257.63
OVERCHUTE CROSSING		258.59
TURNOUT	L	258.61
PHONE LINE CROSSING		259.45
PIPELINE CROSSING		259.64
BRIDGE (2)		259.65
SUNSET RAIL ROAD SIPHON		259.65
PIPELINE CROSSING (2)		260.01
POWERLINE CROSSING		260.11
TURNOUT	L	260.44
PIPELINE CROSSING (3)		260.45
POWERLINE CROSSING (2)		260.66
PIPELINE CROSSING		261.47
STILLING WELL	L	261.68
PIPELINE CROSSING		261.72
SANTIAGO CREEK SIPHON		261.72
BRIDGE (2)		261.72
CHECK NUMBER 32		261.72

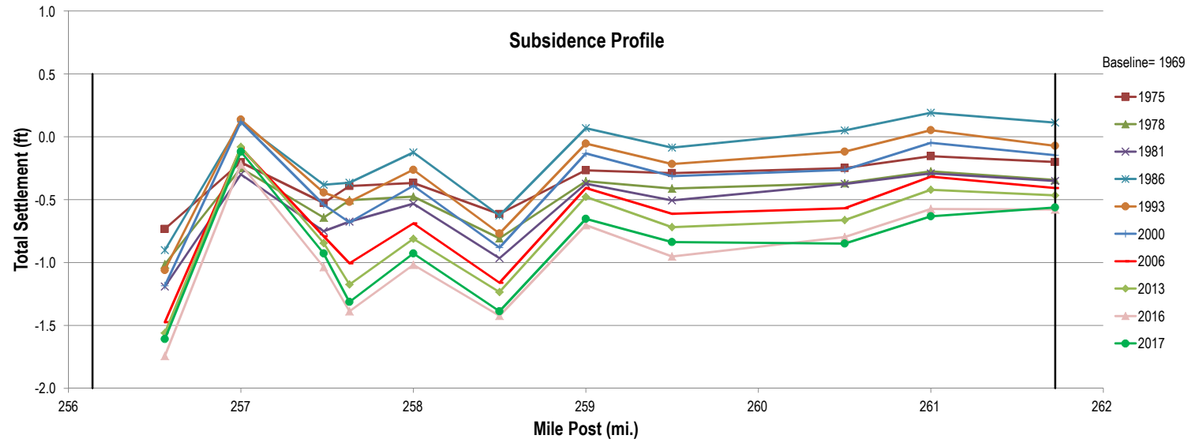

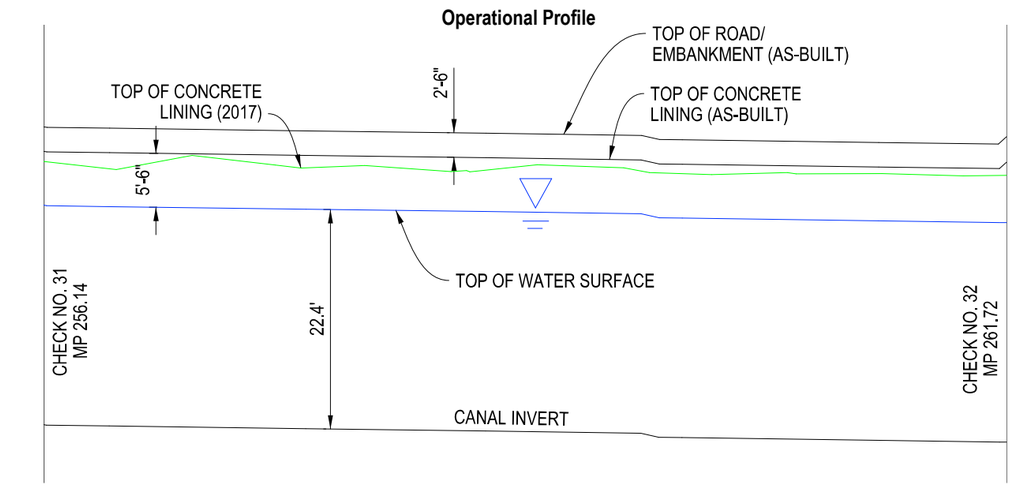

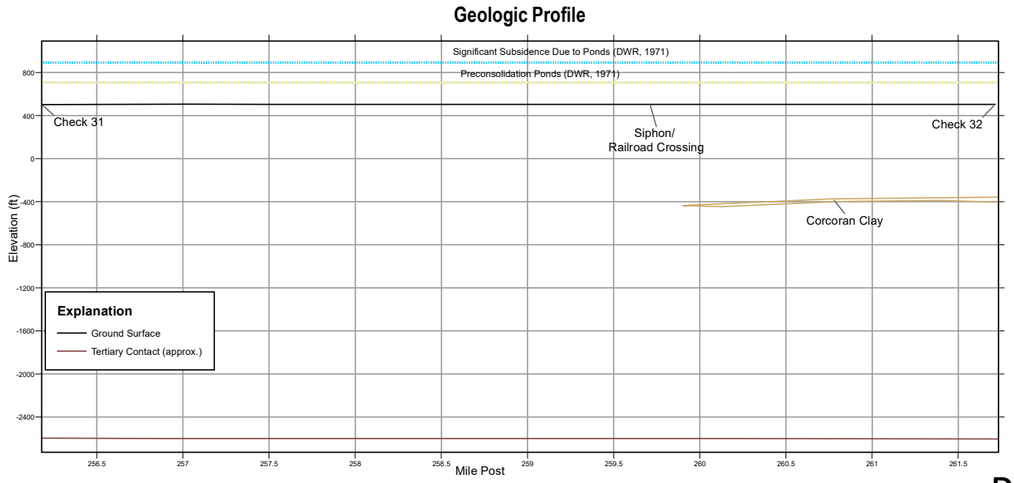

PLATE 21

DEPARTMENT OF WATER RESOURCES
STATE WATER PROJECT
CALIFORNIA AQUEDUCT SUBSIDENCE STUDY

SUBSIDENCE, OPERATION, & GEOLOGIC PROFILES

POOL 32: MP 256.14 – 261.72

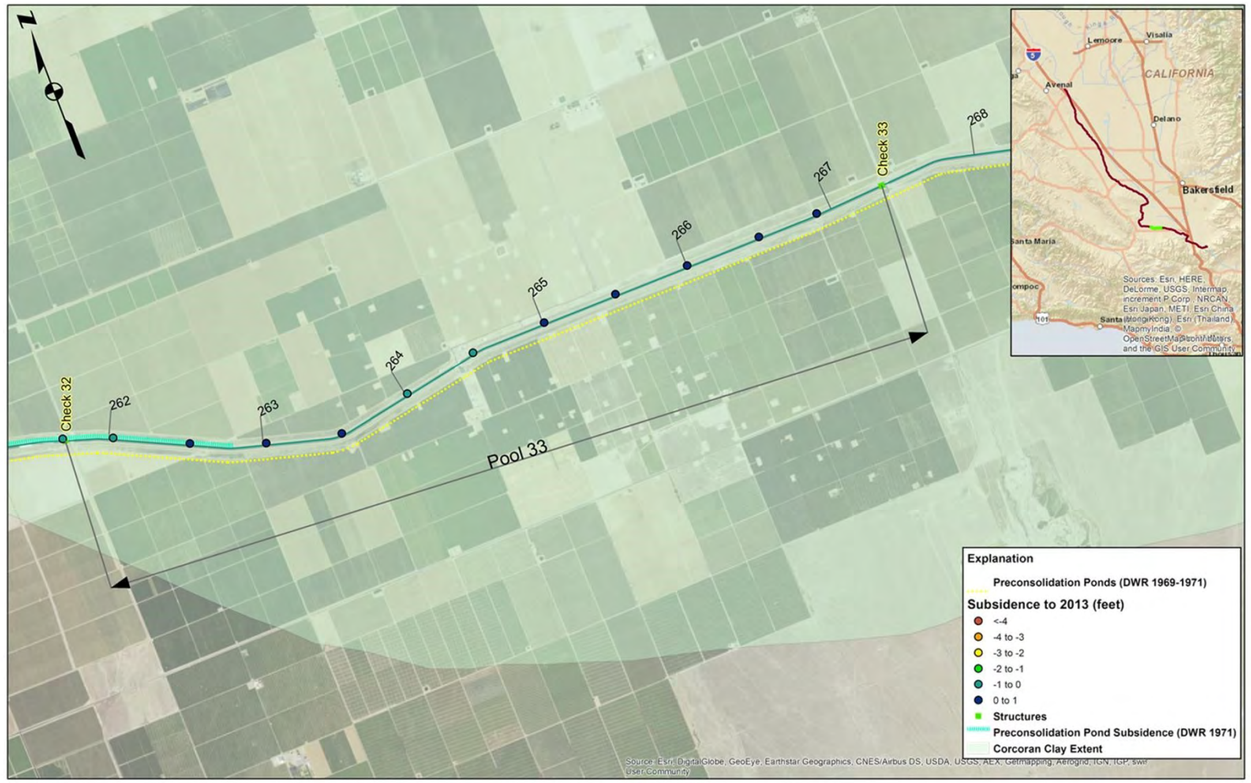

STRUCTURE	SIDE OF EMBANKMENT	MP
CHECK NUMBER 32		261.72
POWERLINE CROSSING		261.74
STILLING WELL	L	261.8
PHONE LINE CROSSING		262.5
PIPELINE CROSSING		262.61
BRIDGE		262.61
POWERLINE CROSSING		263.6
BRIDGE		264.37
POWERLINE CROSSING		264.37
LOS LOBOS SIPHON/BRIDGE		264.37
PIPELINE CROSSING		264.38
TURNOUT	L	264.42
POWERLINE CROSSING		264.9
POWERLINE CROSSING		265.12
TURNOUT	R	266.91
PIPELINE CROSSING		267.14
POWERLINE CROSSING		267.14
SAN EMIGDIO CREEK SIPHON		267.36
STILLING WELL	L	267.36
CHECK NUMBER 33		267.36

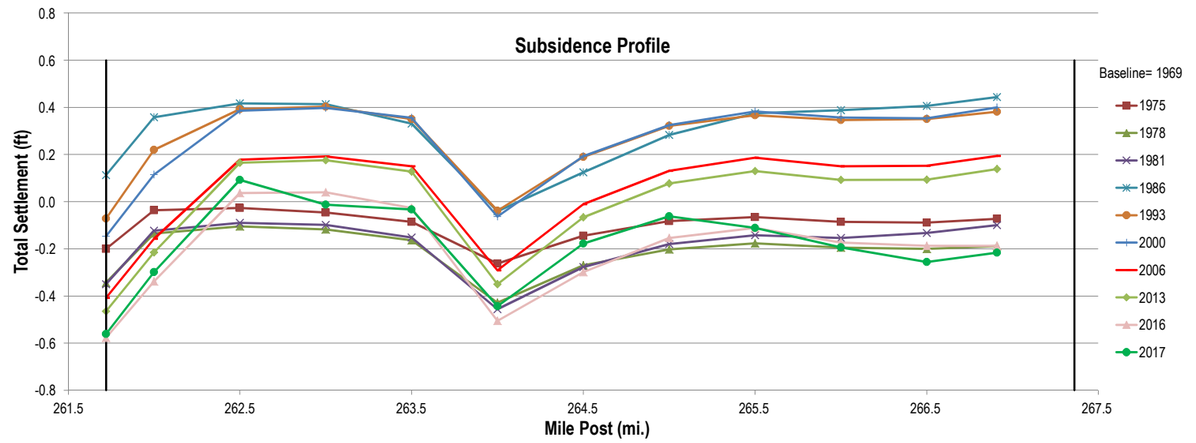

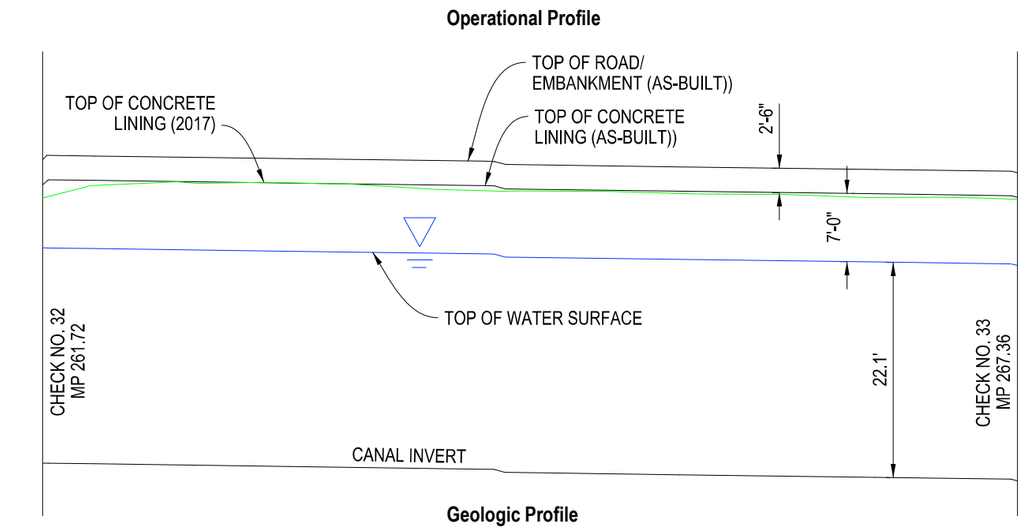

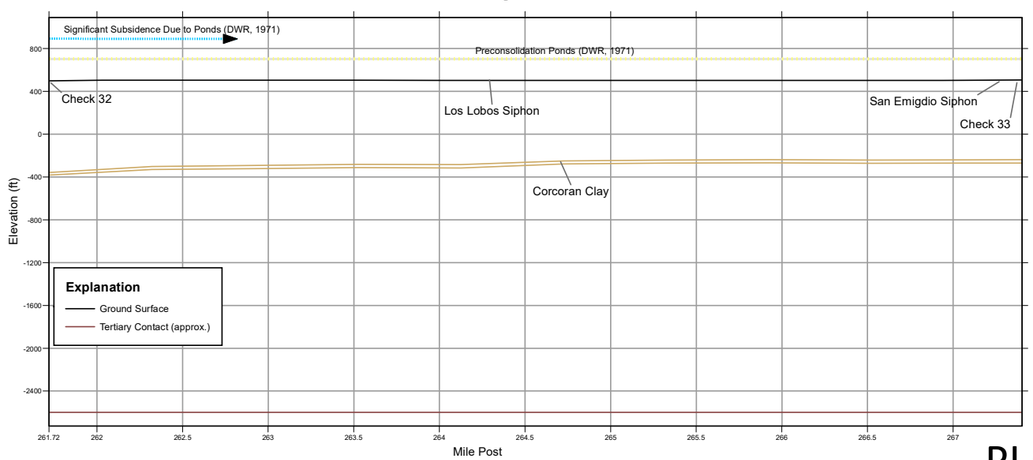

PLATE 22

DEPARTMENT OF WATER RESOURCES
STATE WATER PROJECT
CALIFORNIA AQUEDUCT SUBSIDENCE STUDY

SUBSIDENCE, OPERATION, & GEOLOGIC PROFILES

POOL 33: MP 261.72 – 267.36

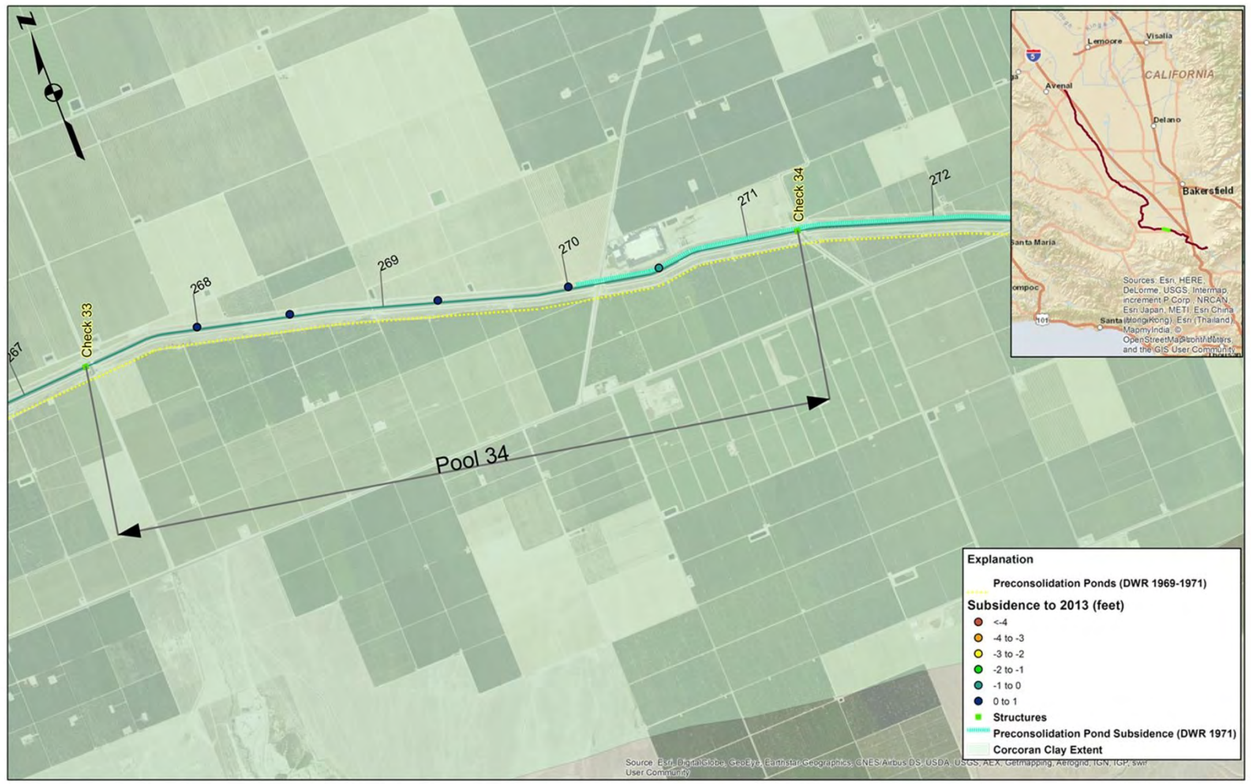

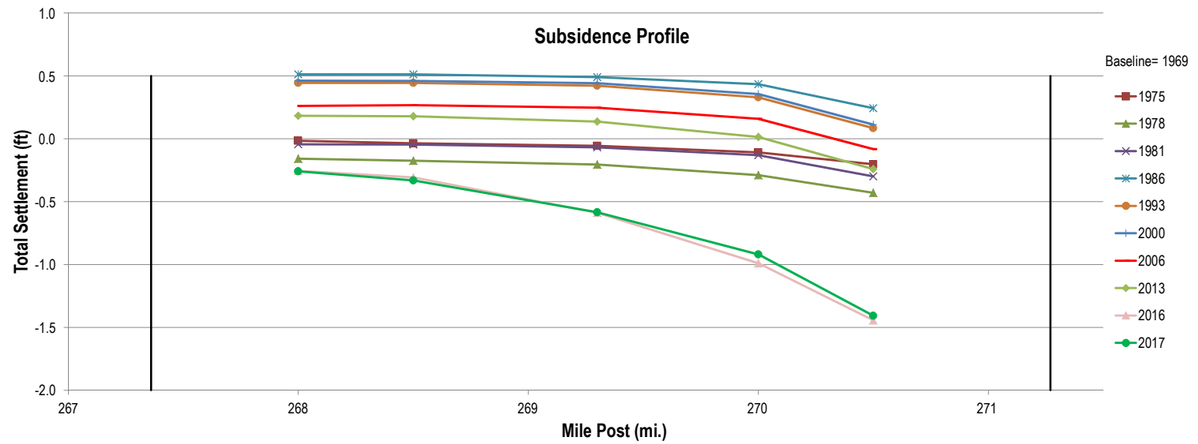

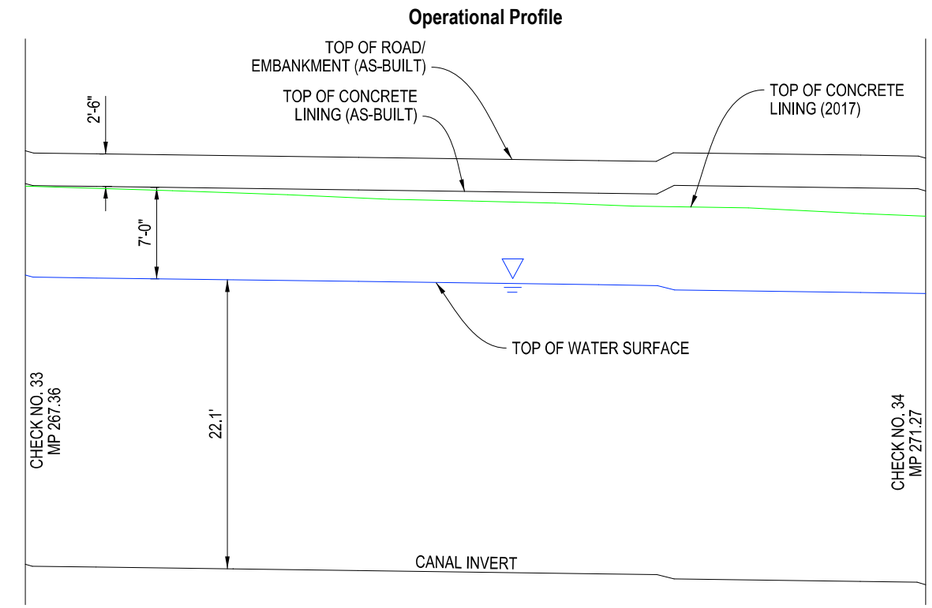

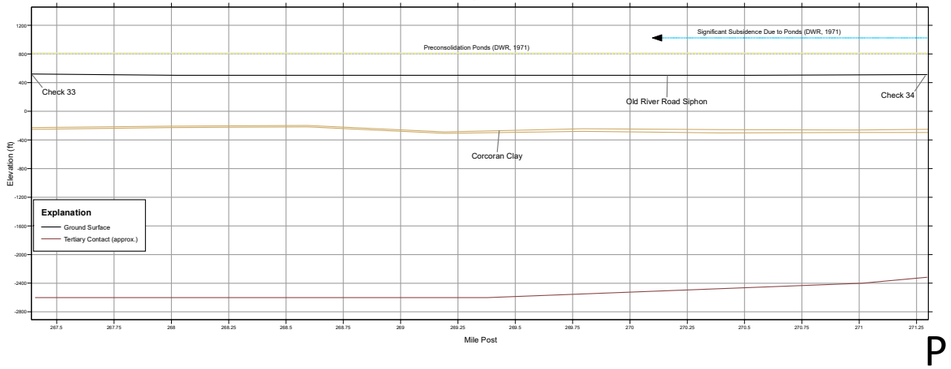

STRUCTURE	SIDE OF EMBANKMENT	MP
CHECK NUMBER 33		267.36
BRIDGE (2)		267.39
PHONE LINE CROSSING		267.44
STILLING WELL	L	267.47
POWERLINE CROSSING		267.58
PIPELINE CROSSING (3)		267.6
PIPELINE CROSSING (2)		268.54
BRIDGE		268.94
PHONE LINE CROSSING		268.95
PIPELINE CROSSING		269.3
PIPELINE CROSSING		269.66
OLD RIVER ROAD SIPHON		270.14
BRIDGE (2)		270.16
POWERLINE CROSSING		270.17
PIPELINE CROSSING		270.18
TURNOUT	L	270.24
STILLING WELL	L	271.26
PLEITITO CREEK SIPHON		271.27
CHECK NUMBER 34		271.27

PLATE 23

DEPARTMENT OF WATER RESOURCES
STATE WATER PROJECT
CALIFORNIA AQUEDUCT SUBSIDENCE STUDY

SUBSIDENCE, OPERATION, & GEOLOGIC PROFILES

POOL 34: MP 267.36 – 271.27

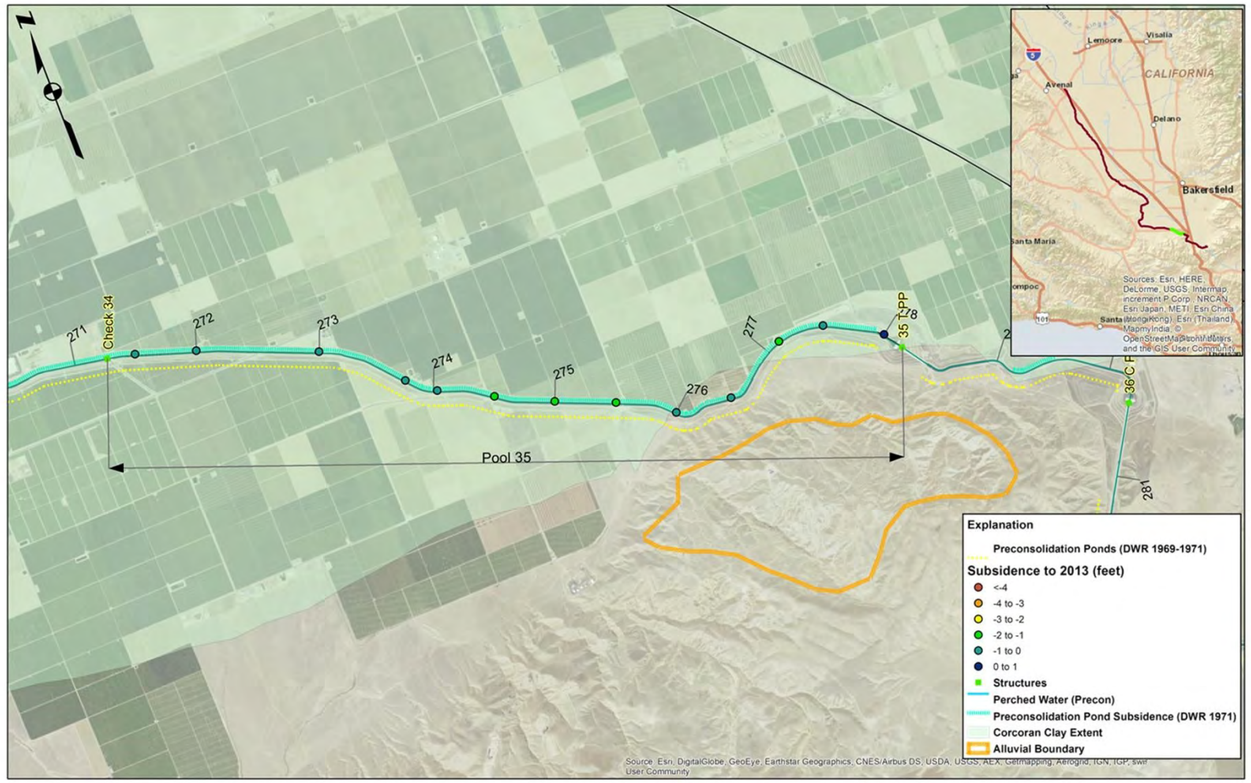

STRUCTURE	SIDE OF EMBANKMENT	MP
CHECK NUMBER 34		271.27
BRIDGE		271.3
STILLING WELL	L	271.37
PIPELINE CROSSING		271.85
TURNOUT	L	272.39
PIPELINE CROSSING (4)		272.4
HIGHWAY 166 BRIDGE		272.53
POWERLINE CROSSING		272.59
PIPELINE CROSSING (2)		273.09
PIPELINE CROSSING (2)		273.48
PIPELINE CROSSING		273.75
POWERLINE CROSSING		273.85
OVERCHUTE CROSSING		274.04
KELLY STATION ROAD BRIDGE		274.45
PIPELINE CROSSING		274.45
OVERCHUTE CROSSING		275.56
TURNOUT	L	276.09
OVERCHUTE CROSSING		276.5
PIPELINE CROSSING		276.71
PHONE LINE CROSSING		276.73
SAND TRAP		276.84
OVERCHUTE CROSSING		277.13
TURNOUT	L	277.31
TEERINK PUMPING PLANT		278.13

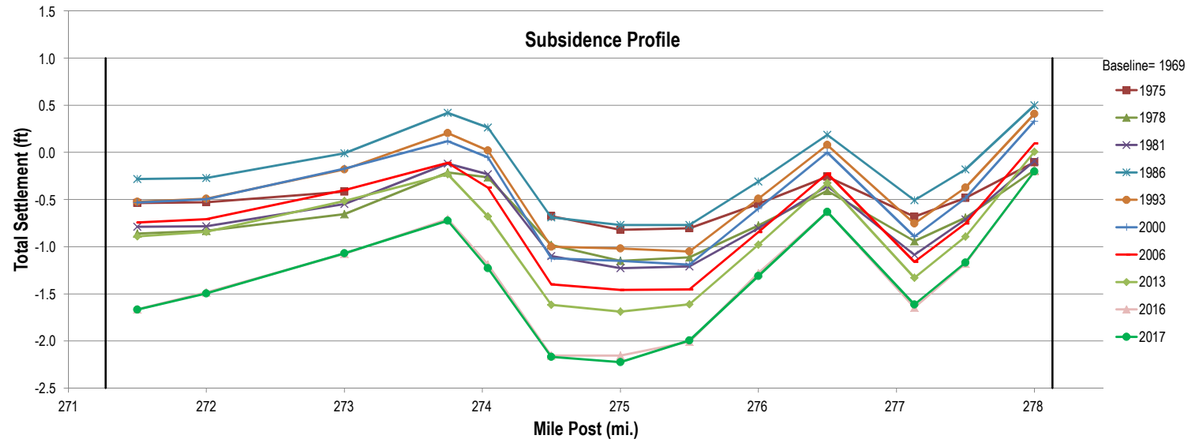

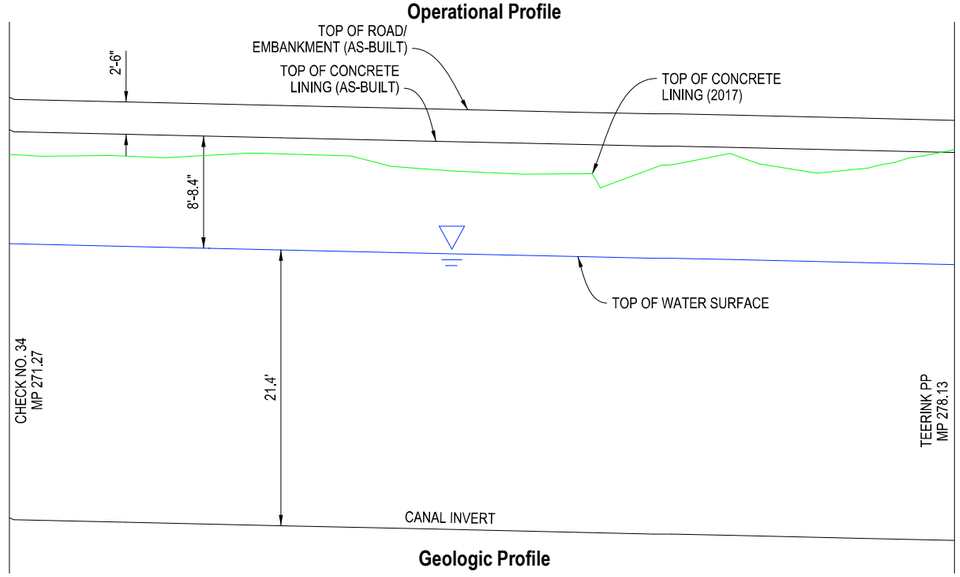

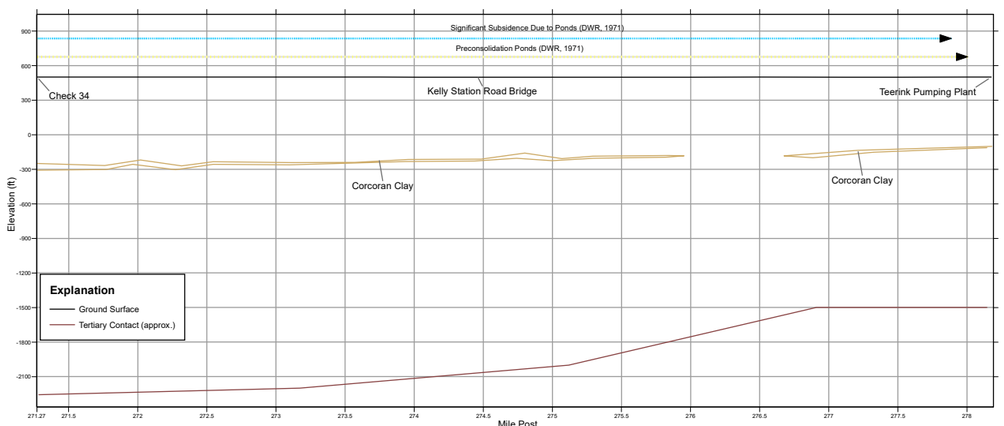

PLATE 24

DEPARTMENT OF WATER RESOURCES
STATE WATER PROJECT
CALIFORNIA AQUEDUCT SUBSIDENCE STUDY

SUBSIDENCE, OPERATION, & GEOLOGIC PROFILES

POOL 35: MP 271.27 – 278.13

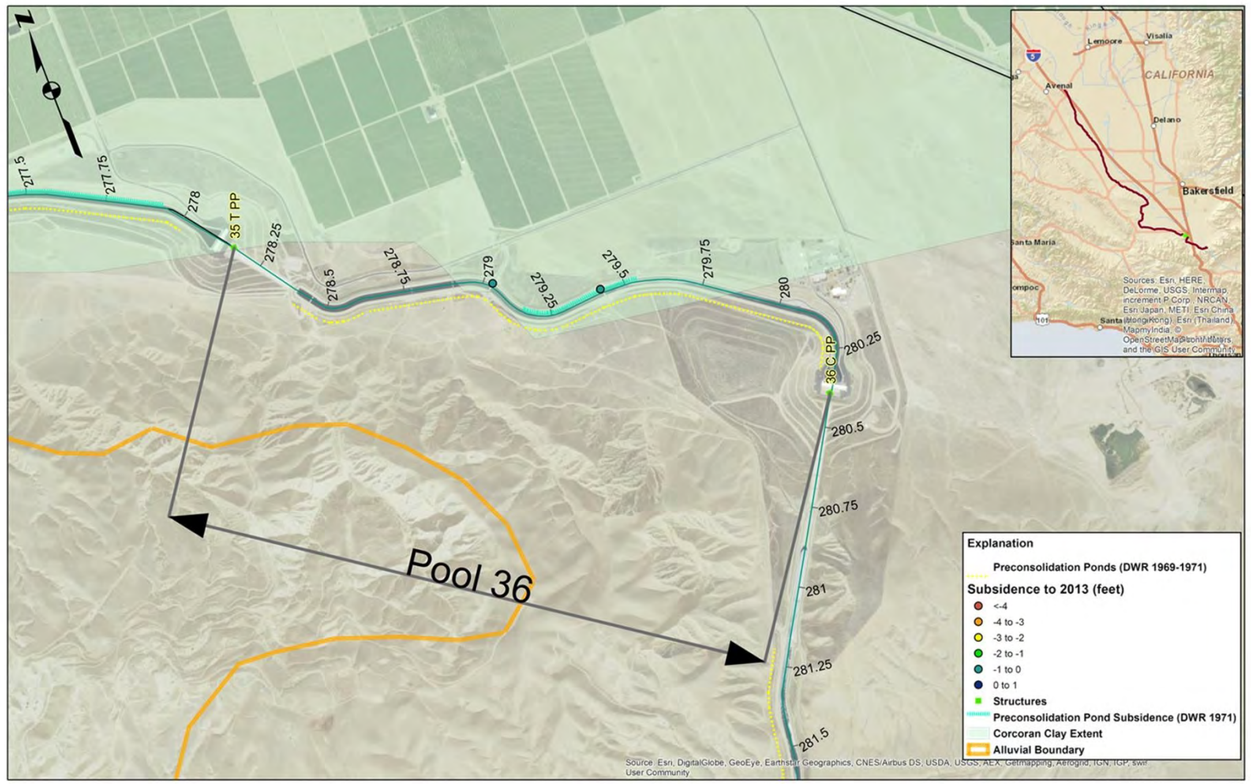

STRUCTURE	SIDE OF EMBANKMENT	MP
TEERINK PUMPING PLANT		278.13
PIPELINE CROSSING		278.41
OVERCHUTE CROSSING		278.47
SUMP PUMP	R	278.78
OVERCHUTE CROSSING		278.8
POWERLINE CROSSING		278.85
OVERCHUTE CROSSING		278.93
TURNOUT	L	279.03
BRIDGE		279.05
POWERLINE CROSSING		279.21
CULVERT CROSSING		279.39
SUMP PUMP	R	279.42
PIPELINE CROSSING		279.44
OVERCHUTE CROSSING		279.44
SUMP PUMP	R	280.03
TURNOUT	L	280.06
SAN JOAQUIN O&M CENTER	L	280.06
CHRISMAN PUMPING PLANT		280.36

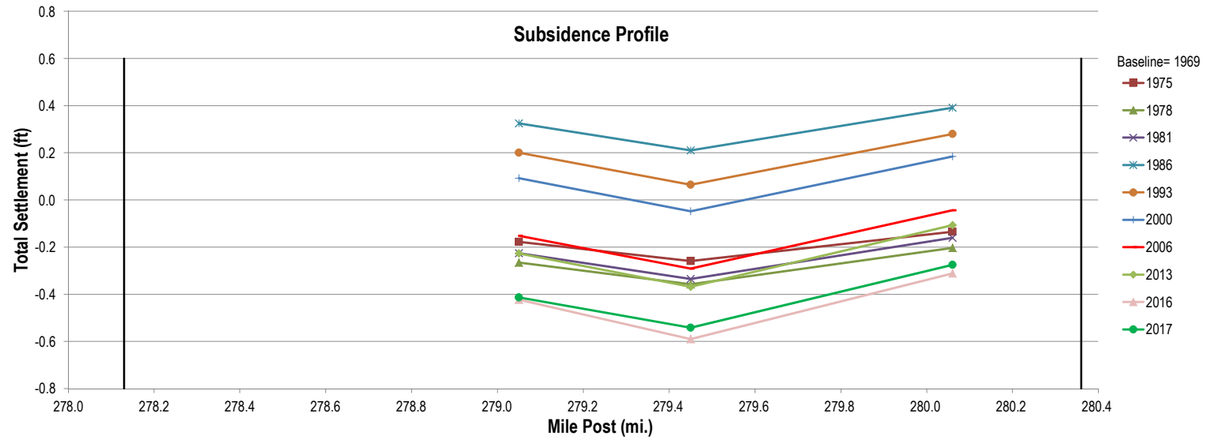

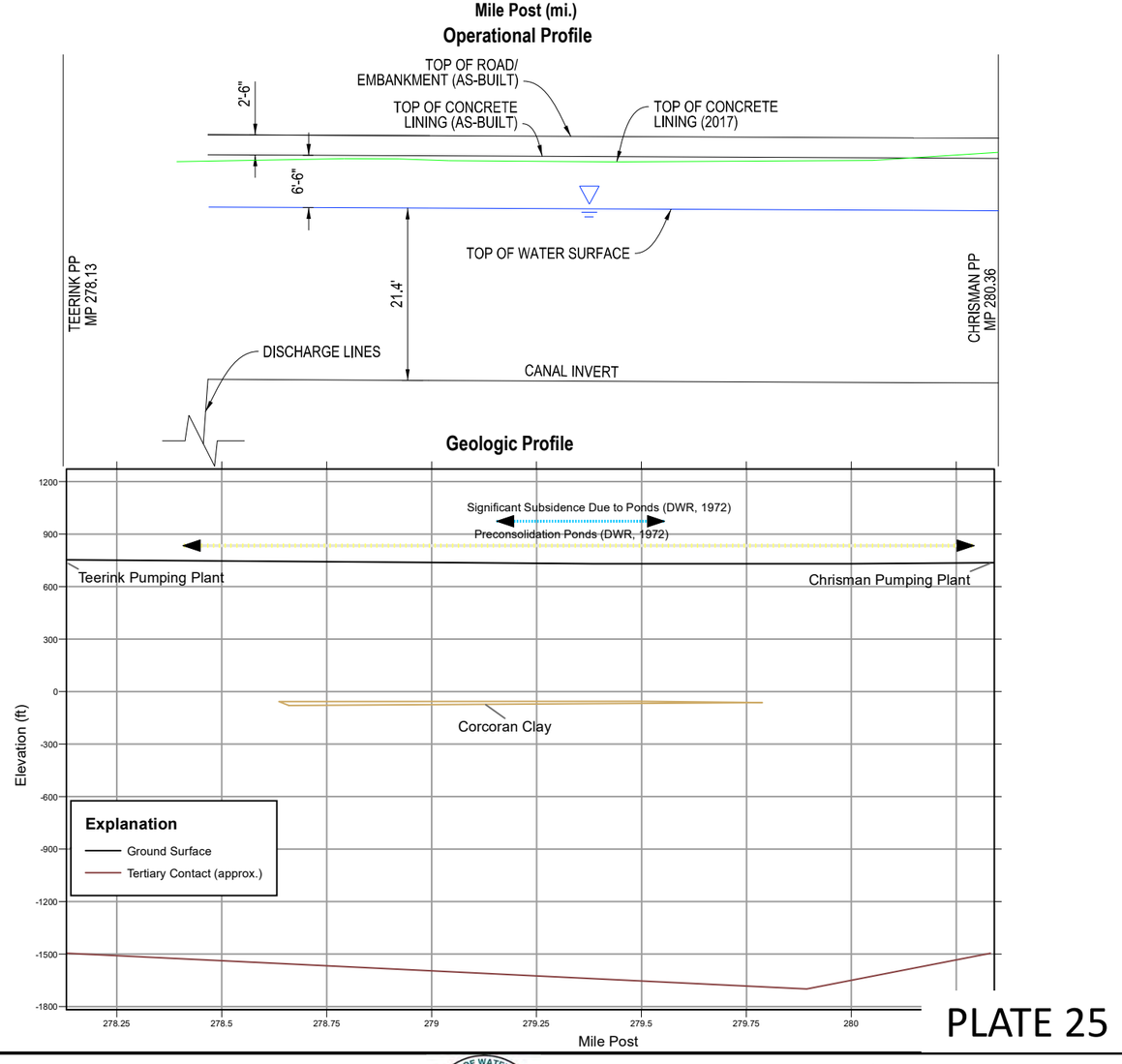

PLATE 25

DEPARTMENT OF WATER RESOURCES
STATE WATER PROJECT
CALIFORNIA AQUEDUCT SUBSIDENCE STUDY

SUBSIDENCE, OPERATION, & GEOLOGIC PROFILES

POOL 36: MP 278.13 – 280.36

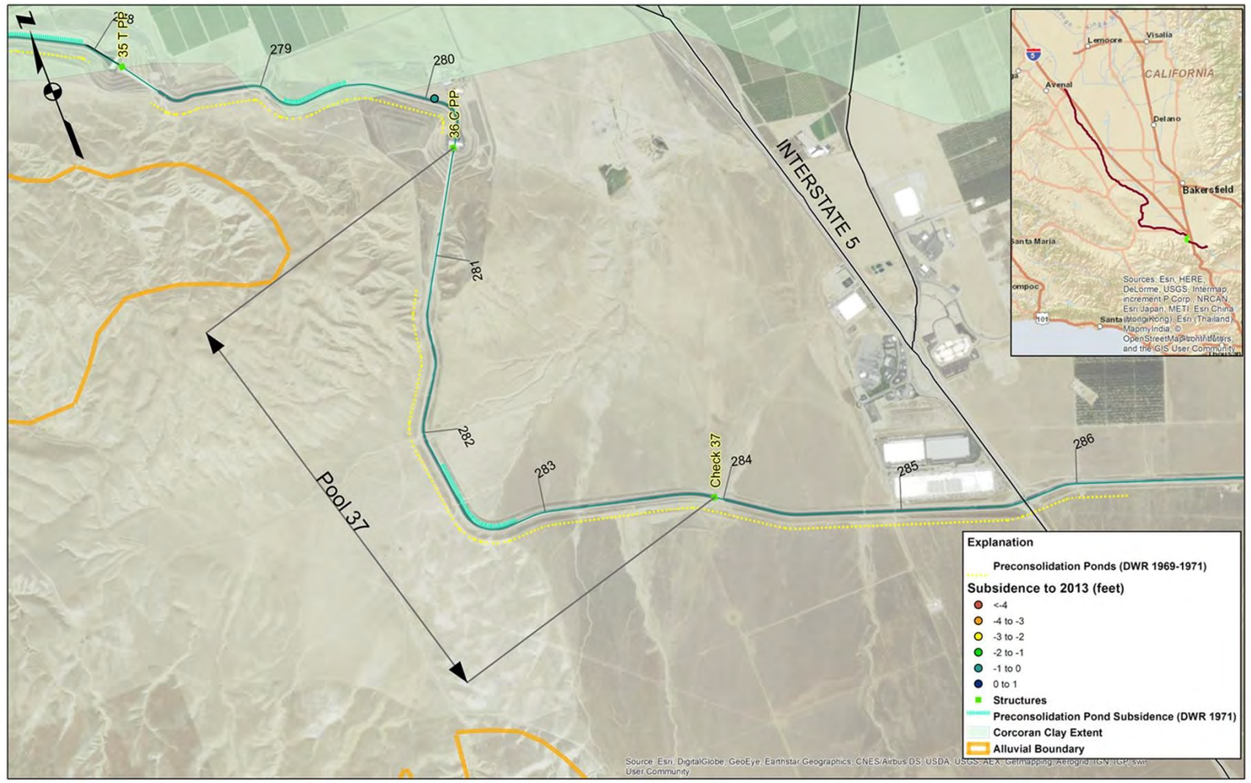

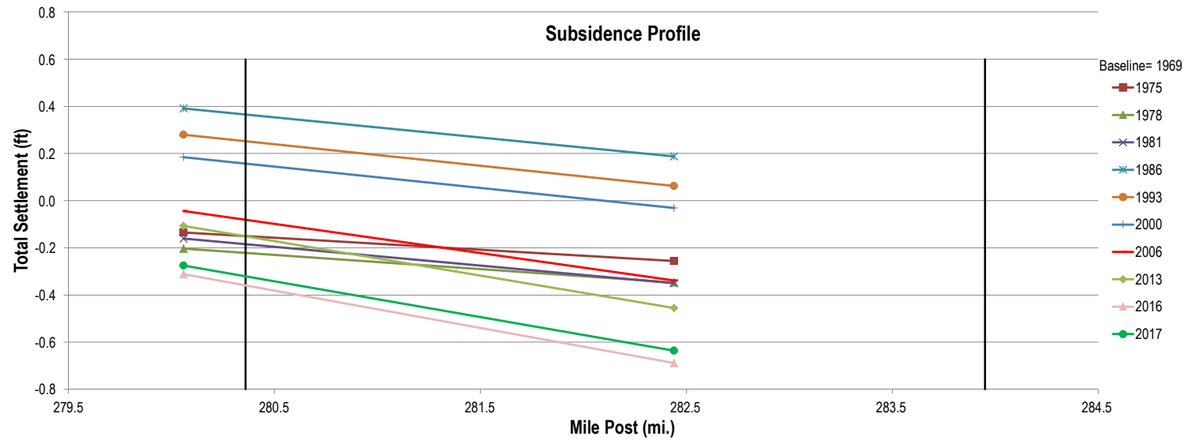

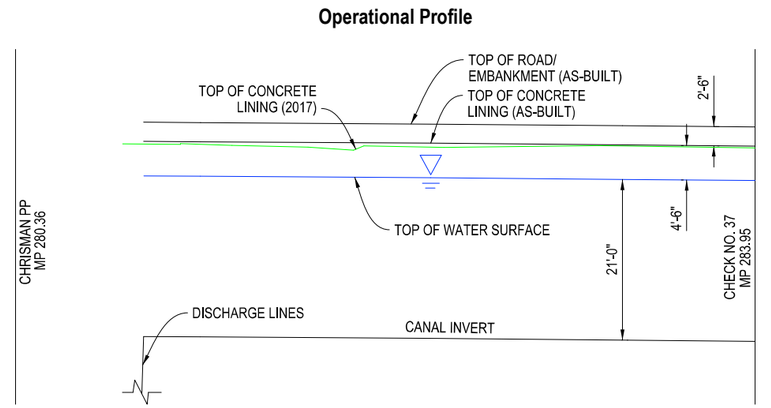

STRUCTURE	SIDE OF EMBANKMENT	MP
CHRISMAN PUMPING PLANT		280.36
BRIDGE		281.16
SUMP PUMP	R	281.18
OVERCHUTE /PIPELINE		281.41
POWERLINE CROSSING		281.72
OVERCHUTE CROSSING		281.78
PIPELINE CROSSING (3)		281.78
SUMP PUMP	R	281.92
OVERCHUTE CROSSING		282
BRIDGE		282.03
PIPELINE CROSSING (3)		282.03
PIPELINE CROSSING		282.04
TURNOUT	L	282.06
OVERCHUTE CROSSING		282.44
OVERCHUTE CROSSING		283.19
STILLING WELL	L	283.93
BRIDGE		283.95
SALT CREEK SIPHON		283.95
CHECK NUMBER 37		283.95

Geologic Profile

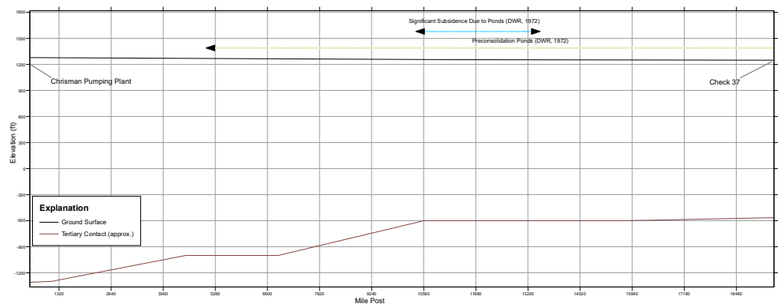

PLATE 26

DEPARTMENT OF WATER RESOURCES
STATE WATER PROJECT
CALIFORNIA AQUEDUCT SUBSIDENCE STUDY

SUBSIDENCE, OPERATION, & GEOLOGIC PROFILES

POOL 37: MP 280.36 – 283.95

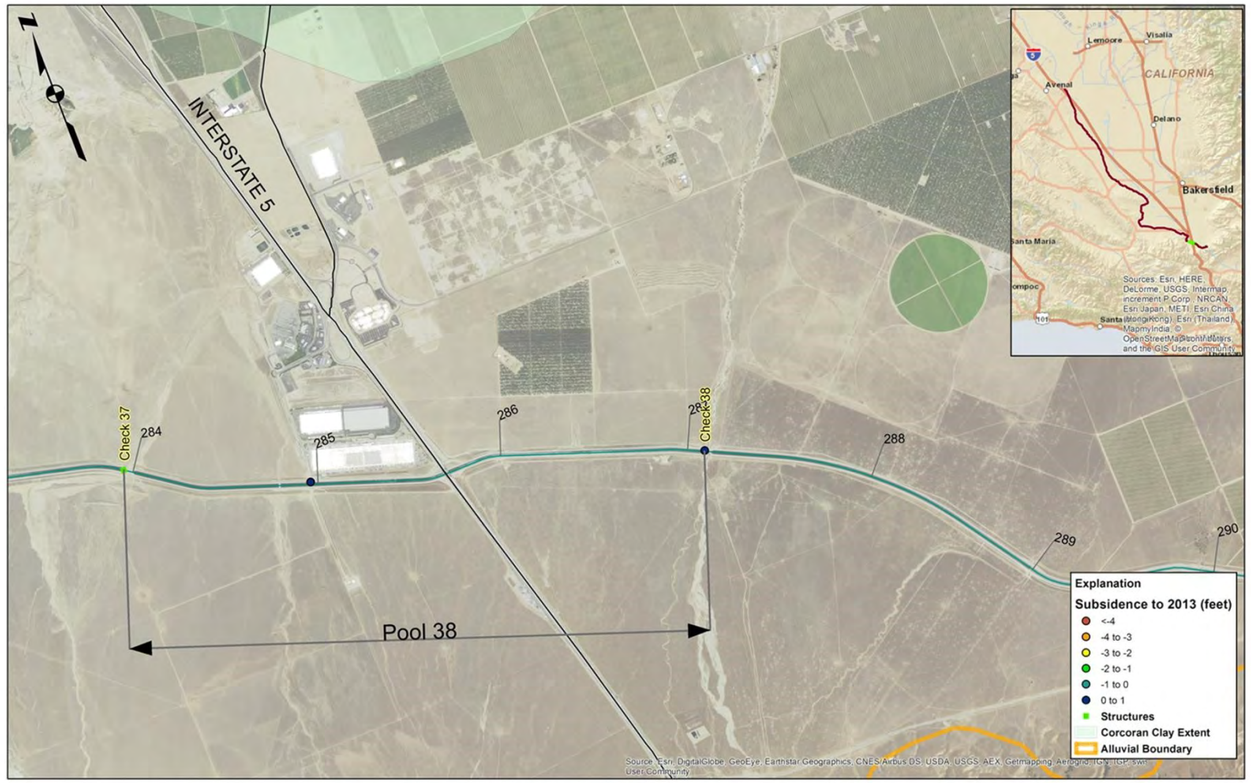

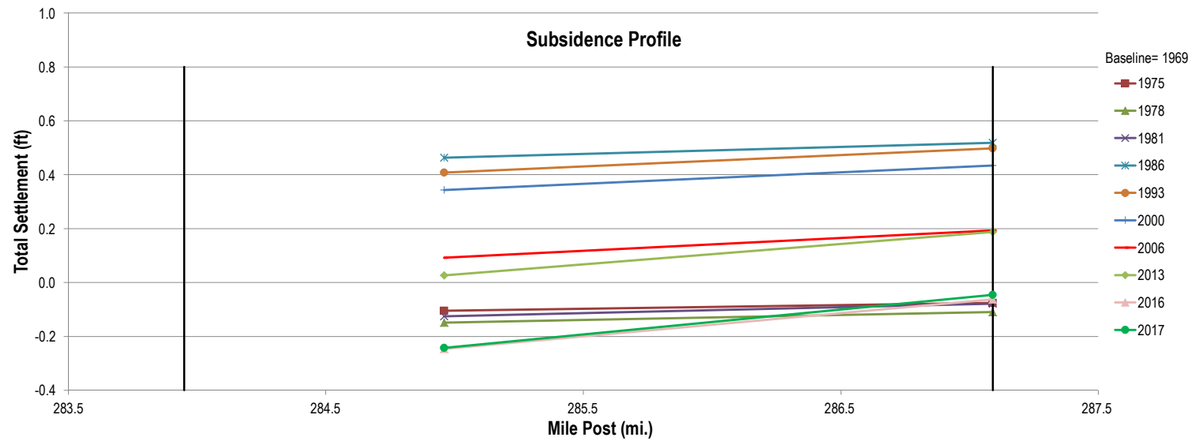

STRUCTURE	SIDE OF EMBANKMENT	MP
CHECK NUMBER 37		283.95
PIPELINE CROSSING		283.97
STILLING WELL	L	284.05
OVERCHUTE CROSSING		284.8
POWERLINE CROSSING		284.95
BRIDGE		284.97
PIPELINE CROSSING		284.97
TURNOUT	L	285.01
INTERSTATE 5 OVERPASS		285.69
INTERSTATE 5 BRIDGE		285.71
POWERLINE CROSSING		285.76
PIPELINE CROSSING (3)		285.99
PHONE LINE CROSSING		285.99
TURNOUT	L	286.39
CULVERT CROSSING		286.42
PIPELINE CROSSING		286.56
STILLING WELL	L	287.02
TURNOUT	L	287.06
GRAPEVINE CREEK SIPHON		287.09
CHECK NUMBER 38		287.09

Operational Profile

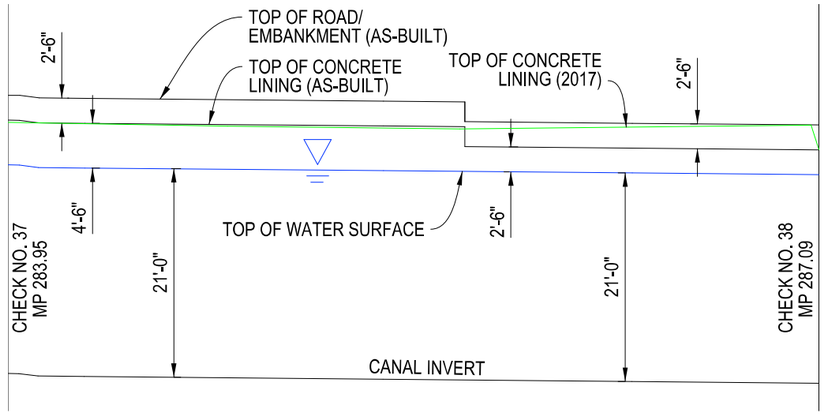

Geologic Profile

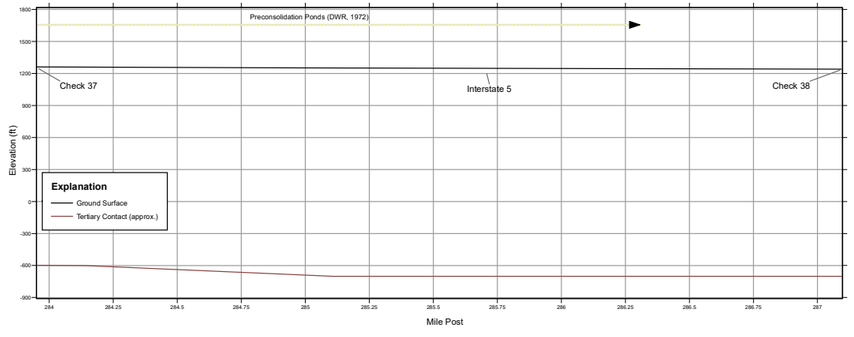

PLATE 27

DEPARTMENT OF WATER RESOURCES
STATE WATER PROJECT
CALIFORNIA AQUEDUCT SUBSIDENCE STUDY

SUBSIDENCE, OPERATION, & GEOLOGIC PROFILES

POOL 38: MP 283.95 – 287.09

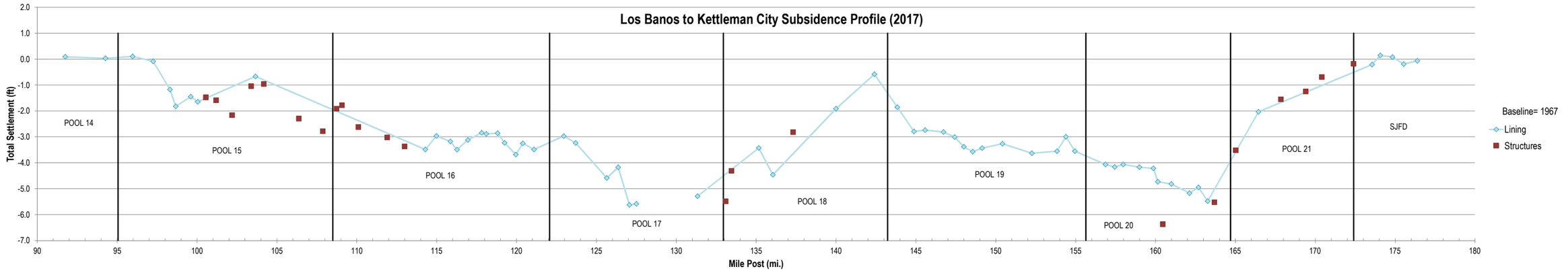

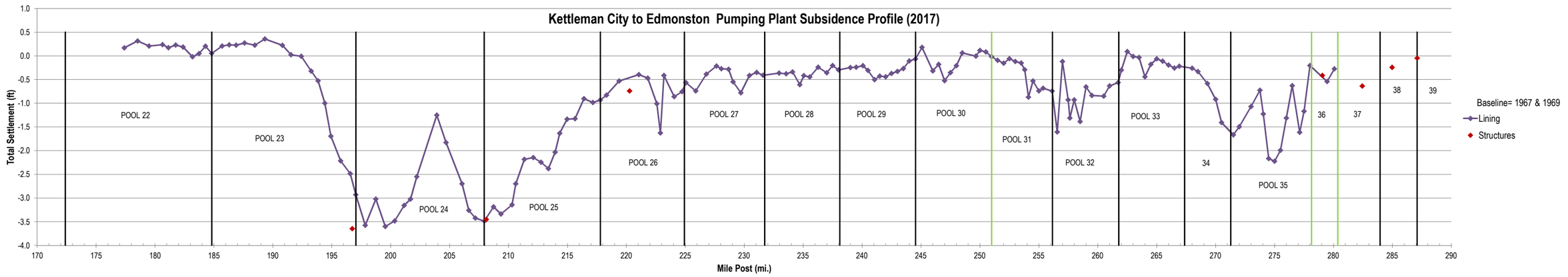

PLATE 28

DEPARTMENT OF WATER RESOURCES
STATE WATER PROJECT
CALIFORNIA AQUEDUCT SUBSIDENCE STUDY

SLFD & SJFD SUBSIDENCE
PROFILES 2017
MP 91.75 – 287.09

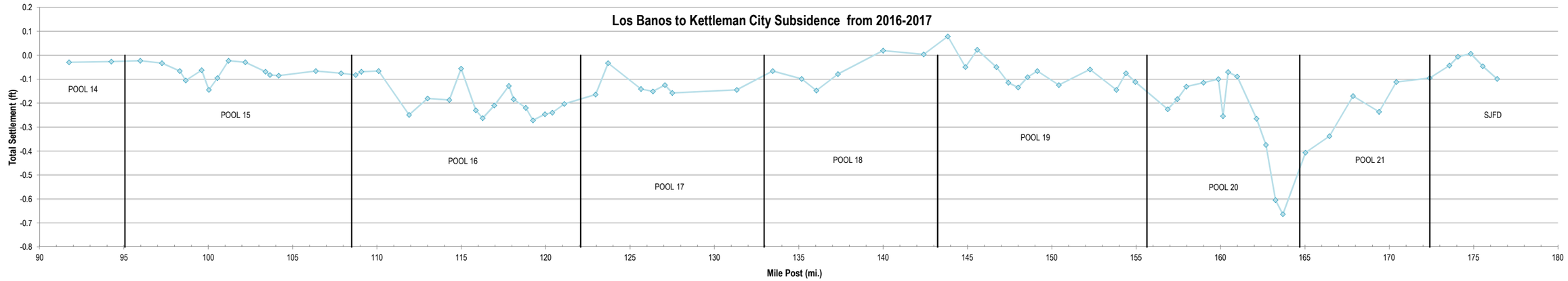

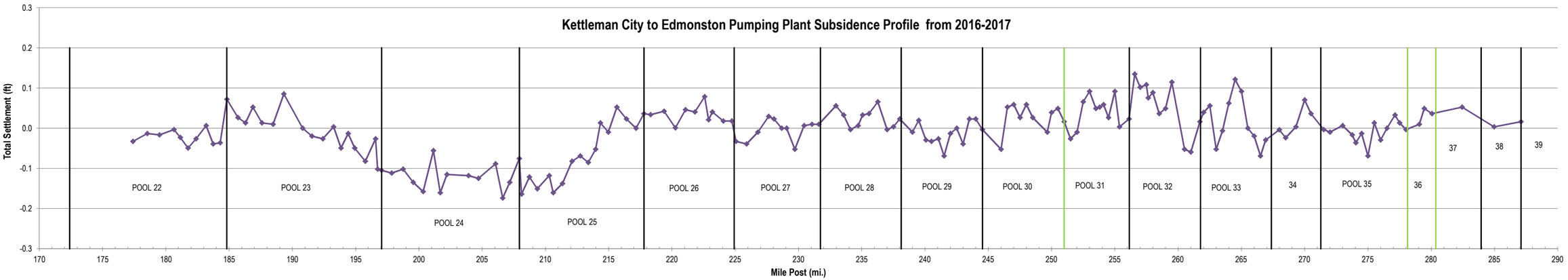

PLATE 29

DEPARTMENT OF WATER RESOURCES
STATE WATER PROJECT
CALIFORNIA AQUEDUCT SUBSIDENCE STUDY

SLFD & SJFD SUBSIDENCE PROFILES
FROM 2016-2017
MP 91.75 – 287.09

Los Banos to Kettleman City Top of Lining Subsidence Profile from 1967-2017

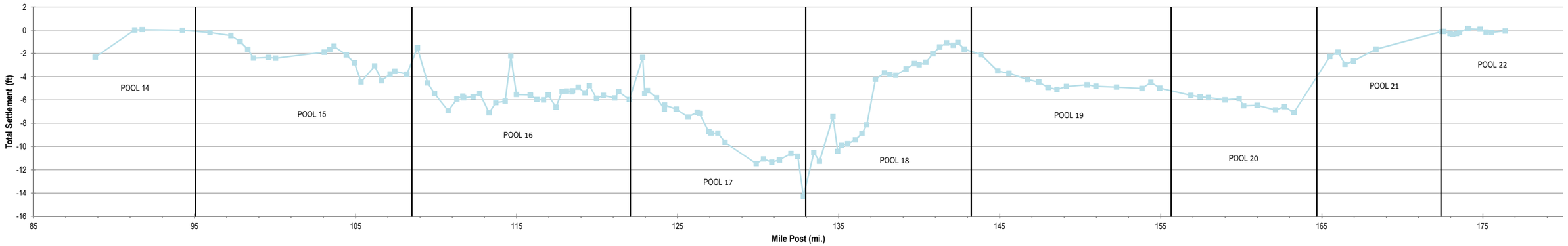

Kettleman City to Edmonston Pumping Plant Top of Lining Subsidence Profile from 1967/1969 to 2017

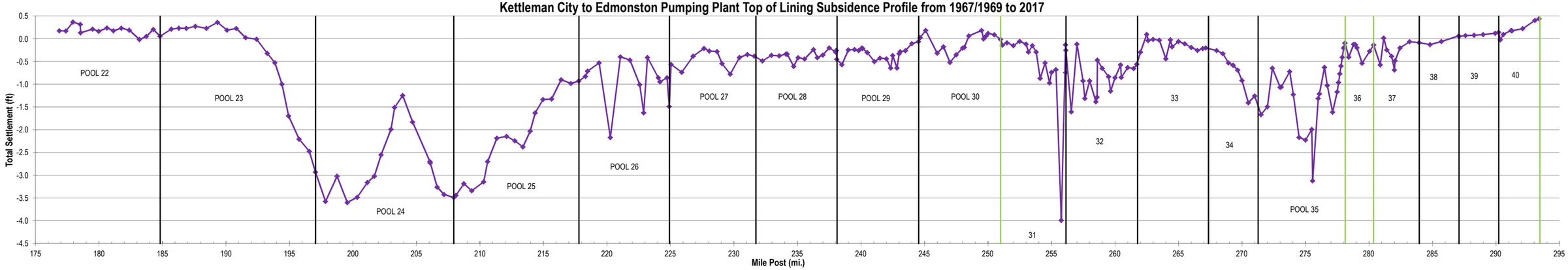

PLATE 31

DEPARTMENT OF WATER RESOURCES
STATE WATER PROJECT
CALIFORNIA AQUEDUCT SUBSIDENCE STUDY

SLFD & SJFD TOP OF LINING MAGNITUDE OF SUBSIDENCE FROM AS-BUILT TO 2017

Los Banos to Kettleman City Top of Lining: 1967 As-Built Elev. vs. 2017 Elev.

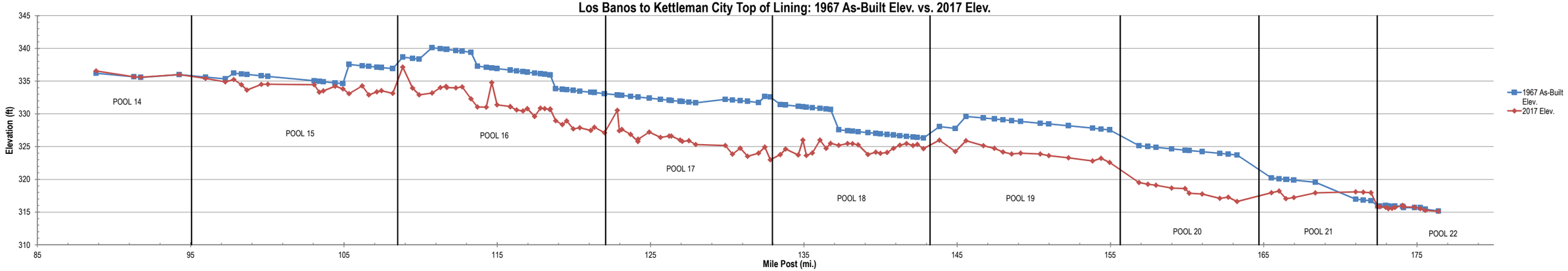

Kettleman City to Edmonston Pumping Plant Top of Lining: As-Built Elev. vs. 2017 Elev. (1 of 4)

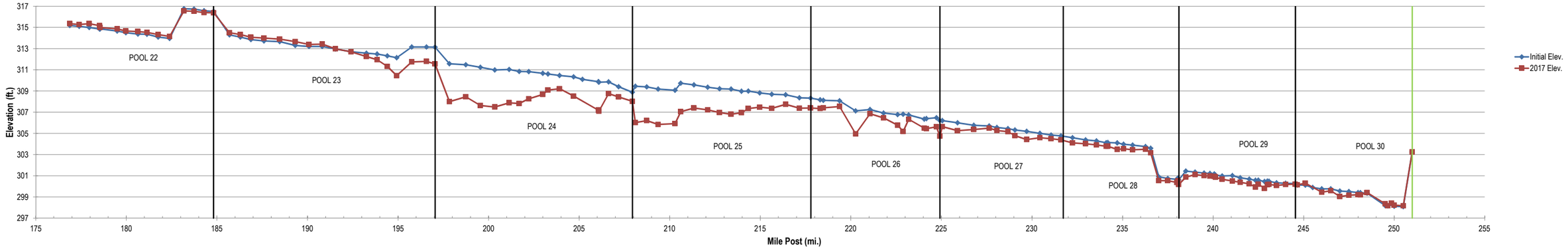

Kettleman City to Edmonston Pumping Plant Top of Lining: As-Built Elev. vs. 2017 Elev. (2 of 4)

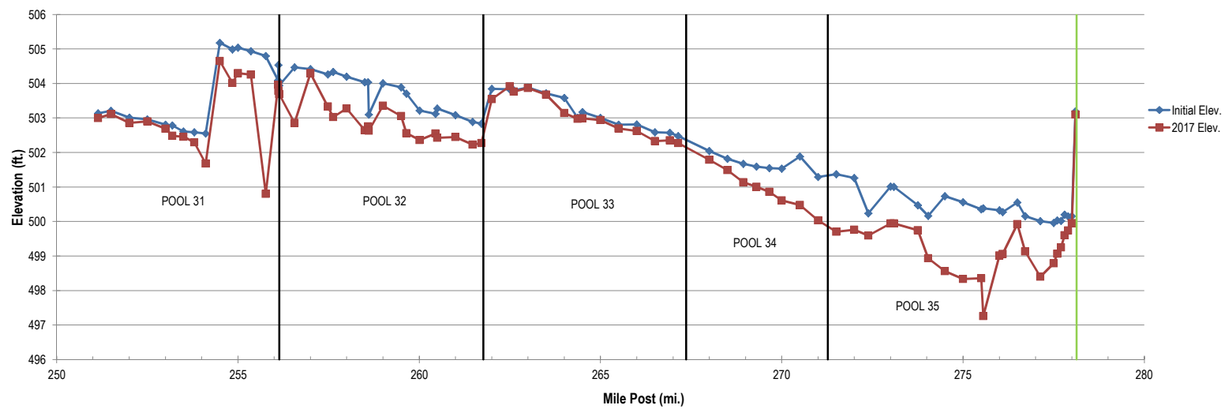

Kettleman City to Edmonston Pumping Plant Top of Lining: As-Built Elev. vs. 2017 Elev. (3 of 4)

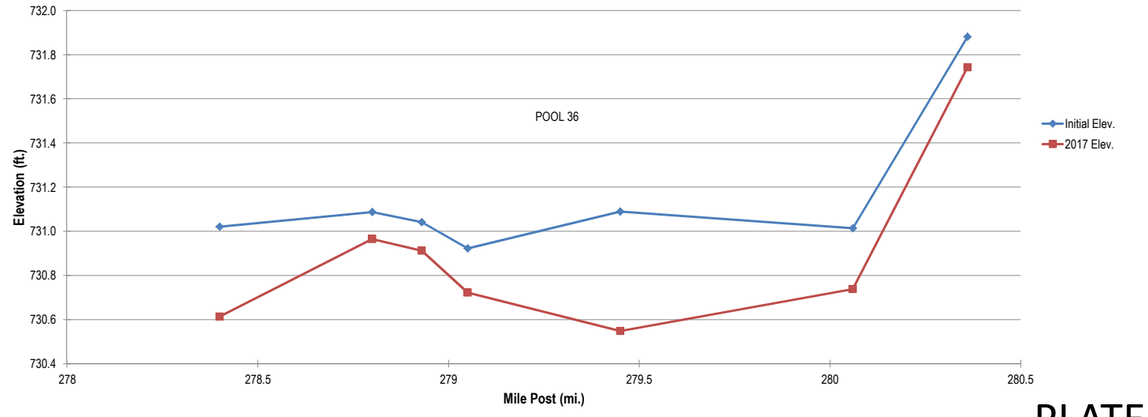

PLATE 32

DEPARTMENT OF WATER RESOURCES
STATE WATER PROJECT
CALIFORNIA AQUEDUCT SUBSIDENCE STUDY

SLFD & SJFD TOP OF LINING SUBSIDENCE PROFILES FROM AS-BUILT TO 2017 (1 of 2)

MP 88 – 294

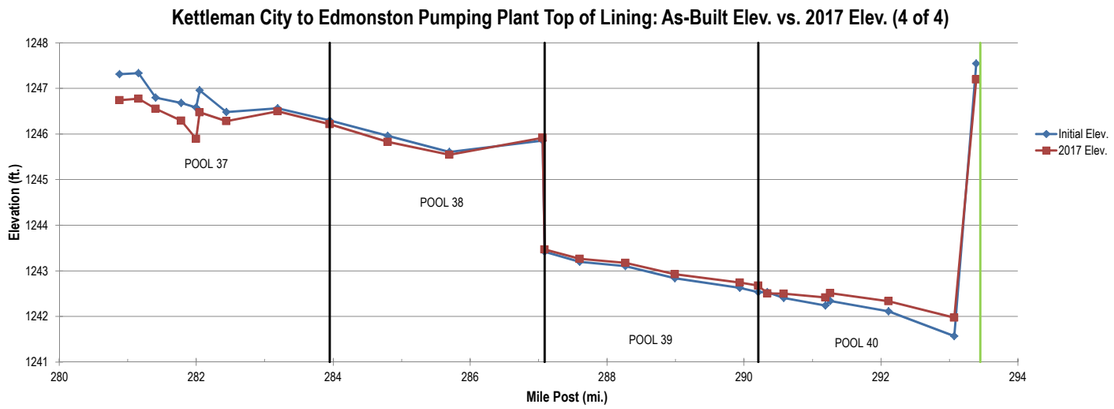

PLATE 33

DEPARTMENT OF WATER RESOURCES
STATE WATER PROJECT
CALIFORNIA AQUEDUCT SUBSIDENCE STUDY

SLFD & SJFD TOP OF LINING SUBSIDENCE
PROFILES FROM AS-BUILT TO 2017 (2 of 2)
MP 88 – 294

March 2019